

Université de Montréal

**Investigation of the Non-Canonical Roles and Regulation Mechanisms  
of  $\beta$ -arrestin 1/2**

*Par*

**Badr Sokrat**

Département de Biochimie et Médecine Moléculaire

Faculté de Médecine

Thèse présentée en vue de l'obtention du grade de

Philosophiae Doctor (Ph.D.)

En Biochimie, Cheminement libre

Avril 2023

© Badr Sokrat, 2023

Université de Montréal

Département de Biochimie et Médecine Moléculaire, Faculté de Médecine

---

*Cette thèse intitulée*

**Investigation of the Non-Canonical Roles and Regulation Mechanisms of  $\beta$ -arrestin 1/2**

*Présenté par*

**Badr Sokrat**

*A été évalué(e) par un jury composé des personnes suivantes*

**Nikolaus Heveker**

Président-rapporteur

**Michel Bouvier**

Directeur de recherche

**Patrick Giguère**

Membre du jury

**Jean-Philippe Pin**

Examineur externe

## Résumé

Les récepteurs couplés aux protéines G (RCPG) constituent la plus grande famille de récepteurs à domaines transmembranaires et sont impliqués dans divers processus biologiques, ce qui en fait une cible privilégiée pour le développement de médicaments. Parmi les protéines qui régulent la signalisation des RCPG, les  $\beta$ -arrestines sont impliquées dans plusieurs fonctions canoniques telles que la désensibilisation, l'internalisation et le trafic des récepteurs. En outre, la  $\beta$ -arrestine accomplit aussi des fonctions non-canoniques en agissant comme un échafaudage pour des complexes de signalisation notamment pour la voie MAPK et ainsi favorise certaines voies de signalisation intracellulaire. La présente thèse visait à explorer des fonctions non-canoniques et de nouveaux mécanismes possibles de régulation de la  $\beta$ -arrestine induite par l'activation des RCPG.

Le premier projet visait à mettre en évidence le mécanisme de trafic des protéines G de la membrane plasmique vers les endosomes et le rôle que joue la  $\beta$ -arrestine dans ce processus. Nous avons montré que la sous-unité  $G_{\alpha s}$  se dissocie de la membrane plasmique indépendamment de la  $\beta$ -arrestine après l'activation des récepteurs, alors que le dimère  $G\beta\gamma$  nécessite la présence de la  $\beta$ -arrestine. Nous avons également mis en évidence la formation d'un complexe composé du récepteur V2 de la vasopressine, de la  $\beta$ -arrestine et de l'hétérodimère  $G\beta\gamma$  et que ce complexe est crucial pour la translocation des protéines G vers les endosomes. Cette étude met en évidence le rôle de la  $\beta$ -arrestine dans le trafic endosomal des protéines G et établit les bases pour expliquer sa contribution dans la médiation de la signalisation soutenue des protéines G dans les endosomes.

Le second projet avait pour objectif d'explorer le rôle de l'ubiquitination du récepteur du glucagon (GCGR) sur sa signalisation et les fonctions de la  $\beta$ -arrestine. Nous avons montré que l'état d'ubiquitination de ce récepteur cause un biais de signalisation, car le GCGR déubiquitiné présente une diminution du couplage et de l'activité des protéines G alors que la liaison à la  $\beta$ -arrestine est augmentée. Ceci contribue à l'activation de la voie de signalisation MAPK p38 de manière dépendante de la  $\beta$ -arrestine 1. Nous avons également montré que le biais en faveur de

la  $\beta$ -arrestine ne réduit pas la sécrétion d'insuline médiée par le GCGR dans les cellules  $\beta$  pancréatiques. Cette étude suggère que la sécrétion d'insuline dépendante du GCGR implique à la fois une signalisation dépendante des protéines G, mais aussi de la  $\beta$ -arrestine. Le statut d'ubiquitination du GCGR oriente la signalisation du récepteur par différents effecteurs pour réguler la sécrétion d'insuline et l'homéostasie du glucose.

Le troisième projet visait à identifier de nouveaux interacteurs des  $\beta$ -arrestines 1/2 et à caractériser le rôle de ces interactions dans le contexte de la signalisation des RCPG. Nous avons identifié plus de 100 nouveaux interacteurs potentiels des  $\beta$ -arrestines 1/2 en utilisant l'approche protéomique BioID. Nous avons confirmé l'interaction de l'enzyme atypique de conjugaison de l'ubiquitine UBE2O avec les  $\beta$ -arrestines. Nous avons également montré que UBE2O module le trafic des  $\beta$ -arrestines entre la membrane plasmique et les endosomes. Cette étude ouvre de nouvelles voies pour explorer des fonctions potentielles des  $\beta$ -arrestines médiées par leurs liaisons à des interacteurs jusqu'alors non identifiés.

Les résultats compilés dans cette thèse permettent de dresser un tableau plus étendu des mécanismes régulant les fonctions de la  $\beta$ -arrestine ainsi que de nouveaux rôles potentiels que cette protéine joue dans la signalisation des RCPG. La caractérisation des fonctions non-canoniques et des mécanismes de régulation de la  $\beta$ -arrestine est une avenue prometteuse qui pourrait mener au développement de thérapies ciblant les RCPG.

**Mots-clés :** RCPG,  $\beta$ -arrestine, signalisation cellulaire, complexe protéique, modifications post-traductionnelles, trafic cellulaire



## Abstract

G protein-coupled receptors (GPCRs) are the largest family of transmembrane receptors and are involved in various biological processes, making them an interesting target for drug discovery. GPCR signaling is regulated by various proteins, including the  $\beta$ -arrestin family that mediate various canonical functions such as receptor desensitization, internalization, and trafficking.  $\beta$ -arrestin also fulfills certain non-canonical roles and has been shown to trigger intracellular signaling by acting as a scaffold for signaling complexes such as for the MAPK pathway. The present thesis aimed to explore non-canonical functions and possible novel mechanism of regulation of  $\beta$ -arrestin following GPCR activation.

The objective of the first project was to uncover G protein trafficking mechanism from the plasma membrane to the endosomes and the role that  $\beta$ -arrestin plays in this process. We showed that the  $G_{\alpha s}$  subunit dissociates from the plasma membrane independently of  $\beta$ -arrestin after receptor activation while the  $G\beta\gamma$  dimer requires  $\beta$ -arrestin for its trafficking. We also revealed the formation of a complex composed of the vasopressin V2 receptor,  $\beta$ -arrestin, and the  $G\beta\gamma$  heterodimer and that this complex is critical for G protein translocation to the endosomes. This study highlights the role of  $\beta$ -arrestin in  $G\beta\gamma$  trafficking and lays the basis for explaining the role of  $\beta$ -arrestin in mediating sustained endosomal G protein signaling.

The aim of the second project was to explore the role of the glucagon receptor (GCGR) ubiquitination on signaling and  $\beta$ -arrestin functions. We showed that the ubiquitination state of the receptor controls signaling bias as a deubiquitinated GCGR exhibits decreased G protein coupling and activity while  $\beta$ -arrestin binding is enhanced. Deubiquitinated GCGR signaling is also redirected to a  $\beta$ -arrestin 1-dependent p38 MAPK pathway. We also revealed that this  $\beta$ -arrestin bias does not reduce GCGR-mediated insulin secretion in pancreatic  $\beta$ -cells. This study suggests that GCGR-dependent insulin secretion involves both G-protein and  $\beta$ -arrestin-dependent signaling. The ubiquitination status of GCGR directs signaling through different effectors to regulate insulin secretion and glucose homeostasis.

The third project aimed to identify novel interactors of  $\beta$ -arrestin 1/2 and characterize the role of these interactions in the context of GPCR signaling. We identified over 100 new  $\beta$ -arrestin 1/2 potential interactions using the BioID proteomic approach. We confirmed the interaction of the atypical ubiquitin conjugating enzyme UBE2O with  $\beta$ -arrestin by co-immunoprecipitation and by BRET. We also showed that UBE2O modulates  $\beta$ -arrestin trafficking between the plasma membrane and early endosomes. The results of this study open new avenues to explore novel functions and regulation mechanisms of  $\beta$ -arrestin mediated by their interactions with previously unidentified interactors.

The findings compiled in this thesis shed light on a broader picture of the mechanisms regulating  $\beta$ -arrestin functions, as well as the potential novel roles this protein plays in GPCR signaling. The characterization of non-canonical functions and regulatory mechanisms of  $\beta$ -arrestin is an exciting avenue that could be important in the development of future therapies targeting GPCRs.

**Keywords:** GPCR,  $\beta$ -arrestin, cell signaling, protein complex, post-translational modifications, cell trafficking

# Table of Contents

Résumé.....	3
Abstract.....	5
Table of Contents.....	7
List of Figures.....	11
List of Abbreviations.....	12
Acknowledgements.....	16
Foreword.....	18
Introduction.....	19
1 Chapter 1: G Protein-Coupled Receptors.....	20
1.1 Generality.....	20
1.2 GPCR classification.....	22
1.2.1 Kolakowski.....	22
1.2.2 GRAFS.....	23
1.3 GPCR structure.....	25
1.4 GPCR signaling.....	29
1.4.1 G proteins.....	29
1.4.2 G proteins structure.....	29
1.4.3 G $\alpha$ signaling.....	31
1.4.4 G $\beta\gamma$ signaling.....	32
1.4.5 GPCR regulators.....	32
1.5 GPCR models.....	34
1.5.1 $\beta$ 2-adrenergic receptor ( $\beta$ 2AR).....	34

1.5.2	Vasopressin V2 receptor (V2R)	34
1.5.3	Chemokine receptor type 4 (CXCR4)	35
1.5.4	Glucagon receptor (GCGR)	35
2	Chapter 2: $\beta$ -arrestin	36
2.1	Generality	36
2.2	Visual arrestins	37
2.3	$\beta$ -arrestin structure	37
2.4	$\beta$ -arrestin regulation	40
2.5	$\beta$ -arrestin localization	40
2.6	GPCR desensitization and trafficking	44
2.6.1	Heterologous and homologous desensitization	44
2.6.2	$\beta$ -arrestin recruitment	46
2.6.3	$\beta$ -arrestin-dependent internalization	47
2.6.4	$\beta$ -arrestin-independent internalization	48
2.6.5	GPCR intracellular trafficking	49
2.7	$\beta$ -arrestin dependent signaling	52
2.7.1	Src kinase	52
2.7.2	ERK1/2 pathway	52
2.7.3	JNK pathway	53
2.7.4	p38 MAPK pathway	53
2.7.5	PI3K pathway	53
2.7.6	NF- $\kappa$ B	54
2.7.7	$\beta$ -arrestin vs G protein	54
2.7.8	Biased signaling	56

2.8	Endosomal signaling.....	58
2.9	$\beta$ -arrestin interactors .....	60
3	Chapter 3: Post-Translational Modifications .....	61
3.1	Generality.....	61
3.2	Phosphorylation .....	63
3.2.1	GPCR phosphorylation .....	63
3.2.2	$\beta$ -arrestin phosphorylation .....	66
3.3	Ubiquitination .....	67
3.3.1	GPCR ubiquitination .....	68
3.3.2	$\beta$ -arrestin ubiquitination .....	70
3.4	SUMOylation .....	71
3.4.1	GPCR SUMOylation .....	72
3.4.2	$\beta$ -arrestin SUMOylation .....	72
	Thesis statement and objectives.....	74
	Results.....	75
4	Chapter 4: The V2R- $\beta$ -arrestin-G $\beta\gamma$ Complex Promotes G Protein Translocation to Endosomes .....	76
5	Chapter 5: The Ubiquitination Status of the Glucagon Receptor Determines Signal Bias ..	116
6	Chapter 6: The E2/E3 Ubiquitin-Conjugating Enzyme UBE2O is a $\beta$ -arrestin1/2 Binding Partner and Trafficking Regulator .....	172
7	Chapter 7: Discussion .....	199
7.1	Sustained GPCR signaling .....	199
7.2	G protein trafficking .....	200
7.3	Role of GCGR ubiquitination on signaling bias.....	202

7.4	GCGR-mediated insulin secretion .....	203
7.5	Advantages and limitations of the BioID proteomic approach.....	204
7.6	$\beta$ -arrestin interactome studies.....	205
7.7	Differential localization and binding partners of $\beta$ -arrestin 1/2.....	207
7.8	$\beta$ -arrestin interaction with the atypical E2/E3 ubiquitin-conjugating enzyme UBE2O 207	
7.9	UBE2O accelerates $\beta$ -arrestin endosomal translocation .....	208
7.10	Conclusion .....	209
	References.....	212
	Annexes .....	228
	Annex I: Genetically Encoded Intrabody Sensors Report the Interaction and Trafficking of $\beta$ - arrestin 1 Upon Activation of G-Protein–Coupled Receptors.....	229
	Annex II: The RanBP2/RanGAP1-SUMO Complex Gates $\beta$ -arrestin2 Nuclear Entry to Regulate the Mdm2-p53 Signaling Axis .....	245
	Annex III: Computationally Designed GPCR Quaternary Structures Bias Signaling Pathway Activation .....	261

## List of Figures

<b>Figure 1.</b> – GPCR activation and signaling. ....	22
<b>Figure 2.</b> – GPCR families and classes. ....	24
<b>Figure 3.</b> – $\beta$ 2AR three-dimensional structure.....	28
<b>Figure 4.</b> – GPCR transducers and effectors. ....	33
<b>Figure 5.</b> – $\beta$ -arrestin structure and recruitment.....	39
<b>Figure 6.</b> – $\beta$ -arrestin subcellular localization. ....	43
<b>Figure 7.</b> – Role of $\beta$ -arrestin in GPCR internalization and trafficking. ....	51
<b>Figure 8.</b> – Examples of $\beta$ -arrestin dependent signaling pathways. ....	55
<b>Figure 9.</b> – GPCR biased signaling. ....	57
<b>Figure 10.</b> – GPCR post-translational modifications. ....	62
<b>Figure 11.</b> – GPCR phosphorylation barcode. ....	65
<b>Figure 12.</b> – V2R- $\beta$ arr1/2-G $\beta$ y complex formation monitored by BRETfect assay. ....	201
<b>Figure 13.</b> – $\beta$ -arrestin interactome identified by BioID and APEX2. ....	206
<b>Figure 14.</b> – Role of the SIM of $\beta$ -arrestin 2 in its translocation. ....	210

## List of Abbreviations

AMP	Adenosine monophosphate
AT1R	Angiotensin type 1 receptor
ATP	Adenosine triphosphate
AVP	Arginine vasopressin
$\beta$ 2AR	$\beta$ 2-Adrenergic Receptor
$\beta$ 2V2R	Chimeric $\beta$ 2-adrenergic receptor harboring V2R C terminus
$\beta$ ARKct	$\beta$ -adrenergic receptor kinase carboxyl-terminus
$\beta$ arr1	$\beta$ -arrestin 1
$\beta$ arr2	$\beta$ -arrestin 2
BioID	Proximity-dependent biotin identification
BRET	Bioluminescence resonance energy transfer
BRETfect	Bioluminescence resonance energy transfer with fluorescence enhancement by combined transfer
cAMP	Cyclic adenosine monophosphate
CB1R	Cannabinoid receptor type 1
CREB	cAMP Response Element-Binding Protein
CRISPR	Clustered Regularly Interspaced Short Palindromic Repeats
Cryo-EM	Cryogenic electron microscopy
CXCR4	C-X-C chemokine receptor type 4
CXCR7	C-X-C chemokine receptor type 7



DOR	$\delta$ -opioid receptor
ebBRET	Enhanced bystander bioluminescence resonance energy transfer
ECL	Extracellular loop
ER	Endoplasmic reticulum
ERK	Extracellular signal-regulated kinase
ESCRT	Endosomal sorting complexes required for transport
GCG	Glucagon
GCGR	Glucagon receptor
GDP	Guanosine diphosphate
GFP	Green fluorescent protein
GIRK	G protein-coupled inwardly-rectifying potassium channel
GLP-1R	Glucagon-like peptide-1 receptor
GPCR	G protein-coupled receptor
GRK	G protein-coupled receptor kinase
GSIS	Glucose-Stimulated Insulin Secretion
GTP	Guanosine triphosphate
ICL	Intracellular loop
ISO	Isoproterenol
ITC	Isothermal titration calorimetry
MAPK	Mitogen-activated protein kinase
MOR	$\mu$ -opioid receptor
NES	Nuclear export signal

NK1R	Neurokinin-1 receptor
NLS	Nuclear localization signal
NMR	Nuclear magnetic resonance
NTSR1	Neurotensin receptor 1
OXT	Oxytocin
PDE	Phosphodiesterase
PKA	Protein kinase A
PKC	Protein kinase C
PTM	Post-translational modification
RGS	Regulators of G protein signaling
RTK	Receptor tyrosine kinase
SIM	SUMO-interacting motif
SUMO	Small Ubiquitin-like Modifier
T2D	Type 2 diabetes
TM	Transmembrane
V2R	Vasopressin V2 receptor
WT	Wild type
YFP	Yellow fluorescent protein

*Impossible is not a fact. It's an opinion.  
Impossible is potential. Impossible is temporary.  
Impossible is nothing.*

Muhammad Ali

## Acknowledgements

Although my name appears on the front page of this document, there are a lot of people behind this thesis. I am deeply grateful to all those who have generously shared their wisdom, expertise, and resources, and have played a significant role in the completion of this thesis.

First, I would like to thank my supervisor, Dr. Michel Bouvier, for welcoming me into his lab and trusting me to lead so many different research projects and to participate in great scientific collaborations. His expertise, dedication, and constructive feedback have been instrumental in shaping the direction and quality of this work. I would also like to extend my appreciation to the members of my thesis committee, Dr. Nikolaus Heveker and Dr. Sylvie Mader, for their insightful comments, suggestions, and expertise in reviewing my work.

Thank you to my lab colleagues for their camaraderie, intellectual discussions, and support during this research endeavor. Their friendship and collaborative spirit have been truly cherished, and I am fortunate to have been a part of such an exceptional team. As the Bouvier lab has seen numerous members come and go over the years, I will try my best to not forget anyone. Thank you to Justine Paradis, my original mentor in the lab, who provided me with the tools and guidance that allowed me to begin my Ph.D. on the right foot. To the French gang, Pierre, Charlotte, Alan, and Élodie, your friendship, sense of humor, and team spirit have made our office a hard place to leave (also a hard place to focus sometimes). To Nick, Ruth, Diego and Julian, your time in the lab left a lasting impression, not only for scientific reasons but also for the memorable moments we shared outside the lab. Thank you to Monique, Mireille, Christian, Hiro, André, Marie-José, Marie-Ève, Supriya, Lucas, Pedro 1, Pedro 2, Suli, all past and present lab members.

I am also grateful for the friendships born and those that have further blossomed throughout the course of my Ph.D. journey. The after-work moments shared with Shane, Gaby, Laia, Guillem, Roger, Maria, Layane, Jamil, and Sam have been a source of joy and support, providing much-needed moments of laughter, relaxation, and camaraderie amidst the rigors of academic research. A big shout-out to the Phoenix family, my teammates, coach Leo and coach Whitney for pushing me beyond my limits and for supporting me during training camps and fight nights. The

OGs, Jade, Joe, Rawan, Oumnia, Abdel, who believed I might never be done with school, thank you for your unwavering support throughout the years. The memories we have shared have been truly amazing, and I am sure the bonds we have formed will never fade.

To my parents and siblings, thank you for your support, motivation, encouragements, and for always believing in me. This thesis belongs to all of us. Finally, to my partner, Maria, I am grateful for the joy and fulfillment I have experienced in living this Ph.D. journey alongside you. You have been an incredible source of inspiration to me over the past three years. Thank you for everything!

## Foreword

Cells are the building blocks of our organs and tissues. They can sense their immediate environment and trigger reactions to adapt to it by integrating information provided by various extracellular signals. An obvious example is that of cells that can sense the presence of nutrients in their environment and migrate to an area where they can grow better and proliferate. Cells can also secrete chemical signals to communicate with each other. The distance between the signal transmitting and the signal receiving cells determines the type of signaling. Paracrine signaling describes the transmission of signal between neighboring cells, autocrine signaling refers to the same cell sending and receiving its own signal, and endocrine signaling occurs when the chemical message is sent through the circulatory system.

To receive the extracellular message, cells express receptor proteins at their plasma membrane that recognize and bind signaling molecules to initiate an intracellular response. Plasma membrane receptor families include G-protein-coupled receptors (GPCRs), receptor tyrosine kinases (RTKs), and ligand-gated ion channels. Our laboratory focuses on the study of GPCRs which constitute the largest transmembrane receptor family and represent an important pharmacological target. In the context of my thesis, I took an interest in the study of the  $\beta$ -arrestin family of proteins that was initially identified for its role in blocking GPCR intracellular signaling. Through different projects, I had the opportunity to investigate lesser-known roles and regulation mechanisms of  $\beta$ -arrestin. I was able to expand our knowledge regarding  $\beta$ -arrestin and illustrate a clearer picture of the role this protein plays in the regulation of GPCR signaling. I hope that this modest contribution to the field of GPCRs will help advance our understanding of the intricate relationship between GPCRs and  $\beta$ -arrestin and possibly provide new insights that could lead to the development of novel therapies targeting GPCRs.

# Introduction

# 1 Chapter 1: G Protein-Coupled Receptors

## 1.1 Generality

G Protein-Coupled Receptors (GPCRs) are the largest family of membrane-bound proteins in humans with more than 800 members and account for approximately 4% of the human genome (1, 2, 3). GPCRs are ubiquitously expressed and can be found in virtually all cell and tissue types (4). They are the target of a wide variety of extracellular ligands such as photons, ions, small molecules, peptides, and hormones. Ligand binding to GPCRs induces its coupling to heterotrimeric G proteins and the production of intracellular second messengers that activate different signaling pathways regulating biological responses such as cell growth, proliferation, division, differentiation, migration, and death (**Figure 1**) (5, 6). Due to their ubiquitous expression and the diversity of their ligands, GPCRs act as regulators or modulators in a broad array of biological processes like sight, taste, smell, chemotaxis, neurotransmission, cardiac, and pulmonary functions, gastric regulation, and many others (7, 8). As a result, dysregulation of GPCRs is also an important trigger for many pathologies for instance, cardiovascular diseases, diabetes, immune syndromes, obesity, cancer, reproductive and metabolic disorders (9, 10, 11). Thus, GPCRs constitute a very important drug target for the treatment of various diseases. Thirty-four percent of FDA-approved drugs target over 100 therapeutically pertinent GPCRs, leaving many potentially relevant receptors whose therapeutic potential is yet to be clearly established (12, 13).

GPCRs are also known as seven-transmembrane (7TM) receptors due to their common and distinctive three-dimensional structure. These membrane-anchored receptors have an extracellular amino terminus and an intracellular carboxyl terminus that differ greatly in size and in sequence homology. GPCRs also possess seven helical transmembrane hydrophobic domains (TM1 to TM7) connected by three intracellular loops (ICL1, ICL2, ICL3) and three extracellular loops (ECL1, ECL2, ECL3). Generally speaking, GPCRs share a high sequence homology within their characteristic transmembrane domains (14). The structural similarities that exist between



eukaryotic GPCRs and several bacterial photoreceptor families indicate a common evolutionary origin of these two groups of receptors (15).

The interest in GPCRs study began in the 1970s but the concept of receptor biology dates back to the early 1900s with the works of Ehrlich, Clark, Ariens, Stephenson, Furchgott and Black (16, 17). Decades later, the investigations of Earl Sutherland on the hormonal effects of glucagon and epinephrine led to the discovery of adenylate cyclase and the second messenger cyclic AMP (cAMP). He stipulated that cellular receptors could be acting as regulators for enzyme activation but the precise mechanism remained elusive at the time (18). Later in the 1970s, several research groups hypothesized the existence of an intermediary between the receptor and the effector enzymes until this was demonstrated by Alfred G. Gilman. Indeed, the identification of the heterotrimeric G protein G<sub>s</sub>, which acts as an activator of adenylate cyclase (19) and the subsequent discovery of other G proteins of the same family that regulate the activity of different cellular effectors confirmed this hypothesis (20, 21, 22). The striking similarities between the mechanism of hormone-stimulated adenylate cyclase activation and the photoactivation of the visual receptor rhodopsin were further investigated, but the purification followed by the cloning of rhodopsin (23, 24, 25) and the  $\beta$ -adrenergic receptor (26, 27, 28) led to the unexpected realization that these receptors share sequence homology and similar three-dimensional structure. This signaled the birth of the GPCR family of proteins as in the following years, numerous novel GPCRs were identified with the improvement of sequencing technologies (29).

Later in the 2000s, the advancement in the field of structural biology allowed the structure resolution of both rhodopsin (30) and  $\beta$ 2AR (31). Today, over 400 GPCR structures have been published in active or inactive states and in association with various effectors allowing a better understanding of the relationship between structure and function of GPCRs (32). Another recent development in the GPCR field is the introduction of the concept of functional selectivity or biased signaling which is the idea that different ligands induce the activation of different effectors downstream of the receptor with different efficacies (33). The development of novel GPCR ligands as well as allosteric modulators using structural and functional insights is an emerging approach for the treatment of GPCR-related disorders.

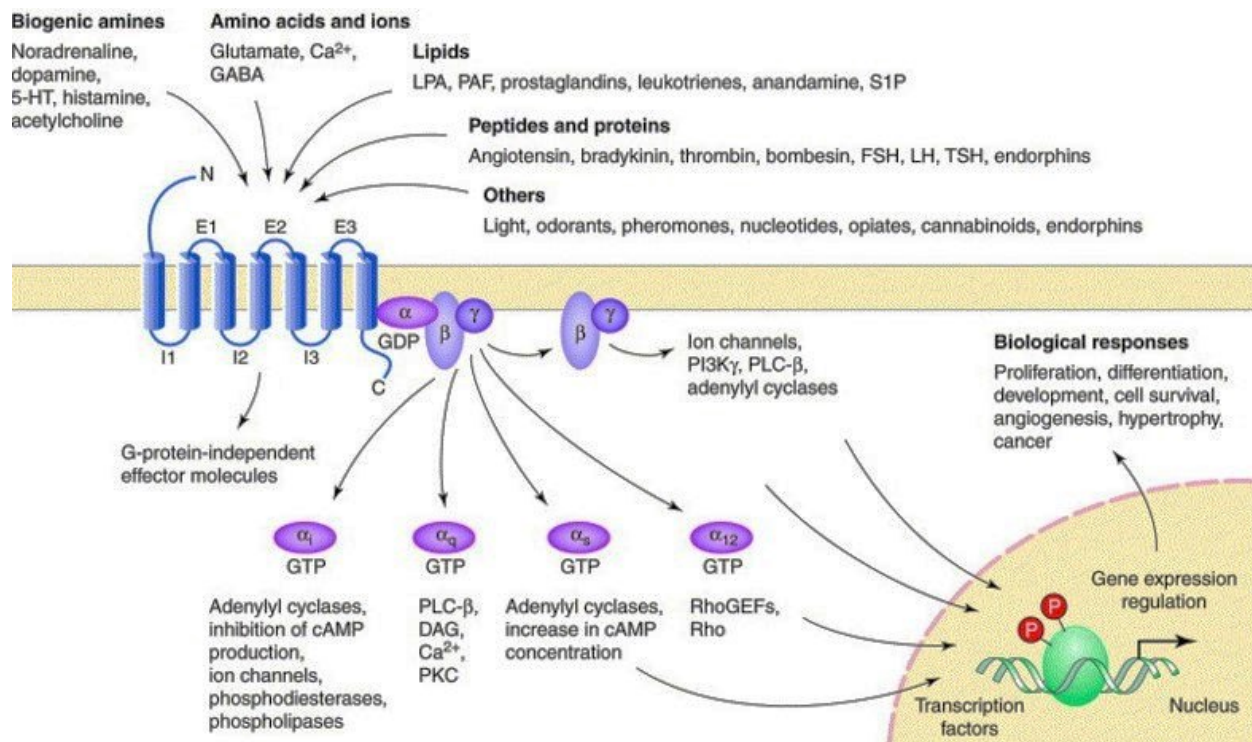


**Figure 1.** – GPCR activation and signaling.

GPCR activation by various extracellular ligands and triggering of heterotrimeric G proteins signaling pathways regulating different biological responses (34).

## 1.2 GPCR classification

Of the 800 identified GPCRs, more than half are sensory receptors that mediate olfaction, taste, light perception, and pheromone signaling (35, 36). Different sorting systems have been proposed to classify GPCRs. The first one proposed by L.F. Kolakowski Jr is based on the sequence homology between receptors to divide them into 7 classes (A-F) (37). Another classification system is based on phylogenetic studies and divides GPCRs into 5 classes: Glutamate, Rhodopsin, Adhesion, Frizzled/Taste2, and Secretin (GRAFS) (38). Finally, GPCRs can also be classified according to their internalization profile and their interaction with  $\beta$ -arrestins (discussed in chapter 2).

### 1.2.1 Kolakowski

The Kolakowski classification (A-F) serves as the basis for the widely used GPCR database (GPCRdb) and is built on receptors sequence homology (**Figure 2A**).

Class A or rhodopsin-like family is the largest family of GPCRs (over 80% of all GPCRs) and includes most of the sensory receptors. Non-sensory class A receptors bind ligands like small molecules, neurotransmitters, peptides, and hormones. They possess some common structural characteristics: a short N-terminal domain, a conserved cysteine bridge, E/DRY and NPxxY motifs. Dopamine, adrenergic, vasopressin and chemokine receptors are among the class A family of GPCRs(39, 40).

Class B or secretin-like family receptors have low sequence homology to class A GPCRs and bind large hormone peptides such as secretin, parathyroid hormone, glucagon, calcitonin, and growth hormone-releasing hormone. They have a characteristically long N-terminal domain that is important for ligand binding and lack the conserved motifs present in class A receptors. Calcitonin, corticotropin-releasing factor, glucagon, and parathyroid hormone receptors are class B receptors. Adhesion GPCRs are also considered part of the class B family (41, 42).

Class C or metabotropic glutamate receptors are activated by small ligands like calcium ions or glutamate and possess a uniquely large extracellular lobe at the N-terminus that serves as an orthosteric ligand binding site. They form constitutive dimers that are necessary for receptor activation. Metabotropic glutamate,  $\gamma$ -aminobutyric acid and calcium-sensing receptors are members of the class C family of GPCRs (43, 44).

Class D and E receptors are not present in the human genome. They are pheromone and cAMP receptors expressed in some simple organisms and serve as chemical sensors for cellular communication and signaling (45, 46).

Class F family includes 10 Frizzled proteins and one Smoothed protein. They mediate Wnt and hedgehog signaling and are key regulators of animal development by acting on cell proliferation, migration, cell polarity, and embryonic development (47).

### **1.2.2 GRAFS**

The GRAFS classification divides human GPCRs into five families: Glutamate (G), Rhodopsin (R), Adhesion (A), Frizzled/Taste2 (F), and Secretin (S) (**Figure 2B**). It is based on phylogenetic analyses of the human genome and on comparison of the similarities of the transmembrane sequences. It

also aims to elucidate the evolutionary history of GPCRs. The main difference with the Kolakowski classification is the division of the class B into two groups, Adhesion (A) and Secretin (S) GPCRs. Phylogenetic analyses also showed that the Rhodopsin family can be further divided into subgroups ( $\alpha$ ,  $\beta$ ,  $\gamma$  et  $\delta$ ) (38).

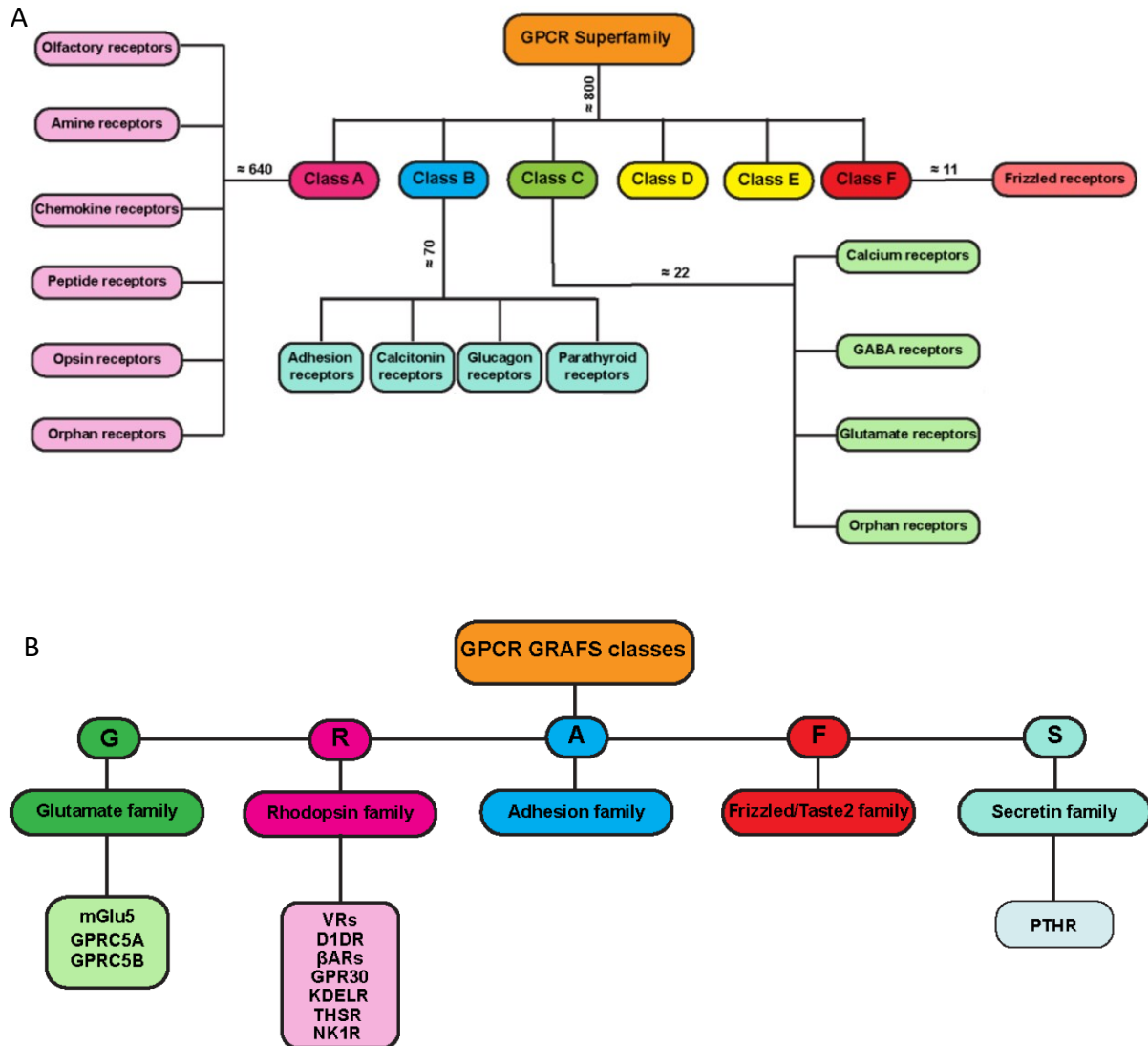


**Figure 2.** – GPCR families and classes.

GPCRs classification according to the Kolakowski (A) or GRAFS models (B). Adapted from (48).

### 1.3 GPCR structure

Structural biology is the study of the assembly of biological macromolecules and the conformations they assume in relation to each other. It also aims to study the impact of the three-dimensional structure of these molecules on their biological functions. Over the last 25 years, different methods have been developed to investigate protein structure. X-ray crystallography necessitates the formation of protein crystals and the exposure of the sample to an X-ray beam. The resulting diffraction pattern provides information about atom location and different thermodynamic models are used to refine the three-dimensional model (49). NMR spectroscopy aims to study proteins in solution by exposing the sample to pulses of radio waves and measuring how atoms nuclei interact with these wavelengths to map the structure of the protein (50). For Cryo-EM, an electron microscope is used to expose a frozen macromolecule sample to an electron beam to image individual proteins. The individual images are reconstituted to form a three-dimensional protein structure (51).

The examination of GPCRs structure is an important step in understanding GPCRs roles and functions and thus in developing therapeutic avenues targeting these receptors. However, GPCRs structure study comes with its load of challenges. The first issue is the generally low expression level of GPCRs and the fact that protein structure resolution requires a large amount of protein. In addition, GPCRs are very unstable once extracted from the lipid membrane as they are very hydrophobic. They also adopt very flexible conformations that must be stabilized in the hope of capturing a snapshot conformation and they lack in the formation of crystal contacts (52). Different tools have been developed to facilitate GPCRs structure resolution including the use of soluble tags, antibody stabilization, innovations in protein purification, development of new detergents as well as breakthroughs in DEER spectroscopy, NMR, and computational simulation (53).

The study of the structure of GPCRs began with rhodopsin which is a light-sensitive receptor expressed in the outer segment of retinal rod cells. Rhodopsin represents the major protein at the rods plasma membrane and covers over half of the membrane surface (40). Rhodopsin is covalently bound to its ligand, 11-cis-retinal, which acts as an inverse agonist and is converted to

all-trans-retinal upon exposure to light, resulting in rhodopsin change of conformation and downstream G protein activation (54). Due to the high level of expression of rhodopsin in retinal cells, it was possible to purify large amounts of protein, which led to its proteomic sequencing. This allowed the prediction of the secondary structure of rhodopsin with the presence of seven hydrophobic transmembrane domains linked by intracellular and extracellular loops (24). The first high-resolution three-dimensional structure (2.8Å) of rhodopsin confirmed the seven transmembrane domain model and provides new insights into the conformation and organization of the extracellular domain, binding pocket, and intracellular effectors interface (55). It would take seven more years before the structure of another GPCR, the  $\beta$ 2AR, was resolved (31) but since then, hundreds of new GPCRs structures have been published and brought new understanding to receptor structure-function relation.

We will discuss the structural characteristics of class A receptors as they are the largest family of GPCRs and that most receptor structures are from this family. The general structure of GPCRs consists of an extracellular N-terminal domain, seven transmembrane helices connected by three intracellular and three extracellular loops, and an intracellular C-terminal domain. The ligand binding process involves at once, the transmembrane domains that form the ligand binding pocket, the N-terminus domain, and the extracellular loops. In most GPCRs, a disulfide bridge between two cysteines in the ECL1 and ECL2 stabilizes the ligand binding pocket. The conformation of the 7TM varies between receptors and results in the formation of binding pockets of very different sizes and shapes. The lengths of the loops, the N-terminus, and the C-terminus domains also vary between receptors. Class A GPCRs typically possess a few conserved motifs important for receptor activation such as the E/DRY, PIF, CWxP and NPxxY motifs. The intracellular loops are in turn involved in the interaction interface with the cytoplasmic effectors. The C-terminal tail possesses a palmitoylation site that anchors this domain to the plasma membrane (56, 57).

Comparing the structures of inactive and active receptors has allowed to identify key molecular switches that control GPCR activation. Indeed, ligand binding associated with effector coupling stabilizes the receptor active conformation. The main structural switches are the outward movement of TM6 away from TM3, the inward movement of TM7 and the rotation of TM5 that

allow coupling on the cytoplasmic side to cellular effectors such as G proteins and  $\beta$ -arrestins (**Figure 3**) (14, 58). In particular,  $G_{\alpha s}$  coupling to the receptor requires the insertion of an alpha helix domain in the transmembrane domain of the receptor and the disruption of a key GPCR molecular switch, the ionic lock consisting of the interaction between the E/DRY motif of TM3 and a glutamate of TM6 (58). This ionic lock serves to stabilize the inactive conformation of the receptor. The NPxxY motif creates a network of polar bonds with different residues stabilizing the active conformation of the receptor (59). A sodium ion coordinated by TM2, TM3 and TM7 is present in the inactive structure of most GPCRs and is displaced in the active structure after agonist binding (60). The CWxP motif is a conserved motif located within the ligand binding pocket that undergoes a switch during activation enabling TM movement and receptor activation (61). The active receptor also exhibits a tightening of the ligand binding pocket mediated by the PIF motif consisting of the hydrophobic interaction between a proline in TM5, isoleucine in TM3, and phenylalanine in TM6 (62). Even though these conformational changes are characteristic for class A receptors, some resolved structures of class B receptors show similar properties. However, they lack the motifs described here (42). Regarding the mechanism of functional selectivity, studies suggest that different ligands might stabilize different conformations of the receptor engaging different effectors (63).

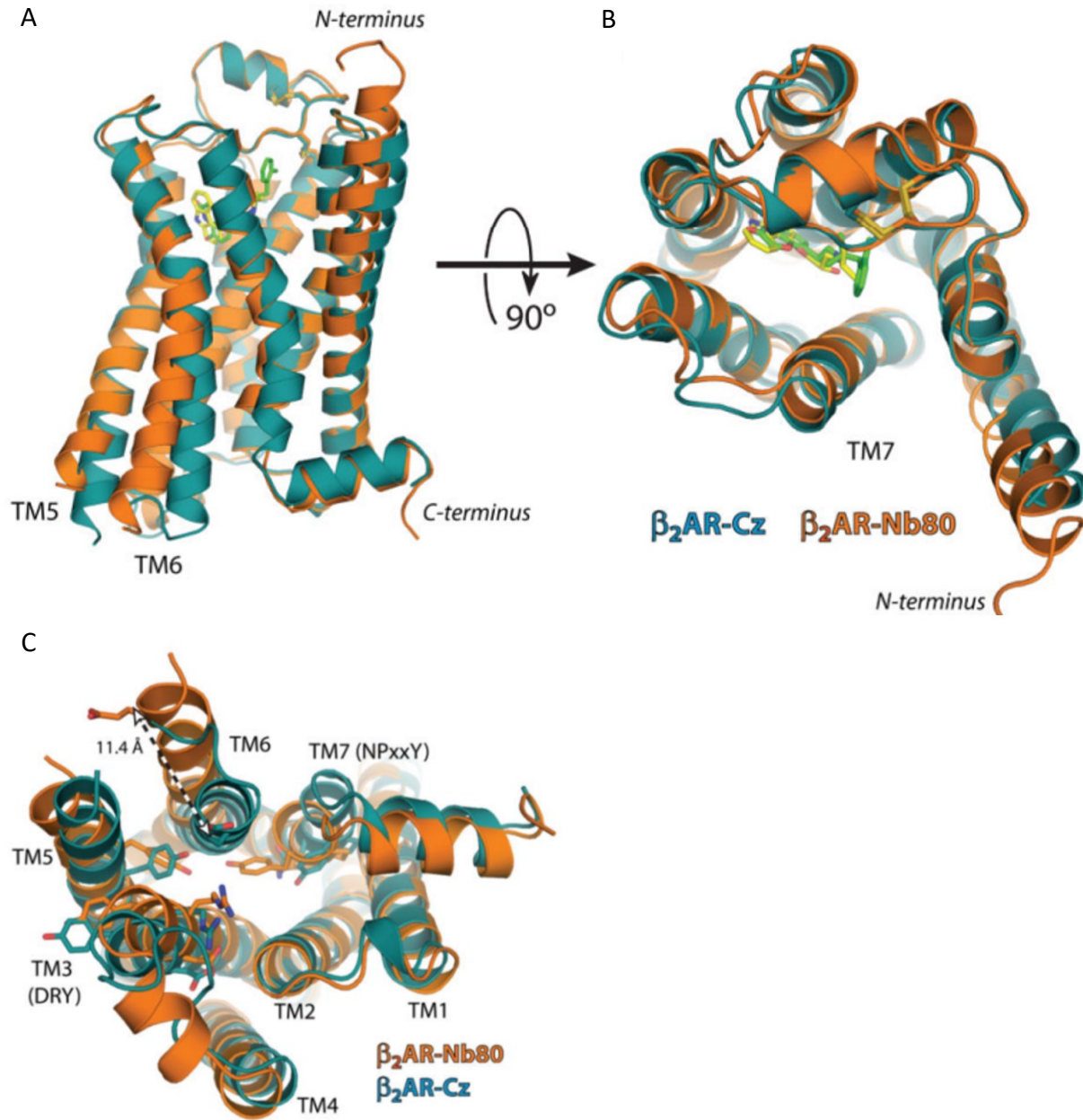


**Figure 3.** –  $\beta_2$ AR three-dimensional structure.

Comparison of agonist-occupied  $\beta_2$ AR in orange with inverse agonist occupied receptor in blue. (A) Side view of the superimposed structures. (B) Extracellular view of the ligand binding pocket. (C) Cytoplasmic view illustrating the NPxxY and DRY motifs. Adapted from (64).



## 1.4 GPCR signaling

### 1.4.1 G proteins

As mentioned previously, ligand binding to the extracellular part of a GPCR induces a conformational change triggering intracellular signaling cascades. These signaling events are canonically mediated by the receptor engaging heterotrimeric guanine nucleotide-binding G proteins that are constituted of three protein subunits,  $G\alpha$ ,  $G\beta$  and  $G\gamma$ . G proteins are highly conserved throughout evolution and are found in a wide range of simple and complex organisms. As a result, many bacterial toxins bind and alter G proteins functions and are still used in GPCR and G proteins research. Alfred G. Gilman was awarded the physiology or medicine Nobel Prize in 1994 for the purification and characterization of the  $G\alpha$  protein and the discovery  $G\beta$  and  $G\gamma$  subunits that coprecipitate with it. The last two subunits form a constitutive dimer  $G\beta\gamma$  (65). The human genome codes for 16  $G\alpha$ , 5  $G\beta$  and 12  $G\gamma$  proteins (66).

The  $G\alpha$  subunit has a nucleotide binding site occupied in the inactive state by a guanosine diphosphate (GDP). Ligand-induced receptor activation induces an exchange of the GDP for a guanosine triphosphate nucleotide (GTP). This results in further conformation change of the heterotrimeric G proteins and dissociation of  $G\alpha$  from  $G\beta\gamma$  (67). The free  $G\alpha$  and  $G\beta\gamma$  dimer interact with numerous effectors such as adenylate cyclase, phospholipase C, tyrosine kinases, mitogen-activated protein kinases (MAPK), GPCR kinases, and ionic channels. These effectors control the release of second messengers like cyclic AMP (cAMP), diacylglycerol (DAG), PIP2 phospholipids and ions (66). The  $G\alpha$  subunit possesses an intrinsic GTPase activity that hydrolyzes the terminal phosphate of the GTP nucleotide to return the G protein to its inactive state and allows reassociation with  $G\beta\gamma$  dimer to complete the activation cycle. The kinetics of this reaction can be further tuned by Regulators of G protein Signaling proteins (RGS) (**Figure 4**) (68).

### 1.4.2 G proteins structure

$G\alpha$  proteins have a conserved three-dimensional structure consisting of a GTPase domain responsible for GTP hydrolysis and a helical domain forming the main interaction interface with receptors and other effectors. The helical domain of different  $G\alpha$  subunits shows the most

sequence diversity as it controls interaction specificity with different receptors and effectors whereas the GTPase domain is very well conserved. It is homologous to the family of small GTPases and is composed of 5  $\alpha$ -helices, 6  $\beta$ -sheets, and a consensus sequence for guanine nucleotide binding. The helical domain is formed by 6  $\alpha$ -helices and covers the nucleotide binding site, keeping the bound GDP buried in the core of the  $G\alpha$  subunit. The  $G\beta$  subunit structure is a  $\beta$ -propeller formed with seven  $\beta$ -sheets and the  $G\gamma$  subunit is formed by 2  $\alpha$ -helices. The  $G\beta\gamma$  dimer is associated by an interaction of the N-terminus of  $G\gamma$  along the base of the  $G\beta$  subunit and the  $G\alpha$  subunit interacts via its  $\alpha 2$ -helix,  $\beta 3/\alpha 2$  loop and N-terminus with the  $\beta$ -propeller strands of the  $G\beta$  subunit (69, 70, 71, 72).

The mechanism of G protein activation by GPCRs has long been a mystery and considering the distance between the G protein-GPCR interface and the nucleotide binding site (30Å), it was hypothesized that the agonist-induced conformational change of the receptor mediates an allosteric structural shift of the  $G\alpha$  subunit causing GDP-GTP exchange. The answer came with the resolution of the  $\beta 2$  adrenergic receptor-Gs heterotrimeric protein complex (73). This study along with others published structures revealed that GPCR activation induces a movement of the  $G\alpha$  subunit's helical domain relative to the inactive state without any conformational change to the core of this domain. Another key conformational change is the movement of the  $\alpha 5$ -helix of the  $G\alpha$  subunit towards the cytoplasmic core of the receptor that is open after the agonist-induced TM6 outwards motion. Residues in the C-terminus of the  $\alpha 5$ -helix interact with conserved GPCR motifs such as the DRY motif stabilizing the receptors' active state. The displacement of the helical domain and in particular the  $\alpha 5$ -helix allows access to the nucleotide binding site and GDP-GTP exchange. In absence of receptor, the  $\alpha 5$ -helix is disordered and fails to exhibit a stable structure.  $G\alpha$  binding to the receptor induce stabilization of a helix conformation linked to the conserved guanine binding motif. Interestingly, mutations of this motif cause spontaneous GDP release (73, 74).

### 1.4.3 G $\alpha$ signaling

G proteins are classified according to the identity of the G $\alpha$  subunit in the heterotrimer. The human genome encodes 16 different G $\alpha$  proteins clustered into 4 groups on the basis of their sequence homology: G $\alpha$ s, G $\alpha$ i/o, G $\alpha$ q/11, and G $\alpha$ 12/13. Each G protein family plays different functions in the cell and binds different effectors.

The G $\alpha$ s family is composed of two proteins: G $\alpha$ s and G $\alpha$ olf (olfactory system). This G protein family mediates GPCR-induced adenylyl cyclase catalytic conversion of ATP to intracellular cyclic adenosine monophosphate (cAMP). cAMP is a second messenger that activates various cellular effectors such as Protein Kinase A (PKA), Exchange Protein Activated by cAMP (Epac) and cAMP-response element binding protein (CREB). Activated PKA phosphorylates different targets including GPCRs, MAPK, and ion channels. Epac activates small monomeric G protein and CREB regulates gene expression in response to GPCR activation (75, 76).

The G $\alpha$ i/o family is composed of G $\alpha$ i1, G $\alpha$ i2, G $\alpha$ i3, G $\alpha$ o, G $\alpha$ z, G $\alpha$ t<sub>rod</sub> (visual system), G $\alpha$ t<sub>cone</sub> (visual system), and G $\alpha$ gust (gustative system). Receptors coupled to G $\alpha$ i/o are associated with inhibition of adenylyl cyclase and decreased cAMP production. G $\alpha$ i1, G $\alpha$ i2, G $\alpha$ i3, G $\alpha$ o, and G $\alpha$ z interact directly with adenylyl cyclase to inhibit its function whereas G $\alpha$ t and G $\alpha$ gust regulate phosphodiesterase (PDE) activity to hydrolyze cAMP (77, 78).

The G $\alpha$ q/11 family is composed of G $\alpha$ q, G $\alpha$ 11, G $\alpha$ 14 and G $\alpha$ 15 and their activation stimulates the  $\beta$ -isoform of phospholipase C (PLC- $\beta$ ). This enzyme catalyzes the hydrolysis of phosphatidylinositol bisphosphate (PIP<sub>2</sub>) and the production of the second messengers inositol-triphosphate (IP<sub>3</sub>) and diacylglycerol (DAG). IP<sub>3</sub> regulates calcium mobilization from intracellular compartments such as the endoplasmic reticulum and DAG activates protein kinase C (PKC) to phosphorylate various cellular effectors (79).

The G $\alpha$ 12/13 family is composed of G $\alpha$ 12 and G $\alpha$ 13 proteins. This G protein family mediates the activation of RhoGTPase nucleotide exchange factor (RhoGEF). This intracellular effector regulates the function of small monomeric GTPases of the RhoA family. G $\alpha$ 12/13 activation has been linked to actin and cytoskeleton organization, cell adhesion, microtubule dynamics, cell polarity, and cell migration (80, 81).

#### **1.4.4 Gβγ signaling**

The Gβγ subunit was initially described as responsible only for the inactivation of the Gα subunit by reassociation with Gα-GDP after GTP hydrolysis and restoration of the G protein heterotrimer ready for a new cycle of GPCR activation. However, several studies over the past 25 years have shown that the Gβγ dimer governs several signaling events independently of the Gα subunit.

The Gβγ dimer is formed by a combination of 5 Gβ proteins (β1-β5) and 12 Gγ proteins (Gγ1-Gγ5 and Gγ7-Gγ13). Gβ1, Gβ2, Gβ3, and Gβ4 share high sequence homology (~78-88%) and similar tissue expression profiles while Gβ5 is different in sequence (~50%) and tissue expression. The Gγ subunits are more diverse in their sequences (27-76% homology) and can be divided into different groups either on the basis of their sequence or on the basis of their post-translational lipid modifications that modulate anchorage to the plasma membrane. Thus, this creates a diversity of possible Gβγ dimers, each capable of activating or fine-tuning the intensity or kinetics of different signaling pathways. Gβγ have been shown to interact with and activate numerous effectors such as phospholipase C, adenylyl cyclase, GPCR kinases, G protein-activated inwardly rectifying potassium channels (GIRK), calcium channels, phosphoinositide 3-kinase (PI3k) and MAPK pathway (65, 71, 82).

#### **1.4.5 GPCR regulators**

Several cellular effectors are regulated by GPCRs and some even provide a feedback regulation of GPCR signaling. Indeed, following GPCR activation, GPCR kinases (GRKs) recognize the active state of the receptor and are recruited to phosphorylate serine and threonine residues within the C-terminal domain and intracellular loops of the receptor. There are seven GRKs expressed in humans (GRK1-GRK7) that are grouped in three families. The GRK1 family is comprised of GRK1 and GRK7 and is restricted to the visual system (rhodopsins and cones). The GRK2 family is composed of GRK2 and GRK3. The GRK4 family includes GRK4, GRK5, and GRK6. GRK1 and GRK4 families are respectively prenylated and palmitoylated to ensure their localization at the plasma membrane. The GRK2 family is cytoplasmic and its recruitment to the active receptor at the plasma membrane is mediated by the dissociated Gβγ as the members of this GRK family possess a Gβγ binding site. Other kinases like PKA and PKC have also been shown to phosphorylate GPCRs

(83). Receptor phosphorylation is considered the first step in receptor desensitization as although it does not result in G protein uncoupling from the receptor, it triggers the recruitment of arrestin proteins to the phosphorylated receptor. The arrestin family is composed of four proteins (arrestin 1-4) that recognize, engage the active receptor, and uncouple the active G protein from the receptor (84, 85, 86). Chapter 2 is devoted to discussing arrestins and more specifically the  $\beta$ -arrestin 1 and  $\beta$ -arrestin 2 isoforms.

G protein regulation is also dependent of the intrinsic GTPase activity of the  $G\alpha$  subunit that hydrolyzes GTP to GDP to stop downstream signaling. The regulator of G protein signaling (RGS) family of proteins controls the kinetics of this enzymatic reaction by acting as GTPase-accelerating proteins (GAPs) that promote  $G\alpha$ -GDP reassociation with  $G\beta\gamma$  in the inactive form of the heterotrimer and thereby modulate the duration and extent of cellular responses to GPCR activation. Twenty RGS proteins have been identified in mammals and they act on different  $G\alpha$  subunits with different levels of specificity to terminate G protein signaling (85, 87).

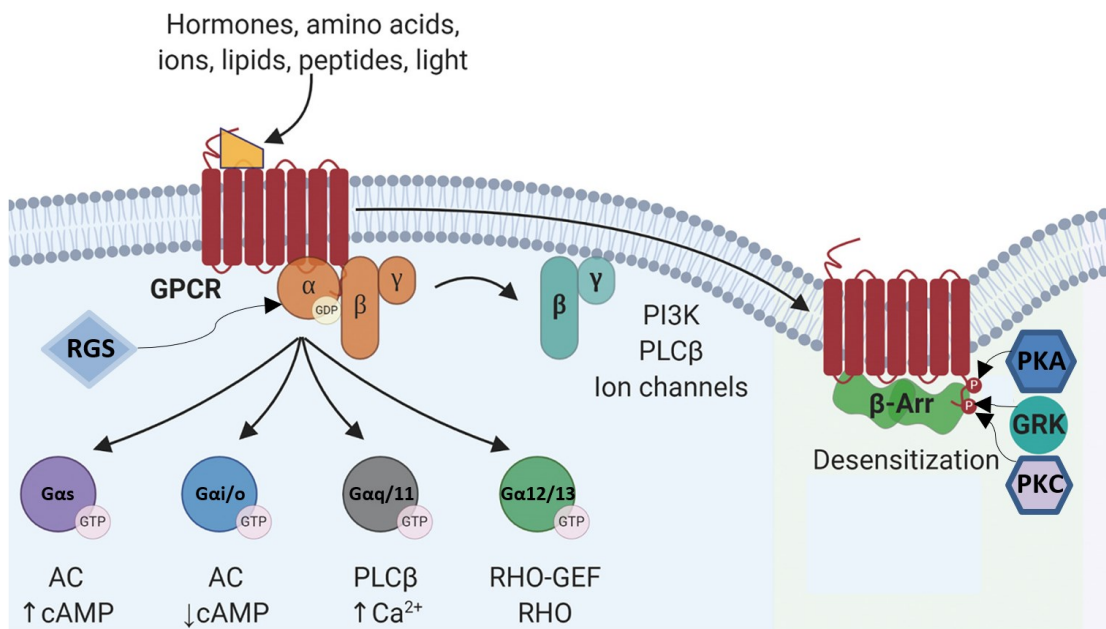


**Figure 4.** – GPCR transducers and effectors.

GPCR signaling via heterotrimeric G proteins and recruitment of various effectors (GRK,  $\beta$ -arrestin, PKA, PKC and RGS) to regulate receptor activation. Adapted from (88).

## 1.5 GPCR models

In this section, we will discuss some of the GPCRs used in the context of this thesis as models to study receptor-mediated cellular signaling as well as the functions and regulatory mechanisms of  $\beta$ -arrestin 1/2.

### 1.5.1 $\beta$ 2-adrenergic receptor ( $\beta$ 2AR)

The  $\beta$ 2AR is a prototypical class A (rhodopsin-like) GPCR and has been for a long time one of the main models for GPCR structure and function research. In the early years of GPCR research, it was used as a study model to understand epinephrine-induced cAMP production.  $\beta$ 2AR is mainly expressed in pulmonary, cardiac, and skeletal tissue and mediates bronchodilatation, muscle contraction, and cardiac output. In addition to the hormones epinephrine and norepinephrine which are endogenous ligands for the  $\beta$ 2AR, other molecules such as salbutamol and salmeterol activate the  $\beta$ 2AR and are used to treat respiratory disorders. Coupling to Gs mediates the  $\beta$ 2AR-mediated cAMP production which acts as a second messenger targeting various cellular substrates such as PKA. Interestingly,  $\beta$ 2AR phosphorylation by PKA reduces its affinity for Gs coupling and increases its affinity for Gi coupling. This switch in coupling decreases levels of cAMP production and increases Gi-dependent MAPK activation.  $\beta$ -arrestins are also recruited to the phosphorylated  $\beta$ 2AR, with  $\beta$ -arrestin 2 having a higher affinity for this receptor than  $\beta$ -arrestin 1, and mediate receptor desensitization, internalization, and trafficking (89, 90, 91).

### 1.5.2 Vasopressin V2 receptor (V2R)

The V2R is another prototypical rhodopsin-like GPCR and is a receptor for arginine-vasopressin peptide (AVP). The V2R is primarily expressed in the kidney and regulates osmotic homeostasis by modulating water reabsorption from urine through aquaporin channels. This process is mediated by the coupling of the receptor to Gs, cAMP production and PKA activation. This results in increased aquaporin expression and trafficking to the apical cell membrane. Failures of the AVP-V2R system due to loss of function mutations are the predominant cause of nephrogenic diabetes insipidus. In addition to the canonical Gs coupling, the V2R also couples to Gq and recruits both  $\beta$ -arrestins (92, 93).

### **1.5.3 Chemokine receptor type 4 (CXCR4)**

Chemokine receptors are a family of GPCRs activated by chemokine peptides that control immune and hematopoietic cells activity by mediating cell adhesion and chemotaxis. The CXCR4 is a rhodopsin-like member of this receptor family and is activated by stromal-derived-factor-1 (SDF-1 also known as CXCL12). Higher expression levels of CXCR4 in various cancers reveal an important role for this receptor in promoting tumor growth and correlates with poor prognosis. Ligand binding induces activation of Gi signaling pathways and recruitment of  $\beta$ -arrestins to the receptor (94).

### **1.5.4 Glucagon receptor (GCGR)**

The GCGR is a class B GPCR expressed in pancreatic  $\beta$  cells and in liver hepatocytes and is stimulated by the peptide hormone glucagon. GCGR activation results in Gs coupling, recruitment of  $\beta$ -arrestins and downstream signaling that regulates glycogenolysis, gluconeogenesis, and insulin secretion. As such, GCGR is a major therapeutic drug target for the treatment of type II diabetes (T2D). Indeed, the use of antagonist ligands is investigated to determine their effect as glucose regulating drugs (95, 96).

## 2 Chapter 2: $\beta$ -arrestin

### 2.1 Generality

The arrestin family of proteins is composed of 4 homologous proteins divided into two groups: the visual arrestins (arrestin 1 and arrestin 4) and the non-visual arrestins (arrestin 2 also known as  $\beta$ -arrestin 1 and arrestin 3 also known as  $\beta$ -arrestin 2). Initially identified as part of the retinal photoreceptor system, the protein previously referred to as retinal S antigen (soluble antigen) has been implicated in allergic uveitis (97). Other contemporary studies discovered a “48 kDa protein” that binds to the light-activated phosphorylated rhodopsin receptor (98) and is essential for stopping signal transduction (99). Similar studies conducted with purified  $\beta$ 2AR showed that receptor desensitization was dependent on the addition of the S antigen protein (100). This led to the purification and cloning of the ubiquitously expressed  $\beta$ -arrestin 1 (101) and  $\beta$ -arrestin 2 (102). Subsequently,  $\beta$ -arrestins were shown to desensitize GPCRs not only by G protein uncoupling but also by acting as an adaptor for the endocytic machinery and mediating GPCRs endocytosis (103). Surprisingly, it has also been described that GPCRs and  $\beta$ -arrestin 1/2 complexes trigger signaling cascades distinct from the signaling pathways mediated by G proteins (104, 105).

$\beta$ -arrestin 1 and  $\beta$ -arrestin 2 share high sequence homology (78%), but they differ in tissue expression, cellular localization, affinity for each GPCR, and protein interactions (102). Knockout in mice of either  $\beta$ -arrestin 1 or  $\beta$ -arrestin 2 is viable although exhibiting specific phenotypes. However knockout of both isoforms is lethal at the embryonic stage indicating a redundancy for their essential functions (106). Several cellular functions have been shown to be mediated by  $\beta$ -arrestins. For instance,  $\beta$ -arrestins regulate cilia formation by interacting with several proteins such as KIF3A and 14-3-3 protein (107). Finally, recruitment to different GPCRs allows  $\beta$ -arrestins to modulate cell proliferation, cell migration and other functions via receptor desensitization and endocytosis or by scaffolding specific signaling cascades.



## 2.2 Visual arrestins

Visual arrestins are found in the retina and are expressed at high levels in both cone and rod photoreceptor cells. Arrestin 1 is expressed at comparable levels in rods and cones whereas arrestin 4 is expressed primarily in cones. Visual receptors rhodopsin and opsin activation by light induces their phosphorylation by GRKs followed by arrestin binding. Mammals express two types of visual GRKs, GRK 1 mediates phosphorylation in rods and cones while GRK 7 is exclusive to cones. Visual arrestins play an important role in the accurate, rapid, and sensitive quenching of receptor activation which is essential as vision requires high temporal resolution of signal modulation and termination (108, 109).

## 2.3 $\beta$ -arrestin structure

The three-dimensional structures of all four arrestin proteins have been resolved and show a conserved backbone. We will focus on studies describing the structures of  $\beta$ -arrestin 1/2.

$\beta$ -arrestin structures reveal a conserved two domains conformation (N-domain and C-domain) where each domain forms a lobe composed of antiparallel  $\beta$ -sheets linked by small loops. The  $\beta$ -arrestin C-terminus extremity is flexible and is buried inside the N-domain stabilizing its inactive conformation. Several structural motifs are characteristic of  $\beta$ -arrestins such as the polar core region that separates the N-domain from the C-domain and the three-element motif interaction between the  $\beta$ -arrestin C-tail,  $\beta$ -sheet I and  $\alpha$ -helix of the N-domain (**Figure 5A**). These two motifs are essentials in maintaining the  $\beta$ -arrestins in the inactive conformation as mutational studies have shown that disruption of these interactions results in a pre-activated conformation of  $\beta$ -arrestin (110, 111).

Studies describing the structure of  $\beta$ -arrestins in complex with phosphorylated peptides mimicking the C-tail of different GPCRs or with a full-length receptor provide structural details explaining the conformational change undergone by activated  $\beta$ -arrestins as it's binding to the active receptor (112, 113, 114). The major conformation change is a 20° rotation of the N-domain relative the C-domain and a rearrangement of several  $\beta$ -arrestins motifs. First, the phosphorylated C-tail of the GPCR interacts with  $\beta$ -arrestin's N-domain via the formation of salt

bridges between the lysine and arginine residues of the N-domain and the phosphates on the receptor. This interaction displaces the C-terminus of  $\beta$ -arrestin from the N-domain and destabilizes the polar core motif as well as the three-element interaction. Another key feature of  $\beta$ -arrestin activation is the formation of an  $\alpha$ -helix at the finger loop region that can insert into the intracellular GPCR pocket characteristic of receptor activation and created by the opening of the transmembrane domains. There is also a shift of the middle loop towards the N-domain and rearrangement of the lariat loop creating a gap to accommodate the intracellular loop 2 of the receptor (110, 111). Structural studies describing the conformation of  $\beta$ -arrestin 1 bound to the  $\beta$ 2V2R ( $\beta$ 2AR with its C-tail truncated and replaced with the V2R C-tail to strengthen the interaction with  $\beta$ -arrestin) show two possible states. The first conformation is when  $\beta$ -arrestin 1 is loosely bound through its N-domain to the receptor's C-tail and the second is a higher affinity bond where  $\beta$ -arrestin 1 is bound to the core of the receptor (**Figure 5B**). Whether the first conformation is an intermediary state or whether the two states co-exist is still undetermined (113).

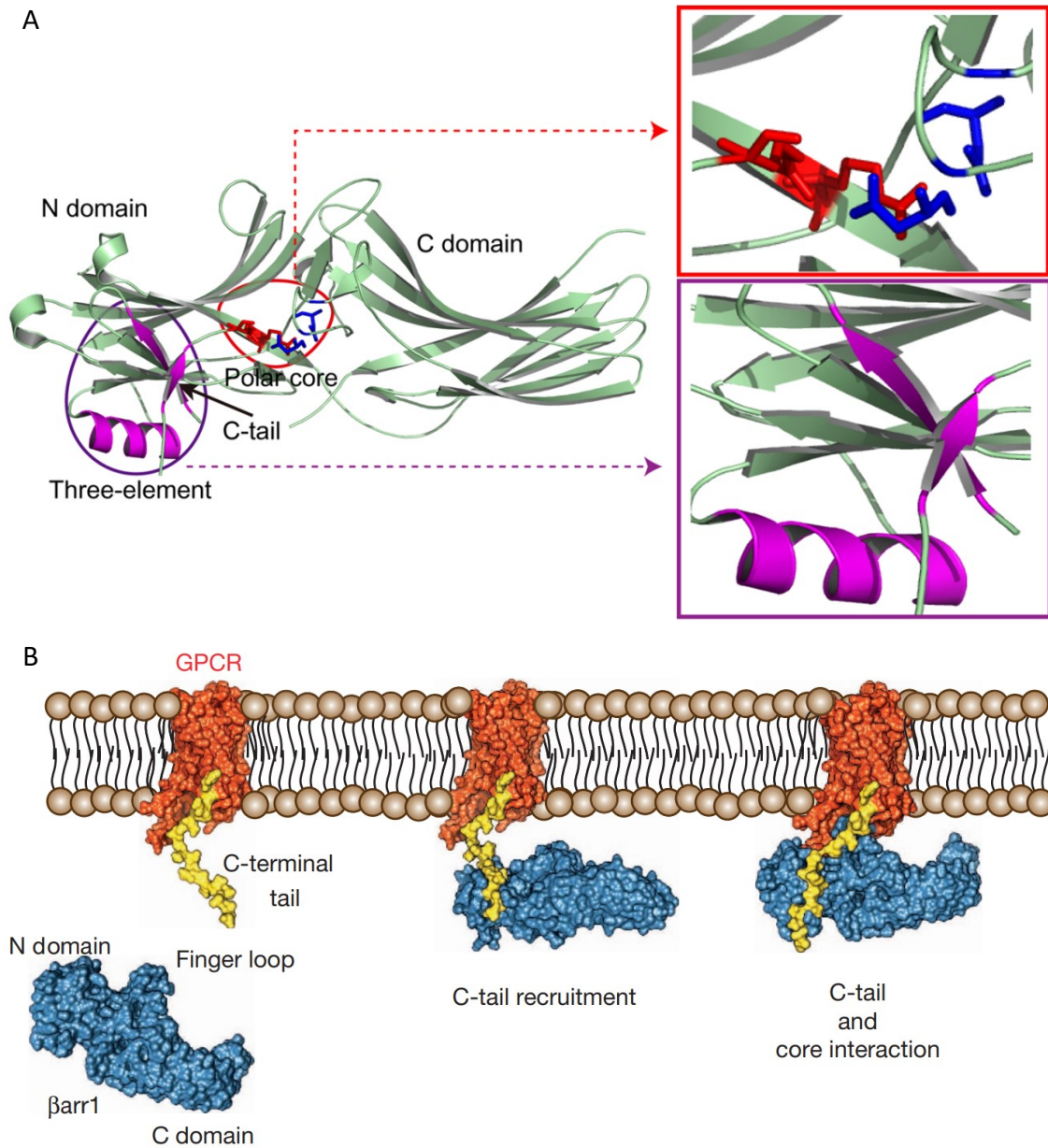


**Figure 5.** –  $\beta$ -arrestin structure and recruitment

(A) Three-dimensional structure of inactive  $\beta$ -arrestin 1 with an inset highlighting the three-element motif and the polar core. (B) Illustration of the two modes of binding (C-tail vs core) of  $\beta$ -arrestin to the receptor. Adapted from (113, 115).

## 2.4 $\beta$ -arrestin regulation

The expression levels of  $\beta$ -arrestin 1/2 are regulated by multiple factors at the transcriptional, translational, and post-translational stages. Considering that the amount of  $\beta$ -arrestin 1/2 expressed is altered in certain physiological disorders such as Parkinson's disease, multiple sclerosis, coronary disease, and cancers (116), it is primordial to consider the factors regulating  $\beta$ -arrestin 1/2 expression and functions.

In humans, the gene coding for  $\beta$ -arrestin 1 is located on chromosome 11 and the gene coding for  $\beta$ -arrestin 2 is located on chromosome 17. There are at least two known variants for each  $\beta$ -arrestin due to alternative exon splicing (117). Transcription of  $\beta$ -arrestin 1/2 genes is regulated by glucocorticoid receptors as they bind Glucocorticoid Response Element to activate  $\beta$ -arrestin 1 expression and bind Negative Glucocorticoid Response Element to repress  $\beta$ -arrestin 2 expression. This reveals a unique crosstalk between plasma membrane receptors and nuclear receptors through this mechanism where glucocorticoids can regulate GPCR response as a study shows that  $\beta$ -arrestin 1 upregulation by glucocorticoid directs GPCR signaling away from G protein-dependent pathways and more towards  $\beta$ -arrestin-dependent signaling (116). Protein translation regulation can be modulated by microRNAs (miRNAs) that bind to mRNA transcripts to inhibit their translation. It has been shown that miRNAs such as miR-525-3p and miR-365 target respectively  $\beta$ -arrestin 1 and  $\beta$ -arrestin 2 to interfere with their translation (118, 119).  $\beta$ -arrestin 1/2 are also modulated by post-translational modifications that will be discussed in chapter 3.

## 2.5 $\beta$ -arrestin localization

$\beta$ -arrestin 1 and  $\beta$ -arrestin 2 share a high degree of sequence homology, a conserved structure and achieve GPCR regulatory functions at the plasma membrane. However, they differ in their subcellular localization, as  $\beta$ -arrestin 1 is distributed at the basal level in both the cytoplasm and the nucleus, whereas  $\beta$ -arrestin 2 is located mainly in the cytoplasm. Cell treatment with a nuclear export inhibitor, Leptomycin B (LMB), results in nuclear accumulation of  $\beta$ -arrestin 2 but has no effect on  $\beta$ -arrestin 1. This indicates that  $\beta$ -arrestin 2 can localize in the nucleus but undergoes constitutive nuclear export (**Figure 6**) (120).

Given the large molecular size of  $\beta$ -arrestin 1/2 (~48 kDa), they cannot passively diffuse across the nuclear membrane and thus necessitate specific transporter to shuttle between the cytoplasm and the nucleus.  $\beta$ -arrestin 1 has a classical bipartite Nuclear Localization Signal (NLS) that allows interaction with importin- $\alpha$  and subsequent binding to importin- $\beta$ 1, which mediates import through the nuclear pores in a GTP hydrolysis-dependent process (121). Mutation of this NLS excludes  $\beta$ -arrestin 1 from the nucleus without affecting its recruitment to GPCRs at the plasma membrane. The mechanisms of nuclear import of  $\beta$ -arrestin 2 were poorly understood as a possible NLS has only recently been proposed (122). However, in a recent study (**annex II**), we reported that a SUMO-Interacting Motif (SIM) in  $\beta$ -arrestin 2 promotes its interaction with the RanBP2/RanGAP1-SUMO nuclear pore complex and mutation of the SIM excludes  $\beta$ -arrestin 2 from the nucleus (123). This suggests that nuclear import of  $\beta$ -arrestin 2 is a two-step process involving both the SIM and the NLS.

The nuclear localization of  $\beta$ -arrestins has been shown to play a critical role in regulation of gene transcription. It has been shown that  $\beta$ -arrestin 1 scaffolds different protein complexes to either activate or repress the expression of specific genes. For instance,  $\delta$ -opioid receptor (DOR) activation induces  $\beta$ -arrestin 1 nuclear accumulation and its binding to p27 and c-fos promoters where it enables recruitment of histone acetyltransferase p300, histones H4 acetylation, and increased gene transcription (124).  $\beta$ -arrestin 1 nuclear accumulation is also important for mediating NF- $\kappa$ B transcriptional response, by recruiting a p65 kinase and other acetyltransferases to regulate the transcription of genes activated by the NF- $\kappa$ B pathway. Thus, the regulation of the nuclear import of  $\beta$ -arrestin is crucial as it impacts gene transcription in response to extracellular signaling pathways.

In addition to having an NLS,  $\beta$ -arrestin 2 also possesses a Nuclear Export Signal (NES) as a hydrophobic region (VXXXFXXLXL) in the C-terminus is responsible for mediating  $\beta$ -arrestin 2 nuclear export.  $\beta$ -arrestin 2 undergoes continuous cycles of nuclear import and export but the NES dominates as  $\beta$ -arrestin 2 looks to be predominantly cytoplasmic when observed at basal level. Leptomycin B inhibits nuclear export by binding irreversibly a cysteine of the exportin CRM1 and blocking its binding to the NES. Mutation of a single leucine in the NES results in the almost complete delocalization of  $\beta$ -arrestin 2 in the nucleus. Interestingly, in the sequence of  $\beta$ -arrestin

1, there is a single amino acid difference (Glutamate instead of Leucine) resulting in a loss of interaction of  $\beta$ -arrestin 1 with CRM1 that explains the difference in subcellular localization.

The localization of  $\beta$ -arrestin 2 regulates the functions of various proteins. For instance,  $\beta$ -arrestin 2 interacts with the E3 ubiquitin ligase Mdm2 (murine double minute 2) in the nucleus and when  $\beta$ -arrestin 2 is exported to the cytoplasm, so is Mdm2. As Mdm2 ubiquitinates and induces the degradation of the transcription factor p53, the nucleocytoplasmic shuttling of  $\beta$ -arrestin 2 and by association Mdm2 stabilizes p53 in the nucleus and allows gene transcription. In addition, cytoplasmic accumulation of Mdm2 promotes ubiquitination and degradation of its cytoplasmic targets.  $\beta$ -arrestin 2 also regulates subcellular localization of JNK that is mainly cytoplasmic. However, mutation of the NES of  $\beta$ -arrestin 2 results in nuclear colocalization of  $\beta$ -arrestin 2 and JNK. This indicates a regulatory role of  $\beta$ -arrestin 2 in the cytoplasmic localization of JNK and the scaffolding of this signaling cascade (120, 125). Taken together, this reveals important roles of  $\beta$ -arrestin 1/2 in the nucleus related to gene transcription and regulation of protein localization.

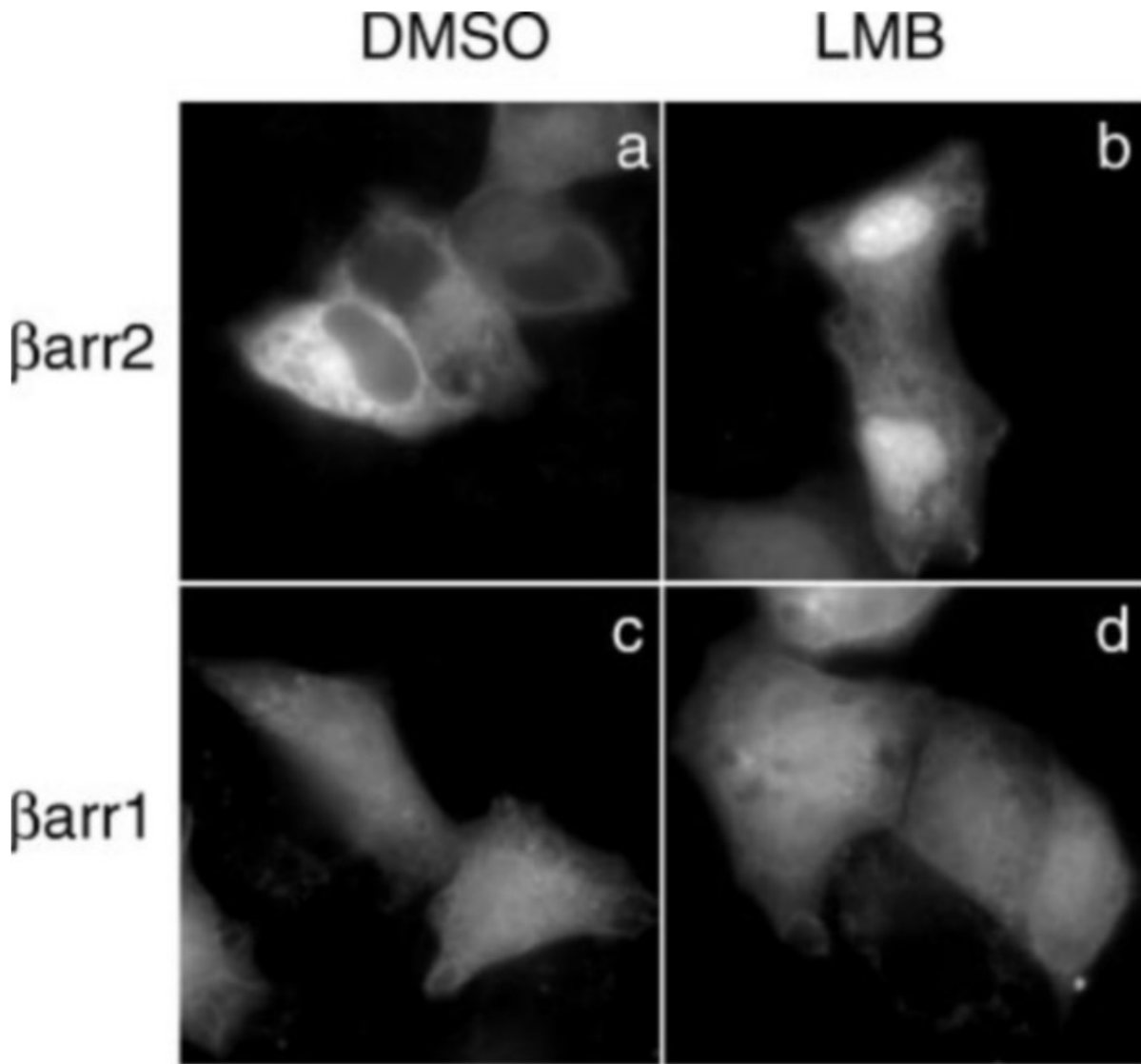


**Figure 6.** –  $\beta$ -arrestin subcellular localization.

$\beta$ -arrestin 2 is localized mainly in the cytoplasm and treatment with 20nM LMB blocks its nucleocytoplasmic shuttling.  $\beta$ -arrestin 1 is distributed in the cytoplasm and the nucleus and LMB has no noticeable effect on its localization (120).

## 2.6 GPCR desensitization and trafficking

GPCR stimulation by a ligand induces G protein activation characterized by dissociation of the  $G\alpha$  from the  $G\beta\gamma$  subunits, GDP to GTP exchange, and regulation of downstream effectors and signaling pathways. In parallel, another process is triggered to control the duration and extent of a signaling event initiated by ligand binding. GPCR desensitization is a negative feedback process coordinating multiple steps and involving different enzymes and scaffolding proteins. The first desensitization step is the phosphorylation of intracellular serine/threonine residues in the GPCR C-tail or intracellular loops, mainly ICL3. Receptor phosphorylation increases their affinity for the arrestin family of proteins that are then recruited to the GPCR and uncouple the activated G protein from the receptor. Arrestins also play a role in regulation of the number of receptors expressed at the cell surface as they recruit proteins of the endocytic machinery such as clathrin and AP2 complex to trigger GPCR internalization from the plasma membrane. The internalized receptor is trafficked through the endocytic pathway and can be sorted towards degradation in the lysosomes or recycled back to plasma membrane. Long-term desensitization caused by a prolonged exposition to a receptor agonist results in downregulation and decrease of *de novo* GPCR synthesis by unelucidated mechanisms. Paradoxically, in addition to avoiding overstimulation, GPCR desensitization process also triggers the transition from canonical G protein signaling to  $\beta$ -arrestin-dependent signaling (126).

### 2.6.1 Heterologous and homologous desensitization

GPCR phosphorylation is initiated within seconds of receptor activation and is achieved by two types of kinases: GPCR kinases (GRKs) or second messenger-activated kinases such as PKA and PKC. GRK-mediated phosphorylation initiates what is known as homologous desensitization and specifically targets ligand-bound activated receptors as opposed to PKA/PKC phosphorylation which induces heterologous desensitization and targets receptors at the plasma membrane without discrimination as to their activation status. Phosphorylation by PKA/PKC does not significantly increase the affinity of the receptor for  $\beta$ -arrestins. However, it does result in G protein uncoupling. PKA has also been shown to act directly on G protein effectors. For instance, phosphorylation of adenylate cyclase by PKA inhibits cAMP production revealing a different mode



of desensitization. Furthermore, the heterologous desensitization process can result in the decrease of signaling of a certain pathway in favor of another. Indeed, it has been shown that phosphorylation of the  $\beta$ 2AR by PKA results in a switch from Gs to Gi coupling and thus inhibiting further adenylate cyclase activation (127, 128, 129).

GRK phosphorylation by itself does not have a big impact on G protein coupling to the receptor, but it does increase GPCR affinity for the arrestin family of proteins that are recruited to the phosphorylated receptor and sterically hinder G protein coupling (130, 131). GRKs can also mediate GPCR desensitization through processes independent of phosphorylation. GRKs share three conserved functional domains: an RGS homology domain, a serine/threonine kinase domain, and a C-terminal domain. The C-terminal domain is responsible of directing GRKs to the plasma membrane and varies between the GRK proteins as GRK1, GRK 4, GRK5, GRK6, and GRK7 are anchored at the plasma membrane by different post-translational modifications (palmitoylation, prenylation) or by the interaction of a polybasic domain with phospholipids. On the other hand, GRK2 and GRK3 possess a pleckstrin homology (PH) domain that binds PIP2 and G $\beta\gamma$  to translocate from the cytoplasm to the receptor at the plasma membrane. A peptide mimicking the C-terminal PH domain of GRK2/3 (known as  $\beta$ ARKct for  $\beta$ -adrenergic receptor kinase C-tail) can be used as a competition peptide to inhibit G $\beta\gamma$  mediated recruitment of GRK2 and receptor phosphorylation. It has also been shown that GRK2 and GRK3 can disrupt Gq protein signaling by binding G $\alpha_q$  via its RGS domain and G $\beta\gamma$  via its PH domain resulting in the uncoupling of the heterotrimeric Gq protein from the receptor. GRK2/3 have also been shown to inhibit Gs and Gi function although the mechanism is unclear as G $\alpha_s$  and G $\alpha_i$  have not been shown to bind GRK2 or GRK3 (86, 126).

Regulator of G protein-signaling (RGS) proteins are also an important part of the desensitization process. They act as GTPase Accelerating Proteins (GAPs) for the G $\alpha$  subunits and increase the rate of GTP hydrolysis by the intrinsic GTPase activity of the G protein. This results in a shorter time span of G protein activation and signaling as the GDP-bound G $\alpha$  subunit reassociates with G $\beta\gamma$  dimer to return to the inactive state and reveals a mechanism of GPCR desensitization independent of receptor phosphorylation (87).

## 2.6.2 $\beta$ -arrestin recruitment

GPCR phosphorylation is a key trigger for  $\beta$ -arrestin recruitment to the plasma membrane as numerous studies have shown that  $\beta$ -arrestin binding to the receptor relies both on the interaction with the active conformation of the receptor via its activation sensor and on the interaction with phosphorylated intracellular residues via its phosphate sensor. As a matter of fact, *in vitro* studies have shown that phosphorylation of rhodopsin's C-tail results in a 10-fold increase in its affinity for the visual arrestin 1 (132). Arrestins compete for the site of G protein coupling and displace the G protein from the receptor by steric hindrance. Interestingly, two arrestins (arrestin 1 and arrestin 4) are recruited to rhodopsin and opsin in the visual system. For the other over 800 non-visual GPCRs, only two other arrestins ( $\beta$ -arrestin 1 and  $\beta$ -arrestin 2) have been characterized for their role in GPCR desensitization.

Considering the low sequence homology of GPCRs intracellular loops and C-tails, the variability of phosphorylated residues, and the different kinases potentially involved in GPCR phosphorylation,  $\beta$ -arrestin 1/2 are still able to recognize and bind the different receptor interfaces. However, GPCRs recruits  $\beta$ -arrestins with different affinities hence the notion of classifying GPCRs according to their interaction with  $\beta$ -arrestin 1/2. Class A GPCRs bind  $\beta$ -arrestin 2 with greater affinity than  $\beta$ -arrestin 1 and the formed complex is transient as it dissociates after receptor internalization in the endosomes and  $\beta$ -arrestins returns to the cytosolic pool. Class A GPCRs include the  $\beta$ 2 adrenergic ( $\beta$ 2AR),  $\mu$  opioid (MOR), endothelin A (ETAR) and dopamine D1A (D1AR) receptors. Class B GPCRs bind both  $\beta$ -arrestin 1 and  $\beta$ -arrestin 2 with similar affinity. They form stable complexes as  $\beta$ -arrestin 1/2 internalizes with the receptor targeted to the endosomes. Class B GPCRs include the angiotensin (AT1R), neurotensin 1 (NTSR1), vasopressin 2 (V2R), thyrotropin-releasing hormone (THR) and neurokinin NK-1 (NK1R) receptors. The phosphorylation of specific serine/threonine clusters in the intracellular loops and C-tail of the receptor dictates the stability of the GPCR- $\beta$ -arrestin interaction. Interestingly, replacement of the C-tail of a class A receptor with the C-tail of a class B receptor strengthens and stabilizes its interaction with  $\beta$ -arrestins. The opposite is also possible as substitution of the C-tail of a class B receptor for the C-tail of class A receptor converts the nature of its interaction with  $\beta$ -arrestins highlighting the importance of the C-tail in the formation of the receptor- $\beta$ -arrestin complex (133).

GPCR post-translational modification of intracellular serines/threonines by different kinases (GRKs, PKA and PKC) creates various phosphorylation patterns. The selection of specific residues to be phosphorylated depends on a multitude of factors such as specific ligands, GPCR type, and kinases expression level in a specific cell line. Studies have revealed that phosphorylation patterns function as barcodes that trigger different structural changes in the conformation of  $\beta$ -arrestins. Furthermore, each  $\beta$ -arrestin conformational state could direct a different functional outcome by scaffolding distinct protein complexes. For example, V2R phosphorylation by GRK2/3 leads to receptor desensitization and internalization while phosphorylation by GRK5/6 is important for initiating  $\beta$ -arrestin-dependent signaling pathways (134). Biased agonists of  $\beta$ 2AR have been shown to induce phosphorylation of different residues compared to a balanced agonist explaining the different functional consequences of receptor activation bias (135).

Moreover, some GPCRs recruit  $\beta$ -arrestins independently of phosphorylation as mutating the serine and threonine residues in their intracellular domains does not affect recruitment of  $\beta$ -arrestins. Negatively charged residues in the C-tail of these receptors act as phosphomimetic and facilitate  $\beta$ -arrestin recruitment. For instance, an aspartic acid residue in the ICL3 of the luteinizing hormone receptor mediates  $\beta$ -arrestin 2 recruitment, GPCR desensitization and internalization in a process independent of receptor phosphorylation (136, 137).

### **2.6.3 $\beta$ -arrestin-dependent internalization**

In addition to mediating GPCR desensitization,  $\beta$ -arrestin 1/2 promote receptor internalization to block further activation by extracellular ligands. The two main GPCR internalization pathways are through clathrin-coated pits or the caveolae pathway. Although receptor internalization has been linked to an agonist-induced response, some GPCRs undergo constitutive endocytosis to regulate the basal activity of the receptor as in the case of the melanocortin MC4 receptor or to redistribute the GPCR into different cellular compartments as in the case of the cannabinoid CB1 receptors (138). Dysregulation of the constitutive internalization of the V2R has been linked with familial nephrogenic diabetes insipidus (139). It remains that the rate of constitutive internalization is much slower than agonist-promoted internalization.

The canonical and most studied mode of GPCR endocytosis is the clathrin-coated vesicles mediated internalization.  $\beta$ -arrestins act as protein adaptors to target the receptor to clathrin-coated pits and recruit proteins such as clathrin and the AP2 complex to initiate receptor endocytosis. Clathrin is composed of three light and three heavy chains that coat and create an invagination of the plasma membrane in the form of pits destined for internalization. The AP2 complex is a tetrameric adaptor complex comprised of four adaptin subunits:  $\alpha$ ,  $\beta$ 2,  $\mu$ 2 and  $\sigma$ 2.  $\beta$ -arrestin activation releases its C-terminal domain, which interacts with clathrin heavy chains and the  $\beta$ 2-adaptin subunit of the AP2 complex. Deletion of the last 25 residues in the C-terminal domain of  $\beta$ -arrestin results in loss of interaction with AP2 and clathrin blocking GPCR internalization. AP2 also binds clathrin and other accessory proteins (epsin, amphiphysin, endophilin) to regulate the maturation of the clathrin pits. The GTPase dynamin mediates the detachment of the clathrin-coated vesicles from the plasma membrane. Dynamin possesses a PH domain that allows binding to the lipids of the plasma membrane and a GTPase domain that catalyzes the fission of the clathrin-coated vesicles from the plasma membrane. The released vesicles lose their clathrin coating and can fuse with early endosomes where the GPCR can undergo dephosphorylation and ligand dissociation (140, 141).

#### **2.6.4 $\beta$ -arrestin-independent internalization**

Evidence that some GPCRs can internalize independently of  $\beta$ -arrestins was obtained using  $\beta$ -arrestin 1/2 KO cells where receptor internalization was not inhibited. Some membrane proteins including some GPCRs like the  $\alpha$ 1b-adrenergic and thromboxane receptors possess a tyrosine-based internalization motif recognized directly by the  $\mu$ 2-adaptin subunit of the AP2 complex while the  $\alpha$ -adaptin subunit interacts with plasma membrane phospholipids. AP2 mediates GPCR interaction with clathrin and initiates the receptors internalization (142).

Another non-canonical route of GPCR endocytosis independent of  $\beta$ -arrestins and clathrin is the internalization via the caveolae pathway. Caveolae are portions of the plasma membrane enriched in cholesterol and sphingomyelin. Recruitment of caveolin, cavin, and pacsin creates invagination in the membrane while the fission of the endocytic vesicle is dependent on dynamin. It is suggested that receptor post-translational modification by the attachment of fatty acids could

direct GPCRs to the caveolae pits. Somatostatin SST2, muscarinic M2, endothelins ETAA, and bradykinin B2 receptors have been shown to internalize via the caveolae pathway although they can also use the classical clathrin mode (143).

### **2.6.5 GPCR intracellular trafficking**

After detachment from the plasma membrane, the endocytic vesicle undergoes depolymerization of the clathrin coating, if present, and fuses with the early endosomes. The early endosomes are organelles responsible of acting as the sorting center of the cell and directing the internalized receptor towards degradation or recycling (**Figure 7**). The acidic environment in the lumen of the endosomes affects the ligands binding and results in their dissociation from the receptor (144).

The GTPases of the Rab family localized in the endosomal compartments contribute to the structure and function of these organelles. Each Rab protein can recruit specific effectors to the different endosomes. For instance, Rab5, Rab13, Rab21, Rab22, and Rab23 are associated with the early endosomes and play a role in the fusion of the internalized vesicle with the early endosome. Rab4, Rab8 and Rab11 localize in the recycling endosomes where they regulate transport of dephosphorylated GPCRs back to the plasma membrane. Rab7, Rab9, and Rab12 are characteristic of late endosomes and lysosome and thus regulate GPCR degradation (145). Biomolecular tools using these proteins as markers of the different cellular compartments have been developed to monitor GPCR localization by microscopy or more recently by Bioluminescence Resonance Energy Transfer (BRET).

$\beta$ -arrestins play an important role in the sorting of GPCRs, as it has been shown that class A receptors that have a weaker affinity for  $\beta$ -arrestins are more likely to be selected for recycling, whereas class B receptors that internalize forming a stable complex with  $\beta$ -arrestins are more susceptible to be directed to lysosomal degradation.

Recycling of some internalized membrane proteins, such as transferrin receptors, occurs via bulk recycling tubules. This process is triggered by the fission of narrow tubules that contain a high concentration of membrane proteins from the endosomes and provides a general mechanism for returning these proteins to the plasma membrane. For most of the studied GPCRs, recycling is mediated by a specific endosomal microdomain enriched in actin/sorting nexin/retromer

complex (ASRT). This highly regulated mechanism is dependent on a PDZ-binding sequence in the C-terminal domain and mutation of this sequence results in inhibition of receptor recycling to the plasma membrane (146). GPCR recycling also requires the action of two phosphatases PP2A and PP2B that dephosphorylate the residues in the intracellular loops and C-terminal domain of the receptor (147).

GPCR lysosomal degradation was first demonstrated for the yeast receptor sterile 2  $\alpha$ -factor receptor (Ste2). It has been shown that Ste2 ubiquitination is critical to its internalization and subsequent degradation (148). However, in mammals the ubiquitination signal is not essential for receptor internalization but does regulate receptor degradation. Lysosomal degradation of GPCRs is mediated by the highly conserved endosomal-sorting complex required for transport (ESCRT) pathway, composed of four protein complexes. ESCRT-0 contains a FYVE zinc-finger domain that enables recruitment and binding to the endosomal endomembrane. It also recognizes ubiquitinated cargo proteins through multiple ubiquitin binding domains. ESCRT-I is enriched in late endosomes and is recruited by ESCRT-0 which allows recognition of the ubiquitinated receptor. ESCRT-II and ESCRT-III are recruited sequentially and mediate membrane invagination, fission, and fusion with lysosomes. CXCR4, PAR2 and  $\mu$ OR have been shown to be degraded by a ubiquitin and ESCRT regulated mechanism (149, 150). Ubiquitination of GPCRs will be further discussed in chapter 3.

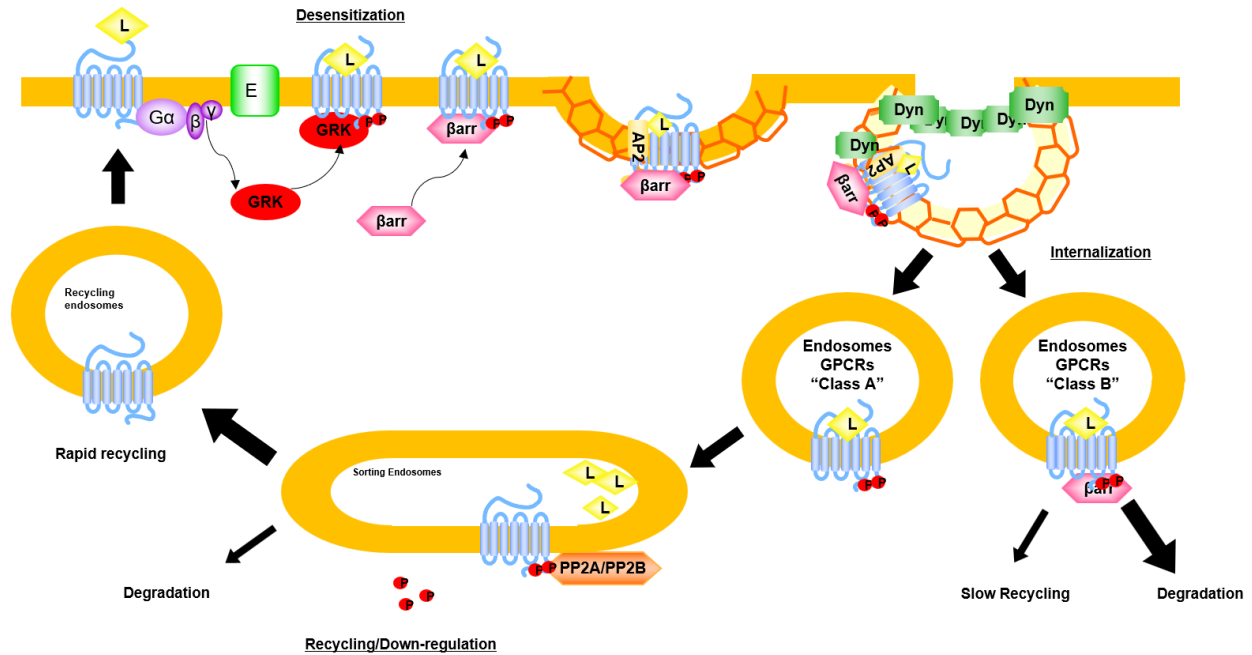


**Figure 7.** – Role of  $\beta$ -arrestin in GPCR internalization and trafficking.

After receptor phosphorylation by GRKs,  $\beta$ -arrestin is recruited to the receptor and mediates desensitization and internalization by scaffolding the proteins of the AP2 complex and clathrin.  $\beta$ -arrestin dissociates from class A GPCRs in the endosomes and these receptors are more prone to be recycled to the plasma membrane. Class B receptors have a stable interaction with  $\beta$ -arrestin and are more likely to be sent towards degradation pathways. Adapted from (133).

## 2.7 $\beta$ -arrestin dependent signaling

$\beta$ -arrestins are misnamed as they do not only “arrest” receptor signaling, but they also promote certain signaling pathways. Although  $\beta$ -arrestins do not possess an enzymatic activity, they can trigger signaling events by scaffolding different signalosomes. Numerous biochemical and proteomic studies identified  $\beta$ -arrestin interactors that form signaling complexes (**Figure 8**).

### 2.7.1 Src kinase

The first discovery of a  $\beta$ -arrestin-mediated mode of signaling came from a study showing an interaction between  $\beta$ -arrestin 1 and the Src family of non-receptor tyrosine kinases.  $\beta$ 2AR activation promotes recruitment of  $\beta$ -arrestin in complex with activated Src at the plasma membrane. Src kinases are cytoplasmic proteins responsible of phosphorylation of various substrates and activate pathways such as the RAS/MAPK pathway to regulate cell proliferation, differentiation, survival, and motility. GPCR activation also induces Src-mediated phosphorylation of dynamin to modulate receptor internalization (104, 151). Other GPCRs such as the neurokinin-1 receptor have also been shown to activate Src through the interaction with  $\beta$ -arrestins (105).

### 2.7.2 ERK1/2 pathway

Mitogen-Activated Protein Kinase (MAPK) signaling regulates cell proliferation, mitosis, differentiation, and apoptosis by modulating the phosphorylation of cytoplasmic substrates and nuclear transcription factors. The ERK1/2 pathway is a prototypical MAPK pathway and consist of a signaling cascade composed of three serine/threonine kinases: MAPK kinase kinase (MAPKKK), MAPK kinase (MAPKK), and MAPK. Activation of cell surface receptors (GPCRs and RTKs among others) promotes activation of RAS GTPases that recruits MAPKKK Raf isoforms to the plasma membrane and induces its phosphorylation. This acts as an activation event and triggers the phosphorylation of MAPKK MEK1/2 by Raf. In turn, MEK1/2 activates MAPK ERK1/2 by phosphorylation (152). Several studies using GPCR internalization inhibitors or  $\beta$ -arrestin dominant negative mutants suggested an important role of  $\beta$ -arrestin in ERK1/2 activation. Furthermore, *in vitro* studies have shown  $\beta$ -arrestin 1/2 binding to all three components of the ERK/12 signaling cascade. Also, formation of receptor- $\beta$ -arrestin-Raf-MEK1/2-ERK1/2 in an agonist-promoted manner shows a clear role of  $\beta$ -arrestin in mediating ERK1/2 signaling after



receptor activation. This suggests that  $\beta$ -arrestin acts as a scaffold that creates proximity between the three kinases and allows a more efficient transduction of the ERK1/2 signaling (153).

### **2.7.3 JNK pathway**

JNK signaling is involved in cellular stress response, apoptosis, differentiation, proliferation, and migration. Similar to the ERK1/2 pathway, a signaling cascade composed of three kinases participates in JNK signaling: MAPKKK (Ask1), MAPKK (MKK4/7), MAPK (JNK1/2/3).  $\beta$ -arrestin 2 has been shown to bind all three JNK cascade kinases and regulates transcription by retaining JNK3 in the cytoplasm. AT1R stimulation results in JNK pathway activation and  $\beta$ -arrestin 2 scaffolding of the JNK pathway in endosomal vesicles. Thus,  $\beta$ -arrestin 2 regulates activation and spatial distribution of the JNK signaling pathway (154).

### **2.7.4 p38 MAPK pathway**

p38 is another MAPK signaling pathway where  $\beta$ -arrestin has been shown to play a role. Several MAPK kinase kinases have been shown to converge and activate MKK3/6 that phosphorylates p38 MAPK.  $\beta$ -arrestin has been shown to be critical in promoting CXCR4 activation of p38 MAPK-mediated chemotaxis. The kappa opioid receptor also activates p38 MAPK by a mechanism that requires  $\beta$ -arrestin 2 and triggers formation of  $\beta$ -arrestin-p38 MAPK signalosomes (155, 156).

### **2.7.5 PI3K pathway**

Phosphatidylinositol 3 kinase (PI3K) is activated by GPCRs and RTKs. Its activation induces conversion of phosphatidylinositol-4,5-bisphosphate (PIP2) to phosphatidylinositol-3,4,5 triphosphate (PIP3). PIP3 recruits Akt kinase to the plasma membrane where it recruits various substrates regulating cell growth and apoptosis. The insulin-like growth factor 1 receptor (IGF1R) activates Akt through a  $\beta$ -arrestin 1 dependent mechanism that does not involve GPCRs and promotes anti-apoptotic responses. Protease-activated receptors (PAR) have been shown to activate Akt by a mechanism distinct from G proteins and  $\beta$ -arrestin. Dopamine D2 receptor promotes  $\beta$ -arrestin 2 binding to Akt and phosphatase 2A (PP2A) to inhibit the anti-apoptotic functions of the PI3K pathway (157, 158, 159).

### 2.7.6 NF- $\kappa$ B

Nuclear Factor kappa B (NF- $\kappa$ B) is a transcription factor regulating the expression of many genes that control cell proliferation and inflammation. I $\kappa$ B $\alpha$  is an inhibitory protein that interacts with NF- $\kappa$ B to limit its localization to the cytoplasm. Phosphorylation of I $\kappa$ B $\alpha$  by I $\kappa$ B kinase promotes its ubiquitination and degradation, freeing NF- $\kappa$ B and allowing its translocation to the nucleus.  $\beta$ 2AR activation promotes  $\beta$ -arrestin 2 association with I $\kappa$ B $\alpha$  and prevents its degradation resulting in inhibition of NF- $\kappa$ B nuclear translocation. On the other hand,  $\beta$ -arrestin 1 acts as a NF- $\kappa$ B activator as it enhances nuclear localization of NF- $\kappa$ B (121, 160).

### 2.7.7 $\beta$ -arrestin vs G protein

$\beta$ -arrestin role in acting as a scaffolding protein for MAPK activation has been repeatedly demonstrated in numerous studies and has been tightly linked to GPCR activation. Indeed, ERK1/2 phosphorylation was utilized as a functional readout of  $\beta$ -arrestin dependent signaling without necessarily considering the contributions of G proteins. It has been shown that class A receptors that bind weakly to  $\beta$ -arrestin induce ERK1/2 activation and translocation to the nucleus to phosphorylate nuclear substrates, while class B receptors that form a stable complex with  $\beta$ -arrestin promote cytoplasmic functions of ERK1/2 by retaining the GPCR- $\beta$ -arrestin-ERK1/2 complex in the cytosol (161). Meanwhile, G proteins were found to mediate early-phase MAPK activation, with AT1R stimulation inducing transient and rapid ERK1/2 activation, while  $\beta$ -arrestin mediated a later and longer lasting ERK1/2 activation (162). Yet, the role of G proteins in this process is a controversial matter. A study using G protein depleted cells showed that  $\beta$ -arrestin is still recruited to the receptor in absence of G protein activation, but no  $\beta$ -arrestin-mediated ERK1/2 activation was observed (163). This suggests that  $\beta$ -arrestin does mediate ERK1/2 activity but needs an initial trigger from G proteins. Another study using  $\beta$ -arrestin depleted cells came to the surprising conclusion that in different KO cell lines,  $\beta$ -arrestin can promote or inhibit ERK1/2 signaling. CRISPR generated cell lines may be randomly selected for their ability to compensate for the eliminated protein by different pathways (164). All taken together, the evidence points to a collaborative effort between G proteins and  $\beta$ -arrestin in promoting MAPK signaling.

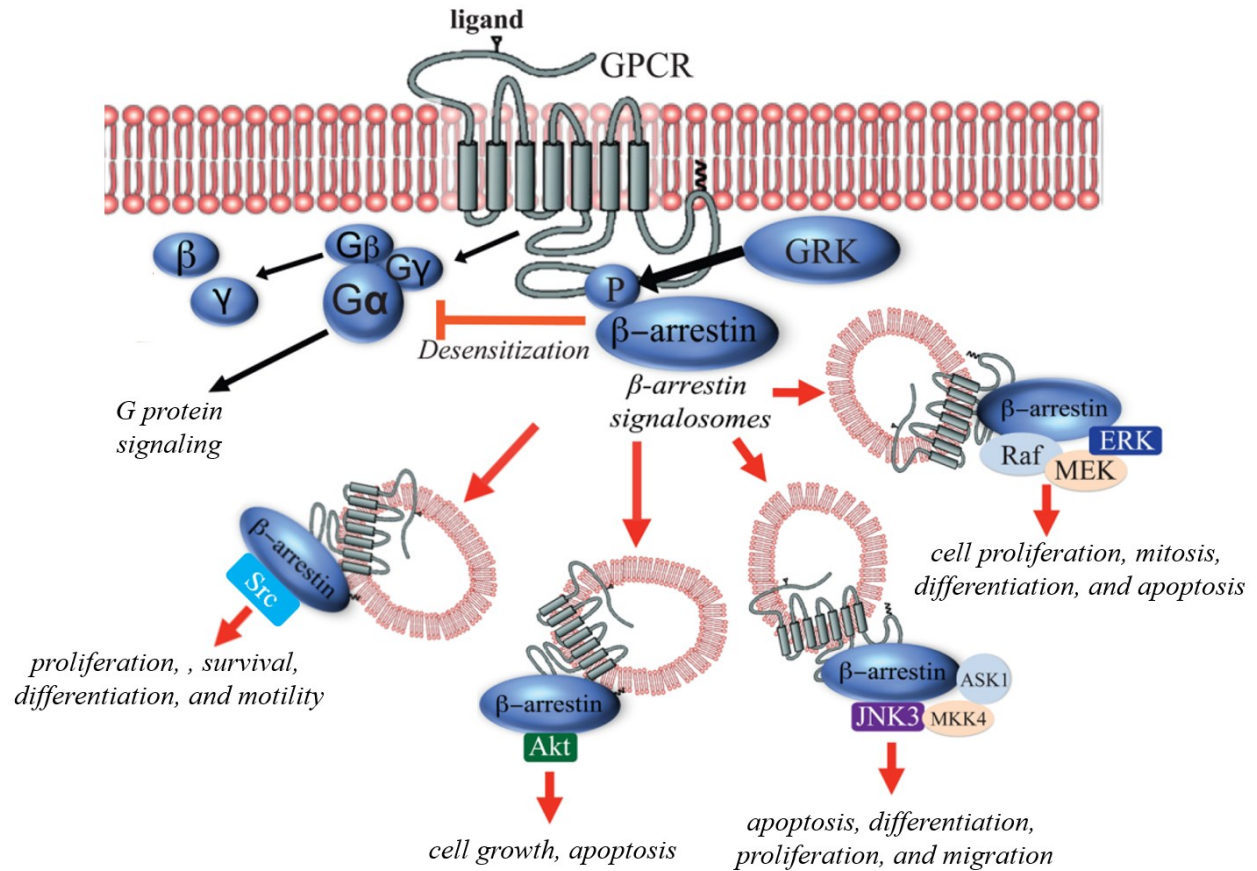


**Figure 8.** – Examples of β-arrestin dependent signaling pathways.

GPCR stimulation by a ligand leads to the recruitment and scaffolding of various signaling proteins by β-arrestin. Adapted from (165).

### 2.7.8 Biased signaling

The finding that a single GPCR can couple to and activate multiple heterotrimeric G proteins and that  $\beta$ -arrestin recruitment to the receptor triggers non-canonical signaling pathways has expanded our view of GPCR signaling. The old notion that an agonist binds to a receptor and induces a structural change to a unique active conformation has been replaced by the concept of functional selectivity or signaling bias. This paradigm shift describes the idea that different ligands can stabilize different active conformations of the receptor, each leading to the activation of different signaling pathways. Biased agonists have the capacity to activate some signaling effectors while blocking others, as opposed to balanced agonists that stabilize receptor conformations competent for activating all coupled effectors without discrimination. Numerous studies describe ligands that show a bias for G protein signaling pathways (G protein-biased) or  $\beta$ -arrestin-mediated signaling pathways ( $\beta$ -arrestin-biased). Some ligands even exhibit a bias between G proteins favoring a single G protein subtype over others that might couple to the receptor (**Figure 9**) (166).

Biased signaling has important physiological and therapeutical implications as activation of some signaling pathways can have beneficial or detrimental effects. For instance, a balanced agonist could activate G protein signaling mediating beneficial cellular outcomes but also activate  $\beta$ -arrestin signaling mediating detrimental side effects. The use of a G protein biased agonist targeting the same receptor would allow to activate only the desired signaling pathways and avoid negative side effects. A study on the  $\mu$ -opioid receptor showed that the  $\beta$ -arrestin biased ligand TRV130 presents greater analgesia effects compared to the balanced agonist morphine, but in addition, it showed lesser adverse effects such as nausea, respiratory depression, and vomiting (167). Similar studies on the AT1R lead to the development of a  $\beta$ -arrestin-biased agonist TRV120027 for the treatment of acute decompensated heart failure by stimulating cardiac contractility while diminishing side effects caused by balanced AT1R agonists (168). Other GPCRs such as  $\beta$ 2AR, PTHR, CXCR4, and D2R are the targets of studies and clinical trials in order to develop biased ligands with an optimal therapeutic outcome compared to balanced ligands(166).

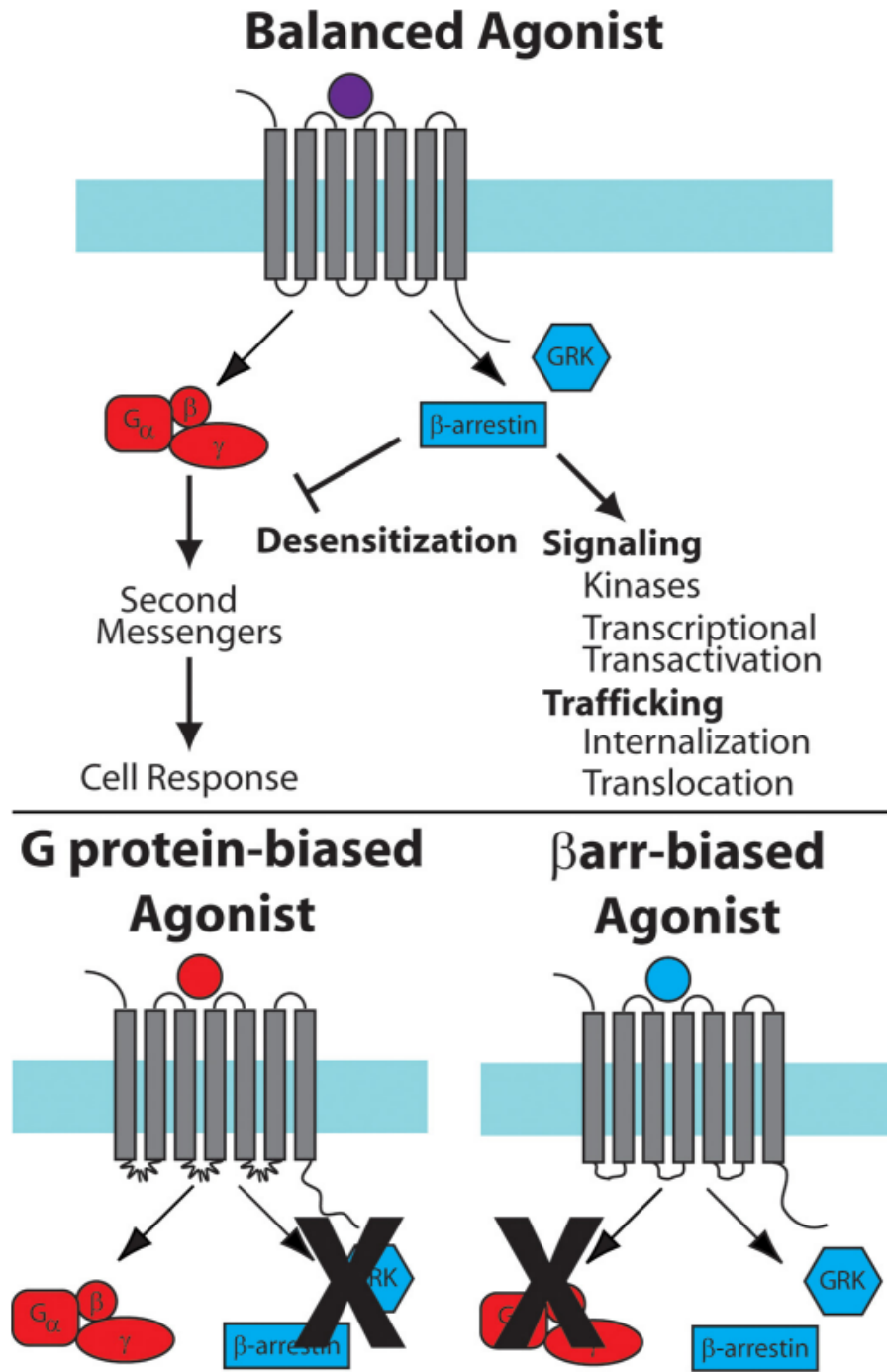


**Figure 9.** – GPCR biased signaling.

Balanced agonists promote equally activation of G protein and  $\beta$ -arrestin mediated signaling pathways, whereas biased agonists promote preferentially one or some signaling pathways over others (169).

## 2.8 Endosomal signaling

Classically, GPCRs are described to trigger signaling at the plasma membrane by coupling heterotrimeric G proteins. Subsequent  $\beta$ -arrestin recruitment to the receptor sterically hinders G protein coupling leading to desensitization and receptor internalization. This concept has been revisited over the past decade as many GPCRs have been shown to support long-lasting and sustained G protein signaling after receptor internalization. The number of GPCRs displaying sustained endosomal signaling profiles is growing and includes the parathyroid hormone receptor (PTHrP), vasopressin type 2 receptor (V2R), thyroid stimulating hormone receptor (TSHR), luteinizing hormone receptor (LHR), sphingosine-1-phosphate 1 receptor (S1PR1), neurokinin type 1 receptor (NK1R), calcitonin receptor-like receptor (CLR), and C-C chemokine receptor-1 (CCR1) (170).

The first evidence for GPCR sustained signaling was shown in transgenic mice where thyroid-stimulating hormone (TSH) stimulation led to  $\beta$ -arrestin-dependent TSHR internalization but was not associated with receptor desensitization or inhibition of cAMP production. Moreover, heterotrimeric Gs protein and adenylate cyclase were also found in the endocytic compartment explaining the sustained signaling mediated by the internalized TSHR (171). PTHrP has also been shown to mediate sustained signaling as PTHrP(1-36) stimulation resulted in exclusively plasma membrane cAMP response while PTH(1-34) remained associated with PTHrP coupled to Gs heterotrimeric protein after internalization resulting in sustained endosomal signaling. Difference in PTHrP(1-36) and PTH(1-34) binding kinetic is an important parameter in modulating the duration of the PTHrP sustained signaling (172). A follow-up study showed that  $\beta$ -arrestin enhances Gs endosomal signaling as PTHrP,  $\beta$ -arrestin, and G $\beta\gamma$  form a complex that allows rapid heterotrimeric Gs formation and reactivation in the endosomes after G $\alpha_s$  subunit GTP hydrolysis (173). A study on V2R-mediated sustained signaling also showed that  $\beta$ -arrestin extends the duration of cAMP generation after receptor internalization in contrast to the canonical role of desensitization it usually plays at the plasma membrane (174).

These studies highlight the role of  $\beta$ -arrestin in endosomal GPCR signaling, first by mediating receptor translocation from the plasma membrane to the endosomes and by enhancing G protein

activity in the endosomes. Previously, G protein and  $\beta$ -arrestin engagement to the receptor were considered mutually exclusive until the discovery of an endosomal mega-complex composed of a single GPCR binding simultaneously to both a heterotrimeric Gs protein and to  $\beta$ -arrestin. Structural studies have shown that G proteins engage the receptor intracellular loops while  $\beta$ -arrestin displaces this interaction by binding the transmembrane core of the receptor. However,  $\beta$ -arrestin can also be partially coupled by binding only to the C-tail of the receptor and this conformation is sufficient to trigger its internalization. This conformation frees the core of the receptor permitting G protein coupling. The visualization of this 'megaplex' by cryo-EM confirmed the formation of a  $\beta$ 2V2R-Gs- $\beta$ -arrestin complex where the heterotrimeric Gs protein is bound to the core of the receptor and  $\beta$ -arrestin is bound to the C-tail. Biochemical and cellular assays showed endosomal localization of the megaplex and sustained Gs-mediated cAMP production (175). This study provides a mechanism and an explanation for the paradoxical role of  $\beta$ -arrestin in facilitating sustained signaling for class B GPCRs. Class A GPCRs interact transiently with  $\beta$ -arrestin and do not remain in complex once they reach the endosomes, so it is not expected that they form megaplex-like structure. The question remains open to find out if class A GPCRs such as the  $\beta$ 2AR can give rise to G protein-mediated endosomal sustained signaling and whether  $\beta$ -arrestin is involved in such process.

GPCR endosomal signaling has been linked with several physiological and pathophysiological processes. In cardiac ganglia neurons, pituitary adenylate cyclase 1 receptor (PAC1R) activates MEK/ERK signaling in the endosomes to modulate neuronal excitability (176). Protease-activated receptor-2 (PAR2) is implicated in the triggering of persistent pain associated with irritable bowel syndrome. A study showed that PAR2 sustained signaling from the endosomes resulting in continuous hyperexcitability of nociceptors and chronic pain. An endosome-targeted PAR2 antagonist is being developed to inhibit endosomal signaling and could be used as a potential treatment for the chronic pain of irritable bowel syndrome (177). V2R expression in the kidneys regulates water homeostasis in the body. The agonist arginine vasopressin (AVP) binds strongly to the V2R and mediates internalization and endosomal signaling while the agonist oxytocin (OXT) has a lower affinity dissociates from the internalized V2R. This explains the stronger antidiuretic

effect of AVP compared to OXT (174). A more comprehensive understanding of endosomal signaling mechanisms will provide new opportunities of GPCR based treatments.

## 2.9 $\beta$ -arrestin interactors

$\beta$ -arrestin proteins were initially identified for their role in receptor desensitization and as such, GPCRs were considered as their main interactor.  $\beta$ -arrestin was also shown to mediate receptor internalization by interacting with proteins of the endocytic machinery such as clathrin, AP-2 complex, N-ethylmaleimide-sensitive fusion protein (NSF), ADP-ribosylation factor 6 (ARF6), and guanine nucleotide exchange factor ARNO. In addition, many novel  $\beta$ -arrestin functions were identified growing the number of interactors and effectors of  $\beta$ -arrestin. Most notably,  $\beta$ -arrestin interaction with signaling molecules such as Src, ERK1/2, JNK3, p38, and AKT has been characterized in depth (178).  $\beta$ -arrestin has also been shown to interact and regulate the functions of receptors other than GPCRs such as the tyrosine kinase IGF1 receptor, TGF $\beta$  III receptor, nicotinic cholinergic receptor, and Notch (179).

Thus, it is now understood that  $\beta$ -arrestin acts as a multifunctional adaptor and scaffolds multiple protein complexes regulating diverse cellular responses. A proteomic analysis of  $\beta$ -arrestin 1/2 interactome under basal and AT1R-stimulated conditions and led to the identification of 71 interactors for  $\beta$ -arrestin 1, 164 interactors for  $\beta$ -arrestin 2, and 102 interactors common to both isoforms (180). Curation of interaction databases such as NetPath (181), BioGRID (182), and Mentha (183) compile more  $\beta$ -arrestin interactors identified in other studies. The identified interactors are broadly distributed in the cell and are found in the cytoplasm, nucleus, plasma membrane, mitochondria, endoplasmic reticulum, and Golgi apparatus among other cellular compartments illustrating the widespread functions played by  $\beta$ -arrestin in the cell. These interaction partners are involved in many functions including intracellular trafficking, signal transduction, post-translational modifications, gene transcription, RNA processing, protein biosynthesis, and cytoskeleton remodeling (184). The identification of each new  $\beta$ -arrestin interactors helps understand novel functions that these proteins might be playing in the cell as it is evident that  $\beta$ -arrestin is implicated in many more functions than initially thought.



## 3 Chapter 3: Post-Translational Modifications

### 3.1 Generality

The complexity of proteome study is amplified due to protein post-translational modifications (PTMs) that increase the functional diversity of the proteome. PTMs are covalent modifications of amino acid side chains after protein biosynthesis and these modifications play a central role in modulating protein functions. PTMs modulate a broad spectrum of protein behaviors including protein activity, localization, trafficking, solubility, folding, and interactions with other cellular partners. As well, PTMs regulate various biological processes like signal transduction, cell cycle control, gene expression, and DNA repair (185).

Over 200 types of PTMs have been described in the literature, some of the most commonly studied are phosphorylation, acetylation, ubiquitination, N- and O-glycosylation, methylation, SUMOylation, nitrosylation and palmitoylation (186). It is estimated that these modifications are catalyzed by the activity of various enzymes that account for 5% of the entire proteome, including kinases, phosphatases, ligases, and transferases (187). PTMs are categorized into three main groups. The first group includes modifications that add a chemical group to an amino acid residue like glycosylation, prenylation, myristoylation and palmitoylation. The second group represents PTMs that induce the addition of a polypeptide to the substrate protein such as ubiquitination and SUMOylation for example. And the third group consists of cleavage of peptide bonds and protein degradation like proteolysis. Protein modifications occur at the different time points of protein life cycle. Some modifications occur as the proteins go along the translation process to ensure proper folding, stability, and cellular localization. Other PTMs are required to regulate or activate protein functions. They can also be modified to be targeted towards protein degradation systems. Many pathophysiologicals and diseases exhibit dysregulation of PTMs; neurodegenerative diseases such as Alzheimer's, Parkinson's, and Huntington's diseases in addition to various cancers are impacted by disruptions of proteins PTMs (185).

In the context of studying GPCRs (**Figure 10**) and  $\beta$ -arrestins in this thesis, we will focus on three post-translational modifications: phosphorylation, ubiquitination, and SUMOylation.

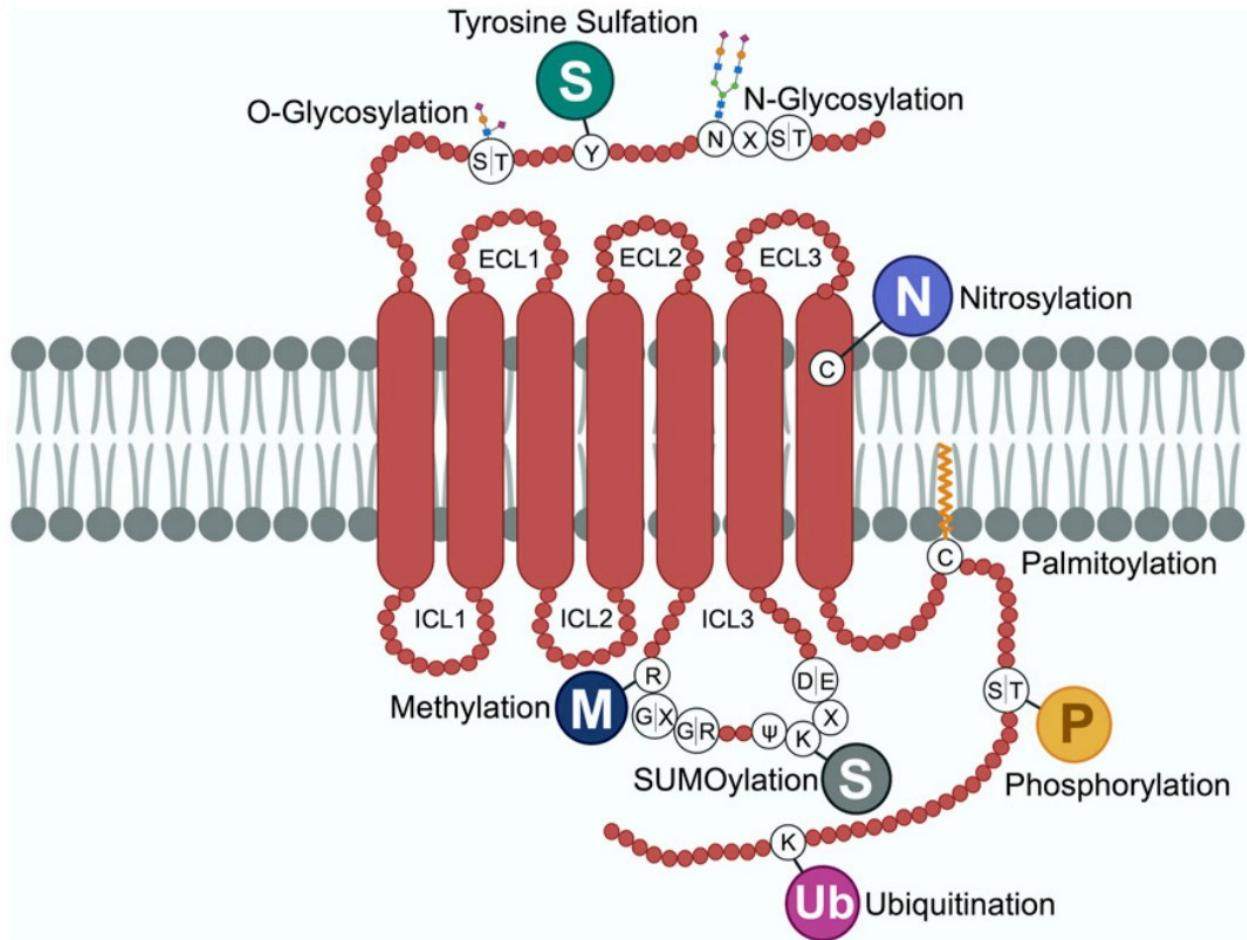


**Figure 10.** – GPCR post-translational modifications.

GPCRs undergo multiple intracellular and extracellular post-translational modification such as sulfation, glycosylation, nitrosylation, palmitoylation, methylation, SUMOylation, phosphorylation, and ubiquitination (188).

## 3.2 Phosphorylation

Phosphorylation is one of the most extensively studied PTMs and plays a critical role in many biological processes. It is a reversible protein modification modulated by the catalytic action of two sets of enzymes, kinases and phosphatases that represent 2%-5% of the human genome. Over 500 kinases have been characterized in the human proteome as the enzymes catalyzing the transfer of a terminal phosphate group ( $\text{PO}_4$ ) from ATP to the nucleophilic-OH group on the side chain of threonine, serine, and tyrosine residues. Kinases target specific amino acids flanked by different consensus sequences and can recognize one specific substrate or hundreds of proteins to phosphorylate. They can also phosphorylate a single residue or multiple residues on the same protein (189).

Phosphorylation acts as a rapid molecular switch (milliseconds to seconds) to regulate cellular processes like the cell cycle, cell growth, signal transduction, differentiation, and apoptosis. Phosphorylation positively or negatively regulates substrate activity by inducing protein conformational change that alters the protein catalytic activity or modifies the protein affinity for interaction partners that bind to the phosphorylated motifs. The modulation of protein phosphorylation is very complex as a multitude of intracellular and extracellular signals converge to regulate this process (190). In turn, phosphatases are part of a family of approximately 150 enzymes responsible for protein dephosphorylation. They regulate the duration and intensity of phosphorylation-dependent functions by catalyzing the hydrolysis of the phosphate group from the protein substrate. Kinases and phosphatases balance the phosphorylated state of proteins and dysregulation of this system can lead to disease development (191).

### 3.2.1 GPCR phosphorylation

GPCR phosphorylation has been known for a long time to play a role in GPCR regulation. Rhodopsin was first shown to be phosphorylated after activation to induce receptor desensitization and visual arrestin recruitment (98). This was followed by studies on the  $\beta$ 2AR that showed receptor phosphorylation by both GRKs and PKA (131, 192). Virtually all the investigated GPCRs have been shown to undergo phosphorylation at basal levels or induced by agonist activation. GPCRs act as dynamic scaffolds capable of binding a multitude of cellular

effectors to trigger different biological outcomes. The combination of the different active conformations that a receptor can take, and the phosphorylation of different cytoplasmic residues allows the receptor to select a specific binding partner. As previously discussed (**section 2.6.2**), the arrestin family of protein recruitment is closely linked to receptor phosphorylation as the arrestin phosphate sensor detects and binds to the receptor's phosphorylated residues. Phosphorylated rhodopsin affinity with arrestin is increased 10-fold compared to the inactive state, but non-visual receptors exhibit only a 2—to 3-fold increase in arrestin affinity (193). Moreover, it is critical to consider that non-visual arrestins are responsible for recognizing and binding hundreds of different GPCRs that present low sequence homology highlighting the role of phosphorylation in  $\beta$ -arrestin recruitment to the receptor. The differences in GPCR phosphorylation profiles create a wide spectrum of affinities for  $\beta$ -arrestin which allowed to categorize receptors with weaker affinity for  $\beta$ -arrestin as class A GPCRs and receptors with stronger affinity for  $\beta$ -arrestin as class B GPCRs (194). Conversely, receptor dephosphorylation is mediated in the endosomes by different phosphatases (PP2A, PP2B, PP1B) and is critical for receptor resensitization and recycling (147, 195).

GPCR phosphorylation has been shown to occur on serine and threonine residues in the C-terminal tail as well as ICL1 and ICL3. Several kinases have been shown to mediate receptor phosphorylation, mainly GPCR kinases, but also second-messenger dependent kinases such as protein kinase A (PKA) and protein kinase C (PKC) (196). Other enzymes such as casein kinase and protein kinase B have also been shown to phosphorylate GPCRs. Recent evidence led to the postulation of a signaling barcode hypothesis (**Figure 11**) that proposes that receptor phosphorylation by different kinases on different residues translates into different cellular outcomes (197, 198). Several factors modulate GPCR phosphorylation. For instance, different ligands can induce various conformations of the receptor and trigger different phosphorylation patterns. Similarly, kinases are expressed at different levels within cells and tissues such that the levels of protein kinases have an impact on GPCR phosphorylation profile.

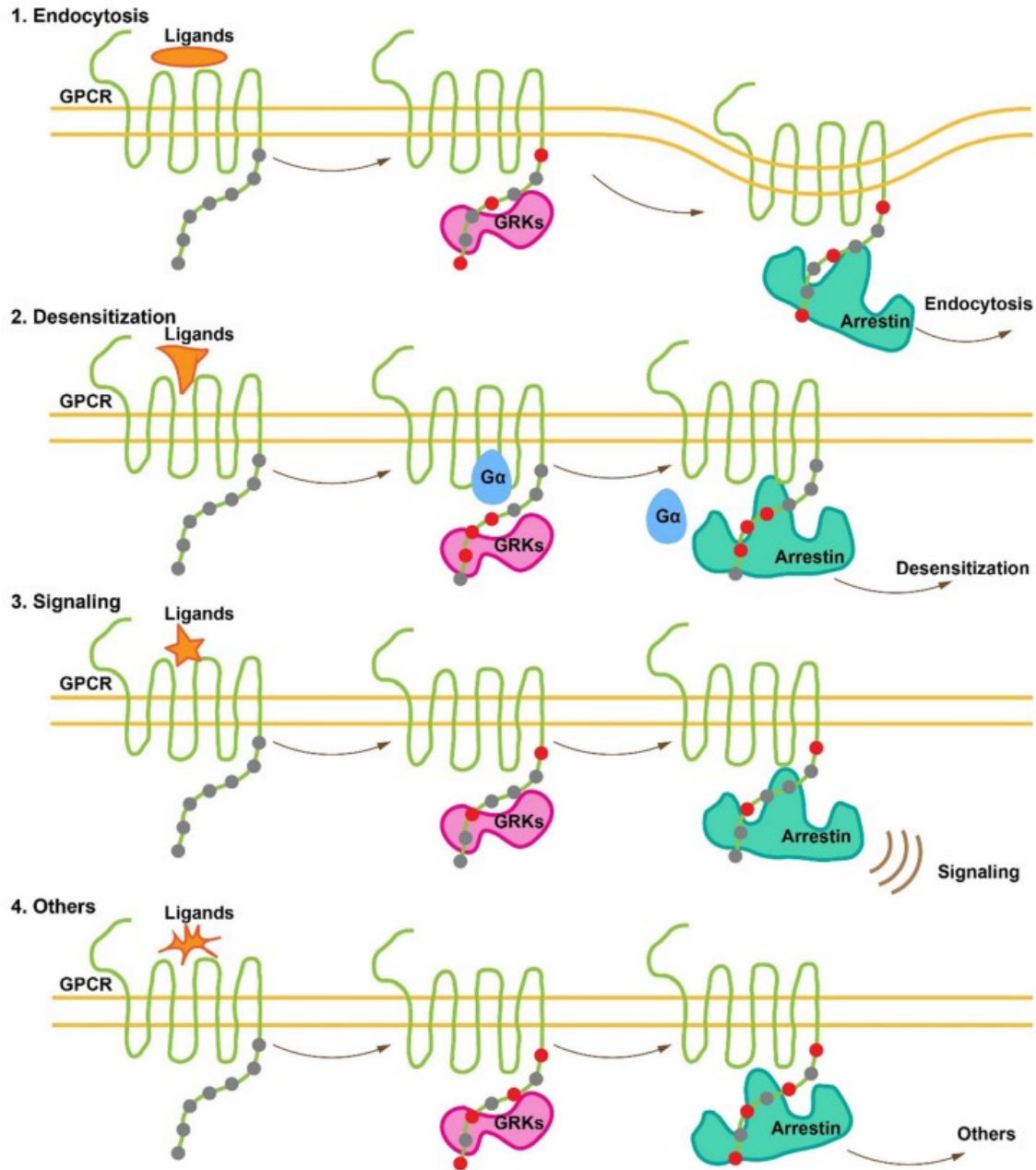


**Figure 11.** – GPCR phosphorylation barcode.

Integration of several factors such as ligand, GPCR type, and kinase into a phosphorylation barcode. Phosphorylation of different residues (indicated in red) leads to the different cellular outcomes (endocytosis, desensitization, signaling, etc.) (198).

Studies on the  $\beta$ 2AR have shown that both PKA/PKC- and GRK-mediated phosphorylation of the receptor induce receptor desensitization, with only GRK phosphorylation promoting  $\beta$ -arrestin recruitment (199). As well, only PKA phosphorylation of  $\beta$ 2AR switches its coupling from Gs to Gi proteins and creates a negative feedback loop for cAMP generation (200). Other studies on the V2R and AT1R have shown that their phosphorylation is mediated by GRK2 and GRK5/6, but while GRK5/6 is critical to trigger ERK signaling, GRK2 controls desensitization and internalization (134, 201). This suggests that each phosphorylation pattern promotes a state favorable to certain functions. Indeed, GRK2 and GRK6 induce differential kinetics of  $\beta$ -arrestin recruitment and BRET assays showed a difference in the conformation of activated  $\beta$ -arrestin (135, 202). Several other receptors have been shown to be differentially phosphorylated with various resulting outcomes such as the C-C motif chemokine receptor 7 (203), the free fatty acid receptor G-protein coupled receptor 120 (204), and the ghrelin receptor (205).

### **3.2.2 $\beta$ -arrestin phosphorylation**

$\beta$ -arrestin undergoes cycles of phosphorylation and dephosphorylation that regulate its GPCR-related functions. Both  $\beta$ -arrestin 1 and  $\beta$ -arrestin 2 have been shown to be constitutively phosphorylated by various kinases and at different residues.  $\beta$ -arrestin 1 is phosphorylated at Ser412 in unstimulated cells and undergoes agonist-promoted dephosphorylation by an unidentified phosphatase once it is recruited to the plasma membrane. The phosphorylation state of  $\beta$ -arrestin 1 has no effect on its recruitment to the plasma membrane and on receptor desensitization as phosphodeficient or phosphomimetic mutants did not exhibit any effect on these processes. However,  $\beta$ -arrestin 1 dephosphorylation regulates receptor internalization as phosphorylated  $\beta$ -arrestin 1 is unable to interact with clathrin and a phosphodeficient mutant enhances  $\beta$ 2AR internalization (206).

$\beta$ -arrestin 2 has also been shown to be phosphorylated under basal conditions at Ser361 and Thr383. Phosphorylation of Thr383 is mediated by casein kinase II while Ser361 is phosphorylated by an unidentified kinase.  $\beta$ -arrestin 2 undergoes agonist-promoted dephosphorylation of these two residues by an uncharacterized mechanism. Point mutation of Ser361 and Thr383 to aspartic acid to act as phosphomimetics decreased  $\beta$ -arrestin 2 interaction with clathrin and  $\beta$ 2AR

internalization further illustrating the importance of  $\beta$ -arrestin dephosphorylation for receptor internalization (207).

Interestingly, MAPK pathway activation by constitutively active mutants of MEK and Ras, GPCR or RTK stimulation, or pharmacological molecules stimulation was shown to trigger  $\beta$ -arrestin 2 phosphorylation on Ser14 and Thr276 by ERK1/2. For several receptors such as CXCR4, AT1R and V2R,  $\beta$ -arrestin 2 phosphorylation diminishes G protein activation and effector recruitment. Indeed, ERK1/2 phosphorylation of  $\beta$ -arrestin 2 causes intracellular sequestration of GPCRs and reduces their cell surface expression uncovering a novel mechanism of negative regulation of GPCR activation (208).

### **3.3 Ubiquitination**

Ubiquitination is an enzymatic cascade that results in the covalent attachment of a ubiquitin peptide on lysine residues of a protein substrate to regulate its function and fate. Early studies in the 1970s identified a heat-stable protein ubiquitously expressed and essential for protein degradation. They also observed that proteins destined for proteolysis increased in molecular weight before degradation (209) and that these proteins were in fact modified by the addition of at least four ubiquitin chains by an ATP-dependent mechanism (210).

Ubiquitin was further characterized and found to be a 76 amino acids protein that is highly conserved in sequence and structure among eukaryotic species. Its structure consists of a  $\beta$ -grasp fold protein, composed of 3.5 turns of an amphipathic  $\alpha$ -helix and a short  $3_{10}$ -helix packed against a five-strand  $\beta$ -sheet with seven reverse turns (211). Four human genes (RPS27A, UBA52, UBB, and UBC) code for the ubiquitin precursor from which deubiquitination enzymes generate free ubiquitin (212). Ubiquitin's C-terminal Gly76 forms an isopeptide bond with the side chain amino group of the target lysine. In addition, ubiquitin also possesses seven intrinsic lysine residues (Lys6, Lys11, Lys27, Lys29, Lys33, Lys48 and Lys63) that can themselves be further modified to form different ubiquitin chains. Therefore, a protein can be modified by the addition of a single ubiquitin moiety (monoubiquitination), the addition of one ubiquitin on multiple residues (multi-monoubiquitination), or addition of ubiquitin chains on the substrate (polyubiquitination). The modification or linkage type takes on distinct conformations that mediate different functions.

For instance, monoubiquitination has been associated with the regulation of protein interaction, sorting, and trafficking while Lys48-polyubiquitination has been associated with targeting substrates to the 26S proteasome for protein degradation (213).

Ubiquitination is a multi-step process involving three enzymes: E1 ubiquitin-activating enzyme, E2 ubiquitin-conjugating enzyme, and E3 ubiquitin-protein ligase. The first step is the activation of ubiquitin as the E1 enzyme catalyzes the adenylation of its C-terminal carboxyl group in an ATP-dependent reaction. Then, the activated ubiquitin is transferred to the active site cysteine of the E2 enzyme where it forms a thioester bond. Finally, the E3 enzyme mediates the transfer of ubiquitin to the substrate lysine by interacting simultaneously with the E2 enzyme and the substrate protein. The human genome codes for a single E1 enzyme, about 60 E2 enzymes and over 400 E3 enzymes. This suggests that the specificity of the ubiquitin reaction is driven by the specific interaction between the E3 and the protein substrate (214). Ubiquitination is a reversible modification as over 100 deubiquitination enzymes (DUBs) catalyze the depolymerization and removal of ubiquitin moieties from the substrate proteins (215).

### **3.3.1 GPCR ubiquitination**

The role of GPCR ubiquitination in receptor function and trafficking was initially discovered in yeast with the sterile 2  $\alpha$ -factor receptor protein (Ste2) as its ubiquitination triggers internalization and vacuolar degradation (148). In contrast, mammalian GPCRs ubiquitination has been shown to be important for receptor degradation but is not required for receptor internalization. For example, a  $\beta$ 2AR mutant lacking all lysine residues successfully internalizes with similar kinetic to the WT receptor. However, the mutant fails to undergo lysosomal degradation (216). Similar observations were made on the CXCR4 and V2R as abrogation of their ubiquitination did not affect receptor internalization but increased receptor half-life as a result of the lack of lysosomal degradation (217, 218). Receptor degradation in the lysosomes is controlled by the endosomal-sorting-complex-required-for-transport (ESCRT) machinery. This pathway comprised of four distinct protein complexes (ESCRT-0, -I, -II and -III) facilitates the trafficking of GPCRs from early endosomes, to late endosomes where receptors are sorted and sent for degradation into the lumen of the lysosomes (219).



The type of ubiquitin conjugation also serves to direct different protein functions and although GPCR ubiquitination types are largely not well defined, it has been hypothesized that monoubiquitination and K63-linked polyubiquitination regulate lysosomal sorting and cell surface retention, while K48-linked polyubiquitination directs the receptor to proteasomal degradation (220). Several receptors such as the delta opioid receptor (DOR) and thyrotropin-releasing hormone receptor (TRHR) have been shown to be ubiquitinated shortly after being translated to go through the quality control exerted in the ER and to trigger degradation of misfolded receptors (221, 222). Constitutive ubiquitination of GPCRs also plays an important role in the control of receptor cell surface expression. CXCR7 is ubiquitinated at the basal level and undergoes deubiquitination after activation and phosphorylation. Once internalized and after ligand detachment, CXCR7 is again ubiquitinated which initiates receptor recycling back to the plasma membrane (223). GCGR is also ubiquitinated at basal level and undergoes deubiquitination mediated by two DUBs (STAMBP and USP33) to facilitate Rab4a-dependent recycling (224). Ubiquitination of GPCRs is a highly dynamic process that regulates at once the proper GPCR folding, cell surface expression of the receptor and transport to the lysosomes for degradation.

Prior receptor phosphorylation has also been shown to be critical to allow agonist-promoted receptor ubiquitination, suggesting a role for  $\beta$ -arrestin in mediating GPCR ubiquitination (225).  $\beta$ -arrestin scaffolds E3 ligases to allow ubiquitin conjugation to GPCRs.  $\beta$ 2AR and V2R activation does not lead to receptor ubiquitination in  $\beta$ -arrestin KO cells unless they are transfected with exogenous  $\beta$ -arrestin. In fact, it was demonstrated that  $\beta$ 2AR ubiquitination is mediated by the E3 ligase Nedd4 (Neural Precursor Cell Expressed Developmentally Down-Regulated Protein 4) and that  $\beta$ -arrestin serves as an adaptor to recruit Nedd4 to the receptor (226). Other GPCRs are ubiquitinated by various E3 ligases, for instance, CXCR4 ubiquitination is mediated by AIP4 (Atrophin-1 Interacting Protein 4) (217), PAR2 is ubiquitinated by c-Cbl (Cbl Proto-Oncogene), and (227), and mGluR is ubiquitinated by Siah1A (Seven In Absentia Homolog 1) (228). This highlights the role of  $\beta$ -arrestin and the various E3 ligases that can participate in the ubiquitination and regulation of GPCRs.

### 3.3.2 $\beta$ -arrestin ubiquitination

As stated above, mammalian GPCR internalization does not depend on the receptor ubiquitination status, but  $\beta$ -arrestin ubiquitination is critical for triggering receptor internalization.  $\beta$ -arrestin is rapidly ubiquitinated by the RING domain E3 ubiquitin ligase Mdm2 following stimulation of numerous GPCRs (216). In Mdm2-depleted cells, GPCRs still undergo ubiquitination, but their internalization is impaired, indicating that  $\beta$ -arrestin ubiquitination by Mdm2 is critical to trigger receptor internalization. Interestingly,  $\beta$ -arrestin ubiquitination kinetics differ depending on the activated receptor.  $\beta$ 2AR activation induces transient  $\beta$ -arrestin ubiquitination while AT1R activation results in sustained  $\beta$ -arrestin ubiquitination. These ubiquitination profiles correlate with the clustering of GPCR into class A and B receptors according to the stability of their interaction with  $\beta$ -arrestin (229). Dissociation of  $\beta$ -arrestin from the receptor appears to correlate with the deubiquitination of  $\beta$ -arrestin since a chimeric fusion of  $\beta$ -arrestin 2 C-tail with ubiquitin remains associated with the internalized receptor. This change in  $\beta$ -arrestin trafficking pattern is illustrated by the strong binding of this chimera with the  $\beta$ 2AR after its internalization in the endosomes.  $\beta$ -arrestin deubiquitination is mediated by USP33 and the deubiquitinated state dissociates from the receptor and inhibits the formation of  $\beta$ -arrestin signalosome (230).

Sustained ubiquitination of  $\beta$ -arrestin supports the ability of class B receptors to form endosomal signalosomes. Agonist stimulation of AT1R leads to sustained ubiquitination of Lys11 and Lys12 in  $\beta$ -arrestin. Mutating these two sites results in impaired  $\beta$ -arrestin ubiquitination, loss of  $\beta$ -arrestin colocalization with the receptor in the endosomes, and failure to scaffold  $\beta$ -arrestin mediated ERK signalosomes. These results highlight the critical role of  $\beta$ -arrestin ubiquitination in the regulation of  $\beta$ -arrestin-dependent signaling (231).  $\beta$ -arrestin 1 has 35 lysine residues and  $\beta$ -arrestin 2 has 31 lysine residues with different GPCR inducing ubiquitination at distinct sites. Indeed, AT1R stimulation induces sustained ubiquitination on Lys11 and Lys12, but other class B GPCRs such as V2R and NK1R can still form stable interaction with  $\beta$ -arrestin lacking these two sites. The question remains whether Mdm2 is the only E3 ligase responsible for  $\beta$ -arrestin ubiquitination or whether different GPCRs trigger the recruitment of various E3 ligases to mediate selective ubiquitination of  $\beta$ -arrestin.

### 3.4 SUMOylation

SUMOylation is a post-translational modification that refers to the covalent attachment of a SUMO (Small Ubiquitin-like MOdifier) molecule to lysine residues of a protein substrate. SUMOs are a family of proteins that share structural similarities with ubiquitin but have little amino acid sequence identity (232). Four different SUMO proteins are expressed in mammals (SUMO1/2/3/4) and they were historically shown to primarily modify nuclear proteins such as transcription factors and nuclear membrane proteins to regulate nuclear translocation or function. The first SUMOylation substrate identified was the nuclear pore protein RanGAP1 (Ran-GTPase-activating protein 1) (233).

SUMO proteins are initially translated as inactive precursors that require C-terminal cleavage by SENP enzymes (sentrin/SUMO-specific protease) to expose the di-glycine motif required for conjugation to target lysine residues. Similar to ubiquitination, SUMOylation is catalyzed by a cascade of three enzymes (E1 activating, E2 conjugating, and E3 ligase). The SUMOylation cascade consists of two E1 enzymes, SAE1 and SAE2, that function as a heterodimer to activate SUMO and bind it to the active site cysteine on SAE2. This is followed by the transfer of SUMO to the active site of Ubc9, the only known SUMO E2 conjugating enzyme in humans. Ubc9 can bind directly to target proteins in some cases, but the SUMO system also possesses a dozen SUMO E3 ligases that mediate isopeptide binding between the C-terminal di-glycine of SUMO and the target lysine (234). SUMO modification usually occurs within a consensus sequence determined as  $\Psi\text{KX(D/E)}$ , where  $\Psi$  represents an aliphatic residue followed by a target lysine, and where X is any amino acid adjacent to an acidic residue, although several proteins have been shown to be SUMOylated in the absence of such sequence (235). SUMOylation is a reversible modification and the SUMO removal from proteins is mediated by a group of six SENP proteases, each with different specificity for the SUMO isoforms (236). Several proteins have also been shown to bind non-covalently to SUMO using SUMO-interacting motifs (SIM) such that SUMOylation regulates the function of SIM-containing proteins (237). SUMOylation plays a critical role in various physiological functions as Ubc9 KO cells suffer abnormal chromosome segregation, defective nuclear organization, and cell death (238). However, mutations or KO of individual SUMO isoforms do not cause any apparent phenotype as the other isoforms can effectively compensate for the lost one (239).

### 3.4.1 GPCR SUMOylation

Very few studies have focused on GPCR regulation by SUMOylation. The first study on GPCR SUMOylation showed that metabotropic glutamate receptors (mGluRs) bind, in a yeast two-hybrid screen, to SUMO1 and the SUMO E3 ligase Pias1. They also showed *in cellulo* SUMOylation of mGluR8a on Lys882 within a SUMO consensus motif (240). The cannabinoid receptor type 1 (CB1R) is also SUMOylated at basal level but undergoes deSUMOylation in response to  $\Delta^9$ -Tetrahydrocannabinol ( $\Delta^9$ -THC) stimulation (241). Conversely, acute stimulation of the serotonin1A receptor (5-HT1AR) increases SUMOylation levels of the receptor to regulate its subcellular distribution (242). A recent study also showed that the M1 muscarinic acetylcholine receptor (M1 mAChR) is constitutively SUMOylated on Lys327. This modification increases the receptor ligand binding affinity, signaling efficiency, and receptor endocytosis (243). These studies indicate a potentially important role for SUMOylation in GPCR function and regulation, but this needs to be demonstrated for a larger number of receptors.

### 3.4.2 $\beta$ -arrestin SUMOylation

An initial study investigated bovine  $\beta$ -arrestin 2 SUMOylation and found two possible SUMO consensus sequences flanking Lys295 and Lys400. Mutagenesis experiments showed that Lys400 is the major site of SUMOylation on bovine  $\beta$ -arrestin 2 and that  $\beta$ 2AR activation increases  $\beta$ -arrestin 2 SUMOylation. They also showed by Ubc9 KO and Lys400 mutagenesis that  $\beta$ -arrestin 2 SUMOylation is critical for GPCR internalization as SUMOylation promotes  $\beta$ -arrestin binding to the AP2 complex (244). Another study found that human  $\beta$ -arrestin 2 contains only one SUMO consensus motif flanking the main SUMOylation site Lys295. They also showed that the SUMO-specific protease 1 (SEN1) is responsible for  $\beta$ -arrestin 2 deSUMOylation. This study revealed a role for  $\beta$ -arrestin SUMOylation in TRAF6-mediated NF- $\kappa$ B/AP-1 activation (245). An additional study confirmed that loss of Lys295 SUMOylation inhibits receptor internalization without affecting  $\beta$ -arrestin recruitment to the plasma membrane. However, a  $\beta$ -arrestin-SUMO1 chimera stabilized receptor- $\beta$ -arrestin complexes but also localized at the nuclear membrane where it binds to RanGAP1 hinting to potential novel functions of SUMOylated  $\beta$ -arrestin (246). This is in line with our study showing colocalization of  $\beta$ -arrestin 2 with the RanBP2/RanGAP1-SUMO nuclear pore complex and where we revealed an additional role for the SIM in  $\beta$ -arrestin 2 nuclear

import (123). These studies highlight the importance of SUMOylation in the regulation of canonical  $\beta$ -arrestin functions such as receptor internalization, but also non-canonical roles in the nucleus.

## Thesis statement and objectives

$\beta$ -arrestin interacts with numerous proteins and acts as a scaffold to support various cellular functions. Initially identified for its role in GPCR desensitization,  $\beta$ -arrestin was also shown to recruit proteins required to promote receptor internalization and trafficking. Historically, GPCR phosphorylation had been linked to  $\beta$ -arrestin recruitment, however many studies have also shown that different factors such as other post-translational modifications also play a role in  $\beta$ -arrestin-GPCR interaction.  $\beta$ -arrestin has also been shown to mediate non-canonical functions, and to be involved in intracellular signaling by scaffolding signaling complexes for the MAPK, Jnk, and PI3K pathways among others.

This thesis aims to explore novel functions and regulation mechanisms of  $\beta$ -arrestin in the context of GPCR signaling.

The first aim of this thesis was to characterize the role of  $\beta$ -arrestin in G protein trafficking. The specific objectives of this study were to:

1. Investigate the role of  $\beta$ -arrestin and the mechanism of G protein endosomal trafficking.
2. Characterize the formation and regulation of a novel  $\beta$ -arrestin complex involved in G protein trafficking.

The second aim of this thesis was to investigate how the ubiquitination status of the GCGR affects receptor signaling and  $\beta$ -arrestin functions. The specific objectives of this study were to:

1. Characterize the GCGR signaling bias in ubiquitinated vs deubiquitinated state.
2. Characterize the effect of GCGR ubiquitination state on  $\beta$ -arrestin signaling and trafficking.
3. Investigate the impact of GCGR ubiquitination on its physiological functions.

The third aim of this thesis was to identify novel proteins interacting with  $\beta$ -arrestin and the role of these interactions. The specific objectives of this study were to:

1. Identify novel  $\beta$ -arrestin 1/2 interactors using the BioID proteomic approach.
2. Confirm the identified interaction with biochemical and cellular assays.
3. Test the role of the identified interactor on  $\beta$ -arrestin 1/2 trafficking.

## Results

## **4 Chapter 4: The V2R- $\beta$ -arrestin-G $\beta\gamma$ Complex Promotes G Protein Translocation to Endosomes**

Context:

In recent years, our understanding of G protein-coupled receptor (GPCR) signaling has evolved beyond the traditional paradigm of G protein activation at the plasma membrane followed by  $\beta$ -arrestin-mediated desensitization and internalization. It has become increasingly clear that some GPCRs can continue to signal from internalized compartments, leading to unique cellular responses compared to plasma membrane signaling. However, the role of  $\beta$ -arrestin in mediating sustained GPCR endosomal signaling remains poorly understood. Here, we showed that formation of a V2R- $\beta$ -arrestin-G $\beta\gamma$  complex enables G $\beta\gamma$  translocation to the endosomes where it potentiates G $\alpha_s$  translocation, presumably leading to reformation of heterotrimeric G proteins in this compartment. These findings provide new insights into the intricate interplay between  $\beta$ -arrestin, G $\beta\gamma$ , and G $\alpha_s$  in mediating sustained GPCR signaling from endosomes.

Contribution:

I designed this study in collaboration with Anthony Nguyen under the guidance of Dr. Michel Bouvier and Dr. Robert J. Lefkowitz. I performed, analyzed, and interpreted all the BRET and BRETfect experiments. I also wrote the manuscript with Anthony Nguyen under the guidance of Dr. Michel Bouvier and Dr. Robert J. Lefkowitz. This manuscript will shortly be submitted to Nature Communications.



# The V2R- $\beta$ -arrestin-G $\beta$ $\gamma$ complex promotes G protein translocation to endosomes

**Sokrat Badr**<sup>1,2\*</sup>, Anthony Nguyen<sup>3\*</sup>, Alex R. B. Thomsen<sup>3,4†</sup>, Li-Yin Huang<sup>3</sup>, Hiroyuki Kobayashi<sup>2</sup>, Alem W. Kahsai<sup>4</sup>, Jihee Kim<sup>3</sup>, Bing X. Ho<sup>3</sup>, Symon Ma<sup>3</sup>, John Little IV<sup>3</sup>, Catherine Ehrhart<sup>3</sup>, Ian Pyne<sup>3</sup>, Emmerly Hammond<sup>3</sup>, Michel Bouvier<sup>1,2#</sup>

1 Department of Biochemistry and Molecular Medicine, University of Montreal, Montreal, Quebec, H3T 1J4 Canada

2 Institute for Research in Immunology and Cancer, University of Montreal, Montreal, Quebec, H3T 1J4 Canada

3 Department of Biochemistry, Duke University School of Medicine, Durham, NC 27710, USA

4 Department of Medicine, Duke University Medical Center, Durham, NC 27710, USA

5 Howard Hughes Medical Institute, Duke University School of Medicine, Durham, NC 27710, USA

\* These authors contributed equally to the manuscript

† Present address: Department of Molecular Pathology, New York University School of Dentistry, New York, NY 10010

# Corresponding author

## **Abstract**

Classically, G protein-coupled receptors (GPCRs) promote signaling at the plasma membrane through activation of heterotrimeric  $G\alpha\beta\gamma$  proteins. This is followed by the recruitment of GPCR kinases (GRK) and  $\beta$ arrestins ( $\beta$ arrs) that facilitate receptor desensitization and internalization. However, recent studies have shown that some GPCRs continue to signal from internalized compartments. This additional mode of sustained G protein signaling leads to distinct downstream cellular responses compared to those elicited by signaling at the plasma membrane. Interestingly,  $\beta$ arrs appear to potentiate sustained G protein signaling. However, the role of  $G\beta\gamma$  and  $\beta$ arr in internalized G protein signaling remains poorly understood. Here, we demonstrate that the vasopressin V2 receptor (V2R)- $\beta$ arr complex scaffolds plasma membrane  $G\beta\gamma$  through  $\beta$ arr and transports it to endosomes, and that said  $G\beta\gamma$  potentiates  $G\alpha$ s endosomal translocation to presumably regenerate an endosomal pool of heterotrimeric Gs. This work demonstrates the mechanism mediating G protein translocation from the plasma membrane to the endosomes and provides a basis for understanding the role of  $\beta$ arr in mediating sustained endosomal G protein signaling.

## Introduction

G protein-coupled receptors (GPCRs) are the largest class of membrane receptor encoded by the human genome and are involved in the regulation of virtually every physiological process (1,2). These receptors share a common hepta-helical transmembrane structure and are activated by a large variety of extracellular stimuli, including small molecules, hormones, neurotransmitters, lipids, and peptides (3,4). Upon binding to an agonist at its extracellular orthosteric binding site, GPCRs adopt an active conformation that enables the intracellular engagement of heterotrimeric  $G\alpha\beta\gamma$  proteins by the receptor (2). This engagement catalyzes the exchange of GDP for GTP in the  $G\alpha$  subunit, leading to the dissociation of the  $G\beta\gamma$  heterodimer from the  $G\alpha$  subunit (2). The GTP-bound  $G\alpha$  subsequently interacts with effectors such as adenylyl cyclase to generate second messengers like cyclic AMP (cAMP) in order to propagate a wave of signaling that eventually results in a cellular response (1,5,6).

To prevent over-activation of these signaling pathways, GPCRs ultimately undergo a desensitization mechanism mediated by  $\beta$ arrestins ( $\beta$ arrestins). This process is initiated by the phosphorylation of a GPCR at specific serine and threonine residues located within the intracellular cytoplasmic loops (ICLs) and/or C-terminal tail of the receptor by GPCR kinases (GRKs) process (7). The phosphorylated receptor enables the recruitment and coupling of  $\beta$ arrestins, thus sterically hindering G protein coupling to the receptor (8,9). Notably, we have demonstrated that GPCR- $\beta$ arrestin complexes can adopt two distinct conformations: (1) whereby  $\beta$ arrestin engages the phosphorylated tail of the receptor (deemed the 'tail' conformation) or (2) whereby  $\beta$ arrestin additionally engages the intracellular core of the GPCR via its finger loop region (deemed the 'core' conformation) (10). Additionally, we and others demonstrate that a GPCR- $\beta$ arrestin complex in the tail conformation can carry out most functions expected of an activated  $\beta$ arrestin with the exception of desensitization, which is exclusively carried out by the core conformation (11-13).

$\beta$ arrestins also recruit endocytic proteins such as AP2 and clathrin to facilitate receptor internalization into early endosomes where some receptors rapidly lose their interaction with  $\beta$ arrestin (class A GPCRs) whereas others maintain a sustained interaction with  $\beta$ arrestin (class B GPCRs) (14-16). In addition to their roles in G protein desensitization and receptor trafficking,  $\beta$ arrestins initiate several

signaling cascades through scaffolding a variety of other enzymes, such as various kinases (17-21). Several class B GPCRs such as the parathyroid hormone receptor (PTHrP), neurokinin 1 receptor (NK1R) and the vasopressin type 2 receptor (V2R) have been observed to continue signaling within internalized compartments instead of staying desensitized. Initially, this mode of sustained signaling has been difficult to integrate into the classical model of signaling, which states that  $\beta$ arr sterically hinders additional G protein coupling at receptors. However, additional investigations by us and others show that sustained signaling is mediated by the formation of a GPCR–Gs– $\beta$ arr megacomplex in endosomes (22-25). This ‘megaplex’ comprises a  $\beta$ arr which engages the receptor in a tail conformation, thus leaving the receptor intracellular core free to couple to and activate a heterotrimeric G protein within endosomes (22,23). The megaplex provides a potential biophysical explanation for how certain GPCRs continue to signal within internalized compartments.

While  $\beta$ arr classically serves as a desensitizer of G protein signaling at the plasma membrane, it serves to potentiate sustained G protein signaling from within internalized compartments. Interestingly,  $\beta$ arr1 has also been shown to interact with G $\beta\gamma$  to promote Akt phosphorylation and NF- $\kappa$ B activation (26). Additional reports demonstrate that the G $\beta\gamma$  heterodimers significantly influence sustained G protein signaling at the PTHrP, a prototypical class B GPCR, through the formation of a PTHrP– $\beta$ arr–G $\beta\gamma$  complex (24,27,28). Five distinct G protein beta subunits and twelve G protein gamma subunits have been identified, which can pair to form distinct heterodimeric G $\beta\gamma$  combinations. Several studies have shown that specific G $\beta\gamma$  heterodimers are found in different intracellular membranes such as the Golgi, ER, mitochondria and endosomes (29-31). Also, although G $\alpha$ s is anchored at the plasma membrane via palmitoylation, receptor activation leads to G $\alpha$ s dissociation from the plasma membrane to the cytoplasm (32-36).

These observations raise several questions: (1) despite its classical role in receptor desensitization, how does  $\beta$ arr enhance sustained G protein signaling, particularly at class B GPCRs? (2) Within the GPCR– $\beta$ arr–G $\beta\gamma$  complex, what is the role of G $\beta\gamma$  in mediating said signaling? To answer these questions, we employ a variety of cellular and biochemical techniques to elucidate the mechanism of endosomal trafficking of G $\alpha$ s and G $\beta\gamma$ . Using the V2R, a prototypical class B GPCR, we reveal the ability of  $\beta$ arr and G $\beta\gamma$  to promote endosomal G $\alpha$ s

translocation, the association of G $\beta\gamma$  and  $\beta$ arr to the V2R in a stable complex, and the impact of  $\beta$ arr on the formation of GPCR signaling complexes in endosomes.

## Results

### *Gas dissociates from the plasma membrane after V2R activation and translocates to endosomes*

To investigate Gas trafficking from the plasma membrane to the endosomal compartment, we monitored Gas translocation using an enhanced bystander bioluminescence resonance energy transfer (ebBRET) approach (37). First, we assessed Gas dissociation from the plasma membrane in HEK293T cells at AVP-stimulated V2R by measuring the signal between BRET donor Gas67-RlucII and BRET acceptor Renilla reniformis GFP (rGFP) anchored at the plasma membrane via a prenylated CAAX motif. As expected, V2R activation caused a decrease in BRET signal indicating dissociation of Gas from the plasma membrane into the cytosol (Fig. 1A). Interestingly, expression of a plasma membrane anchored GRK2 C-terminal peptide ( $\beta$ ARKct-CAAX) that acts as an inhibitory scavenger of G $\beta\gamma$  (38,39) caused a significant decrease in Gas dissociation from the plasma membrane. In contrast, overexpression of G $\beta$  and G $\gamma$  increased the level of dissociation of Gas from the plasma membrane; this effect is reduced by the addition of  $\beta$ ARKct-CAAX. These results suggest that the formation of heterotrimeric Gs and dissociation of Gas from the plasma membrane is dependent on the presence of free G $\beta\gamma$ . The effect of scavenging free G $\beta\gamma$  with  $\beta$ ARKct on Gas release from the plasma membrane was found to be restricted to this compartment since anchoring  $\beta$ ARKct to the endosomes using the FYVE targeting domain of endofin (40) had little impact on Gas dissociation from the plasma membrane with or without G $\beta\gamma$  overexpression (Fig. 1B). To assess the role of  $\beta$ arr in Gas dissociation from the plasma membrane, we used CRISPR  $\beta$ arr1/2 knock-out (KO) HEK293T cells.  $\beta$ arr depletion had no impact on the decrease in BRET between Gas67-RlucII and rGFP-CAAX, suggesting that  $\beta$ arr is not required for Gas dissociation from the plasma membrane (Fig. 1A). Similarly,  $\beta$ ARKct-CAAX inhibited Gas capacity to leave the plasma membrane in this KO cell line to a similar extent as observed in the parental WT cells (Fig. 1A).

We then investigated the role of G $\beta\gamma$  and  $\beta$ arr in Gas trafficking to early endosomes by measuring the BRET signal between donor Gas67-RlucII and acceptor rGFP fused to FYVE (37). We observed

an agonist-promoted increase in BRET signal indicating accumulation of G $\alpha$ s in endosomes (Fig. 1C).  $\beta$ ARKct-CAAX as well as  $\beta$ ARKct-FYVE completely blocked G $\alpha$ s trafficking to the endosomes while overexpression of G $\beta\gamma$  significantly enhanced G $\alpha$ s endosomal translocation (Fig. 1C-D). Strikingly, we observed a significant reduction in G $\alpha$ s translocation to endosomes in  $\beta$ arr1/2 KO cells (Fig. 1C), whereas G $\alpha$ s dissociation from the plasma membrane was not impaired by  $\beta$ arr1/2 depletion (Fig. 1A). Taken together, these results show that sequestration of G $\beta\gamma$  impairs both G $\alpha$ s dissociation from the plasma membrane and endosomal translocation while increasing free G $\beta\gamma$  enhances G $\alpha$ s trafficking. However, depletion of  $\beta$ arr only impairs G $\alpha$ s endosomal translocation, not its dissociation from the plasma membrane.

#### *$\beta$ arr mediates G $\beta\gamma$ trafficking from the plasma membrane to the endosomes*

Given that both scavenging of G $\beta\gamma$  and loss of  $\beta$ arr significantly impairs the translocation of G $\alpha$ s to endosomes, we hypothesized that  $\beta$ arr may be involved in the shuttling of G $\beta\gamma$  from the plasma membrane to endosomes. Endosomal G $\beta\gamma$  could then attract the G $\alpha$ s released from the plasma membrane allowing the reconstitution of a trimeric G protein in the endosomal compartment. To test this hypothesis, we measured the BRET signal between Gy2-RlucII and the plasma membrane marker rGFP-CAAX at AVP-stimulated V2R in both parental and  $\beta$ arr1/2 KO cells. In the parental cell line, we observed an AVP-induced decrease in BRET at the plasma membrane reflecting a loss of plasma membrane G $\beta\gamma$  most likely resulting from its internalization. This loss of plasma membrane G $\beta\gamma$  was largely abolished in  $\beta$ arr1/2 KO cells but restored by transfection of  $\beta$ arr1/2 suggesting that  $\beta$ arr mediates G $\beta\gamma$  internalization from the plasma membrane (Fig. 1E).

Concomitant with the loss of G $\beta\gamma$  from the plasma membrane, we observed an increase in BRET between Gy2-RlucII and the endosomal marker rGFP-FYVE, indicating an influx of G $\beta\gamma$  into this compartment (Fig. 1F). Again, this signal was greatly blunted in  $\beta$ arr-depleted cells while overexpression of  $\beta$ arr1/2 restored G $\beta\gamma$  trafficking to the endosomes to similar levels to the one observed in parental cells. Taken together, these data suggest that G $\beta\gamma$  undergoes  $\beta$ arr-mediated endocytosis upon V2R activation.

To determine whether G $\beta\gamma$  trafficking to endosomes is truly dependent on  $\beta$ arr-mediated endocytosis, we assessed the G $\beta\gamma$  trafficking upon activation of CXCR4, a GPCR that although

couples to  $\beta$ arrs (41,42), can be internalized via a number of  $\beta$ arr-dependent and independent pathways. In contrast to what is observed for the V2R, for which the loss of plasma membrane receptor upon activation requires  $\beta$ arrs (Fig. 2A), CXCR4 undergoes agonist-promoted internalization in  $\beta$ arr1/2 KO HEK293T cells (Fig. 2B) upon CXCL12 stimulation. Despite this  $\beta$ arr-independent internalization of CXCR4, which is comparable in  $\beta$ arr1/2 KO cells and parental cells, we observed a significant reduction in CXCL12-induced  $G\beta\gamma$  dissociation from the plasma membrane in  $\beta$ arr1/2 KO cells compared to that in parental cells. The blunted  $G\beta\gamma$  trafficking was readily rescued with overexpression of either  $\beta$ arr1 or  $\beta$ arr2 (Fig. 2C). These results confirm that  $G\beta\gamma$  trafficking from the plasma membrane to the endosomes is  $\beta$ arr-dependent and, that receptor internalization is not sufficient to promote  $G\beta\gamma$  translocation from the plasma membrane.

#### *V2R, $\beta$ arr and $G\beta\gamma$ form a complex in cells*

Our previous data suggest that  $\beta$ arrs mediates the trafficking of  $G\beta\gamma$  from the plasma membrane to the endosomes while  $G\alpha$ s dissociates from the plasma membrane via a  $\beta$ arr-independent mechanism. Considering that  $\beta$ arr is also essential for V2R internalization, we investigated whether a complex composed of V2R,  $\beta$ arr2, and  $G\beta\gamma$  could form in the absence of  $G\alpha$  and be responsible for the endocytosis of  $G\beta\gamma$ . To this end, we took advantage of BRET with fluorescence enhancement by combined transfer (BRETfect). This approach tracks the formation of ternary protein complexes by measuring the increase in energy transfer from a luciferase energy donor to a fluorescent energy acceptor in presence of a fluorescent intermediate (43). To assess the formation of the complex, we used RlucII fused to  $\beta$ arr2 as an energy donor (D), mTFP fused to the V2R as an energy intermediate (I) and YFP fused to  $G\gamma$ 2 as an energy acceptor (A) (Fig. 3A).

In parental HEK293T (Fig. 3B), expression of  $\beta$ arr2-RlucII with V2R-mTFP (D + I) resulted in an AVP-induced increase in signal indicative of recruitment of  $\beta$ arr2 to the receptor. Expression of  $\beta$ arr2-RlucII with  $G\gamma$ 2-YFP (D + A) did not result in an agonist-induced response in the absence of overexpressed V2R. Overexpression of unlabelled V2R with  $\beta$ arr2-RlucII and  $G\gamma$ 2-YFP (D + A) results only in a small increase in signal (Fig. S1). However, expression of all three plasmids (D + I

+ A) produced a significantly higher increase in AVP-induced signal indicating the formation of a ternary complex between V2R,  $\beta$ arr2 and  $G\beta\gamma$  (Fig. 3B).

To assess whether the V2R- $\beta$ arr- $G\beta\gamma$  complex detected by BRETfect can be formed in the absence of  $G\alpha$  subunit, we monitored V2R- $\beta$ arr2- $G\beta\gamma$  complex formation in  $G\alpha$ s-depleted cells (44),  $G\alpha$ s being the primary  $G\alpha$  subunit engaged by V2R. We observed a similar agonist-induced BRETfect signal that the one observed in parental cells indicating the formation of a V2R- $\beta$ arr2- $G\beta\gamma$  complex in  $G\alpha$ s-depleted cells (Fig. 3C). Since a recent study showed that the V2R also activates  $G\alpha_q$ ,  $G\alpha_{11}$ ,  $G\alpha_{13}$ ,  $G\alpha_{14}$  and  $G\alpha_{15}$  (45), we tested complex formation in a cell line lacking all  $G\alpha$  proteins to eliminate the possibility of the formation of the previously described V2R- $\beta$ arr-Gs megaplex (22) formation confounding our BRETfect results. As seen in Fig. 3D, V2R- $\beta$ arr2- $G\beta\gamma$  complex could still form in the total absence of  $G\alpha$  proteins. Taken together, these results show that V2R- $\beta$ arr- $G\beta\gamma$  complex can exist as a unique entity without the incorporation of  $G\alpha$  subunits.

#### *Agonist-promoted V2R- $\beta$ arr2- $G\beta\gamma$ complex formation occurs at the plasma membrane*

The BRETfect approach also allows for real-time imaging of ternary complexes formation using BRET microscopy as described previously (46). A moderate agonist-promoted increase in signal could be observed between  $\beta$ arr2-RlucII and V2R-mTFP at the plasma membrane reflecting the recruitment of  $\beta$ arr2 to the receptor. As was the case for the spectrometric experiments described above, the AVP-promoted signal increase observed at the plasma membrane was greatly potentiated in the BRETfect configuration (ie: co-expression of  $\beta$ arr2-RlucII, V2R-mTFP and  $G\gamma$ 2-YFP) supporting the notion that a V2R- $\beta$ arr2- $G\beta\gamma$  complex is formed at the plasma membrane (Fig. 4).

Kinetic analysis of the BRETfect signal using both imaging and spectrometric approaches revealed that formation of the V2R- $\beta$ arr2- $G\beta\gamma$  occurs rapidly after stimulation of the receptor ( $t_{1/2}$ : 16.7 sec) in WT parental HEK293T cells (Fig. 5A-C). Although the formation of the V2R- $\beta$ arr2- $G\beta\gamma$  complex was also observed in the total  $G\alpha$  KO, the formation kinetics was much slower ( $t_{1/2}$ : 288.8 sec) in the absence of  $G\alpha$  subunits (Fig. 5B-C). Taken together, these results show V2R-



$\beta$ arr2-G $\beta$  $\gamma$  complex formation at the plasma membrane both in presence and in absence of G $\alpha$  subunits, although the former leads to faster complex formation (Fig. 5C).

To further assess the potential role of the G $\alpha$  subunits in the formation of the V2R- $\beta$ arr-G $\beta$  $\gamma$  complex, we tested the effect of different G $\alpha$  subtypes. Whereas over-expression of the G $\alpha$  subtypes known to be activated by V2R (i.e.: G $\alpha$ s and G $\alpha$ q) did not significantly affect complex formation in the parental HEK293T cells, G $\alpha$ i and G $\alpha$ 12 over-expression resulted in a significant decrease in BRETfect signal reflecting an inhibition of complex formation (Fig. 6A). In cells lacking all G $\alpha$  subunits expression (total G $\alpha$  KO cells), the reintroduction of G $\alpha$ s and G $\alpha$ q potentiated V2R- $\beta$ arr-G $\beta$  $\gamma$  complex formation. In contrast, over-expression of G $\alpha$ i and G $\alpha$ 12, blunted complex formation (Fig. 6B). This observation is consistent with a previous study that showed unproductive coupling between V2R and G $\alpha$ 12 resulting in an inhibition of agonist-promoted effector recruitment to the receptor and downstream signaling (47). Another study also showed formation of a V2R- $\beta$ arr-G $\alpha$ i complex that does not mediate canonical G protein signaling (48). Taken together, these data indicate that G protein activation is a prerequisite for a V2R- $\beta$ arr-G $\beta$  $\gamma$  complex formation.

To assess whether V2R- $\beta$ arr-G $\beta$  $\gamma$  complex formation occurs at the plasma membrane immediately following receptor activation or may require endocytosis we investigated the effect of a dominant-negative mutant of dynamin (DynK44A) that inhibits receptor endocytosis (49) and of  $\beta$ ARKct peptide that can sequester G $\beta$  $\gamma$  either at the plasma membrane ( $\beta$ ARKct-CAAX) or in the endosomes ( $\beta$ ARKct-FYVE). DynK44A had no impact on complex formation (Fig. 6C) whereas it blocked V2R internalization (Fig. S2). In contrast, plasma membrane-anchored but not endosomal targeted  $\beta$ ARKct drastically blocked complex formation (Fig. 6C-D), indicating that the V2R- $\beta$ arr-G $\beta$  $\gamma$  complex forms at the plasma membrane before receptor internalization.

#### *Molecular Determinants of the G $\beta$ $\gamma$ - $\beta$ arr interaction*

Structural analysis of G $\beta$  $\gamma$  bound to three effectors: GRK2, GIRK2, and phosducin, revealed that G $\beta$  $\gamma$  typically binds its effectors via its inner toroidal surface (Fig. 7A) (50-52). This same surface is occupied by the GDP-bound G $\alpha$ s within the heterotrimeric Gs (53), suggesting that G protein activation by receptor is critical in freeing up G $\beta$  $\gamma$  and allowing for G $\beta$  $\gamma$ - $\beta$ arr association. With this

in mind, we asked if G $\beta\gamma$  binds preferentially to either inactive or active forms of  $\beta$ arr. To biochemically test the ability of G $\beta\gamma$  to directly associate with  $\beta$ arr1, we performed in vitro pull-down between purified G $\beta\gamma$  and GST-tagged  $\beta$ arr1, which shows that G $\beta\gamma$  binds to  $\beta$ arr1 in its inactive conformation (Fig. 7B). Subsequently, to test if G $\beta\gamma$  can also bind to  $\beta$ arr1 in its active conformation, we additionally performed a pull-down between purified G $\beta\gamma$  and the Flag-tagged  $\beta$ 2V2R- $\beta$ arr-Fab30 complex in the presence of the  $\beta$ 2AR agonist BI-167107. G $\beta\gamma$  was found to also associate with  $\beta$ arr in the context of a GPCR- $\beta$ arr complex, indicating that the activated  $\beta$ arr associated to the receptor can also bind G $\beta\gamma$  (Fig. 7C).

To quantitatively probe the G $\beta\gamma$ - $\beta$ arr interaction, we employed isothermal titration calorimetry (ITC) to obtain binding constants between G $\beta\gamma$  and various forms of active or inactive  $\beta$ arr. G $\beta\gamma$  associates specifically with inactive  $\beta$ arr1 with an affinity of 9.4  $\mu$ M (Fig. 8A). Similarly, G $\beta\gamma$  binds specifically to an active  $\beta$ arr1-V2Rpp-Fab30 complex, where V2Rpp is a previously validated phosphorylated carboxy-terminal peptide derived from the human V2R (54), with an affinity of 3.8  $\mu$ M (Fig. 8B). G $\beta\gamma$  displayed the same propensity to bind to both  $\beta$ arr2 (Fig. 8C) and  $\beta$ arr2 in the presence of 4-fold molar excess of V2Rpp (Fig. 8D), with an affinity of 5.6  $\mu$ M and 7.3  $\mu$ M, respectively. These experiments reveal that G $\beta\gamma$  is capable of specifically binding both  $\beta$ arr1 and  $\beta$ arr2 either in the inactive or active conformation, at low micromolar affinity without  $\beta$ arr conformational or ortholog preference.

Finally, we asked if the prenylation site on G $\gamma$ 2 influences binding of  $\beta$ arr. To that end, we expressed and purified G $\beta\gamma$  with a C68S point mutation in G $\gamma$ 2 (here forward referred to as G $\beta\gamma$  C68S), abrogating the prenylation site on G $\gamma$ 2 to generate unprenylated G $\beta\gamma$  (55-57). ITC experiments reveal that G $\beta\gamma$  C68S maintains its capacity to bind to inactive  $\beta$ arr1 and  $\beta$ arr2 with affinities of 1.1 and 3.2  $\mu$ M, respectively (Fig. S3 A-B). Given that the phosphorylated C-terminal tail of the V2R should serve as a critical feature that allows for recruitment of  $\beta$ arr on the way to assembling the V2R- $\beta$ arr-G $\beta\gamma$  complex, we wondered if G $\beta\gamma$  synergistically interact with the phosphorylated V2R tail in addition to  $\beta$ arr1. To answer this question, we performed ITC between G $\beta\gamma$  and the V2Rpp. No saturable and specific binding could be observed between these two proteins (Fig. S4) indicating that G $\beta\gamma$  interacts with the V2R- $\beta$ arr complex primarily through

binding at a portion of  $\beta$ arr that does not involve phosphorylated C-terminal GPCR tail recognition.

## Discussion

It has long been observed that second messenger molecules such as cAMP are cellularly compartmentalized, thus creating a molecular gradient that is most concentrated in the immediate vicinity of where they were synthesized (58,59). These compartmentalized cAMP molecules modulate enzymes within the local cytosolic milieu, potentially lead to differential physiological responses compared to those elicited by cAMP at the plasma membrane (60,61). Some GPCRs exhibit sustained signaling from within endosomes rather than assuming an inactive desensitized state (24,62,63). Furthermore,  $\beta$ arr, classically known for its role in the desensitization of receptor-mediated G protein signaling at the plasma membrane, has been implicated in potentiating this non-canonical mode of endosomal signaling. Various studies by us and others have demonstrated that (1)  $\beta$ arr potentiates endosomal G protein signaling in class B GPCRs, as the tail conformation of the GPCR- $\beta$ arr complex can accommodate additional binding of a heterotrimeric G protein (11,22,23), and (2) two complexes, a GPCR- $\beta$ arr-Gs megaplex and a GPCR- $\beta$ arr-G $\beta\gamma$  complex can contribute to sustained signaling. Previous cellular experiments suggested an interaction between  $\beta$ arr and G $\beta\gamma$ , and that increases in free cellular G $\beta\gamma$  leads to enhanced cAMP generation from internalized compartments (24,26,28,64).

Our previous structural studies have illustrated that within a megaplex, a single active GPCR can simultaneously accommodate both a G protein and a  $\beta$ arr. However, the exact mechanism by which  $\beta$ arr and G $\beta\gamma$  enhances endosomal G protein signaling remains unknown. Through experiments outlined above, we demonstrate that (1) the ternary V2R- $\beta$ arr-G $\beta\gamma$  complex form at the plasma membrane, that the presence of a G $\alpha$  subunit is not required for its formation and subsequent internalization in endosomes, that (2) free G $\beta\gamma$  which has dissociated from G $\alpha$ s binds specifically to both active and inactive  $\beta$ arr1 and  $\beta$ arr2 at low micromolar affinity, without preference for  $\beta$ arr conformation or ortholog and that (3) the V2R- $\beta$ arr-G $\beta\gamma$  complex enhances G $\alpha$ s endosomal translocation, likely to reform competent heterotrimeric Gs in order to potentiate additional signaling from the endosomal compartment.

The use of BRETfect both in spectrometric and imaging configurations allowed us to distinguish the V2R- $\beta$ arr-G $\beta\gamma$  from the previously described megaplex. Indeed, although with a slower kinetics, the V2R- $\beta$ arr-G $\beta\gamma$  can readily form in cells lacking all G $\alpha$  subunits. Our data also show that dissociation of G $\beta\gamma$  from G $\alpha$  is required for the agonist-promoted formation and endocytosis of the V2R- $\beta$ arr-G $\beta\gamma$  complex. Indeed, scavenging of G $\beta\gamma$  by the plasma membrane-tethered  $\beta$ ARKct significantly impaired V2R- $\beta$ arr-G $\beta\gamma$  complex formation and G $\beta\gamma$  endosomal trafficking. As endosome-anchored  $\beta$ ARKct did not impact complex formation, this suggests that this complex forms at the plasma membrane and we further confirmed this by blocking receptor internalization which had no effect on complex formation. In vitro experiments also confirm binding of G $\beta\gamma$  and  $\beta$ arr, further lending credence to the existence of the V2R- $\beta$ arr-G $\beta\gamma$  complex as a separate entity from the megaplex.

Our study shows that the trafficking of G $\beta\gamma$  into endosomes is largely dependent on its ability to associate with  $\beta$ arr, as  $\beta$ arr depletion greatly reduced agonist-promoted translocation of G $\beta\gamma$  from the plasma membrane to the endosomes. This is in sharp contrast with the trafficking of G $\alpha$ s that can dissociate from the plasma membrane to the similar extent in WT and  $\beta$ arr KO cells indicating that it can occur independently of  $\beta$ arr and of receptor endocytosis. This clearly indicates that the G $\alpha$  and G $\beta\gamma$  subunits used different trafficking routes to reach the endosomes.

An important mechanistic element of our work concerns the generation of competent Gs heterotrimers in internalized compartments. Building on previous reports showing the de-palmitoylation, dissociation of G $\alpha$ s from the plasma membrane, and endomembrane association after receptor-mediated G protein activation (65,66), we show that the presence of G $\beta\gamma$  and by extension the V2R- $\beta$ arr-G $\beta\gamma$  complex in endosomes serves to promote G $\alpha$ s endosomal translocation, giving rise to competent Gs heterotrimers that can be activated by the GPCR and propagate second messenger generation from internalized compartments. Interestingly, there seems to be cooperativity between V2R- $\beta$ arr-G $\beta\gamma$  complexes and G $\alpha$ , as BRETfect experiments in total G $\alpha$  knockout cells displayed markedly diminished BRETfect signal kinetics. Although G $\alpha$ s is not necessary for V2R- $\beta$ arr-G $\beta\gamma$  complex formation, activation of a heterotrimeric G protein by a receptor leads to free G $\beta\gamma$  that is able to bind to  $\beta$ arr when it is recruited to the receptor, which may hasten the G $\beta\gamma$ - $\beta$ arr interaction. In total G alpha KO cells, the membrane-bound G $\beta\gamma$

will likely associate with  $\beta$ arr through free diffusion, which may explain the slower kinetics of V2R- $\beta$ arr-G $\beta\gamma$  complex formation.

We posit that (1) receptor-mediated catalytic activation of G protein is necessary to generate free heterodimeric, plasma membrane-bound G $\beta\gamma$  and (2) recruitment of  $\beta$ arr to the phosphorylated C-terminal tail of the receptor are both critical to facilitate the G $\beta\gamma$ - $\beta$ arr interaction. In addition, our ITC experiment demonstrate low-micromolar affinity binding of G $\beta\gamma$  in vitro to both orthologs of  $\beta$ arr without clear conformational or ortholog preference. These data suggest that G $\beta\gamma$  binds promiscuously to all  $\beta$ arrs, likely at a site on  $\beta$ arr that does not undergo conformational binding to a phosphorylated C-terminal receptor tail. Taken together with a recent report which demonstrates distinct subcellular localization of specific combinations of G protein  $\beta$  and  $\gamma$  subunits, we speculate that G $\beta\gamma$  subtypes may lead to G $\alpha$  translocation to different intracellular compartments to facilitate sustained signaling (31).

We summarize our findings, as well as our current understanding of endosomal signaling in the attached schematic (Fig. 9). Initially, the V2R is activated by an agonist, allowing for the binding of G protein followed by nucleotide exchange at the G $\alpha$  subunit and dissociation of G $\beta\gamma$ . The GTP-bound G $\alpha$  subunit interacts with effectors to generate second messenger molecules that constitute the first wave of plasma membrane signaling. G $\alpha$ s is then de-palmitoylated, forming a pool of cytoplasmic G $\alpha$  subunits that probes endomembrane compartments. Upon receptor phosphorylation by GRK, and recruitment of  $\beta$ arr, GPCR- $\beta$ arr-G $\beta\gamma$  complexes form at the plasma membrane. The complex is then internalized into endosomes via  $\beta$ arr-mediated endocytosis. The presence of G $\beta\gamma$  in the endosomes spurs the translocation of G $\alpha$ s, thus regenerating competent Gs heterotrimers and reassociation with an activated receptor in this compartment. Newly activated endosomal G $\alpha$ s subsequently generates second messenger molecules from internalized compartments enabling a second wave of GPCR-mediated signaling. Presumably, the continued presence of the V2R- $\beta$ arr-G $\beta\gamma$  complexes hasten endosomal signaling by promoting regeneration of Gs heterotrimers. These pathways result in persistent endosomal signaling until the GPCR complex is eventually degraded in lysosomes. Given that each of these transducers were classically thought to function independently, our results add to the growing body of evidence that signal transducers can function in a co-dependent manner.

In conclusion, our work confirms the existence of the V2R- $\beta$ arr-G $\beta$  $\gamma$  complex in living cells, biochemically illustrate an interaction between G and  $\beta$ arr, as well as highlight the endosomal presence of G $\beta$  $\gamma$  as an enhancer of endosomal signaling by promoting endosomal G $\alpha$ s translocation. Our work provides an explanation for how  $\beta$ arr enhances G protein signaling from within internalized compartments.

## **Methods:**

### *Reagents:*

Dulbecco's phosphate-buffered saline (PBS), Hanks' Balanced Salt Solution (HBSS), Dulbecco's modified Eagle's medium (DMEM), Trypsin, penicillin/streptomycin, fetal bovine serum (FBS), and newborn calf serum (NCS) were purchased from Wisent Bioproducts. Polyethylenimine (PEI) was purchased from Alfa Aesar (Thermo Fisher Scientific). Arginine vasopressin (AVP) was from Sigma-Aldrich. Coelenterazine H, and Prolume Purple were purchased from Nanolight Technologies. The V2R phosphopeptide (V2Rpp) was synthesized by the Tufts University peptide synthesis core facility.

### *Cell lines:*

Parental HEK293SL and  $\beta$ arr1/2 KO cells were gifted from Dr Stephane Laporte (McGill University, Montreal, Quebec, Canada). HEK293T, G $\alpha$ s KO and total G $\alpha$  KO cells were gifted from Dr Asuka Inoue (Tohoku University, Sendai, Miyagi, Japan).

### *Enhanced bystander Bioluminescence Resonance Energy Transfer:*

Cells were cultured in DMEM supplemented with 10% fetal bovine serum (FBS), 100 units of penicillin, and 100  $\mu$ g/ml streptomycin. Cells in suspension were transiently transfected at a density of 0.4 million cells/ml using 25 kDa linear polyethylenimine (PEI) as transfecting agent, at a ratio of 4:1 PEI/DNA.

For G $\alpha$ s trafficking, parental HEK293SL and  $\beta$ arr1/2 KO cells were transfected with FLAG-V2R, G $\alpha$ s67-RlucII (BRET donor) and rGFP-CAAX or rGFP-FYVE (BRET acceptor), and co-transfected with  $\beta$ ARKct-CAAX,  $\beta$ ARKct-FYVE, G $\beta$ 1 and G $\gamma$ 2 as indicated in the figure's legends.

For G $\beta\gamma$  trafficking assays, parental HEK293SL and  $\beta$ arr1/2 KO cells were transfected with FLAG-V2R or HA-CXR4, Gy2-RlucII (BRET donor) and rGFP-CAAX or rGFP-FYVE (BRET acceptor). Cells are supplemented with  $\beta$ arr1/2 as indicated.

For receptor trafficking assays, parental HEK293SL and  $\beta$ arr1/2 KO cells were transfected with V2R-RlucII or CXCR4-Rluc (BRET donor) and rGFP-CAAX or rGFP-FYVE (BRET acceptor). Cells are supplemented with  $\beta$ arr1/2 as indicated. DynK44A is co-transfected to block receptor internalization.

Transfected cells were seeded in 96-well microplates (Greiner) (100  $\mu$ l/well). Forty-eight hours post-transfection, DMEM was removed, and cells were washed with PBS and replaced by HBSS. Cells were then treated with vehicle or agonists for the indicated time in the figure's legends and Prolume Purple (1 $\mu$ M) was added for 6min. BRET readings were done on a Tecan Spark multimode microplate reader equipped with filters for BRET2 (400/70 nm (donor) and 515/20 nm (acceptor)). The BRET signal was calculated as the ratio of light emitted at the energy acceptor wavelengths over the light emitted at the energy donor wavelengths. The agonist-induced BRET response is calculated by deducting the BRET signal obtained in presence of vehicle from the BRET signal obtained in presence of agonist.

*BRET with fluorescence enhancement by combined transfer:*

For BRETfect assays, HEK293T, G $\alpha$ s KO or total G $\alpha$  KO cells were transfected with  $\beta$ arr2-RlucII, V2R-mTFP and Gy2-YFP. G $\alpha$  proteins, DynK44A and  $\beta$ ARKct peptides are co-expressed in the indicated experiments. Transfected cells were seeded in 96-well microplates (Greiner) (100  $\mu$ l/well). Forty-eight hours post-transfection, DMEM was removed, and cells were washed with PBS and replaced by HBSS. Cells were then treated with vehicle or 100nM AVP for 20min and Coelenterazine H (2,5 $\mu$ M) was added 10min before reading on a Mithras LB940 photon-counting plate reader (Berthold Technologies) equipped with donor filter (480/20 nm) and acceptor filter (530/20 nm). The BRETfect signal was calculated as the ratio of light detected at the acceptor wavelengths over the light emitted at the energy donor wavelengths from which the signal calculated from the donor only condition was subtracted.

*BRETfect microscopy*

Microscopic imaging of BRET signals was performed with an inverted microscope (Eclipse Ti-E, Nikon), and EMCCD camera (HNU512, Nuvu Cameras) as described previously (46). HEK293T cells were seeded on 35mm glass bottom dishes and transfected with the BRETfect constructs for 48 hours. Cells were washed with HBSS. Luciferase substrate (Coelenterazine H, 10  $\mu$ M) was diluted with HBSS and added just before the measurement. Binary photon counting frames were continuously recorded with 100 msec exposure. Filter before the camera was switched every 10s (100 frames) to alternately obtain total luminescence frames (without filter) and acceptor frames (with 510 nm long-pass filter). Final images were obtained by integrating the same numbers of total luminescence frames and acceptor frames until the average photon count of the total luminescence image reaches 100 counts/pixel. BRET image was obtained by dividing acceptor photon counts by total photon counts, pixel by pixel. To reduce the shot noise level, BM3D filter adapted for Poisson noise reduction (67) was applied and contrast was slightly compressed ( $\gamma = 1.5$ ) for all BRET images. The details of the image treatment is described elsewhere (68). BRET level was described using pseudocolor allocated with 'jet' colormap of MATLAB 2021b.

#### *Protein Purification*

For in vitro pulldown experiments, G $\beta\gamma$  from bovine brain and the Flag-tagged  $\beta$ 2V2R- $\beta$ arr-Fab30 complex were purified as previously described (10,69).

For isothermal titration calorimetry experiments, recombinant WT G $\beta$ 1 $\gamma$ 2 and were used and purified as previously described (53). G $\beta$ 1 $\gamma$ 2 with a C68S mutation in G $\gamma$ 2 was generated using the Quikchange method (Agilent) and purified as previously described (57). Finally, GST- $\beta$ arr1, untagged  $\beta$ arr1/2, the  $\beta$ arr1-V2Rpp-Fab30 complex and the Flag-tagged, BI-occupied  $\beta$ 2V2R- $\beta$ arr1-Fab30 complex were purified as described (10,54,70).

#### *Structural Comparison of G $\beta\gamma$ -effector complexes*

Previously published structures of G $\beta\gamma$  bound to various effectors, in this case G protein-gated inward rectifier potassium channel 2 (GIRK2; PDB: 4KFM), GPCR kinase 2 (GRK2; PDB: 1OMW), and phosducin (PDB: 2TRC) were visualized in PyMol and aligned by their G protein beta subunits (50-52). Subsequently, the interface between G $\beta$  and the effectors were calculated using the InterfaceResidues script within PyMol.



### *In vitro Pull-down*

Flag-tagged, BI-occupied  $\beta 2V2R$ -  $\beta$  arr1-Fab30 complex was mixed with  $G\beta\gamma$  from bovine brain in a 1:3 ratio in an assay buffer containing 20 mM HEPES, pH 7.4, 150 mM NaCl, 0.01% LMNG, 100 nM BI and left to incubate for 30 min. Next, M1 anti-FLAG agarose beads and 2mM  $CaCl_2$  was added followed by another 30 min incubation. Subsequently, the beads were washed five times using the same assay buffer + 2mM  $CaCl_2$ . The protein was eluted using an elution buffer containing 1 mg/ml FLAG peptide (Sigma-Aldrich), 20mM HEPES, pH 7.4, 150mM NaCl, 0.01% LMNG, 100 nM BI, 5 mM EDTA. Eluted samples were visualized by gel electrophoresis.

Similarly, GST-  $\beta$  arr1 was mixed with  $G\beta\gamma$  from bovine brain in a 1:3 ratio in an assay buffer containing 20 mM HEPES, pH 8.0, 100 mM NaCl, 0.01% DDM and left to incubate for 30 min. Next, glutathione Sepharose beads (GE Healthcare) was added followed by another 30 min incubation. Subsequently, the beads were washed five times using the same assay buffer and eluted with an elution buffer comprising 20 mM HEPES, pH 8.0, 100 mM NaCl, 0.01% DDM, 5mg/ml reduced glutathione, 5mM DTT. Eluted samples were visualized by gel electrophoresis.

### *Isothermal Titration Calorimetry (ITC)*

ITC measurements were made using the MicroCal PEAQ-ITC (Malvern Panalytical). Purified  $\beta$ arr1,  $\beta$ arr2, or  $G\beta\gamma$  were dialyzed overnight in 20mM HEPES, 150 mM NaCl, 0.02% DDM, pH 7.4. The dialysis buffer was subsequently used to wash each component of the ITC instrument. Six ITC experiment were performed with: (1) 40  $\mu$ M of  $\beta$ arr1 loaded into the sample cell and 400  $\mu$ M of  $G\beta\gamma$  in the injection syringe, (2) 25  $\mu$ M  $\beta$ arr1-V2Rpp-Fab30 loaded in the sample cell and 250  $\mu$ M  $G\beta\gamma$  in the injection syringe, (3) 25  $\mu$ M of  $\beta$ arr2 loaded into the sample cell and 250  $\mu$ M of  $G\beta\gamma$  in the injection syringe, (4) 25  $\mu$ M of  $\beta$ arr2 with 1mM V2Rpp loaded into the sample cell and 250  $\mu$ M of  $G\beta\gamma$  with 1mM V2Rpp in the injection syringe, (5) 40  $\mu$ M of  $\beta$ arr1 loaded into the sample cell and 400  $\mu$ M of  $G\beta\gamma$  C68S in the injection syringe, and (6) 30  $\mu$ M of  $\beta$ arr2 loaded into the sample cell and 300  $\mu$ M of  $G\beta\gamma$  C68S in the injection syringe. The sample cell was equilibrated to 25°C, the reference power was set to 5.5  $\mu$ cal·s<sup>-1</sup> and the sample cell was stirred continuously at 750 rpm. Each titration experiment was initiated by a 0.4  $\mu$ L injection from the syringe, followed by eighteen 2.0  $\mu$ L injections at 180 second intervals. Raw data excluding the first injection were

baseline corrected, and each peak area was integrated and normalized. Data was analyzed using the MicroCal PEAQ-ITC analysis software (Malvern Panalytical) to obtain a dissociation constant (K<sub>d</sub>), stoichiometry, and thermodynamic parameters such as enthalpy ( $\Delta H$ ) and entropy ( $\Delta S$ ) of binding.

### **Acknowledgement**

This work was supported by NIH grants R01HL016037 (R.J.L) and F30HL149213 (A.H.N.). R.J.L. is an Investigator of the Howard Hughes Medical Institute (HHMI). A.H.N. was additionally supported by a fellowship through the HHMI Medical Research Fellows Program.

### **Author contributions**

A.H.N., B.S., A.R.B.T., M.B., and R.J.L. conceived the project and designed experiments. B.S. and H.K. performed BRET, BRETfect, and microscopy experiments. A.H.N, A.R.B.T, L.-Y.H., A.K., J.K., B.H., S.M., J.L.IV, C.E., I.P., and E.H. purified protein, performed structural analysis, in vitro pull-down, and ITC experiments. B.S., A.H.N, A.R.B.T., M.B. and R.J.L wrote the manuscript. M.B. and R.J.L supervised the project.

### **Competing interests**

M.B. is the president of the scientific advisory board of Domain Therapeutics. All other authors declare no competing interests.

## References

- 1 Pierce, K. L., Premont, R. T. & Lefkowitz, R. J. Seven-transmembrane receptors. *Nat Rev Mol Cell Biol* 3, 639-650, doi:10.1038/nrm908 (2002).
- 2 Weis, W. I. & Kobilka, B. K. The Molecular Basis of G Protein-Coupled Receptor Activation. *Annu Rev Biochem* 87, 897-919, doi:10.1146/annurev-biochem-060614-033910 (2018).
- 3 Marinissen, M. J. & Gutkind, J. S. G-protein-coupled receptors and signaling networks: emerging paradigms. *Trends Pharmacol Sci* 22, 368-376, doi:10.1016/s0165-6147(00)01678-3 (2001).
- 4 Armstrong, J. F. et al. The IUPHAR/BPS Guide to PHARMACOLOGY in 2020: extending immunopharmacology content and introducing the IUPHAR/MMV Guide to MALARIA PHARMACOLOGY. *Nucleic Acids Res* 48, D1006-D1021, doi:10.1093/nar/gkz951 (2020).
- 5 Gilman, A. G. G PROTEINS: TRANSDUCERS OF RECEPTOR-GENERATED SIGNALS. *Annual Review of Biochemistry* 56, 615-649, doi:10.1146/annurev.bi.56.070187.003151 (1987).
- 6 Rosenfeldt, H., Vázquez-Prado, J. & Gutkind, J. S. P-REX2, a novel PI-3-kinase sensitive Rac exchange factor. *FEBS Lett* 572, 167-171, doi:10.1016/j.febslet.2004.06.097 (2004).
- 7 Moore, C. A., Milano, S. K. & Benovic, J. L. Regulation of receptor trafficking by GRKs and arrestins. *Annu Rev Physiol* 69, 451-482, doi:10.1146/annurev.physiol.69.022405.154712 (2007).
- 8 Lohse, M. J., Benovic, J. L., Codina, J., Caron, M. G. & Lefkowitz, R. J. beta-Arrestin: a protein that regulates beta-adrenergic receptor function. *Science* 248, 1547-1550 (1990).
- 9 Shukla, A. K. et al. Visualization of arrestin recruitment by a G-protein-coupled receptor. *Nature* 512, 218-222, doi:10.1038/nature13430 (2014).
- 10 Shukla, A. K. et al. Visualization of arrestin recruitment by a G-protein-coupled receptor. *Nature* 512, 218-222, doi:10.1038/nature13430 (2014).
- 11 Cahill, T. J., 3rd et al. Distinct conformations of GPCR-beta-arrestin complexes mediate desensitization, signaling, and endocytosis. *Proc Natl Acad Sci U S A* 114, 2562-2567, doi:10.1073/pnas.1701529114 (2017).
- 12 Kumari, P. et al. Functional competence of a partially engaged GPCR-beta-arrestin complex. *Nat Commun* 7, 13416, doi:10.1038/ncomms13416 (2016).
- 13 Kumari, P. et al. Core engagement with beta-arrestin is dispensable for agonist-induced vasopressin receptor endocytosis and ERK activation. *Mol Biol Cell* 28, 1003-1010, doi:10.1091/mbc.E16-12-0818 (2017).
- 14 Mettlen, M., Chen, P. H., Srinivasan, S., Danuser, G. & Schmid, S. L. Regulation of Clathrin-Mediated Endocytosis. *Annu Rev Biochem* 87, 871-896, doi:10.1146/annurev-biochem-062917-012644 (2018).
- 15 Moo, E. V., van Senten, J. R., Brauner-Osborne, H. & Moller, T. C. Arrestin-Dependent and -Independent Internalization of G Protein-Coupled Receptors: Methods, Mechanisms, and Implications on Cell Signaling. *Mol Pharmacol* 99, 242-255, doi:10.1124/molpharm.120.000192 (2021).
- 16 Oakley, R. H., Laporte, S. A., Holt, J. A., Caron, M. G. & Barak, L. S. Differential affinities of visual arrestin, beta arrestin1, and beta arrestin2 for G protein-coupled receptors delineate two major classes of receptors. *J Biol Chem* 275, 17201-17210, doi:10.1074/jbc.M910348199 (2000).
- 17 McDonald, P. H. et al. Beta-arrestin 2: a receptor-regulated MAPK scaffold for the activation of JNK3. *Science* 290, 1574-1577, doi:10.1126/science.290.5496.1574 (2000).

- 18 Lefkowitz, R. J., Rajagopal, K. & Whalen, E. J. New Roles for  $\beta$ -Arrestins in Cell Signaling: Not Just for Seven-Transmembrane Receptors. *Molecular Cell* 24, 643-652, doi:<https://doi.org/10.1016/j.molcel.2006.11.007> (2006).
- 19 Lefkowitz, R. J. & Shenoy, S. K. Transduction of Receptor Signals by  $\beta$ -Arrestins. *Science* 308, 512-517, doi:[doi:10.1126/science.1109237](https://doi.org/10.1126/science.1109237) (2005).
- 20 Latorraca, N. R. et al. How GPCR Phosphorylation Patterns Orchestrate Arrestin-Mediated Signaling. *Cell* 183, 1813-1825.e1818, doi:[doi:10.1016/j.cell.2020.11.014](https://doi.org/10.1016/j.cell.2020.11.014) (2020).
- 21 Luttrell, L. M. et al. Manifold roles of  $\beta$ -arrestins in GPCR signaling elucidated with siRNA and CRISPR/Cas9. *Sci Signal* 11, eaat7650, doi:[doi:10.1126/scisignal.aat7650](https://doi.org/10.1126/scisignal.aat7650) (2018).
- 22 Thomsen, A. R. B. et al. GPCR-G Protein- $\beta$ -Arrestin Super-Complex Mediates Sustained G Protein Signaling. *Cell* 166, 907-919, doi:[doi:10.1016/j.cell.2016.07.004](https://doi.org/10.1016/j.cell.2016.07.004) (2016).
- 23 Nguyen, A. H. et al. Structure of an endosomal signaling GPCR-G protein-beta-arrestin megacomplex. *Nat Struct Mol Biol* 26, 1123-1131, doi:[doi:10.1038/s41594-019-0330-y](https://doi.org/10.1038/s41594-019-0330-y) (2019).
- 24 Wehbi, V. L. et al. Noncanonical GPCR signaling arising from a PTH receptor-arrestin-Gbetagamma complex. *Proc Natl Acad Sci U S A* 110, 1530-1535, doi:[doi:10.1073/pnas.1205756110](https://doi.org/10.1073/pnas.1205756110) (2013).
- 25 Jensen, D. D. et al. Neurokinin 1 receptor signaling in endosomes mediates sustained nociception and is a viable therapeutic target for prolonged pain relief. *Sci Transl Med* 9, doi:[doi:10.1126/scitranslmed.aal3447](https://doi.org/10.1126/scitranslmed.aal3447) (2017).
- 26 Yang, M., He, R. L., Benovic, J. L. & Ye, R. D. beta-Arrestin1 interacts with the G-protein subunits beta1gamma2 and promotes beta1gamma2-dependent Akt signalling for NF-kappaB activation. *Biochem J* 417, 287-296, doi:[doi:10.1042/BJ20081561](https://doi.org/10.1042/BJ20081561) (2009).
- 27 Jean-Alphonse, F. G. et al. beta(2)-adrenergic receptor control of endosomal PTH receptor signaling via Gbetagamma. *Nat Chem Biol* 13, 259-261, doi:[doi:10.1038/nchembio.2267](https://doi.org/10.1038/nchembio.2267) (2017).
- 28 White, A. D. et al. G(q/11)-dependent regulation of endosomal cAMP generation by parathyroid hormone class B GPCR. *Proc Natl Acad Sci U S A* 117, 7455-7460, doi:[doi:10.1073/pnas.1918158117](https://doi.org/10.1073/pnas.1918158117) (2020).
- 29 Saini, D. K., Kalyanaraman, V., Chisari, M. & Gautam, N. A family of G protein  $\beta\gamma$  subunits translocate reversibly from the plasma membrane to endomembranes on receptor activation. *J Biol Chem* 282, 24099-24108, doi:[doi:10.1074/jbc.M701191200](https://doi.org/10.1074/jbc.M701191200) (2007).
- 30 Ajith Karunarathne, W. K., O'Neill, P. R., Martinez-Espinosa, P. L., Kalyanaraman, V. & Gautam, N. All G protein  $\beta\gamma$  complexes are capable of translocation on receptor activation. *Biochem Biophys Res Commun* 421, 605-611, doi:[doi:10.1016/j.bbrc.2012.04.054](https://doi.org/10.1016/j.bbrc.2012.04.054) (2012).
- 31 Masuho, I., Skamangas, N. K., Muntean, B. S. & Martemyanov, K. A. Diversity of the G $\beta\gamma$  complexes defines spatial and temporal bias of GPCR signaling. *Cell Syst* 12, 324-337.e325, doi:[doi:10.1016/j.cels.2021.02.001](https://doi.org/10.1016/j.cels.2021.02.001) (2021).
- 32 Wedegaertner, P. B. & Bourne, H. R. Activation and depalmitoylation of Gs alpha. *Cell* 77, 1063-1070, doi:[doi:10.1016/0092-8674\(94\)90445-6](https://doi.org/10.1016/0092-8674(94)90445-6) (1994).
- 33 Degtyarev, M. Y., Spiegel, A. M. & Jones, T. L. Increased palmitoylation of the Gs protein alpha subunit after activation by the beta-adrenergic receptor or cholera toxin. *J Biol Chem* 268, 23769-23772 (1993).
- 34 Mumby, S. M., Kleuss, C. & Gilman, A. G. Receptor regulation of G-protein palmitoylation. *Proc Natl Acad Sci U S A* 91, 2800-2804, doi:[doi:10.1073/pnas.91.7.2800](https://doi.org/10.1073/pnas.91.7.2800) (1994).

- 35 Yu, J. Z. & Rasenick, M. M. Real-time visualization of a fluorescent G( $\alpha$ )(s): dissociation of the activated G protein from plasma membrane. *Mol Pharmacol* 61, 352-359, doi:10.1124/mol.61.2.352 (2002).
- 36 Duncan, J. A. & Gilman, A. G. A cytoplasmic acyl-protein thioesterase that removes palmitate from G protein alpha subunits and p21(RAS). *J Biol Chem* 273, 15830-15837, doi:10.1074/jbc.273.25.15830 (1998).
- 37 Namkung, Y. et al. Monitoring G protein-coupled receptor and beta-arrestin trafficking in live cells using enhanced bystander BRET. *Nat Commun* 7, 12178, doi:10.1038/ncomms12178 (2016).
- 38 Koch, W. J., Hawes, B. E., Inglese, J., Luttrell, L. M. & Lefkowitz, R. J. Cellular expression of the carboxyl terminus of a G protein-coupled receptor kinase attenuates G beta gamma-mediated signaling. *J Biol Chem* 269, 6193-6197 (1994).
- 39 Koch, W. J. et al. Cardiac function in mice overexpressing the beta-adrenergic receptor kinase or a beta ARK inhibitor. *Science* 268, 1350-1353 (1995).
- 40 Schink, K. O., Raiborg, C. & Stenmark, H. Phosphatidylinositol 3-phosphate, a lipid that regulates membrane dynamics, protein sorting and cell signalling. *Bioessays* 35, 900-912, doi:10.1002/bies.201300064 (2013).
- 41 D'Agostino, G. et al. beta-Arrestin1 and beta-Arrestin2 Are Required to Support the Activity of the CXCL12/HMGB1 Heterocomplex on CXCR4. *Front Immunol* 11, 550824, doi:10.3389/fimmu.2020.550824 (2020).
- 42 Cheng, Z. J. et al. beta-arrestin differentially regulates the chemokine receptor CXCR4-mediated signaling and receptor internalization, and this implicates multiple interaction sites between beta-arrestin and CXCR4. *J Biol Chem* 275, 2479-2485, doi:10.1074/jbc.275.4.2479 (2000).
- 43 Cotnoir-White, D. et al. Monitoring ligand-dependent assembly of receptor ternary complexes in live cells by BRETfect. *Proc Natl Acad Sci U S A* 115, E2653-E2662, doi:10.1073/pnas.1716224115 (2018).
- 44 Stallaert, W. et al. Purinergic Receptor Transactivation by the  $\beta$ (2)-Adrenergic Receptor Increases Intracellular Ca(2+) in Nonexcitable Cells. *Mol Pharmacol* 91, 533-544, doi:10.1124/mol.116.106419 (2017).
- 45 Avet, C. et al. Effector membrane translocation biosensors reveal G protein and betaarrestin coupling profiles of 100 therapeutically relevant GPCRs. *Elife* 11, doi:10.7554/eLife.74101 (2022).
- 46 Kobayashi, H., Picard, L. P., Schönegge, A. M. & Bouvier, M. Bioluminescence resonance energy transfer-based imaging of protein-protein interactions in living cells. *Nat Protoc* 14, 1084-1107, doi:10.1038/s41596-019-0129-7 (2019).
- 47 Okashah, N. et al. Agonist-induced formation of unproductive receptor-G(12) complexes. *Proc Natl Acad Sci U S A* 117, 21723-21730, doi:10.1073/pnas.2003787117 (2020).
- 48 Smith, J. S. et al. Noncanonical scaffolding of Galphai and beta-arrestin by G protein-coupled receptors. *Science* 371, doi:10.1126/science.aay1833 (2021).
- 49 Damke, H., Baba, T., Warnock, D. E. & Schmid, S. L. Induction of mutant dynamin specifically blocks endocytic coated vesicle formation. *J Cell Biol* 127, 915-934, doi:10.1083/jcb.127.4.915 (1994).

- 50 Gaudet, R., Bohm, A. & Sigler, P. B. Crystal structure at 2.4 angstroms resolution of the complex of transducin betagamma and its regulator, phosducin. *Cell* 87, 577-588 (1996).
- 51 Lodowski, D. T., Pitcher, J. A., Capel, W. D., Lefkowitz, R. J. & Tesmer, J. J. Keeping G proteins at bay: a complex between G protein-coupled receptor kinase 2 and Gbetagamma. *Science* 300, 1256-1262, doi:10.1126/science.1082348 (2003).
- 52 Whorton, M. R. & MacKinnon, R. X-ray structure of the mammalian GIRK2-beta gamma G-protein complex. *Nature* 498, 190-197, doi:10.1038/nature12241 (2013).
- 53 Rasmussen, S. G. et al. Crystal structure of the beta2 adrenergic receptor-Gs protein complex. *Nature* 477, 549-555, doi:10.1038/nature10361 (2011).
- 54 Shukla, A. K. et al. Structure of active beta-arrestin-1 bound to a G-protein-coupled receptor phosphopeptide. *Nature* 497, 137-141, doi:10.1038/nature12120 (2013).
- 55 Iniguez-Lluhi, J. A., Simon, M. I., Robishaw, J. D. & Gilman, A. G. G protein beta gamma subunits synthesized in Sf9 cells. Functional characterization and the significance of prenylation of gamma. *J Biol Chem* 267, 23409-23417 (1992).
- 56 Simonds, W. F., Butrynski, J. E., Gautam, N., Unson, C. G. & Spiegel, A. M. G-protein beta gamma dimers. Membrane targeting requires subunit coexpression and intact gamma C-A-A-X domain. *J Biol Chem* 266, 5363-5366 (1991).
- 57 Zheng, S., Abreu, N., Levitz, J. & Kruse, A. C. Structural basis for KCTD-mediated rapid desensitization of GABAB signalling. *Nature* 567, 127-131, doi:10.1038/s41586-019-0990-0 (2019).
- 58 Zhang, J. F., Mehta, S. & Zhang, J. Signaling Microdomains in the Spotlight: Visualizing Compartmentalized Signaling Using Genetically Encoded Fluorescent Biosensors. *Annu Rev Pharmacol Toxicol* 61, 587-608, doi:10.1146/annurev-pharmtox-010617-053137 (2021).
- 59 Zaccolo, M., Zerio, A. & Lobo, M. J. Subcellular Organization of the cAMP Signaling Pathway. *Pharmacol Rev* 73, 278-309, doi:10.1124/pharmrev.120.000086 (2021).
- 60 Bock, A. et al. Optical Mapping of cAMP Signaling at the Nanometer Scale. *Cell* 182, 1519-1530 e1517, doi:10.1016/j.cell.2020.07.035 (2020).
- 61 Anton, S. E. et al. Receptor-associated independent cAMP nanodomains mediate spatiotemporal specificity of GPCR signaling. *Cell* 185, 1130-1142 e1111, doi:10.1016/j.cell.2022.02.011 (2022).
- 62 Calebiro, D. et al. Persistent cAMP-signals triggered by internalized G-protein-coupled receptors. *PLoS Biol* 7, e1000172, doi:10.1371/journal.pbio.1000172 (2009).
- 63 Mullershausen, F. et al. Persistent signaling induced by FTY720-phosphate is mediated by internalized S1P1 receptors. *Nat Chem Biol* 5, 428-434, doi:10.1038/nchembio.173 (2009).
- 64 Jean-Alphonse, F. G. et al. beta2-adrenergic receptor control of endosomal PTH receptor signaling via Gbetagamma. *Nat Chem Biol* 13, 259-261, doi:10.1038/nchembio.2267 (2017).
- 65 Martin, B. R. & Lambert, N. A. Activated G Protein Galphas Samples Multiple Endomembrane Compartments. *J Biol Chem* 291, 20295-20302, doi:10.1074/jbc.M116.729731 (2016).
- 66 Wan, Q. et al. Mini G protein probes for active G protein-coupled receptors (GPCRs) in live cells. *J Biol Chem* 293, 7466-7473, doi:10.1074/jbc.RA118.001975 (2018).
- 67 Azzari, L. & Foj, A. Variance Stabilization for Noisy+Estimate Combination in Iterative Poisson Denoising. *IEEE Signal Processing Letters* 23, 1086-1090, doi:10.1109/LSP.2016.2580600 (2016).

- 68 Kobayashi, H. & Bouvier, M. Bioluminescence Resonance Energy Transfer (BRET) Imaging in Living Cells: Image Acquisition and Quantification. *Methods Mol Biol* 2274, 305-314, doi:10.1007/978-1-0716-1258-3\_26 (2021).
- 69 Pitcher, J. A. et al. Role of beta gamma subunits of G proteins in targeting the beta-adrenergic receptor kinase to membrane-bound receptors. *Science* 257, 1264-1267, doi:10.1126/science.1325672 (1992).
- 70 Nobles, K. N., Guan, Z., Xiao, K., Oas, T. G. & Lefkowitz, R. J. The active conformation of beta-arrestin1: direct evidence for the phosphate sensor in the N-domain and conformational differences in the active states of beta-arrestins1 and -2. *J Biol Chem* 282, 21370-21381, doi:10.1074/jbc.M611483200 (2007).

## Figures legends:

### **Figure 1: Regulation of G proteins trafficking from the plasma membrane to the endosomes by G $\beta\gamma$ and $\beta$ -arrestin.**

A) AVP-induced G $\alpha$ s dissociation from the plasma membrane after 20-minute stimulation monitored by ebBRET between G $\alpha$ s67-RlucII and rGFP-CAAX in parental HEK293SL cells and  $\beta$ -arrestin1/2 KO cells. Overexpression of  $\beta$ ARKct-CAAX and G $\beta$ 1 $\gamma$ 2 modulates G $\alpha$ s dissociation. B) AVP-induced G $\alpha$ s dissociation from the plasma membrane after 20 min stimulation monitored by ebBRET between G $\alpha$ s67-RlucII and rGFP-CAAX in parental HEK293SL cells. Overexpression of  $\beta$ ARKct-FYVE and G $\beta$ 1 $\gamma$ 2 modulates G $\alpha$ s dissociation. C) AVP-induced G $\alpha$ s trafficking to the endosomes after 20min stimulation monitored by ebBRET between G $\alpha$ s67-RlucII and rGFP-FYVE in parental HEK293SL cells and  $\beta$ -arrestin1/2 KO cells. Overexpression of  $\beta$ ARKct-CAAX and G $\beta$ 1 $\gamma$ 2 modulates G $\alpha$ s translocation. D) AVP-induced G $\alpha$ s trafficking to the endosomes after 20min stimulation monitored by ebBRET between G $\alpha$ s67-RlucII and rGFP-FYVE in parental HEK293SL cells. Overexpression of  $\beta$ ARKct-FYVE and G $\beta$ 1 $\gamma$ 2 modulates G $\alpha$ s dissociation. E) AVP-induced G $\beta\gamma$  internalization after 20 min stimulation monitored by ebBRET between G $\gamma$ 2-RlucII and rGFP-CAAX in parental HEK293SL cells and  $\beta$ -arrestin1/2 KO cells with or without  $\beta$ -arrestin1/2 supplementation. F) AVP-induced G $\beta\gamma$  endosomal trafficking after 20 min stimulation monitored by ebBRET between G $\gamma$ 2-RlucII and rGFP-FYVE in parental HEK293SL cells and  $\beta$ -arrestin1/2 KO cells with or without  $\beta$ -arrestin1/2 supplementation. Data are represented as the mean  $\pm$  SEM (n=5). ns nonsignificant; \* P  $\leq$  0.05; \*\* P  $\leq$  0.01; \*\*\* P  $\leq$  0.001; \*\*\*\* P  $\leq$  0.0001 (unpaired t-test).

### **Figure 2: CXCR4-mediated G $\beta\gamma$ trafficking is $\beta$ -arrestin-dependent.**

A) V2R internalization is monitored by ebBRET using V2R-RlucII and rGFP-CAAX in parental HEK293SL cells and  $\beta$ -arrestin1/2 KO cells with or without  $\beta$ -arrestin1/2 supplementation after 20min 100nM AVP stimulation. B) CXCR4 internalization is monitored by ebBRET using CXCR4-Rluc and rGFP-CAAX in parental HEK293SL cells and  $\beta$ -arrestin1/2 KO cells with or without  $\beta$ -arrestin1/2 supplementation after 20min 100nM CXCL12 stimulation. C) CXCL12-induced G $\beta\gamma$  internalization after 20 min stimulation monitored by ebBRET between G $\gamma$ 2-RlucII and rGFP-CAAX in parental HEK293SL cells and  $\beta$ -arrestin1/2 KO cells with or without  $\beta$ -arrestin1/2 supplementation. Data are represented



as the mean  $\pm$  SEM (n=4-5). ns nonsignificant; \*  $P \leq 0.05$ ; \*\*  $P \leq 0.01$ ; \*\*\*  $P \leq 0.001$ ; \*\*\*\*  $P \leq 0.0001$  (unpaired t-test).

**Figure 3: V2R- $\beta$ arr2-G $\beta$  complex formation monitored by BRETfect assay.** A) Illustration of the design of the BRETfect assay with transfer of energy between RlucII donor (D) fused to  $\beta$ -arrestin2, mTFP intermediate (I) fused to V2R and energy acceptor YFP (A) fused to G $\gamma$ 2. B) Co-expression of BRETfect constructs in parental HEK293T followed by vehicle or AVP stimulation for 20min. C) Co-expression of BRETfect constructs in G $\alpha$ s KO cells followed by AVP stimulation for 20min. D) Co-expression of BRETfect constructs in total G $\alpha$  proteins KO cells followed by AVP stimulation for 20min. Data are represented as the mean  $\pm$  SEM (n=3-5). ns nonsignificant; \*  $P \leq 0.05$ ; \*\*  $P \leq 0.01$ ; \*\*\*  $P \leq 0.001$ ; \*\*\*\*  $P \leq 0.0001$  (unpaired t-test).

**Figure 4: V2R- $\beta$ arr2-G $\beta$  complex formation monitored by BRETfect microscopy.** Co-expression of BRETfect constructs  $\beta$ -arrestin2-RlucII, V2R-mTFP and G $\gamma$ 2-YFP in parental HEK293T followed by 100nM AVP stimulation and image acquisition by luminescence microscopy. Scale bar: 5 $\mu$ m.

**Figure 5: V2R- $\beta$ arr2-G $\beta$  complex formation monitored by BRETfect microscopy and kinetics in parental HEK293T and G $\alpha$ KO cells.** A) Co-expression of  $\beta$ -arrestin2-RlucII, V2R-mTFP and G $\gamma$ 2-YFP in parental HEK293T cells followed by AVP stimulation and image acquisition by luminescence microscopy. B) Co-expression of  $\beta$ -arrestin2-RlucII, V2R-mTFP and G $\gamma$ 2-YFP in total G $\alpha$ KO cells followed by AVP stimulation and image acquisition by luminescence microscopy. C) Co-expression of  $\beta$ -arrestin2-RlucII, V2R-mTFP and G $\gamma$ 2-YFP in parental HEK293T cells or total G $\alpha$ KO cells followed by vehicle or 100nM AVP treatment and BRETfect reading. Scale bar: 5 $\mu$ m.

**Figure 6: GPCR and G proteins activation induces V2R- $\beta$ arr2-G $\beta$  complex formation at the plasma membrane.** A) AVP-promoted V2R- $\beta$ arr2-G $\beta$  complex formation monitored by BRETfect measurement between  $\beta$ -arrestin2-RlucII, V2R-mTFP and G $\gamma$ 2-YFP and co-expression of different G $\alpha$  proteins (G $\alpha$ s, G $\alpha$ i, G $\alpha$ q and G $\alpha$ 12) in parental HEK293T. B) AVP-promoted V2R- $\beta$ arr2-G $\beta$  complex formation monitored by BRETfect measurement between  $\beta$ -arrestin2-RlucII, V2R-mTFP and G $\gamma$ 2-YFP and co-expression of different G proteins (G $\alpha$ s, G $\alpha$ i, G $\alpha$ q and G $\alpha$ 12) in G $\alpha$  proteins depleted cells. C) AVP-promoted V2R- $\beta$ arr2-G $\beta$  complex formation monitored by BRETfect measurement between  $\beta$ -arrestin2-RlucII, V2R-mTFP and G $\gamma$ 2-YFP and co-expression of internalization inhibitor

DynK44A or plasma membrane anchored  $\beta$ ARKct-CAAX peptide. D) AVP-promoted V2R- $\beta$ arr2- $G\beta\gamma$  complex formation monitored by BRETfect measurement between  $\beta$ -arrestin2-RlucII, V2R-mTFP and Gy2-YFP and co-expression of increasing amounts of plasma membrane anchored  $\beta$ ARKct peptide ( $\beta$ ARKct-CAAX) or endosomes anchored  $\beta$ ARKct peptide ( $\beta$ ARKct-FYVE). Data are represented as the mean  $\pm$  SEM (n=3). ns nonsignificant; \*  $P \leq 0.05$ ; \*\*  $P \leq 0.01$ ; \*\*\*  $P \leq 0.001$ ; \*\*\*\*  $P \leq 0.0001$  (unpaired t-test).

**Figure 7:  $G\beta\gamma$  binds to inactive and active  $\beta$ arr1 in vitro.** A) Structural analysis of  $G\beta\gamma$ -effector complex structures illustrate variable interaction between residues at the  $G\beta\gamma$  inner toroidal surface with those of effectors. Each  $\beta$  sheet of  $G\beta$  is numbered 1 through 7. B) In vitro pull-down between GST- $\beta$ arr1 and  $G\beta\gamma$ . C) In vitro pull-down between Flag- $\beta$ 2V2R- $\beta$ arr1-Fab30 and  $G\beta\gamma$ .

**Figure 8:  $G\beta\gamma$  displays promiscuous, micromolar affinity binding against inactive and active  $\beta$ arr1/2.** Isothermogram between  $G\beta\gamma$  and A) inactive  $\beta$ arr1, B)  $\beta$ arr1-V2Rpp-Fab30 complex, C) inactive  $\beta$ arr2, and D) active  $\beta$ arr2 in excess V2Rpp.

**Figure 9: Schematic illustrating mechanism of sustained endosomal G protein signaling.**

**Supplementary Figure 1: V2R- $\beta$ arr2- $G\beta\gamma$  complex formation monitored by BRETfect assay.** Co-expression of BRETfect constructs in parental HEK293T followed by vehicle or AVP stimulation for 20min. Unlabeled V2R is co-transfected with the D + A condition. Data are represented as the mean  $\pm$  SEM (n=4). ns nonsignificant; \*  $P \leq 0.05$ ; \*\*  $P \leq 0.01$ ; \*\*\*  $P \leq 0.001$ ; \*\*\*\*  $P \leq 0.0001$  (unpaired t-test).

**Supplementary Figure 2: V2R internalization is inhibited by DynK44A.** A) Receptor internalization in HEK293SL cells is monitored by ebBRET between V2R-RlucII and rGFP-CAAX with co-expression of increasing amounts of DynK44A. Data are represented as the mean  $\pm$  SEM (n=3). ns nonsignificant; \*  $P \leq 0.05$ ; \*\*  $P \leq 0.01$ ; \*\*\*  $P \leq 0.001$ ; \*\*\*\*  $P \leq 0.0001$  (unpaired t-test).

**Supplementary Figure 3:  $G\beta\gamma$  C68S maintains ability to bind to inactive  $\beta$ arr1 and  $\beta$ arr2.** Isothermogram demonstrate saturable, specific binding between  $G\beta\gamma$  and A)  $\beta$ arr1 or B)  $\beta$ arr2.

**Supplementary Figure 4:  $G\beta\gamma$  does not bind to the V2R phosphopeptide.** Isothermogram demonstrate lack of saturable binding between  $G\beta\gamma$  and V2R phosphopeptide (V2Rpp).

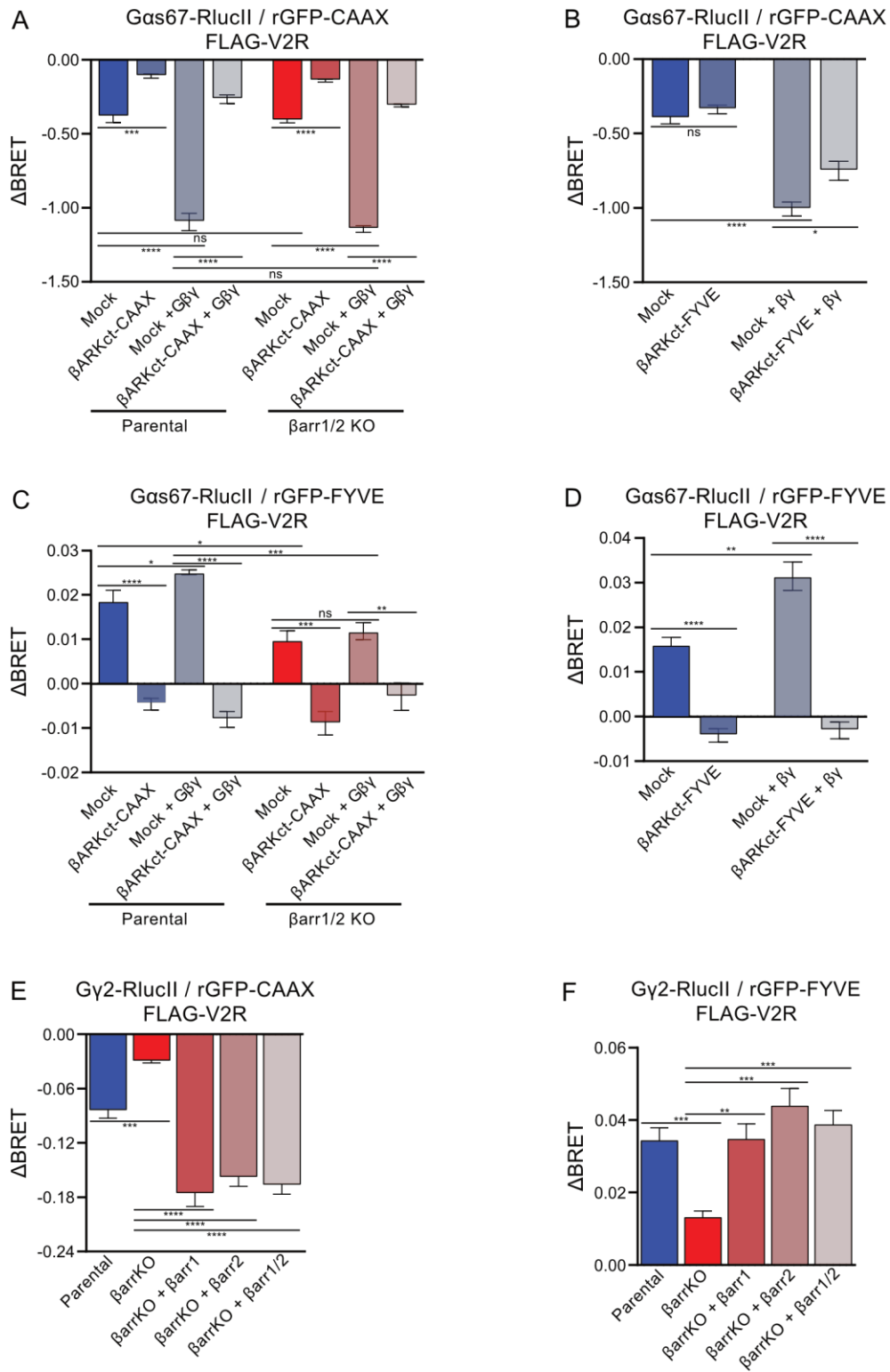


**Figure 1**

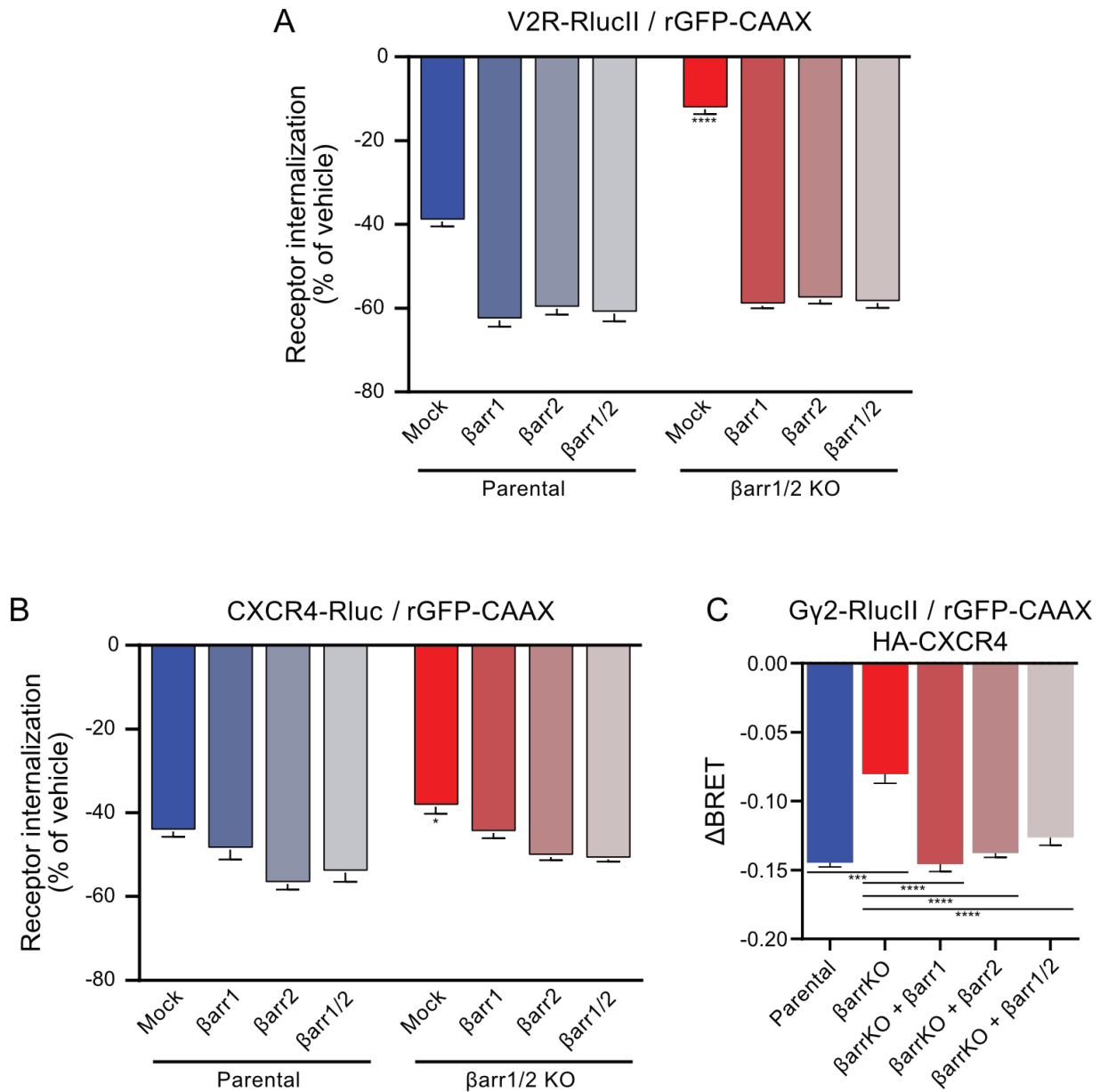


**Figure 2**

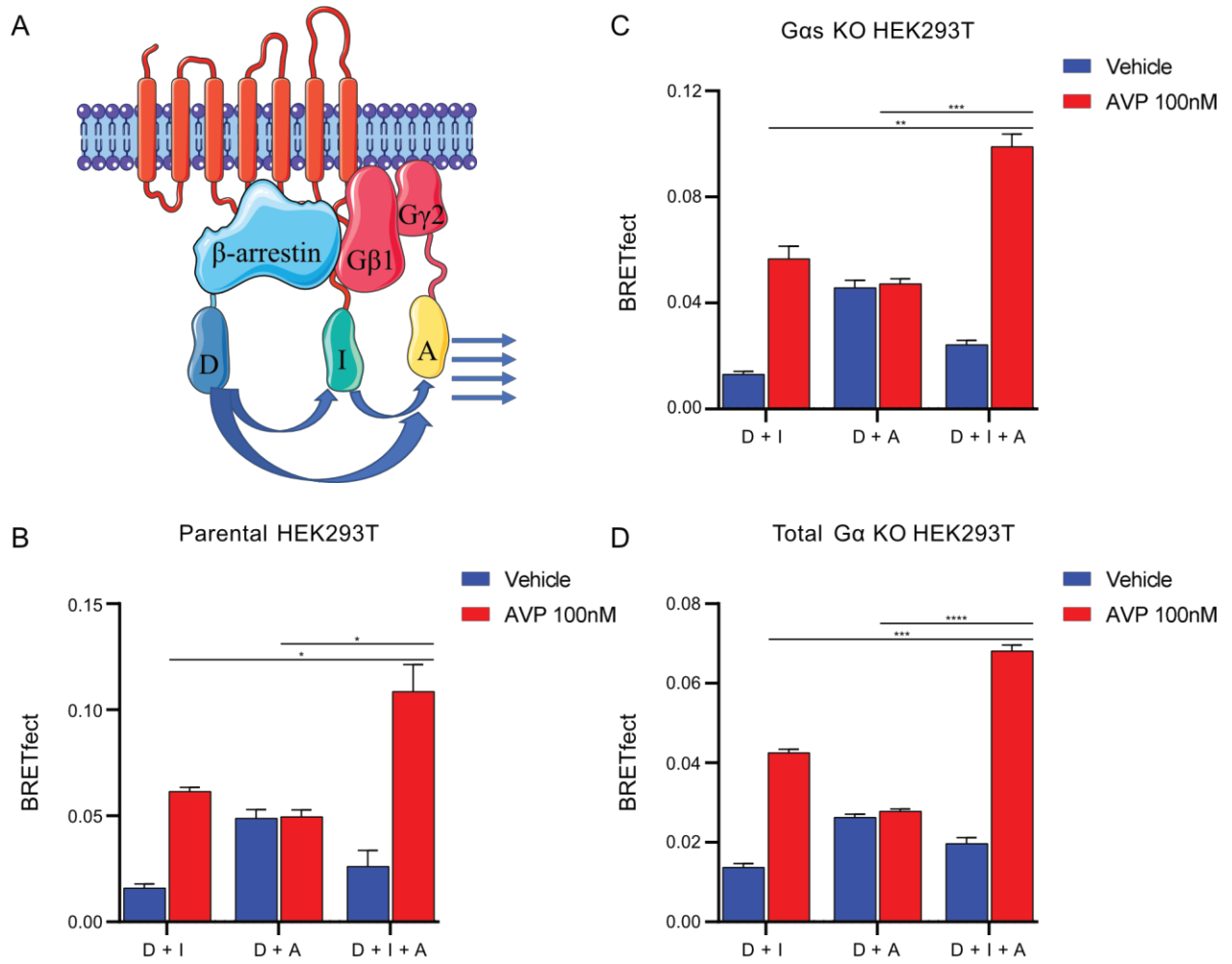


**Figure 3**

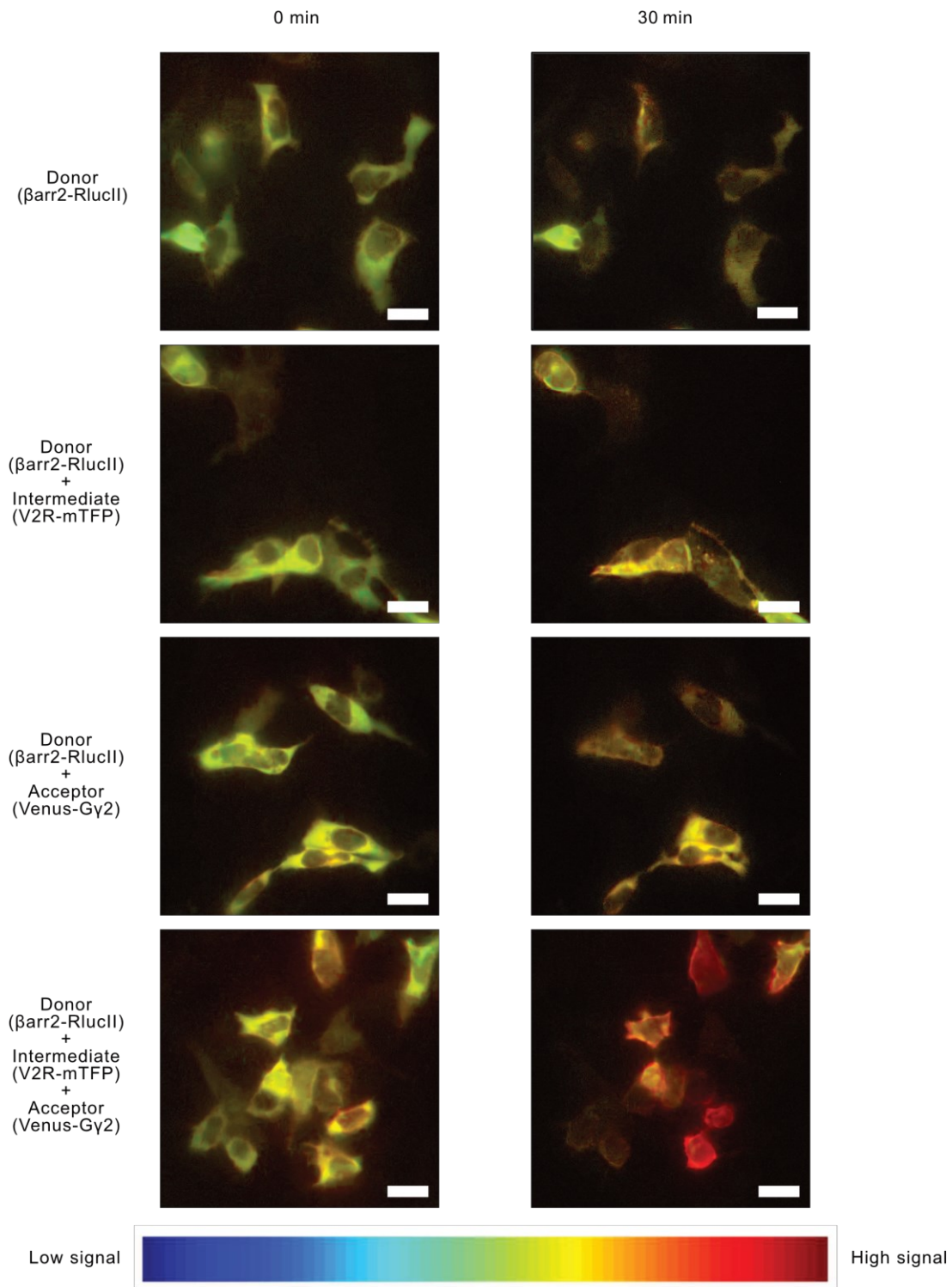


**Figure 4**

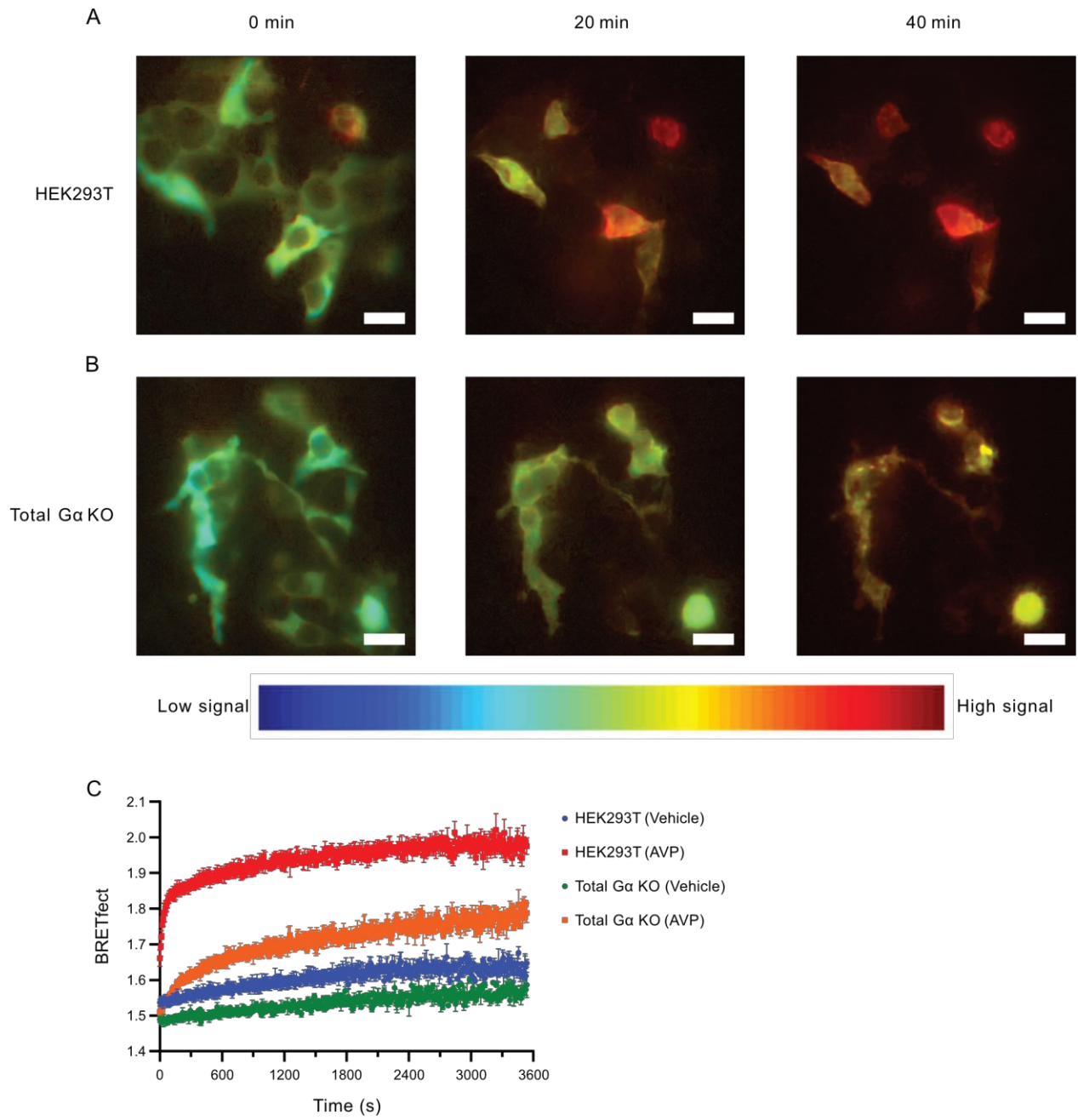


**Figure 5**

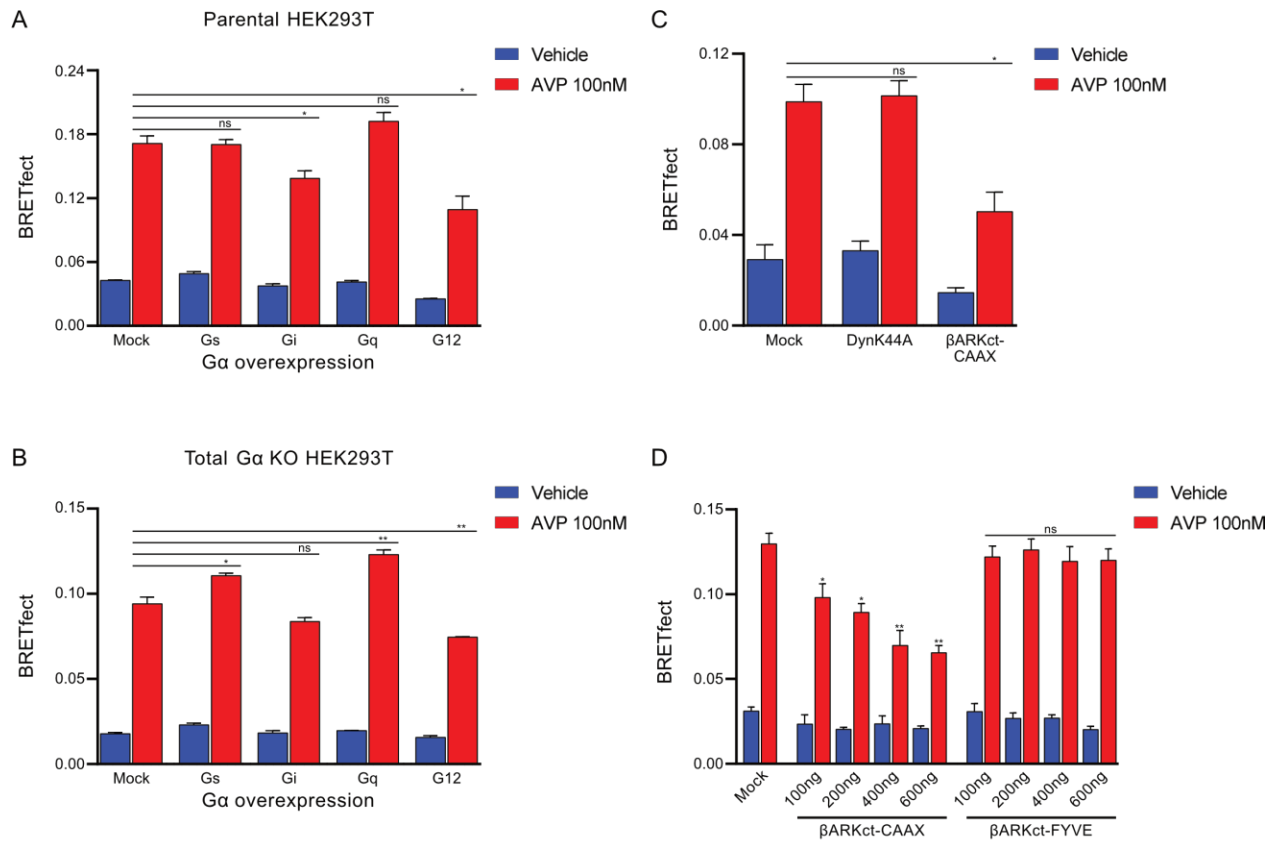


**Figure 6**



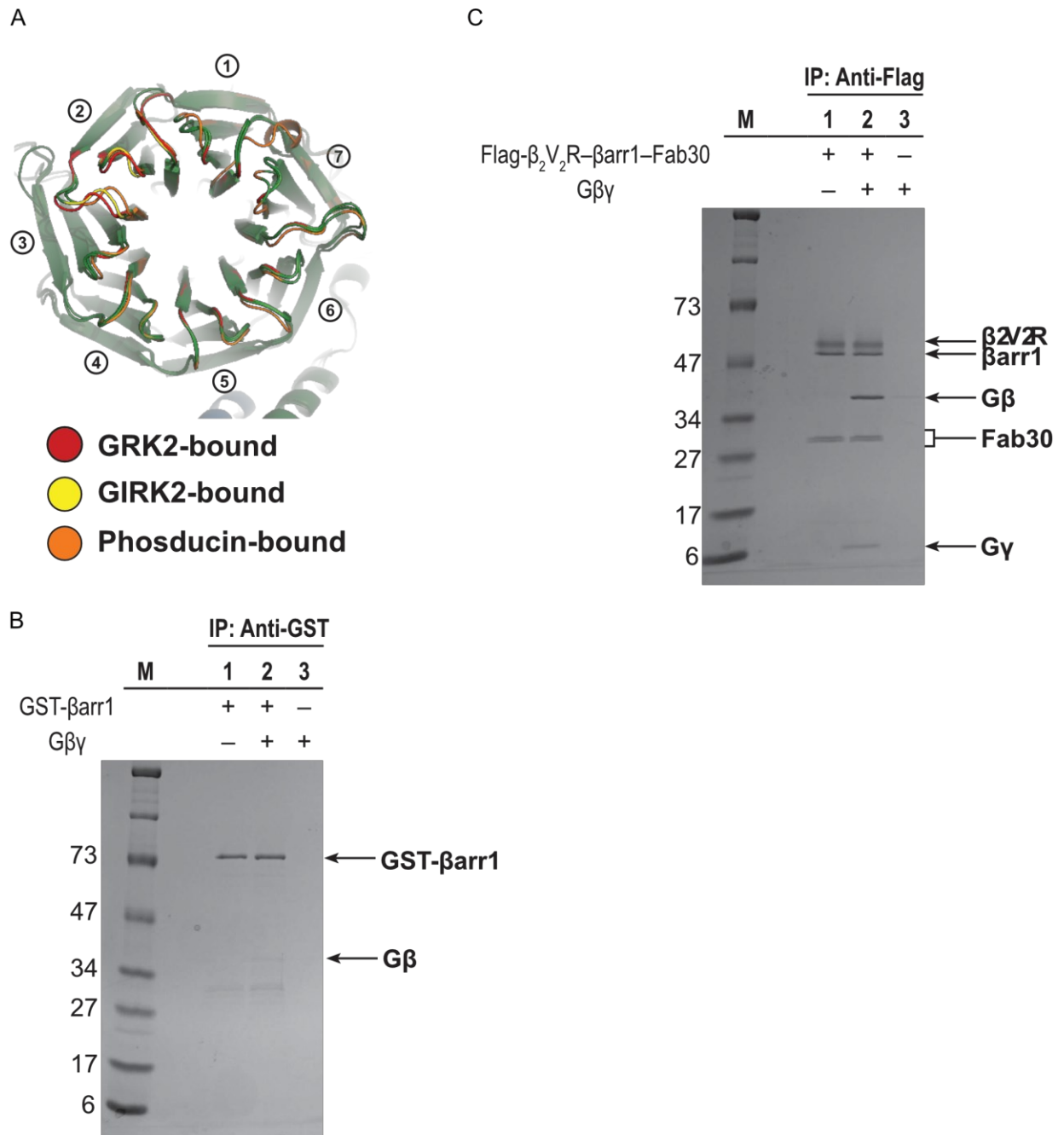
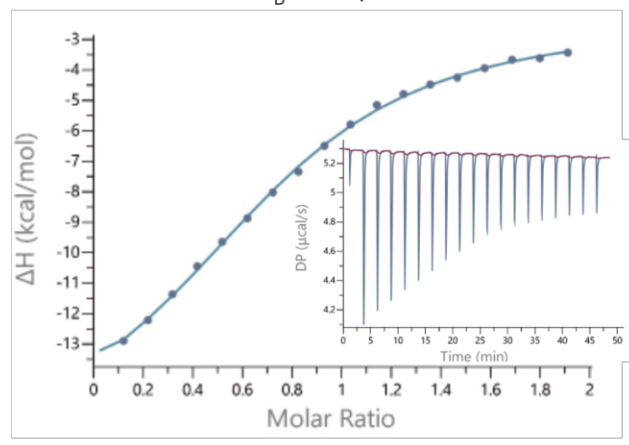


**Figure 7**

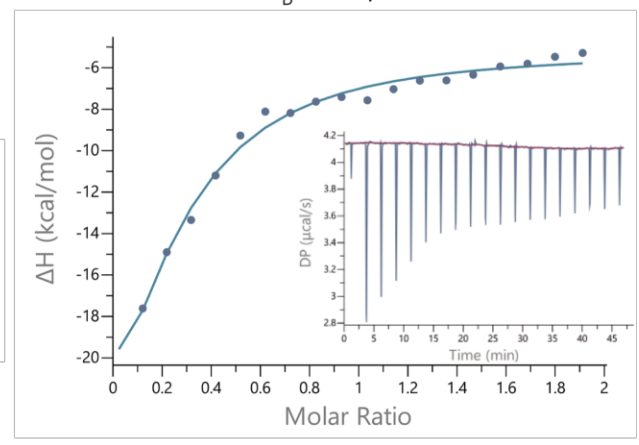
A

$G\beta_1\gamma_2:\beta arr1$   
 $K_D = 9.4 \mu M$



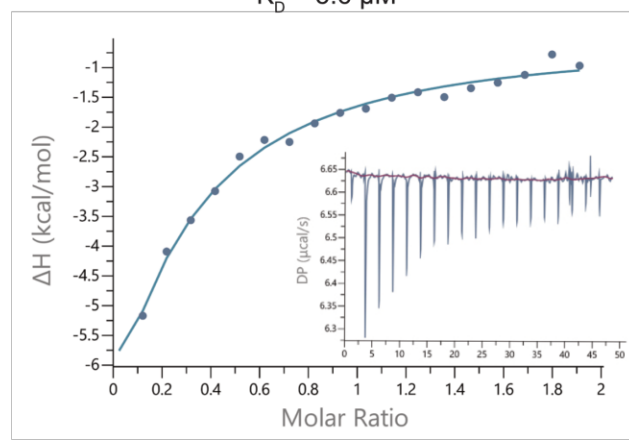
B

$G\beta_1\gamma_2:\beta arr1-V_2Rpp-Fab30$   
 $K_D = 3.8 \mu M$



C

$G\beta_1\gamma_2:\beta arr2$   
 $K_D = 5.6 \mu M$



D

$G\beta_1\gamma_2:\beta arr2-V_2Rpp$   
 $K_D = 7.3 \mu M$

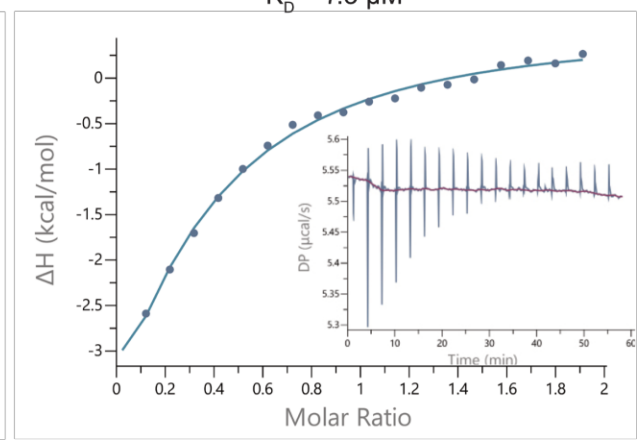


Figure 8

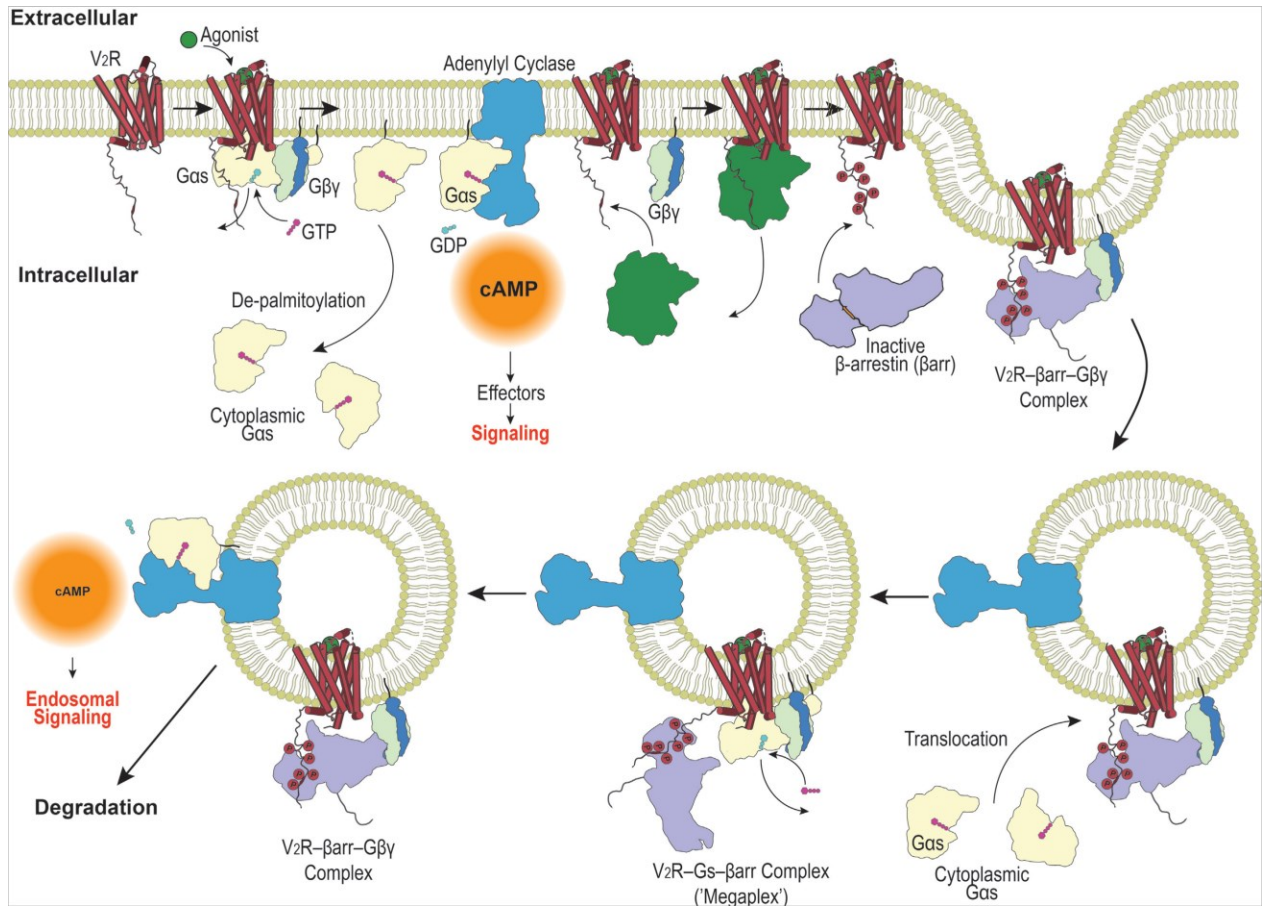
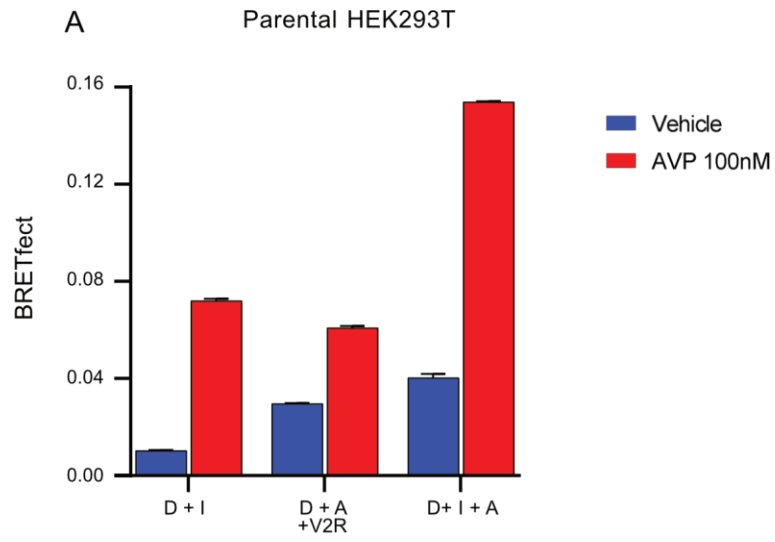


Figure 9



**Figure S1**

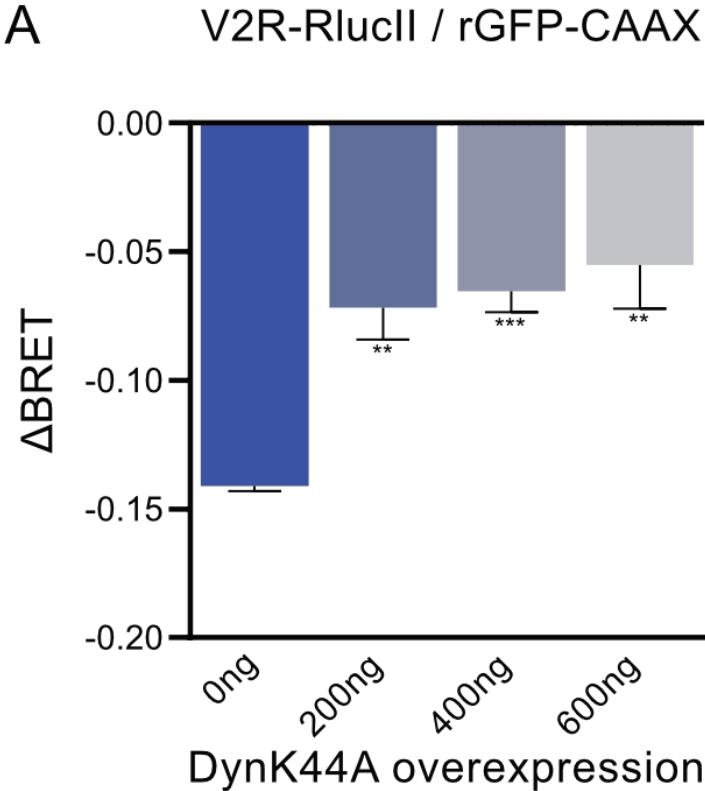
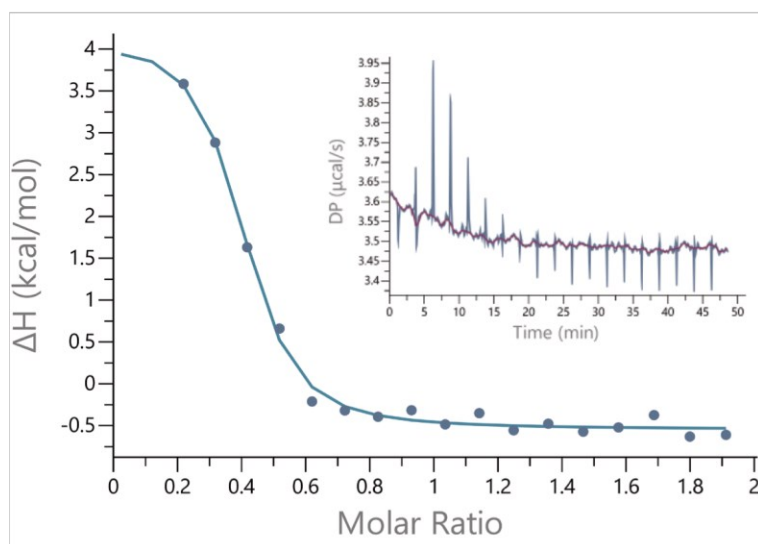


Figure S2

A

$G\beta_1\gamma_2$  C68S: $\beta$ arr1  
 $K_D = 1.1 \mu\text{M}$



B

$G\beta_1\gamma_2$  C68S: $\beta$ arr2  
 $K_D = 3.2 \mu\text{M}$

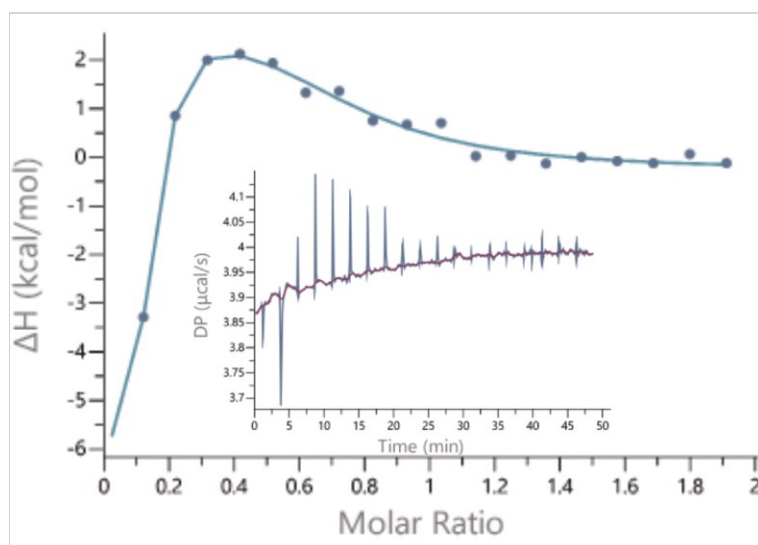


Figure S3

# $G\beta_1\gamma_2:V\alpha Rpp$

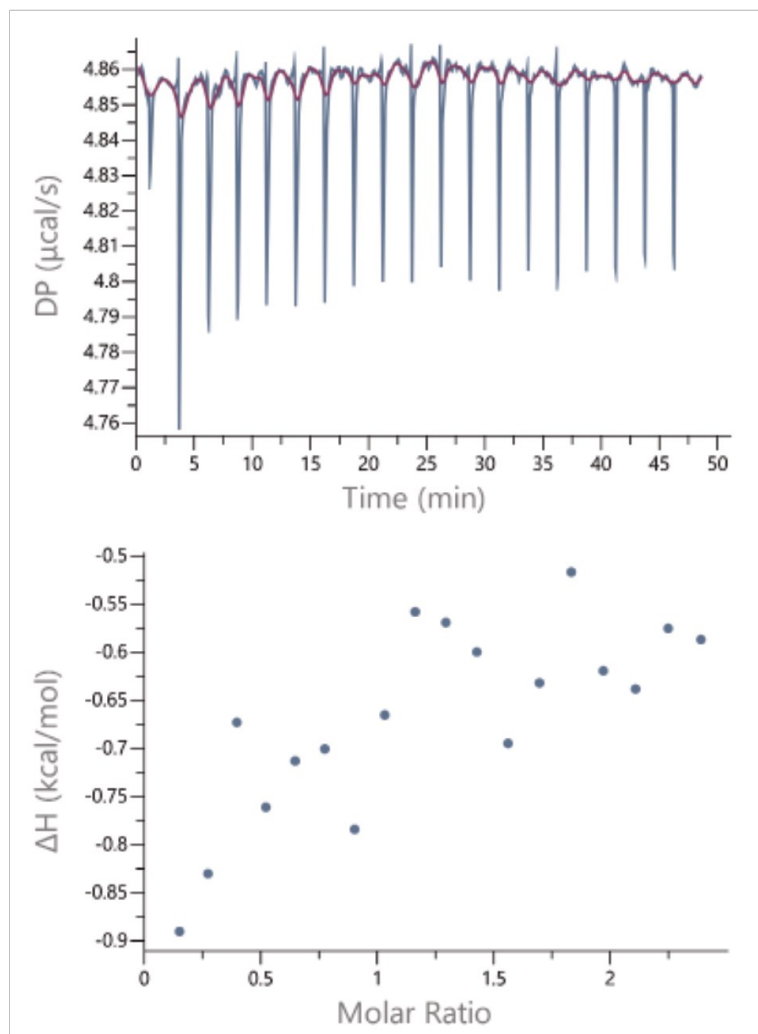


Figure S4

## 5 Chapter 5: The Ubiquitination Status of the Glucagon Receptor Determines Signal Bias

### Context:

Post-translational modifications play a crucial role in GPCR regulation, trafficking, and degradation. A previous study showed that GCGR is constitutively ubiquitinated at the plasma membrane and undergoes glucagon-stimulated endocytosis and deubiquitination in the endosomes. Here, we showed that K333 is the main ubiquitination site for the GCGR, and that the ubiquitination status of this receptor regulates its signal transduction mechanism. In the deubiquitinated state, GCGR exhibits decreased G protein activation, an increase in  $\beta$ -arrestin recruitment, as well as increase in p38 MAPK pathway activation. Despite this signaling bias, deubiquitinated GCGR is fully efficient at promoting glucagon-mediated insulin secretion. This study reveals the critical role of ubiquitination in defining the engagement of the GCGR to different signaling transducers.

### Contribution:

I contributed to the design of this study and performed, analyzed, and interpreted the BRET experiments. I also contributed to the writing of the manuscript under the guidance of Dr. Michel Bouvier and Dr. Sudha Shenoy. This study was published in the Journal of Biological Chemistry (Kaur S, Sokrat B, Capozzi ME, et al. The Ubiquitination Status of the Glucagon Receptor determines Signal Bias. Journal of Biological Chemistry. 2023:104690).



# The Ubiquitination Status of the Glucagon Receptor determines Signal Bias

Suneet Kaur<sup>1,7\*</sup>, **Badr Sokrat**<sup>3,4\*</sup>, Megan E. Capozzi<sup>5\*</sup>, Kimberley El<sup>5</sup>, Yushi Bai<sup>1</sup>, Aeva Jazic<sup>1</sup>, Bridgette Han<sup>1</sup>, Kaavya Krishnakumar<sup>6</sup>, David A. D'Alessio<sup>5</sup>, Jonathan E. Campbell<sup>5</sup>, Michel Bouvier<sup>3,4</sup>, and Sudha K. Shenoy<sup>1,2,#</sup>

1 Division of Cardiology, Department of Medicine, Duke University Medical Center, Durham, NC 27710, USA

2 Department of Cell Biology, Duke University Medical Center, Durham, NC 27710, USA

3 Department of Biochemistry and Molecular Medicine, University of Montreal, Montreal, Quebec, H3T 1J4 Canada.

4 Institute for Research in Immunology and Cancer, University of Montreal, Montreal, Quebec, H3T 1J4 Canada.

5 Division of Endocrinology, Department of Medicine, Duke Molecular Physiology Institute, Duke University, Durham, NC 27710, USA

6 Department of Molecular and Cellular Physiology, Stanford University School of Medicine, Stanford CA 94305

7 Present Address: Laboratory of Signal Transduction, National Institute of Environmental Health Sciences, NIH, Research Triangle Park, NC 27709

\*: These authors have contributed equally to the manuscript

#: Corresponding author

## Abstract

The pancreatic hormone glucagon activates the glucagon receptor (GCGR), a class B seven-transmembrane G protein-coupled receptor (GPCR) that couples to the stimulatory heterotrimeric Gs protein and provokes protein kinase A-dependent signaling cascades vital to hepatic glucose metabolism and islet insulin secretion. Glucagon-stimulation also initiates recruitment of the endocytic adaptors,  $\beta$ -arrestin1 and  $\beta$ -arrestin2, which regulate desensitization and internalization of the GCGR. Unlike many other GPCRs, the GCGR expressed at the plasma membrane is constitutively ubiquitinated and upon agonist-activation, internalized GCGRs are deubiquitinated at early endosomes and recycled via Rab4-containing vesicles. Herein we report a novel link between the ubiquitination status and signal transduction mechanism of the GCGR. In the deubiquitinated state, coupling of the GCGR to Gs is diminished, while binding to  $\beta$ -arrestin is enhanced with signaling biased to a  $\beta$ -arrestin1-dependent p38 mitogen activated protein kinase (MAPK) pathway. This ubiquitin-dependent signaling bias arises through the modification of lysine333 (K333) on the cytoplasmic face of transmembrane helix V. Compared with the GCGR-WT, the mutant GCGR-K333R has impaired ubiquitination, diminished G protein coupling and protein kinase A signaling, but unimpaired potentiation of glucose-stimulated-insulin secretion in response to agonist-stimulation, which involves p38 MAPK signaling. Both WT and GCGR-K333R promote the formation of glucagon-induced  $\beta$ -arrestin1-dependent p38 signaling scaffold that requires canonical upstream MAPK-Kinase3, but is independent of Gs, Gi and  $\beta$ -arrestin2. Thus ubiquitination/deubiquitination at K333 in the GCGR defines the activation of distinct transducers with the potential to influence various facets of glucagon signaling in health and disease.

## Introduction

The peptide hormone glucagon secreted by the pancreatic  $\alpha$ -cells and the class B seven-transmembrane G protein-coupled receptors (GPCRs) that are activated by glucagon play a fundamental role in regulating blood glucose levels. Glucagon activates two class B GPCRs, namely, the glucagon receptor (GCGR) and the glucagon-like peptide 1 receptor (GLP-1R) (1). These two receptors are expressed in pancreatic beta-cells and can promote insulin secretion in response to glucagon stimulation, although GLP-1R is activated by glucagon with a lower potency than GCGR (2, 3, 4, 5). The ability of these receptors to regulate insulin release have established both the GLP-1R and GCGR as major targets for developing new treatments for type II diabetes (T2D). Additionally, secreted glucagon acts on the GCGR expressed in hepatocytes and not only enhances glucose production, but also regulates amino acid and lipid metabolism (6, 7, 8).

Agonist-stimulation of the GCGR provokes coupling of stimulatory  $G_{\alpha s}$  proteins, and subsequent increase in cellular cAMP leading to activation of Protein Kinase A (PKA)-dependent signaling cascades that have been linked to glycogenolysis and gluconeogenesis in liver hepatocytes and insulin secretion in pancreatic islets (2, 9). In addition to inducing G protein signaling, activated GCGR engages additional versatile transducer proteins, namely, (i) GPCR kinases (GRKs) that phosphorylate seryl/threonyl residues in the GCGR, and (ii)  $\beta$ -arrestins ( $\beta$ arrs) that serve as multifunctional endocytic adaptors (10, 11, 12, 13, 14). Two highly homologous isoforms of  $\beta$ arr ( $\beta$ arr1 and  $\beta$ arr2) bind to agonist-activated GPCRs to block G protein coupling and attenuate G protein signaling (10, 14, 15).  $\beta$ ArRs also promote internalization and trafficking of activated GPCRs and serve as signal transducers to promote endosomal signaling (14, 16).

The post-translational modification known as ubiquitination has been shown to regulate the intracellular trafficking and signaling of a growing list of GPCRs, by modifying either the GPCR itself, GRK2,  $\beta$ arr2 or other associated proteins (17, 18, 19). Although ubiquitination of mammalian GPCRs and its functional role was reported two decades ago (20, 21), ubiquitination of the GCGR was uncovered only recently (22). GCGR localized at the plasma membrane is ubiquitinated in quiescent cells, and agonist-stimulation provokes rapid deubiquitination of internalized GCGRs by two distinct enzymes: (1) ubiquitin-specific peptidase 33 (USP33) and (2)

signal transducing adaptor molecule-binding protein (STAMBP) (22). For a handful of GPCRs, ubiquitination of either the receptor or of  $\beta$ arr2 has been shown to promote mitogen-activated protein kinase (MAPK) signaling through canonical or non-canonical activation mechanisms (23, 24, 25, 26). We therefore evaluated signaling properties of the GCGR constructs impaired in ubiquitination and found a novel link between the ubiquitination profile and signal transduction competency of the GCGR: when basally ubiquitinated, the GCGR signals through Gs protein coupling as well as via  $\beta$ -arr1 signaling, whereas when locked in a deubiquitinated state, the GCGR couples poorly to Gs and the signaling is biased toward a  $\beta$ arr1-dependent mechanism.

## Results

### *GCGR-5KR provokes diminished G protein-mediated signaling, but enhanced $\beta$ arrestin association and p38 MAPK activation*

To evaluate whether the ubiquitination status of the GCGR affects its signaling properties, we compared GCGR-5KR (Fig 1A) with GCGR-wild type (WT) for its ability to activate the heterotrimeric G protein Gs and generate cyclic adenosine 3',5'-monophosphate (cAMP) after agonist stimulation. We observed a rightward shift of the cAMP concentration-response curve (5-fold change in EC50) for GCGR-5KR relative to GCGR-WT, in addition to a 3-fold reduction in the maximal response (E-max) (Fig 1B). This substantial decrease in G protein activation by GCGR-5KR is not attributed to differences in receptor expression as revealed by confocal microscopy (Fig 1C) and western blotting (Fig 1D). Additionally, we observed a corresponding reduction of glucagon-induced phosphorylation of cAMP response element-binding protein (CREB) at Ser133, by GCGR-5KR compared with GCGR-WT (Fig 1E, 1F). Ser133 in CREB is predominantly phosphorylated via the cAMP/protein kinase A (PKA) pathway (27, 28). Taken together, GCGR-5KR displays deficiency in ubiquitination (22), cAMP generation and PKA activity (Fig 1A-F). Despite these deficiencies in Gs activation, we detected an augmentation in the association of endogenous  $\beta$ arrestin ( $\beta$ arr) with the GCGR-5KR compared to GCGR-WT as assessed by co-immunoprecipitation (Fig 1G-H).  $\beta$ -arr 1 and  $\beta$ arr2 are not only involved in the desensitization and internalization of GPCR proteins, but are also known to scaffold MAP kinases leading to  $\beta$ -arr-mediated signaling (10, 16, 29, 30, 31, 32). Our assays revealed a more robust activation of p38 MAPK by GCGR-5KR than by GCGR-

WT upon agonist-stimulation (Fig 1I-J), while agonist-induced p42/p44 ERK activation was only minimally augmented by GCGR-5KR compared to GCGR-WT (Fig S1). Accordingly, differential ubiquitination status of the GCGR promotes differences at transducer coupling of the GCGR. A deubiquitinated state of the GCGR facilitates binding of  $\beta$ arrs and activation of p38 MAPK while concomitantly reducing G protein coupling.

*Lysine333 is a critical site in the GCGR for engendering ubiquitin-dependent signal bias between cAMP production and p38 MAPK activation*

To evaluate the contribution of each of the five lysine residues that are putative target sites for ubiquitination, we generated and tested five separate GCGR mutants, each with one of the lysines (K169, K333, K406, K423, or K451) mutated to arginine. In our ubiquitination assays, all of these mutants with only a single lysine changed to arginine, recapitulated the pattern of glucagon-induced deubiquitination possessed by the WT, except the mutant GCGR-K333R, which showed markedly less ubiquitination at baseline and no further decrease after glucagon stimulation (Fig 2A and 2B). The GCGR mutants, K423R and K451R presented greater basal ubiquitination compared with GCGR-WT, but nonetheless were rapidly deubiquitinated with agonist stimulation (Fig 2A and 2B). Each of the GCGR single lysine mutant showed normal expression at the cell membrane, which was equivalent to the pattern obtained for GCGR-WT as assessed by immunostaining and confocal microscopy (Fig 2C). As observed with the GCGR-5KR, glucagon-induced cAMP accumulation was also significantly reduced in cells expressing GCGR-K333R compared with GCGR-WT and the other four lysine mutants as shown by both a reduced potency (6-fold increase in EC<sub>50</sub> for GCGR-K333R) and efficacy (30% decrease in E-max), suggesting a direct correlation between GCGR ubiquitination status and G protein activation (Fig 2D-F). In stark contrast to the blunted effect on cAMP response, GCGR-K333R promoted a much more robust p38 MAPK activation than GCGR-WT and all other single GCGR single lysine mutants (Fig 2G-H). In essence, the signal bias between G protein coupling and p38 MAPK activation invoked by the GCGR-5KR, was replicated by the GCGR-K333R, suggesting that Lys333 is the site targeted for GCGR ubiquitination at the basal state and for deubiquitination after agonist activation. Our results suggest that ubiquitin tag appended at Lys333 in the GCGR can define its potency for G

protein coupling. Our data also suggest that in a deubiquitinated state (as mimicked by the ubiquitin-impaired GCGR-K333R), the GCGR is poised for promoting robust p38 MAPK signaling.

To ascertain if the ubiquitination status of GCGR influences its interaction with G protein complexes and  $\beta$ arr isoforms, we utilized the recently developed enhanced bystander bioluminescence resonance energy transfer (ebBRET) assay (33, 34, 35). We employed mini-Gs (35) and  $\beta$ arr, which are tagged with Renilla Luciferase (RLucII) and assessed their agonist-induced translocation to rGFP-tagged plasma membrane marker (rGFP-CAAX) in HEK-293 cells expressing WT or mutant GCGR (Fig 2I-K). Agonist concentration-dependent recruitment of mini-Gs to the plasma membrane in cells expressing GCGR-K333R or GCGR-5KR was significantly impaired as compared with cells expressing GCGR-WT or all other lysine mutants as reflected by a decrease in both the potency and efficacy of glucagon to promote mini-Gs recruitment (Fig 2I). Accordingly, we infer that the association of mini-Gs is weakened when the GCGR is in a deubiquitinated state. We next assessed agonist-induced BRET between  $\beta$ arr1-RLucII and rGFP-CAAX (Fig 2J) as well as  $\beta$ arr2-RLucII and rGFP-CAAX (Fig 2K) in HEK-293 cells expressing GCGR-WT or each GCGR lysine mutant construct. GCGR-K333R, and GCGR-5KR, that were impaired in coupling to mini Gs, showed enhanced  $\beta$ arr1 (Fig 2J) as well as  $\beta$ arr2 recruitment (Fig 2K) than either GCGR-WT or other GCGR single lysine mutants. This was reflected by an increase in potency and efficacy for  $\beta$ arr1 and potency only for  $\beta$ arr2 for glucagon-promoted recruitment to the plasma membrane. These results support our inference that in a deubiquitinated state, the GCGR is poised for increased  $\beta$ arr association, and decreased Gs coupling than in a ubiquitinated state.

*GCGR-induced p38 MAPK activation is dependent on  $\beta$ arrestin1 and canonical upstream kinase MKK3, but not on  $\beta$ arrestin2 or non-canonical upstream kinase TAB1*

$\beta$ arrs are multifunctional adaptor proteins, and not only do they block G protein coupling, but also promote GPCR endocytosis, and act as scaffolds for propagating and localizing MAPK activities (14, 15, 32, 36). Despite sharing 78% amino acid identity and overlapping functions in GPCR desensitization and trafficking, the two  $\beta$ arr isoforms can have non-redundant roles in signal transduction (37, 38, 39). Thus, to delineate the contribution of individual  $\beta$ arr in the activation of p38 MAPK we silenced their gene expression using previously validated small

interfering RNA (siRNA) targeting each isoform (16) and analyzed the effect on GCGR-induced phosphorylation of p38 MAPK. In our assays, 48 hours after transient transfection with respective siRNA oligonucleotides the abundance of the targeted isoform(s) was reduced by 85% for  $\beta$ arr1 and by 80% for  $\beta$ arr2. Knockdown of  $\beta$ arr1 led to statistically significant reduction in GCGR-stimulated p38 MAPK activation compared to control knockdown conditions whereas  $\beta$ arr2 knockdown in the continuous presence of  $\beta$ arr1 produced little change compared to samples with control siRNA knockdown (Fig 3A-B). We tested the same experimental samples for the levels of GCGR-induced phospho-CREB and found that neither  $\beta$ arr1 or  $\beta$ arr2 knockdown affected glucagon-activated CREB (Fig S2 A-B). In order to ascertain whether the  $\beta$ -arrestin-mediated p38 MAPK activation is applicable to other model systems, we also tested the effect of siRNA-mediated knockdown of each  $\beta$ -arr isoform in the widely used incretin-responsive INS-1  $\beta$ -cell line 832/3 (40). The knockdown efficiency for each  $\beta$ -arr isoform in INS-1 cells was comparable to what we obtained in HEK-293 cells. As in HEK-293 cells, GCGR-induced p38 MAPK activity was almost completely abolished in INS-1 cells with  $\beta$ -arr1 knockdown as compared with cells transfected with control siRNA or a  $\beta$ -arr2 targeting siRNA (Fig 3C-D). These data indicate that  $\beta$ arr1 selectively promotes GCGR-induced p38 MAPK activity, while  $\beta$ arr2 appears to have no major role in this signaling pathway.

p38 MAPK is activated via a cascade of phosphorylation events involving at least two other kinases acting sequentially. The first step is activation of one of ten potential MAP3Ks, which can in turn phosphorylate and activate one of three potential MAP2Ks (41) thus leading p38 MAPK phosphorylation. When activated, MAP2Ks directly phosphorylate the activation loop of p38 on Thr and Tyr residues, leading to a conformational change that results in kinase activation (41). Of the three MAP2Ks, namely, MKK3, MKK4 and MKK6 expressed in mammalian cells, MKK3 is a commonly employed upstream kinase that specifically targets p38 activation. p38 MAPK is also activated through a non-canonical mechanism that is independent of the MAP2Ks and involves autophosphorylation triggered by the binding of TGF- $\beta$ -activated protein kinase 1 (TAK1) binding protein 1 (TAB1) to p38 MAPK (42). To elucidate the pathways responsible for the phosphorylation of p38 MAPK induced by glucagon, we employed siRNA targeting MKK3 and TAB1 which led to >85% knockdown of target protein in each case and tested their effects on

GCGR-induced p38 phosphorylation. GCGR-induced phosphorylation of p38 MAPK was significantly reduced when we knocked down MKK3 in comparison to cells transfected with control siRNA (Fig 3C-D). Conversely, knockdown of TAB1 had no effect on glucagon-induced p38 MAPK activation (Fig 3E-F). Additionally, MKK3 knockdown had no effect on GCGR-induced CREB activity (Fig S2 C-D).

For the GCGR-K333R,  $\beta$ arr1 knockdown caused a significant reduction in p38 MAPK activation compared with control knockdown conditions, whereas  $\beta$ arr2 knockdown had no discernable effect on agonist-induced p38 MAPK activity (Fig 4A-B). Our experiments revealed substantial reduction in not only MKK3 expression, but also p38 phosphorylation with MKK3 siRNA transfection, compared with control siRNA transfections (Fig 4C-D). These data indicate that GCGR-induced p38 MAPK activity proceeds through canonical mechanisms involving MKK3 and  $\beta$ arr1 and that CREB activation stimulated by glucagon, which is unaffected by  $\beta$ arr1 knockdown proceeds through mechanisms independent of MKK3.

*GCGR-induced p38 MAPK activation is independent of PKA and inhibitory heterotrimeric G protein, Gi*

Prior studies have shown that p38 MAPK activity induced by  $\beta$ 2AR agonist-stimulation proceeds in a biphasic manner, where the initial activation of p38 MAPK is  $\beta$ arr1-dependent, while the later phase is G-protein/cAMP/PKA dependent (43). Therefore, to further address the mechanism of p38 MAPK activation via the GCGR, we silenced the expression of PKA isoforms, PKA $\alpha$  and PKA $\beta$  using previously validated siRNA (44, 45). While we obtained >80-85% reduction of respective PKA isoform with siRNA transfections, agonist-induced p38 MAPK activation was significantly increased compared with cells transfected with control siRNA (Fig. 5A and 5B). Additionally pretreatment with the PKA inhibitor, 6-22, also augmented p-38 MAPK phosphorylation by ~35% when compared with samples that were not treated with the inhibitor (Fig S3A-B). These data suggest that cAMP/PKA pathway might be inhibitory to GCGR-induced p38 MAPK activity. Using the same PKA knockdown experimental samples, we tested if GCGR-induced CREB activity is dependent on PKA expression (Fig S2 E-F). We obtained a ~40% decrease in the glucagon induced activation of CREB with the silencing of PKA $\alpha$  and no reduction with PKA $\beta$  knockdown as



compared with CREB activity in control knockdown samples (Fig S2 E-F). Additionally, PKA inhibition significantly reduced CREB activation (Fig S3C-D) with GCGR agonist stimulation. Accordingly, we infer that in HEK-293 cells, PKA activity may impede GCGR-induced p38 MAPK activity, and that PKA $\alpha$  is involved in GCGR-induced CREB activation.

As MAPK activity generally triggered by GPCRs and by  $\beta$ arr-dependent mechanisms is sensitive to Bordetella pertussis toxin (PTX) treatment and linked with the recruitment and/or activation of the inhibitory Gi/o proteins (16, 46, 47, 48, 49) we also assessed the effect of PTX pre-incubation on GCGR-induced p38 MAPK activity (Fig. 5C and 5D). Glucagon-induced p38 MAPK activity remained unchanged in cells pre-treated with PTX, suggesting that GCGR-induced p38 MAPK phosphorylation is independent of Gi/o activity. Since the extent of PTX sensitivity of MAPK relies on the clonal properties of HEK-293 cells (50), we also tested the same cells that we used for glucagon stimulation, to assess p38 MAPK activity triggered by endogenously expressed  $\beta$ 2ARs. Isoproterenol-stimulated phosphorylation of p38 MAPK was reduced by 60% in the presence of PTX, confirming that  $\beta$ 2AR-induced p38 activity involves Gi proteins (Fig 5E-F). Overall, our data show that GCGR-induced p38 MAPK activation is not promoted by either Gs/PKA or Gi proteins in HEK-293 cells.

*Diverse roles of  $\beta$ arr in promoting desensitization, trafficking and deubiquitination in the overall framework of  $\beta$ arr bias at the GCGR*

$\beta$ arrs were originally discovered for their ability to block G protein coupling and dampen second messenger responses triggered by GPCR activation (10, 15). To dissect the role of  $\beta$ arr1 and  $\beta$ arr2 in dampening GCGR-induced cAMP generation, we undertook a gain of function approach, by reconstituting the expression of individual  $\beta$ arr in a  $\beta$ arr1/2 null background (16). We also used corresponding parental cells to evaluate the cAMP response in cells with endogenous  $\beta$ arrs (16). Compared with cAMP generated in the parental cells, the signals from CRISPR  $\beta$ arr1 /2 KO were significantly increased, as evident from the increase in E-max; however, in the KO cells in which  $\beta$ arr expression was rescued, cAMP generation closely matched the pattern obtained in the parental cells (Fig S4A and S4B). We also confirmed the expression of endogenous, and exogenous  $\beta$ arrs as well as that of GCGR-WT, in all samples (Fig S4C). These data indicate that  $\beta$ arr1 and  $\beta$ arr2

have a redundant role in desensitizing G protein mediated cAMP signaling triggered by GCGR activation.

We next assessed the contribution of individual  $\beta$ arr isoforms in mediating internalization, and endosomal trafficking of GCGR-WT and the ubiquitin-impaired GCGR-K333R. We generated RLuc8-tagged GCGR constructs and confirmed that their signaling profiles were comparable to that of untagged GCGR (Fig S5). To measure internalization, we determined disappearance of the GCGR from the plasma membrane leading to a decrease in ebBRET with rGFP-CAAX (33) co-expressed in parental versus  $\beta$ arr1/2 KO CRISPR cells that were reconstituted with individual, or both  $\beta$ arr1/2 constructs (Fig 6A-B). Internalization of GCGR-WT and of GCGR-K333R was impaired in the  $\beta$ arr1/2 KO cells, compared with parental cells or with cells re-expressing  $\beta$ arrs. The trafficking of GCGR-WT as well as GCGR-K333R to FYVE-endosomes was defective in  $\beta$ arr1/2 KO cells as compared with parental cells, and reconstitution with  $\beta$ arr1 and/or  $\beta$ arr2 led to more internalization than in parental cells (Fig 6C-D). Additionally, GCGR-K333R endosomal trafficking was significantly increased compared to that of GCGR-WT in parental cells (Fig 6E). We next evaluated if the activation of GCGR-WT and GCGR-K333R induced differential recruitment of each  $\beta$ arr isoform to early endosomes. We measured agonist-induced ebBRET between RLucII tagged  $\beta$ arr1 or  $\beta$ arr2, rGFP-FYVE in cells expressing GCGR-WT, or GCGR-K333R (Fig 6F-G). Association of  $\beta$ arr1 with FYVE endosomes was significantly enhanced in cells expressing GCGR-K333R compared with WT (Fig 6F). Recruitment of  $\beta$ arr2 with FYVE endosomes was also better with GCGR-K333R than GCGR-WT, but failed to reach statistical significance as compared with the association induced by GCGR-WT (Fig 6G). Taken together, these results suggest that the internalization of GCGR-K333R and localization in early endosomes is enhanced as compared with the GCGR-WT, and this trafficking is supported by the increased recruitment of  $\beta$ arr1 to the activated receptor in early endosomes.

$\beta$ arrs act as important adaptors for promoting ubiquitination and deubiquitination of GPCRs and non-GPCR proteins (17, 32, 51). To define the contribution of  $\beta$ arr in facilitating deubiquitination we first tested the ubiquitination profile of GCGR-WT in the presence and in the complete lack of both  $\beta$ -arr isoforms. We used three independent CRISPR  $\beta$ arr1/2 KO (16) and their cognate parental HEK-293 cells (labelled as HR, SL or AI CRISPR) which were stably transfected with GCGR-

WT (Fig S6 A-F). In these assays glucagon-induced deubiquitination was obtained not only in all the three parental cells, but also in the respective CRISPR  $\beta$ -arr1/2 KO cells (Fig S6 A-F). Interestingly, the GCGR protein band displays a retarded mobility in SDS gels with agonist stimulation (Fig S6), which can be attributed to agonist-induced phosphorylation (52, 53). The exact role of GCGR phosphorylation in the context of agonist-induced deubiquitination remains to be defined. Correlating with the agonist-induced deubiquitination of GCGR obtained in the absence of  $\beta$ arrs, recruitment of cognate deubiquitinases (22), namely, ubiquitin specific protease 33 (USP33) and STAM binding protein (STAMBP) to GCGRs occurs efficiently in the absence of  $\beta$ arr expression (Fig S7). These data collectively suggest that although GCGRs in a deubiquitinated state favor  $\beta$ arr interaction and possess signaling bias,  $\beta$ arrs are not critical to induce a conformational change by facilitating deubiquitination.

*Signaling and insulin secretion by GCGR-WT and GCGR-K333R in INS-1  $\beta$ -cell line and isolated pancreatic islets*

To evaluate whether the ubiquitin-driven signal bias obtained in HEK-293 cells is applicable to physiologically relevant systems, we expressed either GCGR-WT or GCGR K333R using adenovirus in the  $\beta$ -cell line 832/3 (40, 54). The adenoviral vectors in which gene expression is controlled by rat insulin promoter (Figure S8A), were generated by utilizing a recently developed versatile cloning platform (55). The transduction efficiency and protein expression levels of GCGR-WT and GCGR-K333R were equivalent as detected by imaging and western blotting (Fig 7A, Fig S8B-C). INS-1  $\beta$ -cells express endogenous GCGRs (56), and glucagon-stimulation of cells infected with control adenovirus produced a weak response for p38 MAPK and  $\sim$ 1.5 fold increase in CREB phosphorylation (Figure 7A-C). p38 MAPK activation was significantly increased by exogenous GCGR-K333R than GCGR-WT (Fig 7A-B). In contrast, the phospho-CREB induced by GCGR-K333R was significantly decreased compared to that provoked by GCGR-WT (Fig 7A, C). These results affirm the preferential coupling of the deubiquitinated GCGR K333R to p38 MAPK signaling versus Gs/PKA signaling that we obtained in HEK-293 cells to be prevalent in the  $\beta$ -cells.

Glucagon stimulates insulin secretion through both the GLP-1R and GCGR, both expressed in islet  $\beta$ -cells and INS-1 cells, prompting us to utilize a GCGR specific agonist, 44-0410 to assess insulin

secretion independent of GLP-1R activation (2). Prior studies in the  $\beta$ -cell line INS-1 832/3 have shown that endogenous GCGR expressed in these cells have negligible effect in potentiating glucose-stimulated insulin secretion (GSIS), and insulin secretion is mostly attributed to the activation of endogenous GLP-1R in INS-1 cells (12, 57). In keeping with these reports, while high glucose led to a significant increase in insulin secretion, there was no potentiation of this GSIS with increasing doses of 44-0410 in INS-1 832/3 cells, with and without control adenovirus transduction (Fig 7D). On the other hand, agonist-stimulation of overexpressed GCGR-WT, and GCGR-K333R provoked significantly more insulin secretion than induced by high glucose conditions (Fig 7D). Accordingly, in INS-1 832/3 despite the differences in signaling via the GCGR-WT and GCGR-K333R (Fig 7A-C), the effect on GSIS by both GCGR constructs was equivalent (Fig 7D). To discern if p38 MAPK activation by GCGR-WT and GCGR-K333R (Fig 7A-C) is linked to the augmentation of GSIS induced by GCGR agonism (Fig 7D), we pretreated INS-1 cells expressing these constructs with the p38 inhibitor SB 203580 or corresponding vehicle and assessed insulin secretion (Fig 7E, Fig S8D). Indeed, for both GCGR-WT and GCGR-K333R p38 inhibition eliminated the GCGR-induced augmentation of GSIS, while the inhibitor had no effect on GSIS itself (Fig 7E & Fig S8D). These results suggest that in INS-1 cells, the acute activation of p38 MAPK is important for GCGR-induced insulin secretion. Taken together these results support the notion that the observed agonist-promoted GSIS for both wild-type and K333R-GCGR likely results from p38 activation in the INS-1  $\beta$ -cells.

Although the  $\beta$ -cell Gcgr is a less insulinotropic receptor compared to the  $\beta$ -cell Glp1r, it is still required for the full insulinotropic effects of native glucagon in vivo (2, 3). Importantly, the GCGR agonist 44-0410 fails to stimulate insulin secretion in pancreatic islets from Gcgr $\beta$ cell<sup>-/-</sup> mice despite the presence of the Glp1r (2). Therefore, we utilized isolated islets from Gcgr $\beta$ cell<sup>-/-</sup> islets transfected with either GCGR-WT or GCGR-K333R and 44-0410 agonist activation as a functional assay in primary  $\beta$ -cells to test the ability of either receptor to stimulate insulin secretion (Fig 8 and Fig S9). Although adenoviral transduction of INS-1 832/3 cells produced equivalent expression of GCGR-WT and GCGR-K333R (Fig 8A and S9), for reasons unknown there was repeatedly much lesser expression of GCGR-K333R than GCGR-WT in isolated islets; in most experimental replicates, GCGR-WT expression was 3-5 fold higher than the mutant (Fig 8, and Fig S9). While the

transduction efficiency of GCGR-K333R was similar to that of GCGR-WT virus, immunostaining revealed weaker expression of the mutant as compared with the WT (Fig S9B). Remarkably, expression of either GCGR-WT or GCGR-K333R provoked an insulinotropic response to 44-0410 in a manner that was proportional to the amount of GCGR expression (Fig 8A and Fig S9). Since overall GCGR-WT expression was much higher than the mutant, we observed the greater rate of insulin secretion in response to 44-0410 than in samples expressing the mutant (Fig S9 C-D). However, normalization of the insulin secretion response produced by 44-0410 agonist as a function of the level of GCGR showed the rate of insulin secretion was equivalent between GCGR-WT and GCGR-K333R (Fig 8B). The response to glucose or KCl was also the same between groups (Fig 8C-D). Accordingly, these results suggest that despite its impaired G protein coupling, the deubiquitinated GCGR-K333R is functionally competent in promoting insulin secretion in pancreatic islets, which might proceed through  $\beta$ -arrestin-mediated mechanisms.

*$\beta$ arr1 isoform exclusively scaffolds p38 MAPK cascade promoted by GCGR agonist-stimulation*

According to our analyses (Fig 2) and that of others (58) both  $\beta$ arrs are effectively recruited to the GCGR, and furthermore both isoforms are able to transduce MAPK activation promoted by multiple GPCRs (14); hence the mechanism that constrains GCGR-mediated activation of p38 MAPK to be selective for  $\beta$ arr1 is perhaps an intrinsic property of the proteins assembling as a signaling complex (15). Therefore, we analyzed whether the scaffolding of p38 MAPK and MKK3 by the two  $\beta$ arr isoforms is different when cells are activated by glucagon. We immunoprecipitated HA-tagged  $\beta$ arr1 and  $\beta$ arr2 from HEK-293 cells expressing either GCGR-WT or GCGR-K333R with and without agonist stimulation and analyzed binding of phospho-p38, p38 and MKK3 (Fig 9 A-H). In these experiments,  $\beta$ arr1 but not  $\beta$ arr2 emerged as an efficient scaffold for phospho-p38 activated by the GCGR-WT. Notably,  $\beta$ -arr1 formed complexes with phospho-p38 with GCGR activation, but no agonist-promoted interaction was detected with  $\beta$ -arr2 (Fig 9A-D). The immunoprecipitation assay conducted with cells expressing the GCGR-K333R, which is a  $\beta$ arr-biased mutant, presented a clear distinction for  $\beta$ arr1 scaffolding activity (Fig 9 E-H). We not only detected a more robust association of phospho-p38 with  $\beta$ arr1 than with  $\beta$ arr2, but with the GCGR-K333R activation,  $\beta$ arr1 evidently showed increased agonist-induced binding with unphosphorylated p38, as well as with MKK3. Just as with the GCGR-WT activation, GCGR-K333R

activation decreased  $\beta$ arr2 association with each of the above components that form a p38 MAPK scaffold. Accordingly, our data indicates that upon associating with the GCGR in its deubiquitinated state,  $\beta$ arr1 assumes an activated conformation that enables it to function as an exclusive and efficient scaffold to propagate p38 MAPK signaling (Fig 9I).

## Discussion

Our results reveal a novel link between the ubiquitination profile and signal transduction mechanism of the GCGR: when ubiquitinated, the GCGR signals through G protein coupling as well as  $\beta$ arr recruitment, whereas in the deubiquitinated condition the signaling is biased to  $\beta$ arr1-dependent p38 MAPK activity (Fig 9I). Our data suggests that ubiquitin-driven signaling at the GCGR engages K333 on the cytoplasmic face of transmembrane helix V and furthermore, crystal structure maps K333 at the interface of TM5's collocation with alpha5 helix of G protein in the GCGR-G $\alpha$ s protein complex (59). The exact molecular role of ubiquitin moieties in promoting GCGR-G protein coupling remains to be defined. While the GCGR-K333R is impaired in both ubiquitination and G protein coupling,  $\beta$ -arr recruitment induced by this mutant was significantly increased compared with the wild type GCGR as determined by ebBRET. Accordingly, ubiquitination at K333 may function as a molecular switch for engaging specific transducer pathway(s), which may be further fine-tuned by the balance between ubiquitinated and deubiquitinated GCGR species in cells.

GCGR-K333R overexpression in INS-1 cells promoted signal bias with increased p38 activity, and decreased Gs/PKA dependent CREB activity compared to GCGR-WT overexpression. Prior studies consign cAMP/G protein activity as the sole trigger for glucagon-induced insulin secretion as well as CREB activation (60); however insulin secretion induced by agonism of GCGR-K333R or GCGR-WT overexpression were equivalent in INS-1 cells and in islets. It is likely that when locked in a  $\beta$ -arr biased conformation, the GCGR may engage additional mechanisms aside from PKA activation to promote insulin release.

Bimodal activation of ERK1/2 activation via G protein and  $\beta$ -arr-dependent mechanisms by various GPCRs has been an area of intense investigation for nearly two decades (14, 16). Indeed, a predominant focus of such studies has been on ERK1/2 signaling and its spatio-temporal

regulation by  $\beta$ arr2 (33), and interestingly constitutive activation of ERK1/2 leads to sequestration of GPCRs at endosomes reducing their ability to signal through G proteins (61). Recent investigations on biased agonists of receptors in the secretin-glucagon family have evaluated  $\beta$ arr2 (not  $\beta$ arr1) recruitment and cAMP response and despite a favorable increase in cAMP by GCG-derived ligands, corresponding increases were not obtained for either GCGR-induced insulin secretion in INS-1 cells or glucose production in hepatocytes (57). Phenotyping of missense variants of the GCGR indicates that  $G_{\alpha s}$  is the main signaling pathway that preserves physiological role of the GCGR since defects in cAMP were associated with metabolic syndromes, although the signaling defect was most often associated with reduced binding capacity of the endogenous ligand to GCGR variant (58). Interestingly, the most common missense variant in the GCGR, G40S in the extra cellular domain, which has been linked with non-insulin-dependent diabetes and male adiposity in certain populations has preserved  $G_s$ /cAMP and  $\beta$ arr2 association, but impaired  $\beta$ arr1 recruitment (58).

Together with or independently of GPCR activation, the  $\beta$ arr isoforms can play critical roles in insulin secretion by  $\beta$ -cells and in the pathogenesis of insulin resistance in vivo (62, 63, 64, 65).  $\beta$ arr1 associates with the GLP-1R and mediates agonist-induced signaling to cAMP, CREB, ERK and insulin receptor substrate2 (IRS-2), and augments GSIS in INS-1 cells (12). M3-muscarinic receptor-stimulated increase in insulin release is mediated by receptor phosphorylation/arrestin signaling independent of heterotrimeric G proteins and, mediated by  $\beta$ arr1 activation of protein kinase D1 (66).  $\beta$ -cell  $\beta$ arr1 can enhance sulfonylurea-stimulated insulin secretion by promoting the activation of Epac2-Rap1 signaling that affects insulin vesicle trafficking (67). While there is increasing evidence for distinct roles of  $\beta$ arr isoforms in  $\beta$ -cell health, insulin release, and in hepatocyte glucose production, future elaborate studies are needed to determine the contributions of  $\beta$ arr1 and  $\beta$ arr2 in these paradigms as provoked by the biased GCGR-K333R.

Initially discovered as a protein tag for mobilizing unwanted proteins for degradation by 26S proteasomal machinery (68), ubiquitination has been shown to trigger a plethora of cellular effects (18, 69, 70, 71). The non-proteasomal functions of ubiquitination include protein-protein interaction, protein localization, kinase activation and intracellular trafficking of membrane proteins. While ubiquitination of  $\beta$ arr2 has been linked with GPCR association, endocytosis and

scaffolding functions (32), the role of receptor ubiquitination in engaging MAPK signaling has also been reported for a few GPCRs (19). For the type 1 parathyroid hormone receptor (PTH1R), ubiquitination at the two mapped lysines does not regulate PTH-induced G protein coupling, trafficking or degradation of the receptor, but produces differences in the patterns of ERK and p38 phosphorylation induced by the  $\beta$ arr biased ligand PTH7-34 (26). Ubiquitination of protease-activated receptor 1 (PAR1) and the purinergic receptor P2Y1 engages the kinase TAB2 at endosomes, which can engender autophosphorylation of p38 MAPK (72). The atypical p38 activation by PAR1 does not involve  $\beta$ arr recruitment and is different from the canonical p38 activation by a three-tier kinase cascade that we have identified to be triggered by the GCGR, as facilitated by  $\beta$ arr1 recruitment and scaffolding of MKK3 and p38.

Previous studies have shown that the actions of glucagon on lipid metabolism are mediated through p38 MAPK, AMPK, and peroxisome proliferator-activated receptor  $\alpha$  (PPAR $\alpha$ ) dependent manner, but independent of PKA activity (73, 74, 75). On the other hand, others have argued that chronic glucagon treatment (8 h) does not influence AMPK activity (76), suggesting that this signaling pathway may be more important for the acute, immediate response to glucagon agonism. Other studies have shown that p38 activity occurring in series with cAMP activation promotes hepatic gluconeogenesis by promoting transcription of PPAR  $\gamma$  coactivator 1 as well as phosphorylation of CREB (77). Future studies are needed to define whether glucagon-dependent lipid and glucose homeostasis are regulated by the ubiquitin-dependent bias between G $\alpha$ s and  $\beta$ arr1 signaling. Akin to ERK1/2, p38 MAPK phosphorylates a wide variety of downstream substrates allowing its influence on aspects of cell growth, proliferation and differentiation and the activation of p38 MAPK is balanced by multiple forms of positive and negative control (78). The roles of each  $\beta$ -arrestin isoform in endocytosis and signaling (15, 79) and the relevance of endocytosis in biased signaling of the glucagon family receptors remains a complex issue that deserves future detailed investigations. Future studies that identify the set of specific p38 substrates regulated by  $\beta$ arr1 in GCGR signaling should help to elucidate how insulin release, or gluconeogenesis could be regulated by ubiquitin-driven biased signaling. Furthermore, understanding the mechanisms that regulate GCGR has direct implications for novel GLP-1R/GCGR co-agonists being developed for the treatment of T2D.



## Experimental Procedures

### *Reagents*

Anti-FLAG M2 affinity agarose gel, N-ethylmaleimide, poly-lysine, Triton X-100, and BSA were purchased from Sigma. Lipofectamine 2000™ was purchased from Thermo Fisher Scientific. Glosensor plasmid 22F, and Luciferin reagent were from Promega Inc. The following IgGs were procured from the sources listed: mouse monoclonal c-Myc (catalog no. SC-40), rabbit polyclonal p38 (catalog no. SC-535), anti-PKA $\alpha$  (catalog no. sc-903), anti-PKA $\beta$  (catalog no. sc-904) from Santa Cruz Biotechnology, Inc.; mouse monoclonal anti- $\beta$ -actin (catalog no. A5441) from Sigma; anti-ubiquitin FK1 (BML-PW8805) from Enzo Life Sciences. rabbit polyclonal anti-phospho-p44/42 ERK1/2 (catalog no. 9101), Rabbit polyclonal anti-ERK1/2 (catalog no. 9102), Rabbit polyclonal anti-phospho p38 (catalog no. 9102), MKK3 (catalog no. 8535), TAB1 (catalog no. 3226), STAMBP (catalog no. 5245), rabbit polyclonal Myc tag (catalog no. 2272), rabbit monoclonal GAPDH (HRP conjugate, catalog no. 3683) from Cell Signaling Technology, rabbit polyclonal anti-USP33 (A300-925A) from Bethyl Laboratories. HRP-conjugated secondary antibodies were purchased from GE Biosciences, Cell Signaling Technology and Bethyl Laboratories, Inc. Alexa Fluor 488 or 594-conjugated secondary antibodies were obtained from Invitrogen and used at a dilution of 1:500 for immunofluorescence labeling. PKA inhibitor fragment (6, 7, 8, 9, 10, 11, 12, 13, 14, 15, 16, 17, 18, 19, 20, 21, 22) amide was from Bachem Americas Inc; p38 inhibitor SB 203580 was from Millipore Sigma.

### *Cell lines and plasmids*

HEK-293 cells obtained from American Type Culture Collection were cultured in minimal essential media supplemented with 10% fetal bovine serum and 1 % penicillin/streptomycin. INS-1 832/3 cells were generously provided by Dr. Christopher Newgard, and were cultured according to published protocols (40, 54). Parental and CRISPR  $\beta$ -arr1/2 KO cells were cultured as reported before (16). GCGR-MYC-FLAG plasmid was purchased from Origene Technologies and GCGR-5KR-MYC-FLAG has been reported before (22). GCGR-K169R-MYC-FLAG, GCGR-K333R-MYC-FLAG, GCGR-K406R-MYC-FLAG, GCGR-K423R-MYC-FLAG, and GCGR-K451R-MYC-FLAG were generated by substituting lysine with arginine at position 169 or 333 or 406 or 423 or 451 using a

QuikChange™ site-directed mutagenesis kit (Stratagene). Although each of the above mutant construct expressed to comparable levels of the WT construct as assessed by immunostaining of the MYC tag, and by western blotting of solubilized lysate proteins, we observed minor differences between different constructs in successive experiments. Thus, in some experiments GCGR-K168R detection was slightly at higher levels and GCGR-K333R and GCGR-K451R were detected at slightly lower levels as compared to the GCGR-WT transfections. Gateway® Technology was used to mobilize cDNA sequences of GCGR-MYC-FLAG and GCGR-K333R-MYC-FLAG, along with RIP promoter sequence, and IRES-GFP insert into the adenoviral vector pAd/PL-DEST and recombinant adenoviral stocks were produced by using published methods (55). All plasmids were verified by DNA sequencing. Transfections were performed using Lipofectamine 2000™ (Thermo Fisher Scientific) as per manufacture's protocol.

#### *Immunoprecipitation*

HEK-293 cells expressing GCGR-WT or desired GCGR mutant were stimulated with glucagon after starvation for 1 h in serum free media. Following stimulation cells were solubilized in ice-cold lysis buffer containing 50 mM HEPES (pH 7.5), 2 mM EDTA (pH 8.0), 250 mM NaCl, 10% (v/v) glycerol, and 0.5% (v/v) IGEPAL CA-630 or using RIPA buffer (150 mM NaCl, 50 mM Tris, pH 8.0, 5 mM EDTA, 1% Nonidet P-40 [NP-40], and 0.5% deoxycholate), supplemented with phosphatase and protease inhibitors (1 mM sodium orthovanadate, 10 mM sodium fluoride, 100 μM phenylmethylsulfonyl fluoride, 5 μg/ml leupeptin, 5 μg/ml aprotinin, 1 μg/ml pepstatin A, and 1 mM benzaminidine; buffer was also supplemented with 10 mM N-ethylmaleimide. Lysates were centrifuged for 10 min at 13,000 rpm and protein was measured using Bradford reagent (Bio-Rad). Protein amount between 800-1500 μg was taken for setting up co-immunoprecipitation assays. Within each immunoprecipitation experiment, equivalent protein was used for all samples. The solubilized proteins were rotated end-over-end with the M2-FLAG-agarose (Sigma) or Ant-HA magnetic beads (Pierce) at 4 °C for overnight. The immunoprecipitated complexes were washed 3-4 times with cold lysis buffer and eluted in 2× Laemmli sample buffer.

#### *Assessment of p38, ERK1/2 and CREB activation*

HEK-293 cells requiring signaling analysis (GCGR stables, or cells with knockdown) were plated on 6-well dishes to be at <60% confluent next day. 24 h later cells were incubated in respective serum-free starvation media containing 10 mM HEPES, pH 7.5, and 0.1% BSA. 1 h post-serum starvation, desired stimulation was performed and cells were harvested in 2× Laemmli sample buffer. Samples were centrifuged, cooled on ice and then sonicated briefly before SDS-PAGE and immunoblotting.

#### *Immunoblotting*

Solubilized protein samples were resolved on 4-20% Tris Glycine gels or 10% custom acrylamide gels (ProtoGel, National Diagnostics), and then transferred on 0.2 um Nitrocellulose membrane for western blotting. For blocking of membrane and dilution of secondary antibodies 5% (w/v) dried skim milk powder dissolved in TTBS (0.2% (v/v) Tween 20, 10 mM Tris-HCl (pH 8.0), and 150 mM NaCl) was utilized, while primary antibodies were diluted in 5% (w/v) BSA prepared in TTBS. The enhanced chemiluminescence substrate, Super Signal West Pico Plus reagent was used to detect proteins through charge coupled device camera system (Bio-Rad Chemidoc-XRS). The quantification of protein bands was done by using Image Lab™ software (Bio-Rad).

#### *GloSensor Assay for determining cAMP production*

HEK-293 cells transiently transfected either with GCGR-WT, GCGR single lysine mutants or GCGR-5KR and GloSensor 22F plasmid (Promega) in 6-well dishes. Parallel transfections were set up in 6-well dishes and cells were used at the experiment end-point for preparing extracts that were subjected to SDS-PAGE and Western blot analysis to detect GCGR expression as well as for plating on confocal dishes to complete immunostaining and confocal detection of GCGR expression. For the cAMP assay, cells were detached 4h post-transfection resuspended in clear MEM media containing 2% FBS+1%PS+ 10 mM HEPES and reseeded in 96-well white clear bottomed plates that were previously coated with poly-D-lysine. 18-20h later, cells were washed with Hanks' Balanced Salt Solution (HBSS), GloSensor reagent diluted in HBSS was added and incubation was continued for 1h at 26 °C. Subsequently, GloSensor reagent was replaced with 90 uL of HBSS supplemented with 10 mM HEPES, pH 7.5 and plates were subjected to a baseline pre-read for luminescence on a Synergy Neo2 plate reader driven by Gen5 Software (BioTek Instruments). 10

uL of vehicle or agonist glucagon at desired concentration was added to respective wells, and the plates were immediately read for luminescence at 26 °C.

### *Confocal Microscopy*

HEK-293 cells stably or transiently expressing GCGR construct were seeded on poly-D-lysine coated 20-mm confocal glass bottom dish. Cells were fixed using 5% formaldehyde diluted in Dulbecco's PBS (DPBS) for 20 min. Cells were then permeabilized for 20 min with 0.1% Triton X-100 in 2% BSA and subsequently incubated in anti-MYC 9E10 (Santa Cruz Biotechnology) primary antibody, at 4 °C for overnight. Cells were stained by incubating with secondary antibody conjugated to Alexa fluorophore 488 or 594 at room temperature for 1–2 h. After cell fixation and antibody incubations Cells were washed with DPBS. 2% BSA prepared in DPBS was used for making permeabilizing solution and antibody dilutions. Confocal images were captured with LSM-510 META confocal microscope with filter settings for the respective fluorophores; excitation was at 488 nm (Alexa 488) and 561 nm (Alexa 594).

### *RNA Interference*

Double-stranded siRNA oligonucleotides for control non-targeting sequence or targeting TAB1, MKK3, PKA $\alpha$ , PKA $\beta$ ,  $\beta$ -arr1 or  $\beta$ arr2 were purchased from Dharmacon Inc as described previously (16). Sequences of siRNA oligonucleotides were as follows: control non-targeting sequence: 5'-AAUUCUCCGAACGUGUCACGU-3';  $\beta$ -arrestin1: 5'-AAAGCCUUCUGCGCG-GAGAAU-3';  $\beta$ -arrestin 2: 5' -AAGGA-CCGCAAAGUGUUUGUG-3'; PKA $\alpha$ : 5'-CGUCCUGACCUUUGAGUAU-3'; PKA $\beta$ : 5'-GGUCACAGACUUUGGGUUU-3'; TAB1: 5'CGCAAUUGCCAGAGGGAGU3' ; MKK3: 5'UGGACAAGUUCUACCGG-AA-3'. For siRNA experiments early passage cells at the confluence of 40-50% were transfected with 20 ug of siRNA using Lipofectamine 2000TM in respective serum-free medium. After four hours of transfection cells were supplemented with complete media and incubated at 37 °C for 48 h before assay was performed.

### *INS-1 cell assays*

INS-1 832/3 cells were cultured according to published protocols (40, 54). Cells were seeded on 12-well Corning® BioCoat™ poly-D-Lysine coated dishes and 24 h later were transduced with Ad-

RIP- $\beta$ -Gal-IRES-GFP (5 $\mu$ L/mL), Ad-RIP-GCGR-IRES-GFP (5 $\mu$ L/mL) or Ad-RIP-GCGR-K333R-IRES-GFP (10  $\mu$ L/mL) to obtain equivalent MOI for different constructs. 4 h after infection, media was replaced with complete growth medium, and cells were allowed to recover for 48 h. Cells were serum-starved and stimulated with vehicle or agonist for 15 min and solubilized extracts were analyzed for desired protein expression by western blotting. For measuring insulin secretion, cells were washed with PBS and then incubated in HBSS buffer (114 mM NaCl, 4.7 mM KCl, 1.2 mM KH<sub>2</sub>PO<sub>4</sub>, 1.16 mM MgSO<sub>4</sub>, 20 mM HEPES, 2.5 mM CaCl<sub>2</sub>, 0.2% BSA, pH 7.2) containing 2.5mM glucose. After 1 h, cells in duplicate wells were further treated for 1h for the following conditions: low glucose (2.5 mM), high glucose (12.5 mM), or high glucose + agonist 44-0410 agonist (1 nM, 10 nM, 100 nM). Cell supernatant was carefully collected, and assayed for insulin secretion with the Lumit™ Insulin Immunoassay Kit (Promega #CS3037A01). Insulin content in each sample was normalized to total protein. The monolayers of cells were solubilized in 2 $\times$  Laemmli sample buffer, and total protein in each sample was determined using Pierce 660nm Protein Assay Reagent supplemented with Ionic Detergent Compatibility Reagent (Pierce) according to the manufacturer's protocol.

#### *Islet Isolation and Perifusion*

All animal experiments were performed in accordance with protocols approved by Duke University Institutional Animal Care and Use Committee.

Gcgr  $\beta$ cell<sup>-/-</sup> mice were generated as previously described (2). Briefly, mice with LoxP sites in the Gcgr allele (Gcgr<sup>fl</sup>) were crossed with MIP-CreERT mice and administered tamoxifen for four consecutive days to generate Gcgr $\beta$ cell<sup>-/-</sup> mice. Islets were isolated from mice at least 4 weeks after tamoxifen administration. Islet isolation was performed using a histopaque gradient as previously described (2). Immediately after isolation, islets from a single mouse were incubated with either Ad-RIP-GCGR-IRES-GFP (5 $\mu$ L/mL) or Ad-RIP-K333R-IRES-GFP (10 $\mu$ L/mL) in RPMI for 24 hours. Islets were then allowed to recover for 48-72 hours in RPMI before being perifused. After recovery, 75 islets were handpicked into KRPH buffer (140mM NaCl, 4.7mM KCl, 1.5mM CaCl<sub>2</sub>, 1mM NaH<sub>2</sub>PO<sub>4</sub>, 1mM MgSO<sub>4</sub>, 2mM NaHCO<sub>3</sub>, 5mM HEPES, and 0.1% BSA; pH= 7.4) containing 2.7mM glucose and 100 $\mu$ L Bio-Gel P4 Media (Bio-Rad). Islets were equilibrated for 48 min and

then perfused in experimental conditions shown in Fig S4. Insulin secretion was assessed by Lumit Immunoassay (Promega) and assayed using the EnVision plate reader (Perkin Elmer).

### *BRET assays*

HEK-293 cells were cultured in Dulbecco's Modified Eagle's Medium (DMEM) supplemented with 10% newborn calf serum, 100 units of penicillin, and 100 µg/ml streptomycin. Transient transfections were performed on suspended cells at a density of 0.4 million cells/ml using 25 kDa linear polyethylenimine (PEI) as transfecting agent, at a ratio of 4:1 PEI/DNA. Enhanced bystander BRET (ebBRET) experiments were performed as reported before (33).

Briefly, for  $\beta$ -arrestin1/2 recruitment, cells were transfected with  $\beta$ -arrestin1/2-RlucII (BRET donor) and rGFP-CAAX (BRET acceptor) along with each GCGR construct (WT, single lysine or 5KR mutant construct). For Gs engagement, cells were transfected with mGs-Rluc8 (BRET donor) and rGFP-CAAX (BRET acceptor) to monitor the translocation of mini-G protein to active receptor at the plasma membrane. For receptor trafficking, parental HEK-293 cells or  $\beta$ -arrestin1/2 KO cells were transfected with WT or mutant forms of GCGR-MYC-FLAG fused to Rluc8 (GCGR-MYC-FLAG-Rluc8) along with either rGFP-CAAX (plasma membrane) or rGFP-FYVE (early endosomes).

For ebBRET readings, transfected cells were seeded in 96-well microplates (Greiner) (100 µl/well). Forty-eight hours later, DMEM media was removed, and cells were washed with DPBS (Dulbecco's Phosphate Buffered Saline) and replaced by HBSS (Hank's Balanced Salt Solution). For concentration-response experiments, increasing concentrations of glucagon (GCG) were added and cells were incubated for 10 minutes before adding coelenterazine 400a (2.5µM). BRET values were collected 5 minutes after coelenterazine addition. For kinetic experiments, Prolume Purple (2.5µM) was added for 6 minutes before cell stimulation with 1µM GCG or vehicle and BRET measurement was started immediately after and continued for the indicated times. BRET values were collected on a Tecan Spark multimode microplate reader equipped with filters for BRET2 (400/70 nm (donor) and 515/20 nm (acceptor)). The BRET signal was calculated as the ratio of light emitted by the energy acceptor over the light emitted by the energy donor and the agonist-promoted BRET was calculated by subtracting the BRET signal obtained in presence of vehicle from the BRET signal obtained in presence of agonist.

### *Statistical Analyses*

The quantification for all the experiments is presented as means  $\pm$  S.E.M from experimental replicates indicated in the figure legends. The type of statistical analysis and post-hoc test used are included in each figure legend. We have used GraphPad PRISM version 9 (GraphPad Inc.), and considered a p value of  $< 0.05$  as significant.

### **Declaration of Interests**

M.B. is the president of the scientific advisory Board of Domain Therapeutics which licensed-in some of the BRET-based biosensors, used in this study. All other authors declare no competing interests.

### **Acknowledgements**

We thank Wenli Zhang, Thomas Becker, Mette Johnson and Pavitra Murali for their help and discussions. We are grateful to Caroline Ray for her generous help in generating Rluc8 tagged GCGR plasmid. We gratefully acknowledge Drs. Howard Rockman, and Christopher Newgard for generously providing cell lines and for helpful suggestions. We thank Drs. Asuka Inoue and Stephane Laporte for generously sharing CRISPR cell lines and Dr. Nevin Lambert for providing miniGs-Rluc8 plasmid. We express our gratitude to Drs. Robert J. Lefkowitz and Brian Kobilka for generously sharing reagents. We dedicate this manuscript to the memory of our dear colleague Dr. Marc Caron whose generous help with reagents and access to equipment immensely helped this work.

## References

1. Brubaker, P.L. and Drucker, D.J., (2002) Structure-function of the glucagon receptor family of G protein-coupled receptors: the glucagon, GIP, GLP-1, and GLP-2 receptors. *Recept Channels*. 8(34): p. 179-88.
2. Capozzi, M.E., Svendsen, B., Encisco, S.E., Lewandowski, S.L., Martin, M.D., Lin, H., et al., (2019) beta Cell tone is defined by proglucagon peptides through cAMP signaling. *JCI Insight*. 4(5).
3. Svendsen, B., Larsen, O., Gabe, M.B.N., Christiansen, C.B., Rosenkilde, M.M., Drucker, D.J., et al., (2018) Insulin Secretion Depends on Intra-islet Glucagon Signaling. *Cell Rep*. 25(5): p. 1127-1134 e2.
4. Capozzi, M.E., D'Alessio, D.A., and Campbell, J.E., (2022) The past, present, and future physiology and pharmacology of glucagon. *Cell Metab*. 34(11): p. 1654-1674.
5. El, K., Gray, S.M., Capozzi, M.E., Knuth, E.R., Jin, E., Svendsen, B., et al., (2021) GIP mediates the incretin effect and glucose tolerance by dual actions on alpha cells and beta cells. *Sci Adv*. 7(11).
6. Campbell, J.E. and Drucker, D.J., (2015) Islet alpha cells and glucagon—critical regulators of energy homeostasis. *Nat Rev Endocrinol*. 11(6): p. 329-38.
7. Finan, B., Capozzi, M.E., and Campbell, J.E., (2020) Repositioning Glucagon Action in the Physiology and Pharmacology of Diabetes. *Diabetes*. 69(4): p. 532-541.
8. Galsgaard, K.D., Pedersen, J., Knop, F.K., Holst, J.J., and Wewer Albrechtsen, N.J., (2019) Glucagon Receptor Signaling and Lipid Metabolism. *Front Physiol*. 10: p. 413.
9. Miller, R.A. and Birnbaum, M.J., (2016) Glucagon: acute actions on hepatic metabolism. *Diabetologia*. 59(7): p. 1376-1381.
10. DeWire, S.M., Ahn, S., Lefkowitz, R.J., and Shenoy, S.K., (2007) Beta-arrestins and cell signaling. *Annu Rev Physiol*. 69: p. 483-510.
11. Merlen, C., Fabrega, S., Desbuquois, B., Unson, C.G., and Authier, F., (2006) Glucagon-mediated internalization of serine-phosphorylated glucagon receptor and G $\alpha$  in rat liver. *FEBS Lett*. 580(24): p. 5697-704.
12. Sonoda, N., Imamura, T., Yoshizaki, T., Babendure, J.L., Lu, J.C., and Olefsky, J.M., (2008) Beta-Arrestin-1 mediates glucagon-like peptide-1 signaling to insulin secretion in cultured pancreatic beta cells. *Proc Natl Acad Sci U S A*. 105(18): p. 6614-9.
13. Krilov, L., Nguyen, A., Miyazaki, T., Unson, C.G., Williams, R., Lee, N.H., et al., (2011) Dual mode of glucagon receptor internalization: role of PKC $\alpha$ , GRKs and beta-arrestins. *Exp Cell Res*. 317(20): p. 2981-94.
14. Ahn, S., Shenoy, S.K., Luttrell, L.M., and Lefkowitz, R.J., (2020) SnapShot: betaArrestin Functions. *Cell*. 182(5): p. 1362-1362 e1.
15. Peterson, Y.K. and Luttrell, L.M., (2017) The Diverse Roles of Arrestin Scaffolds in G Protein-Coupled Receptor Signaling. *Pharmacol Rev*. 69(3): p. 256-297.
16. Luttrell, L.M., Wang, J., Plouffe, B., Smith, J.S., Yamani, L., Kaur, S., et al., (2018) Manifold roles of beta-arrestins in GPCR signaling elucidated with siRNA and CRISPR/Cas9. *Sci Signal*. 11(549).
17. Jean-Charles, P.Y., Rajiv, V., and Shenoy, S.K., (2016) Ubiquitin-Related Roles of betaArrestins in Endocytic Trafficking and Signal Transduction. *J Cell Physiol*. 231(10): p. 2071-80.
18. Jean-Charles, P.Y., Snyder, J.C., and Shenoy, S.K., (2016) Chapter One – Ubiquitination and Deubiquitination of G Protein-Coupled Receptors. *Prog Mol Biol Transl Sci*. 141: p. 1-55.



19. Dores, M.R. and Trejo, J., (2019) Endo-lysosomal sorting of G-protein-coupled receptors by ubiquitin: Diverse pathways for G-protein-coupled receptor destruction and beyond. *Traffic*. 20(2): p. 101-109.
20. Marchese, A. and Benovic, J.L., (2001) Agonist-promoted ubiquitination of the G protein-coupled receptor CXCR4 mediates lysosomal sorting. *J Biol Chem*. 276(49): p. 45509-12.
21. Shenoy, S.K., McDonald, P.H., Kohout, T.A., and Lefkowitz, R.J., (2001) Regulation of receptor fate by ubiquitination of activated beta 2-adrenergic receptor and beta-arrestin. *Science*. 294(5545): p. 1307-13.
22. Kaur, S., Chen, Y., and Shenoy, S.K., (2020) Agonist-activated glucagon receptors are deubiquitinated at early endosomes by two distinct deubiquitinases to facilitate Rab4a-dependent recycling. *J Biol Chem*. 295(49): p. 16630-16642.
23. Shenoy, S.K., Barak, L.S., Xiao, K., Ahn, S., Berthouze, M., Shukla, A.K., et al., (2007) Ubiquitination of beta-arrestin links seven-transmembrane receptor endocytosis and ERK activation. *J Biol Chem*. 282(40): p. 29549-62.
24. Shenoy, S.K. and Lefkowitz, R.J., (2005) Receptor-specific ubiquitination of betaarrestin directs assembly and targeting of seven-transmembrane receptor signalosomes. *J Biol Chem*. 280(15): p.15315-24.
25. Grimsey, N.J., Aguilar, B., Smith, T.H., Le, P., Soohoo, A.L., Puthenveedu, M.A., et al., (2015) Ubiquitin plays an atypical role in GPCR-induced p38 MAP kinase activation on endosomes. *J Cell Biol*. 210(7): p. 1117-31.
26. Zhang, Q., Xiao, K., Liu, H., Song, L., McGarvey, J.C., Sneddon, W.B., et al., (2018) Site-specific polyubiquitination differentially regulates parathyroid hormone receptor-initiated MAPK signaling and cell proliferation. *J Biol Chem*. 293(15): p. 5556-5571.
27. Gonzalez, G.A. and Montminy, M.R., (1989) Cyclic AMP stimulates somatostatin gene transcription by phosphorylation of CREB at serine 133. *Cell*. 59(4): p. 675-80.
28. Delghandi, M.P., Johannessen, M., and Moens, U., (2005) The cAMP signalling pathway activates CREB through PKA, p38 and MSK1 in NIH 3T3 cells. *Cell Signal*. 17(11): p. 1343-51.
29. Reiter, E., Ahn, S., Shukla, A.K., and Lefkowitz, R.J., (2012) Molecular mechanism of beta-arrestin-biased agonism at seven-transmembrane receptors. *Annu Rev Pharmacol Toxicol*. 52: p. 179-97.
30. Delgado-Peraza, F., Ahn, K.H., Nogueras-Ortiz, C., Mungrue, I.N., Mackie, K., Kendall, D.A., et al., (2016) Mechanisms of Biased beta-Arrestin-Mediated Signaling Downstream from the Cannabinoid 1 Receptor. *Mol Pharmacol*. 89(6): p. 618-29.
31. Carr, R., 3rd, Schilling, J., Song, J., Carter, R.L., Du, Y., Yoo, S.M., et al., (2016) betaarrestin-biased signaling through the beta2-adrenergic receptor promotes cardiomyocyte contraction. *Proc Natl Acad Sci U S A*. 113(28): p. E4107-16.
32. Shenoy, S.K. and Lefkowitz, R.J., (2011) beta-Arrestin-mediated receptor trafficking and signal transduction. *Trends Pharmacol Sci*. 32(9): p. 521-33.
33. Namkung, Y., Le Gouill, C., Lukashova, V., Kobayashi, H., Hogue, M., Khoury, E., et al., (2016) Monitoring G protein-coupled receptor and beta-arrestin trafficking in live cells using enhanced bystander BRET. *Nat Commun*. 7: p. 12178.
34. Avet, C., Mancini, A., Breton, B., Le Gouill, C., Hauser, A.S., Normand, C., et al., (2022) Effector membrane translocation biosensors reveal G protein and betaarrestin coupling profiles of 100 therapeutically relevant GPCRs. *Elife*. 11.

35. Wan, Q., Okashah, N., Inoue, A., Nehme, R., Carpenter, B., Tate, C.G., et al., (2018) Mini G protein probes for active G protein-coupled receptors (GPCRs) in live cells. *J Biol Chem.* 293(19): p. 7466-7473.
36. Caron, M.G. and Barak, L.S., (2019) A Brief History of the beta-Arrestins. *Methods Mol Biol.* 1957: p. 3-8.
37. Ahn, S., Wei, H., Garrison, T.R., and Lefkowitz, R.J., (2004) Reciprocal regulation of angiotensin receptor-activated extracellular signal-regulated kinases by beta-arrestins 1 and 2. *J Biol Chem.* 279(9): p. 7807-11.
38. Oakley, R.H., Laporte, S.A., Holt, J.A., Caron, M.G., and Barak, L.S., (2000) Differential affinities of visual arrestin, beta arrestin1, and beta arrestin2 for G protein-coupled receptors delineate two major classes of receptors. *J Biol Chem.* 275(22): p. 17201-10.
39. Ghosh, E., Dwivedi, H., Baidya, M., Srivastava, A., Kumari, P., Stepniewski, T., et al., (2019) Conformational Sensors and Domain Swapping Reveal Structural and Functional Differences between beta-Arrestin Isoforms. *Cell Rep.* 28(13): p. 3287-3299 e6.
40. Hohmeier, H.E., Mulder, H., Chen, G., Henkel-Rieger, R., Prentki, M., and Newgard, C.B., (2000) Isolation of INS-1-derived cell lines with robust ATP-sensitive K<sup>+</sup> channel-dependent and -independent glucose-stimulated insulin secretion. *Diabetes.* 49(3): p. 424-30.
41. Trempelec, N., Dave-Coll, N., and Nebreda, A.R., (2013) SnapShot: p38 MAPK signaling. *Cell.* 152(3): p. 656-656 e1.
42. Ge, B., Gram, H., Di Padova, F., Huang, B., New, L., Ulevitch, R.J., et al., (2002) MAPKK-independent activation of p38alpha mediated by TAB1-dependent autophosphorylation of p38alpha. *Science.* 295(5558): p. 1291-4.
43. Gong, K., Li, Z., Xu, M., Du, J., Lv, Z., and Zhang, Y., (2008) A novel protein kinase A-independent, beta-arrestin-1-dependent signaling pathway for p38 mitogen-activated protein kinase activation by beta2-adrenergic receptors. *J Biol Chem.* 283(43): p. 29028-36.
44. Kommaddi, R.P., Jean-Charles, P.Y., and Shenoy, S.K., (2015) Phosphorylation of the deubiquitinase USP20 by protein kinase A regulates post-endocytic trafficking of beta2 adrenergic receptors to autophagosomes during physiological stress. *J Biol Chem.* 290(14): p. 8888-903.
45. Yu, S.M., Jean-Charles, P.Y., Abraham, D.M., Kaur, S., Gareri, C., Mao, L., et al., (2019) The deubiquitinase ubiquitin-specific protease 20 is a positive modulator of myocardial beta1-adrenergic receptor expression and signaling. *J Biol Chem.* 294(7): p. 2500-2518.
46. Daaka, Y., Luttrell, L.M., and Lefkowitz, R.J., (1997) Switching of the coupling of the beta2-adrenergic receptor to different G proteins by protein kinase A. *Nature.* 390(6655): p. 88-91.
47. Zamah, A.M., Delahunty, M., Luttrell, L.M., and Lefkowitz, R.J., (2002) Protein kinase A-mediated phosphorylation of the beta 2-adrenergic receptor regulates its coupling to G<sub>s</sub> and G<sub>i</sub>. Demonstration in a reconstituted system. *J Biol Chem.* 277(34): p. 31249-56.
48. Wang, J., Hanada, K., Staus, D.P., Makara, M.A., Dahal, G.R., Chen, Q., et al., (2017) Galphai is required for carvedilol-induced beta1 adrenergic receptor beta-arrestin biased signaling. *Nat Commun.* 8(1): p. 1706.
49. Smith, J.S., Pack, T.F., Inoue, A., Lee, C., Zheng, K., Choi, I., et al., (2021) Noncanonical scaffolding of Galphai and beta-arrestin by G protein-coupled receptors. *Science.* 371(6534).
50. Lefkowitz, R.J., Pierce, K.L., and Luttrell, L.M., (2002) Dancing with different partners: protein kinase a phosphorylation of seven membrane-spanning receptors regulates their G protein-coupling specificity. *Mol Pharmacol.* 62(5): p. 971-4.

51. Jean-Charles, P.Y., Zhang, L., Wu, J.H., Han, S.O., Brian, L., Freedman, N.J., et al., (2016) Ubiquitin-specific Protease 20 Regulates the Reciprocal Functions of beta-Arrestin2 in Toll-like Receptor 4-promoted Nuclear Factor kappaB (NFkappaB) Activation. *J Biol Chem.* 291(14): p. 7450-64.
52. Stadel, J.M., Nambi, P., Shorr, R.G., Sawyer, D.F., Caron, M.G., and Lefkowitz, R.J., (1983) Catecholamine-induced desensitization of turkey erythrocyte adenylate cyclase is associated with phosphorylation of the beta-adrenergic receptor. *Proc Natl Acad Sci U S A.* 80(11): p. 3173-7.
53. Komolov, K.E., Sulon, S.M., Bhardwaj, A., van Keulen, S.C., Duc, N.M., Laurinavichyute, D.K., et al., (2021) Structure of a GRK5-Calmodulin Complex Reveals Molecular Mechanism of GRK Activation and Substrate Targeting. *Mol Cell.* 81(2): p. 323-339 e11.
54. Ronnebaum, S.M., Jensen, M.V., Hohmeier, H.E., Burgess, S.C., Zhou, Y.P., Qian, S., et al., (2008) Silencing of cytosolic or mitochondrial isoforms of malic enzyme has no effect on glucose-stimulated insulin secretion from rodent islets. *J Biol Chem.* 283(43): p. 28909-17.
55. Haldeman, J.M., Conway, A.E., Arlotto, M.E., Slentz, D.H., Muoio, D.M., Becker, T.C., et al., (2019) Creation of versatile cloning platforms for transgene expression and dCas9-based epigenome editing. *Nucleic Acids Res.* 47(4): p. e23.
56. Kieffer, T.J., Heller, R.S., Unson, C.G., Weir, G.C., and Habener, J.F., (1996) Distribution of glucagon receptors on hormone-specific endocrine cells of rat pancreatic islets. *Endocrinology.* 137(11): p. 5119-25.
57. Jones, B., McGlone, E.R., Fang, Z., Pickford, P., Correa, I.R., Jr., Oishi, A., et al., (2021) Genetic and biased agonist-mediated reductions in beta-arrestin recruitment prolong cAMP signaling at glucagon family receptors. *J Biol Chem.* 296: p. 100133.
58. van der Velden, W.J.C., Lindquist, P., Madsen, J.S., Stassen, R., Wewer Albrechtsen, N.J., Holst, J.J., et al., (2022) Molecular and in vivo phenotyping of missense variants of the human glucagon receptor. *J Biol Chem.* 298(2): p. 101413.
59. Hilger, D., Kumar, K.K., Hu, H., Pedersen, M.F., O'Brien, E.S., Giehm, L., et al., (2020) Structural insights into differences in G protein activation by family A and family B GPCRs. *Science.* 369(6503).
60. Sandoval, D.A. and D'Alessio, D.A., (2015) Physiology of proglucagon peptides: role of glucagon and GLP-1 in health and disease. *Physiol Rev.* 95(2): p. 513-48.
61. Paradis, J.S., Ly, S., Blondel-Tepaz, E., Galan, J.A., Beautrait, A., Scott, M.G., et al., (2015) Receptor sequestration in response to beta-arrestin-2 phosphorylation by ERK1/2 governs steady-state levels of GPCR cell-surface expression. *Proc Natl Acad Sci U S A.* 112(37): p. E5160-8.
62. Wess, J., (2022) The Two beta-Arrestins Regulate Distinct Metabolic Processes: Studies with Novel Mutant Mouse Models. *Int J Mol Sci.* 23(1).
63. Luan, B., Zhao, J., Wu, H., Duan, B., Shu, G., Wang, X., et al., (2009) Deficiency of a beta-arrestin-2 signal complex contributes to insulin resistance. *Nature.* 457(7233): p. 1146-9.
64. Zhu, L., Almaca, J., Dadi, P.K., Hong, H., Sakamoto, W., Rossi, M., et al., (2017) betaarrestin-2 is an essential regulator of pancreatic beta-cell function under physiological and pathophysiological conditions. *Nat Commun.* 8: p. 14295.
65. Pydi, S.P., Barella, L.F., Zhu, L., Meister, J., Rossi, M., and Wess, J., (2022) betaArrestins as Important Regulators of Glucose and Energy Homeostasis. *Annu Rev Physiol.* 84: p. 17-40.

66. Kong, K.C., Butcher, A.J., McWilliams, P., Jones, D., Wess, J., Hamdan, F.F., et al., (2010) M3-muscarinic receptor promotes insulin release via receptor phosphorylation/arrestin-independent activation of protein kinase D1. *Proc Natl Acad Sci U S A.* 107(49): p. 21181-6.
67. Barella, L.F., Rossi, M., Zhu, L., Cui, Y., Mei, F.C., Cheng, X., et al., (2019) beta-Cell intrinsic beta-arrestin 1 signaling enhances sulfonylurea-induced insulin secretion. *J Clin Invest.* 129(9): p. 3732-3737.
68. Hershko, A. and Ciechanover, A., (1998) The ubiquitin system. *Annu Rev Biochem.* 67: p. 425-79.
69. Komander, D. and Rape, M., (2012) The ubiquitin code. *Annu Rev Biochem.* 81: p. 203-29.
70. Yau, R. and Rape, M., (2016) The increasing complexity of the ubiquitin code. *Nat Cell Biol.* 18(6): p. 579-86.
71. Jean-Charles, P.Y., Freedman, N.J., and Shenoy, S.K., (2016) Chapter Nine – Cellular Roles of Beta-Arrestins as Substrates and Adaptors of Ubiquitination and Deubiquitination. *Prog Mol Biol Transl Sci.* 141: p. 339-69.
72. Burton, J.C. and Grimsey, N.J., (2019) Ubiquitination as a Key Regulator of Endosomal Signaling by GPCRs. *Front Cell Dev Biol.* 7: p. 43.
73. Longuet, C., Sinclair, E.M., Maida, A., Baggio, L.L., Maziarz, M., Charron, M.J., et al., (2008) The glucagon receptor is required for the adaptive metabolic response to fasting. *Cell Metab.* 8(5): p. 359-71.
74. Berglund, E.D., Lee-Young, R.S., Lustig, D.G., Lynes, S.E., Donahue, E.P., Camacho, R.C., et al., (2009) Hepatic energy state is regulated by glucagon receptor signaling in mice. *J Clin Invest.* 119(8): p. 2412-22.
75. Kimball, S.R., Siegfried, B.A., and Jefferson, L.S., (2004) Glucagon represses signaling through the mammalian target of rapamycin in rat liver by activating AMP-activated protein kinase. *J Biol Chem.* 279(52): p. 54103-9.
76. Huet, C., Boudaba, N., Guigas, B., Viollet, B., and Foretz, M., (2020) Glucose availability but not changes in pancreatic hormones sensitizes hepatic AMPK activity during nutritional transition in rodents. *J Biol Chem.* 295(18): p. 5836-5849.
77. Cao, W., Collins, Q.F., Becker, T.C., Robidoux, J., Lupo, E.G., Jr., Xiong, Y., et al., (2005) p38 Mitogen-activated protein kinase plays a stimulatory role in hepatic gluconeogenesis. *J Biol Chem.* 280(52): p. 42731-7.
78. Canovas, B. and Nebreda, A.R., (2021) Diversity and versatility of p38 kinase signalling in health and disease. *Nat Rev Mol Cell Biol.* 22(5): p. 346-366.
79. Gurevich, V.V. and Gurevich, E.V., (2015) Arrestins: Critical Players in Trafficking of Many GPCRs. *Prog Mol Biol Transl Sci.* 132: p. 1-14.

## Figure legends

**Figure 1. GCGR-5KR is significantly impaired in cAMP generation and G protein-dependent signaling, but enhanced in  $\beta$ -arrestin association as well as p38 MAP Kinase activation compared with wild type GCGR.** (A) Snake-plot (gpcrdb.org) of glucagon receptor (GCGR) highlighting intracellular lysines in blue that are mutated to arginine in GCGR-5KR. (B) cAMP production of WT and 5KR plotted as a percent normalized to maximal level of cAMP generated by GCGR-WT. Data are comprised of means  $\pm$  S.E.M from six independent experiments. Representative confocal images (C) and immunoblots (D) that reveal comparable receptor expression levels of WT and 5KR. Scale Bar = 10  $\mu$ m. (E) PKA phosphorylation of CREB (Ser133) by WT and 5KR. (F) Quantification for phospho-CREB, normalized to total CREB shown are means  $\pm$  SEM of three independent experiments. \*  $p < 0.05$  WT versus 5KR, Two-way ANOVA, Holm-Šídák's multiple comparisons test. (G) GCGR-WT or GCGR-5KR were immunoprecipitated using M2 anti-Flag affinity agarose (Sigma-Aldrich) and eluted samples as well as lysate inputs were immunoblotted for the indicated proteins. GCGR was detected using a MYC IgG (Cell Signaling Technology). (H) The scatter plot with bar represents the quantification for the binding of  $\beta$ arr1/2 to WT or mutant 5KR receptor from three independent experiments. \*  $p < 0.05$  versus Veh, WT; #,  $p < 0.05$  versus all other samples, two-way ANOVA and Holm-Šídák's multiple comparisons test. (I) GCGR-WT or GCGR-5KR expressing HEK-293 cells were stimulated with 100 nM glucagon for the indicated times after serum starvation and whole cell extracts were analyzed by immunoblotting. (J) Line graphs summarize data for phospho-p38 normalized to cognate total p38 from three independent experiments. \*  $p < 0.05$  versus WT, two-way ANOVA and Holm-Šídák's multiple comparisons test. The mobility of molecular weight markers (kDa) are shown beside each blot panel.

**Figure 2. Lysine 333 in GCGR is a critical site for engendering ubiquitin-dependent signal bias between G protein recruitment/cAMP production and  $\beta$ -arrestin association/p38 MAPK activation.** (A) GCGR ubiquitination for WT and constructs with single lysine mutation was detected using the anti-ubiquitin antibody, FK1 (Enzo Life Sciences). The blot was then reprobed with an antibody that detects the MYC tag (Cell Signaling Technology). (B) Ubiquitinated smear was quantitated and normalized to cognate receptor bands and plotted as ratio. The scatter graph

with bars represents the means  $\pm$  S.E.M. from six (WT, K169R), five (K333R, K406R), or four (K423R, K451R) independent experiments. \*,  $p < 0.05$  versus respective non-stimulated, §,  $p < 0.05$  versus WT non-stimulated, two-way ANOVA, Holm-Šídák's multiple comparisons test. (C) Confocal images of immunostaining of single lysine mutant expressing stable HEK-293 cells with anti-MYC IgG followed by secondary IgG conjugated with Alexa594 (Red channel). DAPI staining was used to label nuclei. Scale bar = 10  $\mu$ m. (D-F) HEK-293 cells were transiently transfected with the GCGR-WT or the indicated GCGR lysine mutant and cAMP generation was determined as in Fig 1B. Concentration-response curves are comprised of means  $\pm$  S.E.M from three independent experiments. \*  $p < 0.05$ , WT versus K333R, two-way ANOVA, Holm-Šídák's multiple comparisons test. (G) HEK-293 cells stably expressing WT or indicated single lysine mutants were stimulated with 100 nM glucagon for 15 minutes and solubilized cell extracts were immunoblotted as indicated. (H) The scatter plot with bar summarize the quantification of phospho p38 normalized to total p38, from four independent experiments represented as means  $\pm$  S.E.M. \* $p < 0.05$  versus all the other samples, Holm-Šídák's multiple comparisons test. (I) Enhanced bystander BRET measured between Rluc8-miniGs and the plasma membrane marker rGFP-CAAX to monitor mini-Gs recruitment to the active GCGR WT, single lysine mutants or 5KR mutant after 10 minutes of GCG stimulation at indicated doses. Data are shown as means  $\pm$  SEM (N=3). \*  $p < 0.01$  for WT versus 5KR, K333R, and K169R, two-way ANOVA, Holm-Šídák's multiple comparisons test. Enhanced bystander BRET between (J)  $\beta$ -arrestin1-RlucII or (K)  $\beta$ -arrestin2-RlucII and the plasma membrane marker rGFP-CAAX to monitor  $\beta$ -arrestin recruitment to the active GCGR-WT, single lysine mutants or 5KR mutant after 10 minutes of GCG at indicated doses. Data are represented as the means  $\pm$  SEM (N=3). \*  $p < 0.01$  for 5KR, K333R, versus WT in panel J and \*  $p < 0.01$  for WT versus 5KR and K333R as indicated in panel K; two-way ANOVA, Holm-Šídák's multiple comparisons test. The mobility of molecular weight markers (kDa) are shown beside each blot panel.

**Figure 3. GCGR-induced p38 activation is dependent on  $\beta$ -arrestin1 and canonical upstream kinase MKK3.** (A) HEK-293 cells expressing GCGR-WT were transfected with siRNA targeting either no mRNA (CTL),  $\beta$ arr1 or  $\beta$ arr2. Serum-starved cells were stimulated with 100 nM GCG for 15' and lysates were immunoblotted sequentially for the indicated proteins. (B) Phospho-p38

bands were normalized to cognate p38 bands and summarized as a percent of experimental maximum from four independent experiments \* $p < 0.05$  versus respective 0 min; # $p < 0.05$  versus  $\beta$ arr1 knockdown samples; two-way ANOVA and Holm-Šídák's multiple comparisons test. (C-D) INS-1 832/3 cells were transfected with siRNA as in panel A along with GCGR-WT plasmid, and stimulation and analyses were as in panels A & B. \* $p < 0.05$  versus respective 0 min; # $p < 0.05$  versus  $\beta$ arr1 knockdown samples; two-way ANOVA and Holm-Šídák's multiple comparisons test. (E-H) HEK-293 cells expressing GCGR-WT were transfected with control (CTL) siRNA that has no mRNA target or siRNA targeting MKK3 (E, F) or TAB1 (G, H). Serum-starved cells were stimulated with 100 nM GCG for 15' and lysates were immunoblotted sequentially as indicated. (F, H) Phospho-p38 bands were normalized to cognate p38 bands and summarized as a percent of experimental maximum from four (F) or three (H) independent experiments \* $p < 0.05$  as indicated; two-way ANOVA and Holm-Šídák's multiple comparisons test. HEK-293 cells expressing GCGR-K333R were transfected with siRNA targeting either no mRNA (control, CTL),  $\beta$ -arr1 or  $\beta$ arr2 (G, H); or siRNA targeting CTL, or MKK3 (I, J). (H) \*  $p < 0.05$  versus respective 0 min samples; #  $p < 0.05$  versus  $\beta$ -arr1, 15 min GCG samples. (J) \*  $p < 0.05$  as indicated, two-way ANOVA, and Holm-Šídák's multiple comparisons test. The mobility of molecular weight markers (kDa) are shown beside each blot panel.

**Figure 4.  $\beta$ -arrestin1 is required for p38 activation induced by GCGR-K333R.** HEK-293 cells expressing GCGR-K333R were transfected with siRNA targeting either no mRNA (control, CTL),  $\beta$ -arr1 or  $\beta$ arr2 (A, B); or siRNA targeting CTL, or MKK3 (C, D) and analyzed by western blotting as indicated. (B) \*  $p < 0.05$  versus respective 0 min samples; #  $p < 0.05$  versus  $\beta$ -arr1, 15 min GCG samples. (D) \*  $p < 0.05$  as indicated, two-way ANOVA, and Holm-Šídák's multiple comparisons test. The mobility of molecular weight markers (kDa) are shown beside each blot panel.

**Figure 5. GCGR-induced p38 MAPK activation is independent of PKA and Gi.** (A) HEK-293 cells stably expressing GCGR were transfected with siRNA targeting no mRNA (CTL), PKA $\alpha$  or PKA $\beta$ . 48h post-transfection the cells were serum-starved, stimulated  $\pm$  GCG for 15' and lysates were immunoblotted as indicated. (B) Phospho-p38 bands were normalized to cognate p38 bands and summarized as a percent of experimental maximum from four independent experiments \* $p < 0.05$  versus respective 0 min; # $p < 0.05$  versus CTL, 15'; two-way ANOVA, Holm-Šídák's multiple

comparisons test. (C) HEK-293 cells expressing GCGR were treated  $\pm 100$  ng/mL pertussis toxin (PTX) for 16 h and then stimulated  $\pm 100$  nM GCG for 15'. Whole cell extracts were immunoblotted for indicated proteins. (D) Quantification of phospho-p38 was performed as in (B). \*  $p < 0.05$  as indicated, two-way ANOVA, Holm-Šidák's multiple comparisons test. (E, F) Assay and analyses were conducted as in C & D, but cells were stimulated with 100 nM isoproterenol (ISO) to trigger endogenous  $\beta 2AR$ -induced p38 activation. The mobility of molecular weight markers (kDa) are shown beside each blot panel.

**Figure 6.  $\beta$ -arrestin-dependent internalization and early endosomal trafficking kinetics of GCGR-WT and GCGR-K333R.** Enhanced bystander BRET (ebBRET) was measured between GCGR-Rluc8 (WT or K333R) and either the plasma membrane marker rGFP-CAAX (A, B) to monitor glucagon-induced receptor internalization, the marker for early endosomes, rGFP-FYVE (C, D) to monitor glucagon-induced receptor trafficking to early endosomes. In panels A-D, receptor trafficking was measured in  $\beta$ arr 1/2 CRISPR (SL) knock out and cognate parental HEK-293 cells with and without  $\beta$ arr1 and/or  $\beta$ arr2 rescue. In panels A-D, delta-BRET data are summarized as means  $\pm$  SEM (N=4). (E) Net BRET maximum obtained at 20 min of GCG stimulation in parental cells for WT, and K333R Rluc8 tagged constructs with acceptors rGFP-FYVE. \* $p < 0.05$ , t-test comparison. (F, G) ebBRET between  $\beta$ arr1-RlucII and rGFP-FYVE or  $\beta$ arr2-Rluc II and rGFP-FYVE, upon stimulating for 15 minutes with GCG at indicated doses. \*  $p < 0.05$ , two-way ANOVA, Tukey's multiple comparisons test. ns, not significant.

**Figure 7. Signaling and insulin secretion by GCGR-WT and GCGR-K333R in INS-1  $\beta$ -cell line.** (A) INS-1  $\beta$ -cell line 832/3 was transduced with adenovirus encoding control, GCGR-WT or GCGR-K333R, and 48 h post-infection were stimulated with 10 nM GCG. Cells were solubilized and lysates were immunoblotted to detect phospho-p38, p38, phospho-CREB, CREB, MYC and  $\beta$ -actin as indicated. The mobility of molecular weight markers (kDa) are shown beside each blot panel. The scatter plot with bar shown represents the quantification for the phosphorylation of p38 normalized to total p38 (B), and phospho-CREB normalized to CREB (C) represented as means  $\pm$  S.E.M. \* $p < 0.05$ , \*\*  $p < 0.01$ , \*\*\*  $p < 0.001$  as indicated, Holm-Šidák's multiple comparisons test. (D) Insulin secretory responses in 832/3 cells with no virus, control virus, GCGR-WT or GCGR-K333R treated with 12.5 mM glucose alone or with GCGR selective agonist compound 44-0410 for 1 h.



\* $p < 0.05$ , \*\*  $p < 0.01$ , as indicated, Holm-Šídák's multiple comparisons test. (E) INS-1 832/3 cells transduced with GCGR-WT virus were treated  $\pm$  p38 inhibitor SB 203580 (100 nM, for 1h) and then GSIS assay and analyses were performed as in panel D. \* $p < 0.05$ , \*\*  $p < 0.01$ , as indicated, Holm-Šídák's multiple comparisons test.

**Figure 8. Signaling and insulin secretion by GCGR-WT and GCGR-K333R islets isolated from *Gcgr* $\beta$ cell<sup>-/-</sup> mice.** (A) A correlation between insulin secretion rates in response to GCGR agonism by 44-0410 and the expression levels of GCGR. (B) The area under the curves for the insulin secretion rates by WT and K333R induced by GCGR agonist stimulation (plot area between mins 22-73, Fig S9C), in the presence of 12 mM glucose and normalized to the level of GCGR protein. (C) The area under the curve for glucose-stimulated insulin secretion in islets transduced with WT or K333R virus (plot area between mins 6-22, Fig S9C). (D) The area under the curve for the KCl-stimulated insulin secretion in islets transduced with WT or K333R virus (plot area between mins 81-96, Fig S9C).

**Figure 9.  $\beta$ -arrestin1 isoform exclusively scaffolds p38 kinase cascade promoted by GCGR agonist-stimulation.** HEK-293 cells stably expressing GCGR-WT (A-D) or GCGR-K333R (E-H) were transfected transiently with HA-tagged  $\beta$ arr1 or  $\beta$ arr2. 48 h post-transfection, cells were stimulated with 100 nM GCG for 15 min. Samples were immunoprecipitated using anti-HA affinity magnetic beads and both eluted proteins and cognate lysates were immunoblotted sequentially for the indicated proteins. Band signals for p-p38, p38 or MKK3 were normalized to respective  $\beta$ arr bands and presented in the scatter plots with bars in panels B, C, and D for GCGR-WT and panels F, G, and H for GCGR-K333R. \* $p < 0.05$  between indicated samples, two-way ANOVA and Tukey's multiple-comparison test. The mobility of molecular weight markers (kDa) are shown beside each blot panel. (I) GCGR deubiquitination status potentiates bias toward  $\beta$ arr1-dependent p38 MAPK signaling. The left side of the schematic displays activation of GCGR-WT that retains ubiquitin tag before agonist activation. Glucagon stimulation promotes several immediate events: G protein activation, cAMP production,  $\beta$ arr recruitment and internalization into early endosomes where the GCGR is rapidly deubiquitinated by USP33 and STAMBIP (not shown). With the GCGR-WT, we observe equivalent potential to signal through Gs and  $\beta$ -arr1-p38 signaling. However, our results suggest that Gs/PKA attenuates glucagon-induced p38 MAPK

phosphorylation. The right side of the schematic displays activation of GCGR-K333R that is impaired in ubiquitination and retains a deubiquitinated state. Glucagon stimulation promotes similar trafficking itinerary as for the GCGR-WT, but we observe enhanced mobilization of the receptor at early endosomes. The major differences from the WT pathway are not only a significantly decreased coupling to Gs leading to impaired cAMP production, but also greater p38 MAPK scaffolding by  $\beta$ -arr1 increasing the bias toward  $\beta$ arr1-dependent signal transduction.

**Figure S1. p42/44 ERK MAPK activation by GCGR-WT and GCGR-5KR.** HEK-293 cells stably expressing WT or 5KR GCGR were stimulated with 100 nM glucagon for the indicated times after serum starvation and whole cell extracts were analyzed by immunoblotting. Panels A, B show data summarized from three independent experiments for phospho-ERK normalized to cognate total ERK. The quantification is represented as a percent normalized to maximal signal obtained for GCGR-WT. \*  $p < 0.05$  versus WT, two-way ANOVA and Holm-Šídák's multiple comparisons test. The mobility of molecular weight markers (kDa) are shown beside each blot panel.

**Figure S2. GCGR-induced CREB activation is unaffected by knockdown of individual  $\beta$ arrestin and canonical upstream kinase MKK3, but is dependent on PKA $\alpha$ .** (A) HEK-293 cells expressing GCGR WT were transfected with siRNA targeting either no mRNA (CTL),  $\beta$ arrestin 1 or  $\beta$ -arrestin2. Serum-starved cells were stimulated with 100 nM GCG for 15' and lysates were immunoblotted sequentially for the indicated proteins. (B) Phospho-CREB bands were normalized to cognate CREB bands and summarized as a percent of experimental maximum from three independent experiments. (C) HEK-293 cells expressing GCGR-WT were transfected with control (CTL) siRNA that has no mRNA target or siRNA targeting MKK3. Serum-starved cells were stimulated with 100 nM GCG for 15' and lysates were immunoblotted sequentially for the indicated proteins. (D) Phospho-CREB was quantified as in (B). (E) HEK293 cells stably expressing GCGR were transfected with siRNA targeting no mRNA (CTL), PKA $\alpha$  or PKA $\beta$ . 48h post-transfection the cells were serum-starved, stimulated  $\pm$  GCG for 15' and lysates were immunoblotted for the indicated proteins. (F) Phospho-CREB bands were normalized to cognate CREB bands and summarized as a percent of experimental maximum from four independent experiments \* $p < 0.05$  versus respective 0 min; #  $p < 0.05$  versus CTL, 15' and PKA $\beta$ , 15' samples; two-way ANOVA, Holm-Šídák's multiple

comparisons test. The mobility of molecular weight markers (kDa) are shown beside each blot panel.

**Figure S3. Effects of PKA inhibitor (6-22) on GCGR-induced signaling.** HEK-293 cells expressing GCGR WT were serum-starved, treated  $\pm$  6-22 (100 nM) 15 min, and then stimulated  $\pm$  100 nM GCG for 15 min. Solubilized lysates were analyzed for phospho-p38 (A-B), and phospho-CREB (C-D). (B) Phospho-p38 bands were normalized to cognate p38 bands and summarized as a percent of control maximum from three independent experiments \* $p < 0.05$ , \*\*\* $p < 0.001$  as indicated; two-way ANOVA, Holm-Šídák's multiple comparisons test. (D) Phospho-CREB bands were normalized to cognate CREB bands and summarized as a percent of control maximum from three independent experiments \*\*\*\* $p < 0.0001$  as indicated; two-way ANOVA, Holm-Šídák's multiple comparisons test. The mobility of molecular weight markers (kDa) are shown beside each blot panel.

**Figure S4.  $\beta$ -arrestins 1 and 2 are equipotent in promoting GCGR desensitization.**  $\beta$ arr 1/2 CRISPR knock out (HR) and cognate parental HEK-293 cells were transfected with GCGR and GloSensor 22F, along with vector,  $\beta$ arr1 or  $\beta$ arr2 plasmids. cAMP levels were determined using GloSensor assay as described in Fig. 1B, after stimulating cells with increasing concentrations of GCG. (A) and (B) Dose-response curves and bar graphs showing area under curves, respectively. Data in A are normalized to maximum response obtained in parental cells in each experiment as 100%. The plots are comprised of means  $\pm$  SD from three independent experiments, \*\* $p < 0.05$  versus all other samples, one-way ANOVA. (C) Representative immunoblots from one of the three experiments showing the expression levels of GCGR, endogenous and overexpressed  $\beta$ arr1 or  $\beta$ arr2. The mobility of molecular weight markers (kDa) are shown beside each blot panel.

**Figure S5. Comparison of GCGR and GCGR-RLuc8 constructs for agonist-induced cAMP production.** HEK-293 cells were transiently transfected with GCGR wild type (WT) or GCGR5KR mutant along with GloSensor 22F plasmid and stimulated with increasing doses of glucagon to determine cAMP production plotted as a percent normalized to maximal level of cAMP generated by GCGR WT. Data shown here are comprised of means  $\pm$  SD from two independent experiments done in duplicates.

**Figure S6. Agonist-induced deubiquitination of the GCGR ensues in the absence of  $\beta$ arrestins.**

Three independently derived CRISPR  $\beta$ arr1/2 KO HEK-293 cells and their cognate parental lines were stably transfected with GCGR-MYC-FLAG, and ubiquitination of the receptor  $\pm$  glucagon (GCG, 200 nM, 15 min) was determined as in Figure 3 A-B. In panels B, D and F, \*  $p < 0.05$  as indicated; two-way ANOVA, Holm-Šídák's multiple comparisons test. The mobility of molecular weight markers (kDa) are shown beside each blot panel.

**Figure S7. GCGR-Deubiquitinase interaction proceeds in the absence of  $\beta$ -arrestins.**

CRISPR  $\beta$ arr1/2 KO (HR) HEK-293 cells and their cognate parental lines were stably transfected with GCGR-MYC-FLAG were serum starved for 1 h and stimulated with 200 nM GCG for the indicated times followed by immunoprecipitation with anti-FLAG agarose beads. The immunoprecipitates were resolved on 4-20% Tris-Glycine gels and immunoblotted for the indicated proteins. The graph represents the quantification for USP33 and STAMBP normalized to the respective receptor and represented as means  $\pm$  SD from two independent experiments. The mobility of molecular weight markers (kDa) are shown beside each blot panel.

**Figure S8. Adenoviral transduction of INS-1  $\beta$ -cell line 832/3.**

(A) Schematic showing the cloning of mGCGR (WT and K333R) to obtain Adenoviral construct encoding RIP-GCGRIRES-GFP. (B) INS-1  $\beta$ -cell line 832/3 was infected with adenoviruses at equivalent MOI to express  $\beta$ -galactosidase (control), GCGR-WT, or GCGR-K333R. Cells were plated on confocal dishes and immunostained with a MYC IgG. Images show distribution of GFP (green) and GCGR (Red). Nuclei stained with DAPI are shown in blue. Scale Bar = 10  $\mu$ m. (C) INS-1  $\beta$ cell line 832/3 was infected with adenoviruses at equivalent MOI to express  $\beta$ -galactosidase (control), GCGR-WT, or GCGR-K333R. Whole cell extracts were prepared by solubilizing in 2 $\times$  Laemmli sample buffer and expression of GCGR was detected by immunoblotting with an antiMYC IgG. Lower panel shows reprobe of the blot for  $\beta$ -actin levels. (D) INS-1 832/3 cells transduced with GCGR-K333R virus were treated  $\pm$  p38 inhibitor SB 203580 (100 nM, for 1h)

**Figure S9. Expression and insulin secretion of GCGR-WT and GCGR-K333R in pancreatic islets isolated from *Gcgr $\beta$ cell*<sup>-/-</sup> mice.**

(A) Solubilized islets transduced with either WT or K333R adenovirus that were used in perfusion assay in C, and purified hGCGR (100, 200, 300 and 500

femtomoles) were immunoblotted with anti-Flag IgG to detect and estimate GCGR expression levels by densitometry. The blot was reprobbed to detect GAPDH in islets as shown in the lower panel. (B) Islets were transduced with control, GCGR-WT, or GCGRK333R virus. To analyze expression islets were dispersed into single cells and plated on confocal dishes. Immunostaining and confocal imaging were carried out as in Fig S8. Scale Bar = 10  $\mu$ m. (C) Insulin secretion in islets stimulated with 12 mM glucose starting at minute 6, glucose + GCGR agonist 44-0410 stimulation from min 22-73, and 30 mM KCl at minute 81. (D) Area under the curve (not normalized for GCGR expression) for insulin secretion in response to the GCGR agonist 44-0410 (min 22-73). The mobility of molecular weight markers (kDa) are shown beside each blot panel. and then GSIS assay and analyses were performed as in Fig 7. \* $p < 0.05$ , as indicated, HolmŠídák's multiple comparisons test. The mobility of molecular weight markers (kDa) are shown beside each blot panel.

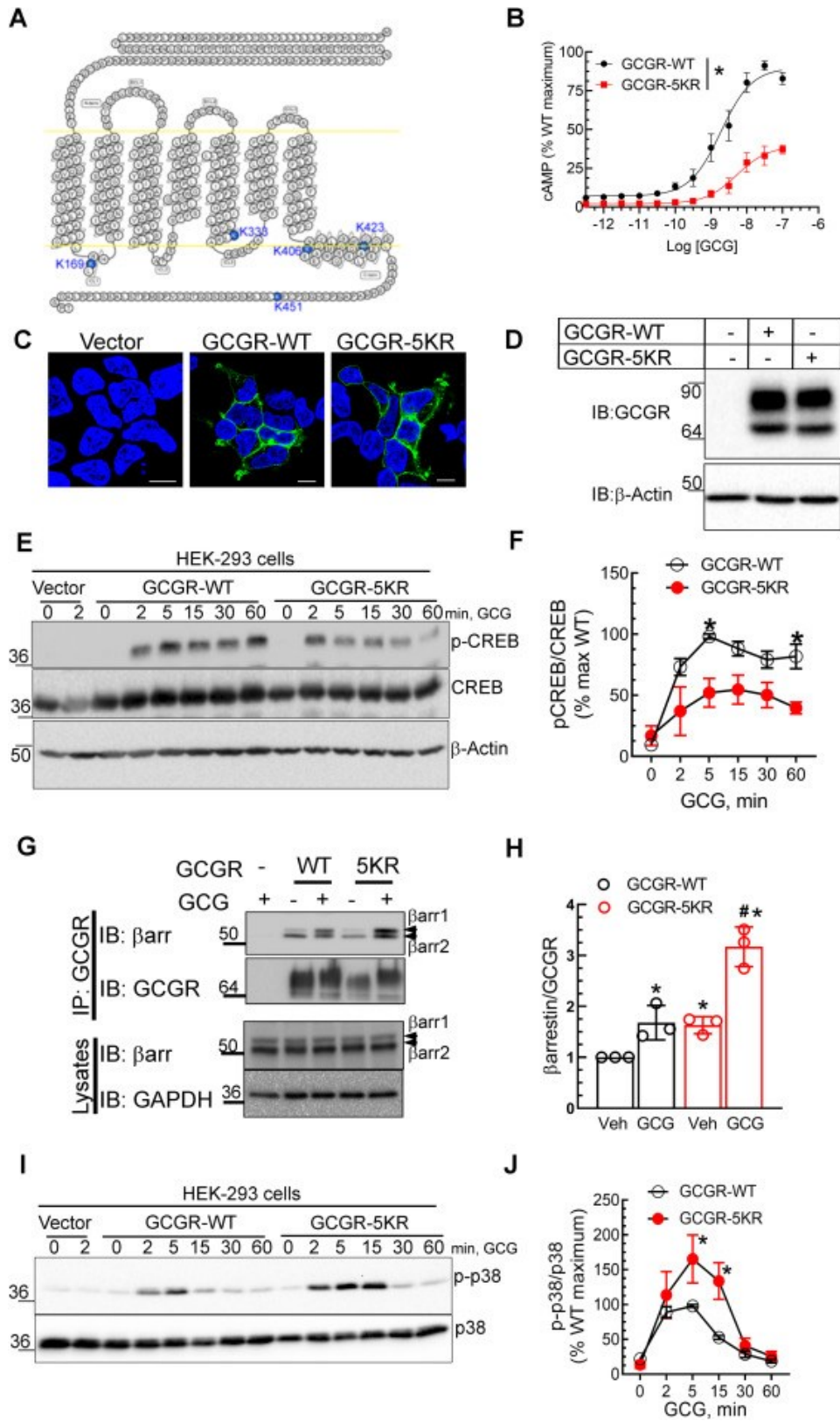


Figure 1

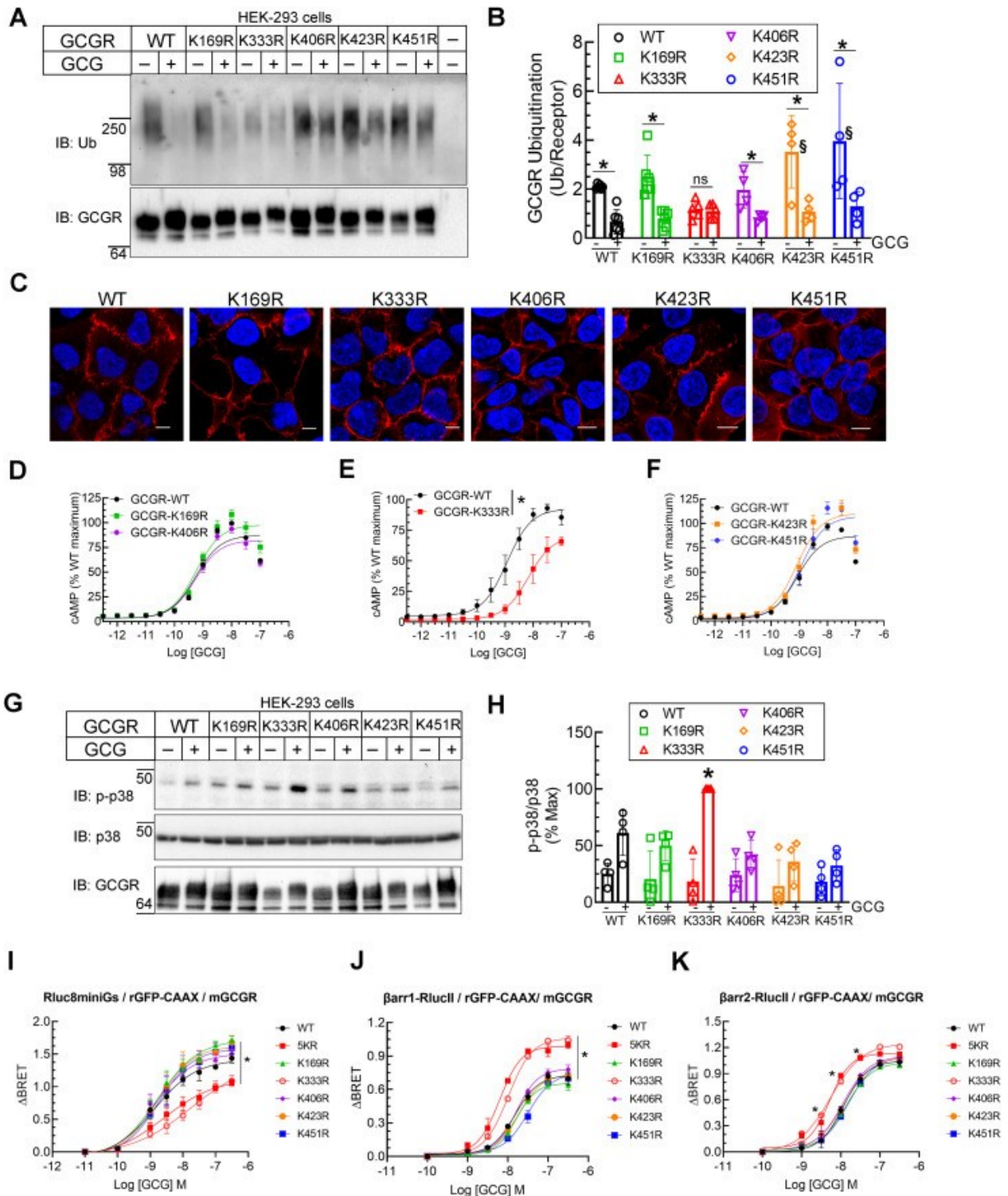


Figure 2

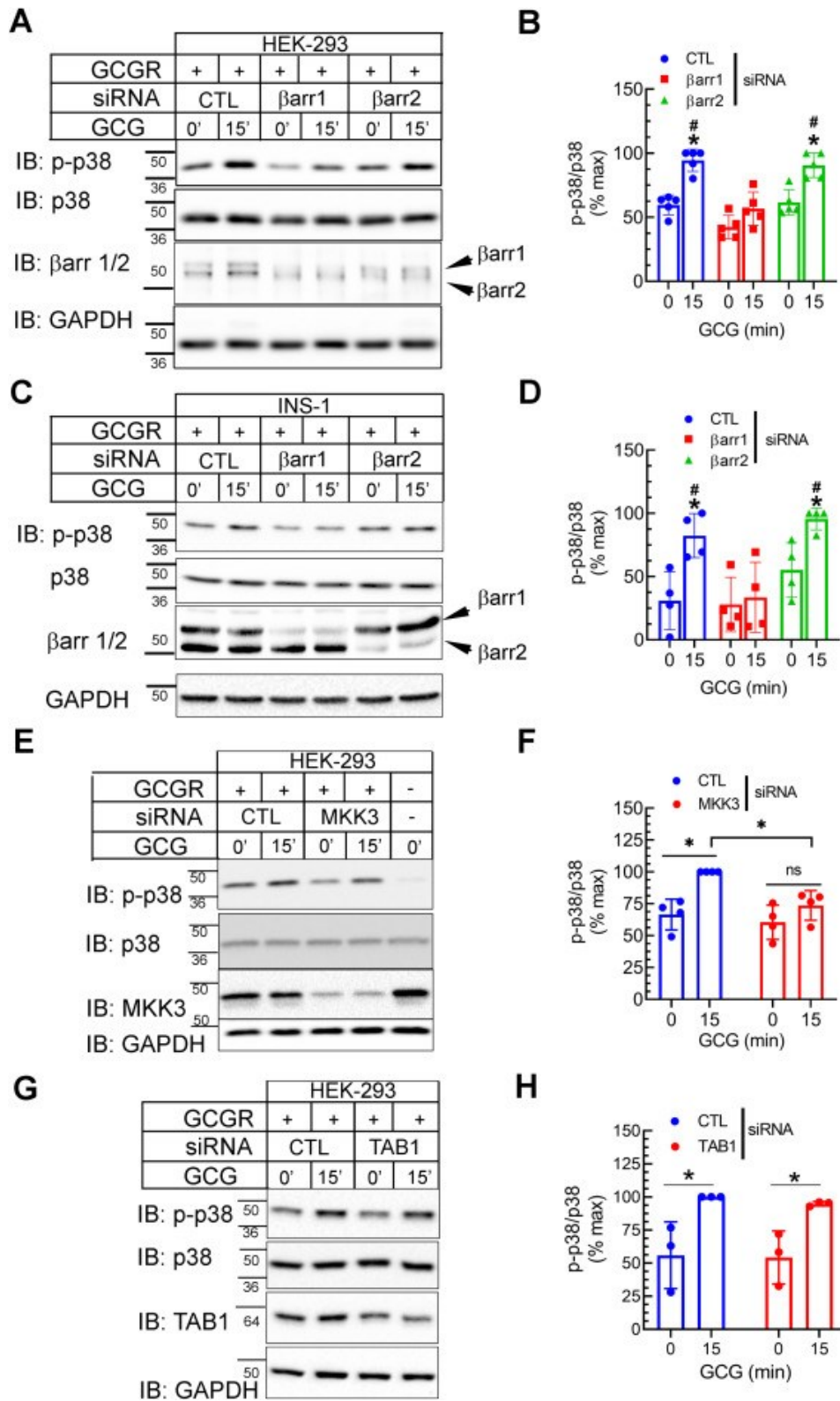


Figure 3



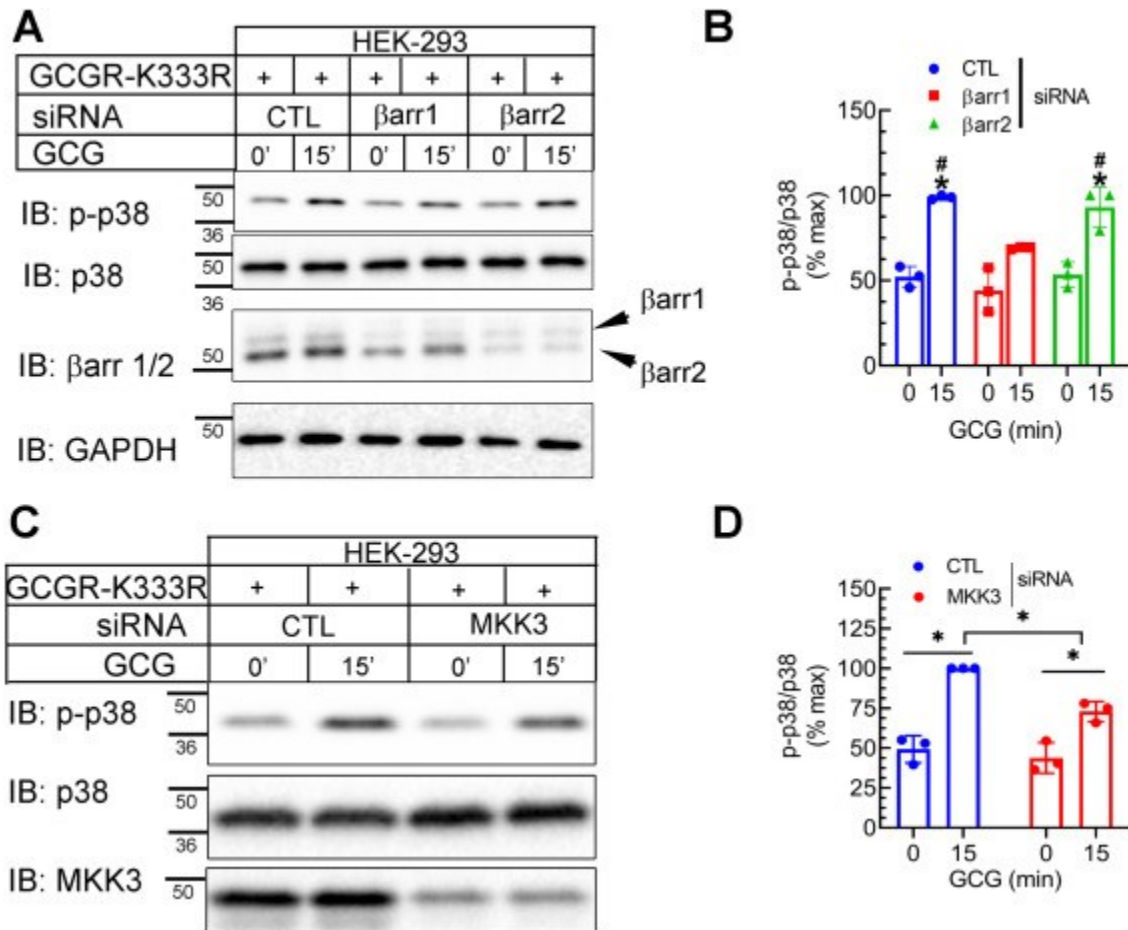


Figure 4

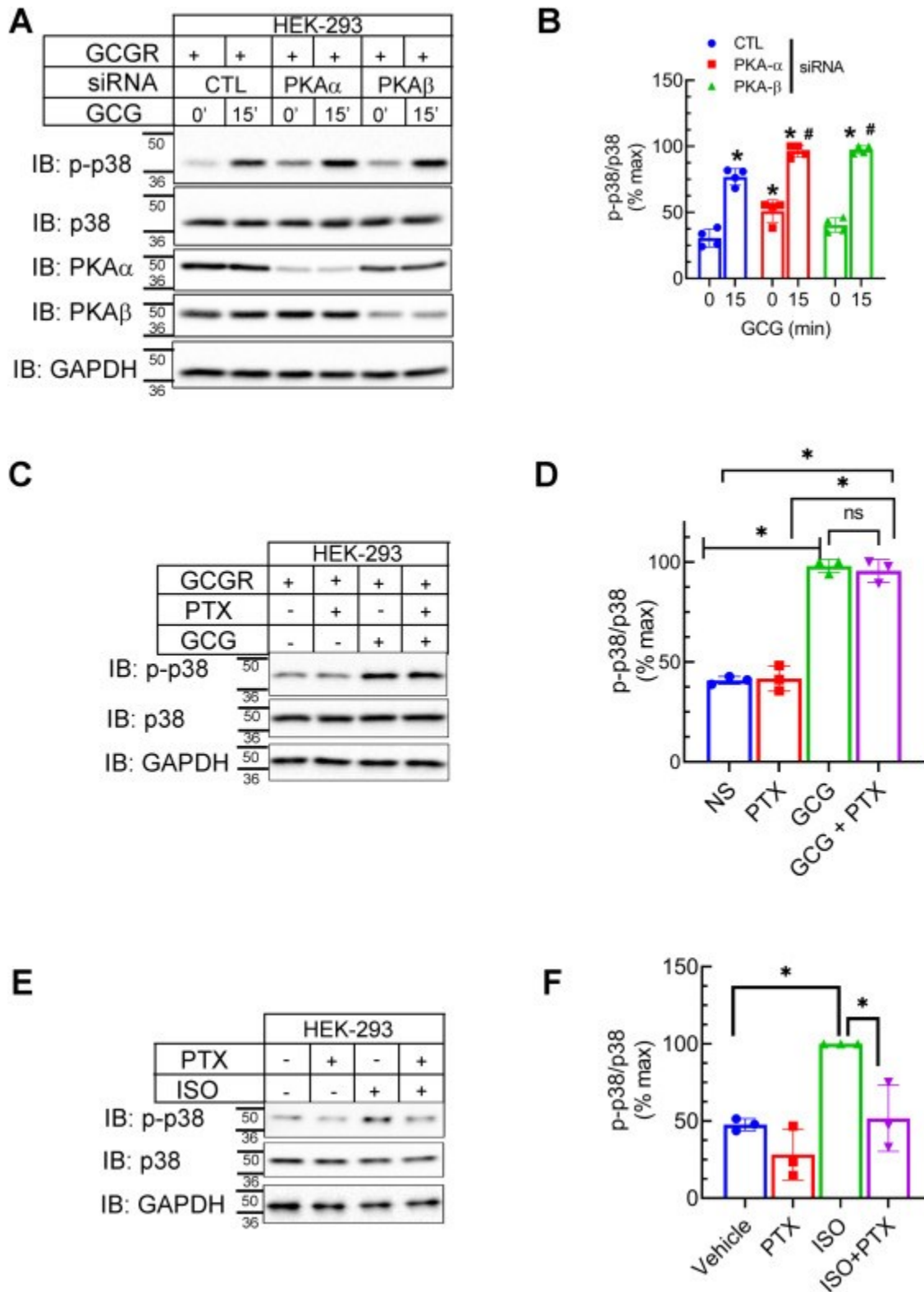


Figure 5

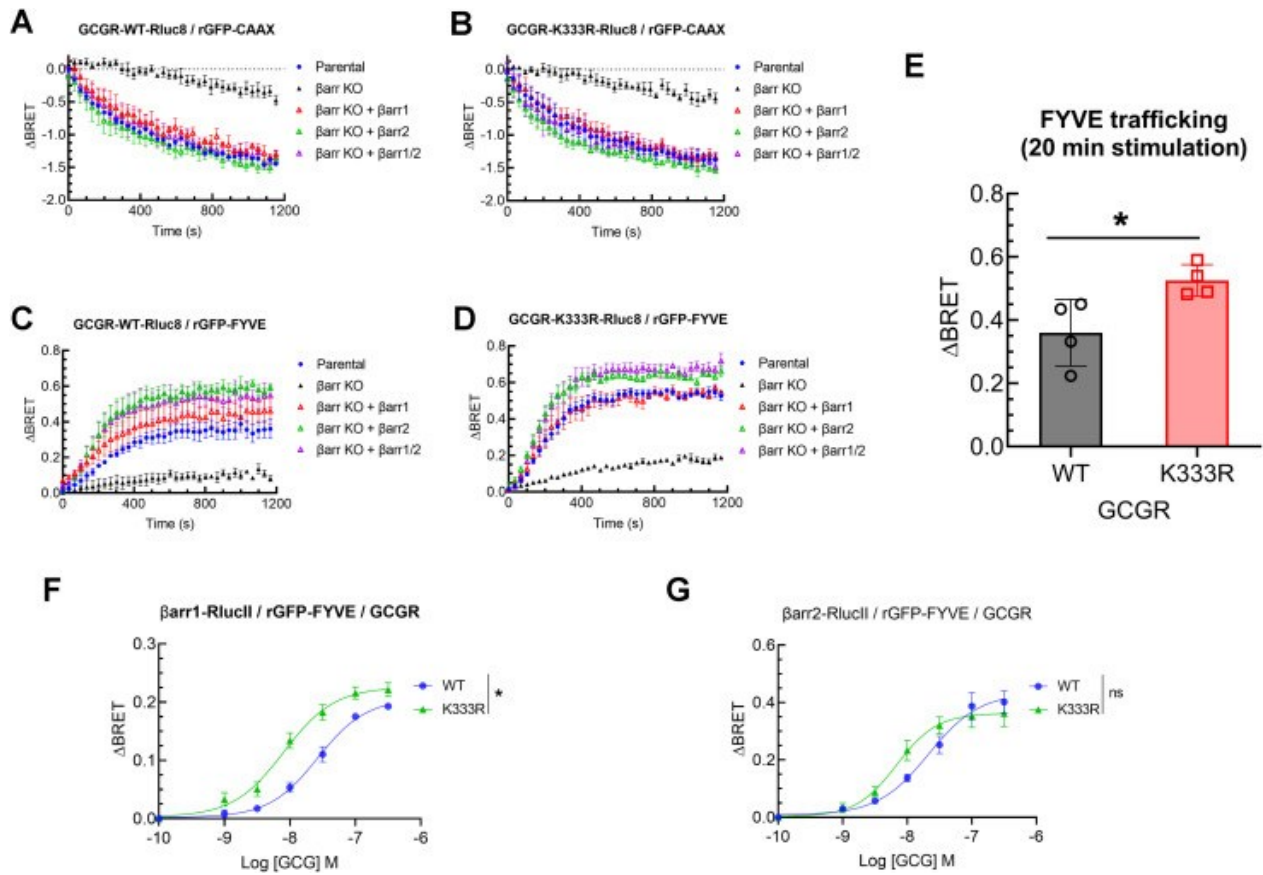
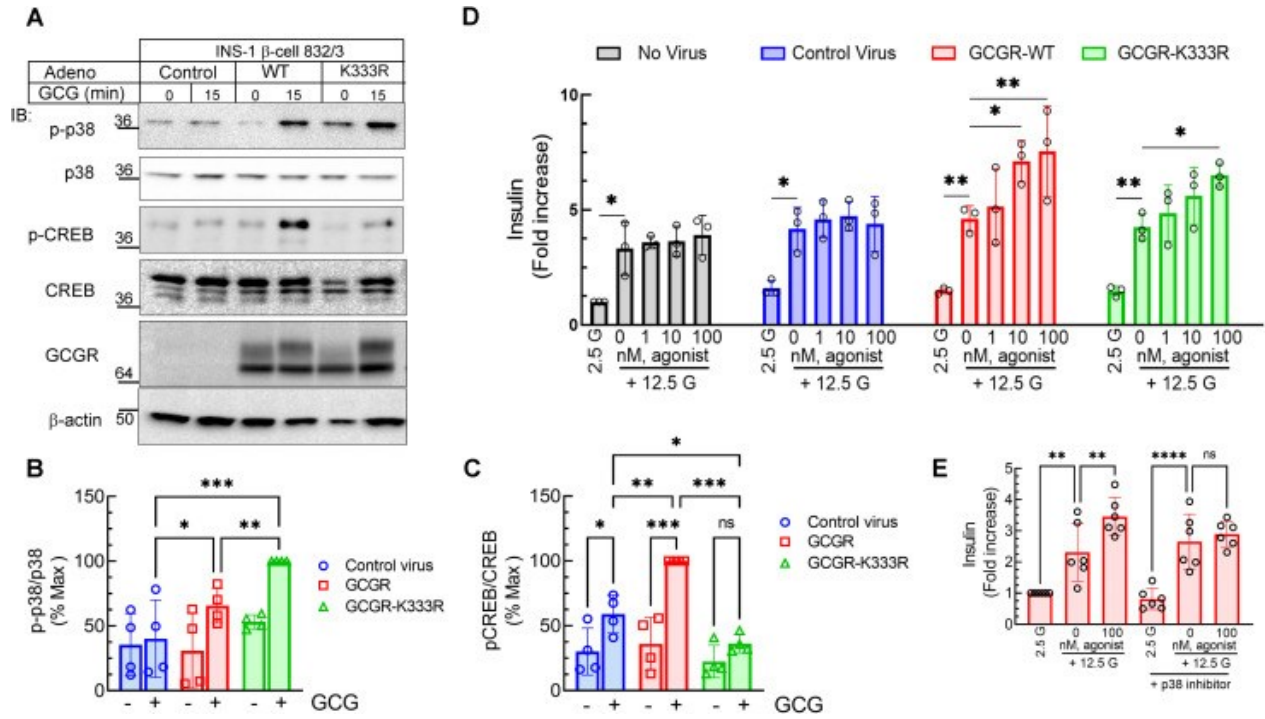
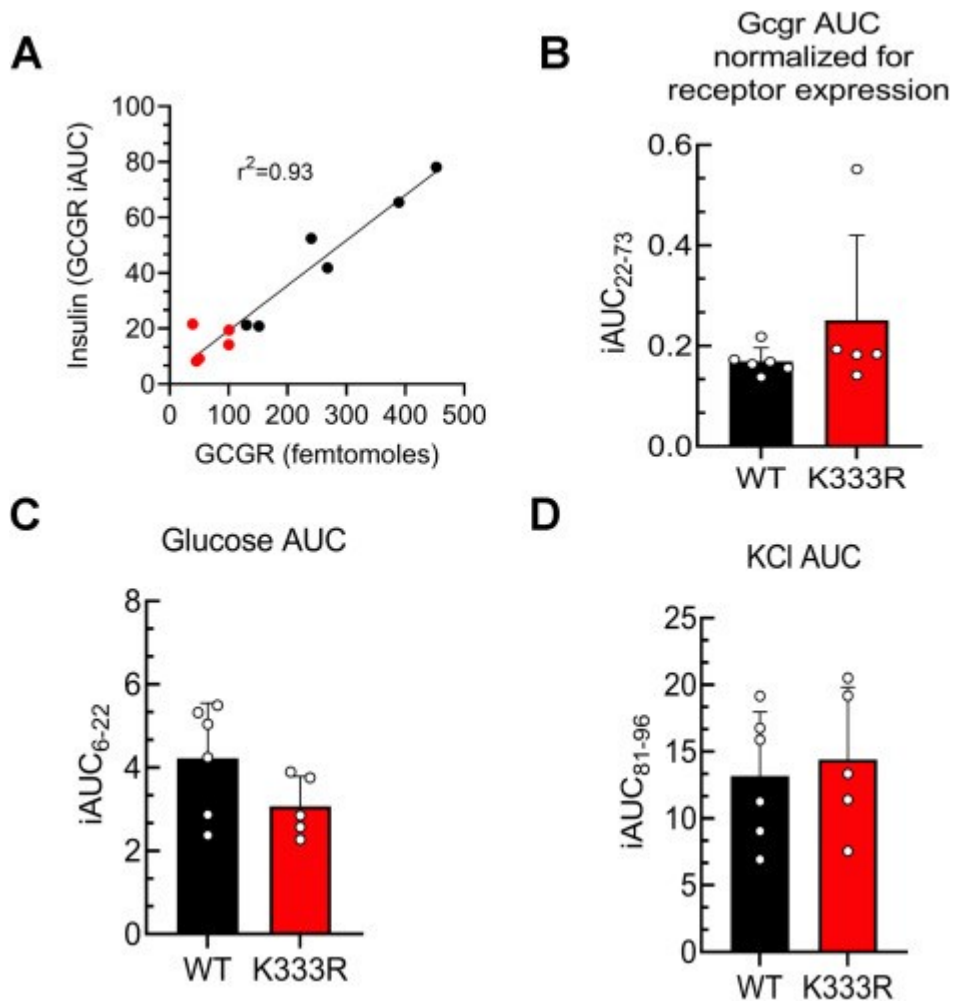


Figure 6



**Figure 7**



**Figure 8**

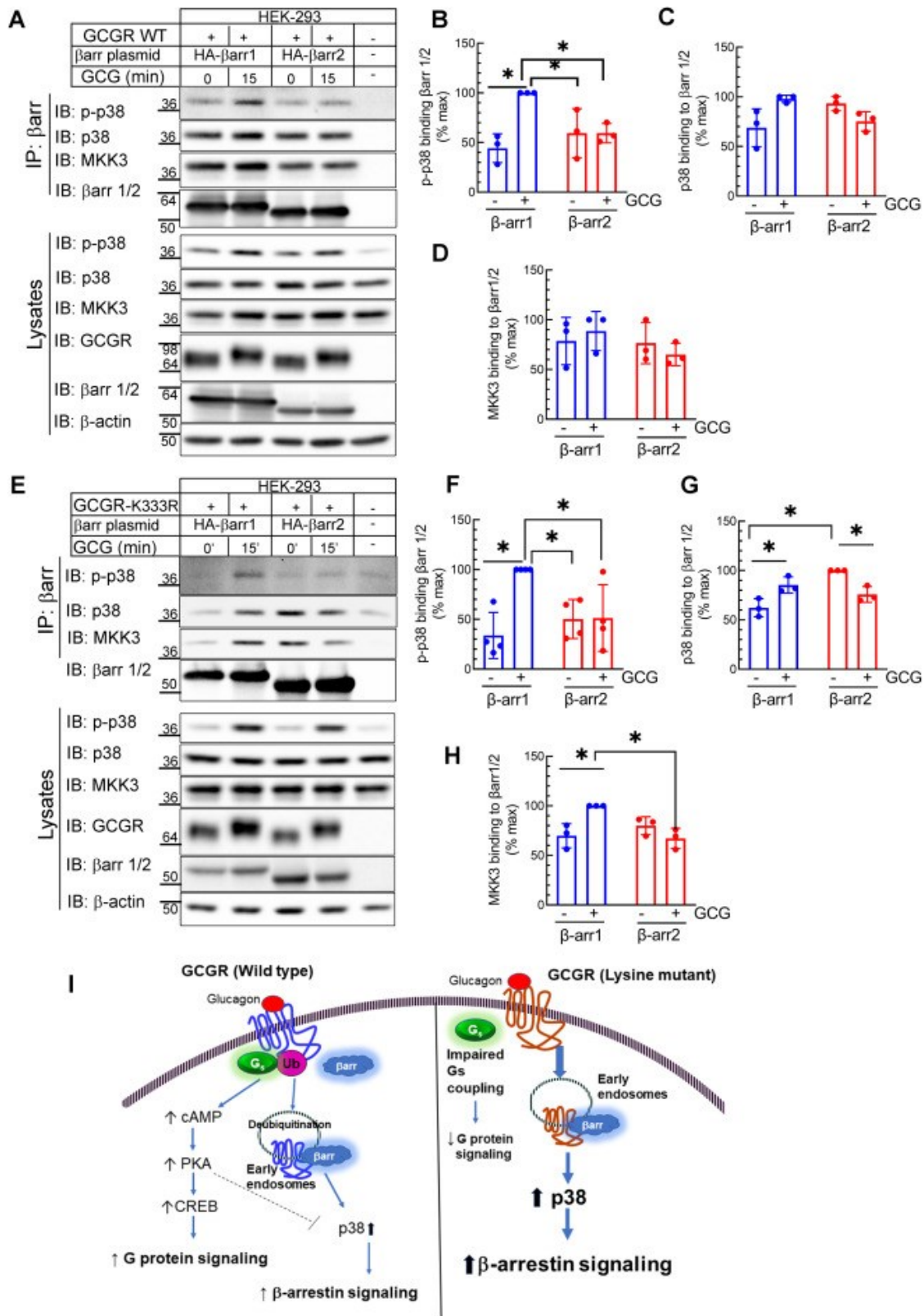


Figure 9

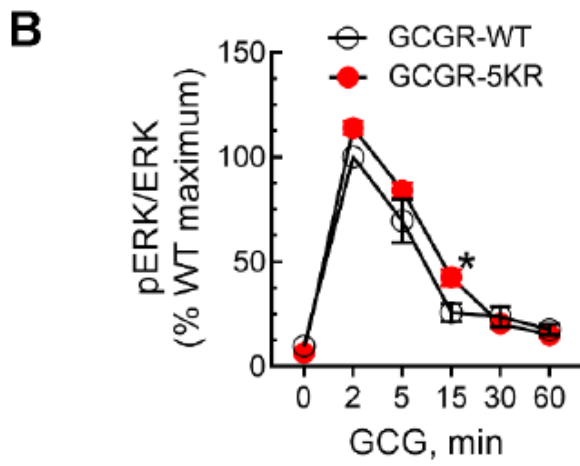
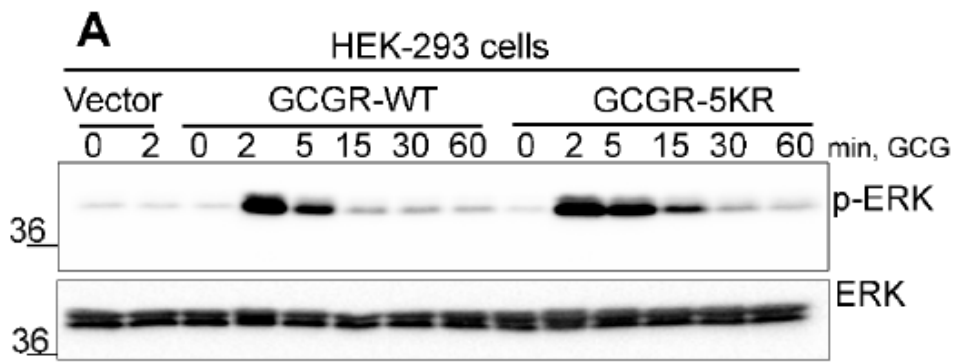


Figure S1

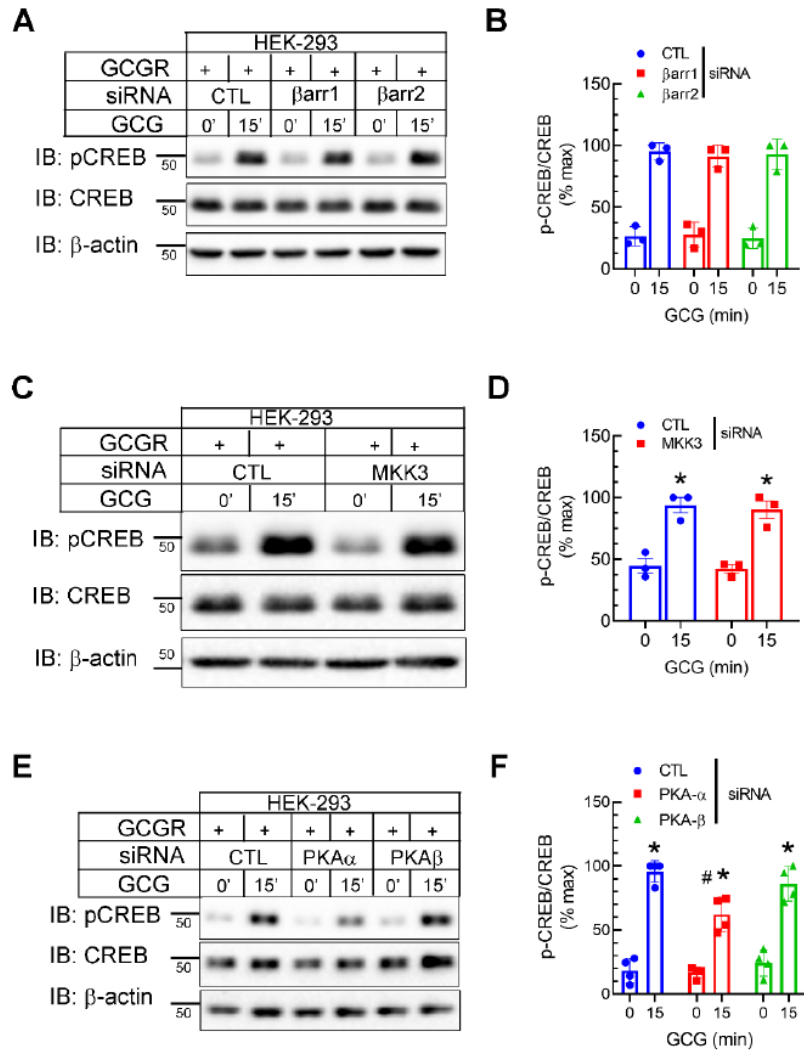


Figure S2



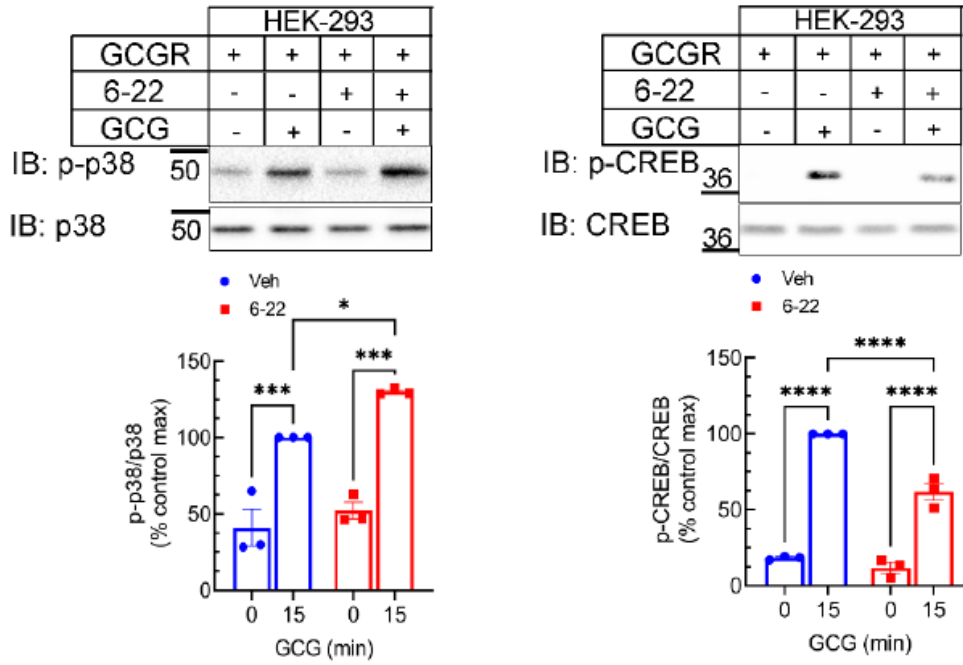
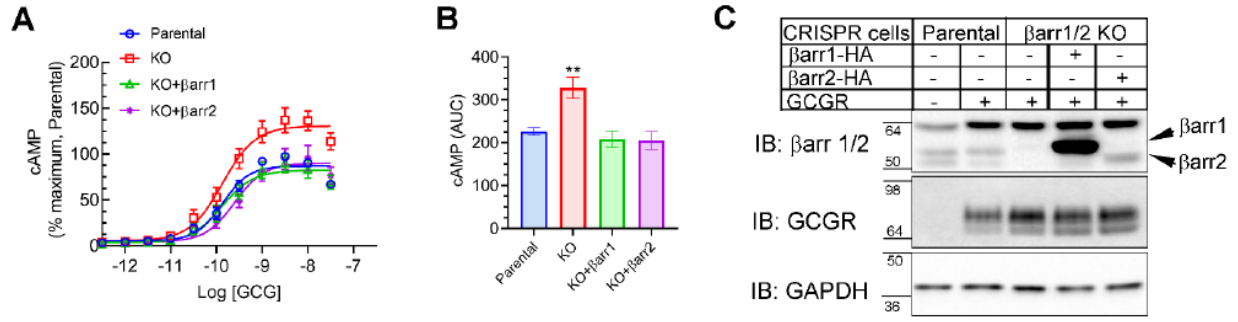


Figure S3



**Figure S4**

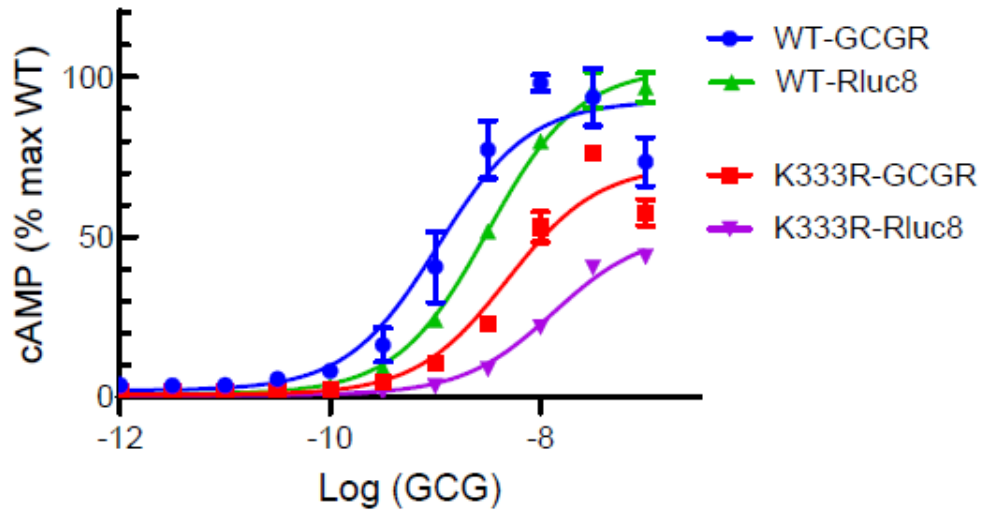


Figure S5

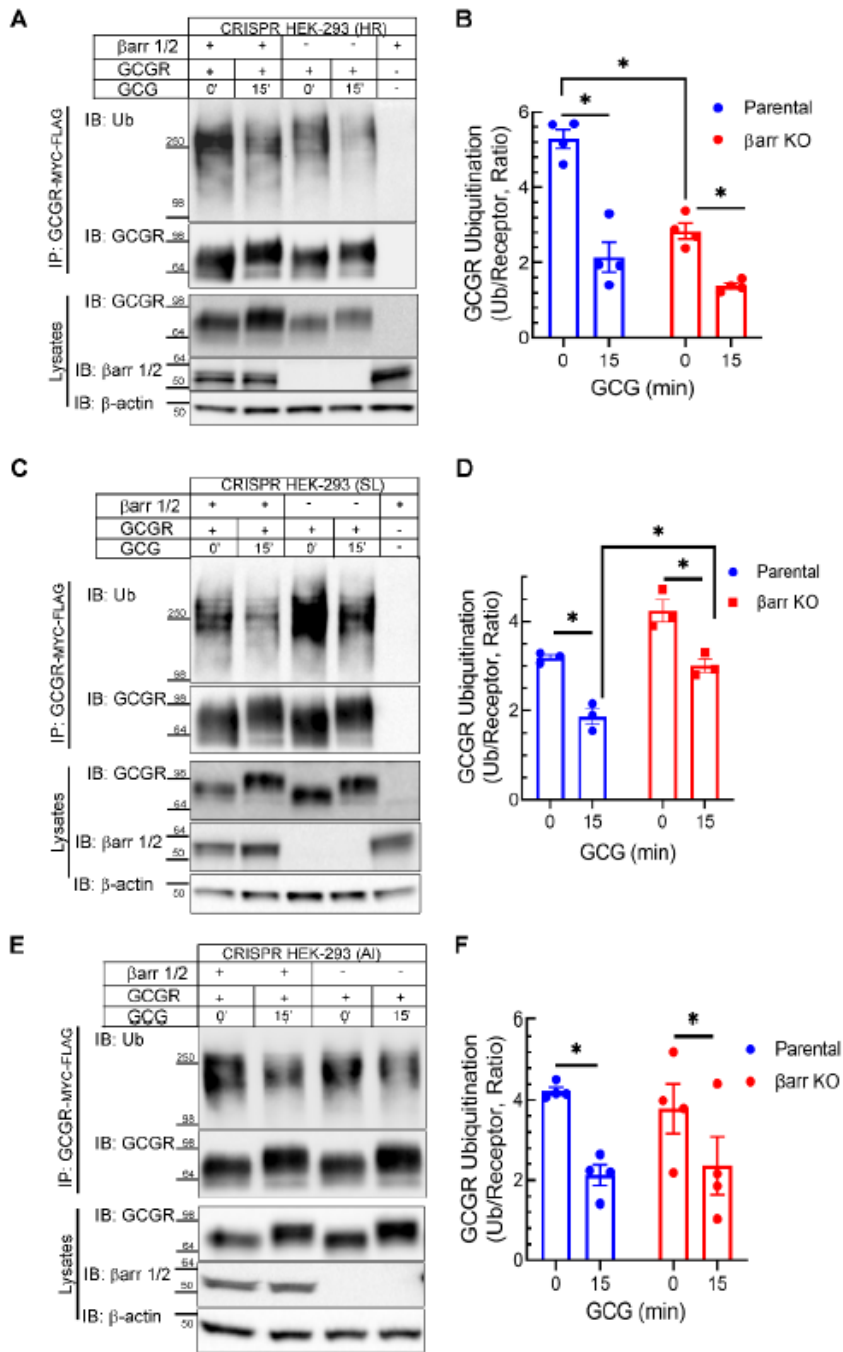
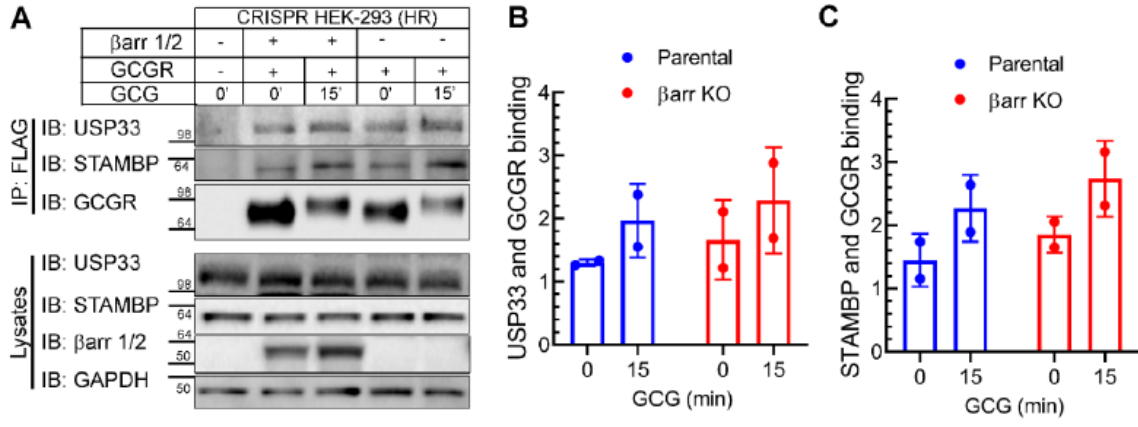


Figure S6



**Figure S7**

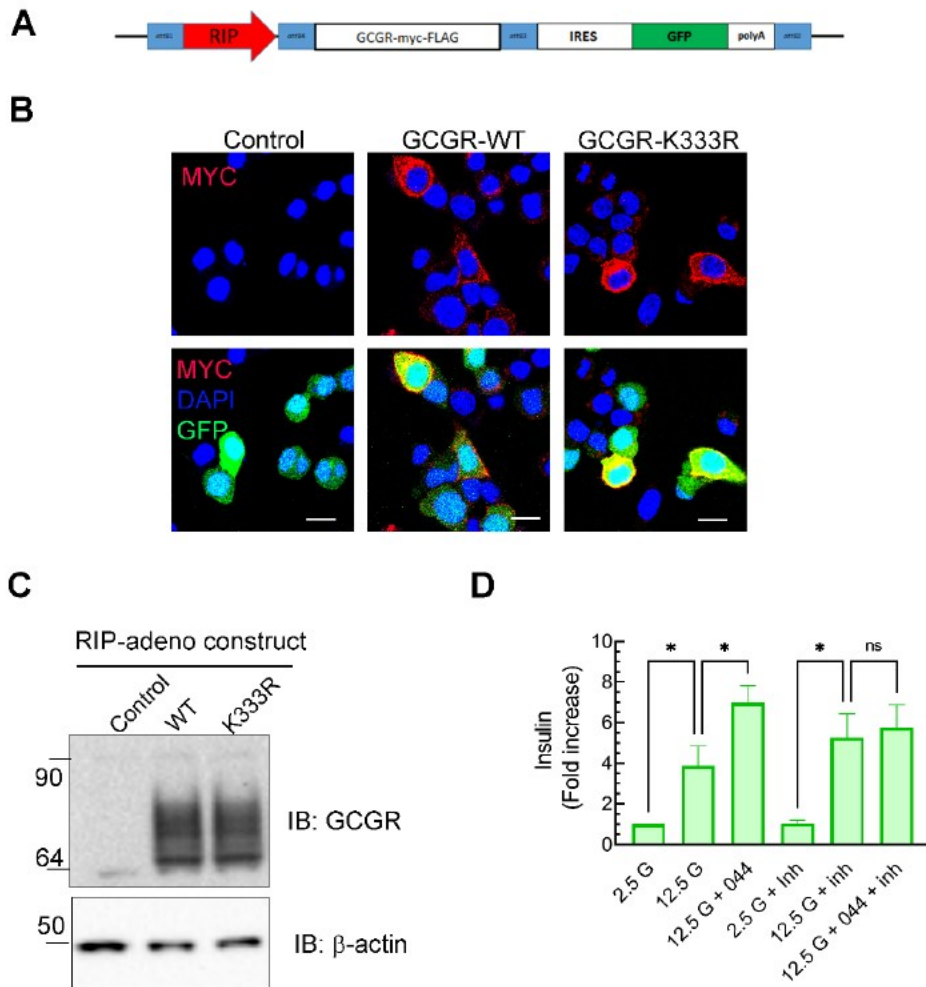


Figure S8

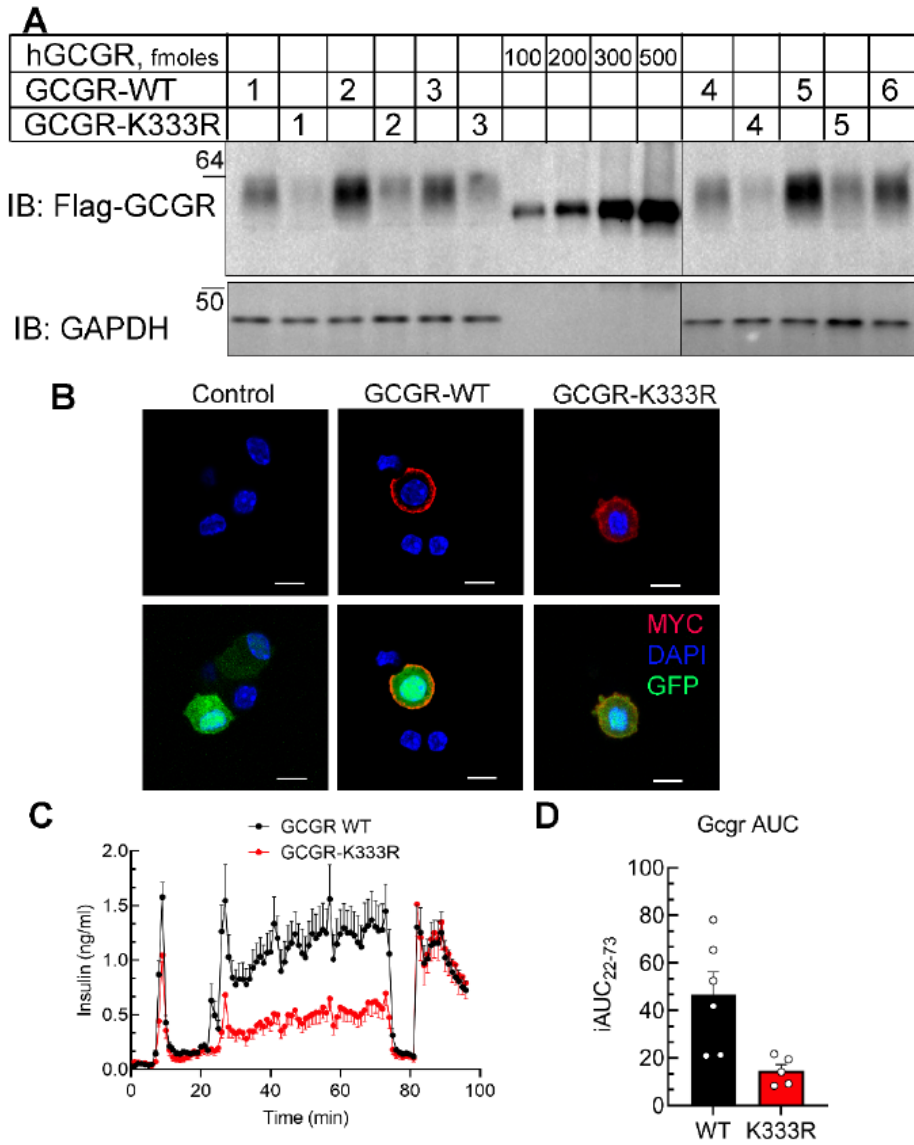


Figure S9

## **6 Chapter 6: The E2/E3 Ubiquitin-Conjugating Enzyme UBE2O is a $\beta$ -arrestin1/2 Binding Partner and Trafficking Regulator**

Context:

$\beta$ -arrestin is a scaffolding protein first identified for its role in desensitization and endocytosis of G-protein coupled receptors (GPCR). In recent years, publications from many teams including the laboratory of Dr. Bouvier showed that  $\beta$ -arrestin also has non-canonical functions as it acts as a scaffolding protein that assembles diverse protein complexes allowing intracellular signaling. In this study, we used a BioID approach to identify novel  $\beta$ -arrestin 1/2 interactors. We also confirmed the interaction between  $\beta$ -arrestin 1/2 and a E2/E3 ubiquitin-conjugating enzyme UBE2O and showed that this enzyme modulates  $\beta$ -arrestin trafficking. Our results shed light on novel interactions that could play an important role in GPCR regulation in addition of highlighting the function of UBE2O in  $\beta$ -arrestin trafficking.

Contribution:

I performed the BioID experiments in collaboration with Justine Paradis and Antoine Méant. The mass spectrometry data acquisition was carried out at the MS platform of IRIC. I analyzed and interpreted the BioID results under the supervision of Dr. Philippe Roux and Dr. Michel Bouvier. I designed, performed, analyzed, and interpreted all the other experiments. An undergrad intern, Stella Cellier, did some of the BRET experiments under my supervision. Finally, I wrote the manuscript under the guidance of Dr. Michel Bouvier.



# The E2/E3 ubiquitin-conjugating enzyme UBE2O is a $\beta$ -arrestin1/2 binding partner and trafficking regulator

**Badr Sokrat**<sup>1,2</sup>, Justine Paradis<sup>2</sup>, Stella Cellier<sup>1,2</sup>, Antoine Méant<sup>2</sup>, Philippe Roux<sup>2</sup>, Michel Bouvier<sup>1,2#</sup>

1 Department of Biochemistry and Molecular Medicine, University of Montreal, Montreal, Quebec, H3T 1J4 Canada

2 Institute for Research in Immunology and Cancer, University of Montreal, Montreal, Quebec, H3T 1J4 Canada

#: Corresponding author

## **Abstract**

$\beta$ -arrestin is a multifunctional scaffolding protein involved in the regulation of G protein-coupled receptor (GPCR) signaling. Upon GPCR activation,  $\beta$ -arrestin is recruited to the plasma membrane where it plays an important role in receptor desensitization and internalization. In addition,  $\beta$ -arrestin is involved in non-canonical functions by acting as a scaffold protein for several signaling cascades such as the MAPK pathway and by mediating nuclear functions such as the nucleocytoplasmic shuttling of Mdm2. Therefore, characterization of the  $\beta$ -arrestin interactome is critical to gain a comprehensive understanding of the diverse roles and regulation mechanisms of  $\beta$ -arrestin. Here, we employed a BioID proteomic approach to identify over 100 potential  $\beta$ -arrestin 1/2 interactors. Notably, we validated an interaction between  $\beta$ -arrestin 1/2 and an atypical E2/E3 ubiquitin conjugating enzyme, UBE2O. We also revealed that UBE2O accelerates  $\beta$ -arrestin translocation from the plasma membrane to early endosomes. Our study uncovers a comprehensive analysis of  $\beta$ -arrestin interactome using BioID and provides novel insight into the regulation of  $\beta$ -arrestin trafficking by a previously unreported interaction with UBE2O.

## Introduction

G protein-coupled receptors (GPCRs) are a large family of seven transmembrane domain receptors (over 800 members in humans) that play an important role in patient therapy as it is estimated that 34% of FDA-approved drugs target GPCRs or their effectors (1). After activation by its ligand, the receptor undergoes a conformational change leading to the activation of the coupled G protein and the generation of second messengers such as cAMP, DAG or IP3 (2, 3, 4). This is followed by phosphorylation of specific intracellular residues in the C-terminal tail and intracellular loop regions of the receptor by second messenger-regulated kinases (PKA and PKC) as well as GPCR kinases (GRKs) (5). GRK-mediated phosphorylation of receptors induces the recruitment of  $\beta$ -arrestin proteins that have been initially identified for their role in GPCR desensitization (6). There are two isoforms of  $\beta$ -arrestin,  $\beta$ -arrestin 1 and  $\beta$ -arrestin 2, that are ubiquitously expressed and share high sequence homology (80%) but differ in their expression profile and selectivity for different GPCRs (7). Moreover, the two isoforms contrast in their subcellular localization at basal level as  $\beta$ -arrestin 1 localizes in both the cytoplasm and the nucleus, while  $\beta$ -arrestin 2 localizes mainly in the cytoplasm with a transient shuttling to the nucleus (8, 9).

$\beta$ -arrestin plays a role in GPCR internalization by acting as a scaffolding protein linking the receptor to the AP2 complex (10) and clathrin (11) of the endocytic machinery.  $\beta$ -arrestin has similarly been shown to interact with other proteins involved in GPCR trafficking and recycling processes such as NSF, ARF6, and ARNO (12, 13, 14).  $\beta$ -arrestin also interacts with E3 ubiquitin ligases and deubiquitinases to control its own post-translational modifications or to regulate GPCR ubiquitination status. For instance,  $\beta$ -arrestin 2 has been shown to be ubiquitinated by Mdm2 to trigger agonist-induced receptor endocytosis. Additionally,  $\beta$ -arrestin serves as an adaptor to mediate  $\beta$ 2AR ubiquitination by Nedd4 and direct the receptor to lysosomal degradation (15, 16, 17).

There are different patterns of  $\beta$ -arrestin binding to GPCRs. Oakley et al. (18), identified two classes of GPCRs with different affinities for  $\beta$ -arrestin1/2. They showed that class A receptors like  $\beta$ 2 adrenergic,  $\mu$ -opioid, endothelin type A and dopamine D1A receptors recruit  $\beta$ -arrestin 2

with higher affinity than  $\beta$ -arrestin 1. On the other hand, class B receptors like vasopressin V2, angiotensin II type 1A, neurotensin 1 and thyrotropin-releasing hormone receptors recruit both  $\beta$ -arrestins with similar high affinities. Furthermore, class A receptors form transient complexes with  $\beta$ -arrestin as they dissociate upon internalization, whereas class B receptors form more stable complexes during internalization in endosomal compartments (19, 20).

Over the last 20 years, numerous studies have shown that  $\beta$ -arrestin plays non-canonical functions by scaffolding signaling cascade events. Indeed, it has been shown that  $\beta$ -arrestin 1 promotes the c-Src cascade following GPCR activation (21, 22).  $\beta$ -arrestin also forms a complex with Raf-1, MEK1, and ERK1/2 of the MAPK pathway to promote ERK1/2 signaling in an agonist-dependent manner (23). Similar studies have shown that  $\beta$ -arrestin binds or has an important function in JNK3, p38 and Akt activation (24, 25, 26). Hence, the identification of novel  $\beta$ -arrestin interactors could give new insights into  $\beta$ -arrestin non-canonical functions and regulation mechanisms. To do so, we used a proximity-dependent biotin identification approach (BioID) (27) and we identified 21 potential interactors for  $\beta$ -arrestin 1, 70 potential interactors for  $\beta$ -arrestin 2 and 16 potential interactors common for both isoforms. Considering that the importance of ubiquitination in GPCR regulation has been highlighted in numerous research papers (15, 28, 29, 30), we focused on the E2/E3 ubiquitin-conjugating enzyme UBE2O as a  $\beta$ -arrestin binding partner. We confirmed the interaction between  $\beta$ -arrestin 1/2 and UBE2O using co-immunoprecipitation and BRET assays and showed a role for UBE2O in regulating  $\beta$ -arrestin trafficking. Taken together, we have developed a BioID approach adapted to the identification of novel  $\beta$ -arrestin interactors and characterized UBE2O as binding partner and trafficking regulator of  $\beta$ -arrestin.

## Results

### *Development of a BioID approach to identify $\beta$ -arrestin 1/2 interaction partners*

To identify interaction partners of  $\beta$ -arrestin 1/2, we developed a BioID approach based on the biotinylation of endogenous proteins in the proximity of the bait protein (Fig. 1A, methods). To this end, we fused BirA-R118G from *Escherichia coli* with a FLAG tag to the C-terminus of  $\beta$ -arrestin 1 and  $\beta$ -arrestin 2. Next, we monitored expression of the fusion proteins in HEK293 stable

cell lines by western blot using an anti-FLAG antibody and observed bands for BirA-FLAG (~35 kDa), GFP-BirA-FLAG (~60 kDa), and  $\beta$ -arrestin 1/2 fused to BirA-FLAG (~85 kDa) at the expected molecular weights (Fig. 1B). Second, labeling with streptavidin-HRP marker revealed a smear pattern indicative of the biotinylation of numerous endogenous proteins resulting from proximity to BirA. Consistent with the anti-FLAG blot where  $\beta$ -arrestin 1 was revealed to be more highly expressed than  $\beta$ -arrestin 2, there seemed to be fewer biotinylated proteins in the case of  $\beta$ -arrestin 2 compared to  $\beta$ -arrestin 1.

Next, we wanted to confirm that BirA does not affect  $\beta$ -arrestin native cellular localization ( $\beta$ -arrestin 1 localizes in both the cytoplasm and the nucleus whereas  $\beta$ -arrestin 2 is mostly cytoplasmic). To do so, we used confocal microscopy to evaluate cellular localization of  $\beta$ -arrestin 1/2 fused to BirA. We cotransfected previously characterized  $\beta$ -arrestin 1 or  $\beta$ -arrestin 2 constructs fused to YFP and observed that  $\beta$ -arrestin 1 fused to BirA colocalizes with the YFP construct in the cytoplasm and the nucleus (Fig. 1C - Top). We also observed that  $\beta$ -arrestin 2 fused to BirA colocalizes with the YFP construct in the cytoplasm and is excluded from the nucleus (Fig. 1C - Bottom). Taken together, these results show that  $\beta$ -arrestin 1/2 constructs fused to BirA are properly expressed, exhibit proper cellular localization, and enable biotinylation of endogenous proteins.

#### *BioID results and analysis of $\beta$ -arrestin 1/2 proximity partners*

Subsequently, we carried the BioID experiment and identified 21 potential interactors for  $\beta$ -arrestin 1, 70 potential interactors for  $\beta$ -arrestin 2 and 16 potential interactors common for both isoforms (Fig. 2A). Comparing the list of interactors that we identified by BioID to proteins listed on the general repository for interaction datasets BioGrid as previously identified interactors of  $\beta$ -arrestin 1/2 (31), we noted that 13 proteins in our list have already been identified as  $\beta$ -arrestin 1/2 interactors in previous studies (KIF3A, NAA15, AP3B1, AHCYL1, AHCYL2, NSF, SPTBN1, TTN, AP2B1, ARRB1, KANK1, AP2A2, RAD18) (Fig. 2B). GO term analysis using STRING (32) revealed that the proteins identified by BioID are ubiquitously distributed throughout the cell but are enriched in cellular compartments where  $\beta$ -arrestin is known to shuttle like the cytoplasm (EIF3A, FXR1, UBE2O), nucleus (CDC27, NUP88), plasma membrane (ERBB2IP, RAPGEF6) and clathrin-coated

vesicles (AP2A2, AP2B1, AP3B1) (Fig. 2C). This indicates that the identified interactors could play a role in  $\beta$ -arrestin 1/2 functions in these compartments for instance in GPCR trafficking. Moreover, the proteins identified by BioID are associated with biological functions such as the regulation of protein localization (BCAS3, SPTBN1), clathrin-coated endocytosis (AP2A2, AP2B1, FCHO2), import into the nucleus (NUP88, SMN2), plasma membrane localization (TNIK, RAPGEF6), and protein kinase activity (MAP4K4, NCK1, MAPK6) (Fig. 2D). These categories of interactors are consistent with established functions of  $\beta$ -arrestin, suggesting that the newly identified binding partners may participate in protein complexes with  $\beta$ -arrestin to achieve these roles.

#### *Interaction of $\beta$ -arrestin 1/2 with UBE2O*

The identification of a potential interaction between  $\beta$ -arrestin and UBE2O, an atypical E2/E3 ubiquitin conjugating enzyme, is intriguing as GPCR and  $\beta$ -arrestin ubiquitination has been shown to be an important regulator of their functions (15, 16, 17). UBE2O is a large enzyme that displays both E2 and E3 activity (33) and has been shown to mediate ubiquitination of several proteins such as SMAD6 (34) and BAP1 (35) to regulate their stability, interaction, and trafficking. Until now, no relationship between UBE2O and GPCR/ $\beta$ -arrestin function has been described. We sought to investigate and confirm the interaction between  $\beta$ -arrestin and UBE2O by co-immunoprecipitation. First, we transfected HEK293 cells with FLAG-tagged  $\beta$ -arrestin 2 and Myc-tagged UBE2O followed by FLAG immunoprecipitation and immunoblotting. Our results revealed the co-immunoprecipitation of UBE2O with  $\beta$ -arrestin 2, suggesting the formation of a protein complex between these two proteins (Fig. 3A). To further confirm this interaction, we conducted a reciprocal experiment by immunoprecipitating Myc-UBE2O in presence of FLAG- $\beta$ -arrestin 2 which yielded similar results confirming the interaction of these two proteins (Fig. 3B).

Although UBE2O was not enriched as a potential interactor of  $\beta$ -arrestin 1 in our BioID experiment, we investigated the possibility of an interaction between these two proteins. We performed a FLAG- $\beta$ -arrestin 1 immunoprecipitation and showed that UBE2O does co-precipitate with  $\beta$ -arrestin 1 (Fig. 3C). Additionally, our results were further confirmed by the reciprocal experiment with Myc-UBE2O immunoprecipitation, which demonstrated that  $\beta$ -arrestin 1 forms a complex with UBE2O (Fig. 3D). Finally, we quantitatively measured the interaction between

UBE2O and  $\beta$ -arrestin 1/2 in living cells by Bioluminescence Resonance Energy Transfer (BRET) (35). We used  $\beta$ -arrestin 1/2 fused to a luminescent energy donor (RlucII) and UBE2O fused to a green fluorescent protein (GFP10), and we observed saturation of the BRET signal indicative of a specific interaction between  $\beta$ -arrestin 1/2 and UBE2O. Furthermore, vasopressin V2 receptor (V2R) stimulation caused a decrease in signal possibly indicating an agonist-promoted loss of interaction between  $\beta$ -arrestin 1/2 and UBE2O (Fig. 3E, 3F). Taken together, these results confirm a constitutive interaction between  $\beta$ -arrestin 1/2 and UBE2O which is dampened following V2R activation.

#### *UBE2O regulates $\beta$ -arrestin 1/2 trafficking*

To test UBE2O involvement in  $\beta$ -arrestin 1/2 functions, we used enhanced bystander BRET (ebBRET) to monitor  $\beta$ -arrestin 1/2 trafficking in living cells (36). First, we assessed recruitment of  $\beta$ -arrestin 1/2 to the plasma membrane after V2R activation, a prototypical class B GPCR, in the presence of overexpressed UBE2O WT or UBE2O CD (Catalytically Dead mutant) (37). We observed that overexpression of UBE2O WT, but not UBE2O CD, decreases  $\beta$ -arrestin 1/2 recruitment to the plasma membrane (Fig. 4A, 4B). This effect was not due to differences in receptor expression as controlled by cell surface ELISA (Fig. 4C) and overexpression of UBE2O WT and UBE2O CD is monitored by western blot (Fig. 4D). UBE2O has a similar effect upon activation of a class A receptor, the  $\beta$ 2-adrenergic receptor ( $\beta$ 2AR) but it does not only reduce the agonist-promoted recruitment of  $\beta$ -arrestin 1/2 to the plasma membrane, but also diminishes  $\beta$ -arrestin 1/2 basal level of plasma membrane recruitment (Fig. S1). This suggests that UBE2O may either impede  $\beta$ -arrestin 1/2 trafficking to the plasma membrane or accelerates its internalization in the endosomes following interaction with the receptor.

To distinguish between these two possibilities, we monitored  $\beta$ -arrestin 1/2 internalization after V2R stimulation and we observed that UBE2O WT overexpression enhances  $\beta$ -arrestin 1/2 endosomal localization suggesting a possible acceleration of  $\beta$ -arrestin 1/2 trafficking from the plasma membrane to early endosomes (Fig. 5A, 5B). Here again, receptor expression in the different conditions was compared by cell surface ELISA (Fig. 5C) and UBE2O overexpression was confirmed by western blot (Fig. 5D). Finally, we investigated the kinetics of  $\beta$ -arrestin 2

recruitment to the plasma membrane in cells expressing increasing amounts of UBE2O WT (Fig. 6A) and observed a decrease in the level of recruitment to the plasma membrane. Moreover, we noted a significant increase in the dissociation rate from the plasma membrane after reaching its maximum (Fig. 6C). The kinetics of  $\beta$ -arrestin 2 endosomal trafficking also revealed that UBE2O accelerates the movement of  $\beta$ -arrestin 2 from the plasma membrane to the endosomes (Fig. 6B, 6D). These results provide new evidence that UBE2O plays a significant role in regulating the recruitment and trafficking of  $\beta$ -arrestin 1/2.

## Discussion

$\beta$ -arrestin plays an important role in the regulation of GPCR signaling, desensitization and trafficking. The present study aimed to identify novel binding partners of  $\beta$ -arrestin 1/2 to help expand our understanding of non-canonical  $\beta$ -arrestin functions and regulation mechanisms. Using a BioID proteomic approach, we identified over 100 potential  $\beta$ -arrestin interactions. We also characterized the interaction and function of a novel binding partner of  $\beta$ -arrestin 1/2, the E2/E3 conjugating-enzyme UBE2O, which we found to regulate  $\beta$ -arrestin 1/2 trafficking by accelerating its translocation from the plasma membrane to early endosomes. These findings uncover new potential interactions that could be involved in  $\beta$ -arrestin functions and suggest a new regulation mechanism of  $\beta$ -arrestin trafficking mediated by UBE2O.

$\beta$ -arrestin has been shown to interact with several non-GPCR proteins including enzymes, signaling proteins, and structural proteins, expanding the spectrum of its functional roles. To date, the  $\beta$ -arrestin interactome includes more than 400 proteins. However, it should be noted that most of these proteins were identified in a single proteomic study based on the immunoprecipitation of  $\beta$ -arrestin 1/2 followed by mass spectrometry protein identification (IP-MS) which identified 337 potential interactors (38). The main limitation of IP-MS when it comes to identifying protein-protein interaction is the difficulty to identify weak or transient interactions, and insoluble proteins. Our approach overcomes these challenges as BioID enables the biotin labeling of weak and transient interactions in their native cellular context. Additionally, it was suggested that BioID is more efficient in identifying insoluble proteins compared to IP-MS (27). It is interesting to note that only 13 of the proteins identified by BioID were already reported



as  $\beta$ -arrestin interactors in previous studies suggesting that different methods may reveal distinct interactors. Combining the results of various approaches aiming to investigate the interactome of  $\beta$ -arrestin could provide insight into new functions played by these proteins.

Our analysis showed that BioID enables the identification of proteins distributed throughout different cellular compartments.  $\beta$ -arrestin 1/2 translocation from the cytoplasm to the plasma membrane followed by trafficking to early endosomes has been extensively studied. Interactors identified by BioID may form a complex with  $\beta$ -arrestin to contribute to these functions or engage in other roles in these cellular compartments. Notably, our BioID approach found the AP2 adaptor complex (39) and NSF (12) that have both been previously shown to interact with  $\beta$ -arrestin and to be involved in GPCR internalization. It is conceivable that other potential interactors identified by BioID may also be involved in trafficking functions. For instance, we identified AP3B1, a subunit of the AP3 complex that is important for protein sorting in the endosomes and trans-Golgi network (40). An investigation of the interaction of  $\beta$ -arrestin with the AP3 complex and its potential role in GPCR trafficking would be an interesting avenue to explore.

We also identified nuclear interactors that could involve  $\beta$ -arrestin in some of its lesser studied roles. For instance,  $\beta$ -arrestin 2 has been shown to mediate Mdm2 translocation from the nucleus to the cytoplasm resulting in increased p53-mediated signaling (41, 42). Similarly,  $\beta$ -arrestin could be involved in the nucleocytoplasmic shuttling of some of the identified interactors or that said interactors, such as NUP88 (a nuclear pore complex protein), mediate  $\beta$ -arrestin complexes shuttling. Another function found to be enriched in the interactors of  $\beta$ -arrestin is the regulation of protein phosphorylation and kinase activity. As  $\beta$ -arrestin has been shown to act as a scaffold for the ERK1/2 cascade, it is interesting to note its interaction with two other MAPK proteins (MAP4K4, MAPK6). Further investigation into the role of  $\beta$ -arrestin in signaling cascades involving these two kinases is necessary.

Ubiquitination serves as a critical regulation mechanism of GPCR and  $\beta$ -arrestin function. Thus, identification of UBE2O as an interactor of both  $\beta$ -arrestin 1/2 is of particular interest. Another study published just recently used APEX2-based proximity labeling and also found UBE2O among the identified  $\beta$ -arrestin 1 interactors (43). It is interesting to observe that GPCR activation results

in a decrease in this interaction possibly due to the recruitment of  $\beta$ -arrestin 1/2 to the receptor at the plasma membrane. It is also possible that the decrease in BRET signal is indicative of changes in the conformation of the complex between  $\beta$ -arrestin and UBE2O. While we cannot exclude that the interaction between UBE2O and  $\beta$ -arrestin is indirect, we clearly demonstrate that UBE2O accelerates  $\beta$ -arrestin translocation from the plasma membrane to the endosomes. It remains to be determined whether this is due to the ubiquitination of  $\beta$ -arrestin, or another protein involved in the endocytosis process. Of note, several ubiquitin ligases including Mdm2, Nedd4, and AIP4 have been shown to mediate GPCR/ $\beta$ -arrestin ubiquitination to regulate receptor internalization and lysosomal degradation (15, 44, 45, 46). Further investigation is required to fully understand the underlying mechanisms of UBE2O's role in  $\beta$ -arrestin and GPCR translocation.

In summary, our study highlights the potential of the BioID proteomic approach to identify potential protein interactors within their native cellular context. The identification of over 100 potential  $\beta$ -arrestin 1/2 interactions opens interesting avenues to study their role in the regulation and signaling mediated by this protein. Additionally, we demonstrated a novel interaction between  $\beta$ -arrestin 1/2 and an atypical E2/E3 ubiquitin conjugating enzyme UBE2O that regulates  $\beta$ -arrestin function by accelerating its translocation from the plasma membrane to the endosomes. It would be expected that in-depth investigation of other proteins identified in the BioID experiment to show novel functions and regulation mechanisms of  $\beta$ -arrestin and provide valuable insight into GPCR-mediated signaling and cellular response.

## **Material and Methods**

### *Reagents:*

Dulbecco's phosphate-buffered saline (PBS), Hanks' Balanced Salt Solution (HBSS), Dulbecco's modified Eagle's medium (DMEM), Trypsin, penicillin/streptomycin, and newborn calf serum (NCS) were purchased from Wisent Bioproducts. Polyethylenimine (PEI) was purchased from Alfa Aesar (Thermo Fisher Scientific). (-)-Isoproterenol hydrochloride (ISO) and Arginine vasopressin (AVP) were purchased from Sigma Aldrich. Coelenterazine 400A, and Prolume Purple were purchased from Nanolight Technologies.

### *DNA Constructs:*

The pcDNA5-FRT/TO-FLAG-BirAR118G construct encoding Flag-BirA-R118G was provided by Dr. Anne-Claude Gingras (University of Toronto, Toronto, Canada). The myc-UBE2O-WT and myc-UBE2O-CD were provided by Dr. El Bachir Affar. The BRET and ebBRET biosensors used were described previously (36).

### *Generation of BioID stable cell lines and BioID experiment:*

Stable cell lines expressing BirA fusions were generated as previously described (47). Cells were grown in presence of 200 µg/ml hygromycin and protein expression was induced by addition of 1 µg/ml tetracycline for 24 hours. 50 µM biotin was added to enable endogenous proteins biotinylation for 24 hours. Cells were centrifuged, washed with ice-cold PBS and frozen at -80 °C. Pellets were then thawed in ice cold RIPA buffer. Lysates were centrifuged and supernatants were transferred to a microfuge tubes, followed by addition of prewashed streptavidin-agarose beads for 3 hours under rotation. Beads were washed twice in RIPA buffer, three times in 50 mM ammonium bicarbonate, resuspended in ammonium bicarbonate with 1 µg of trypsin, and incubated at 37 °C overnight with agitation. After centrifugation, the supernatant was transferred to a fresh tube and vacuum dried. Tryptic peptides were resuspended in 5% formic acid. Mass spectrometry data acquisition and analysis was performed as described previously (48).

### *Immunofluorescence Microscopy*

HeLa cells were seeded on a coverslip in 12-well plates and transfected with the described plasmids. Forty-eight hours later, cells were washed with PBS and fixed with formaldehyde for 5 minutes at room temperature. Cells were washed twice in PBS-0.3% Triton X-100 and incubated for 1 hour with primary antibodies, washed twice with PBS, and incubated for 1 h with secondary Alexa fluor 555-conjugated goat anti-mouse antibody and DAPI. Images were acquired on a confocal microscope Zeiss LSM700 using a 63X objective.

#### *Immunoprecipitation and western blot*

Transfected cells were lysed in RIPA buffer during 30min, followed by centrifugation at 14 000 rpm. Pellets were discarded and the supernatant was incubated with the indicated antibody for 2 hours followed by 1 hour incubation with protein G-Sepharose. Immunoprecipitates were washed three times in lysis buffer, and beads were eluted and boiled in 2×Laemmli buffer. Total lysates and immunoprecipitated samples were analyzed using a 10% SDS-PAGE, followed by transfer to PVDF membranes and immunoblotting.

#### *BRET and enhanced bystander BRET*

Transfected HEK293 cells were seeded in 96-well plates (Greiner) (100 µl/well). Forty-eight hours post-transfection, culture media was removed, cells were washed with PBS, and incubated with HBSS for 1 hour. Cells were then treated with vehicle or different concentrations of agonists. For Kinetics experiments, Prolume Purple (1µM) was added for 6 minutes and for dose-response experiments, Coelenterazine 400A was added for 5 minutes before readings were collected on a Tecan Spark multimode microplate reader or a Berthold Technologies Multilabel Reader Mithras LB 940. The BRET signal was calculated as the ratio of light emitted at the energy acceptor wavelengths (515 ± 20 nm) over the light emitted at the energy donor wavelengths (400 ± 70 nm).

#### *ELISA*

Transfected HEK293 cells were seeded in 96-well plates (Greiner) (100 µl/well). Forty-eight hours post-transfection, culture media was removed, cells were washed with PBS, and fixed with 3% PFA for 10 minutes at room temperature. Cells were washed again with PBS-0.5%BSA, incubated

with an anti-FLAG-HRP antibody for 1 hour, washed 3 times and incubated with ECL before luminescence reading on a Berthold Technologies Multilabel Reader Mithras LB 940.

### **Acknowledgement**

We thank all lab members for their insightful discussions and comments. We also thank Dr. Shane Wright for critical reading of the manuscript.

### **Author contribution**

B.S., P.R., and M.B. conceptualized and designed the study; B.S., J.P., S.C., and A.M. performed the experiments under the supervision of P.R. and M.B.; B.S. wrote the manuscript under the supervision of M.B.

### **Conflict of interest**

M.B. is the president of the scientific advisory board of Domain Therapeutics. All other authors declare no competing interests.

## Reference

1. Hauser AS, Chavali S, Masuho I, Jahn LJ, Martemyanov KA, Gloriam DE, et al. Pharmacogenomics of GPCR Drug Targets. *Cell*. 2018;172(1-2):41-54.e19.
2. Gilman AG. G PROTEINS: TRANSDUCERS OF RECEPTOR-GENERATED SIGNALS. *Annual Review of Biochemistry*. 1987;56(1):615-49.
3. Pierce KL, Premont RT, Lefkowitz RJ. Seven-transmembrane receptors. *Nat Rev Mol Cell Biol*. 2002;3(9):639-50.
4. Rosenfeldt H, Vázquez-Prado J, Gutkind JS. P-REX2, a novel PI-3-kinase sensitive Rac exchange factor. *FEBS Lett*. 2004;572(1-3):167-71.
5. Benovic JL, Strasser RH, Caron MG, Lefkowitz RJ. Beta-adrenergic receptor kinase: identification of a novel protein kinase that phosphorylates the agonist-occupied form of the receptor. *Proc Natl Acad Sci U S A*. 1986;83(9):2797-801.
6. Lohse MJ, Benovic JL, Codina J, Caron MG, Lefkowitz RJ. beta-Arrestin: a protein that regulates beta-adrenergic receptor function. *Science (New York, NY)*. 1990;248(4962):1547-50.
7. Attramadal H, Arriza JL, Aoki C, Dawson TM, Codina J, Kwatra MM, et al. Beta-arrestin2, a novel member of the arrestin/beta-arrestin gene family. *J Biol Chem*. 1992;267(25):17882-90.
8. Smith JS, Rajagopal S. The  $\beta$ -Arrestins: Multifunctional Regulators of G Protein-coupled Receptors. *The Journal of biological chemistry*. 2016;291(17):8969-77.
9. Scott MG, Le Rouzic E, Perianin A, Pierotti V, Enslin H, Benichou S, et al. Differential nucleocytoplasmic shuttling of beta-arrestins. Characterization of a leucine-rich nuclear export signal in beta-arrestin2. *The Journal of biological chemistry*. 2002;277(40):37693-701.
10. Laporte SA, Miller WE, Kim KM, Caron MG. beta-Arrestin/AP-2 interaction in G protein-coupled receptor internalization: identification of a beta-arrestin binding site in beta 2-adaptin. *J Biol Chem*. 2002;277(11):9247-54.
11. Krupnick JG, Goodman OB, Jr., Keen JH, Benovic JL. Arrestin/clathrin interaction. Localization of the clathrin binding domain of nonvisual arrestins to the carboxy terminus. *J Biol Chem*. 1997;272(23):15011-6.
12. McDonald PH, Cote NL, Lin FT, Premont RT, Pitcher JA, Lefkowitz RJ. Identification of NSF as a beta-arrestin1-binding protein. Implications for beta2-adrenergic receptor regulation. *J Biol Chem*. 1999;274(16):10677-80.
13. Claing A, Chen W, Miller WE, Vitale N, Moss J, Premont RT, et al. beta-Arrestin-mediated ADP-ribosylation factor 6 activation and beta 2-adrenergic receptor endocytosis. *J Biol Chem*. 2001;276(45):42509-13.
14. Mukherjee S, Gurevich VV, Jones JC, Casanova JE, Frank SR, Maizels ET, et al. The ADP ribosylation factor nucleotide exchange factor ARNO promotes beta-arrestin release necessary for luteinizing hormone/choriogonadotropin receptor desensitization. *Proc Natl Acad Sci U S A*. 2000;97(11):5901-6.
15. Shenoy SK, McDonald PH, Kohout TA, Lefkowitz RJ. Regulation of receptor fate by ubiquitination of activated beta 2-adrenergic receptor and beta-arrestin. *Science*. 2001;294(5545):1307-13.
16. Shenoy SK, Modi AS, Shukla AK, Xiao K, Berthouze M, Ahn S, et al.  $\beta$ -Arrestin-dependent signaling and trafficking of 7-transmembrane receptors is reciprocally regulated by the

- deubiquitinase USP33 and the E3 ligase Mdm2. *Proceedings of the National Academy of Sciences*. 2009;106(16):6650-5.
17. Shenoy SK, Xiao K, Venkataramanan V, Snyder PM, Freedman NJ, Weissman AM. Nedd4 mediates agonist-dependent ubiquitination, lysosomal targeting, and degradation of the beta2-adrenergic receptor. *The Journal of biological chemistry*. 2008;283(32):22166-76.
  18. Oakley RH, Laporte SA, Holt JA, Caron MG, Barak LS. Differential affinities of visual arrestin, beta arrestin1, and beta arrestin2 for G protein-coupled receptors delineate two major classes of receptors. *The Journal of biological chemistry*. 2000;275(22):17201-10.
  19. Zhang J, Barak LS, Anborgh PH, Laporte SA, Caron MG, Ferguson SS. Cellular trafficking of G protein-coupled receptor/beta-arrestin endocytic complexes. *J Biol Chem*. 1999;274(16):10999-1006.
  20. Oakley RH, Laporte SA, Holt JA, Barak LS, Caron MG. Molecular determinants underlying the formation of stable intracellular G protein-coupled receptor-beta-arrestin complexes after receptor endocytosis\*. *J Biol Chem*. 2001;276(22):19452-60.
  21. Luttrell LM, Ferguson SS, Daaka Y, Miller WE, Maudsley S, Della Rocca GJ, et al. Beta-arrestin-dependent formation of beta2 adrenergic receptor-Src protein kinase complexes. *Science*. 1999;283(5402):655-61.
  22. Miller WE, Maudsley S, Ahn S, Khan KD, Luttrell LM, Lefkowitz RJ. beta-arrestin1 interacts with the catalytic domain of the tyrosine kinase c-SRC. Role of beta-arrestin1-dependent targeting of c-SRC in receptor endocytosis. *J Biol Chem*. 2000;275(15):11312-9.
  23. Luttrell LM, Roudabush FL, Choy EW, Miller WE, Field ME, Pierce KL, et al. Activation and targeting of extracellular signal-regulated kinases by beta-arrestin scaffolds. *Proc Natl Acad Sci U S A*. 2001;98(5):2449-54.
  24. McDonald PH, Chow CW, Miller WE, Laporte SA, Field ME, Lin FT, et al. Beta-arrestin 2: a receptor-regulated MAPK scaffold for the activation of JNK3. *Science (New York, NY)*. 2000;290(5496):1574-7.
  25. Sun Y, Cheng Z, Ma L, Pei G. Beta-arrestin2 is critically involved in CXCR4-mediated chemotaxis, and this is mediated by its enhancement of p38 MAPK activation. *The Journal of biological chemistry*. 2002;277(51):49212-9.
  26. Povsic TJ, Kohout TA, Lefkowitz RJ. Beta-arrestin1 mediates insulin-like growth factor 1 (IGF-1) activation of phosphatidylinositol 3-kinase (PI3K) and anti-apoptosis. *The Journal of biological chemistry*. 2003;278(51):51334-9.
  27. Roux KJ, Kim DI, Raida M, Burke B. A promiscuous biotin ligase fusion protein identifies proximal and interacting proteins in mammalian cells. *J Cell Biol*. 2012;196(6):801-10.
  28. Shenoy SK, Lefkowitz RJ. Trafficking patterns of beta-arrestin and G protein-coupled receptors determined by the kinetics of beta-arrestin deubiquitination. *J Biol Chem*. 2003;278(16):14498-506.
  29. Shenoy SK, Lefkowitz RJ. Receptor-specific ubiquitination of beta-arrestin directs assembly and targeting of seven-transmembrane receptor signalosomes. *J Biol Chem*. 2005;280(15):15315-24.
  30. Hicke L, Zanolari B, Riezman H. Cytoplasmic tail phosphorylation of the alpha-factor receptor is required for its ubiquitination and internalization. *J Cell Biol*. 1998;141(2):349-58.
  31. Stark C, Breitkreutz BJ, Reguly T, Boucher L, Breitkreutz A, Tyers M. BioGRID: a general repository for interaction datasets. *Nucleic acids research*. 2006;34(Database issue):D535-9.

32. von Mering C, Jensen LJ, Snel B, Hooper SD, Krupp M, Foglierini M, et al. STRING: known and predicted protein-protein associations, integrated and transferred across organisms. *Nucleic Acids Res.* 2005;33(Database issue):D433-7.
33. Berleth ES, Pickart CM. Mechanism of ubiquitin conjugating enzyme E2-230K: catalysis involving a thiol relay? *Biochemistry.* 1996;35(5):1664-71.
34. Zhang X, Zhang J, Bauer A, Zhang L, Selinger DW, Lu CX, et al. Fine-tuning BMP7 signalling in adipogenesis by UBE2O/E2-230K-mediated monoubiquitination of SMAD6. *EMBO J.* 2013;32(7):996-1007.
35. Hamdan FF, Percherancier Y, Breton B, Bouvier M. Monitoring protein-protein interactions in living cells by bioluminescence resonance energy transfer (BRET). *Curr Protoc Neurosci.* 2006;Chapter 5:Unit 5 23.
36. Namkung Y, Le Gouill C, Lukashova V, Kobayashi H, Hogue M, Khoury E, et al. Monitoring G protein-coupled receptor and beta-arrestin trafficking in live cells using enhanced bystander BRET. *Nat Commun.* 2016;7:12178.
37. Mashtalir N, Daou S, Barbour H, Sen NN, Gagnon J, Hammond-Martel I, et al. Autodeubiquitination protects the tumor suppressor BAP1 from cytoplasmic sequestration mediated by the atypical ubiquitin ligase UBE2O. *Mol Cell.* 2014;54(3):392-406.
38. Xiao K, McClatchy DB, Shukla AK, Zhao Y, Chen M, Shenoy SK, et al. Functional specialization of beta-arrestin interactions revealed by proteomic analysis. *Proc Natl Acad Sci U S A.* 2007;104(29):12011-6.
39. Laporte SA, Oakley RH, Zhang J, Holt JA, Ferguson SS, Caron MG, et al. The beta2-adrenergic receptor/betaarrestin complex recruits the clathrin adaptor AP-2 during endocytosis. *Proc Natl Acad Sci U S A.* 1999;96(7):3712-7.
40. Drake MT, Zhu Y, Kornfeld S. The assembly of AP-3 adaptor complex-containing clathrin-coated vesicles on synthetic liposomes. *Mol Biol Cell.* 2000;11(11):3723-36.
41. Blondel-Tepaz E, Leverve M, Sokrat B, Paradis JS, Kosic M, Saha K, et al. The RanBP2/RanGAP1-SUMO complex gates beta-arrestin2 nuclear entry to regulate the Mdm2-p53 signaling axis. *Oncogene.* 2021;40(12):2243-57.
42. Wang P, Wu Y, Ge X, Ma L, Pei G. Subcellular localization of beta-arrestins is determined by their intact N domain and the nuclear export signal at the C terminus. *J Biol Chem.* 2003;278(13):11648-53.
43. Zhuo Y, Robleto VL, Marchese A. Proximity Labeling to Identify beta-Arrestin1 Binding Partners Downstream of Ligand-Activated G Protein-Coupled Receptors. *Int J Mol Sci.* 2023;24(4).
44. Martin NP, Lefkowitz RJ, Shenoy SK. Regulation of V2 vasopressin receptor degradation by agonist-promoted ubiquitination. *J Biol Chem.* 2003;278(46):45954-9.
45. Marchese A, Benovic JL. Agonist-promoted ubiquitination of the G protein-coupled receptor CXCR4 mediates lysosomal sorting. *J Biol Chem.* 2001;276(49):45509-12.
46. Hurley JH, Hanson PI. Membrane budding and scission by the ESCRT machinery: it's all in the neck. *Nat Rev Mol Cell Biol.* 2010;11(8):556-66.
47. Kean MJ, Couzens AL, Gingras AC. Mass spectrometry approaches to study mammalian kinase and phosphatase associated proteins. *Methods.* 2012;57(4):400-8.



48. Meant A, Gao B, Lavoie G, Nourredine S, Jung F, Aubert L, et al. Proteomic Analysis Reveals a Role for RSK in p120-catenin Phosphorylation and Melanoma Cell-Cell Adhesion. *Mol Cell Proteomics*. 2020;19(1):50-64.

## Figure legends

**Figure 1: BioID experiment and cell line characterization.** (A) Schematic representation of the BioID experiment. Three control cell lines (FLAG alone, BirA-FLAG, GFP-BirA-FLAG) and two cell lines expressing  $\beta$ -arrestin 1/2 fused to BirA-FLAG are processed through the described pipeline. (B) Cell lysates are analyzed by western blot using an anti-FLAG antibody and streptavidin-HRP to monitor protein expression and endogenous protein biotinylation by BirA. (C) Cells cotransfected with  $\beta$ -arrestin 1/2 fused to BirA-FLAG or YFP were imaged by confocal microscopy. An anti-FLAG antibody is used to stain the BirA constructs and DAPI is used for nucleus visualization.

**Figure 2: BioID results and analysis.** Potential interactors identified by the BioID experiment.  $\beta$ -arrestin 1 interactors are shown in green,  $\beta$ -arrestin 2 in blue and interactors common to both isoforms in yellow. (B) Venn diagram comparing the proteins identified by BioID to proteins listed in the BioGRID database as previously identified  $\beta$ -arrestin 1/2 interactors. (C, D) Go-term analysis of proteins identified by BioID as  $\beta$ -arrestin 1/2 interactors.

**Figure 3: Confirmation of the interaction between  $\beta$ -arrestin 1/2 and UBE2O by Co-IP and BRET.** A) HEK293 cells transfected with Flag- $\beta$ -arrestin 2 and myc-UBE2O are lysed followed by immunoprecipitation of  $\beta$ -arrestin 2 using an anti-FLAG antibody. Samples are analyzed by western blot using a Myc antibody and a  $\beta$ -arrestin 1/2 antibody. (B) HEK293 cells transfected with Flag- $\beta$ -arrestin 2 and myc-UBE2O are lysed followed by immunoprecipitation of UBE2O using an anti-Myc antibody. Samples are analyzed by western blot using a Myc antibody and a  $\beta$ -arrestin 1/2 antibody. (C) HEK293 cells transfected with Flag- $\beta$ -arrestin 1 and myc-UBE2O are lysed followed by immunoprecipitation of  $\beta$ -arrestin 1 using an anti-FLAG antibody. Samples are analyzed by western blot using a Myc antibody and a  $\beta$ -arrestin 1/2 antibody. (D) HEK293 cells transfected with Flag- $\beta$ -arrestin 1 and myc-UBE2O are lysed followed by immunoprecipitation of UBE2O using an anti-Myc antibody. Samples are analyzed by western blot using a Myc antibody and a  $\beta$ -arrestin 1/2 antibody. (E, F) HEK293 cells are cotransfected with Flag-V2R, a constant amount of  $\beta$ -arrestin1/2-RlucII and increasing amounts of GFP10-UBE2O. Basal fluorescence is measured, and cells are then stimulated for 10 min with 100nM AVP before BRET measurement.

**Figure 4:  $\beta$ -arrestin 1/2 recruitment to the Vasopressin V2 receptor at the plasma membrane.**

(A, B) HEK293 cells are cotransfected with  $\beta$ -arrestin 1/2-RlucII, rGFP-CAAX and FLAG-V2R to monitor  $\beta$ -arrestin 1/2 recruitment to the plasma membrane. Cells are stimulated for 10 min with 100nM AVP before BRET measurement. (C) Receptor expression for the BRET experiments is monitored by cell surface ELISA using an anti-FLAG-HRP antibody. (D) Western blot analysis to monitor UBE2O expression using an anti-myc antibody.

**Figure 5:  $\beta$ -arrestin 1/2 internalization into the early endosomes after Vasopressin V2 receptor stimulation.**

(A, B) HEK293 cells are cotransfected with  $\beta$ -arrestin 1/2-RlucII, rGFP-FYVE and FLAG-V2R to monitor  $\beta$ -arrestin 1/2 endocytosis. Cells are stimulated for 10 min with 100nM AVP before BRET measurement. (C) Receptor expression for the BRET experiments is monitored by cell surface ELISA using an anti-FLAG-HRP antibody. (D) Western blot analysis to monitor UBE2O expression using an anti-myc antibody.

**Figure 6: UBE2O effect on  $\beta$ -arrestin 2 trafficking kinetics.**

(A) HEK293 cells are cotransfected with  $\beta$ -arrestin 2-RlucII, rGFP-CAAX and FLAG-V2R to monitor the kinetic of  $\beta$ -arrestin 2 recruitment to the plasma membrane. Cells are stimulated with 100nM AVP prior to BRET measurement. (B) HEK293 cells are cotransfected with  $\beta$ -arrestin 2-RlucII, rGFP-FYVE and FLAG-V2R to monitor the kinetic of  $\beta$ -arrestin 2 endocytosis. Cells are stimulated with 100nM AVP prior to BRET measurement. (C) Rate of  $\beta$ -arrestin 2 dissociation from the plasma membrane by quantification of the hill slope of the plasma membrane recruitment curve. (D) Rate of  $\beta$ -arrestin 2 endocytosis by quantification of the hill slope of the early endosomes internalization curve.

**Figure S1:  $\beta$ -arrestin 1/2 recruitment to the  $\beta$ 2-adrenergic receptor at the plasma membrane.**

(A, B) HEK293 cells are cotransfected with  $\beta$ -arrestin 1/2-RlucII, rGFP-CAAX and FLAG- $\beta$ 2AR to monitor  $\beta$ -arrestin 1/2 recruitment to the plasma membrane. Cells are stimulated for 10 min with 10 $\mu$ M Isoproterenol before BRET measurement. (C) Receptor expression for the BRET experiments is monitored by cell surface ELISA using an anti-FLAG-HRP antibody. (D) Western blot analysis to monitor UBE2O expression using an anti-myc antibody.

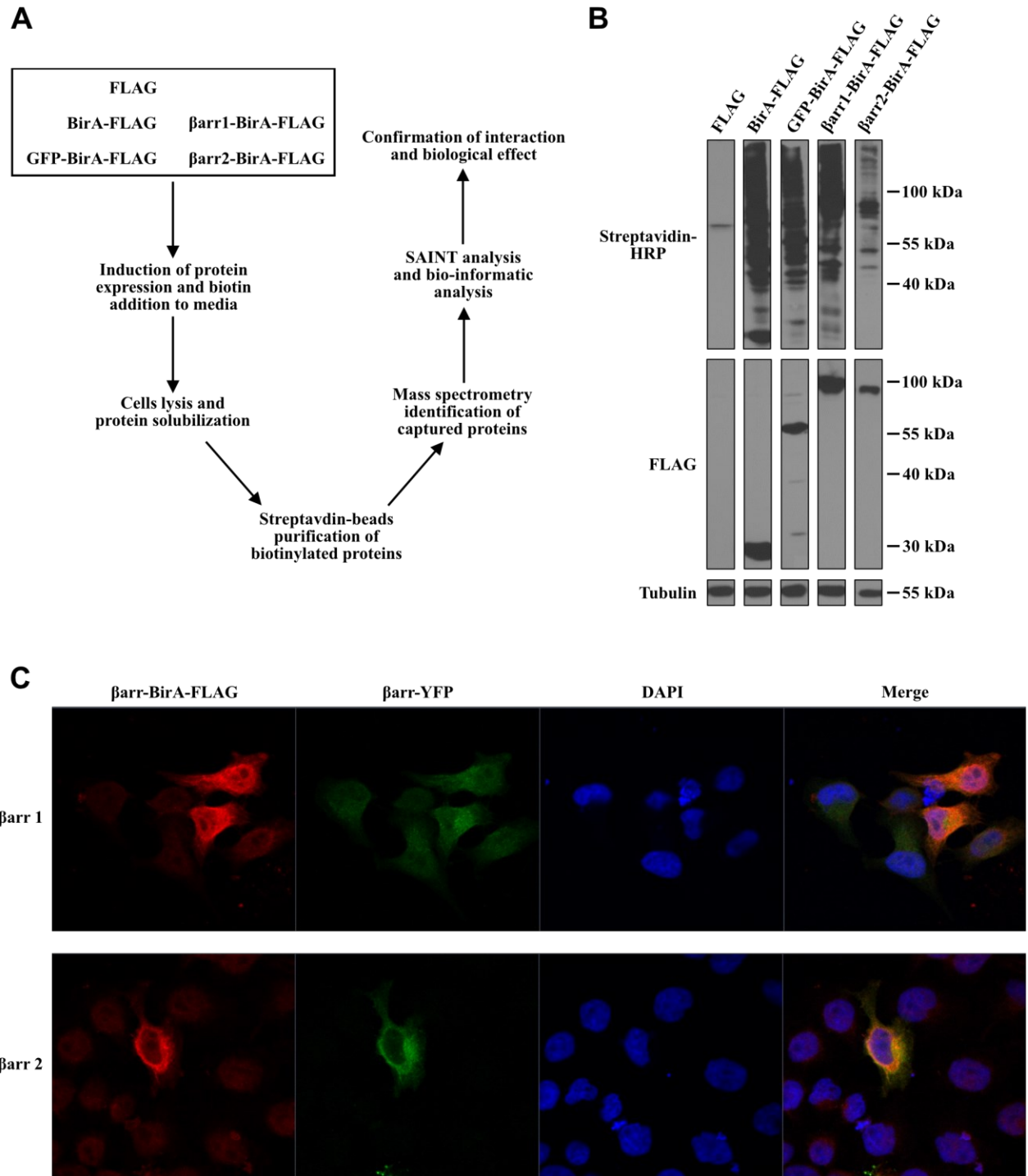
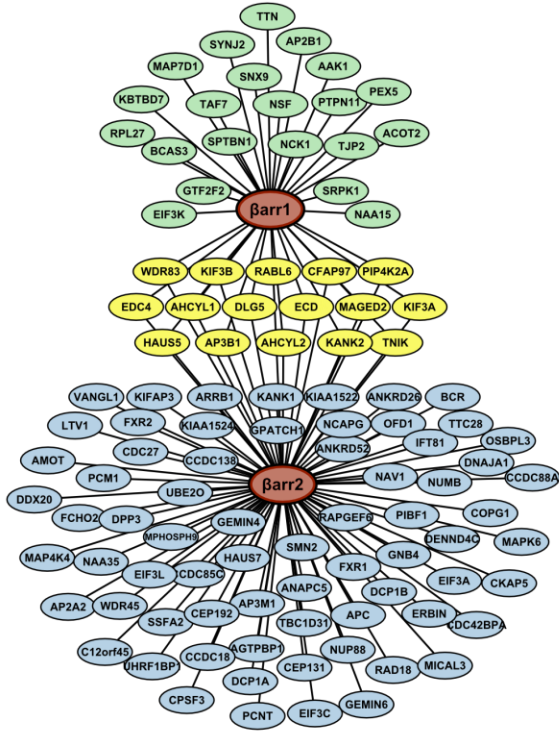


**Figure 1**

**A**



**B**

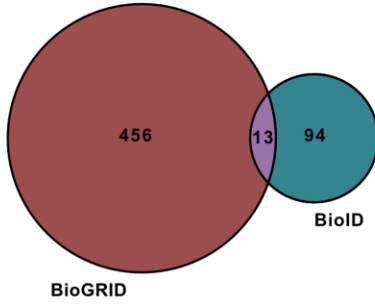
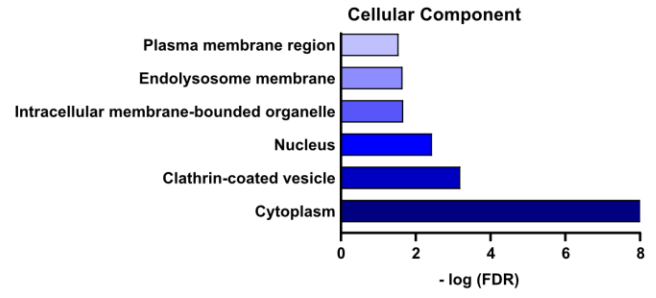
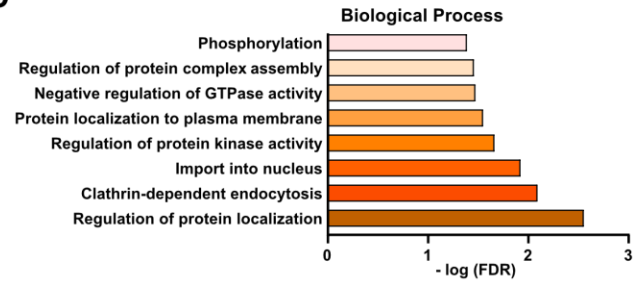


**Figure 2**

**C**



**D**



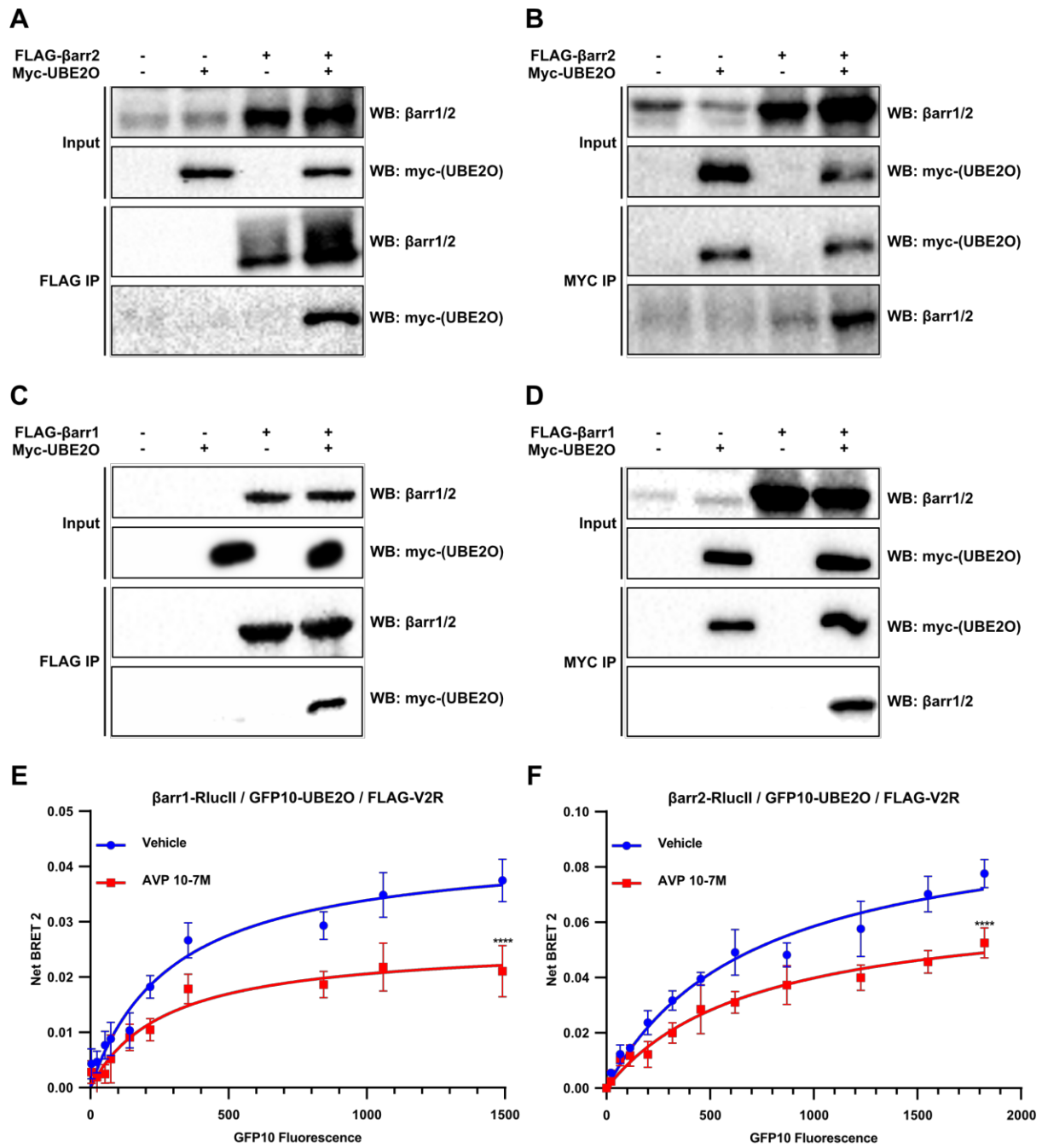


Figure 3

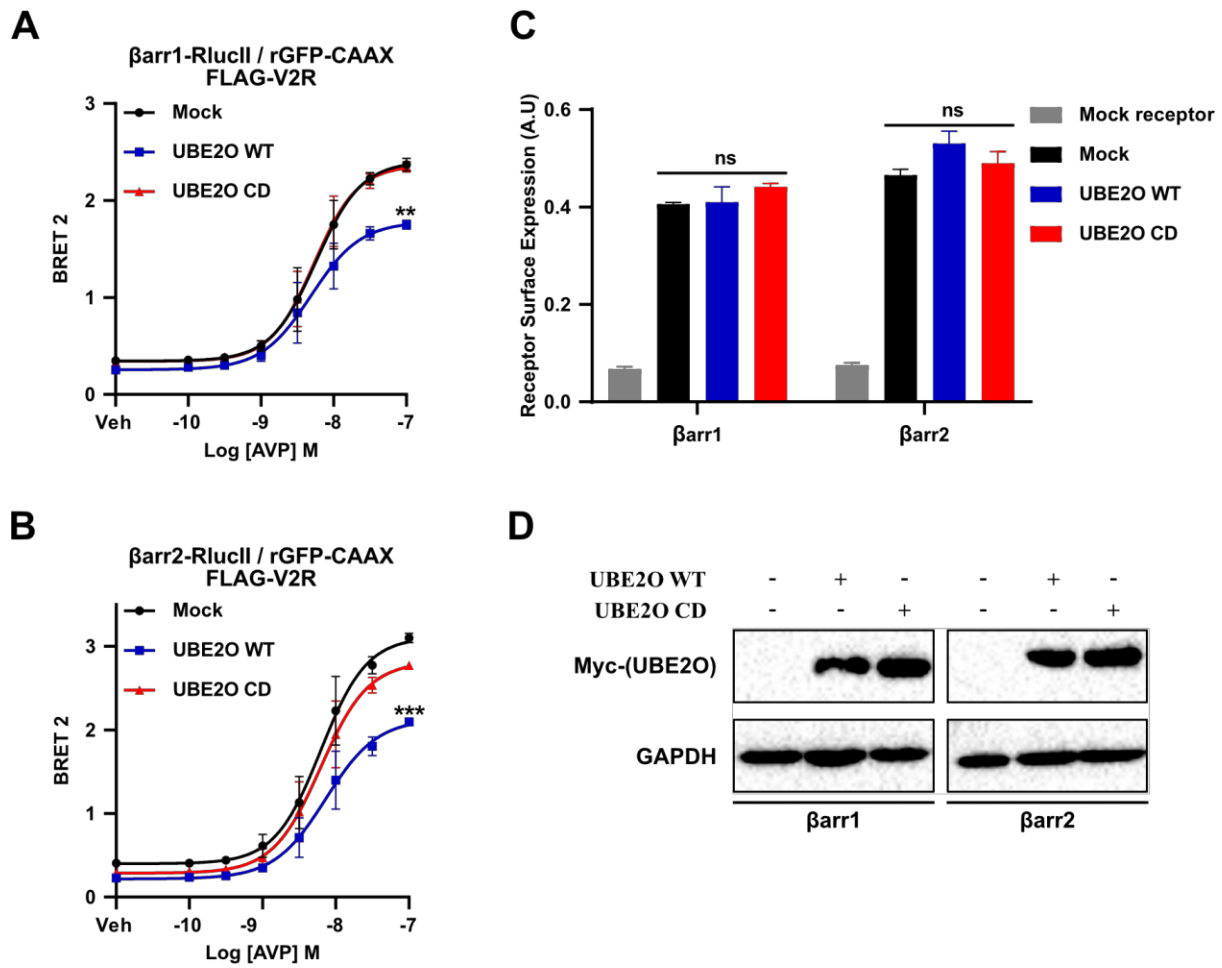


Figure 4

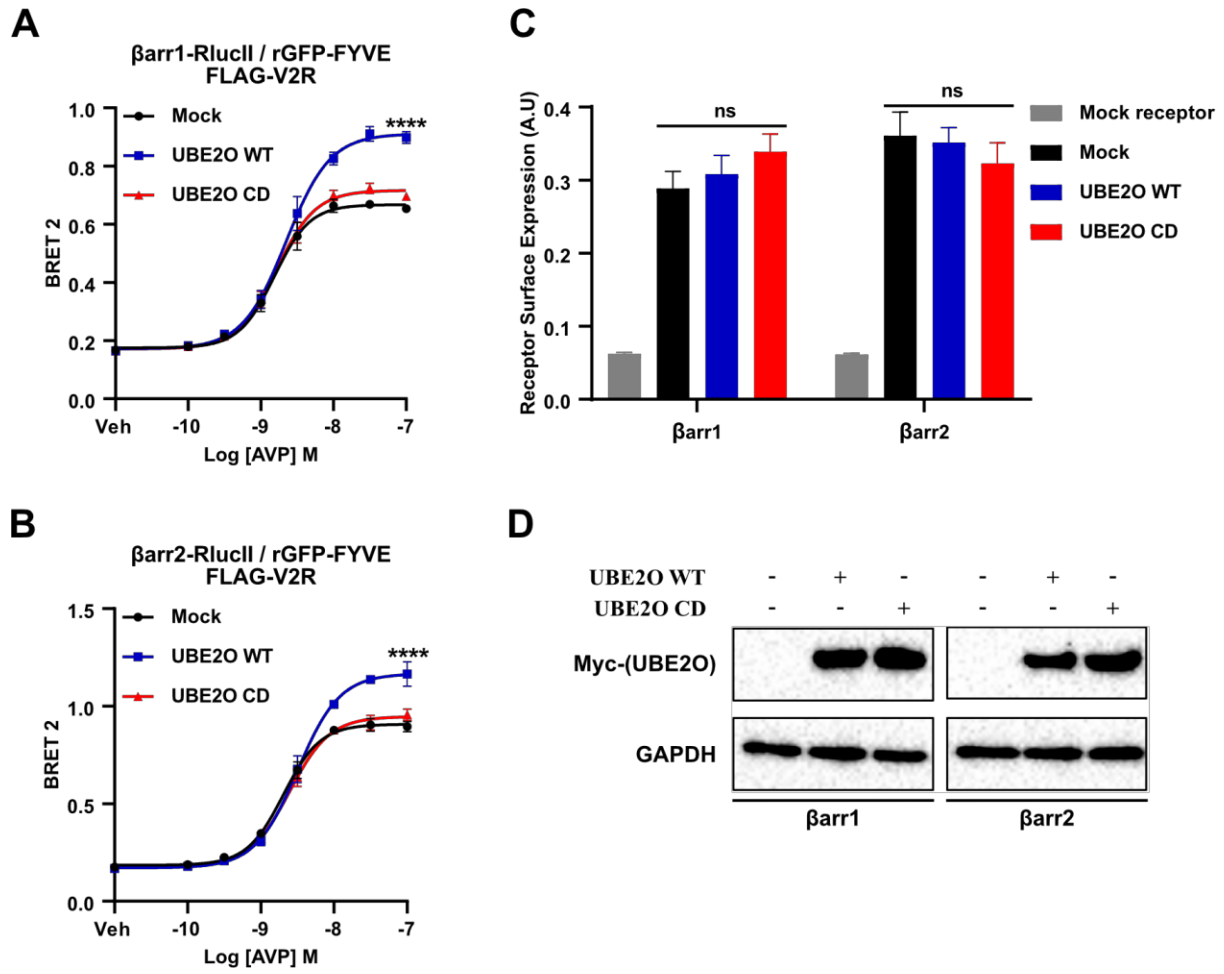


Figure 5



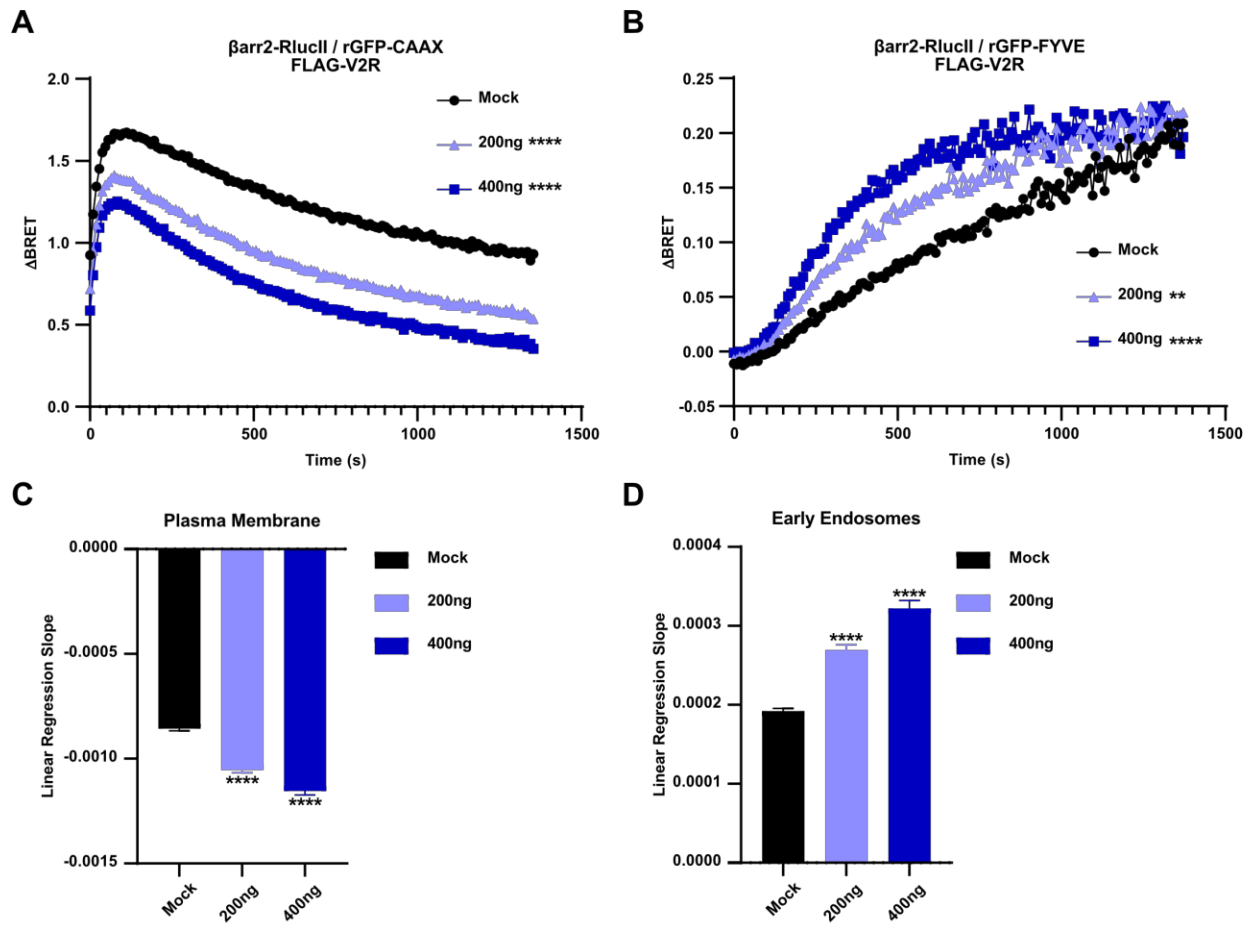


Figure 6

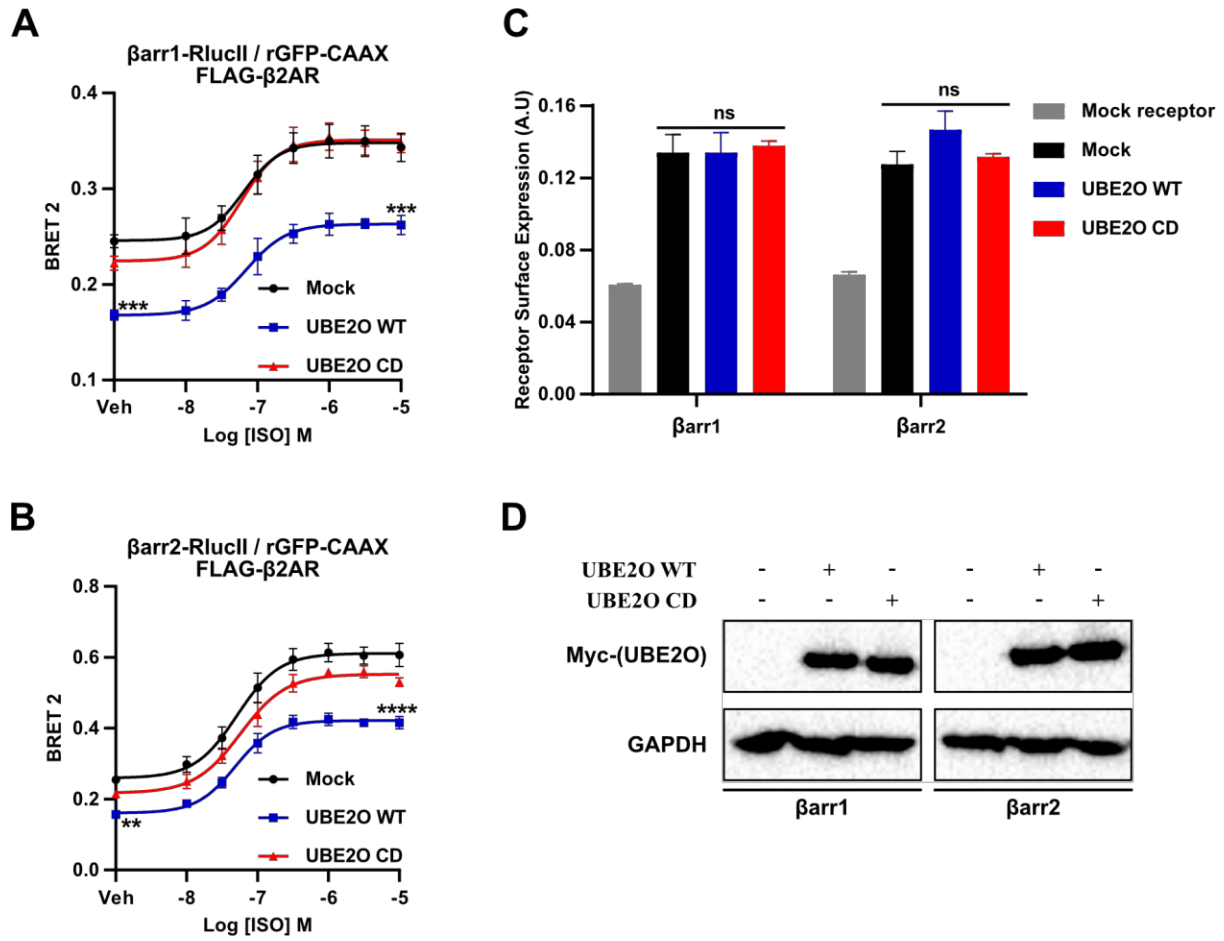


Figure S1

## 7 Chapter 7: Discussion

$\beta$ -arrestin is an important GPCR regulator as it mediates receptor desensitization and endocytosis to attenuate downstream signaling. It has also been shown to play critical non-canonical functions such as the scaffolding of intracellular signaling cascades and executing various nuclear roles. The complexity and diversity of the roles accomplished by  $\beta$ -arrestin suggest that it could present an interesting therapeutic target for the development of drugs aimed at modulating GPCR signaling. In this context, my Ph.D. work sought to expand our understanding of some novel roles and regulation mechanisms of  $\beta$ -arrestin. Among the various themes that I explored is the formation of novel complexes, interaction of  $\beta$ -arrestin with new binding partners, the impact of post-translational modifications and receptor dimerization.

### 7.1 Sustained GPCR signaling

Historically, GPCRs were described to signal from the plasma membrane by coupling with heterotrimeric G proteins, which in turn activate downstream effectors.  $\beta$ -arrestin was thought to terminate this signaling by promoting receptor desensitization and endocytosis. However, recent studies have demonstrated that several class B receptors such as the parathyroid hormone receptor (PTHrP), neurokinin 1 receptor (NK1R) and the vasopressin type 2 receptor (V2R) remain active and trigger a second wave of signaling from endosomes (173, 247, 248, 249). The discovery of a mega-complex formed by a GPCR, heterotrimeric G protein and  $\beta$ -arrestin gave a mechanistic explanation to the origin of sustained endosomal signaling (175). This highlights the critical role that  $\beta$ -arrestin plays in regulating GPCR signaling, not only from the plasma membrane, but also from endosomes.

Moreover, G proteins have been shown to localize in different intracellular compartments including the Golgi apparatus, endoplasmic reticulum, mitochondria, and endosomes (250, 251, 252), yet the mechanisms regulating G protein trafficking to these compartments is not fully elucidated. Here, we showed that the formation of a novel complex composed of the V2R,  $\beta$ -arrestin and G $\beta\gamma$  enables G protein trafficking from the plasma membrane to early endosomes. Indeed, we demonstrated that  $\beta$ -arrestin is required for G $\beta\gamma$  dissociation from the plasma

membrane and translocation to endosomes and that the presence of G $\beta\gamma$  at early endosomes is a prerequisite for the endosomal accumulation of G $\alpha_s$ . Our findings shed new light on the role of  $\beta$ -arrestin in enabling sustained signaling from subcellular organelles. It would be interesting to monitor second-messenger production both at the plasma membrane and in the endosomes to evaluate how compartmentalized cAMP regulates specific cellular effectors. Also, G protein interaction with effectors specific to each intracellular compartment could add a layer of complexity to the investigation of GPCR intracellular signaling.

## 7.2 G protein trafficking

Another one of our key findings is that  $\beta$ -arrestin is not required for G $\alpha_s$  dissociation from the plasma membrane. Previous studies showed that G $\alpha_s$  is covalently modified with a palmitic acid which anchors it at the plasma membrane under basal conditions. Following receptor activation, G $\alpha_s$  is then depalmitoylated by an enzyme acyl-protein thioesterase leading to its translocation from the plasma membrane to the cytoplasm (253, 254, 255, 256, 257). Our data suggests that the presence of G $\beta\gamma$  with an activated receptor in the endosomes is required for the recruitment of G $\alpha_s$  to this compartment. We speculate that cytoplasmic G $\alpha_s$  probes intracellular compartments (258) in the search for an active receptor and that the presence of G $\beta\gamma$  in complex with a GPCR in the endosomes contributes to the reformation of heterotrimeric G protein complex that enables endosomal signaling. Subsequent cycles of activation/deactivation of the G protein may occur, where G $\alpha_s$  dissociates from G $\beta\gamma$ , binds effectors to trigger second messenger production while  $\beta$ -arrestin maintains the V2R- $\beta$ -arrestin-G $\beta\gamma$  complex ready in the endosomes to accelerate reformation of signaling competent heterotrimers. This mechanism results in persistent endosomal signaling until the GPCR complex is eventually degraded in lysosomes or is recycled back to the plasma membrane.

On the other hand,  $\beta$ -arrestin is required for both dissociation of G $\beta\gamma$  from the plasma membrane and for translocation to the endosomes. We showed by various biochemical assays a direct interaction between  $\beta$ -arrestin and G $\beta\gamma$ . It is interesting to note that G $\beta\gamma$  did not exhibit a preference for binding to the active conformation of  $\beta$ -arrestin, suggesting that the interaction is not dependent on a conformational change in  $\beta$ -arrestin following receptor activation. In

addition, our *in vitro* data also revealed that  $\beta$ -arrestin 1 and  $\beta$ -arrestin 2 isoforms can bind  $G\beta\gamma$  and support the formation of a V2R- $\beta$ -arrestin- $G\beta\gamma$  complex (Figure 12).

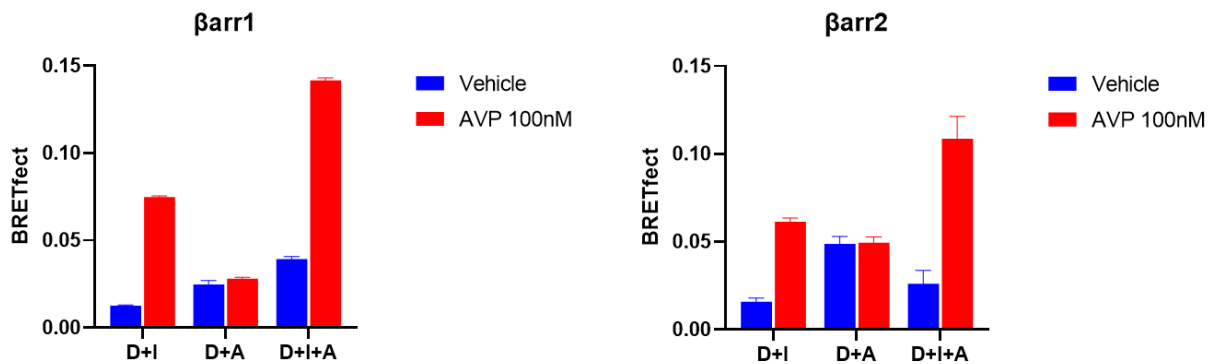


**Figure 12.** – V2R- $\beta$ arr1/2- $G\beta\gamma$  complex formation monitored by BRETfect assay.

Co-expression of BRETfect constructs in parental HEK293T followed by vehicle or 100nM AVP stimulation for 20 min. D:  $\beta$ -arrestin-RlucII, I: V2R-mTFP, A:  $G\gamma$ 2-YFP.

Overall, our data supports the notion that upon V2R activation,  $\beta$ -arrestin 1/2 is recruited to the plasma membrane where it binds both the receptor and  $G\beta\gamma$ . Moreover, our findings demonstrate that both  $\beta$ -arrestin isoforms mediate the endocytosis of the V2R- $\beta$ -arrestin 1/2- $G\beta\gamma$  complex. An interesting direction for future research would be to investigate the formation of similar complexes with other GPCRs. For instance, it would be valuable to explore the ability of  $\beta$ -arrestin 1/2 to bind  $G\beta\gamma$  in the context of GPCRs that have a better affinity for a specific  $\beta$ -arrestin isoform. We could explore the role of each isoform in G protein translocation to the endosomes. We also wonder whether class A GPCRs, which do not colocalize with  $\beta$ -arrestin in the endosomes, can support endosomal signaling and the mechanism enabling G proteins endosomal translocation for these receptors. Moreover, whether the trafficking mechanism described here applies to the trafficking of the other G protein families ( $G_i$ ,  $G_q$  and  $G_{12/13}$ ) remains still to be studied. It is also unknown whether  $\beta$ -arrestin mediates the trafficking of specific  $G\beta\gamma$  dimers to other specific intracellular compartments (Golgi, ER, mitochondria, and nucleus) (252). Further work is required to elucidate the precise role of  $\beta$ -arrestin in this process.

### 7.3 Role of GCGR ubiquitination on signaling bias

Several studies have highlighted the role of GPCR ubiquitination in receptor trafficking and degradation as reviewed in the introduction of this thesis (216, 217). Recently, GCGR was shown to be ubiquitinated and localized at the plasma membrane under basal conditions. Agonist stimulation promotes receptor endocytosis and triggers GCGR deubiquitination in the endosomes by USP33 and STAMBP (224). Here, we identified a novel role of the GCGR ubiquitination status on its signaling and engagement of its effectors. We showed that K333 is the main ubiquitination site for GCGR, and that disruption of this modification creates a signaling bias characterized by a decrease in G protein-mediated signaling and enhanced  $\beta$ -arrestin recruitment and  $\beta$ -arrestin-mediated signaling. Our findings challenge the previous notion that, in the pancreas, GCGR-promoted insulin secretion is exclusively triggered by G protein signaling downstream of the GCGR. Instead, we demonstrate that the  $\beta$ -arrestin-biased GCGR mutant is fully capable of promoting insulin secretion, highlighting the importance of  $\beta$ -arrestin-mediated signaling in this process.

Agonist-promoted ubiquitination of rhodopsin-like GPCRs such as the  $\beta$ 2AR, V2R and CXCR4 has been shown to be critical to trigger receptor degradation in lysosomes by engaging the endosomal-sorting-complex-required-for-transport (ESCRT) machinery (216, 217, 218, 219). On the other hand, constitutive ubiquitination of DOR, TRHR, and CXCR7 plays an important role in the control of correct folding and cell surface expression of these receptors (221, 222, 223). Our findings regarding the impact of GCGR ubiquitination on signaling bias reveal a novel mechanism of GPCR regulation by ubiquitination. However, the precise molecular mechanism by which the addition of a ubiquitin moiety to K333 of GCGR controls the receptor's engagement with transducers remains to be defined. Structural studies of the GCGR-G protein complex situate the K333 on the cytoplasmic side the TM5 at the interaction interface with the  $\alpha$ 5-helix of G $\alpha$ s (259). We speculate that the ubiquitin moiety stabilizes GCGR coupling to G $\alpha$ s and that loss of ubiquitination results in weaker G protein engagement.

Our data also suggests that the deubiquitinated GCGR has an increased affinity for  $\beta$ -arrestin which may sterically hinder or block G protein engagement to the receptor. In addition, the

increased  $\beta$ -arrestin binding favors scaffolding of intracellular signaling pathways as we showed that  $\beta$ -arrestin 1 association with the deubiquitinated GCGR exhibits increased efficiency to scaffold p38 MAPK signaling. It was previously reported that cAMP can inhibit p38 activity (260), suggesting that the decrease in G protein-mediated cAMP production observed for the ubiquitination-deficient GCGR may result in an increase in p38 signaling.

Our results reveal an interesting distinction in the contribution of the two  $\beta$ -arrestin isoforms in the GCGR signaling. While both isoforms exhibit increased recruitment to the deubiquitinated receptor, only  $\beta$ -arrestin 1 promotes p38 MAPK signaling, while  $\beta$ -arrestin 2 appears not to be involved in this signaling pathway. However, we found that both isoforms are capable of promoting GCGR internalization, indicating a divergence in the possible roles of the two isoforms in the regulation of this receptor.

#### **7.4 GCGR-mediated insulin secretion**

GCGR is expressed in pancreatic  $\beta$ -cells and is an important regulator of glucose-stimulated insulin secretion (GSIS). Glucagon stimulation of GCGR and subsequent activation of the  $G\alpha_s$ -cAMP-PKA cascade has been previously linked to insulin secretion in pancreatic islets (261, 262, 263). However, here we showed that a biased GCGR mutant that is deficient in G protein activation and exhibits increased binding to  $\beta$ -arrestin is fully competent at potentiating insulin secretion. Indeed, the ubiquitin-dependent signaling bias that we observed in HEK293 cells was replicated in physiologically relevant cell models, i.e., INS-1  $\beta$ -cell line. Moreover, expression of either GCGR-WT or GCGR-K333R resulted in similar levels of GSIS in INS-1  $\beta$ -cells and in isolated pancreatic islets. Also, p38 inhibition suppressed GCGR-promoted insulin secretion for both the WT and the mutant suggesting that p38 activity, rather than G protein signaling, is the main regulator of GSIS. This contrasts with previous studies which suggested that insulin secretion is solely triggered through G protein signaling (264). It is possible that both G protein and  $\beta$ -arrestin signaling pathways contribute to GSIS, but in a  $\beta$ -arrestin biased situation, the GCGR may accentuate the engagement of the p38 cascade to compensate for the deficit in G protein activity. Interestingly, a common GCGR variant (G40S) in patients diagnosed with non-insulin-dependent diabetes exhibits normal G protein activation and  $\beta$ -arrestin 2 recruitment but impaired  $\beta$ -arrestin 1

binding (265). As our data suggests that GCGR-mediated p38 signaling is scaffolded by activated  $\beta$ -arrestin 1, this may explain the mechanism by which this variant leads to the development of diabetes.

GCGR is also expressed in hepatocytes where it regulates glucose, lipid, and amino acid metabolism. Previous studies suggested that these mechanisms are modulated by G protein signaling (266) but to the best of our knowledge of the literature, the role of  $\beta$ -arrestin in these pathways has not been studied. Therefore, it would be interesting to investigate the role of GCGR ubiquitination on liver cells metabolism and whether the  $\beta$ -arrestin signaling bias observed in the pancreas is also apparent in the liver. Further investigation of the interplay between G protein and  $\beta$ -arrestin signaling in GCGR-mediated metabolism regulation in the liver could reveal novel insights into the mechanisms of metabolic disorders.

## **7.5 Advantages and limitations of the BioID proteomic approach**

To explore novel functions and regulation mechanisms of  $\beta$ -arrestin, we aimed to identify previously unknown interactors of  $\beta$ -arrestin and to characterize the roles of these interactions. For this purpose, we utilized the BioID proteomic approach based on proximity biotinylation in living cells, and we identified over 100 potential interactions for  $\beta$ -arrestin 1/2. BioID offers several advantages over other approaches for detecting protein interactions. First, this method allows identification of endogenous binding partners in living cells. Second, *in cellulo* protein biotinylation and the streptavidin beads that have a high affinity for biotin used to capture the biotinylated proteins allow detection of weak and transient interaction. Third, biotinylated proteins are purified under stringent wash conditions minimizing non-specific interactors. Finally, BioID is applicable to identify insoluble interactors, offering the possibility to detect interactions with membrane proteins that are often missed by other approaches.

Some of the limitations of BioID include the fact that overexpression of the protein of interest fused to the biotin ligase BirA can cause identification of artificial interactions that do not occur at endogenous protein levels. Also, BirA is a 35 kDa protein that is large enough that it could



disturb the stability, function, or localization of the protein of interest. In our study, we did confirm the correct subcellular localization of  $\beta$ -arrestin 1/2 but it would be important to also verify that its function is not affected by the fusion to BirA to further ensure the reliability of our data. This could be achieved by testing the recruitment of  $\beta$ -arrestin-BirA to the plasma membrane after receptor activation or its capacity to mediate receptor desensitization in  $\beta$ -arrestin KO cells. Also, a smaller version of BirA was developed and could limit the issues caused by the size of this enzyme (267). Another limitation is that BioID does not necessarily detect protein interactions but rather protein proximity as BirA is able to biotinylate targets in a radius of 10 nm (268). Hence the need to confirm the potential interactions as we did using multiple complementary techniques such as co-immunoprecipitation and BRET experiments.

## 7.6 $\beta$ -arrestin interactome studies

Several previous studies have investigated  $\beta$ -arrestin protein interactions using other high-throughput methods such as immunoprecipitation followed by mass spectrometry. The group of Dr. Robert Lefkowitz performed a comprehensive IP-MS analysis of the  $\beta$ -arrestin interactome and found a total 337 protein interactors. Of those 124 were found only in the non-stimulated state, 105 were found only after AT1R stimulation, and 210 were found in both conditions (180). Our BioID study focused on basal level interactions but could also be adapted to investigate the  $\beta$ -arrestin interactome after activation of various GPCRs.

Furthermore, of the proteins identified as  $\beta$ -arrestin 1/2 potential interactors in our BioID experiments, 13 were listed in the BioGRID database that curates protein-protein interactions previously reported in the literature. Some of these proteins were identified in high-throughput studies where the interaction with  $\beta$ -arrestin 1/2 was not validated (KIF3A, NAA15, AP3B1, AHCYL1, AHCYL2, SPTBN1, TTN, KANK1, RAD18) but others were confirmed to form complexes with  $\beta$ -arrestin 1/2 (NSF, AP2A2, AP2B1, ARRB1). Indeed, NSF is an ATPase crucial for intracellular vesicle trafficking that was shown to bind to  $\beta$ -arrestin 1 to enhance agonist-promoted  $\beta$ 2AR endocytosis (269). AP2A2 and AP2B1 are part of the AP2 adaptor complex, and it has been previously demonstrated that the  $\beta$ 2-adaptin subunit (AP2B1) mediates the interaction of this complex with  $\beta$ -arrestin to enable GPCR internalization (270). The  $\alpha$ -adaptin subunit (AP2A2) has

not been shown to interact directly with  $\beta$ -arrestin but it was still labeled by BirA due to its proximity in this complex. The identification of  $\beta$ -arrestin 1 (ARRB1) was not surprising as  $\beta$ -arrestin 1/2 have been shown to form homo- and heterodimers to regulate their subcellular localization (271).

While writing this thesis, a new study was published investigating the  $\beta$ -arrestin 1 interactome using APEX2, another proximity-based labeling approach that identified novel interactors under basal and CXCR4-stimulated conditions. Interestingly, in this study we found 14 proteins in common with our BioID experiment with  $\beta$ -arrestin 1 and 19 in common in our experiment with  $\beta$ -arrestin 2 (**Figure 13**). These proteins (AP3B1, AHCYL1, KANK2, MAGED2, PTPN11, SPTBN1, SYNJ2, AP2B1, NAA15, NSF, NCK1, TJP2, MAP7D1, AAK1, KIAA1522, OSBPL3, GEMIN4, FXR1, CDC27, FXR2, BCR, TTC28, AP3M1, UBE2O, PCM1, ERBIN, EIF3C, DENND4C, DDX20) identified by two distinct approaches represent interesting binding partners that warrant further investigation.

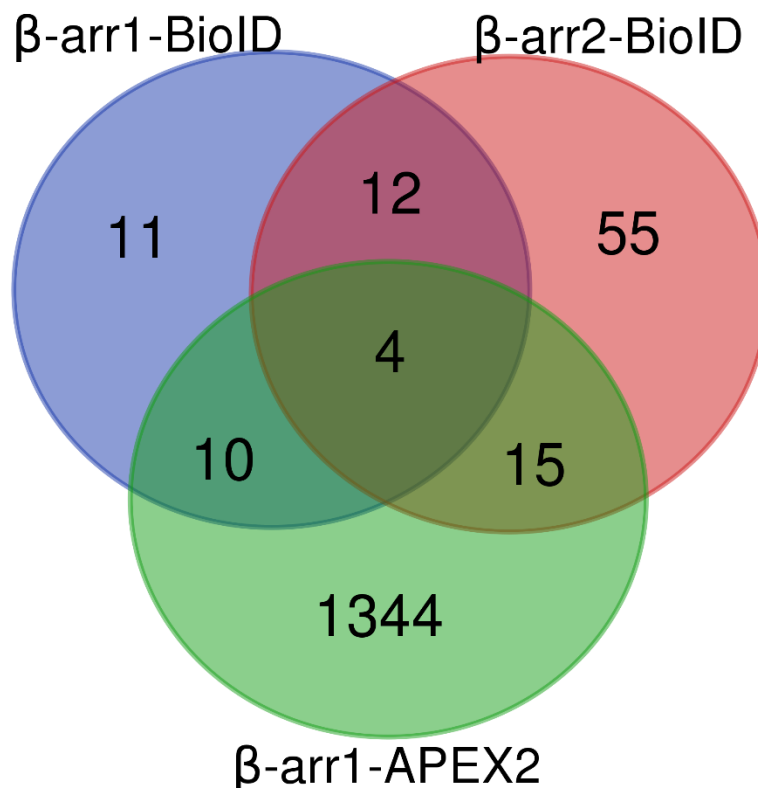


**Figure 13.** –  $\beta$ -arrestin interactome identified by BioID and APEX2.

Venn diagram comparing  $\beta$ -arrestin 1/2 interactors identified by BioID to the  $\beta$ -arrestin 1 interactors identified by APEX2.

Our BioID experiment has uncovered many new potential interactions that could potentially be involved in  $\beta$ -arrestin and GPCR functions. For instance, the identification of two subunits of the AP3-adaptor complex (AP3B1 and AP3M1) requires more validation to confirm this interaction and to determine its potential role. The AP3 complex mediates protein sorting in the Golgi apparatus and trafficking to the lysosomes 37, so it would be fitting to test the impact of this potential interaction on GPCR trafficking and degradation in the lysosomes.

## **7.7 Differential localization and binding partners of $\beta$ -arrestin 1/2**

Our initial hypothesis regarding the BioID experiment was that the difference in subcellular localization of the  $\beta$ -arrestin isoforms may result in major differences in the interactome of  $\beta$ -arrestin 1 compared to  $\beta$ -arrestin 2. As expected, our BioID experiment found only 16 interactors common to both isoforms. However, there was no enrichment of nuclear proteins for  $\beta$ -arrestin 1 compared to  $\beta$ -arrestin 2. This could be explained by the ability of  $\beta$ -arrestin 2 to shuttle to the nucleus allowing biotin labeling of nuclear proteins. To improve the detection of nuclear interactors using BioID, it is possible to use a nuclear export inhibitor such as leptomycin B (LMB) to force  $\beta$ -arrestin accumulation in the nucleus and increase its interaction with nuclear proteins. Alternatively, we could also introduce mutations to nuclear localization or nuclear export signals of  $\beta$ -arrestin to increase the identification of cytoplasmic or nuclear interactors.

## **7.8 $\beta$ -arrestin interaction with the atypical E2/E3 ubiquitin-conjugating enzyme UBE2O**

UBE2O is a large hybrid protein that displays at once E2 and E3 activities and catalyzes the ubiquitination of target proteins. UBE2O has been previously shown to regulate BMP7 signaling by mediating monoubiquitination of SMAD6 (272), to ubiquitinate the nuclear localization signal of the tumor suppressor BAP1 and lead to cytoplasmic retention (273), and to regulate NF- $\kappa$ B activation by inhibiting TRAF6 ubiquitination (274). No link has been proposed between UBE2O and GPCRs or  $\beta$ -arrestin. However,  $\beta$ -arrestin ubiquitination has been reported to regulate receptor internalization, while GPCR ubiquitination is critical for triggering its degradation. Unfortunately, I was unsuccessful at establishing a link between GPCR/ $\beta$ -arrestin ubiquitination

and UBE2O. I tried several combinations of different lysis buffers, ubiquitin antibodies and immunoprecipitation targets as well as ubiquitination BRET sensors but failed to reproduce data reported in the literature that shows ubiquitination of GPCRs or  $\beta$ -arrestin (216, 275).

One of the key findings of this study is that receptor activation results in a decrease in BRET signal between  $\beta$ -arrestin1/2-RlucII and GFP10-UBE2O. We speculate that the recruitment of  $\beta$ -arrestin to the activated receptor at the plasma membrane may lead to a loss of interaction between  $\beta$ -arrestin and UBE2O. It is also possible that the decrease in BRET signal is indicative of changes in the conformation of the complex between  $\beta$ -arrestin and UBE2O since the BRET signal depends on both the distance between the partners but also the orientation of the energy donor relative to the energy acceptor (276). Our results suggest that  $\beta$ -arrestin and UBE2O interact constitutively, and receptor stimulation followed by the subsequent recruitment of  $\beta$ -arrestin to the plasma membrane causes either its dissociation from UBE2O or a conformational change in this complex.

## **7.9 UBE2O accelerates $\beta$ -arrestin endosomal translocation**

Additionally, we showed that UBE2O plays a significant role in regulating  $\beta$ -arrestin trafficking. Specifically, our data suggests that UBE2O overexpression leads to an acceleration of  $\beta$ -arrestin 1/2 translocation from the plasma membrane to the early endosomes. However, the mechanism by which UBE2O modulates  $\beta$ -arrestin trafficking is still unclear and remains to be investigated. We can speculate that UBE2O could ubiquitinate directly  $\beta$ -arrestin altering its trafficking properties or that  $\beta$ -arrestin could act as a scaffold to enable GPCR ubiquitination by UBE2O resulting in the observed trafficking effect. Furthermore, UBE2O may interact and/or ubiquitinate other proteins involved in  $\beta$ -arrestin trafficking such as proteins of the endocytic machinery modulating protein translocation from the plasma membrane to the early endosomes. It is interesting to note that the effect of UBE2O on  $\beta$ -arrestin trafficking was observed upon activation of both a class A ( $\beta$ 2AR) and a class B (V2R) GPCR. This suggests that this regulation mechanism involving UBE2O is not limited to a specific receptor or subtype of GPCRs and could represent a general mechanism of GPCR signaling regulation. Further investigation with a larger number of receptors is needed to confirm the potential implication of UBE2O-mediated GPCR

regulation. If confirmed, this interaction could represent an interesting therapeutic target aiming at modulating GPCR or  $\beta$ -arrestin-mediated signaling as an alternative to the development of signaling biased drugs.

## 7.10 Conclusion

Extensive research on GPCRs over the last 50 years has shed light on the important role that  $\beta$ -arrestin plays in regulating receptor signaling. However, the full scope of  $\beta$ -arrestin functions and regulatory mechanisms are not yet fully understood. The conventional view of GPCR and  $\beta$ -arrestin regulation puts a significant emphasis on receptor phosphorylation as the primary means of regulation of GPCR function and trafficking. Nevertheless, there is still much to be investigated about the intricate relationship between GPCRs and  $\beta$ -arrestin. For instance, our work, along with other studies, continues to highlight the importance and functional significance of novel  $\beta$ -arrestin interactors and novel complexes. In the first chapter of this thesis, we showed that formation of a V2R- $\beta$ -arrestin-G $\beta\gamma$  complex is a critical part of the mechanism enabling G protein translocation from the plasma membrane to early endosomes. Uncovering this mechanism is an important step towards a better understanding of the basis of GPCR sustained endosomal signaling and the potential therapeutic targets that it may provide. In a separate project to which I contributed (**annex I**), we presented the development of single-chain variable fragments used as intrabodies to monitor the localization and trafficking of active  $\beta$ -arrestin 1 in living cells (277). These intrabodies were subsequently shown to potentiate  $\beta$ -arrestin 1 endosomal trafficking and signaling. Whether these intrabodies can modulate G protein translocation to the endosomes remains to be studied.

Another aspect that I investigated in this thesis is the role of post-translational modifications in the regulation of GPCR/ $\beta$ -arrestin functions. In the second chapter, we showed that the ubiquitination status of GCGR regulates signaling bias between G protein and  $\beta$ -arrestin-mediated signaling. Our study provides compelling evidence that the mutant GCGR, which favors  $\beta$ -arrestin-mediated signaling, is functionally capable of promoting insulin secretion. These findings highlight an important link between GCGR ubiquitination and  $\beta$ -arrestin in regulating this physiological

function. We also showed in the third chapter that the atypical ubiquitin-conjugating enzyme UBE2O interacts with  $\beta$ -arrestin and modulates its trafficking. Post-translational modifications play diverse roles as we showed in another study (**annex II**) that  $\beta$ -arrestin 2 possesses a SUMO Interaction Motif (SIM) that is required not only for its binding to the RanBP2/RanGAP1-SUMO nuclear pore complex and cytonuclear trafficking (123) but also for its recruitment to the receptor at the plasma membrane (**Figure 14**). The identification of this dual role of the SIM of  $\beta$ -arrestin 2 highlights the complexity of its regulatory mechanisms and emphasizes the importance of investigating the functional consequences of post-translational modifications.

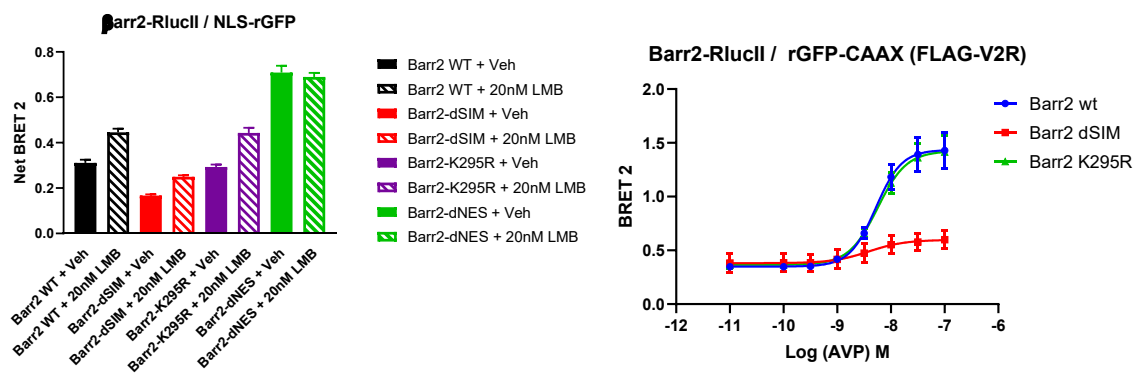


**Figure 14.** – Role of the SIM of  $\beta$ -arrestin 2 in its translocation.

$\beta$ -arrestin 2 nuclear localization and recruitment to the vasopressin V2 receptor at the plasma membrane.

I also contributed to a study (**annex III**) in which we showed that the CXCR4 forms dimers under different conformations and that mutations locking the receptor in a closed-state dimer can activate G proteins similarly to the wild-type receptor. However, CXCR4 in a closed-conformation fails to recruit  $\beta$ -arrestin even though receptor phosphorylation is not affected (278). These findings shed light on another regulatory mechanism that affects the functions of GPCR and  $\beta$ -arrestin, which is modulated by the quaternary structure of the receptor.

In conclusion, my Ph.D. research has contributed to a broader understanding of  $\beta$ -arrestin functions and regulation mechanisms providing new insights into their role in GPCR signaling. Our investigations into various aspects, including the formation of functional complexes, novel interaction partners, post-translational modifications, and receptor oligomerization, have

revealed non-canonical functions and regulatory mechanisms of  $\beta$ -arrestin that could be leveraged in the development of future therapies targeting GPCRs.

## References

1. Fredriksson R, Lagerström MC, Lundin LG, Schiöth HB. The G-protein-coupled receptors in the human genome form five main families. Phylogenetic analysis, paralogon groups, and fingerprints. *Mol Pharmacol*. 2003;63(6):1256-72.
2. Matthews JM, Sunde M. Dimers, oligomers, everywhere. *Adv Exp Med Biol*. 2012;747:1-18.
3. Wess J. Designer GPCRs as Novel Tools to Identify Metabolically Important Signaling Pathways. *Front Endocrinol (Lausanne)*. 2021;12:706957.
4. Atwood BK, Lopez J, Wager-Miller J, Mackie K, Straiker A. Expression of G protein-coupled receptors and related proteins in HEK293, AtT20, BV2, and N18 cell lines as revealed by microarray analysis. *BMC Genomics*. 2011;12:14.
5. Wacker D, Stevens RC, Roth BL. How Ligands Illuminate GPCR Molecular Pharmacology. *Cell*. 2017;170(3):414-27.
6. Kamps AR, Coffman CR. G protein-coupled receptor roles in cell migration and cell death decisions. *Ann N Y Acad Sci*. 2005;1049:17-23.
7. Lattin J, Zidar DA, Schroder K, Kellie S, Hume DA, Sweet MJ. G-protein-coupled receptor expression, function, and signaling in macrophages. *Journal of Leukocyte Biology*. 2007;82(1):16-32.
8. Tzamelis I. GPCRs - Pivotal Players in Metabolism. *Trends Endocrinol Metab*. 2016;27(9):597-9.
9. Schöneberg T, Liebscher I. Mutations in G Protein-Coupled Receptors: Mechanisms, Pathophysiology and Potential Therapeutic Approaches. *Pharmacological Reviews*. 2021;73(1):89.
10. Fernandez-Patron C, Filep JG. GPCRs in cardiovascular pathologies. *Drug Discov Today Dis Mech*. 2012;9(3):e75-e8.
11. Dorsam RT, Gutkind JS. G-protein-coupled receptors and cancer. *Nat Rev Cancer*. 2007;7(2):79-94.
12. Hauser AS, Attwood MM, Rask-Andersen M, Schiöth HB, Gloriam DE. Trends in GPCR drug discovery: new agents, targets and indications. *Nat Rev Drug Discov*. 2017;16(12):829-42.
13. Sriram K, Insel PA. G Protein-Coupled Receptors as Targets for Approved Drugs: How Many Targets and How Many Drugs? *Mol Pharmacol*. 2018;93(4):251-8.
14. Kobilka BK. G protein coupled receptor structure and activation. *Biochim Biophys Acta*. 2007;1768(4):794-807.
15. Shalaeva DN, Galperin MY, Mulikjanian AY. Eukaryotic G protein-coupled receptors as descendants of prokaryotic sodium-translocating rhodopsins. *Biol Direct*. 2015;10:63.
16. Ehrlich P. Chemotherapeutics: scientific principles, methods, and result. *Lancet*. 1913;16:445-51.
17. Limbird LE. *Cell Surface Receptors: A Short Course on Theory and Methods*: Springer US; 1996.
18. SUTHERLAND EW, ROBISON GA, BUTCHER RW. Some Aspects of the Biological Role of Adenosine 3',5'-monophosphate (Cyclic AMP). *Circulation*. 1968;37(2):279-306.



19. Ross EM, Gilman AG. Resolution of some components of adenylate cyclase necessary for catalytic activity. *J Biol Chem.* 1977;252(20):6966-9.
20. Gilman AG. G PROTEINS: TRANSDUCERS OF RECEPTOR-GENERATED SIGNALS. *Annual Review of Biochemistry.* 1987;56(1):615-49.
21. Codina J, Hildebrandt J, Iyengar R, Birnbaumer L, Sekura RD, Manclark CR. Pertussis toxin substrate, the putative Ni component of adenylyl cyclases, is an alpha beta heterodimer regulated by guanine nucleotide and magnesium. *Proc Natl Acad Sci U S A.* 1983;80(14):4276-80.
22. Bokoch GM, Katada T, Northup JK, Ui M, Gilman AG. Purification and properties of the inhibitory guanine nucleotide-binding regulatory component of adenylate cyclase. *J Biol Chem.* 1984;259(6):3560-7.
23. Stryer L. Cyclic GMP Cascade of Vision. *Annual Review of Neuroscience.* 1986;9(1):87-119.
24. Hargrave PA, McDowell JH, Curtis DR, Wang JK, Juszczak E, Fong S-L, et al. The structure of bovine rhodopsin. *Biophysics of structure and mechanism.* 1983;9(4):235-44.
25. Ovchinnikov YA. Rhodopsin and bacteriorhodopsin: structure—function relationships. *FEBS Letters.* 1982;148(2):179-91.
26. Caron MG, Lefkowitz RJ. Solubilization and characterization of the beta-adrenergic receptor binding sites of frog erythrocytes. *J Biol Chem.* 1976;251(8):2374-84.
27. Shorr RG, Lefkowitz RJ, Caron MG. Purification of the beta-adrenergic receptor. Identification of the hormone binding subunit. *J Biol Chem.* 1981;256(11):5820-6.
28. Dixon RAF, Kobilka BK, Strader DJ, Benovic JL, Dohman HG, Frielle T, et al. Cloning of the gene and cDNA for mammalian  $\beta$ -adrenergic receptor and homology with rhodopsin. *Nature.* 1986;321(6065):75-9.
29. Lander ES, Linton LM, Birren B, Nusbaum C, Zody MC, Baldwin J, et al. Initial sequencing and analysis of the human genome. *Nature.* 2001;409(6822):860-921.
30. Okada T, Le Trong I, Fox BA, Behnke CA, Stenkamp RE, Palczewski K. X-Ray diffraction analysis of three-dimensional crystals of bovine rhodopsin obtained from mixed micelles. *J Struct Biol.* 2000;130(1):73-80.
31. Rasmussen SG, Choi HJ, Rosenbaum DM, Kobilka TS, Thian FS, Edwards PC, et al. Crystal structure of the human beta2 adrenergic G-protein-coupled receptor. *Nature.* 2007;450(7168):383-7.
32. Kooistra AJ, Mordalski S, Pandey-Szekeres G, Esguerra M, Mamyrbekov A, Munk C, et al. GPCRdb in 2021: integrating GPCR sequence, structure and function. *Nucleic Acids Res.* 2021;49(D1):D335-D43.
33. Chang SD, Bruchas MR. Functional selectivity at GPCRs: new opportunities in psychiatric drug discovery. *Neuropsychopharmacology.* 2014;39(1):248-9.
34. Marinissen MJ, Gutkind JS. G-protein-coupled receptors and signaling networks: emerging paradigms. *Trends Pharmacol Sci.* 2001;22(7):368-76.
35. Mombaerts P. Genes and ligands for odorant, vomeronasal and taste receptors. *Nat Rev Neurosci.* 2004;5(4):263-78.
36. Alexander SPH, Christopoulos A, Davenport AP, Kelly E, Mathie A, Peters JA, et al. THE CONCISE GUIDE TO PHARMACOLOGY 2019/20: G protein-coupled receptors. *Br J Pharmacol.* 2019;176 Suppl 1:S21-S141.
37. Kolakowski LF, Jr. GCRDb: a G-protein-coupled receptor database. *Recept Channels.* 1994;2(1):1-7.

38. Schioth HB, Fredriksson R. The GRAFS classification system of G-protein coupled receptors in comparative perspective. *Gen Comp Endocrinol*. 2005;142(1-2):94-101.
39. Fridmanis D, Fredriksson R, Kapa I, Schioth HB, Klovins J. Formation of new genes explains lower intron density in mammalian Rhodopsin G protein-coupled receptors. *Mol Phylogenet Evol*. 2007;43(3):864-80.
40. Palczewski K. G protein-coupled receptor rhodopsin. *Annu Rev Biochem*. 2006;75:743-67.
41. Cardoso JC, Pinto VC, Vieira FA, Clark MS, Power DM. Evolution of secretin family GPCR members in the metazoa. *BMC Evol Biol*. 2006;6:108.
42. Bortolato A, Dore AS, Hollenstein K, Tehan BG, Mason JS, Marshall FH. Structure of Class B GPCRs: new horizons for drug discovery. *Br J Pharmacol*. 2014;171(13):3132-45.
43. Das SS, Banker GA. The role of protein interaction motifs in regulating the polarity and clustering of the metabotropic glutamate receptor mGluR1a. *J Neurosci*. 2006;26(31):8115-25.
44. Chun L, Zhang WH, Liu JF. Structure and ligand recognition of class C GPCRs. *Acta Pharmacol Sin*. 2012;33(3):312-23.
45. Nakagawa T, Sakurai T, Nishioka T, Touhara K. Insect sex-pheromone signals mediated by specific combinations of olfactory receptors. *Science*. 2005;307(5715):1638-42.
46. Prabhu Y, Eichinger L. The Dictyostelium repertoire of seven transmembrane domain receptors. *Eur J Cell Biol*. 2006;85(9-10):937-46.
47. Schulte G, Koziellewicz P. Structural insight into Class F receptors - What have we learnt regarding agonist-induced activation? *Basic Clin Pharmacol Toxicol*. 2020;126 Suppl 6:17-24.
48. Liccardo F, Luini A, Di Martino R. Endomembrane-Based Signaling by GPCRs and G-Proteins. *Cells*. 2022;11(3).
49. Smyth MS, Martin JH. x ray crystallography. *Mol Pathol*. 2000;53(1):8-14.
50. Marion D. An introduction to biological NMR spectroscopy. *Mol Cell Proteomics*. 2013;12(11):3006-25.
51. Callaway E. Revolutionary cryo-EM is taking over structural biology. *Nature*. 2020;578(7794):201.
52. Yang D, Zhou Q, Labroska V, Qin S, Darbalaei S, Wu Y, et al. G protein-coupled receptors: structure- and function-based drug discovery. *Signal Transduct Target Ther*. 2021;6(1):7.
53. Jones EM, Lubock NB, Venkatakrisnan AJ, Wang J, Tseng AM, Paggi JM, et al. Structural and functional characterization of G protein-coupled receptors with deep mutational scanning. *Elife*. 2020;9.
54. Sakmar TP, Huber T. Rhodopsin. In: Squire LR, editor. *Encyclopedia of Neuroscience*. Oxford: Academic Press; 2009. p. 365-72.
55. Palczewski K, Kumasaka T, Hori T, Behnke CA, Motoshima H, Fox BA, et al. Crystal structure of rhodopsin: A G protein-coupled receptor. *Science*. 2000;289(5480):739-45.
56. Rosenbaum DM, Rasmussen SG, Kobilka BK. The structure and function of G-protein-coupled receptors. *Nature*. 2009;459(7245):356-63.
57. Qanbar R, Bouvier M. Role of palmitoylation/depalmitoylation reactions in G-protein-coupled receptor function. *Pharmacol Ther*. 2003;97(1):1-33.
58. Zhou Q, Yang D, Wu M, Guo Y, Guo W, Zhong L, et al. Common activation mechanism of class A GPCRs. *Elife*. 2019;8.

59. Ragnarsson L, Andersson A, Thomas WG, Lewis RJ. Mutations in the NPxxY motif stabilize pharmacologically distinct conformational states of the alpha1B- and beta2-adrenoceptors. *Sci Signal*. 2019;12(572).
60. Filipek S. Molecular switches in GPCRs. *Curr Opin Struct Biol*. 2019;55:114-20.
61. Calebiro D, Koszegi Z, Lanoiselee Y, Miljus T, O'Brien S. G protein-coupled receptor-G protein interactions: a single-molecule perspective. *Physiol Rev*. 2021;101(3):857-906.
62. Wacker D, Wang C, Katritch V, Han GW, Huang XP, Vardy E, et al. Structural features for functional selectivity at serotonin receptors. *Science*. 2013;340(6132):615-9.
63. Masureel M, Zou Y, Picard LP, van der Westhuizen E, Mahoney JP, Rodrigues J, et al. Structural insights into binding specificity, efficacy and bias of a beta2AR partial agonist. *Nat Chem Biol*. 2018;14(11):1059-66.
64. Rasmussen SGF, Choi H-J, Fung JJ, Pardon E, Casarosa P, Chae PS, et al. Structure of a nanobody-stabilized active state of the  $\beta(2)$  adrenoceptor. *Nature*. 2011;469(7329):175-80.
65. Dupre DJ, Robitaille M, Rebois RV, Hebert TE. The role of Gbetagamma subunits in the organization, assembly, and function of GPCR signaling complexes. *Annu Rev Pharmacol Toxicol*. 2009;49:31-56.
66. Milligan G, Kostenis E. Heterotrimeric G-proteins: a short history. *Br J Pharmacol*. 2006;147 Suppl 1:S46-55.
67. Lambert NA, Johnston CA, Cappell SD, Kuravi S, Kimple AJ, Willard FS, et al. Regulators of G-protein signaling accelerate GPCR signaling kinetics and govern sensitivity solely by accelerating GTPase activity. *Proc Natl Acad Sci U S A*. 2010;107(15):7066-71.
68. Sprang SR. Invited review: Activation of G proteins by GTP and the mechanism of G $\alpha$ -catalyzed GTP hydrolysis. *Biopolymers*. 2016;105(8):449-62.
69. Lambright DG, Noel JP, Hamm HE, Sigler PB. Structural determinants for activation of the alpha-subunit of a heterotrimeric G protein. *Nature*. 1994;369(6482):621-8.
70. Lambright DG, Sondek J, Bohm A, Skiba NP, Hamm HE, Sigler PB. The 2.0 Å crystal structure of a heterotrimeric G protein. *Nature*. 1996;379(6563):311-9.
71. Cabrera-Vera TM, Vanhauwe J, Thomas TO, Medkova M, Preininger A, Mazzoni MR, et al. Insights into G protein structure, function, and regulation. *Endocr Rev*. 2003;24(6):765-81.
72. Oldham WM, Hamm HE. Structural basis of function in heterotrimeric G proteins. *Q Rev Biophys*. 2006;39(2):117-66.
73. Rasmussen SGF, DeVree BT, Zou Y, Kruse AC, Chung KY, Kobilka TS, et al. Crystal structure of the  $\beta(2)$  adrenergic receptor-Gs protein complex. *Nature*. 2011;477(7366):549-55.
74. Duc NM, Kim HR, Chung KY. Structural mechanism of G protein activation by G protein-coupled receptor. *Eur J Pharmacol*. 2015;763(Pt B):214-22.
75. Wettschureck N, Offermanns S. Mammalian G proteins and their cell type specific functions. *Physiol Rev*. 2005;85(4):1159-204.
76. Wang H, Xu J, Lazarovici P, Quirion R, Zheng W. cAMP Response Element-Binding Protein (CREB): A Possible Signaling Molecule Link in the Pathophysiology of Schizophrenia. *Front Mol Neurosci*. 2018;11:255.
77. Damak S, Margolskee RF. CHAPTER 229 - G Proteins Mediating Taste Transduction. In: Bradshaw RA, Dennis EA, editors. *Handbook of Cell Signaling*. Burlington: Academic Press; 2003. p. 657-61.

78. Hildebrandt JD, Sekura RD, Codina J, Iyengar R, Manclark CR, Birnbaumer L. Stimulation and inhibition of adenylyl cyclases mediated by distinct regulatory proteins. *Nature*. 1983;302(5910):706-9.
79. Mizuno N, Itoh H. Functions and regulatory mechanisms of Gq-signaling pathways. *Neurosignals*. 2009;17(1):42-54.
80. Siehler S. Regulation of RhoGEF proteins by G12/13-coupled receptors. *Br J Pharmacol*. 2009;158(1):41-9.
81. Suzuki N, Hajicek N, Kozasa T. Regulation and physiological functions of G12/13-mediated signaling pathways. *Neurosignals*. 2009;17(1):55-70.
82. Downes GB, Gautam N. The G protein subunit gene families. *Genomics*. 1999;62(3):544-52.
83. Naga Prasad SV. Preface: Changing Paradigms for G-Protein-Coupled Receptor Signaling. *J Cardiovasc Pharmacol*. 2017;70(1):1-2.
84. Moore CA, Milano SK, Benovic JL. Regulation of receptor trafficking by GRKs and arrestins. *Annu Rev Physiol*. 2007;69:451-82.
85. Black JB, Premont RT, Daaka Y. Feedback regulation of G protein-coupled receptor signaling by GRKs and arrestins. *Semin Cell Dev Biol*. 2016;50:95-104.
86. Gurevich VV, Gurevich EV. GPCR Signaling Regulation: The Role of GRKs and Arrestins. *Front Pharmacol*. 2019;10:125.
87. Stewart A, Fisher RA. Introduction: G Protein-coupled Receptors and RGS Proteins. *Prog Mol Biol Transl Sci*. 2015;133:1-11.
88. Pedro MP, Lund K, Iglesias-Bartolome R. The landscape of GPCR signaling in the regulation of epidermal stem cell fate and skin homeostasis. *Stem Cells*. 2020.
89. Johnson M. Molecular mechanisms of beta(2)-adrenergic receptor function, response, and regulation. *J Allergy Clin Immunol*. 2006;117(1):18-24; quiz 5.
90. Martin NP, Whalen EJ, Zamah MA, Pierce KL, Lefkowitz RJ. PKA-mediated phosphorylation of the beta1-adrenergic receptor promotes Gs/Gi switching. *Cell Signal*. 2004;16(12):1397-403.
91. Aldred EM, Buck C, Vall K. Chapter 34 - Respiratory diseases. In: Aldred EM, Buck C, Vall K, editors. *Pharmacology*. Edinburgh: Churchill Livingstone; 2009. p. 267-72.
92. Juul KV, Bichet DG, Nielsen S, Norgaard JP. The physiological and pathophysiological functions of renal and extrarenal vasopressin V2 receptors. *Am J Physiol Renal Physiol*. 2014;306(9):F931-40.
93. Inoue A, Raimondi F, Kadji FMN, Singh G, Kishi T, Uwamizu A, et al. Illuminating G-Protein-Coupling Selectivity of GPCRs. *Cell*. 2019;177(7):1933-47 e25.
94. Bianchi ME, Mezzapelle R. The Chemokine Receptor CXCR4 in Cell Proliferation and Tissue Regeneration. *Front Immunol*. 2020;11:2109.
95. Authier F, Desbuquois B. Glucagon receptors. *Cell Mol Life Sci*. 2008;65(12):1880-99.
96. Galsgaard KD, Pedersen J, Knop FK, Holst JJ, Wewer Albrechtsen NJ. Glucagon Receptor Signaling and Lipid Metabolism. *Front Physiol*. 2019;10:413.
97. Wacker WB, Donoso LA, Kalsow CM, Yankeelov JA, Jr., Organisciak DT. Experimental allergic uveitis. Isolation, characterization, and localization of a soluble uveitopathogenic antigen from bovine retina. *J Immunol*. 1977;119(6):1949-58.
98. Kuhn H, Hall SW, Wilden U. Light-induced binding of 48-kDa protein to photoreceptor membranes is highly enhanced by phosphorylation of rhodopsin. *FEBS Lett*. 1984;176(2):473-8.

99. Miller JL, Fox DA, Litman BJ. Amplification of phosphodiesterase activation is greatly reduced by rhodopsin phosphorylation. *Biochemistry*. 1986;25(18):4983-8.
100. Benovic JL, Kuhn H, Weyand I, Codina J, Caron MG, Lefkowitz RJ. Functional desensitization of the isolated beta-adrenergic receptor by the beta-adrenergic receptor kinase: potential role of an analog of the retinal protein arrestin (48-kDa protein). *Proc Natl Acad Sci U S A*. 1987;84(24):8879-82.
101. Lohse MJ, Benovic JL, Codina J, Caron MG, Lefkowitz RJ. beta-Arrestin: a protein that regulates beta-adrenergic receptor function. *Science*. 1990;248(4962):1547-50.
102. Attramadal H, Arriza JL, Aoki C, Dawson TM, Codina J, Kwatra MM, et al. Beta-arrestin2, a novel member of the arrestin/beta-arrestin gene family. *J Biol Chem*. 1992;267(25):17882-90.
103. Goodman OB, Jr., Krupnick JG, Santini F, Gurevich VV, Penn RB, Gagnon AW, et al. Beta-arrestin acts as a clathrin adaptor in endocytosis of the beta2-adrenergic receptor. *Nature*. 1996;383(6599):447-50.
104. Luttrell LM, Ferguson SS, Daaka Y, Miller WE, Maudsley S, Della Rocca GJ, et al. Beta-arrestin-dependent formation of beta2 adrenergic receptor-Src protein kinase complexes. *Science*. 1999;283(5402):655-61.
105. DeFea KA, Zalevsky J, Thoma MS, Dery O, Mullins RD, Bunnnett NW. beta-arrestin-dependent endocytosis of proteinase-activated receptor 2 is required for intracellular targeting of activated ERK1/2. *J Cell Biol*. 2000;148(6):1267-81.
106. Kohout TA, Lin FS, Perry SJ, Conner DA, Lefkowitz RJ. beta-Arrestin 1 and 2 differentially regulate heptahelical receptor signaling and trafficking. *Proc Natl Acad Sci U S A*. 2001;98(4):1601-6.
107. Green JA, Schmid CL, Bley E, Monsma PC, Brown A, Bohn LM, et al. Recruitment of beta-Arrestin into Neuronal Cilia Modulates Somatostatin Receptor Subtype 3 Ciliary Localization. *Mol Cell Biol*. 2016;36(1):223-35.
108. Hirsch JA, Schubert C, Gurevich VV, Sigler PB. The 2.8 Å crystal structure of visual arrestin: a model for arrestin's regulation. *Cell*. 1999;97(2):257-69.
109. Gurevich VV, Hanson SM, Song X, Vishnivetskiy SA, Gurevich EV. The functional cycle of visual arrestins in photoreceptor cells. *Prog Retin Eye Res*. 2011;30(6):405-30.
110. Chen Q, Iverson TM, Gurevich VV. Structural Basis of Arrestin-Dependent Signal Transduction. *Trends Biochem Sci*. 2018;43(6):412-23.
111. Aydin Y, Coin I. Biochemical insights into structure and function of arrestins. *FEBS J*. 2021;288(8):2529-49.
112. Shukla AK, Manglik A, Kruse AC, Xiao K, Reis RI, Tseng WC, et al. Structure of active beta-arrestin-1 bound to a G-protein-coupled receptor phosphopeptide. *Nature*. 2013;497(7447):137-41.
113. Shukla AK, Westfield GH, Xiao K, Reis RI, Huang LY, Tripathi-Shukla P, et al. Visualization of arrestin recruitment by a G-protein-coupled receptor. *Nature*. 2014;512(7513):218-22.
114. Yin W, Li Z, Jin M, Yin YL, de Waal PW, Pal K, et al. A complex structure of arrestin-2 bound to a G protein-coupled receptor. *Cell Res*. 2019;29(12):971-83.
115. Park JY, Lee SY, Kim HR, Seo MD, Chung KY. Structural mechanism of GPCR-arrestin interaction: recent breakthroughs. *Arch Pharm Res*. 2016;39(3):293-301.

116. Oakley RH, Revollo J, Cidlowski JA. Glucocorticoids regulate arrestin gene expression and redirect the signaling profile of G protein-coupled receptors. *Proc Natl Acad Sci U S A*. 2012;109(43):17591-6.
117. Gurevich EV, Gurevich VV. Arrestins: ubiquitous regulators of cellular signaling pathways. *Genome Biol*. 2006;7(9):236.
118. Kraemer A, Barjaktarovic Z, Sarioglu H, Winkler K, Eckardt-Schupp F, Tapio S, et al. Cell survival following radiation exposure requires miR-525-3p mediated suppression of ARRB1 and TXN1. *PLoS One*. 2013;8(10):e77484.
119. Wang J, Xu W, Zhong T, Song Z, Zou Y, Ding Z, et al. miR-365 targets beta-arrestin 2 to reverse morphine tolerance in rats. *Sci Rep*. 2016;6:38285.
120. Scott MG, Le Rouzic E, Perianin A, Pierotti V, Enslin H, Benichou S, et al. Differential nucleocytoplasmic shuttling of beta-arrestins. Characterization of a leucine-rich nuclear export signal in beta-arrestin2. *J Biol Chem*. 2002;277(40):37693-701.
121. Hoepfner CZ, Cheng N, Ye RD. Identification of a nuclear localization sequence in beta-arrestin-1 and its functional implications. *J Biol Chem*. 2012;287(12):8932-43.
122. Zhang X, Min X, Wang S, Sun N, Kim KM. Mdm2-mediated ubiquitination of beta-arrestin2 in the nucleus occurs in a Gbetagamma- and clathrin-dependent manner. *Biochem Pharmacol*. 2020;178:114049.
123. Blondel-Tepaz E, Lerverve M, Sokrat B, Paradis JS, Kosic M, Saha K, et al. The RanBP2/RanGAP1-SUMO complex gates beta-arrestin2 nuclear entry to regulate the Mdm2-p53 signaling axis. *Oncogene*. 2021;40(12):2243-57.
124. Kang J, Shi Y, Xiang B, Qu B, Su W, Zhu M, et al. A nuclear function of beta-arrestin1 in GPCR signaling: regulation of histone acetylation and gene transcription. *Cell*. 2005;123(5):833-47.
125. Wang P, Wu Y, Ge X, Ma L, Pei G. Subcellular localization of beta-arrestins is determined by their intact N domain and the nuclear export signal at the C terminus. *J Biol Chem*. 2003;278(13):11648-53.
126. Rajagopal S, Shenoy SK. GPCR desensitization: Acute and prolonged phases. *Cell Signal*. 2018;41:9-16.
127. Sibley DR, Peters JR, Nambi P, Caron MG, Lefkowitz RJ. Desensitization of turkey erythrocyte adenylate cyclase. Beta-adrenergic receptor phosphorylation is correlated with attenuation of adenylate cyclase activity. *J Biol Chem*. 1984;259(15):9742-9.
128. Bouvier M, Collins S, O'Dowd BF, Campbell PT, de Blasi A, Kobilka BK, et al. Two distinct pathways for cAMP-mediated down-regulation of the beta 2-adrenergic receptor. Phosphorylation of the receptor and regulation of its mRNA level. *J Biol Chem*. 1989;264(28):16786-92.
129. Pitcher J, Lohse MJ, Codina J, Caron MG, Lefkowitz RJ. Desensitization of the isolated beta 2-adrenergic receptor by beta-adrenergic receptor kinase, cAMP-dependent protein kinase, and protein kinase C occurs via distinct molecular mechanisms. *Biochemistry*. 1992;31(12):3193-7.
130. Sibley DR, Strasser RH, Caron MG, Lefkowitz RJ. Homologous desensitization of adenylate cyclase is associated with phosphorylation of the beta-adrenergic receptor. *J Biol Chem*. 1985;260(7):3883-6.

131. Benovic JL, Strasser RH, Caron MG, Lefkowitz RJ. Beta-adrenergic receptor kinase: identification of a novel protein kinase that phosphorylates the agonist-occupied form of the receptor. *Proc Natl Acad Sci U S A*. 1986;83(9):2797-801.
132. Gurevich VV, Benovic JL. Visual arrestin binding to rhodopsin. Diverse functional roles of positively charged residues within the phosphorylation-recognition region of arrestin. *J Biol Chem*. 1995;270(11):6010-6.
133. Luttrell LM, Lefkowitz RJ. The role of beta-arrestins in the termination and transduction of G-protein-coupled receptor signals. *J Cell Sci*. 2002;115(Pt 3):455-65.
134. Ren XR, Reiter E, Ahn S, Kim J, Chen W, Lefkowitz RJ. Different G protein-coupled receptor kinases govern G protein and beta-arrestin-mediated signaling of V2 vasopressin receptor. *Proc Natl Acad Sci U S A*. 2005;102(5):1448-53.
135. Nobles KN, Xiao K, Ahn S, Shukla AK, Lam CM, Rajagopal S, et al. Distinct phosphorylation sites on the beta(2)-adrenergic receptor establish a barcode that encodes differential functions of beta-arrestin. *Sci Signal*. 2011;4(185):ra51.
136. Mukherjee S, Gurevich VV, Preninger A, Hamm HE, Bader MF, Fazleabas AT, et al. Aspartic acid 564 in the third cytoplasmic loop of the luteinizing hormone/choriogonadotropin receptor is crucial for phosphorylation-independent interaction with arrestin2. *J Biol Chem*. 2002;277(20):17916-27.
137. Galliera E, Jala VR, Trent JO, Bonecchi R, Signorelli P, Lefkowitz RJ, et al. beta-Arrestin-dependent constitutive internalization of the human chemokine decoy receptor D6. *J Biol Chem*. 2004;279(24):25590-7.
138. Scarselli M, Donaldson JG. Constitutive internalization of G protein-coupled receptors and G proteins via clathrin-independent endocytosis. *J Biol Chem*. 2009;284(6):3577-85.
139. Barak LS, Oakley RH, Laporte SA, Caron MG. Constitutive arrestin-mediated desensitization of a human vasopressin receptor mutant associated with nephrogenic diabetes insipidus. *Proc Natl Acad Sci U S A*. 2001;98(1):93-8.
140. Mettlen M, Chen PH, Srinivasan S, Danuser G, Schmid SL. Regulation of Clathrin-Mediated Endocytosis. *Annu Rev Biochem*. 2018;87:871-96.
141. Moo EV, van Senten JR, Brauner-Osborne H, Moller TC. Arrestin-Dependent and -Independent Internalization of G Protein-Coupled Receptors: Methods, Mechanisms, and Implications on Cell Signaling. *Mol Pharmacol*. 2021;99(4):242-55.
142. Diviani D, Lattion AL, Abuin L, Staub O, Cotecchia S. The adaptor complex 2 directly interacts with the alpha 1b-adrenergic receptor and plays a role in receptor endocytosis. *J Biol Chem*. 2003;278(21):19331-40.
143. Chini B, Parenti M. G-protein coupled receptors in lipid rafts and caveolae: how, when and why do they go there? *J Mol Endocrinol*. 2004;32(2):325-38.
144. Yamashiro DJ, Maxfield FR. Acidification of endocytic compartments and the intracellular pathways of ligands and receptors. *J Cell Biochem*. 1984;26(4):231-46.
145. Wandinger-Ness A, Zerial M. Rab proteins and the compartmentalization of the endosomal system. *Cold Spring Harb Perspect Biol*. 2014;6(11):a022616.
146. Puthenveedu MA, Lauffer B, Temkin P, Vistein R, Carlton P, Thorn K, et al. Sequence-dependent sorting of recycling proteins by actin-stabilized endosomal microdomains. *Cell*. 2010;143(5):761-73.

147. Kliewer A, Reinscheid RK, Schulz S. Emerging Paradigms of G Protein-Coupled Receptor Dephosphorylation. *Trends Pharmacol Sci.* 2017;38(7):621-36.
148. Hicke L, Riezman H. Ubiquitination of a yeast plasma membrane receptor signals its ligand-stimulated endocytosis. *Cell.* 1996;84(2):277-87.
149. Raiborg C, Stenmark H. The ESCRT machinery in endosomal sorting of ubiquitylated membrane proteins. *Nature.* 2009;458(7237):445-52.
150. Skieterska K, Rondou P, Van Craenenbroeck K. Regulation of G Protein-Coupled Receptors by Ubiquitination. *Int J Mol Sci.* 2017;18(5).
151. Miller WE, Maudsley S, Ahn S, Khan KD, Luttrell LM, Lefkowitz RJ. beta-arrestin1 interacts with the catalytic domain of the tyrosine kinase c-SRC. Role of beta-arrestin1-dependent targeting of c-SRC in receptor endocytosis. *J Biol Chem.* 2000;275(15):11312-9.
152. Meloche S, Pouyssegur J. The ERK1/2 mitogen-activated protein kinase pathway as a master regulator of the G1- to S-phase transition. *Oncogene.* 2007;26(22):3227-39.
153. Luttrell LM, Roudabush FL, Choy EW, Miller WE, Field ME, Pierce KL, et al. Activation and targeting of extracellular signal-regulated kinases by beta-arrestin scaffolds. *Proc Natl Acad Sci U S A.* 2001;98(5):2449-54.
154. McDonald PH, Chow CW, Miller WE, Laporte SA, Field ME, Lin FT, et al. Beta-arrestin 2: a receptor-regulated MAPK scaffold for the activation of JNK3. *Science.* 2000;290(5496):1574-7.
155. Sun Y, Cheng Z, Ma L, Pei G. Beta-arrestin2 is critically involved in CXCR4-mediated chemotaxis, and this is mediated by its enhancement of p38 MAPK activation. *J Biol Chem.* 2002;277(51):49212-9.
156. Bruchas MR, Macey TA, Lowe JD, Chavkin C. Kappa opioid receptor activation of p38 MAPK is GRK3- and arrestin-dependent in neurons and astrocytes. *J Biol Chem.* 2006;281(26):18081-9.
157. Povsic TJ, Kohout TA, Lefkowitz RJ. Beta-arrestin1 mediates insulin-like growth factor 1 (IGF-1) activation of phosphatidylinositol 3-kinase (PI3K) and anti-apoptosis. *J Biol Chem.* 2003;278(51):51334-9.
158. Goel R, Phillips-Mason PJ, Raben DM, Baldassare JJ. alpha-Thrombin induces rapid and sustained Akt phosphorylation by beta-arrestin1-dependent and -independent mechanisms, and only the sustained Akt phosphorylation is essential for G1 phase progression. *J Biol Chem.* 2002;277(21):18640-8.
159. Beaulieu JM, Sotnikova TD, Marion S, Lefkowitz RJ, Gainetdinov RR, Caron MG. An Akt/beta-arrestin 2/PP2A signaling complex mediates dopaminergic neurotransmission and behavior. *Cell.* 2005;122(2):261-73.
160. Gao H, Sun Y, Wu Y, Luan B, Wang Y, Qu B, et al. Identification of beta-arrestin2 as a G protein-coupled receptor-stimulated regulator of NF-kappaB pathways. *Mol Cell.* 2004;14(3):303-17.
161. Tohgo A, Choy EW, Gesty-Palmer D, Pierce KL, Laporte S, Oakley RH, et al. The stability of the G protein-coupled receptor-beta-arrestin interaction determines the mechanism and functional consequence of ERK activation. *J Biol Chem.* 2003;278(8):6258-67.
162. Ahn S, Shenoy SK, Wei H, Lefkowitz RJ. Differential kinetic and spatial patterns of beta-arrestin and G protein-mediated ERK activation by the angiotensin II receptor. *J Biol Chem.* 2004;279(34):35518-25.
163. Grundmann M, Merten N, Malfacini D, Inoue A, Preis P, Simon K, et al. Lack of beta-arrestin signaling in the absence of active G proteins. *Nat Commun.* 2018;9(1):341.



164. Luttrell LM, Wang J, Plouffe B, Smith JS, Yamani L, Kaur S, et al. Manifold roles of beta-arrestins in GPCR signaling elucidated with siRNA and CRISPR/Cas9. *Sci Signal*. 2018;11(549).
165. Bologna Z, Teoh JP, Bayoumi AS, Tang Y, Kim IM. Biased G Protein-Coupled Receptor Signaling: New Player in Modulating Physiology and Pathology. *Biomol Ther (Seoul)*. 2017;25(1):12-25.
166. Rajagopal S, Rajagopal K, Lefkowitz RJ. Teaching old receptors new tricks: biasing seven-transmembrane receptors. *Nat Rev Drug Discov*. 2010;9(5):373-86.
167. Soergel DG, Subach RA, Burnham N, Lark MW, James IE, Sadler BM, et al. Biased agonism of the mu-opioid receptor by TRV130 increases analgesia and reduces on-target adverse effects versus morphine: A randomized, double-blind, placebo-controlled, crossover study in healthy volunteers. *Pain*. 2014;155(9):1829-35.
168. Boerrigter G, Soergel DG, Violin JD, Lark MW, Burnett JC, Jr. TRV120027, a novel beta-arrestin biased ligand at the angiotensin II type I receptor, unloads the heart and maintains renal function when added to furosemide in experimental heart failure. *Circ Heart Fail*. 2012;5(5):627-34.
169. Smith JS, Rajagopal S. The beta-Arrestins: Multifunctional Regulators of G Protein-coupled Receptors. *J Biol Chem*. 2016;291(17):8969-77.
170. Thomsen ARB, Jensen DD, Hicks GA, Bunnett NW. Therapeutic Targeting of Endosomal G-Protein-Coupled Receptors. *Trends Pharmacol Sci*. 2018;39(10):879-91.
171. Calebiro D, Nikolaev VO, Gagliani MC, de Filippis T, Dees C, Tacchetti C, et al. Persistent cAMP-signals triggered by internalized G-protein-coupled receptors. *PLoS Biol*. 2009;7(8):e1000172.
172. Ferrandon S, Feinstein TN, Castro M, Wang B, Bouley R, Potts JT, et al. Sustained cyclic AMP production by parathyroid hormone receptor endocytosis. *Nat Chem Biol*. 2009;5(10):734-42.
173. Wehbi VL, Stevenson HP, Feinstein TN, Calero G, Romero G, Vilaradaga JP. Noncanonical GPCR signaling arising from a PTH receptor-arrestin-Gbetagamma complex. *Proc Natl Acad Sci U S A*. 2013;110(4):1530-5.
174. Feinstein TN, Yui N, Webber MJ, Wehbi VL, Stevenson HP, King JD, Jr., et al. Noncanonical control of vasopressin receptor type 2 signaling by retromer and arrestin. *J Biol Chem*. 2013;288(39):27849-60.
175. Thomsen ARB, Plouffe B, Cahill TJ, 3rd, Shukla AK, Tarrasch JT, Dosey AM, et al. GPCR-G Protein-beta-Arrestin Super-Complex Mediates Sustained G Protein Signaling. *Cell*. 2016;166(4):907-19.
176. Merriam LA, Baran CN, Girard BM, Hardwick JC, May V, Parsons RL. Pituitary adenylate cyclase 1 receptor internalization and endosomal signaling mediate the pituitary adenylate cyclase activating polypeptide-induced increase in guinea pig cardiac neuron excitability. *J Neurosci*. 2013;33(10):4614-22.
177. Jimenez-Vargas NN, Pattison LA, Zhao P, Lieu T, Latorre R, Jensen DD, et al. Protease-activated receptor-2 in endosomes signals persistent pain of irritable bowel syndrome. *Proc Natl Acad Sci U S A*. 2018;115(31):E7438-E47.
178. Lefkowitz RJ, Shenoy SK. Transduction of receptor signals by beta-arrestins. *Science*. 2005;308(5721):512-7.

179. Lefkowitz RJ, Rajagopal K, Whalen EJ. New roles for beta-arrestins in cell signaling: not just for seven-transmembrane receptors. *Mol Cell*. 2006;24(5):643-52.
180. Xiao K, McClatchy DB, Shukla AK, Zhao Y, Chen M, Shenoy SK, et al. Functional specialization of beta-arrestin interactions revealed by proteomic analysis. *Proc Natl Acad Sci U S A*. 2007;104(29):12011-6.
181. Kandasamy K, Mohan SS, Raju R, Keerthikumar S, Kumar GS, Venugopal AK, et al. NetPath: a public resource of curated signal transduction pathways. *Genome Biol*. 2010;11(1):R3.
182. Stark C, Breitkreutz BJ, Reguly T, Boucher L, Breitkreutz A, Tyers M. BioGRID: a general repository for interaction datasets. *Nucleic Acids Res*. 2006;34(Database issue):D535-9.
183. Calderone A, Castagnoli L, Cesareni G. mentha: a resource for browsing integrated protein-interaction networks. *Nat Methods*. 2013;10(8):690-1.
184. Crepieux P, Poupon A, Langonne-Gallay N, Reiter E, Delgado J, Schaefer MH, et al. A Comprehensive View of the beta-Arrestinome. *Front Endocrinol (Lausanne)*. 2017;8:32.
185. Ramazi S, Zahiri J. Posttranslational modifications in proteins: resources, tools and prediction methods. *Database (Oxford)*. 2021;2021.
186. Khoury GA, Baliban RC, Floudas CA. Proteome-wide post-translational modification statistics: frequency analysis and curation of the swiss-prot database. *Sci Rep*. 2011;1.
187. Ivry SL, Meyer NO, Winter MB, Bohn MF, Knudsen GM, O'Donoghue AJ, et al. Global substrate specificity profiling of post-translational modifying enzymes. *Protein Sci*. 2018;27(3):584-94.
188. Patwardhan A, Cheng N, Trejo J. Post-Translational Modifications of G Protein-Coupled Receptors Control Cellular Signaling Dynamics in Space and Time. *Pharmacol Rev*. 2021;73(1):120-51.
189. Cohen P. The regulation of protein function by multisite phosphorylation--a 25 year update. *Trends Biochem Sci*. 2000;25(12):596-601.
190. Singh V, Ram M, Kumar R, Prasad R, Roy BK, Singh KK. Phosphorylation: Implications in Cancer. *Protein J*. 2017;36(1):1-6.
191. Hunter T. Protein kinases and phosphatases: the yin and yang of protein phosphorylation and signaling. *Cell*. 1995;80(2):225-36.
192. Benovic JL, Pike LJ, Cerione RA, Staniszewski C, Yoshimasa T, Codina J, et al. Phosphorylation of the mammalian beta-adrenergic receptor by cyclic AMP-dependent protein kinase. Regulation of the rate of receptor phosphorylation and dephosphorylation by agonist occupancy and effects on coupling of the receptor to the stimulatory guanine nucleotide regulatory protein. *J Biol Chem*. 1985;260(11):7094-101.
193. Gurevich VV, Gurevich EV. The structural basis of arrestin-mediated regulation of G-protein-coupled receptors. *Pharmacol Ther*. 2006;110(3):465-502.
194. Oakley RH, Laporte SA, Holt JA, Caron MG, Barak LS. Differential affinities of visual arrestin, beta arrestin1, and beta arrestin2 for G protein-coupled receptors delineate two major classes of receptors. *J Biol Chem*. 2000;275(22):17201-10.
195. Poll F, Doll C, Schulz S. Rapid dephosphorylation of G protein-coupled receptors by protein phosphatase 1beta is required for termination of beta-arrestin-dependent signaling. *J Biol Chem*. 2011;286(38):32931-6.

196. Lefkowitz RJ. G protein-coupled receptors: III. New roles for receptor kinases and  $\beta$ -arrestins in receptor signaling and desensitization. *Journal of Biological Chemistry*. 1998;273(30):18677-80.
197. Tobin AB. G-protein-coupled receptor phosphorylation: where, when and by whom. *Br J Pharmacol*. 2008;153 Suppl 1:S167-76.
198. Chen H, Zhang S, Zhang X, Liu H. QR code model: a new possibility for GPCR phosphorylation recognition. *Cell Commun Signal*. 2022;20(1):23.
199. Roth NS, Campbell PT, Caron MG, Lefkowitz RJ, Lohse MJ. Comparative rates of desensitization of beta-adrenergic receptors by the beta-adrenergic receptor kinase and the cyclic AMP-dependent protein kinase. *Proc Natl Acad Sci U S A*. 1991;88(14):6201-4.
200. Daaka Y, Luttrell LM, Lefkowitz RJ. Switching of the coupling of the beta2-adrenergic receptor to different G proteins by protein kinase A. *Nature*. 1997;390(6655):88-91.
201. Wei H, Ahn S, Shenoy SK, Karnik SS, Hunyady L, Luttrell LM, et al. Independent beta-arrestin 2 and G protein-mediated pathways for angiotensin II activation of extracellular signal-regulated kinases 1 and 2. *Proc Natl Acad Sci U S A*. 2003;100(19):10782-7.
202. Violin JD, Ren XR, Lefkowitz RJ. G-protein-coupled receptor kinase specificity for beta-arrestin recruitment to the beta2-adrenergic receptor revealed by fluorescence resonance energy transfer. *J Biol Chem*. 2006;281(29):20577-88.
203. Zidar DA, Violin JD, Whalen EJ, Lefkowitz RJ. Selective engagement of G protein coupled receptor kinases (GRKs) encodes distinct functions of biased ligands. *Proc Natl Acad Sci U S A*. 2009;106(24):9649-54.
204. Prihandoko R, Alvarez-Curto E, Hudson BD, Butcher AJ, Ulven T, Miller AM, et al. Distinct Phosphorylation Clusters Determine the Signaling Outcome of Free Fatty Acid Receptor 4/G Protein-Coupled Receptor 120. *Molecular pharmacology*. 2016;89(5):505-20.
205. Bouzo-Lorenzo M, Santo-Zas I, Lodeiro M, Nogueiras R, Casanueva FF, Castro M, et al. Distinct phosphorylation sites on the ghrelin receptor, GHSR1a, establish a code that determines the functions of  $\beta$ -arrestins. *Sci Rep*. 2016;6:22495.
206. Lin FT, Krueger KM, Kendall HE, Daaka Y, Fredericks ZL, Pitcher JA, et al. Clathrin-mediated endocytosis of the beta-adrenergic receptor is regulated by phosphorylation/dephosphorylation of beta-arrestin1. *J Biol Chem*. 1997;272(49):31051-7.
207. Lin FT, Chen W, Shenoy S, Cong M, Exum ST, Lefkowitz RJ. Phosphorylation of beta-arrestin2 regulates its function in internalization of beta(2)-adrenergic receptors. *Biochemistry*. 2002;41(34):10692-9.
208. Paradis JS, Ly S, Blondel-Tepaz E, Galan JA, Beautrait A, Scott MG, et al. Receptor sequestration in response to beta-arrestin-2 phosphorylation by ERK1/2 governs steady-state levels of GPCR cell-surface expression. *Proc Natl Acad Sci U S A*. 2015;112(37):E5160-8.
209. Ciechanover A, Hod Y, Hershko A. A heat-stable polypeptide component of an ATP-dependent proteolytic system from reticulocytes. *Biochem Biophys Res Commun*. 1978;81(4):1100-5.
210. Ciechanover A, Heller H, Elias S, Haas AL, Hershko A. ATP-dependent conjugation of reticulocyte proteins with the polypeptide required for protein degradation. *Proc Natl Acad Sci U S A*. 1980;77(3):1365-8.
211. Vijay-Kumar S, Bugg CE, Cook WJ. Structure of ubiquitin refined at 1.8 Å resolution. *J Mol Biol*. 1987;194(3):531-44.

212. Kimura Y, Tanaka K. Regulatory mechanisms involved in the control of ubiquitin homeostasis. *J Biochem.* 2010;147(6):793-8.
213. Pickart CM, Eddins MJ. Ubiquitin: structures, functions, mechanisms. *Biochim Biophys Acta.* 2004;1695(1-3):55-72.
214. Li W, Chanda SK, Micik I, Joazeiro CA. Methods for the functional genomic analysis of ubiquitin ligases. *Methods in enzymology.* 2005;398:280-91.
215. Nijman SM, Luna-Vargas MP, Velds A, Brummelkamp TR, Dirac AM, Sixma TK, et al. A genomic and functional inventory of deubiquitinating enzymes. *Cell.* 2005;123(5):773-86.
216. Shenoy SK, McDonald PH, Kohout TA, Lefkowitz RJ. Regulation of receptor fate by ubiquitination of activated beta 2-adrenergic receptor and beta-arrestin. *Science.* 2001;294(5545):1307-13.
217. Marchese A, Benovic JL. Agonist-promoted ubiquitination of the G protein-coupled receptor CXCR4 mediates lysosomal sorting. *J Biol Chem.* 2001;276(49):45509-12.
218. Martin NP, Lefkowitz RJ, Shenoy SK. Regulation of V2 vasopressin receptor degradation by agonist-promoted ubiquitination. *J Biol Chem.* 2003;278(46):45954-9.
219. Hurley JH, Hanson PI. Membrane budding and scission by the ESCRT machinery: it's all in the neck. *Nat Rev Mol Cell Biol.* 2010;11(8):556-66.
220. Dores MR, Trejo J. Ubiquitination of G protein-coupled receptors: functional implications and drug discovery. *Mol Pharmacol.* 2012;82(4):563-70.
221. Petaja-Repo UE, Hogue M, Laperriere A, Bhalla S, Walker P, Bouvier M. Newly synthesized human delta opioid receptors retained in the endoplasmic reticulum are retrotranslocated to the cytosol, deglycosylated, ubiquitinated, and degraded by the proteasome. *J Biol Chem.* 2001;276(6):4416-23.
222. Cook LB, Zhu CC, Hinkle PM. Thyrotropin-releasing hormone receptor processing: role of ubiquitination and proteasomal degradation. *Mol Endocrinol.* 2003;17(9):1777-91.
223. Canals M, Scholten DJ, de Munnik S, Han MK, Smit MJ, Leurs R. Ubiquitination of CXCR7 controls receptor trafficking. *PLoS One.* 2012;7(3):e34192.
224. Kaur S, Chen Y, Shenoy SK. Agonist-activated glucagon receptors are deubiquitinated at early endosomes by two distinct deubiquitinases to facilitate Rab4a-dependent recycling. *J Biol Chem.* 2020;295(49):16630-42.
225. Hicke L, Zanolari B, Riezman H. Cytoplasmic tail phosphorylation of the alpha-factor receptor is required for its ubiquitination and internalization. *J Cell Biol.* 1998;141(2):349-58.
226. Shenoy SK, Xiao K, Venkataramanan V, Snyder PM, Freedman NJ, Weissman AM. Nedd4 mediates agonist-dependent ubiquitination, lysosomal targeting, and degradation of the beta2-adrenergic receptor. *J Biol Chem.* 2008;283(32):22166-76.
227. Jacob C, Cottrell GS, Gehringer D, Schmidlin F, Grady EF, Bunnett NW. c-Cbl mediates ubiquitination, degradation, and down-regulation of human protease-activated receptor 2. *J Biol Chem.* 2005;280(16):16076-87.
228. Moriyoshi K, Iijima K, Fujii H, Ito H, Cho Y, Nakanishi S. Seven in absentia homolog 1A mediates ubiquitination and degradation of group 1 metabotropic glutamate receptors. *Proc Natl Acad Sci U S A.* 2004;101(23):8614-9.
229. Shenoy SK, Lefkowitz RJ. Trafficking patterns of beta-arrestin and G protein-coupled receptors determined by the kinetics of beta-arrestin deubiquitination. *J Biol Chem.* 2003;278(16):14498-506.

230. Shenoy SK, Modi AS, Shukla AK, Xiao K, Berthouze M, Ahn S, et al. Beta-arrestin-dependent signaling and trafficking of 7-transmembrane receptors is reciprocally regulated by the deubiquitinase USP33 and the E3 ligase Mdm2. *Proc Natl Acad Sci U S A*. 2009;106(16):6650-5.
231. Shenoy SK, Lefkowitz RJ. Receptor-specific ubiquitination of beta-arrestin directs assembly and targeting of seven-transmembrane receptor signalosomes. *J Biol Chem*. 2005;280(15):15315-24.
232. Bayer P, Arndt A, Metzger S, Mahajan R, Melchior F, Jaenicke R, et al. Structure determination of the small ubiquitin-related modifier SUMO-1. *Journal of molecular biology*. 1998;280(2):275-86.
233. Matunis MJ, Coutavas E, Blobel G. A novel ubiquitin-like modification modulates the partitioning of the Ran-GTPase-activating protein RanGAP1 between the cytosol and the nuclear pore complex. *J Cell Biol*. 1996;135(6 Pt 1):1457-70.
234. Sampson DA, Wang M, Matunis MJ. The small ubiquitin-like modifier-1 (SUMO-1) consensus sequence mediates Ubc9 binding and is essential for SUMO-1 modification. *J Biol Chem*. 2001;276(24):21664-9.
235. Xu J, He Y, Qiang B, Yuan J, Peng X, Pan XM. A novel method for high accuracy sumoylation site prediction from protein sequences. *BMC Bioinformatics*. 2008;9:8.
236. Mukhopadhyay D, Dasso M. Modification in reverse: the SUMO proteases. *Trends Biochem Sci*. 2007;32(6):286-95.
237. Kerscher O. SUMO junction-what's your function? New insights through SUMO-interacting motifs. *EMBO Rep*. 2007;8(6):550-5.
238. Hayashi T, Seki M, Maeda D, Wang W, Kawabe Y-i, Seki T, et al. Ubc9 is essential for viability of higher eukaryotic cells. *Experimental cell research*. 2002;280(2):212-21.
239. Evdokimov E, Sharma P, Lockett SJ, Lualdi M, Kuehn MR. Loss of SUMO1 in mice affects RanGAP1 localization and formation of PML nuclear bodies, but is not lethal as it can be compensated by SUMO2 or SUMO3. *Journal of cell science*. 2008;121(24):4106-13.
240. Tang Z, El Far O, Betz H, Scheschonka A. Pias1 interaction and sumoylation of metabotropic glutamate receptor 8. *J Biol Chem*. 2005;280(46):38153-9.
241. Gowran A, Murphy CE, Campbell VA. Delta(9)-tetrahydrocannabinol regulates the p53 post-translational modifiers Murine double minute 2 and the Small Ubiquitin MOdifier protein in the rat brain. *FEBS Lett*. 2009;583(21):3412-8.
242. Li Q, Muma NA. Estradiol potentiates 8-OH-DPAT-induced sumoylation of 5-HT(1)A receptor: characterization and subcellular distribution of sumoylated 5-HT(1)A receptors. *Psychoneuroendocrinology*. 2013;38(11):2542-53.
243. Xu J, Tan P, Li H, Cui Y, Qiu Y, Wang H, et al. Direct SUMOylation of M1 muscarinic acetylcholine receptor increases its ligand-binding affinity and signal transduction. *FASEB J*. 2019;33(3):3237-51.
244. Wyatt D, Malik R, Vesecky AC, Marchese A. Small ubiquitin-like modifier modification of arrestin-3 regulates receptor trafficking. *J Biol Chem*. 2011;286(5):3884-93.
245. Xiao N, Li H, Mei W, Cheng J. SUMOylation attenuates human beta-arrestin 2 inhibition of IL-1R/TRAF6 signaling. *J Biol Chem*. 2015;290(4):1927-35.
246. Nagi K, Kaur S, Bai Y, Shenoy SK. In-frame fusion of SUMO1 enhances betaarrestin2's association with activated GPCRs as well as with nuclear pore complexes. *Cell Signal*. 2020;75:109759.

247. Thomsen ARB, Plouffe B, Cahill TJ, 3rd, Shukla AK, Tarrasch JT, Dosey AM, et al. GPCR-G Protein- $\beta$ -Arrestin Super-Complex Mediates Sustained G Protein Signaling. *Cell*. 2016;166(4):907-19.
248. Nguyen AH, Thomsen ARB, Cahill TJ, 3rd, Huang R, Huang LY, Marcink T, et al. Structure of an endosomal signaling GPCR-G protein-beta-arrestin megacomplex. *Nat Struct Mol Biol*. 2019;26(12):1123-31.
249. Jensen DD, Lieu T, Halls ML, Veldhuis NA, Imlach WL, Mai QN, et al. Neurokinin 1 receptor signaling in endosomes mediates sustained nociception and is a viable therapeutic target for prolonged pain relief. *Sci Transl Med*. 2017;9(392).
250. Saini DK, Kalyanaraman V, Chisari M, Gautam N. A family of G protein  $\beta\gamma$  subunits translocate reversibly from the plasma membrane to endomembranes on receptor activation. *J Biol Chem*. 2007;282(33):24099-108.
251. Ajith Karunarathne WK, O'Neill PR, Martinez-Espinosa PL, Kalyanaraman V, Gautam N. All G protein  $\beta\gamma$  complexes are capable of translocation on receptor activation. *Biochem Biophys Res Commun*. 2012;421(3):605-11.
252. Masuho I, Skamangas NK, Muntean BS, Martemyanov KA. Diversity of the G $\beta\gamma$  complexes defines spatial and temporal bias of GPCR signaling. *Cell Syst*. 2021;12(4):324-37.e5.
253. Wedegaertner PB, Bourne HR. Activation and depalmitoylation of Gs alpha. *Cell*. 1994;77(7):1063-70.
254. Degtyarev MY, Spiegel AM, Jones TL. Increased palmitoylation of the Gs protein alpha subunit after activation by the beta-adrenergic receptor or cholera toxin. *J Biol Chem*. 1993;268(32):23769-72.
255. Mumby SM, Kleuss C, Gilman AG. Receptor regulation of G-protein palmitoylation. *Proc Natl Acad Sci U S A*. 1994;91(7):2800-4.
256. Yu JZ, Rasenick MM. Real-time visualization of a fluorescent G(alpha)(s): dissociation of the activated G protein from plasma membrane. *Mol Pharmacol*. 2002;61(2):352-9.
257. Duncan JA, Gilman AG. A cytoplasmic acyl-protein thioesterase that removes palmitate from G protein alpha subunits and p21(RAS). *J Biol Chem*. 1998;273(25):15830-7.
258. Martin BR, Lambert NA. Activated G Protein G $\alpha$ s Samples Multiple Endomembrane Compartments. *J Biol Chem*. 2016;291(39):20295-302.
259. Hilger D, Kumar KK, Hu H, Pedersen MF, O'Brien ES, Giehm L, et al. Structural insights into differences in G protein activation by family A and family B GPCRs. *Science*. 2020;369(6503).
260. Zhang J, Bui TN, Xiang J, Lin A. Cyclic AMP inhibits p38 activation via CREB-induced dynein light chain. *Mol Cell Biol*. 2006;26(4):1223-34.
261. Miller RA, Birnbaum MJ. Glucagon: acute actions on hepatic metabolism. *Diabetologia*. 2016;59(7):1376-81.
262. Capozzi ME, Svendsen B, Encisco SE, Lewandowski SL, Martin MD, Lin H, et al. beta Cell tone is defined by proglucagon peptides through cAMP signaling. *JCI Insight*. 2019;4(5).
263. Capozzi ME, D'Alessio DA, Campbell JE. The past, present, and future physiology and pharmacology of glucagon. *Cell Metab*. 2022;34(11):1654-74.
264. Sandoval DA, D'Alessio DA. Physiology of proglucagon peptides: role of glucagon and GLP-1 in health and disease. *Physiol Rev*. 2015;95(2):513-48.

265. van der Velden WJC, Lindquist P, Madsen JS, Stassen R, Wewer Albrechtsen NJ, Holst JJ, et al. Molecular and in vivo phenotyping of missense variants of the human glucagon receptor. *J Biol Chem.* 2022;298(2):101413.
266. Sekar R, Motzler K, Kwon Y, Novikoff A, Julg J, Najafi B, et al. Vps37a regulates hepatic glucose production by controlling glucagon receptor localization to endosomes. *Cell Metab.* 2022;34(12):2047.
267. Kim DI, Jensen SC, Noble KA, Kc B, Roux KH, Motamedchaboki K, et al. An improved smaller biotin ligase for BioID proximity labeling. *Mol Biol Cell.* 2016;27(8):1188-96.
268. Kim DI, Birendra KC, Zhu W, Motamedchaboki K, Doye V, Roux KJ. Probing nuclear pore complex architecture with proximity-dependent biotinylation. *Proc Natl Acad Sci U S A.* 2014;111(24):E2453-61.
269. McDonald PH, Cote NL, Lin FT, Premont RT, Pitcher JA, Lefkowitz RJ. Identification of NSF as a beta-arrestin1-binding protein. Implications for beta2-adrenergic receptor regulation. *J Biol Chem.* 1999;274(16):10677-80.
270. Schmid EM, Ford MG, Burtey A, Praefcke GJ, Peak-Chew SY, Mills IG, et al. Role of the AP2 beta-appendage hub in recruiting partners for clathrin-coated vesicle assembly. *PLoS Biol.* 2006;4(9):e262.
271. Milano SK, Kim YM, Stefano FP, Benovic JL, Brenner C. Nonvisual arrestin oligomerization and cellular localization are regulated by inositol hexakisphosphate binding. *J Biol Chem.* 2006;281(14):9812-23.
272. Zhang X, Zhang J, Bauer A, Zhang L, Selinger DW, Lu CX, et al. Fine-tuning BMP7 signalling in adipogenesis by UBE2O/E2-230K-mediated monoubiquitination of SMAD6. *EMBO J.* 2013;32(7):996-1007.
273. Mashtalir N, Daou S, Barbour H, Sen NN, Gagnon J, Hammond-Martel I, et al. Autodeubiquitination protects the tumor suppressor BAP1 from cytoplasmic sequestration mediated by the atypical ubiquitin ligase UBE2O. *Mol Cell.* 2014;54(3):392-406.
274. Zhang X, Zhang J, Zhang L, van Dam H, ten Dijke P. UBE2O negatively regulates TRAF6-mediated NF-kappaB activation by inhibiting TRAF6 polyubiquitination. *Cell Res.* 2013;23(3):366-77.
275. Perroy J, Pontier S, Charest PG, Aubry M, Bouvier M. Real-time monitoring of ubiquitination in living cells by BRET. *Nat Methods.* 2004;1(3):203-8.
276. Marullo S, Bouvier M. Resonance energy transfer approaches in molecular pharmacology and beyond. *Trends Pharmacol Sci.* 2007;28(8):362-5.
277. Baidya M, Kumari P, Dwivedi-Agnihotri H, Pandey S, Sokrat B, Sposini S, et al. Genetically encoded intrabody sensors report the interaction and trafficking of beta-arrestin 1 upon activation of G-protein-coupled receptors. *J Biol Chem.* 2020;295(30):10153-67.
278. Paradis JS, Feng X, Murat B, Jefferson RE, Sokrat B, Szpakowska M, et al. Computationally designed GPCR quaternary structures bias signaling pathway activation. *Nat Commun.* 2022;13(1):6826.

## Annexes



**Annex I: Genetically Encoded Intrabody Sensors Report the Interaction and Trafficking of  $\beta$ -arrestin 1 Upon Activation of G-Protein–Coupled Receptors**



# Genetically encoded intrabody sensors report the interaction and trafficking of $\beta$ -arrestin 1 upon activation of G-protein-coupled receptors

Received for publication, May 7, 2020, and in revised form, May 18, 2020. Published, Papers in Press, May 21, 2020, DOI 10.1074/jbc.RA120.013470

Mithu Baidya<sup>1,†</sup>, Punita Kumari<sup>1,†</sup>, Hemlata Dwivedi-Agnihotri<sup>1,†</sup>, Shubhi Pandey<sup>1</sup>, Badr Sokrat<sup>2,3</sup>, Silvia Sposini<sup>4</sup>, Madhu Chaturvedi<sup>1</sup>, Ashish Srivastava<sup>1</sup>, Debarati Roy<sup>1</sup>, Aylin C. Hanyaloglu<sup>4</sup>, Michel Bouvier<sup>2,3</sup>, and Arun K. Shukla<sup>1,\*</sup>

From the <sup>1</sup>Department of Biological Sciences and Bioengineering, Indian Institute of Technology, Kanpur, India, the <sup>2</sup>Institute for Research in Immunology and Cancer, Université de Montréal, Montreal, Quebec, Canada, the <sup>3</sup>Department of Biochemistry and Molecular Medicine, Université de Montréal, Montreal, Quebec, Canada, and the <sup>4</sup>Institute of Reproductive and Developmental Biology, Department of Metabolism, Digestion and Reproduction, Imperial College London, London, United Kingdom

Edited by Henrik G. Dohlman

Agonist stimulation of G-protein-coupled receptors (GPCRs) typically leads to phosphorylation of GPCRs and binding to multifunctional proteins called  $\beta$ -arrestins ( $\beta$ arrs). The GPCR- $\beta$ arr interaction critically contributes to GPCR desensitization, endocytosis, and downstream signaling, and GPCR- $\beta$ arr complex formation can be used as a generic readout of GPCR and  $\beta$ arr activation. Although several methods are currently available to monitor GPCR- $\beta$ arr interactions, additional sensors to visualize them may expand the toolbox and complement existing methods. We have previously described antibody fragments (FABs) that recognize activated  $\beta$ arr1 upon its interaction with the vasopressin V2 receptor C-terminal phosphopeptide (V2Rpp). Here, we demonstrate that these FABs efficiently report the formation of a GPCR- $\beta$ arr1 complex for a broad set of chimeric GPCRs harboring the V2R C terminus. We adapted these FABs to an intrabody format by converting them to single-chain variable fragments and used them to monitor the localization and trafficking of  $\beta$ arr1 in live cells. We observed that upon agonist stimulation of cells expressing chimeric GPCRs, these intrabodies first translocate to the cell surface, followed by trafficking into intracellular vesicles. The translocation pattern of intrabodies mirrored that of  $\beta$ arr1, and the intrabodies co-localized with  $\beta$ arr1 at the cell surface and in intracellular vesicles. Interestingly, we discovered that intrabody sensors can also report  $\beta$ arr1 recruitment and trafficking for several unmodified GPCRs. Our characterization of intrabody sensors for  $\beta$ arr1 recruitment and trafficking expands currently available approaches to visualize GPCR- $\beta$ arr1 binding, which may help decipher additional aspects of GPCR signaling and regulation.

G-protein-coupled receptors (GPCRs) recognize a diverse set of ligands and initiate a broad spectrum of downstream signaling responses (1). Upon agonist stimulation, GPCRs couple to three major subfamilies of cellular proteins namely, the heterotrimeric G-proteins, GPCR kinases, and  $\beta$ -arrestins ( $\beta$ arrs) (1). Of these,  $\beta$ arrs are multifunctional adaptor proteins, which play a central role in regulatory and signaling paradigms of

GPCRs (2, 3).  $\beta$ arrs are evenly distributed in the cytoplasm under basal condition, and upon agonist stimulation, they typically translocate to the plasma membrane to interact with activated and phosphorylated receptors (4).

Binding of  $\beta$ arrs to GPCRs at the plasma membrane results in termination of G-protein coupling and desensitization of receptors through a steric hindrance-based mechanism (5). Subsequently,  $\beta$ arrs either dissociate from the receptors and relocalize back in the cytoplasm or traffic into endosomal vesicles in complex with the receptors (2, 4). These two different patterns are referred to as “class A” and “class B,” respectively (4).  $\beta$ arrs also contribute in a number of downstream GPCR signaling pathways such as ERK1/2 MAP kinase activation, although strict G-protein independence of such mechanisms are currently being discussed and debated (6–9).

Considering the multifaceted roles of  $\beta$ arrs, understanding the details of their interaction with GPCRs continues to be a frontier area in GPCR research (10). The interaction of  $\beta$ arrs with GPCRs involves two distinct components (11, 12). One is receptor phosphorylation, primarily in the C terminus but also in the intracellular loops, and the other is the intracellular side of receptor transmembrane bundle, referred to as the receptor core (11, 12). There are several assays that are currently used to measure GPCR- $\beta$ arr interaction, including those based on resonance energy transfer (13–15), enzyme complementation (16), and reporter responses (17, 18). However, developing novel sensors is desirable to expand the currently available toolbox and complement the existing assays.

Previous studies have suggested that receptor phosphorylation is not only sufficient to promote  $\beta$ arr binding, but it can also induce  $\beta$ arr conformations capable of mediating receptor endocytosis and signaling (19–21). These findings raise the possibility that biochemical reagents such as antibodies, which selectively recognize  $\beta$ arr conformation triggered by the interaction of phosphorylated receptor, may serve as sensors for  $\beta$ arr recruitment and trafficking. Here, we develop and characterize intrabody sensors derived from synthetic antibody fragments (FABs) against  $\beta$ arr1 that report the formation of

<sup>†</sup>These authors contributed equally to this work.

\* For correspondence: Arun K. Shukla, arshukla@iitk.ac.in.

## Intrabody sensors for $\beta$ -arrestin 1

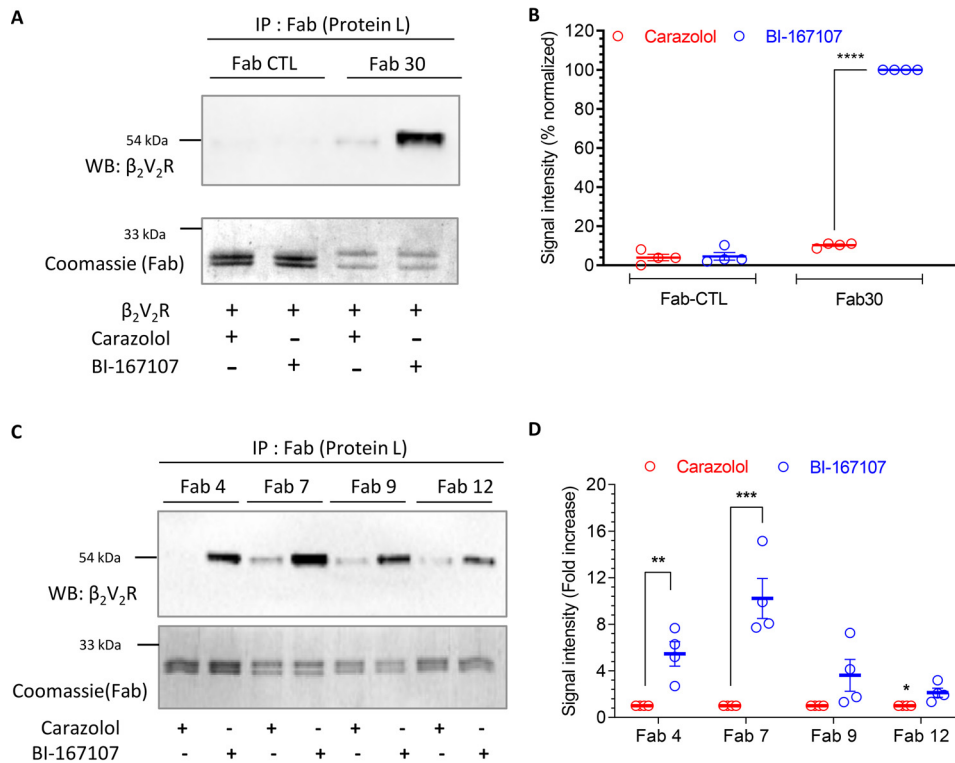


**Figure 1. Synthetic FABs that recognize  $\beta_2V_2R$ - $\beta$ arr1 complex.** *A*, Fab30 selectively recognizes agonist-induced  $\beta_2V_2R$ - $\beta$ arr1 complex as assessed by co-immunoprecipitation. *Sf9* cells expressing FLAG-tagged  $\beta_2V_2R$  and GRK2CAAX were stimulated with either carazolol (1  $\mu$ M) or BI-167107 (100 nM), lysed, and mixed with purified  $\beta$ arr1 and Fab30 (or a control Fab). Subsequently, Fab was immunoprecipitated using protein L-agarose beads, and co-purification of the receptor was visualized by Western blotting (WB) using HRP-coupled anti-FLAG M2 antibody. Fabs were detected by Coomassie staining. *B*, densitometry-based quantification of Western blotting signal in *A* presented as means  $\pm$  S.E. of four independent experiments normalized with respect to maximal response (treated as 100%). *C*, the ability of additional Fabs to recognize agonist-induced  $\beta_2V_2R$ - $\beta$ arr1 complex assessed by co-immunoprecipitation following the protocol mentioned above. *D*, densitometry-based quantification of Western blotting signal in *C* presented as means  $\pm$  S.E. of four independent experiments normalized with respect to carazolol condition (treated as 1). The data in *B* and *D* were analyzed using one-way ANOVA. \*\*\*\*,  $p < 0.0001$ ; \*\*\*,  $p < 0.001$ ; \*\*,  $p < 0.01$ ; \*,  $p < 0.05$ .

GPCR- $\beta$ arr1 complexes and allow us to monitor  $\beta$ arr1 trafficking in cellular context.

## Results

### Synthetic antibody fragments report the formation of $\beta_2V_2R$ - $\beta$ arr1 complex

Agonist-induced receptor phosphorylation is a key determinant for  $\beta$ arr recruitment (11). A phosphopeptide corresponding to the C terminus of the human vasopressin  $V_2$  receptor, referred to as  $V_2Rpp$ , has been used extensively as a surrogate to induce active  $\beta$ arr conformation *in vitro* (22–25). We have previously generated and characterized a set of synthetic FABs that selectively recognize  $V_2Rpp$ -bound  $\beta$ arr1 (26). We have also used one of these FABs, referred to as Fab30, to monitor the interaction of  $\beta$ arr1 with a chimeric  $\beta_2$ -adrenergic receptor harboring  $V_2R$  C terminus (referred to as  $\beta_2V_2R$ ) and  $V_2R$  (25). As the first step toward developing these FABs as potential sensors of GPCR- $\beta$ arr interaction and trafficking, we first confirmed their ability to report the formation of  $\beta_2V_2R$ - $\beta$ arr1 complex *in vitro* (Fig. 1, *A–D*). Here, we used lysates from cells expressing FLAG- $\beta_2V_2R$  mixed with purified  $\beta$ arr1 and FABs, followed by co-immunoprecipitation (co-IP) and detection of the receptor as a readout of complex formation. We observed that Fab30 and the additional FABs selectively pull down  $\beta_2V_2R$  upon agonist stimulation through the formation of receptor- $\beta$

arr1 complex (Fig. 1, *A–D*). A control FAB that does not interact with  $\beta$ arr1 failed to yield any detectable signal in the co-IP experiment (Fig. 1, *A* and *B*).

### Fab30 reports the formation of $\beta$ arr1 complex for multiple chimeric GPCRs

Before proceeding to generate potentially generic intrabody sensors from these FABs, we evaluated their ability to recognize  $\beta$ arr1 complex with other GPCRs. Considering that these FABs were selected against  $V_2Rpp$ -bound  $\beta$ arr1, we reasoned that they should detect  $\beta$ arr1 complex for other chimeric GPCRs harboring the  $V_2R$  C terminus, similar to that in  $\beta_2V_2R$ . We generated six different chimeric GPCRs including the members from different subclasses such as chemokine (CCR2- $V_2R$ ), adrenergic ( $\alpha 2B$ - $V_2R$ ), complement (C5aR1- $V_2R$ ), muscarinic (M5- $V_2R$ ), and dopamine (D2- $V_2R$  and D5- $V_2R$ ) receptors. Some of these receptors, such as M5R,  $\alpha 2BR$ , and D2R, contain large third intracellular loops, whereas others have relatively shorter third intracellular loops. We tested the ability of Fab30, which was most effective among all the FABs, to report the formation of receptor- $\beta$ arr1 complex in co-IP assay for these receptors. As presented in Fig. 2 (*A–F*), we observed that Fab30 efficiently recognized  $\beta$ arr1 for every chimeric GPCR tested here, similar to that of  $\beta_2V_2R$ . This finding allowed us to conceive that these FABs should work as generic intrabody sensors

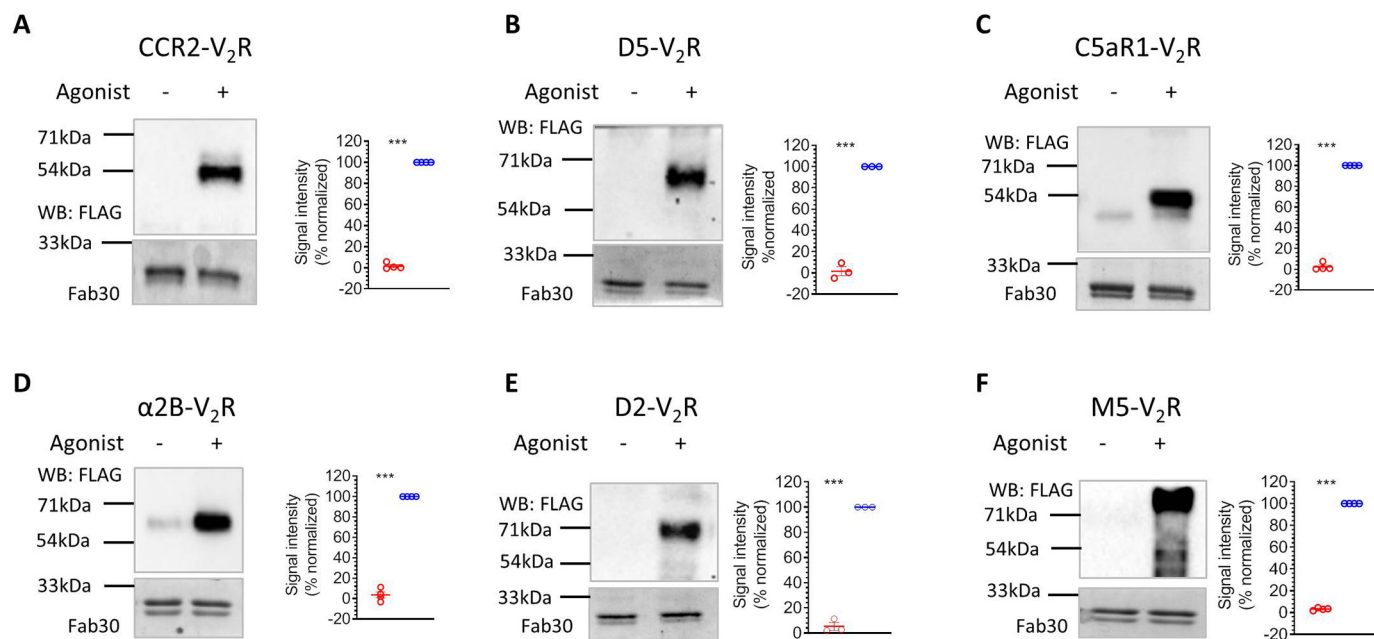


**Figure 2. Fab30 reports agonist-induced interaction of  $\beta$ arr1 with chimeric GPCRs.** A–F, HEK-293 cells expressing N-terminally FLAG-tagged chimeric GPCRs harboring the V<sub>2</sub>R C terminus and  $\beta$ arr1 were stimulated with corresponding agonists (100 nM CCL7, 20  $\mu$ M carbachol, 20  $\mu$ M dopamine, 100 nM C5a, 20  $\mu$ M epinephrine, 20  $\mu$ M dopamine, and 20  $\mu$ M carbachol, respectively), lysed, and mixed with purified Fab30. Subsequently, Fab30 was immunoprecipitated using protein L-agarose beads, and co-purification of the receptor was visualized by Western blotting (WB) using HRP-coupled anti-FLAG M2 antibody. Fabs were detected by Coomassie staining. The graphs in every panel show densitometry-based quantification of Western blotting signal presented as means  $\pm$  S.E. of four independent experiments (three for D<sub>5</sub>V<sub>2</sub>R and D<sub>2</sub>V<sub>2</sub>R) normalized with respect to maximal response (treated as 100%) and analyzed using one-way ANOVA. \*\*\*,  $p < 0.001$ .

of  $\beta$ arr1 interaction and trafficking in cellular context for a broad set of chimeric GPCRs.

### Conversion of FABs into intrabodies and their expression analysis

To develop these FABs into cellular sensors of  $\beta$ arr1 activation and trafficking, it is required to express them in functional form in the cytoplasm as intrabodies. We therefore converted the selected FABs into single-chain variable fragments (ScFvs) by connecting the variable domains of their heavy and light chains through a previously optimized flexible linker (12) and then expressed them in HEK-293 cells as intrabodies, either with a C-terminal HA tag or as YFP fusion (Fig. 3, A–D). We observed robust expression of two of these intrabodies namely intrabody30 (Ib30) and intrabody4 (Ib4) in HEK-293 cells, whereas others displayed relatively weaker expression (Fig. 3B). For YFP-tagged intrabodies, we observed cytoplasmic as well as nuclear localization (Fig. 3C–D). The underlying reason for nuclear localization of the intrabodies is not apparent to us, although a previous study has also reported nuclear localization of an intrabody targeting  $\beta$ <sub>2</sub>-adrenergic receptor (27).

### Ib30 and Ib4 report the interaction of $\beta$ arr1 with $\beta$ <sub>2</sub>V<sub>2</sub>R and trafficking

We next tested whether intrabodies can report the formation of receptor– $\beta$ arr1 complex in a cellular context. We first co-expressed  $\beta$ <sub>2</sub>V<sub>2</sub>R,  $\beta$ arr1, and HA-tagged intrabodies in HEK-293 cells, stimulated the cells with either an agonist

(isoproterenol) or inverse agonist (carazolol), and immunoprecipitated the intrabodies using the HA tag. We observed that both intrabodies, *i.e.* Ib30 and Ib4, recognized the  $\beta$ <sub>2</sub>V<sub>2</sub>R– $\beta$ arr1 complex upon agonist stimulation, although Ib30 was relatively more efficient (Fig. 4, A and B). We also tested the ability of Ib30 to recognize the  $\beta$ <sub>2</sub>V<sub>2</sub>R– $\beta$ arr1 complex formed upon stimulation of the receptor with a set of ligands with varying efficacies. Importantly, we observed that the level of recognition of the  $\beta$ <sub>2</sub>V<sub>2</sub>R– $\beta$ arr1 complex by Ib30 mirrors the efficacy of the ligands (Fig. 4, C and D). This observation underscores the ability of Ib30 to report the formation of pharmacologically relevant receptor– $\beta$ arr1 complex and corroborates its suitability as a reliable sensor of receptor– $\beta$ arr1 interaction.

To probe the utility of intrabodies to monitor  $\beta$ arr1 trafficking upon receptor stimulation, we co-expressed  $\beta$ <sub>2</sub>V<sub>2</sub>R,  $\beta$ arr1–mCherry, and YFP-tagged intrabodies in HEK-293 cells and followed the localization of  $\beta$ arr1 and intrabodies using confocal microscopy after agonist treatment (Fig. 4, E and F). As expected, activation of  $\beta$ <sub>2</sub>V<sub>2</sub>R resulted in a typical class B pattern of  $\beta$ arr1 translocation, and interestingly, the intrabodies followed the localization of  $\beta$ arr1 and displayed robust co-localization (Fig. 4, E and F). We observed that Ib30 and Ib4 were first translocated to the cell surface from the cytoplasm, and upon sustained agonist stimulation, they were localized in the intracellular vesicles. Taken together, these findings demonstrate the usefulness of intrabodies as yet another tool to monitor the formation of the receptor– $\beta$ arr1 complex *in vitro* and  $\beta$ arr1 trafficking in the cellular context.



## Intrabody sensors for $\beta$ -arrestin 1

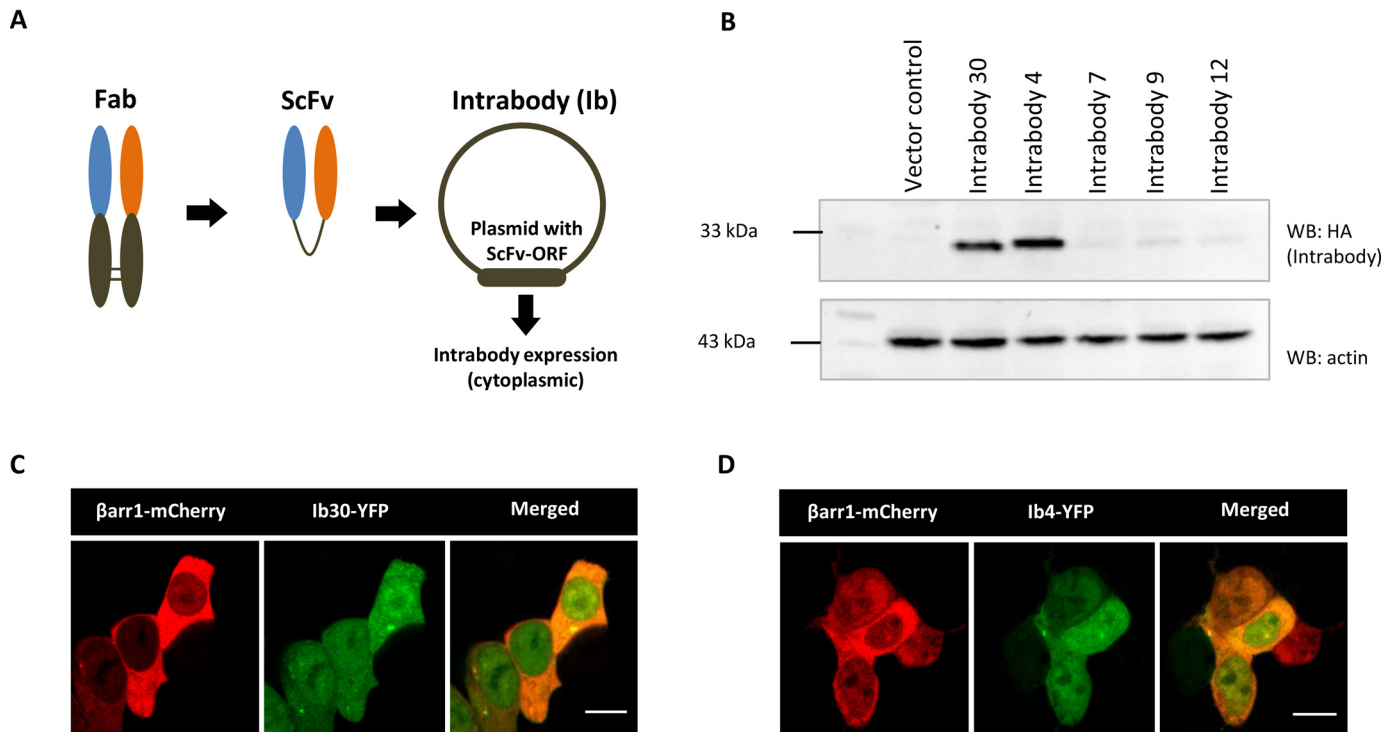


**Figure 3. Conversion of FABS into intrabodies and their expression analysis.** *A*, schematic representation of conversion of FABS into ScFv format for intracellular expression as intrabodies. *B*, expression profile of intrabodies in HEK-293 cells visualized by Western blotting (WB). Lysate prepared from HEK-293 cells expressing the indicated intrabodies with C terminus HA tag were separated on SDS-PAGE followed by visualization using anti-HA antibody. *C* and *D*, intracellular expression of Ib30-YFP/Ib4-YFP and  $\beta$ arr1-mCherry as visualized by confocal microscopy. HEK-293 cells expressing the corresponding plasmids were subjected to live cell imaging, and it revealed localization of Ib30-YFP and Ib4-YFP in both cytoplasm and nucleus. Scale bar, 10  $\mu$ m.

### Intrabodies also report the interaction and trafficking of $\beta$ arr1 upon $V_2R$ stimulation

Because the intrabodies are derived from FABS selected against  $V_2R$ pp-bound  $\beta$ arr1, we anticipated that they should be able to report agonist-induced  $\beta$ arr1 interaction and trafficking for  $V_2R$  as well. Accordingly, we tested the ability of Ib30 and Ib4 to detect the formation of the  $V_2R$ - $\beta$ arr1 complex *in vitro* and report agonist-induced translocation of  $\beta$ arr1 in a cellular context (Fig. 5, *A-E*). We observed a pattern very similar to that of  $\beta_2V_2R$  described above in both the co-immunoprecipitation experiment and confocal microscopy (Fig. 5, *A-E*). That is, Ib30 and Ib4 selectively recognized  $V_2R$ - $\beta$ arr1 complex upon agonist stimulation and followed the localization pattern of  $\beta$ arr1 upon agonist stimulation as reflected by translocation to the cell surface first followed by localization in intracellular vesicles. An additional band was observed on the Western blot in the co-IP experiment, which migrates below the  $V_2R$  band, but its origin is currently not clear to us.

We also measured the ability of Ib30 to recognize endogenous  $\beta$ arr1 upon agonist stimulation of  $V_2R$  and observed a robust interaction in co-immunoprecipitation assay (Fig. 6, *A* and *B*). Furthermore, we evaluated the translocation pattern of Ib30-YFP upon agonist stimulation for  $\beta_2V_2R$  and  $V_2R$  in HEK-293 cells where  $\beta$ arr1 is overexpressed without any modification. As presented in Fig. 6C, Ib30-YFP was robustly localized to intracellular vesicles after agonist stimulation, which is reminiscent of the typical translocation pattern of  $\beta$ arr1 for

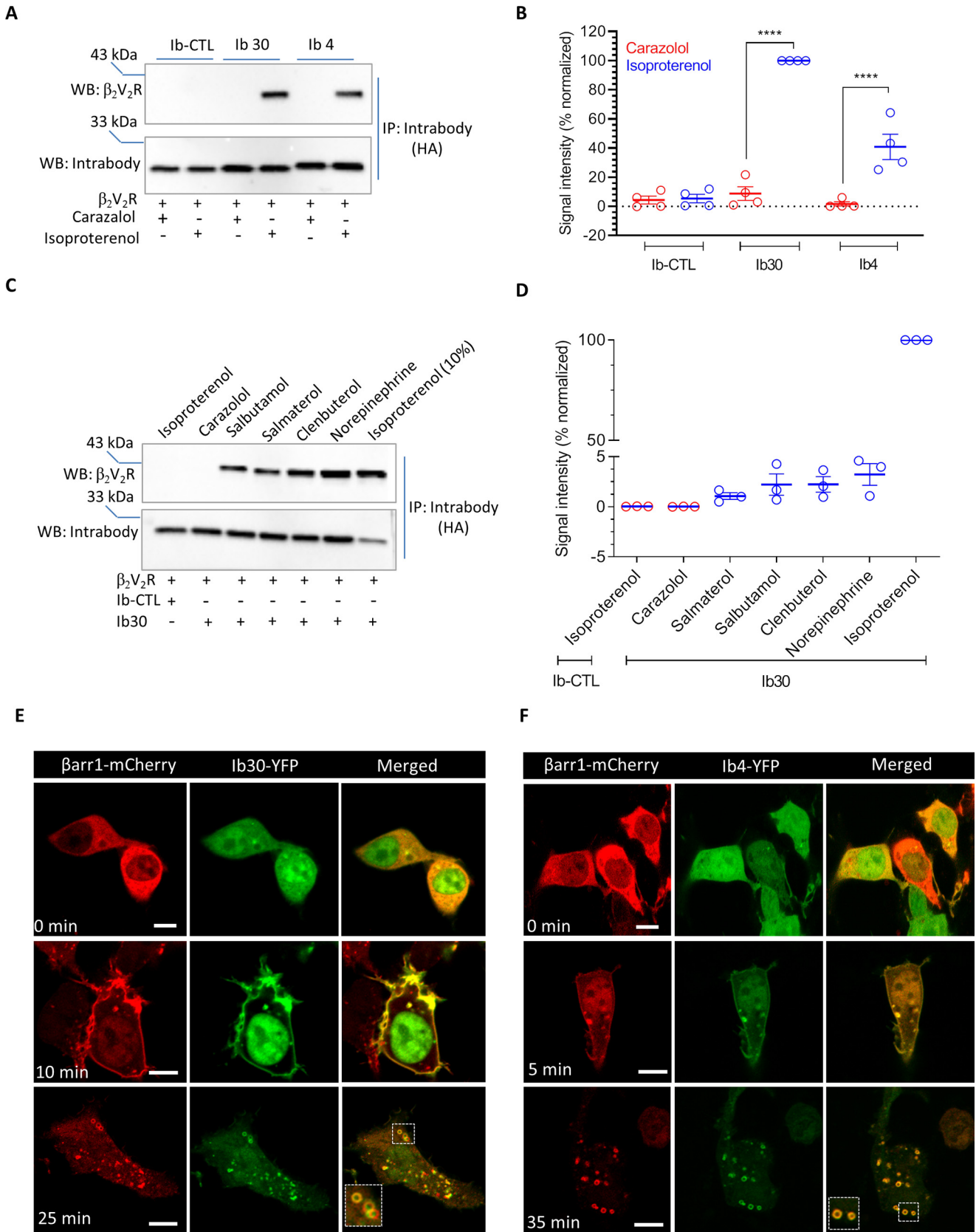
these receptors. These data further strengthen the utility of intrabody sensors described here in monitoring  $\beta$ arr1 recruitment and trafficking.

### Intrabodies do not alter $\beta$ arr recruitment, receptor endocytosis, G-protein coupling, and ERK1/2 phosphorylation

For the intrabodies to be reliable sensors of  $\beta$ arr recruitment and trafficking, it is important that they do not significantly alter  $\beta$ arr recruitment, receptor endocytosis, and G-protein coupling. Therefore, we first measured agonist-induced recruitment of  $\beta$ arr1 to  $V_2R$  in presence of either a control intrabody (Ib-CTL) or Ib30/Ib4 using an intermolecular BRET assay. As presented in Fig. 7A, we did not observe any significant difference in  $\beta$ arr1 recruitment. Next, to probe whether  $V_2R$  is co-localized with Ib30 and  $\beta$ arr1 on intracellular vesicles, we performed three-color confocal imaging on HEK-293 cells expressing FLAG- $V_2R$ ,  $\beta$ arr1-YFP, and Ib30-HA after agonist stimulation (Fig. 7B). Expectedly, we observed a robust co-localization of  $V_2R$ ,  $\beta$ arr1, and Ib30 on intracellular vesicles, suggesting that Ib30 does not alter the normal trafficking pattern of receptor- $\beta$ arr1 complex in a cellular context. This is further corroborated by the pattern of  $V_2R$  co-localization with the early endosomal markers EEA1 and APPL1, which remains unaltered in presence of Ib-CTL versus Ib30 (Fig. 7, *C* and *D*). Furthermore, we also measured  $\beta$ arr1 trafficking to endosomes upon  $V_2R$  activation using an enhanced bystander BRET set-up (15) in presence of either Ib-CTL or Ib4/Ib30. Although we did not observe a significant difference in  $EC_{50}$  values (Fig. 7E),

Ib4/Ib30 appear to stabilize endosomal localization of  $\beta$ arr1 as reflected by  $\Delta$ BRET signal (Fig. 7F). This observation is particularly relevant if the intrabody sensors are used in the context of

receptor recycling where they might slow down receptor recycling to the plasma membrane, and it would be interesting to probe this aspect further in future studies.



## Intrabody sensors for $\beta$ -arrestin 1

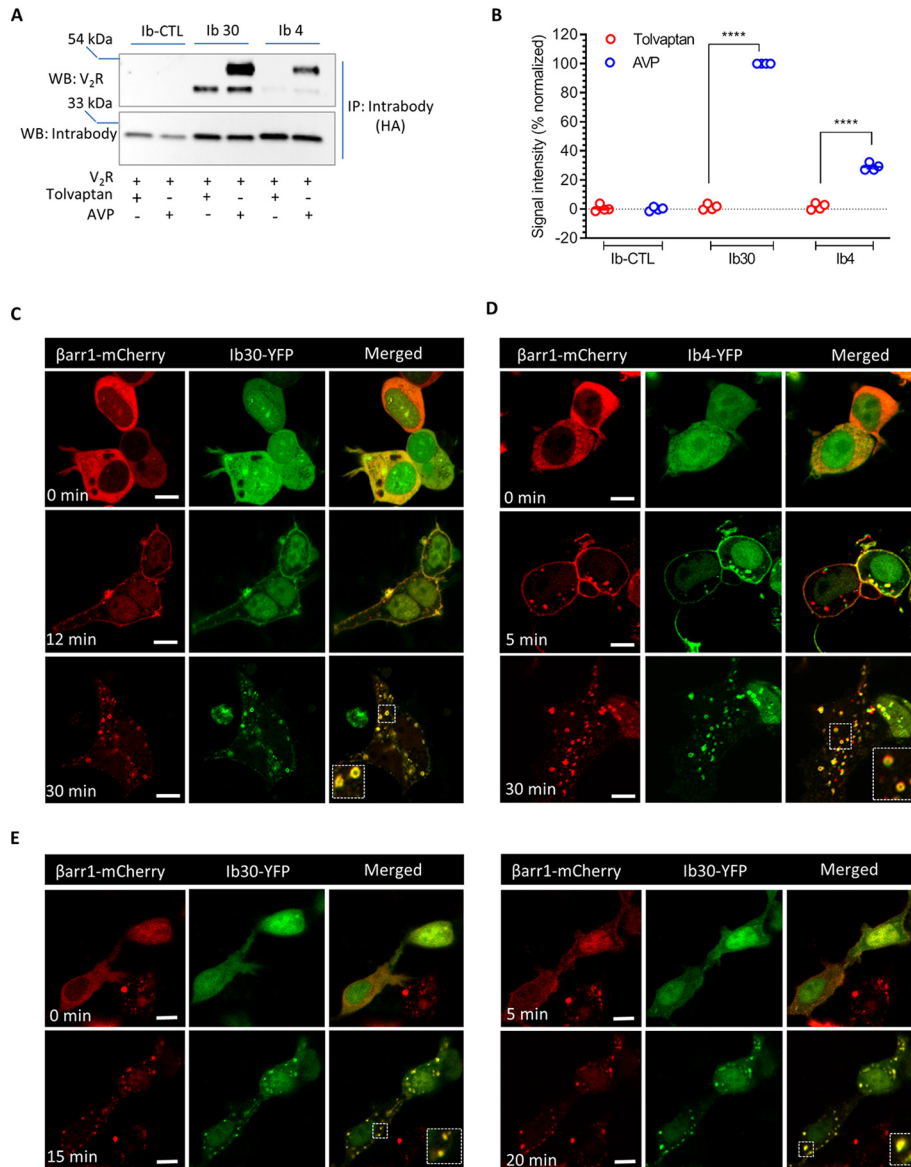


**Figure 5. Intrabodies report the formation of V<sub>2</sub>R- $\beta$ arr1 complex and trafficking of  $\beta$ arr1 upon V<sub>2</sub>R stimulation.** *A*, the ability of intrabodies (Ib30 and Ib4) to recognize V<sub>2</sub>R-bound  $\beta$ arr1 upon agonist stimulation. HEK-293 cells expressing V<sub>2</sub>R,  $\beta$ arr1, and Ib30/Ib4/Ib-CTL were stimulated with either inverse agonist (tolvaptan; 100 nM) or agonist (AVP; 100 nM) followed by co-immunoprecipitation (co-IP) using anti-HA antibody agarose. Subsequently, the proteins were visualized by Western blotting (WB) using anti-FLAG M2 antibody and anti-HA antibody. *B*, densitometry-based quantification of the data in *A* presented as means  $\pm$  S.E. from four independent experiments normalized with maximal response (treated as 100%) and analyzed using one-way ANOVA with Bonferroni post test. \*\*\*\*,  $p < 0.0001$ . *C* and *D*, HEK-293 cells expressing V<sub>2</sub>R,  $\beta$ arr1-mCherry, and YFP-tagged Ib30/Ib4 were stimulated with AVP (100 nM), and the localization of  $\beta$ arr1 and intrabodies was visualized using confocal microscopy at the indicated time points. PCCs were measured to assess the co-localization of  $\beta$ arr1 and Ib30 using JACoP plugin in ImageJ. The following values were obtained: for Ib30,  $0.31 \pm 0.02$  from 16 cells,  $0.81 \pm 0.03$  from 16 cells, and  $0.80 \pm 0.02$  from 20 cells for the upper, middle, and lower panels, respectively, with six independent experiments; and for Ib4,  $0.27 \pm 0.02$  from 20 cells,  $0.74 \pm 0.02$  from 21 cells, and  $0.75 \pm 0.01$  from 47 cells for the upper, middle, and lower panels, respectively, with three independent experiments. *E*, time-lapse confocal imaging of HEK-293 cells expressing V<sub>2</sub>R,  $\beta$ arr1-mCherry, and Ib30-YFP to demonstrate agonist-induced translocation of  $\beta$ arr1 and Ib30 in the same cells over time. A representative image panel from three independent experiments is shown here. Scale bar, 10  $\mu$ m.

**Figure 4. Intrabodies report agonist-induced formation of  $\beta_2$ V<sub>2</sub>R- $\beta$ arr1 complex and trafficking of  $\beta$ arr1 upon  $\beta_2$ V<sub>2</sub>R stimulation.** *A*, the ability of intrabodies (Ib30 and Ib4) to recognize receptor-bound  $\beta$ arr1 upon agonist stimulation. HEK-293 cells expressing  $\beta_2$ V<sub>2</sub>R,  $\beta$ arr1, and Ib30/Ib4/Ib-CTL were stimulated with either inverse agonist (carazolol; 1  $\mu$ M) or agonist (isoproterenol; 10  $\mu$ M) followed by co-IP using anti-HA antibody agarose. Subsequently, the proteins were visualized by Western blotting (WB) using anti-FLAG M2 antibody and anti-HA antibody. *B*, densitometry-based quantification of the data in *A* presented as means  $\pm$  S.E. from four independent experiments normalized with maximal response (treated as 100%) and analyzed using one-way ANOVA. \*\*\*\*,  $p < 0.0001$ . *C*, the ability of Ib30 to report the formation of receptor- $\beta$ arr1 complex mirrors ligand efficacy. HEK-293 cells expressing  $\beta_2$ V<sub>2</sub>R,  $\beta$ arr1, and Ib30 (or Ib-CTL) were stimulated with saturating concentrations of the indicated ligands followed by co-immunoprecipitation and Western blotting as mentioned above. For isoproterenol condition, which yielded maximal signal, only 10% of the total elution from the co-IP is loaded on the gel to avoid signal saturation. *D*, densitometry-based quantification of the data in *C* presented as means  $\pm$  S.E. from three independent experiments normalized with respect to maximal response (treated as 100%). *E* and *F*, HEK-293 cells expressing  $\beta_2$ V<sub>2</sub>R,  $\beta$ arr1-mCherry, and YFP-tagged Ib30/Ib4 were stimulated with isoproterenol (10  $\mu$ M), and the localization of  $\beta$ arr1 and intrabodies was visualized using confocal microscopy at the indicated time points. PCCs were measured to assess the co-localization of  $\beta$ arr1 and Ib30 using JACoP plugin in ImageJ. The following values were obtained: for Ib30,  $0.28 \pm 0.03$  from 13 cells,  $0.74 \pm 0.05$  from 9 cells, and  $0.76 \pm 0.02$  from 29 cells for the upper, middle, and lower panels, respectively, with four independent experiments; and for Ib4,  $0.24 \pm 0.03$  from 10 cells,  $0.84 \pm 0.03$  from 9 cells, and  $0.94 \pm 0.01$  from 20 cells for the upper, middle, and lower panels, respectively, with three independent experiments. Scale bar, is 10  $\mu$ m.

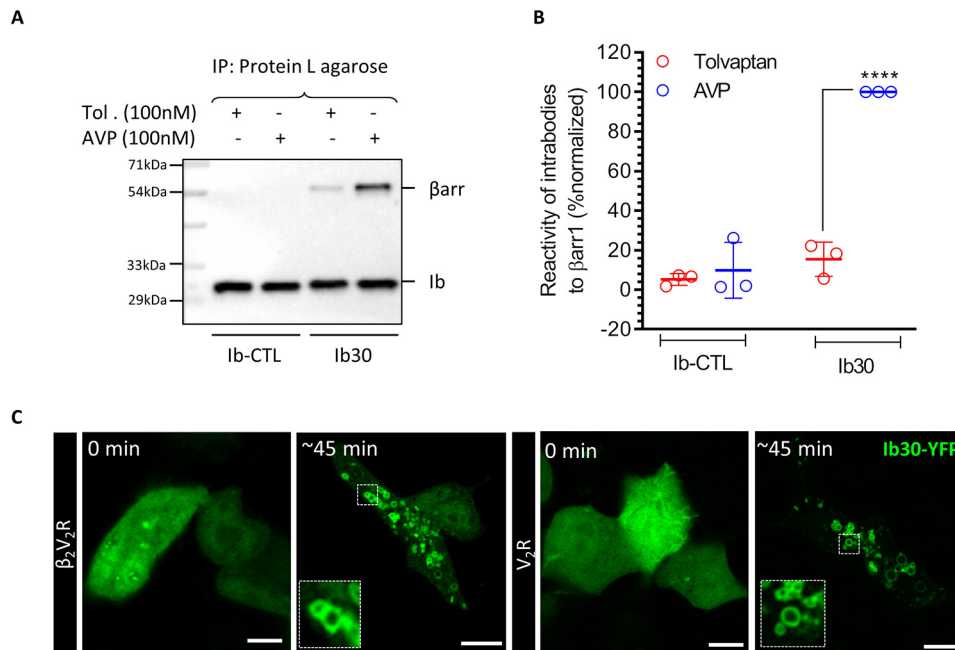


**Figure 6. Intrabody30 recognizes receptor-bound endogenous  $\beta$ arr1 and reports the trafficking of native  $\beta$ arr1.** *A*, the ability of intrabody Ib30 to recognize  $V_2R$ -bound endogenous  $\beta$ arr1 upon agonist stimulation. HEK-293 cells expressing  $V_2R$  and HA-tagged Ib30/Ib-CTL were stimulated with either inverse agonist (tolvaptan; 100 nM) or agonist (AVP; 100 nM) followed by co-IP using anti-HA antibody agarose. Subsequently, the proteins were visualized by Western blotting using anti- $\beta$ arr and anti-HA antibodies. *B*, densitometry-based quantification of the data in *A* presented as means  $\pm$  S.E. from three independent experiments normalized with maximal response (treated as 100%) and analyzed using one-way ANOVA. \*\*\*\*,  $p < 0.0001$ . *C*, HEK-293 cells expressing  $\beta_2V_2R/V_2R$  and Ib30-YFP were stimulated with isoproterenol (10  $\mu$ M) and AVP (100 nM), respectively, and the localization of Ib30-YFP was visualized using confocal microscopy. Representative images from three independent experiments are shown here. Scale bar, 10  $\mu$ m.

We next measured the effect of intrabodies on  $G\alpha_s$  coupling to the  $V_2R$  using cAMP response as a readout. Once again, we did not observe any significant difference in cAMP dose response or time kinetics for Ib-CTL *versus* Ib30/Ib4 conditions (Fig. 8, *A* and *B*). Finally, we also evaluated the effect of intrabodies on agonist-induced ERK1/2 MAP kinase activation, a prototypical readout of  $V_2R$  signaling, and did not detect a significant alteration by the intrabodies (Fig. 8, *C* and *D*). Taken together, these data establish that intrabodies do not have a major effect on transducer coupling and receptor endocytosis, making them suitable sensors to record  $\beta$ arr1 interaction and trafficking for GPCRs.

#### **Ib30 as a generic sensor of agonist-induced $\beta$ arr1 trafficking for multiple chimeric GPCRs**

Taking lead from the ability of Fab30 to recognize  $\beta$ arr1 complex with several chimeric GPCRs as presented in Fig. 2, we next evaluated Ib30 as a sensor to report  $\beta$ arr1 trafficking for these chimeric GPCRs in cellular context. Similar to previous experiments, we co-expressed the chimeric receptors with  $\beta$ arr1-mCherry and Ib30-YFP in HEK-293 cells and followed the localization of  $\beta$ arr1 and intrabodies using confocal microscopy after agonist treatment (Fig. 9, *A-F*). We observed that similar to  $\beta_2V_2R$ , Ib30 followed  $\beta$ arr1 translocation pattern by first localizing to the cell surface followed by trafficking into intracellular vesicles for all of these chimeric receptors (Fig. 9, *A-F*). It is worth noting here that the receptors used in Fig. 9 (*A-C*) contain most of the phosphorylation sites in their C terminus, whereas their third intracellular loops are relatively small. On the other hand, receptors included in Fig. 9 (*D-F*),

harbor a larger third intracellular loop, which also contains most of the potential phosphorylation sites, and their C terminus is relatively smaller. Therefore, the data presented in Fig. 9 not only demonstrate the generality of Ib30 as a sensor to monitor agonist-induced  $\beta$ arr1 recruitment and trafficking for chimeric GPCRs but also its versatility for receptors differing in terms of their C terminus and intracellular loops.

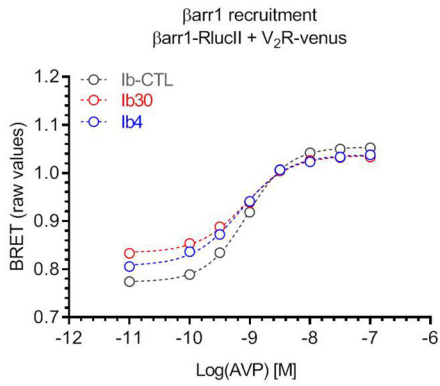
#### **Ib30 sensor suggests conformational diversity in GPCR- $\beta$ arr1 complexes**

Finally, we evaluated the ability of the Ib30 sensor to report the trafficking of  $\beta$ arr1 for a set of GPCRs without the fusion of  $V_2R$ -tail. We observed that Ib30-YFP followed agonist-induced translocation pattern of  $\beta$ arr1 for several different receptors including the complement C5a receptor 1 (C5aR1), the neurotensin receptor 1 (NTSR1), the muscarinic acetylcholine receptor subtype 2 (M2R), and the atypical chemokine receptor subtype 2 (ACKR2) (Fig. 10, *A-D*). We also validated the ability of Ib30 to recognize receptor-bound  $\beta$ arr1 for C5aR1 and ACKR2 by co-immunoprecipitation experiment (Fig. 10, *E* and *F*). These findings suggest that Ib30 can act as a sensor for monitoring agonist-induced  $\beta$ arr1 translocation for at least some GPCRs with their native C terminus as well. Interestingly, however, we observed that Ib30 did not robustly follow  $\beta$ arr1 translocation for the bradykinin subtype 2 receptor ( $B_2R$ ) upon agonist stimulation (Fig. 10*G*), although there was clear translocation of  $\beta$ arr1, first to the plasma membrane and then in intracellular vesicles. Taken together, these data potentially hint at conformational differences in GPCR- $\beta$ arr1 complexes, even if the overall recruitment patterns are apparently similar. Future studies

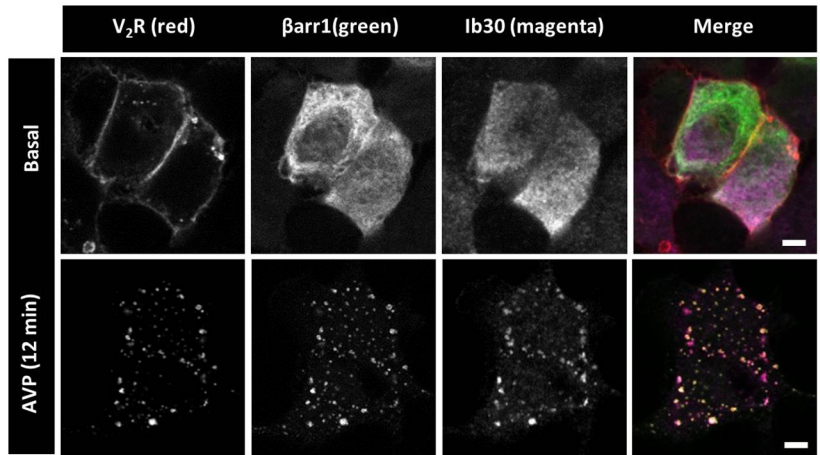


# Intrabody sensors for $\beta$ -arrestin 1

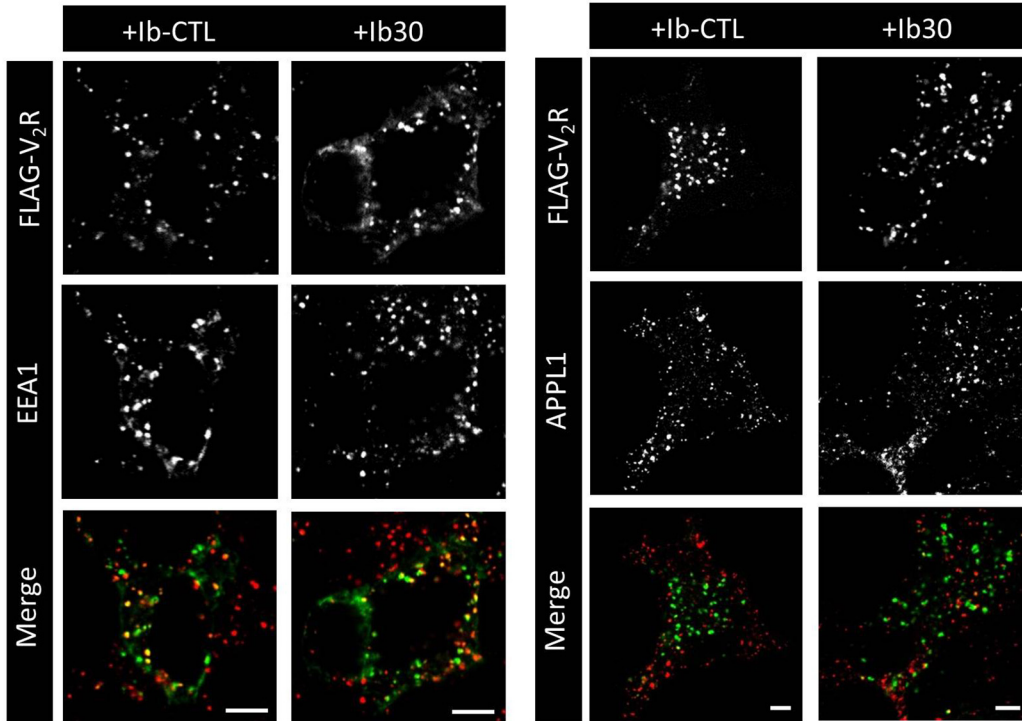
**A**



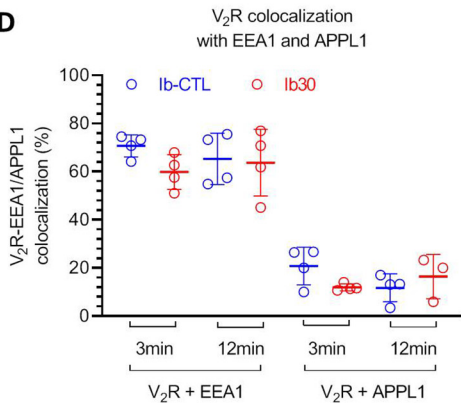
**B**



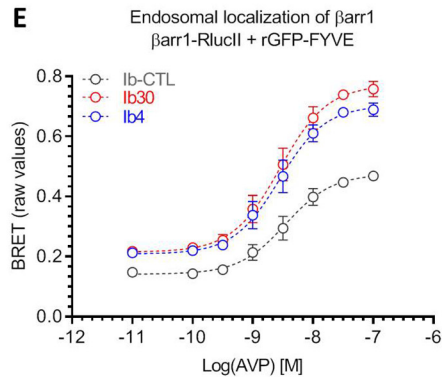
**C**



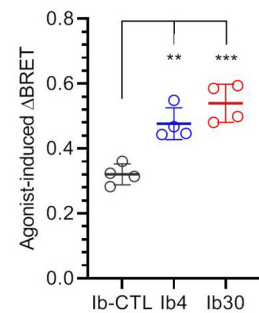
**D**



**E**



**F**



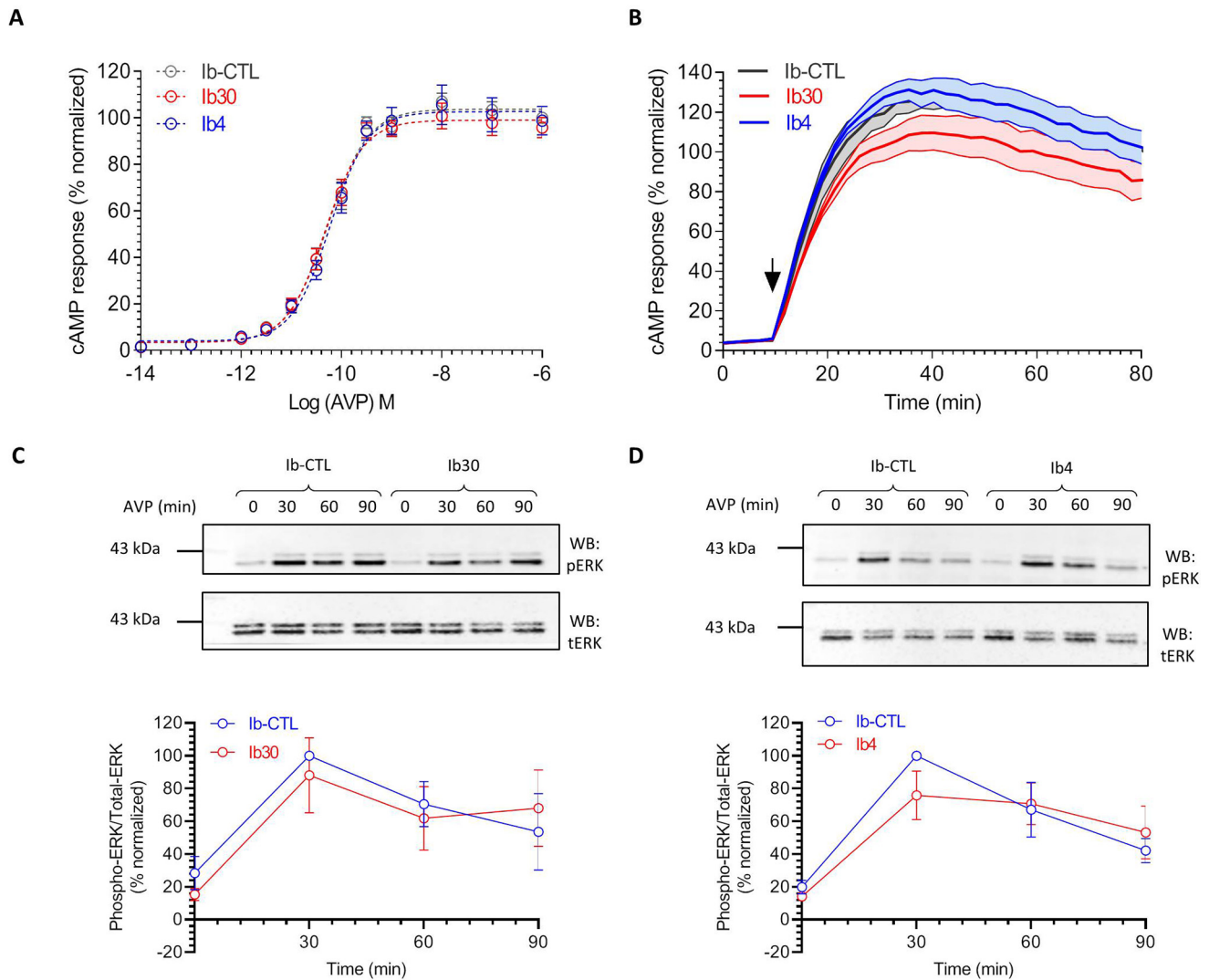


**Figure 8. Effect of intrabodies on G-protein coupling and ERK1/2 phosphorylation.** *A*, Ib30 does not significantly alter  $G_{\alpha_s}$  coupling of  $V_2R$  as reflected by cAMP response. HEK-293 cells expressing  $V_2R$ , the indicated intrabodies, and a luciferase-based cAMP biosensor (F22) were stimulated with varying doses of AVP, and the levels of cAMP were measured in terms of bioluminescence using a microplate reader. The data are normalized with respect to the maximal response obtained in presence of Ib-CTL (treated as 100%), and the graph represents means  $\pm$  S.E. of three independent experiments, each performed in duplicate. *B*, time course of agonist-induced cAMP response in HEK-293 cells expressing  $V_2R$  and the indicated intrabodies. The data are derived from the experiments described in *A* at an AVP concentration of 100 nM. *C* and *D*, intrabodies do not significantly alter agonist-induced ERK1/2 MAP kinase phosphorylation. HEK-293 cells expressing  $V_2R$  and the indicated intrabodies were stimulated with AVP (100 nM) for the indicated time points followed by detection of ERK1/2 phosphorylation using Western blotting (WB). Representative images from four independent experiments are shown here, and densitometry-based quantification of data, normalized with Ib-CTL, with the 30-min condition treated as 100%, is presented in the lower panels.

**Figure 7. Effect of intrabodies on  $\beta$ arr1 recruitment,  $V_2R$  endocytosis, and endosomal localization of  $\beta$ arr1.** *A*, intrabodies do not significantly alter agonist-induced  $\beta$ arr1 recruitment to  $V_2R$  as assessed in intermolecular BRET assay. HEK-293 cells expressing  $V_2R$ -venus,  $\beta$ arr1-RlucII, and the indicated intrabodies were stimulated with varying doses of AVP, and the levels of BRET signal were recorded using a plate reader. The data represent means  $\pm$  S.E.M. from three independent experiments, each performed in triplicate. *B*, Ib30 co-localizes with internalized  $V_2R$  and  $\beta$ arr1 upon agonist stimulation as visualized using confocal microscopy of HEK-293 cells expressing FLAG- $V_2R$ ,  $\beta$ arr1-YFP, and Ib30-HA. The merged image shows co-localization of all three protein upon receptor internalization. The cells were "fed" anti-FLAG M2 antibody prior to agonist stimulation (AVP 100 nM, 12 min) and were subsequently fixed, permeabilized, treated with HA antibody, and imaged (PCC of  $V_2R$  and  $\beta$ arr1 in unstimulated cells = 0.38  $\pm$  0.03 and in stimulated cells = 0.88  $\pm$  0.03, Ib30 and  $V_2R$  in unstimulated cells = 0.29  $\pm$  0.04 and in stimulated cells = 0.83  $\pm$  0.01, and  $\beta$ arr1 with Ib30 in unstimulated cells = 0.43  $\pm$  0.08 and in stimulated cells = 0.63  $\pm$  0.04, no. of cells = 3). A representative image of  $n = 3$  cells/condition is shown here. Scale bar, 5  $\mu$ m. *C*, Ib30 does not significantly alter agonist-induced internalization of  $V_2R$  as assessed by confocal microscopy. Comparative analysis of  $V_2R$  co-localization with two early endosomal markers, EEA1 and APPL1, upon agonist stimulation was performed in the presence of either Ib-CTL or Ib30. Cells expressing FLAG- $V_2R$  and Ib30-HA were treated with anti-FLAG antibody prior to agonist stimulation (AVP, 100 nM, 3–12 min) followed by fixation, permeabilization, and staining for endosomal markers APPL1 or EEA1 (Pearson's coefficient of  $V_2R$  and EEA1 in Ib-CTL cells = 0.70  $\pm$  0.01 and in Ib30 cells = 0.42  $\pm$  0.01, no. of cells = 4, and Pearson's coefficient of  $V_2R$  and APPL1 in Ib-CTL cells = 0.69  $\pm$  0.07 and in Ib30 cells = 0.30  $\pm$  0.07, no. of cells = 4). *D*, co-localization was also measured by manual counting of punctae in confocal images, and quantified data representing means  $\pm$  S.E. from four different cells per condition are presented. *E*, an intermolecular BRET assay to measure the effect of intrabodies on the endosomal localization of  $\beta$ arr1 upon agonist stimulation. HEK-293 cells expressing  $V_2R$ ,  $\beta$ arr1-RlucII, rGFP-FYVE, and the indicated intrabodies were stimulated with varying doses of AVP, and the levels of BRET signal were recorded using a plate reader. The data represent means  $\pm$  S.E.M. from four independent experiments, each performed in triplicate. *F*, agonist-induced change in BRET signal (*i.e.* the difference in BRET signal between the highest and the lowest AVP doses) as measured in panel E is presented as  $\Delta$ BRET and analyzed using one-way ANOVA. \*\*,  $p < 0.01$ ; \*\*\*,  $p < 0.001$ .

## Intrabody sensors for $\beta$ -arrestin 1

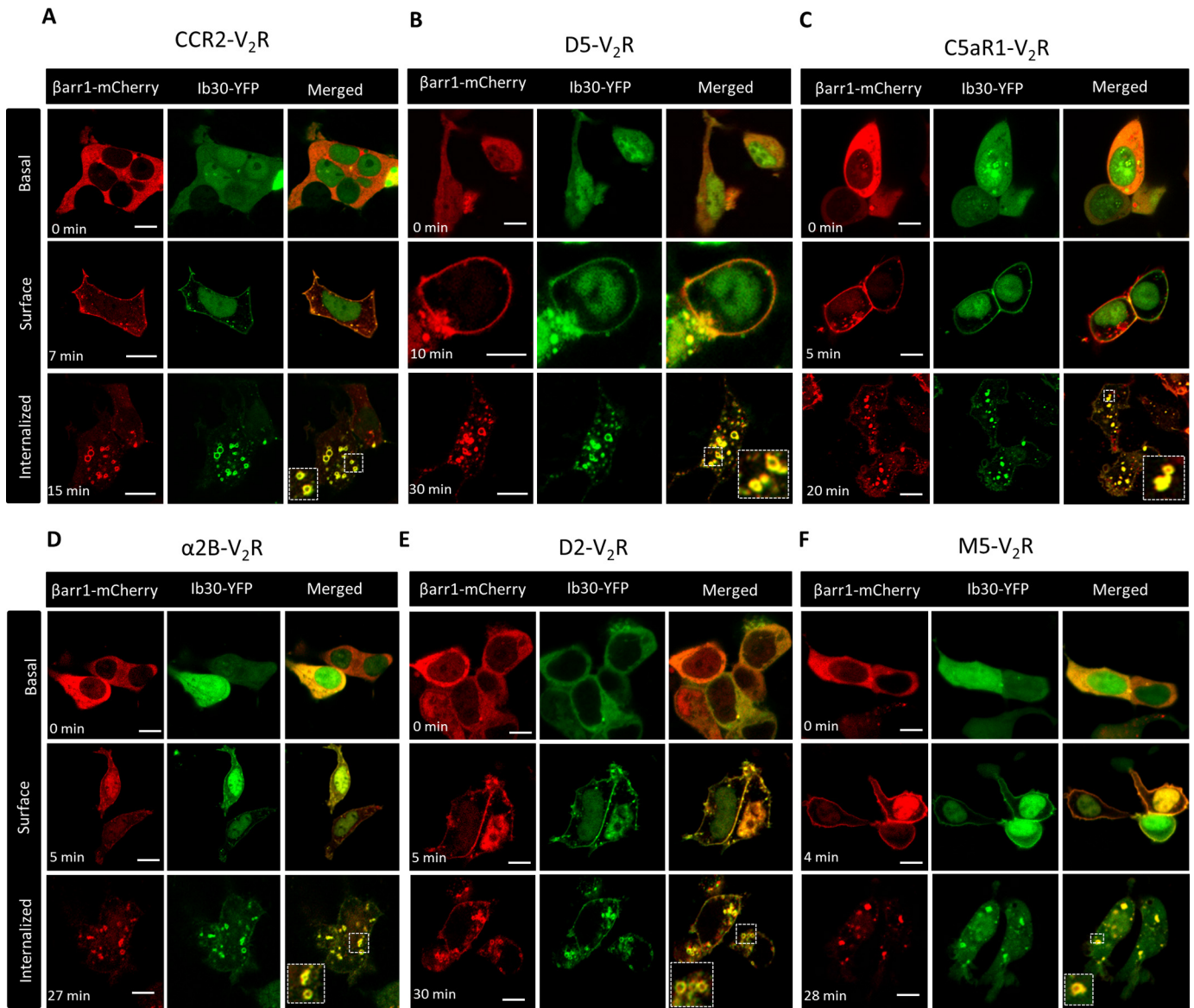


**Figure 9. Ib30 reports agonist-induced trafficking of  $\beta$ arr1 for chimeric GPCRs.** A–F, HEK-293 cells expressing the indicated chimeric GPCRs with V<sub>2</sub>R C terminus,  $\beta$ arr1–mCherry, and Ib30–YFP were stimulated with saturating concentration of respective agonists (100 nM CCL7, 20  $\mu$ M dopamine, and 100 nM C5a, 20  $\mu$ M epinephrine, 20  $\mu$ M dopamine, and 20  $\mu$ M carbachol, respectively), and the localization of  $\beta$ arr1 and Ib30 was visualized using confocal microscopy at the indicated time points. Scale bar, 10  $\mu$ m. PCCs were measured to assess the co-localization of  $\beta$ arr1 and Ib30 using JACoP plugin in ImageJ, and the values for the upper, middle, and lower panels, respectively, are presented here. The following values were obtained: for CCR2V<sub>2</sub>R, 0.21  $\pm$  0.02 from 17 cells, 0.84  $\pm$  0.06 from 5 cells, and 0.83  $\pm$  0.02 from 26 cells, with four independent experiments; for D5V<sub>2</sub>R, 0.36  $\pm$  0.04 from 9 cells, 0.87  $\pm$  0.04 from 6 cells, and 0.82  $\pm$  0.03 from 30 cells, with three independent experiments; for C5aR1V<sub>2</sub>R, 0.31  $\pm$  0.03 from 34 cells, 0.87  $\pm$  0.01 from 40 cells, and 0.85  $\pm$  0.01 from 53 cells with four independent experiments; for  $\alpha$ 2BV<sub>2</sub>R, 0.30  $\pm$  0.04 from 7 cells, 0.90  $\pm$  0.02 from 8 cells, and 0.91  $\pm$  0.02 from 11 cells with four independent experiments; for D2V<sub>2</sub>R, 0.27  $\pm$  0.04 from 18 cells, 0.88  $\pm$  0.02 from 11 cells, and 0.83  $\pm$  0.03 from 13 cells with three independent experiments; and for M5V<sub>2</sub>R, 0.27  $\pm$  0.02 from 15 cells, 0.79  $\pm$  0.04 from 22 cells, and 0.82  $\pm$  0.05 from 9 cells with four independent experiments. Scale bar, 10  $\mu$ m.

focused on measuring conformational differences in different GPCR– $\beta$ arr complexes may provide additional insights and possibly link the conformational diversity to functional outcomes.

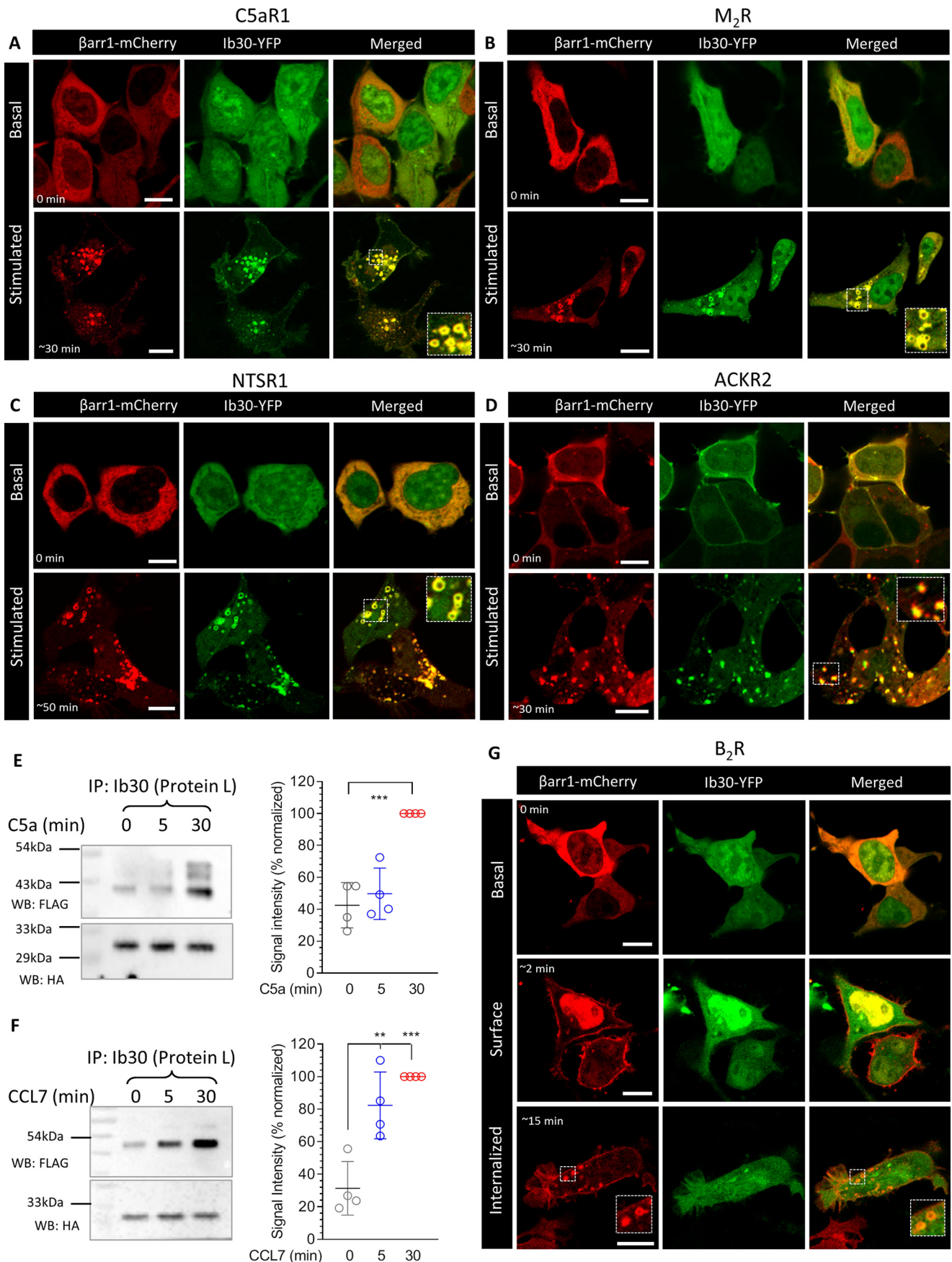
### Discussion

Monitoring  $\beta$ arr interaction and subsequent trafficking has been used extensively to study the activation and regulatory framework of GPCRs. A number of approaches are commonly utilized for this including direct fusion of fluorescent proteins to  $\beta$ arrs (4), resonance energy transfer (FRET/BRET)–based

assays (14, 28), enzyme complementation methods (16), and reporter assays (17, 18). Each of these methods necessitates a significant engineering and modification of the receptor, the  $\beta$ arr, or both. Intrabody sensors described here recognize receptor-bound  $\beta$ arr1 and report its trafficking in cellular context without the need for any modification of  $\beta$ arr1.

Although we observe that the intrabody sensors are capable of recognizing  $\beta$ arr1 for several GPCRs without the modification of their C termini, a potential drawback is that they are not likely to be universal for every GPCR as reflected for B<sub>2</sub>R in Fig. 10G. On the other hand, these intrabody sensors are able to





## Intrabody sensors for $\beta$ -arrestin 1

recognize  $\beta$ arr1 more generally in the context of chimeric GPCRs harboring the  $V_2R$  C terminus. It is conceivable that a similar strategy can be employed for other GPCRs as well by using, for example, phosphopeptides derived from the corresponding receptors. It is also worth noting here that many of the  $\beta$ arr assays such as PRESTO-TANGO also utilize chimeric GPCRs with  $V_2R$  C terminus ( $V_2R$  tail) (18). Engineering  $V_2R$  tail typically imparts a class B pattern on GPCRs and thereby makes the detection of  $\beta$ arr1 interaction more robust compared with the unmodified receptors (29). It is also important to note that of five different FABs tested here, only two expressed efficiently as intrabodies in the cytoplasm. Therefore, starting with a larger number of FABs may be desirable to obtain more functional intrabodies in future endeavors.

Considering that YFP fusion does not alter the ability of intrabodies to interact with  $\beta$ arr1 and follow their translocation, it is also conceivable that they can be adapted in resonance energy transfer assays, or even in NanoBit format, for quantitative measurements of receptor– $\beta$ arr1 interaction. Such strategies may yield even more sensitive versions of these intrabody sensors compared with approaches utilized here. In addition, although the intrabody sensors developed here are specific to  $\beta$ arr1 (25), it is plausible to design and develop similar intrabodies for  $\beta$ arr2 as well. Such an effort may help uncover novel insights into the functional divergence of the two  $\beta$ arr isoforms (30). Another interesting aspect of GPCR– $\beta$ arr1 interaction is the ability of differential receptor phosphorylation patterns to induce distinct functional conformations in  $\beta$ arrs (31, 32). For several GPCRs, different phosphorylation patterns arising in ligand-specific, cell type-specific, and kinase-specific manners have been mapped and correlated with  $\beta$ arr mediated functional outcomes (33–35). Thus, it is tantalizing to hypothesize that intrabodies designed against different phosphopeptides derived from a given receptor may illuminate interesting attributes of receptor signaling and regulation in future. In conclusion, our study expands the currently available toolbox to monitor GPCR– $\beta$ arr interaction and trafficking, and the intrabody sensors described here should facilitate drawing novel insights into GPCR signaling and regulatory paradigms.

## Experimental procedures

### General reagents, plasmids, and cell culture

HEK-293 cells (ATCC) were maintained in Dulbecco's modified Eagle's medium containing 10% FBS and penicillin/streptomycin (100 units/ml) at 37 °C in 5% CO<sub>2</sub>. Transient transfection

of plasmids was performed using PEI, and the cells were typically assayed 48 h post-transfection. The plasmids encoding FLAG– $\beta_2V_2R$ , FLAG– $V_2R$ , Ib–CTL–HA, Ib4–HA, Ib30–HA,  $\beta$ arr1–mCherry have been described previously (25). YFP-tagged intrabodies were generated by subcloning their coding region in pCMV6–AC–YFP vector. The chimeric GPCRs were generated by grafting the  $V_2R$ -tail sequence at residues 324 in CCR2, 443 in  $\alpha$ 2BR, 443 in D2R, 379 in D5R, 514 in M5R, and 326 in C5aR1. All constructs were verified by DNA sequencing. The antibodies were purchased from Sigma (HRP-coupled mouse anti-FLAG M2), Cell Signaling Technology ( $\beta$ arrs), Santa Cruz Biotechnology (rabbit anti-HA), and Thermo Fisher (goat anti-rabbit Alexa Fluor 647 and goat anti-mouse Alexa Fluor 555). Other general chemicals were purchased from Sigma, APEX BIO, and local suppliers. Recombinant human CCL7 was purified following a previously published protocol (36).

### Co-immunoprecipitation assay

To probe the reactivity of FABs toward  $\beta_2V_2R$  (Fig. 1), S9 cells expressing FLAG-tagged receptor were lysed and incubated with purified  $\beta$ arr1 and FABs. For the co-IP data presented in Fig. 2, the plasmids encoding FLAG-tagged receptor and  $\beta$ arr1 were transfected in HEK-293 cells. 48 h post-transfection, the cells were serum-starved for 4–6 h, stimulated with agonist, lysed by Dounce homogenizer, and incubated with FAB30 for 1 h at room temperature. Subsequently, the receptor– $\beta$ arr1–FAB complex were solubilized with 1% MNG for 1 h and centrifuged to collect the clarified solubilized complex, and 20  $\mu$ l of pre-equilibrated (in 20 mM HEPES, 150 mM NaCl, pH 7.4 buffer) Protein L beads (GE Healthcare) were added. After additional 1 h of incubation, the beads were washed three times with wash buffer (20 mM HEPES, 150 mM NaCl, pH 7.4, 0.01% MNG) and eluted with 2 $\times$  SDS loading buffer. Eluted samples were run on 12% SDS-PAGE, and the receptors were detected using HRP-coupled anti-FLAG M2 antibody, whereas the FABs were visualized using Coomassie staining.

To assess the ability of intrabodies to report the formation of receptor– $\beta$ arr1 complex (Figs. 4 and 6, A and B), HEK-293 cells expressing the FLAG-tagged receptor,  $\beta$ arr1, and HA-tagged intrabodies were stimulated with saturating concentration of indicated ligands for 30 min at 37 °C. Afterward, the cells were lysed in Nonidet P-40 lysis buffer (50 mM Tris, 150 mM NaCl, 1 $\times$  PhosStop, 1 $\times$  Protease inhibitor, 1% Nonidet P-40) followed by incubation with 20  $\mu$ l of pre-equilibrated HA beads

**Figure 10. Ib30 reports agonist-induced trafficking of  $\beta$ arr1 for several unmodified GPCRs.** A–D, HEK-293 cells expressing the indicated receptor,  $\beta$ arr1–mCherry and Ib30–YFP were stimulated with saturating concentration of respective agonists (100 nM C5a, 20  $\mu$ M carbachol, 100 nM NTS1, and 100 nM CCL7, respectively), and the localization of  $\beta$ arr1 and Ib30 was visualized using confocal microscopy at the indicated time points. PCCs were measured to assess the co-localization of  $\beta$ arr1 and Ib30 using JACoP plugin in ImageJ, and the values for the unstimulated and stimulated conditions, respectively, are presented here. The following values were obtained: for C5aR1,  $0.27 \pm 0.03$  from 20 cells and  $0.75 \pm 0.03$  from 25 cells with five independent experiments; for M<sub>2</sub>R,  $0.30 \pm 0.04$  from 8 cells and  $0.85 \pm 0.02$  from 25 cells with four independent experiments; for NTSR1,  $0.24 \pm 0.04$  from 15 cells and  $0.87 \pm 0.01$  from 16 cells with three independent experiments; and for ACKR2,  $0.88 \pm 0.02$  from 9 cells and  $0.81 \pm 0.01$  from 29 cells with three independent experiments. Scale bar, 10  $\mu$ m. For ACKR2, we observed significant membrane localization of  $\beta$ arr1 and Ib30, even before agonist treatment, which results into higher PCC values for unstimulated condition. E and F, HEK-293 cells expressing the C5aR1 and ACKR2, respectively, together with  $\beta$ arr1 and Ib30 were stimulated with either respective agonists (100 nM) for the indicated time points followed by co-IP using protein L–agarose beads. Subsequently, the proteins were visualized by Western blotting (WB) using anti-FLAG M2 antibody and anti-HA antibody. The right panels show densitometry-based quantification of four independent experiments normalized with signal at 30 min (treated as 100%) and analyzed using one-way ANOVA. \*\*,  $p < 0.01$ ; \*\*\*,  $p < 0.001$ . G, Ib30 does not follow agonist-induced translocation of  $\beta$ arr1 for the B<sub>2</sub>R as assessed by confocal microscopy on HEK-293 cells expressing B<sub>2</sub>R,  $\beta$ arr1–mCherry, and Ib30–YFP and stimulated with 100 nM bradykinin. The PCCs in the upper, middle, and lower panels were  $0.33 \pm 0.03$  from 15 cells,  $0.34 \pm 0.03$  from 20 cells, and  $0.34 \pm 0.04$  from 16 cells, respectively, based on five independent experiments. Scale bar, 10  $\mu$ m.



(Sigma, A-2095) for 2 h at 4 °C. The beads were washed three times with wash buffer (20 mM HEPES, 150 mM NaCl, pH 7.4), eluted with 2× SDS loading buffer, and proteins were visualized by Western blotting (HRP-coupled anti-FLAG M2 antibody at 1:2000 dilution and anti-HA antibody, sc-805 from Santa Cruz Biotechnology at 1:5000 dilution).

### Confocal microscopy

To monitor the translocation of  $\beta$ arr1 and intrabodies by confocal microscopy (Figs. 3, C and D; 4, E and F; 5, C–E; 6C; 9, A–F; and 10, A–D and G), HEK-293 cells were transfected with plasmids encoding the indicated receptor,  $\beta$ arr1–mCherry, and YFP-tagged intrabodies. 24 h postinfection, the cells were seeded onto confocal dishes (GenetiX; catalog no. 100350) pretreated with 0.01% poly-D-lysine (Sigma). After another 24 h, the cells were serum-starved for 4–6 h prior to stimulation with saturating concentration of indicated agonists. For live cell confocal imaging, we used Zeiss LSM 710 NLO confocal microscope, and samples were housed on a motorized XY stage with a CO<sub>2</sub> enclosure and a temperature-controlled platform equipped with 32× array GaAsP descanned detector (Zeiss). YFP was excited with a diode laser at 488-nm laser line, whereas mCherry was excited at 561 nm. Laser intensity and pinhole settings were kept in the same range for parallel set of experiments, and spectral overlap for any two channels was avoided by adjusting proper filter excitation regions and bandwidths. Images were scanned using the line scan mode, and the images were finally processed in ZEN lite (ZEN-blue/ZEN-black) software suite from ZEISS. Co-localization was analyzed by calculating Pearson's correlation coefficient (PCC) between the indicated channels using JACoP plugin in ImageJ software (37). At least three regions of interest per cell were analyzed, and the means  $\pm$  S.E. of PCCs are presented in the respective figure legends together with the number of cells and independent experiments.

For three-color imaging (Fig. 7B) and co-localization with early endosomal markers (Fig. 7C), receptor imaging of live or fixed cells was monitored by “feeding” cells with anti-FLAG antibody (15 min, 37 °C) in phenol red–free Dulbecco's modified Eagle's medium prior to agonist treatment. Fixed cells were washed three times in PBS, 0.04% EDTA to remove FLAG antibody bound to the remaining surface receptors, fixed using 4% PFA (20 min at room temperature), permeabilized, and stained using HA primary antibody followed by Alexa Fluor 555 or 647 secondary antibodies. For co-localization of FLAG–V<sub>2</sub>R with endosomal markers, the cells were treated as above except incubated with either of the following primary antibodies post-permeabilization: EEA1 (rabbit anti-EEA1 antibody from Cell Signaling Technology) or APPL1 (rabbit anti-APPL1 antibody from Cell Signaling Technology). The cells were imaged using a TCS-SP5 confocal microscope (Leica) with a 63× 1.4 numerical aperture objective and solid-state lasers of 488, 561, and/or 642 nm as light sources. Leica LAS AF image acquisition software was utilized. All subsequent raw-image tiff files were analyzed using ImageJ or LAS AF Lite (Leica), and co-localization was measured by calculating the PCC using JACoP plugin in ImageJ software as mentioned above.

### GloSensor assay and ERK1/2 phosphorylation

To measure the effect of intrabodies on G $\alpha_s$  coupling, if any, we measured agonist-induced cAMP response in GloSensor assay following a previously described protocol (25). Briefly, HEK-293 cells were transfected with plasmids encoding the V<sub>2</sub>R, the luciferase-based cAMP biosensor (pGloSensorTM-22F plasmid), and the intrabodies. 16 h post-transfection, the medium was aspirated, and the cells were flushed and pooled together in assay buffer containing 1× Hanks balanced salt solution, pH 7.4, and 20 mM of HEPES. Cell density was measured and adjusted such as to yield ~125,000 cells in 100  $\mu$ l. The cells were pelleted at 2000 rpm for 3 min to remove the assay buffer, and then the pellet was resuspended in the desired volume of sodium luciferin solution prepared in the same assay buffer. After seeding the cells in a 96-well plate, the plate was incubated at 37 °C for 90 min followed by an additional incubation of 30 min at room temperature. Subsequently, various doses of the indicated ligand were added to the cells, and the luminescence reading was recorded using a microplate reader (Victor  $\times$  4; Perkin Elmer). Agonist-induced phosphorylation of ERK1/2 MAP kinase was measured by Western blotting following a previously described protocol (38).

### BRET assay

For measuring  $\beta$ arr1 recruitment and endosomal localization by BRET (Fig. 7A, E and F), transfections were performed on HEK-293 cells seeded (40,000 cells/100  $\mu$ l/well) in 96-well white microplates (Greiner) using PEI at a ratio of 4:1 (PEI:DNA). To monitor V<sub>2</sub>R– $\beta$ arr1 interaction, we used  $\beta$ arr1–RlucII and V<sub>2</sub>R–YFP plasmids described previously (39). To monitor endosomal translocation of  $\beta$ arr1, we used enhanced bystander BRET, in which the BRET acceptor (*Renilla* GFP; rGFP) is fused to the FYVE domain from endofin protein targeted to early endosomes (rGFP-FYVE) and  $\beta$ arr1 fusion with the BRET donor RlucII (15). 48 h post-transfection, the culture medium was removed, and the cells were washed with Dulbecco's PBS and replaced by Hanks' balanced salt solution. Afterward, the cells were stimulated with increasing concentrations of arginine vasopressin (AVP) for 10 min, and 2.5  $\mu$ M coelenterazine H (BRET1) or coelenterazine 400a (BRET2) was added 5 min before BRET measurement. BRET signals were recorded on a Mithras (Berthold Scientific) microplate reader equipped with the following filters: 480/20 nm (donor) and 530/20 nm (acceptor) for BRET1 and 400/70 nm (donor) and 515/20 nm (acceptor) for BRET2. The BRET signal was determined as the ratio of the light emitted by the energy acceptor over the light emitted by energy donor. Raw BRET values are presented in Fig. 7 (A and E), whereas agonist-induced change in BRET signal ( $\Delta$ BRET) obtained by calculating the difference in BRET values for the highest and lowest concentrations of AVP is presented in Fig. 7F.

### Statistical analysis and data presentation

The quantified data were plotted and analyzed using GraphPad Prism software, and the details of experimental replicates and statistical analysis are mentioned in the corresponding figure legends.

## Data availability

All data are available in the article.

**Acknowledgments**—We thank the members of our laboratories for critical reading of the manuscript.

**Author contributions**—M. Baidya, P. K., H. D.-A., S. P., and A. K. S. conceptualization; M. Baidya, P. K., B. S., S. S., A. C. H., M. Bouvier, and A. K. S. data curation; M. Baidya, P. K., H. D.-A., M. C., A. S., D. R., and A. K. S. validation; M. Baidya, H. D.-A., B. S., S. S., M. C., A. S., D. R., and A. K. S. investigation; M. Baidya and P. K. visualization; M. Baidya, P. K., H. D.-A., S. P., B. S., S. S., M. C., A. S., D. R., A. C. H., M. Bouvier, and A. K. S. methodology; M. Baidya, P. K., H. D.-A., S. P., B. S., S. S., M. C., A. S., D. R., A. C. H., M. Bouvier, and A. K. S. writing-review and editing; A. C. H., M. Bouvier, and A. K. S. supervision; A. K. S. resources; A. K. S. formal analysis; A. K. S. funding acquisition; A. K. S. writing-original draft; A. K. S. project administration.

**Funding and additional information**—This work was supported by DBT Wellcome Trust India Alliance Intermediate Fellowship IA/I/14/1/501285 (to A. K. S.), Innovative Young Biotechnologist Award BT/08/IYBA/2014-3 from the Department of Biotechnology, Government of India (to A. K. S.), a Lady Tata Memorial Trust Young Researcher Award (to A. K. S.), Science and Engineering Research Board Grant SB/SO/BB-121/2013 (to A. K. S.), and Council of Scientific and Industrial Research Grant 37[1637]14/EMR-II. Dr. Shukla is an EMBO Young Investigator. Drs. Hemlata Dwivedi and Mithu Baidya were supported by National Post-Doctoral Fellowship of Science and Engineering Research Board Grants PDF/2016/002930 and PDF/2016/2893. Dr. Ashish Srivastava is supported by Wellcome Trust/DBT India Alliance Early Career Fellowship Grant IA/E/17/1/503687. Dr. Hanyaloglu is supported by Genesis Research Trust Grant P73441 and Biotechnology and Biological Sciences Research Council Grants BB/N016947/1 and BB/S001565/1.

**Conflict of interest**—The authors declare that they have no conflicts of interest with the contents of this article.

**Abbreviations**—The abbreviations used are: GPCR, G-protein-coupled receptor;  $\beta$ arr,  $\beta$ -arrestin; FAB, antibody fragment; BRET, bioluminescence resonance energy transfer; ERK, extracellular signal-regulated kinase; MAP, mitogen-activated protein; ANOVA, analysis of variance; co-IP, co-immunoprecipitation; HA, hemagglutinin; YFP, yellow fluorescent protein; Ib, intrabody; CTL, control; C5aR1, C5a receptor 1; NTSR1, neurotensin receptor 1; M2R, muscarinic acetylcholine receptor subtype 2; ACKR2, atypical chemokine receptor subtype 2; B<sub>2</sub>R, bradykinin subtype 2 receptor; PEI, polyethyleneimine; HRP, horseradish peroxidase; PCC, Pearson's correlation coefficient; RlucII, *Renilla* luciferase II; ScFv, single-chain variable fragment; AVP, arginine vasopressin.

## References

1. Bockaert, J., and Pin, J. P. (1999) Molecular tinkering of G protein-coupled receptors: an evolutionary success. *EMBO J.* **18**, 1723–1729 [CrossRef Medline](#)
2. Kang, D. S., Tian, X., and Benovic, J. L. (2014) Role of  $\beta$ -arrestins and arrestin domain-containing proteins in G protein-coupled receptor trafficking. *Curr. Opin. Cell Biol.* **27**, 63–71 [CrossRef Medline](#)
3. Lefkowitz, R. J., and Shenoy, S. K. (2005) Transduction of receptor signals by  $\beta$ -arrestins. *Science* **308**, 512–517 [CrossRef Medline](#)
4. Oakley, R. H., Laporte, S. A., Holt, J. A., Caron, M. G., and Barak, L. S. (2000) Differential affinities of visual arrestin, beta arrestin1, and beta arrestin2 for G protein-coupled receptors delineate two major classes of receptors. *J. Biol. Chem.* **275**, 17201–17210 [CrossRef Medline](#)
5. Freedman, N. J., and Lefkowitz, R. J. (1996) Desensitization of G protein-coupled receptors. *Recent Prog. Horm. Res.* **51**, 319–351 [Medline](#)
6. Grundmann, M., Merten, N., Malfacini, D., Inoue, A., Preis, P., Simon, K., Rüttiger, N., Ziegler, N., Benkel, T., Schmitt, N. K., Ishida, S., Müller, I., Reher, R., Kawakami, K., Inoue, A., et al. (2018) Lack of beta-arrestin signaling in the absence of active G proteins. *Nat. Commun.* **9**, 341 [CrossRef Medline](#)
7. Gurevich, V. V., and Gurevich, E. V. (2018) Arrestin-mediated signaling: Is there a controversy? *World J. Biol. Chem.* **9**, 25–35 [CrossRef Medline](#)
8. Gutkind, J. S., and Kostenis, E. (2018) Arrestins as rheostats of GPCR signalling. *Nat. Rev. Mol. Cell Biol.* **19**, 615–616 [CrossRef Medline](#)
9. Luttrell, L. M., Wang, J., Plouffe, B., Smith, J. S., Yamani, L., Kaur, S., Jean-Charles, P. Y., Gauthier, C., Lee, M. H., Pani, B., Kim, J., Ahn, S., Rajagopal, S., Reiter, E., Bouvier, M., et al. (2018) Manifold roles of  $\beta$ -arrestins in GPCR signaling elucidated with siRNA and CRISPR/Cas9. *Sci. Signal.* **11**, eaat7650 [CrossRef Medline](#)
10. Ranjan, R., Dwivedi, H., Baidya, M., Kumar, M., and Shukla, A. K. (2017) Novel structural insights into GPCR- $\beta$ -arrestin interaction and signaling. *Trends Cell Biol.* **27**, 851–862 [CrossRef Medline](#)
11. Gurevich, V. V., and Gurevich, E. V. (2004) The molecular acrobatics of arrestin activation. *Trends Pharmacol. Sci.* **25**, 105–111 [CrossRef Medline](#)
12. Shukla, A. K., Westfield, G. H., Xiao, K., Reis, R. I., Huang, L. Y., Tripathi-Shukla, P., Qian, J., Li, S., Blanc, A., Oleskie, A. N., Dosey, A. M., Su, M., Liang, C. R., Gu, L. L., Shan, J. M., et al. (2014) Visualization of arrestin recruitment by a G-protein-coupled receptor. *Nature* **512**, 218–222 [CrossRef Medline](#)
13. Angers, S., Salahpour, A., Joly, E., Hilairiet, S., Chelsky, D., Dennis, M., and Bouvier, M. (2000) Detection of  $\beta_2$ -adrenergic receptor dimerization in living cells using bioluminescence resonance energy transfer (BRET). *Proc. Natl. Acad. Sci. U.S.A.* **97**, 3684–3689 [CrossRef Medline](#)
14. Charest, P. G., Terrillon, S., and Bouvier, M. (2005) Monitoring agonist-promoted conformational changes of  $\beta$ -arrestin in living cells by intramolecular BRET. *EMBO Rep* **6**, 334–340 [CrossRef Medline](#)
15. Namkung, Y., Le Guillou, C., Lukashova, V., Kobayashi, H., Hogue, M., Khoury, E., Song, M., Bouvier, M., and Laporte, S. A. (2016) Monitoring G protein-coupled receptor and  $\beta$ -arrestin trafficking in live cells using enhanced bystander BRET. *Nat. Commun.* **7**, 12178 [CrossRef Medline](#)
16. Bassoni, D. L., Raab, W. J., Achacoso, P. L., Loh, C. Y., and Wehrman, T. S. (2012) Measurements of  $\beta$ -arrestin recruitment to activated seven transmembrane receptors using enzyme complementation. *Methods Mol. Biol.* **897**, 181–203 [CrossRef Medline](#)
17. Barnea, G., Strapps, W., Herrada, G., Berman, Y., Ong, J., Kloss, B., Axel, R., and Lee, K. J. (2008) The genetic design of signaling cascades to record receptor activation. *Proc. Natl. Acad. Sci. U.S.A.* **105**, 64–69 [CrossRef Medline](#)
18. Kroeze, W. K., Sassano, M. F., Huang, X. P., Lansu, K., McCorvy, J. D., Giguère, P. M., Sciak, N., and Roth, B. L. (2015) PRESTO-Tango as an open-source resource for interrogation of the druggable human GPCRome. *Nat. Struct. Mol. Biol.* **22**, 362–369 [CrossRef Medline](#)
19. Kumari, P., Srivastava, A., Banerjee, R., Ghosh, E., Gupta, P., Ranjan, R., Chen, X., Gupta, B., Gupta, C., Jaiman, D., and Shukla, A. K. (2016) Functional competence of a partially engaged GPCR- $\beta$ -arrestin complex. *Nat. Commun.* **7**, 13416 [CrossRef Medline](#)
20. Kumari, P., Srivastava, A., Ghosh, E., Ranjan, R., Dogra, S., Yadav, P. N., and Shukla, A. K. (2017) Core engagement with  $\beta$ -arrestin is dispensable for agonist-induced vasopressin receptor endocytosis and ERK activation. *Mol. Biol. Cell* **28**, 1003–1010 [CrossRef Medline](#)
21. Cahill, T. J., 3rd, Thomsen, A. R., Tarrasch, J. T., Plouffe, B., Nguyen, A. H., Yang, F., Huang, L. Y., Kahsai, A. W., Bassoni, D. L., Gavino, B. J., Lamerdin, J. E., Triest, S., Shukla, A. K., Berger, B., Little, J. T., 4th, et al. (2017) Distinct conformations of GPCR- $\beta$ -arrestin complexes

- mediate desensitization, signaling, and endocytosis. *Proc. Natl. Acad. Sci. U.S.A.* **114**, 2562–2567 [CrossRef Medline](#)
22. Xiao, K., Shenoy, S. K., Nobles, K., and Lefkowitz, R. J. (2004) Activation-dependent conformational changes in  $\beta$ -arrestin 2. *J. Biol. Chem.* **279**, 55744–55753 [CrossRef Medline](#)
  23. Nobles, K. N., Guan, Z., Xiao, K., Oas, T. G., and Lefkowitz, R. J. (2007) The active conformation of  $\beta$ -arrestin1: direct evidence for the phosphate sensor in the N-domain and conformational differences in the active states of  $\beta$ -arrestins1 and -2. *J. Biol. Chem.* **282**, 21370–21381 [CrossRef Medline](#)
  24. Shukla, A. K., Manglik, A., Kruse, A. C., Xiao, K., Reis, R. I., Tseng, W. C., Staus, D. P., Hilger, D., Uysal, S., Huang, L. Y., Paduch, M., Tripathi-Shukla, P., Koide, A., Koide, S., Weis, W. I., *et al.* (2013) Structure of active  $\beta$ -arrestin-1 bound to a G-protein-coupled receptor phosphopeptide. *Nature* **497**, 137–141 [CrossRef Medline](#)
  25. Ghosh, E., Dwivedi, H., Baidya, M., Srivastava, A., Kumari, P., Stepniwski, T., Kim, H. R., Lee, M. H., van Gastel, J., Chaturvedi, M., Roy, D., Pandey, S., Maharana, J., Guixa-Gonzalez, R., Luttrell, L. M., *et al.* (2019) Conformational sensors and domain swapping reveal structural and functional differences between  $\beta$ -arrestin isoforms. *Cell Rep.* **28**, 3287–3299 [CrossRef Medline](#)
  26. Ghosh, E., Srivastava, A., Baidya, M., Kumari, P., Dwivedi, H., Nidhi, K., Ranjan, R., Dogra, S., Koide, A., Yadav, P. N., Sidhu, S. S., Koide, S., and Shukla, A. K. (2017) A synthetic intrabody-based selective and generic inhibitor of GPCR endocytosis. *Nat. Nanotechnol.* **12**, 1190–1198 [CrossRef Medline](#)
  27. Irannejad, R., Tomshine, J. C., Tomshine, J. R., Chevalier, M., Mahoney, J. P., Steyaert, J., Rasmussen, S. G., Sunahara, R. K., El-Samad, H., Huang, B., and von Zastrow, M. (2013) Conformational biosensors reveal GPCR signalling from endosomes. *Nature* **495**, 534–538 [CrossRef Medline](#)
  28. Haider, R. S., Godbole, A., and Hoffmann, C. (2019) To sense or not to sense—new insights from GPCR-based and arrestin-based biosensors. *Curr. Opin. Cell Biol.* **57**, 16–24 [CrossRef Medline](#)
  29. Oakley, R. H., Laporte, S. A., Holt, J. A., Barak, L. S., and Caron, M. G. (2001) Molecular determinants underlying the formation of stable intracellular G protein-coupled receptor- $\beta$ -arrestin complexes after receptor endocytosis. *J. Biol. Chem.* **276**, 19452–19460 [CrossRef Medline](#)
  30. Srivastava, A., Gupta, B., Gupta, C., and Shukla, A. K. (2015) Emerging functional divergence of  $\beta$ -arrestin isoforms in GPCR function. *Trends Endocrinol. Metab.* **26**, 628–642 [CrossRef Medline](#)
  31. Shukla, A. K., Violin, J. D., Whalen, E. J., Gesty-Palmer, D., Shenoy, S. K., and Lefkowitz, R. J. (2008) Distinct conformational changes in  $\beta$ -arrestin report biased agonism at seven-transmembrane receptors. *Proc. Natl. Acad. Sci. U.S.A.* **105**, 9988–9993 [CrossRef Medline](#)
  32. Nobles, K. N., Xiao, K., Ahn, S., Shukla, A. K., Lam, C. M., Rajagopal, S., Strachan, R. T., Huang, T. Y., Bressler, E. A., Hara, M. R., Shenoy, S. K., Gygi, S. P., and Lefkowitz, R. J. (2011) Distinct phosphorylation sites on the  $\beta_2$ -adrenergic receptor establish a barcode that encodes differential functions of  $\beta$ -arrestin. *Sci. Signal.* **4**, ra51 [CrossRef Medline](#)
  33. Butcher, A. J., Prihandoko, R., Kong, K. C., McWilliams, P., Edwards, J. M., Bottrill, A., Mistry, S., and Tobin, A. B. (2011) Differential G-protein-coupled receptor phosphorylation provides evidence for a signaling barcode. *J. Biol. Chem.* **286**, 11506–11518 [CrossRef Medline](#)
  34. Reiter, E., Ahn, S., Shukla, A. K., and Lefkowitz, R. J. (2012) Molecular mechanism of  $\beta$ -arrestin-biased agonism at seven-transmembrane receptors. *Annu. Rev. Pharmacol. Toxicol.* **52**, 179–197 [CrossRef Medline](#)
  35. Tobin, A. B., Butcher, A. J., Kong, K. C. (2008) Location, location, location... site-specific GPCR phosphorylation offers a mechanism for cell-type-specific signalling. *Trends Pharmacol. Sci.* **29**, 413–420 [CrossRef Medline](#)
  36. Goncharuk, M. V., R. D., Dubinnyi, M. A., Nadezhdin, K. D., Srivastava, A., Baidya, M., Agnihotri-Dwivedi, H., As, A., and Shukla, A. K. (2020) Purification of native CCL7 and its functional interaction with selected chemokine receptors. *Protein Expr. Purif.* **171**, 105617 [CrossRef Medline](#)
  37. Bolte, S., and Cordelieres, F. P. (2006) A guided tour into subcellular colocalization analysis in light microscopy. *J. Microsc. (Oxford)* **224**, 213–232 [CrossRef Medline](#)
  38. Kumari, P., Dwivedi, H., Baidya, M., and Shukla, A. K. (2019) Measuring agonist-induced ERK MAP kinase phosphorylation for G-protein-coupled receptors. *Methods Cell. Biol.* **149**, 141–153 [CrossRef Medline](#)
  39. Rochdi, M. D., Vargas, G. A., Carpentier, E., Oligny-Longpré, G., Chen, S., Kovoor, A., Gitelman, S. E., Rosenthal, S. M., von Zastrow, M., and Bouvier, M. (2010) Functional characterization of vasopressin type 2 receptor substitutions (R137H/C/L) leading to nephrogenic diabetes insipidus and nephrogenic syndrome of inappropriate antidiuresis: implications for treatments. *Mol. Pharmacol.* **77**, 836–845 [CrossRef Medline](#)



**Annex II: The RanBP2/RanGAP1-SUMO Complex Gates  $\beta$ -  
arrestin2 Nuclear Entry to Regulate the Mdm2-p53 Signaling**

**Axis**



# The RanBP2/RanGAP1-SUMO complex gates $\beta$ -arrestin2 nuclear entry to regulate the Mdm2-p53 signaling axis

Elodie Blondel-Tepaz<sup>1,2,3</sup> · Marie Leverve<sup>1,2,3</sup> · Badr Sokrat<sup>4,5</sup> · Justine S. Paradis<sup>5,6</sup> · Milena Kosic<sup>7</sup> · Kusumika Saha<sup>1,2,3</sup> · Cédric Auffray<sup>1,2,3</sup> · Evelyne Lima-Fernandes<sup>1,2,3</sup> · Alessia Zamborlini<sup>8</sup> · Anne Poupon<sup>9</sup> · Louis Gaboury<sup>5,10</sup> · Jane Findlay<sup>11</sup> · George S. Baillie<sup>11</sup> · Hervé Enslin<sup>1,2,3</sup> · Michel Bouvier<sup>5,6</sup> · Stéphane Angers<sup>7</sup> · Stefano Marullo<sup>1,2,3</sup> · Mark G. H. Scott<sup>1,2,3</sup>

Received: 2 September 2020 / Revised: 4 February 2021 / Accepted: 5 February 2021 / Published online: 1 March 2021  
© The Author(s), under exclusive licence to Springer Nature Limited 2021

## Abstract

Mdm2 antagonizes the tumor suppressor p53. Targeting the Mdm2-p53 interaction represents an attractive approach for the treatment of cancers with functional p53. Investigating mechanisms underlying Mdm2-p53 regulation is therefore important. The scaffold protein  $\beta$ -arrestin2 ( $\beta$ -arr2) regulates tumor suppressor p53 by counteracting Mdm2.  $\beta$ -arr2 nucleocytoplasmic shuttling displaces Mdm2 from the nucleus to the cytoplasm resulting in enhanced p53 signaling.  $\beta$ -arr2 is constitutively exported from the nucleus, via a nuclear export signal, but mechanisms regulating its nuclear entry are not completely elucidated.  $\beta$ -arr2 can be SUMOylated, but no information is available on how SUMO may regulate  $\beta$ -arr2 nucleocytoplasmic shuttling. While we found  $\beta$ -arr2 SUMOylation to be dispensable for nuclear import, we identified a non-covalent interaction between SUMO and  $\beta$ -arr2, via a SUMO interaction motif (SIM), that is required for  $\beta$ -arr2 cytonuclear trafficking. This SIM promotes association of  $\beta$ -arr2 with the multimolecular RanBP2/RanGAP1-SUMO nucleocytoplasmic transport hub that resides on the cytoplasmic filaments of the nuclear pore complex. Depletion of RanBP2/RanGAP1-SUMO levels result in defective  $\beta$ -arr2 nuclear entry. Mutation of the SIM inhibits  $\beta$ -arr2 nuclear import, its ability to delocalize Mdm2 from the nucleus to the cytoplasm and enhanced p53 signaling in lung and breast tumor cell lines. Thus, a  $\beta$ -arr2 SIM nuclear entry checkpoint, coupled with active  $\beta$ -arr2 nuclear export, regulates its cytonuclear trafficking function to control the Mdm2-p53 signaling axis.

**Supplementary information** The online version contains supplementary material available at <https://doi.org/10.1038/s41388-021-01704-w>.

✉ Mark G. H. Scott  
mark.scott@inserm.fr

<sup>1</sup> Inserm, U1016, Institut Cochin, Paris, France

<sup>2</sup> CNRS, UMR8104, Paris, France

<sup>3</sup> Université de Paris, Paris, France

<sup>4</sup> Institute for Research in Immunology and Cancer (IRIC), Université de Montréal, Montréal, QC, Canada

<sup>5</sup> Department of Biochemistry and Molecular Medicine, Université de Montréal, Montréal, QC, Canada

<sup>6</sup> Molecular Biology Program, Université de Montréal, Montréal, QC, Canada

## Introduction

Initially discovered for the roles they play in the regulation of G protein-coupled receptors (GPCRs), the  $\beta$ -arrestins ( $\beta$ -arr1 and  $\beta$ -arr2) have now been shown to act as scaffolding hubs that control multiple signaling pathways [1–3].

<sup>7</sup> Leslie Dan Faculty of Pharmacy and Department of Biochemistry, University of Toronto, Toronto, ON, Canada

<sup>8</sup> Institute for Integrative Biology of the Cell (I2BC), CEA, CNRS, Université Paris-Saclay, Gif-sur-Yvette, France

<sup>9</sup> PRC, INRA, CNRS, IFCE, Université de Tours, Nouzilly, France

<sup>10</sup> Department of Pathology and Cell Biology, IRIC, Université de Montréal, Montréal, QC, Canada

<sup>11</sup> Institute of Cardiovascular and Medical Sciences, College of Veterinary, Medical and Life Sciences, University of Glasgow, Glasgow, UK

Through their scaffolding properties  $\beta$ -arrestins dynamically regulate the activity and/or subcellular distribution of non-GPCR protein partners such as ERK1/2 [4, 5] JNK3 [6], Mdm2 [7–9], PTEN [10–12], and FAK [13]. While strong sequence homology exists between  $\beta$ -arr1 and  $\beta$ -arr2 they display different subcellular distributions [9, 14]. Whereas  $\beta$ -arr1 is found in both the nucleus and cytoplasm at steady state,  $\beta$ -arr2 shows an apparent cytoplasmic distribution. We previously showed that  $\beta$ -arr2 is constitutively excluded from the nucleus by a leptomycin B (LMB)-sensitive pathway driven by a nuclear export signal (NES) that is absent in  $\beta$ -arr1 [14]. We also found that  $\beta$ -arr2 is actively imported into the nucleus, indicating that it undergoes constitutive nucleocytoplasmic shuttling [14].  $\beta$ -arr2 shuttling displaces nuclear partners, such as JNK3 and Mdm2, from the nucleus to the cytoplasm [9, 14]. In the case of Mdm2, its  $\beta$ -arr2-mediated delocalization results in increased p53 signaling and cell cycle arrest [7]. In contrast to the well-characterized nuclear export mechanism of  $\beta$ -arr2 the entry mechanism(s) of  $\beta$ -arr2 into the nucleus are not completely elucidated.

$\beta$ -arr2 can be SUMOylated [15, 16], but no information is available on how SUMO may regulate  $\beta$ -arr2 nucleocytoplasmic trafficking. SUMOylation is a key dynamic regulatory posttranslational modification that impacts the activity and localization of protein targets including into the nucleus [17–19]. These functional consequences are generally due to modification in protein–protein interactions caused by SUMOylation. Akin to the situation with the ubiquitination pathway, SUMOylation involves a series of sequential enzymatic reactions ultimately leading to covalent conjugation of the 12 kDa protein SUMO on a lysine residue contained within a SUMOylation site ( $\Psi$ -K-X-E;  $\Psi$ , a bulky aliphatic residue, typically L, I, or V) on a target protein [17, 18, 20]. There are four SUMO isoforms in mammals: SUMO1, SUMO2, and SUMO3 are expressed ubiquitously, whereas SUMO4 displays tissue restricted expression and it is not clear whether it is conjugated to cellular proteins [21]. SUMO2 and SUMO3 display 97% homology and contain internal SUMOylation sites allowing them to form poly-SUMO chains. SUMO1 shares 45% homology with SUMO2/3 [17]. SUMOylation is reversible with SUMO-modified targets being subject to cleavage of the isopeptide bond by SUMO-specific proteases that release SUMO molecules that become available for further SUMOylation cycles. SUMOylated proteins can establish non-covalent interaction with protein partners via SUMO interaction motifs (SIMs). Identified via two-hybrid screening and biophysical studies, SIMs are composed of a short stretch of hydrophobic residues (generally V/I-V/I-X-V/I) flanked N- or C-terminally by serine residues and/or several acidic residues [17, 22]. When bound to SUMO, SIMs adopt a parallel or antiparallel  $\beta$ -strand conformation

that permits the hydrophobic side chains of the SIM to interact with a hydrophobic pocket on the surface of SUMO. The acidic flanking residues in the SIM form electrostatic interactions with a basic interface on SUMO, and thus also contribute to the SUMO–SIM interaction. SIMs can be involved in *cis*-SUMOylation or in recruitment/targeting of SIM-containing proteins to SUMOylated partners [17].

Using various *in vitro* and cell-based approaches, we have characterized both a SUMOylation site and SIM in human  $\beta$ -arr2. Whereas  $\beta$ -arr2 SUMOylation is not required for nuclear import, mutation of the SIM prevents  $\beta$ -arr2 nuclear import. The SIM promotes association of  $\beta$ -arr2 with the multimolecular RanBP2/RanGAP1-SUMO nucleocytoplasmic transport hub and depletion of this complex inhibits  $\beta$ -arr2 nuclear import. The  $\beta$ -arr2 $\Delta$ SIM mutant loses its ability to delocalize Mdm2 from the nucleus to the cytoplasm with functional consequences for p53 activity. Combined, our data reveal that a SUMO–SIM nuclear entry checkpoint, coupled with the nuclear export function of  $\beta$ -arr2, cooperate to regulate its cytonuclear trafficking function and subsequent control of the Mdm2–p53 pathway.

## Results

### Human $\beta$ -arr2 is SUMOylated at lysine 295

To investigate the potential role of SUMO in the nucleocytoplasmic trafficking action of  $\beta$ -arr2, we first searched for potential SUMOylation sites within human  $\beta$ -arr2. Ubc9 fusion-directed SUMOylation (UFDS) experiments [23], which permit efficient and selective protein SUMOylation, were conducted by cloning the E2 conjugase Ubc9 coding sequence upstream of the open reading frame of  $\beta$ -arr2 with a C-terminal FLAG-tag, generating a coding sequence for a Ubc9- $\beta$ -arr2-FLAG fusion protein (Fig. 1a). The fusion protein was expressed in HeLa cells in the presence of HA-SUMO1 or HA-SUMO2. Immunoprecipitations of the protein extracts using anti-FLAG antibodies followed by western blotting with anti-FLAG antibodies revealed the presence of a molecular weight (MW) band of ~100 kDa corresponding to the Ubc9- $\beta$ -arr2-FLAG fusion conjugated with HA-SUMO1 or HA-SUMO2 (Fig. 1b, c, lanes 2). The fused Ubc9 catalyzed SUMOylation of  $\beta$ -arr2, as the active site mutant Ubc9C93S fused to  $\beta$ -arr2 (Fig. 1a) failed to promote  $\beta$ -arr2 SUMOylation in the presence of either SUMO1 or SUMO2 (Fig. 1b, c, lanes 3). Similar results were obtained with the fusions in  $\beta$ -arr1/2 knockout-mouse embryonic fibroblasts (Fig. S1). The expected MW of native  $\beta$ -arr2 is 55 kDa. Following highly denaturing lysis, affinity pulldown with Ni-NTA resin greatly enriched

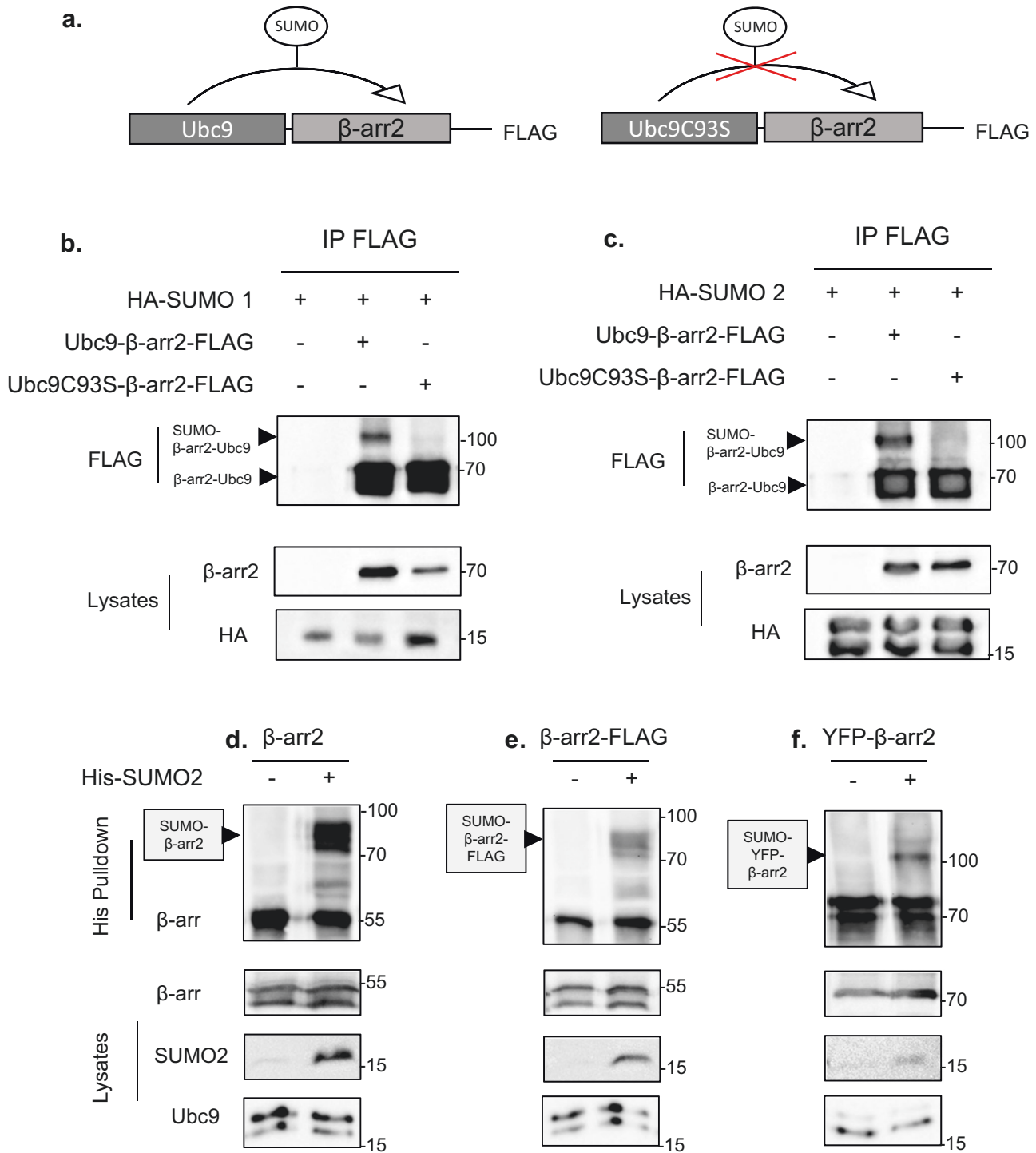


**Fig. 1**  $\beta$ -arr2 is SUMOylated in cells. **a** Schematic diagram details the Ubc9- $\beta$ -arr2-FLAG and catalytically dead Ubc9C93S- $\beta$ -arr2-FLAG UFDS fusions. SUMOylation of  $\beta$ -arr2 assessed by UFDS. Ubc9- $\beta$ -arr2 or Ubc9C93S- $\beta$ -arr2 were coexpressed with HA-SUMO1 (**b**) or HA-SUMO2 (**c**) in HeLa cells as indicated. The protein extracts were subject to immunoprecipitation using EZview Red ANTI-FLAG<sup>®</sup> M2 Affinity Gel, and fusions and SUMOylated fusions were detected by western blot using anti-FLAG antibodies. The top set of arrows

indicates SUMOylated forms of Ubc9- $\beta$ -arr2. HEK-293T cells were co-transfected with plasmids encoding Ubc9, His-tagged SUMO2, or empty vector, and either **d**  $\beta$ -arr2, **e**  $\beta$ -arr2-FLAG, or **f** YFP- $\beta$ -arr2. Forty-eight hours later, cells were lysed in denaturing conditions followed by purification on Ni-NTA beads. Cell lysates and His-SUMO conjugated proteins purified with Ni-NTA agarose beads were analyzed by western blot with the indicated antibodies. The arrow indicates SUMO2-conjugated  $\beta$ -arr2.

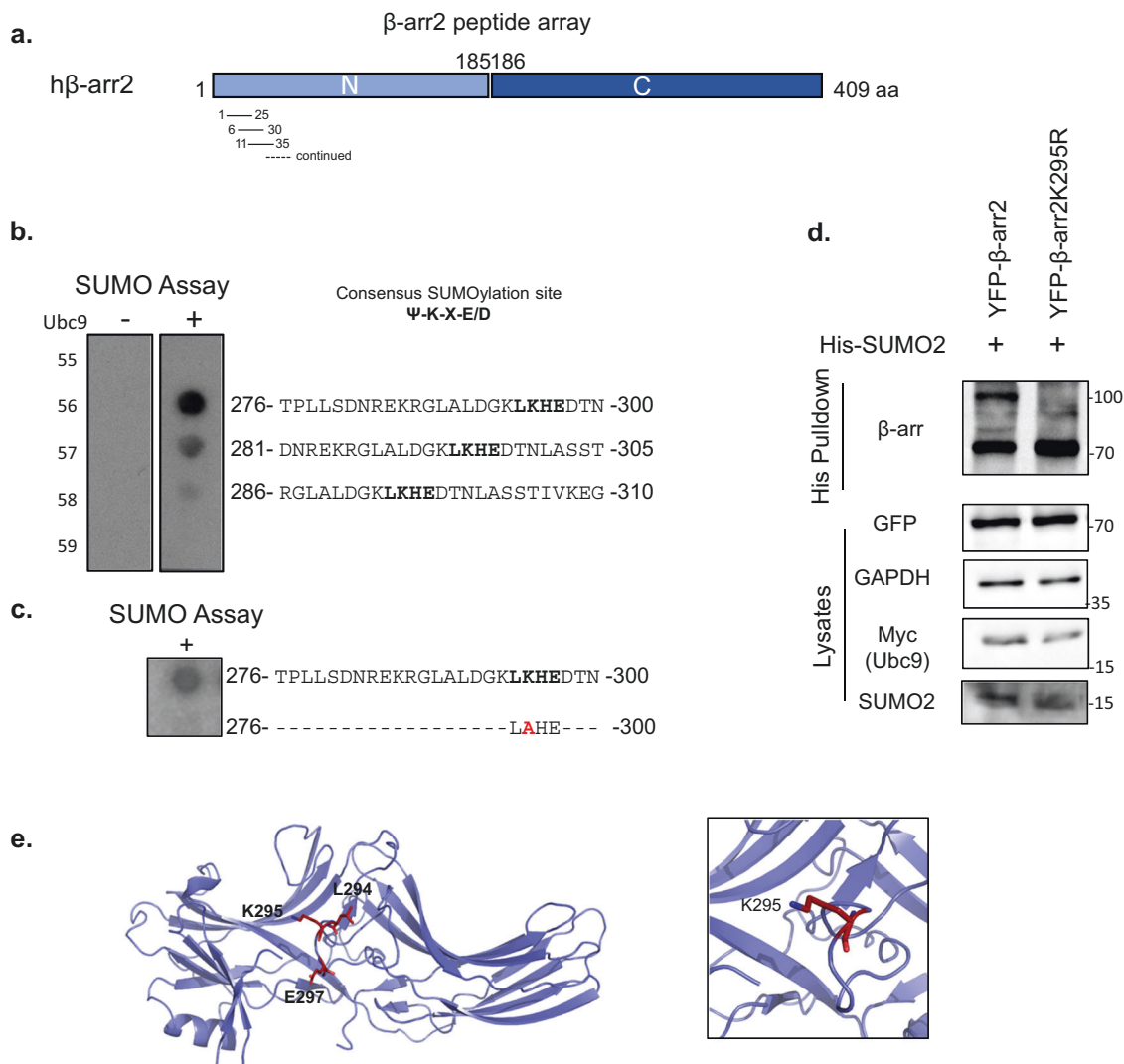


**Fig. 2**  $\beta$ -arr2 is SUMOylated on lysine 295. **a** Schematic diagram showing the library of overlapping 25-mer peptides that cover the entire  $\beta$ -arr2 sequence. **b** The peptide library was overlaid with SUMO conjugation assay mixture (Ubc9+) including recombinant His-SUMO1–His-SUMO3. Dark spots represent a run of peptides that displayed successful conjugation of recombinant SUMO to immobilized peptides that are absent in the control array (Ubc9–). **c** Alanine

substitution at K295 inhibits SUMO conjugation on the immobilized 276–300 peptide. **d** K295R mutation inhibits SUMOylation in cells following lysis in denaturing conditions and purification on Ni-NTA beads. **e** Structure of  $\beta$ -arr2 in cartoon representation, with SUMO site in red sticks representation (left), zoom on K295 residue (right).

SUMOylated human  $\beta$ -arr2 with a MW of  $\sim$ 75 kDa corresponding to  $\beta$ -arr2 covalently conjugated with one molecule of SUMO2 in HEK-293 cells expressing exogenous native  $\beta$ -arr2, Ubc9, and His-SUMO2, or FLAG-tagged  $\beta$ -arr2, Ubc9, and His-SUMO2 (Fig. 1d, e, right lanes). SUMOylated  $\beta$ -arr2 was not observed in control cells lacking His-SUMO2 (Fig. 1d, e, left lanes). Similar results were obtained using a yellow fluorescent protein (YFP)-tagged form of  $\beta$ -arr2 (Fig. 1f, MW band at  $\sim$ 100 kDa).

Human  $\beta$ -arr2 is a 409 amino acid protein composed of N- and C-globular domains linked together by a short hinge region, and a flexible regulatory C-terminal tail (Fig. 2a). To screen for a SUMO acceptor site(s) in  $\beta$ -arr2, a library of

overlapping peptides (25-mers), each shifted by five amino acids across the entire sequence of  $\beta$ -arr2 (Fig. 2a), was SPOT-synthesized on cellulose membranes. The peptide arrays were subjected to *in vitro* SUMOylation assays using a SUMO assay mix containing recombinant forms of E1-activase, E2 conjugase Ubc9, SUMO1–SUMO3, and Mg-ATP solution. Control arrays were performed using SUMO assay mixtures that omitted Ubc9. The arrays were then probed with anti-SUMO antibodies and SUMOylated peptides were identified as dark spots. Using this approach, three consecutive SUMOylated peptides were identified comprising amino acids T276–G310 (Figs. 2b and S2a) that were absent in the control arrays. These peptides contained

a consensus SUMOylation motif in  $\beta$ -arr2 294-L-K-H-E-297 that has previously been documented [15, 16]. Confirming that K295 is indeed SUMOylated in the peptides, its mutation to alanine in a “progeny” 25-mer containing amino acids 276–300 inhibited SUMOylation (Figs. 2c and S2b). To confirm the SUMO acceptor site in cells, HEK-293 cells were co-transfected with YFP- $\beta$ -arr2 or mutant YFP- $\beta$ -arr2K295R in the presence of Myc-Ubc9 and His-SUMO2. While a  $\sim$ 100 kDa band of SUMOylated YFP- $\beta$ -arr2 was observed in Ni-NTA experiments in cells expressing wild-type  $\beta$ -arr2 (Fig. 2d, lane 1), this band was lost with the YFP- $\beta$ -arr2K295R mutant (Fig. 2d, lane 2), consistent with this being a major SUMOylation site for  $\beta$ -arr2. Taken together, the above findings indicate that  $\beta$ -arr2 is SUMOylated both in vitro and in cells, and that K295, located in the regulatory “ariat loop” of the C-domain of  $\beta$ -arr2 (Fig. 2e), represents a major SUMO conjugation site contained within a consensus SUMOylation motif.

### Human $\beta$ -arr2 contains a SIM in its N-domain

In addition to SUMOylation sites for covalent SUMO conjugation on lysine residues, SIMs exist that mediate non-covalent interaction between SUMO and SIM-containing proteins. We used a Joined Advanced Sumoylation Site and SIM Analyzer (JASSA) program [24], which predicts SIMs, to analyze the primary sequence of  $\beta$ -arr2. A potential SIM was predicted in the N-domain of  $\beta$ -arr2 between amino acids 41 and 44: 41-V-V-L-V-44 (Fig. 3a, b). Figure 3a shows the alignment of the potential SIM sequence in  $\beta$ -arr2 against other known SIMs found in Daxx, RanBP2, PML-III, and PIAS1. In addition, the sequence in  $\beta$ -arr2 also contains two aspartic acid residues juxtaposed to the hydrophobic core (Fig. 3a, b), another important feature of functional SIMs. To test whether the potential SIM in  $\beta$ -arr2 is capable of non-covalent interaction with SUMO, we carried out pulldown experiments using SUMO1 and SUMO2 proteins coupled to agarose beads. Whereas wild-type  $\beta$ -arr2 bound to both SUMO1 and SUMO2 beads, a  $\beta$ -arr2 $\Delta$ SIM mutant with the 41-V-V-L-V-44 sequence mutated to 41-A-A-L-A-44 displayed greatly decreased binding (Fig. 3c). Thus, the SIM domain in  $\beta$ -arr2 is functional and provides non-covalent interaction with both SUMO1 and SUMO2.

### $\beta$ -arr2 SIM is required for nuclear import

$\beta$ -arr2 is actively imported into the nucleus and subsequently excluded from the nuclear compartment via active nuclear export [14]. As SUMOylation and non-covalent SUMO interactions are both known to impact protein targeting to the nucleus, we next investigated their possible

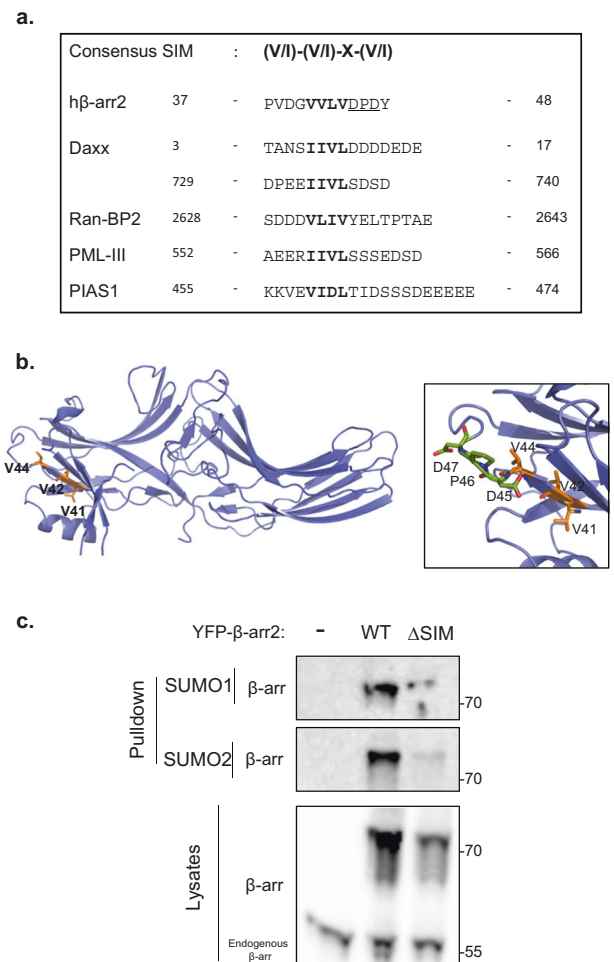


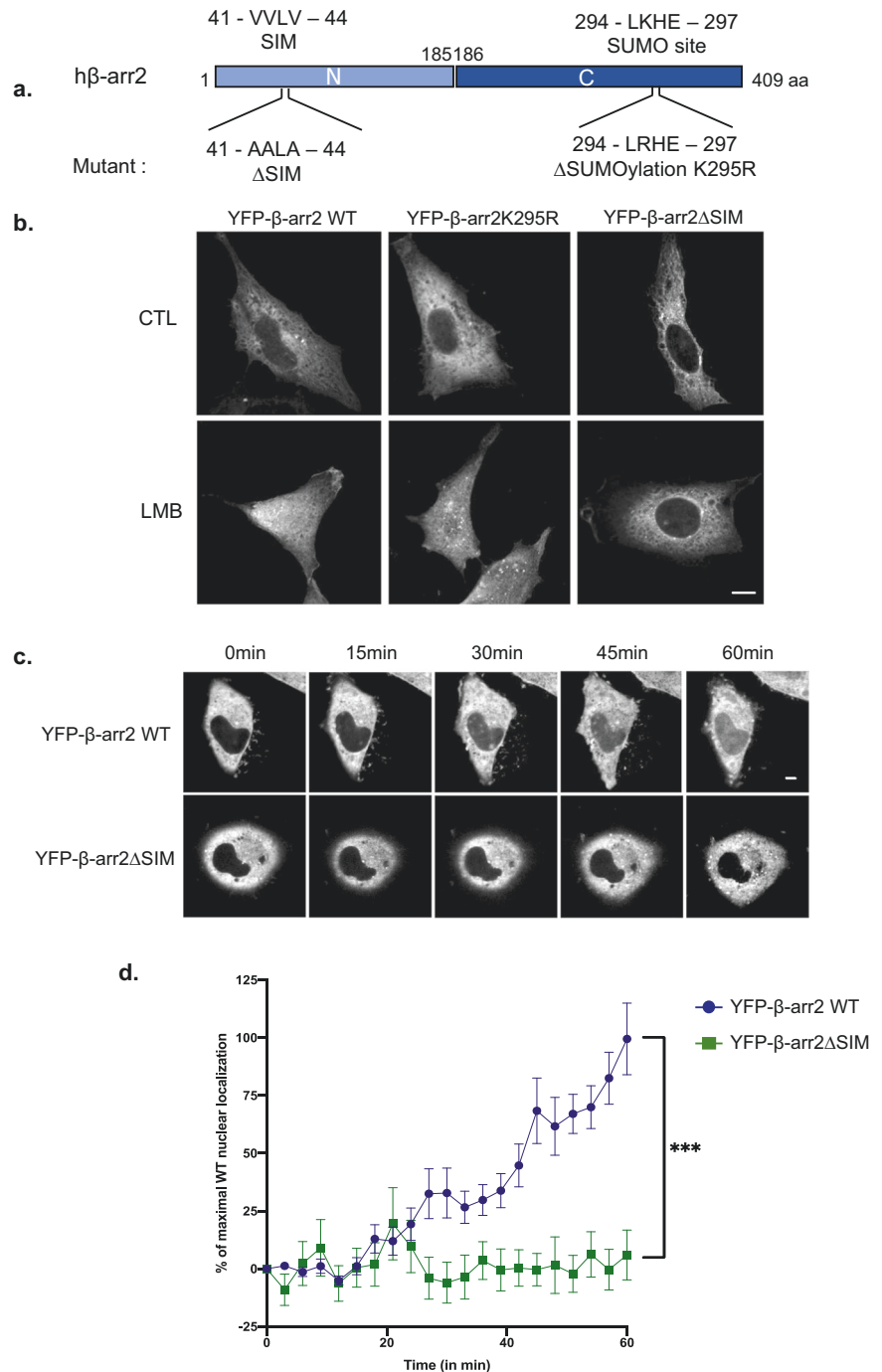
**Fig. 3  $\beta$ -arr2 contains a SIM in its N-domain.** **a** Alignment of the putative SIM sequence in the N-domain of  $\beta$ -arr2 against other known characterized SIMs in Daxx, RanBP2, PML-III, and PIAS1. **b** Structure of  $\beta$ -arr2 in cartoon representation, with SIM site in orange sticks representation (left), zoom on the SIM residues, also highlighting the DPD loop in green sticks (right). **c** Pulldown of wild-type  $\beta$ -arr2 but not  $\beta$ -arr2 $\Delta$ SIM mutant by SUMO1- or SUMO2-agarose beads.

involvement in the coordination of  $\beta$ -arr2 nucleocytoplasmic trafficking. HeLa cells were transfected with YFP-tagged forms of wild-type  $\beta$ -arr2, SUMOylation mutant ( $\beta$ -arr2K295R) or SIM mutant ( $\beta$ -arr2 $\Delta$ SIM) (Fig. 4a). The cells were then incubated with vehicle or LMB, a drug that specifically inhibits nuclear export of proteins containing leucine-rich NES through inactivation of CRM1/exportin1 [25]. All fusions demonstrated a cytoplasmic distribution at steady state (Fig. 4b). As expected, a 1-h incubation with LMB elicited wild-type  $\beta$ -arr2 nuclear accumulation (Fig. 4b);  $\beta$ -arr2K295R also accumulated in the nucleus in the presence of LMB, demonstrating that SUMOylation on K295 is not required for nuclear import. In contrast, the  $\beta$ -arr2 $\Delta$ SIM mutant failed to accumulate in the nucleus suggesting a default in its nuclear import. Similar results were obtained with non-tagged  $\beta$ -arr2 $\Delta$ SIM, FLAG-tagged



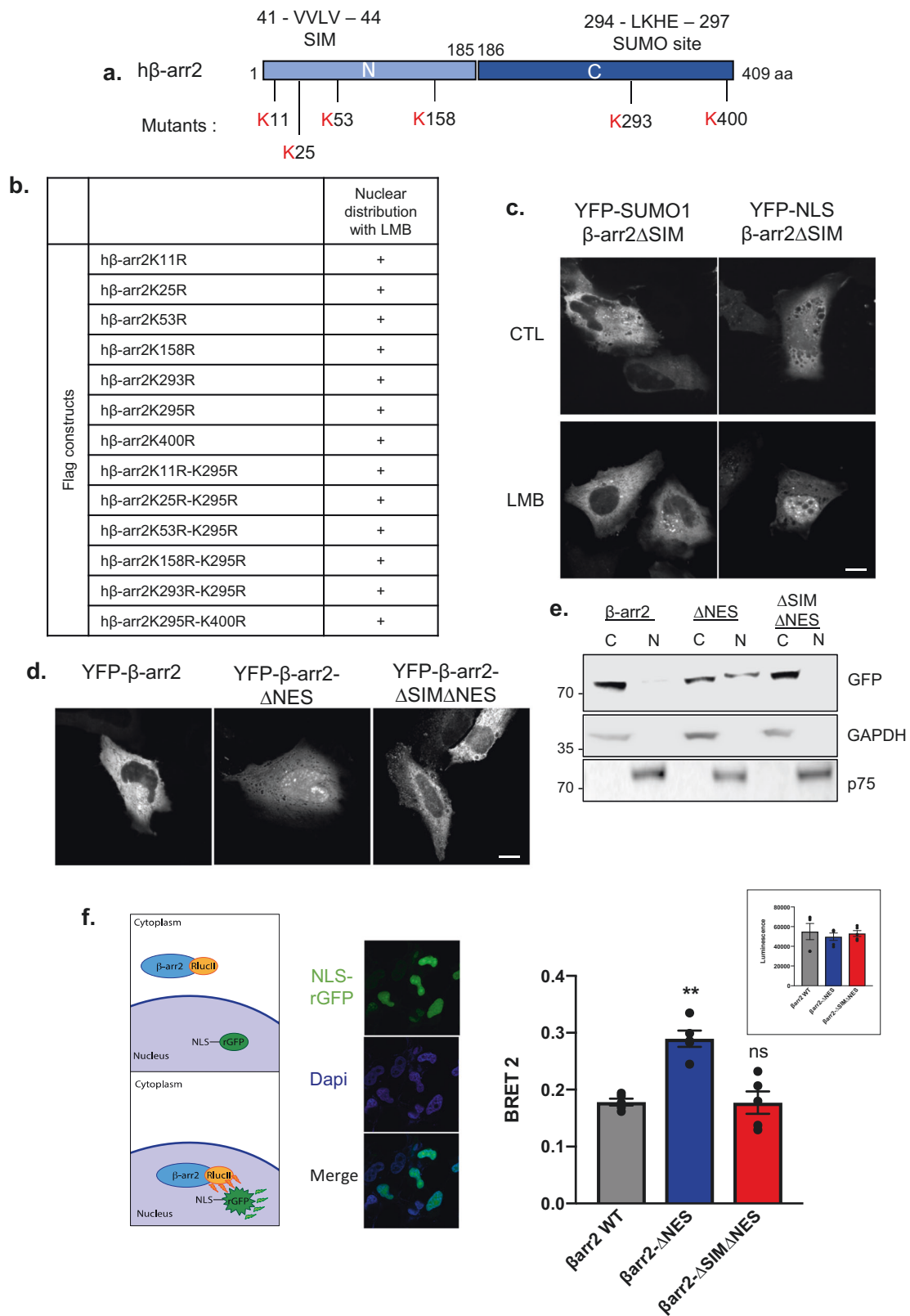
**Fig. 4 The SIM but not SUMOylation on lysine 295 is required for  $\beta$ -arr2 nuclear entry.**

**a** Schematic diagram showing the SIM and K295 SUMOylation site in  $\beta$ -arr2. The SIM was mutated from 41-VVLV-44 to 41-AALA-44 and the SUMOylation site changed from 294-LKHE-297 to 294-LRHE-297. **b** HeLa cells transfected with YFP-tagged  $\beta$ -arr2 wild type,  $\beta$ -arr2K295R, or  $\beta$ -arr2 $\Delta$ SIM were incubated with methanol control (CTL) or 20 nM LMB for 60 min at 37 °C, then fixed and processed for confocal fluorescence microscopy. Representative images are shown. **c** Direct visualization of YFP- $\beta$ -arr2 WT or YFP- $\beta$ -arr2 $\Delta$ SIM nuclear accumulation in live HeLa cells in the presence of 20 nM LMB for 60 min. Images were acquired using a spinning disk confocal microscope equipped with a 37 °C heated control chamber. Images acquired every 15 min are displayed. **d** Quantification of  $\beta$ -arr2 WT or  $\beta$ -arr2 $\Delta$ SIM nuclear accumulation in the presence of LMB in live cells. Fluorescence intensity was quantified using the previously described ImageJ plugin [47] and values were plotted as a percentage of maximal WT response. Data represent mean  $\pm$  SEM ( $n = 10$ ; \*\*\* $P < 0.001$ ). Scale bars, 10  $\mu$ m.



$\beta$ -arr2 $\Delta$ SIM, and mCherry-tagged  $\beta$ -arr2 $\Delta$ SIM (Fig. S3). Live cell imaging in cells transfected with YFP-tagged forms of  $\beta$ -arr2 corroborated results obtained in fixed cells:  $\beta$ -arr2 progressively accumulated in the nucleus during LMB incubation, whereas  $\beta$ -arr2 $\Delta$ SIM did not (Fig. 4c, d), confirming that this mutant presents a defect in nuclear import. Despite this defect in nuclear import, control endocytosis experiments showed that  $\beta$ -arr2 $\Delta$ SIM is still functional as it was able to promote internalization of the GPCR V2 vasopressin receptor (Fig. S4a, b).

SIMs can promote *in cis* SUMOylation of protein targets and this can occur on lysine residues that do not lie in strict consensus SUMOylation sequences [17]. To rule out that potential additional minor SUMOylation on a secondary lysine in  $\beta$ -arr2 could contribute to nuclear import the  $\beta$ -arr2 primary sequence was analyzed using the JASSA program [24]. In addition to the major K295 site, K11, K25, K53, K158, K293, and K400 were predicted as potential SUMOylation conjugation sites (Fig. 5a). We mutated these lysine residues to arginine either individually, or in



combination with the K295R mutation, and tested their impact on nuclear import by incubating HeLa cells expressing the mutant forms of  $\beta$ -arr2 with LMB for 1 h. All

mutants accumulated in the nucleus, like K295R, ruling out the possibility that they are implicated in nuclear import (Figs. 5a, b and S5). Finally, we also created a SUMO1-



◀ **Fig. 5 SUMO1 fusion to  $\beta$ -arr2 $\Delta$ SIM does not rescue nuclear import but an NLS fusion does.** **a** Schematic diagram showing other potential SUMOylation sites predicted by JASSA. **b** HeLa cells were transfected with the indicated constructs and incubated with 20 nM LMB for 60 min. Accumulation of the various fusions in the nucleus is indicated. **c** HeLa cells transfected with plasmids encoding YFP-SUMO1- $\beta$ -arr2 $\Delta$ SIM or YFP-NLS- $\beta$ -arr2 $\Delta$ SIM were incubated with methanol (vehicle control) or 20 nM LMB during 1 h at 37 °C, then fixed and processed for fluorescence microscopy. **d** HeLa cells transfected with plasmids encoding YFP- $\beta$ -arr2, YFP- $\beta$ -arr2 $\Delta$ NES, or YFP- $\beta$ -arr2 $\Delta$ SIM $\Delta$ NES were subsequently fixed and processed for fluorescence microscopy. All cells were visualized on a confocal microscope. Representative images of all conditions are shown. Scale bars, 10  $\mu$ m. **e** Nuclear and cytoplasmic fractions of HeLa cells, transfected with plasmids encoding YFP- $\beta$ -arr2, YFP- $\beta$ -arr2 $\Delta$ NES, or YFP- $\beta$ -arr2 $\Delta$ SIM $\Delta$ NES, were prepared. The fractions were analyzed by western blot. GAPDH was used as a cytoplasmic marker and p75 as a nuclear marker. **f** Schematic representation of the ebBRET system. The RlucII donor is fused to  $\beta$ -arr2, and the rGFP acceptor to a nuclear localization signal (NLS), to target it to the nucleus (see fluorescence panels). Changes in BRET signals indicate changes in nuclear accumulation. HEK-293 cells transfected with plasmids encoding  $\beta$ -arr2-RlucII,  $\beta$ -arr2- $\Delta$ NES-RlucII, or  $\beta$ -arr2- $\Delta$ SIM $\Delta$ NES-RlucII and rGFP-NLS were used to monitor relative  $\beta$ -arrestin2 nuclear localization by ebBRET. The inset shows equivalent expression of the different forms of  $\beta$ -arr2-RucII. Data represent mean  $\pm$  SEM ( $n = 5$ ;  $**P < 0.01$ , ns: nonsignificant).

$\beta$ -arr2 $\Delta$ SIM fusion tagged with YFP, to determine if SUMO fused to  $\beta$ -arr2 $\Delta$ SIM could promote nuclear import. In the presence of LMB this fusion also failed to accumulate in the nucleus, in contrast to a fusion of  $\beta$ -arr2 with the nuclear localization signal (NLS) of SV40, which was able to rescue  $\beta$ -arr2 $\Delta$ SIM nuclear import (Fig. 5c). We next tested the effect of the  $\beta$ -arr2 $\Delta$ SIM mutation in a context where nuclear export of  $\beta$ -arr2 is inhibited through mutation of its NES (L394A). As expected YFP- $\beta$ -arr2 $\Delta$ NES strongly accumulated in the nucleus, however, the  $\Delta$ SIM $\Delta$ NES mutant did not, again confirming the importance of the  $\beta$ -arr2 SIM in nuclear import (Fig. 5d). Similar results were obtained with fractionation experiments, showing marked enrichment of YFP- $\beta$ -arr2 $\Delta$ NES in the nuclear fraction, whereas YFP- $\beta$ -arr2 $\Delta$ SIM $\Delta$ NES, like wild-type  $\beta$ -arr2, was not (Fig. 5e). We also used enhanced bystander bioluminescence resonance energy transfer (ebBRET), based on energy transfer between the naturally occurring chromophores luciferase (Rluc) and green fluorescent protein (rGFP) from Renilla [26] to monitor nuclear accumulation of  $\beta$ -arr2. For this, rGFP was targeted to the nucleus through fusion of an NLS (rGFP-NLS) and relative nuclear residency of Rluc- $\beta$ -arr2 fusions was assessed by their ability to generate BRET signals (Fig. 5f). Rluc- $\beta$ -arr2 $\Delta$ NES generated a stronger BRET signal compared to wild type in agreement with its expected nuclear localization (Fig. 5f). The  $\Delta$ SIM $\Delta$ NES mutant displayed a marked decrease in BRET compared to  $\Delta$ NES indicating reduced nuclear accumulation.

## The RanBP2/RanGAP1-SUMO complex gates $\beta$ -arr2 nuclear entry

The above results indicate that whereas SUMOylation is not required for  $\beta$ -arr2 nuclear import, a non-covalent interaction of the  $\beta$ -arr2 SIM with a SUMOylated protein partner may contribute to its nuclear import. Interestingly, we found that  $\beta$ -arr2 associates with the nucleoporin RanBP2 and RanGAP1-SUMO1 (Fig. 6a), components of a multimolecular SUMO E3 ligase complex that resides on the cytoplasmic filaments of the nuclear pore complex. This complex is involved in substrate SUMOylation and acts as a hub for nucleocytoplasmic transport [27, 28]. RanBP2 is a 358-kDa protein that contains multiple domains including several FG repeats, four Ran-binding domains, and a region that interacts with RanGAP1 [29–32]. The interaction of RanGAP1 with RanBP2 requires RanGAP1 SUMOylation [29]. When the SIM in  $\beta$ -arr2 is mutated there is a marked reduction in coimmunoprecipitation of both RanGAP1-SUMO1 and RanBP2 with  $\beta$ -arr2, indicating the SIM is important for RanBP2 and RanGAP1-SUMO1 association with  $\beta$ -arr2 (Fig. 6a). To determine if RanBP2 may play a role in  $\beta$ -arr2 nuclear import, we subjected HeLa cells to RanBP2 siRNA treatment and subsequently transfected the cells with mCherry- $\beta$ -arr2 $\Delta$ NES. Both RanBP2 and RanGAP1-SUMO1 levels were significantly reduced compared to control cells (Fig. 6b) as previously observed [33]. Under these conditions Cherry- $\beta$ -arr2 $\Delta$ NES shifted from a nuclear to cytoplasmic distribution demonstrating that the RanBP2/RanGAP1-SUMO1 complex plays an important role in promoting  $\beta$ -arr2 nuclear import. These results indicate that the  $\beta$ -arr2 SIM targets  $\beta$ -arr2 to the RanBP2/RanGAP1-SUMO1 complex, which is involved in stimulation of  $\beta$ -arr2 nuclear entry.

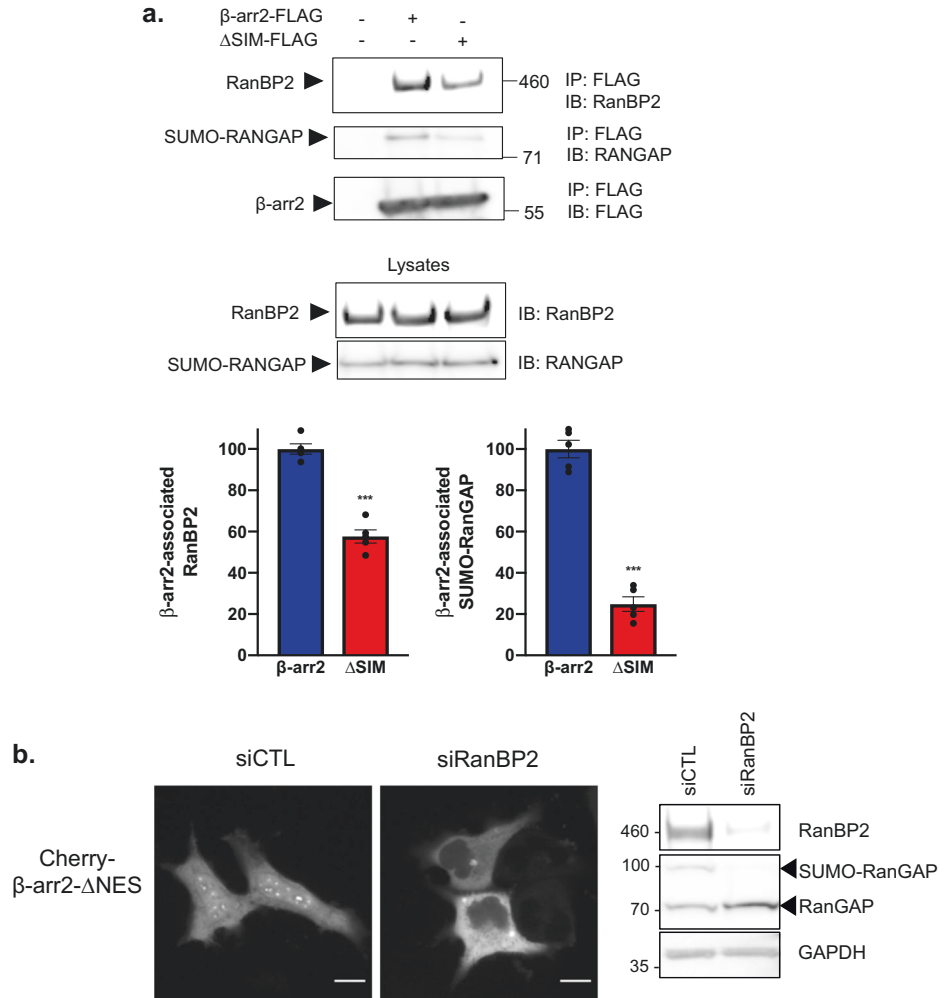
## Coordinated nuclear import and export of $\beta$ -arr2 regulates Mdm2 subcellular localization and p53 activity

The nucleocytoplasmic shuttling function of  $\beta$ -arr2 displaces nuclear binding cargoes from the nucleus to the cytoplasm. It was previously demonstrated that displacement of Mdm2, the major negative regulator of p53, from the nucleus to the cytoplasm results in increased p53 activity [7]. We anticipated that a functional SIM would be essential for Mdm2 displacement by  $\beta$ -arr2. In HEK-293 cells transfected with wild-type  $\beta$ -arr2, GFP-Mdm2 was displaced from the nucleus to the cytoplasm, unlike control cells, where GFP-Mdm2 remained nuclear (Fig. 7a, b). Quantification of Mdm2 displacement by  $\beta$ -arr2 demonstrated ~60% of Mdm2 cytoplasmic relocalization: in ~10% of cells Mdm2 was predominantly cytoplasmic and in ~50% partly cytoplasmic, in agreement with previous studies [7] (Fig. 7c). In the presence of  $\beta$ -arr2 $\Delta$ SIM, the distribution of Mdm2 was similar to control Cherry/Mdm2

**Fig. 6 The  $\beta$ -arr2 SIM enhances association with the RanBP2/RanGAP1-SUMO complex and RanBP2/RanGAP1-SUMO depletion inhibits  $\beta$ -arr2 nuclear entry.**

**a** Western blot of FLAG immunoprecipitates from HEK cells expressing  $\beta$ -arr2-FLAG or  $\beta$ -arr2 $\Delta$ SIM-FLAG showing reduced association of  $\beta$ -arr2 $\Delta$ SIM with RanGAP1-SUMO1 and RanBP2. Data shown represent the mean  $\pm$  SEM of five independent experiments (\*\* $P < 0.001$ ).

**b** HeLa cells were transfected with control siRNA or siRNA targeting RanBP2. Quantification of western blots demonstrated knockdown of  $85 \pm 1.6\%$  for RanBP2, and  $85 \pm 7.8\%$  for RanGAP-SUMO1 (mean  $\pm$  SEM,  $n = 4$ ). The cells were subsequently transfected with Cherry- $\beta$ -arr2 $\Delta$ NES and cytonuclear distribution visualized directly in live HeLa cells. Representative images are shown. Scale bars, 10  $\mu$ m.



expressing cells (Fig. 7a–c). This indicates that due to defective nuclear import,  $\beta$ -arr2 $\Delta$ SIM fails to displace Mdm2 from the nucleus to the cytosol. From a functional viewpoint with regard to Mdm2 displacement, the  $\beta$ -arr2 $\Delta$ SIM therefore behaves like the  $\beta$ -arr2 $\Delta$ NES mutant, which enters in the nucleus but cannot displace Mdm2 due to its defective nuclear export (Fig. 7a–c). The SUMOylation K295R mutant of  $\beta$ -arr2 was still able to displace Mdm2 in line with its normal capacity to shuttle through the nucleus (Fig. 7a–c). Therefore, the SIM in  $\beta$ -arr2, coupled with its nuclear export function, combine to regulate  $\beta$ -arr2 cytonuclear trafficking function with consequences for Mdm2 subcellular localization.

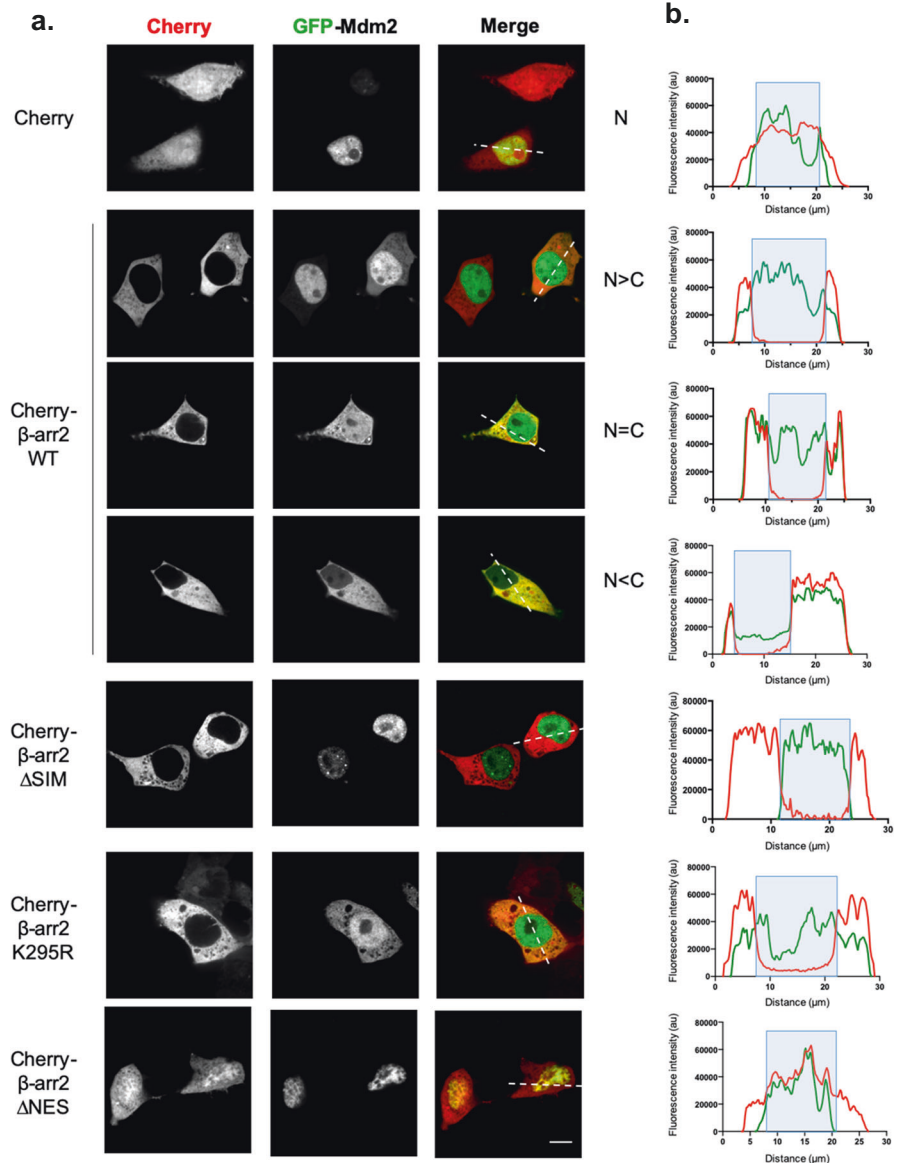
To determine functional consequences of the defect in cytonuclear shuttling found with  $\beta$ -arr2 $\Delta$ SIM on p53 signaling, we first used a H1299 non-small cell lung carcinoma cell line (p53-null) engineered to express p53 using the TETON system [34]. We confirmed that the  $\beta$ -arr2 $\Delta$ SIM defect in nuclear import was also found in these H1299-p53-TETON cells (Fig. 8a). We next transfected H1299-p53-TETON cells with a plasmid coding for luciferase under the control of multiple p53 response elements. As expected,

incubation of the cells with doxycycline, to induce p53 expression comparative to endogenous levels found in MCF-7 breast cancer cells carrying *TP53* (Fig. S6a), robustly stimulated the luciferase signal, which was markedly reduced by exogenous Mdm2 (Fig. 8b). When  $\beta$ -arr2 was co-transfected with Mdm2, there was a significant increase in p53-dependent luciferase activity compared to Mdm2 alone. However, with the  $\beta$ -arr2 $\Delta$ SIM mutant, which is defective in displacing Mdm2 to the cytoplasm (Fig. 7a–c), no significant increase in p53-dependent activity was observed. This indicates that  $\beta$ -arr2 $\Delta$ SIM failed to rescue Mdm2-mediated inhibition of p53 activity.

As an additional cancer cell model, we used MCF-7 cells with endogenous levels of  $\beta$ -arr2, SUMO1, SUMO2, Ubc9, RanBP2, SUMO-RanGAP, Mdm2, and p53 (Fig. S6b) to investigate the effect of  $\beta$ -arr2 $\Delta$ SIM versus wild-type  $\beta$ -arr2 on p53 signaling. We observed a similar defect in  $\beta$ -arr2 $\Delta$ SIM nuclear import in MCF-7 cells (Fig. 8c), to that documented in HeLa, HEK, and H1299-p53-TETON cells. Finally, we performed p53-dependent gene reporter experiments in MCF-7 cells. An enhancing effect on

**Fig. 7 A functional SIM domain is required for  $\beta$ -arr2-mediated cytoplasmic delocalization of Mdm2.**

**a** HEK cells expressing mCherry, mCherry- $\beta$ -arr2, mCherry- $\beta$ -arr2 $\Delta$ SIM, mCherry- $\beta$ -arr2K295R, or mCherry- $\beta$ -arr2 $\Delta$ NES (left column) and GFP-Mdm2 constructs (middle column) were imaged using a spinning disk confocal microscope. Merged images are shown in the right column. Scale bar, 10  $\mu$ m. **b** Line traces generated in ImageJ of the corresponding traces (white dotted lines) in the merged images shown in (a) with Cherry and GFP intensities displayed in red and green, respectively. The blue area defines the nuclear area. **c** Manual quantification of nuclear (N), cytoplasmic (C), or partially displaced Mdm2 localization (N/C). Bars indicate the percentage of cells in each category. Over 100 cells were quantified for each experimental condition (\*\* $P < 0.01$ , \*\*\* $P < 0.001$ , ns: nonsignificant).



p53 signaling by wild-type Rluc-tagged  $\beta$ -arr2, expressed at comparative levels to endogenous  $\beta$ -arr2 (Fig. S6c), was observed (Fig. 8d) and this effect was lost with  $\beta$ -arr2 $\Delta$ SIM.

Taken together, the above data therefore demonstrate the importance of the SIM in  $\beta$ -arr2 for enhancing p53 function in different cancer cell types.

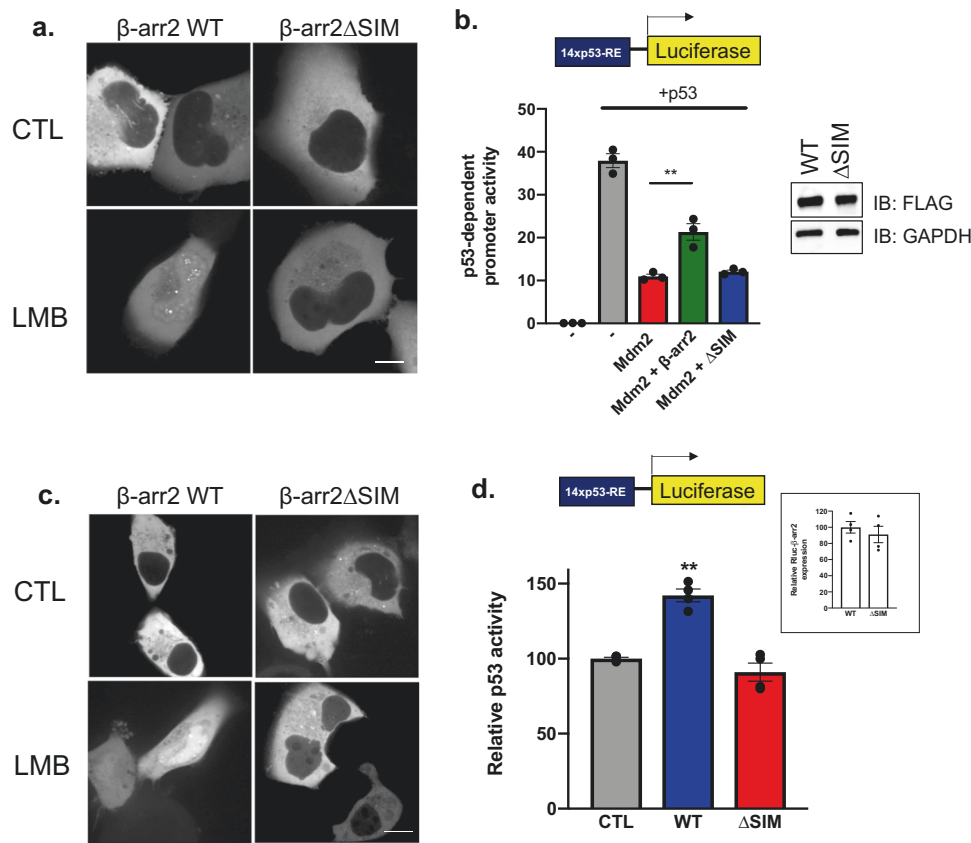


**Fig. 8 The  $\beta$ -arr2 SIM domain is required for increased p53 signaling.** **a** H1299 cells expressing YFP- $\beta$ -arr2 or YFP- $\beta$ -arr2 $\Delta$ SIM were treated with methanol control (CTL) or 20 nM LMB for 60 min and live cells were imaged directly using a spinning disk confocal microscope. Scale bar, 10  $\mu$ m. **b** H1299-p53-TETON cells were stimulated with 100 ng/ml doxycycline to induce p53 expression (+p53) and subsequently transfected with 14xp53-RE-luc and control pRL.TK, in addition to the indicated combinations of empty vector (-), Mdm2, and  $\beta$ -arr2/ $\beta$ -arr2 $\Delta$ SIM plasmids. Promoter activity driven by p53 is expressed as a ratio of firefly luciferase:Renilla luciferase

activity. Equivalent expression of  $\beta$ -arr2 and  $\beta$ -arr2- $\Delta$ SIM is shown in the western blot inset. Data are expressed as mean  $\pm$  SEM,  $n = 3$ ; \*\* $P < 0.01$ . **c** MCF-7 cells expressing Cherry- $\beta$ -arr2 or Cherry- $\beta$ -arr2 $\Delta$ SIM were treated with methanol control (CTL) or 20 nM LMB for 60 min and live cells were directly imaged using a spinning disk confocal microscope. Scale bar, 10  $\mu$ m. **d** MCF-7 cells were transfected with 14xp53-RE-luc and either empty vector, Rluc- $\beta$ -arr2 or Rluc- $\beta$ -arr2 $\Delta$ SIM. Equivalent luciferase expression of Rluc- $\beta$ -arr2 or Rluc- $\beta$ -arr2 $\Delta$ SIM is shown in the inset. Data are expressed as mean  $\pm$  SEM,  $n = 4$ ; \*\* $P < 0.01$ .

## Discussion

Mdm2 is the principal negative regulator of p53. Investigating mechanisms underlying Mdm2 regulation is therefore important in understanding p53 biology.  $\beta$ -arr2 nucleocytoplasmic shuttling serves to titrate Mdm2 from the nucleus to the cytoplasm to enhance p53 signaling [7]. Under steady-state conditions this is a receptor-independent signaling mode of  $\beta$ -arr2. While the active nuclear export mechanism of  $\beta$ -arr2, due to the presence of a NES in its C-terminal tail, has been well characterized [9, 14], the mechanism(s) involved in its nuclear import are not completely elucidated. Previous studies have suggested that the N-domain is likely to play an important role in  $\beta$ -arr2 nuclear import [9, 14]. Here, we demonstrate that SUMO orchestrates  $\beta$ -arr2 cytonuclear traffic. Whereas  $\beta$ -arr2 SUMOylation is not required for  $\beta$ -arr2 nuclear import, a

SIM in the N-terminus of  $\beta$ -arr2 is involved in its nuclear import. Mutation of the SIM inhibits  $\beta$ -arr2 association with the RanBP2/RanGAP1-SUMO1 nucleocytoplasmic transport hub, and  $\beta$ -arr2 nuclear import. As a consequence, the ability of  $\beta$ -arr2 to titrate Mdm2 from the nucleus to the cytoplasm and effect on p53 signaling is impaired. Our data therefore unveil that a SUMO-SIM nuclear entry checkpoint, coupled with the nuclear export function of  $\beta$ -arr2, regulates its cytonuclear trafficking function to control the Mdm2-p53 loop.

We confirmed that K295 is a major SUMOylation site in human  $\beta$ -arr2. Previous studies of  $\beta$ -arr2 SUMOylation have shown that bovine  $\beta$ -arr2 is SUMOylated on both lysines K295 and K400 but that K400 represents the main SUMOylation site in this species [15]. Inhibition of bovine  $\beta$ -arr2 SUMOylation decreased its association with the endocytic partner  $\beta$ 2-adaptin and attenuated  $\beta$ 2-AR



endocytosis [15]. These data suggest that  $\beta$ -arr2 SUMOylation enhances its binding to  $\beta$ 2-adaptin to promote the canonical function of  $\beta$ -arr2 in GPCR endocytosis. Alignment of the bovine and human sequences around K400, however, demonstrates that the human sequence does not fit a strict consensus SUMOylation site here. A subsequent study using human  $\beta$ -arr2 demonstrated that, in contrast to bovine  $\beta$ -arr2, the main SUMOylation site resides at K295 [16]. SUMOylation on this site was found to inhibit  $\beta$ -arr2 binding to TRAF6, permitting enhanced TRAF6 oligomerization and autoubiquitination, and promoting TRAF6-mediated NF- $\kappa$ B signaling [16]. Our results therefore agree with the study on human  $\beta$ -arr2 and confirm K295 as a main SUMOylation site. We found that SUMOylation of  $\beta$ -arr2, however, was not essential for its nuclear import. This finding does not, however, rule out potential intranuclear roles for  $\beta$ -arr2 SUMOylation.

We also identified and characterized a SIM in the N-terminal domain of  $\beta$ -arr2 that we found was required for nuclear delivery. Similar to the role for the  $\beta$ -arr2 SIM in promoting nuclear delivery, SIMs have also been proposed to participate in the nuclear import/accumulation of several other proteins to date. These include the vaccinia virus protein E3 [35], the Epstein–Barr virus protein kinase BGLF4 [36], the viral restriction factor TRIM5 $\alpha$  [37], and the MAPK p38 [38]. This suggests that SIM-SUMO mediated transport may be a wider phenomenon involved in nuclear delivery of protein cargoes. SIMs promote recruitment/targeting of SIM-containing proteins to SUMOylated partners. For example, the transcriptional corepressor Daxx contains a SIM that is crucial for subnuclear targeting of Daxx to PML oncogenic domains and for the transrepression of several SUMOylated transcription factors [17, 39]. Our results point toward a targeting role of the SIM in  $\beta$ -arr2 to RanBP2/RanGAP-SUMO1, which forms part of a SUMO E3 ligase complex, localized at the cytoplasmic nuclear pore complex [40]. It is involved in the SUMOylation of certain substrates including Ran-GDP [27] and provides a hub for nucleocytoplasmic transport [28]. A study investigating a nuclear import enhancement role by RanBP2 analyzed the distribution of ~200 nuclear proteins following RanBP2 depletion [28]. The vast majority did not change subcellular distribution upon RanBP2 depletion, but around 5% were clearly affected, demonstrating cytoplasmic accumulation due to defective nuclear import. RanBP2 can therefore act as a platform for nuclear import for a subset of import cargoes [28]. Our results demonstrating cytoplasmic accumulation of  $\beta$ -arr2 $\Delta$ NES following RanBP2 depletion clearly indicate that this nucleoporin is required for  $\beta$ -arr2 nuclear entry. It was proposed that RanBP2 can enhance nuclear import by at least two mechanisms. First, it reduces the active concentration of import receptors required for efficient transport [41, 42] and

second, import receptor-independent interaction of selected cargoes with RanBP2 can increase efficiency of nuclear import [28]. This suggests that  $\beta$ -arr2 nuclear import probably involves multiple steps coordinated by RanBP2. Indeed, a recent study identified a NLS in  $\beta$ -arr2 and importin  $\beta$ 1-dependent nuclear import [43]. This suggests that  $\beta$ -arr2 has dual nuclear entry signals similar to what has been documented with the nuclear protease Calpain 5 [44]. RanBP2 serves as a binding site for importin  $\beta$ 1 keeping the transport receptor in association with the nuclear pore complex. RanBP2 therefore likely acts as a hub to coordinate spatiotemporal regulation of  $\beta$ -arr2 nuclear import occurring through dual nuclear entry motifs. In summary, our findings demonstrate that the  $\beta$ -arr2 SIM targets it to the RanBP2/RanGAP-SUMO1 complex, which gates  $\beta$ -arr2 nuclear entry.

As mutation of the SIM inhibits  $\beta$ -arr2 nuclear import, its ability to delocalize Mdm2 from the nucleus to the cytoplasm and effect on enhanced p53 signaling is impaired. The  $\Delta$ SIM mutant therefore gives rise to the same impaired p53 signaling effect as the  $\Delta$ NES mutant, which also fails to displace Mdm2 from the nucleus [7]. Our results uncovering the critical role of a  $\beta$ -arr2 SIM in its nuclear entry, coupled with the previously characterized export mechanism, generate an emerging picture of regulatory nodes that impact receptor-independent  $\beta$ -arr2-mediated control of the Mdm2/p53 axis. Future studies will be required to determine if  $\beta$ -arr2 cytonuclear shuttling function is altered in cancer settings.

## Materials and methods

### Reagents, plasmids, and antibodies

A full list of reagents, plasmids, and antibodies is provided in the Supplementary Materials and Methods section.

### Cell culture and transfection

Cell culture and transfection conditions are provided in the Supplementary Materials and Methods section.

### His-tagged protein purification using Ni-NTA beads

Assay conditions for His-tagged protein purification are provided in the Supplementary Materials and Methods section.

### SUMO beads pulldown assay

For isolation and enrichment of SUMO interacting proteins, SUMO agarose beads from ENZO were used. Assay

conditions are provided in the Supplementary Materials and Methods section.

### SPOT synthesis of peptides

A peptide library of overlapping 25-mers, that scan the entire human  $\beta$ -arr2 sequence, was produced by automatic SPOT synthesis and synthesized on continuous cellulose membrane supports on Whatman 50 cellulose membranes using Fmoc (fluoren-9-ylmethoxycarbonyl) chemistry with the AutoSpot-Robot ASS 222 (Intavis Bioanalytical Instruments), as described previously [45].

### In vitro SUMOylation on $\beta$ -arr2 peptide arrays

A SUMOylation kit (Biomol) was used according to the manufacturer's instructions for the SUMOylation of putative SUMO sites contained within the  $\beta$ -arr2 peptide array [46]. The SUMO assay mix was incubated with array membranes at 30 °C with shaking. Membranes were washed with TBS-T (Tris-buffered saline with Tween 20: 137 mM NaCl, 20 mM Tris/HCl, pH7.6, and 0.1% Tween 20) followed by probing the SUMOylated moieties on the peptide array using an anti-SUMO antibody. Control arrays were performed using SUMO assay mixtures that omitted the E2 conjugase Ubc9.

### Coimmunoprecipitation

HEK cells were transiently transfected with plasmids as indicated in the figure legends and following lysis subjected to coimmunoprecipitation as detailed in the Supplementary Materials and Methods section.

### Live cell imaging and Immunofluorescence

Live cell imaging and immunofluorescence experiments were conducted as previously described [47]. Details are provided in the Supplementary Materials and Methods section.

### Flow cytometry

The details of the flow cytometry assay used to monitor  $\beta$ -arr2-dependent endocytosis of HA-V2R-vYFP have been described previously [48]. Details are provided in the Supplementary Materials and Methods section.

### Cytoplasmic and nuclear fractionation

Cytoplasmic and nuclear extracts were prepared from HeLa cells using the Invent Biotechnologies Minute<sup>TM</sup> fractionation kit according to the manufacturer's instructions.

### Enhanced bystander bioluminescence resonance energy transfer (ebBRET)

Endocytosis and nuclear localization ebBRET assays were performed in HEK cells and are described in the Supplementary Materials and Methods section.

### Gene reporter experiments

H1299-p53-TETON cells and MCF-7 cells were co-transfected with p53-luc (Stratagene), containing 14xp53-response elements, and either pRL.TK (H1299 cells) or Rluc-tagged forms of  $\beta$ -arr2 (MCF-7 cells) using Lipo3000 in 12-well plates. Cells were lysed using passive lysis buffer (Promega) and both firefly and Renilla luciferase activities detected using the Dual-Luciferase Reporter Assay System (Promega).

### Molecular modeling

The 3D structure used for  $\beta$ -arr2 is PDB:3P2D. Figures were prepared with PyMol Molecular Graphics System, Version 2.0 Schrödinger, LLC.

### Data analysis and statistics

Data are represented as mean  $\pm$  SEM. Statistical analysis was performed using GraphPad Prism using unpaired *t*-tests or one-way analysis of variance with Tukey's post hoc test.

**Acknowledgements** We thank Dr. A. Benmerah for helpful discussion, Dr. J. Liotard for excellent technical assistance, and the Institut Cochin Imaging (IMAG'IC) and Sequencing platforms (GENOM'IC). The Institut Cochin lab is part of the Who am I? laboratory of excellence (grant ANR-11-LABX-0071), funded by the "Investments for the Future" program operated by The French National Research Agency (grant ANR-11-IDEX-0005-01). This work was funded by grants from the Fondation ARC pour la Recherche sur le Cancer ("Projet ARC" to MGHS), Ligue contre le Cancer (to MGHS), Royal Society ("International Joint Project Scheme" to MGHS and GSB), France Canada Research Fund (to MGHS and SA), CNRS, and INSERM. The work in the laboratory of M.B. was supported by a CIHR Foundation (FDN148431) grant. M.B. holds the Canada Research Chair in Signal transduction and Molecular Pharmacology. EBT was funded by MESR and Fondation ARC pour la Recherche sur le Cancer doctoral fellowships.

**Author contributions** EBT, ML, BS, JSP, GSB, HE, MB, SA, SM, and MGHS designed research. EBT, ML, JSP, BS, MK, KS, JF, AP, and MGHS performed research. EBT, ML, BS, JSP, CA, ELF, AZ, LG, GSB, HE, MB, SA, SM, and MGHS analyzed data. MGHS supervised the project. EBT and MGHS wrote the paper, which was subsequently reviewed by all other authors.

### Compliance with ethical standards

**Conflict of interest** The authors declare no competing interests.

**Publisher's note** Springer Nature remains neutral with regard to jurisdictional claims in published maps and institutional affiliations.

## References

- Enslin H, Lima-Fernandes E, Scott MG. Arrestins as regulatory hubs in cancer signalling pathways. *Handb Exp Pharmacol*. 2014;219:405–25.
- Laporte SA, Scott MGH. beta-Arrestins: multitask scaffolds orchestrating the where and when in cell signalling. *Methods Mol Biol*. 2019;1957:9–55.
- Peterson YK, Luttrell LM. The diverse roles of arrestin scaffolds in G protein-coupled receptor signaling. *Pharmacol Rev*. 2017;69:256–97.
- Luttrell LM, Roudabush FL, Choy EW, Miller WE, Field ME, Pierce KL, et al. Activation and targeting of extracellular signal-regulated kinases by beta-arrestin scaffolds. *Proc Natl Acad Sci USA*. 2001;98:2449–54.
- Luttrell LM, Wang J, Plouffe B, Smith JS, Yamani L, Kaur S, et al. Manifold roles of beta-arrestins in GPCR signaling elucidated with siRNA and CRISPR/Cas9. *Sci Signal*. 2018;11:eaat7650.
- McDonald PH, Chow CW, Miller WE, Laporte SA, Field ME, Lin FT, et al. Beta-arrestin 2: a receptor-regulated MAPK scaffold for the activation of JNK3. *Science*. 2000;290:1574–7.
- Boullaran C, Scott MG, Bourougaa K, Bellal M, Esteve E, Thuret A, et al. beta-arrestin 2 oligomerization controls the Mdm2-dependent inhibition of p53. *Proc Natl Acad Sci USA*. 2007;104:18061–6.
- Shenoy SK, McDonald PH, Kohout TA, Lefkowitz RJ. Regulation of receptor fate by ubiquitination of activated beta 2-adrenergic receptor and beta-arrestin. *Science*. 2001;294:1307–13.
- Wang P, Wu Y, Ge X, Ma L, Pei G. Subcellular localization of beta-arrestins is determined by their intact N domain and the nuclear export signal at the C terminus. *J Biol Chem*. 2003;278:11648–53.
- Javadi A, Deevi RK, Evergren E, Blondel-Tepaz E, Baillie GS, Scott MG, et al. PTEN controls glandular morphogenesis through a juxtamembrane beta-Arrestin1/ARHGAP21 scaffolding complex. *Elife*. 2017;6:e24578.
- Lima-Fernandes E, Enslin H, Camand E, Kotelevets L, Boullaran C, Achour L, et al. Distinct functional outputs of PTEN signalling are controlled by dynamic association with beta-arrestins. *EMBO J*. 2011;30:2557–68.
- Lima-Fernandes E, Misticone S, Boullaran C, Paradis JS, Enslin H, Roux PP, et al. A biosensor to monitor dynamic regulation and function of tumour suppressor PTEN in living cells. *Nat Commun*. 2014;5:4431.
- Alexander RA, Lot I, Saha K, Abadie G, Lambert M, Decosta E, et al. Beta-arrestins operate an on/off control switch for focal adhesion kinase activity. *Cell Mol Life Sci*. 2020;77:5259–79.
- Scott MG, Le Rouzic E, Perianin A, Pierotti V, Enslin H, Benichou S, et al. Differential nucleocytoplasmic shuttling of beta-arrestins. Characterization of a leucine-rich nuclear export signal in beta-arrestin2. *J Biol Chem*. 2002;277:37693–701.
- Wyatt D, Malik R, Vesecky AC, Marchese A. Small ubiquitin-like modifier modification of arrestin-3 regulates receptor trafficking. *J Biol Chem*. 2011;286:3884–93.
- Xiao N, Li H, Mei W, Cheng J. SUMOylation attenuates human beta-arrestin 2 inhibition of IL-1R/TRAF6 signaling. *J Biol Chem*. 2015;290:1927–35.
- Flotho A, Melchior F. Sumoylation: a regulatory protein modification in health and disease. *Annu Rev Biochem*. 2013;82:357–85.
- Geiss-Friedlander R, Melchior F. Concepts in sumoylation: a decade on. *Nat Rev Mol Cell Biol*. 2007;8:947–56.
- Hay RT. SUMO: a history of modification. *Mol Cell*. 2005;18:1–12.
- Rodriguez MS, Dargemont C, Hay RT. SUMO-1 conjugation in vivo requires both a consensus modification motif and nuclear targeting. *J Biol Chem*. 2001;276:12654–9.
- Guo D, Li M, Zhang Y, Yang P, Eckenrode S, Hopkins D, et al. A functional variant of SUMO4, a new I kappa B alpha modifier, is associated with type 1 diabetes. *Nat Genet*. 2004;36:837–41.
- Kerscher O. SUMO junction-what's your function? New insights through SUMO-interacting motifs. *EMBO Rep*. 2007;8:550–5.
- Jakobs A, Koehnke J, Himstedt F, Funk M, Korn B, Gaestel M, et al. Ubc9 fusion-directed SUMOylation (UFDS): a method to analyze function of protein SUMOylation. *Nat Methods*. 2007;4:245–50.
- Beauclair G, Bridier-Nahmias A, Zagury JF, Saib A, Zamborlini A. JASSA: a comprehensive tool for prediction of SUMOylation sites and SIMs. *Bioinformatics*. 2015;31:3483–91.
- Kudo N, Matsumori N, Taoka H, Fujiwara D, Schreiner EP, Wolff B, et al. Leptomycin B inactivates CRM1/exportin 1 by covalent modification at a cysteine residue in the central conserved region. *Proc Natl Acad Sci USA*. 1999;96:9112–7.
- Namkung Y, Le Gouill C, Lukashova V, Kobayashi H, Hogue M, Khoury E, et al. Monitoring G protein-coupled receptor and beta-arrestin trafficking in live cells using enhanced bystander BRET. *Nat Commun*. 2016;7:12178.
- Sakin V, Richter SM, Hsiao HH, Urlaub H, Melchior F. Sumoylation of the GTPase Ran by the RanBP2 SUMO E3 Ligase Complex. *J Biol Chem*. 2015;290:23589–602.
- Walde S, Thakar K, Hutten S, Spillner C, Nath A, Rothbauer U, et al. The nucleoporin Nup358/RanBP2 promotes nuclear import in a cargo- and transport receptor-specific manner. *Traffic*. 2012;13:218–33.
- Mahajan R, Delphin C, Guan T, Gerace L, Melchior F. A small ubiquitin-related polypeptide involved in targeting RanGAP1 to nuclear pore complex protein RanBP2. *Cell*. 1997;88:97–107.
- Matunis MJ, Wu J, Blobel G. SUMO-1 modification and its role in targeting the Ran GTPase-activating protein, RanGAP1, to the nuclear pore complex. *J Cell Biol*. 1998;140:499–509.
- Wu J, Matunis MJ, Kraemer D, Blobel G, Coutavas E. Nup358, a cytoplasmically exposed nucleoporin with peptide repeats, Ran-GTP binding sites, zinc fingers, a cyclophilin A homologous domain, and a leucine-rich region. *J Biol Chem*. 1995;270:14209–13.
- Yokoyama N, Hayashi N, Seki T, Pante N, Ohba T, Nishii K, et al. A giant nucleopore protein that binds Ran/TC4. *Nature*. 1995;376:184–8.
- Hashizume C, Kobayashi A, Wong RW. Down-modulation of nucleoporin RanBP2/Nup358 impaired chromosomal alignment and induced mitotic catastrophe. *Cell Death Dis*. 2013;4:e854.
- Monteith JA, Mellert H, Sammons MA, Kuswanto LA, Sykes SM, Resnick-Silverman L, et al. A rare DNA contact mutation in cancer confers p53 gain-of-function and tumor cell survival via TNFAIP8 induction. *Mol Oncol*. 2016;10:1207–20.
- Gonzalez-Santamaria J, Campagna M, Garcia MA, Marcos-Villar L, Gonzalez D, Gallego P, et al. Regulation of vaccinia virus E3 protein by small ubiquitin-like modifier proteins. *J Virol*. 2011;85:12890–900.
- Li R, Wang L, Liao G, Guzzo CM, Matunis MJ, Zhu H, et al. SUMO binding by the Epstein-Barr virus protein kinase BGLF4 is crucial for BGLF4 function. *J Virol*. 2012;86:5412–21.
- Brandariz-Nunez A, Roa A, Valle-Casuso JC, Biris N, Ivanov D, Diaz-Griffero F. Contribution of SUMO-interacting motifs and SUMOylation to the antiretroviral properties of TRIM5alpha. *Virology*. 2013;435:463–71.
- Wang PY, Hsu PI, Wu DC, Chen TC, Jarman AP, Powell LM, et al. SUMOs mediate the nuclear transfer of p38 and p-p38 during helicobacter pylori infection. *Int J Mol Sci*. 2018;19:2482

39. Lin DY, Huang YS, Jeng JC, Kuo HY, Chang CC, Chao TT, et al. Role of SUMO-interacting motif in Daxx SUMO modification, subnuclear localization, and repression of sumoylated transcription factors. *Mol Cell*. 2006;24:341–54.
40. Werner A, Flotho A, Melchior F. The RanBP2/RanGAP1\*-SUMO1/Ubc9 complex is a multisubunit SUMO E3 ligase. *Mol Cell*. 2012;46:287–98.
41. Hutten S, Flotho A, Melchior F, Kehlenbach RH. The Nup358-RanGAP complex is required for efficient importin  $\alpha$ /beta-dependent nuclear import. *Mol Biol Cell*. 2008;19:2300–10.
42. Hutten S, Walde S, Spillner C, Hauber J, Kehlenbach RH. The nuclear pore component Nup358 promotes transportin-dependent nuclear import. *J Cell Sci*. 2009;122:1100–10.
43. Zhang X, Min X, Wang S, Sun N, Kim KM. Mdm2-mediated ubiquitination of beta-arrestin2 in the nucleus occurs in a Gbetagamma- and clathrin-dependent manner. *Biochem Pharm*. 2020;178:114049.
44. Singh R, Brewer MK, Mashburn CB, Lou D, Bondada V, Graham B, et al. Calpain 5 is highly expressed in the central nervous system (CNS), carries dual nuclear localization signals, and is associated with nuclear promyelocytic leukemia protein bodies. *J Biol Chem*. 2014;289:19383–94.
45. Bolger GB, Baillie GS, Li X, Lynch MJ, Herzyk P, Mohamed A, et al. Scanning peptide array analyses identify overlapping binding sites for the signalling scaffold proteins, beta-arrestin and RACK1, in cAMP-specific phosphodiesterase PDE4D5. *Biochem J*. 2006;398:23–36.
46. Li X, Vadrevu S, Dunlop A, Day J, Advant N, Troeger J, et al. Selective SUMO modification of cAMP-specific phosphodiesterase-4D5 (PDE4D5) regulates the functional consequences of phosphorylation by PKA and ERK. *Biochem J*. 2010;428:55–65.
47. Blondel-Tepaz E, Guilbert T, Scott MGH. Methods to investigate the nucleocytoplasmic shuttling properties of beta-arrestins. *Methods Mol Biol*. 2019;1957:251–69.
48. Paradis JS, Ly S, Blondel-Tepaz E, Galan JA, Beautrait A, Scott MG, et al. Receptor sequestration in response to beta-arrestin-2 phosphorylation by ERK1/2 governs steady-state levels of GPCR cell-surface expression. *Proc Natl Acad Sci USA*. 2015;112:E5160–8.



# **Annex III: Computationally Designed GPCR Quaternary Structures Bias Signaling Pathway Activation**

# Computationally designed GPCR quaternary structures bias signaling pathway activation

Received: 16 March 2022

Accepted: 24 October 2022

Published online: 11 November 2022

 Check for updates


Justine S. Paradis<sup>1,2,7</sup>, Xiang Feng <sup>3,6,7</sup>, Brigitte Murat<sup>1,2</sup>, Robert E. Jefferson <sup>3</sup>, Badr Sokrat<sup>1,2</sup>, Martyna Szpakowska <sup>4</sup>, Mireille Hogue<sup>2</sup>, Nick D. Bergkamp<sup>5</sup>, Franziska M. Heydenreich<sup>1,2</sup>, Martine J. Smit <sup>5</sup>, Andy Chevigné <sup>4</sup>, Michel Bouvier <sup>1,2,8</sup>  & Patrick Barth <sup>3,8</sup> 

Communication across membranes controls critical cellular processes and is achieved by receptors translating extracellular signals into selective cytoplasmic responses. While receptor tertiary structures can be readily characterized, receptor associations into quaternary structures are challenging to study and their implications in signal transduction remain poorly understood. Here, we report a computational approach for predicting receptor self-associations, and designing receptor oligomers with various quaternary structures and signaling properties. Using this approach, we designed chemokine receptor CXCR4 dimers with reprogrammed binding interactions, conformations, and abilities to activate distinct intracellular signaling proteins. In agreement with our predictions, the designed CXCR4s dimerized through distinct conformations and displayed different quaternary structural changes upon activation. Consistent with the active state models, all engineered CXCR4 oligomers activated the G protein Gi, but only specific dimer structures also recruited  $\beta$ -arrestins. Overall, we demonstrate that quaternary structures represent an important unforeseen mechanism of receptor biased signaling and reveal the existence of a bias switch at the dimer interface of several G protein-coupled receptors including CXCR4,  $\mu$ -Opioid and type-2 Vasopressin receptors that selectively control the activation of G proteins vs  $\beta$ -arrestin-mediated pathways. The approach should prove useful for predicting and designing receptor associations to uncover and reprogram selective cellular signaling functions.

A wide range of membrane proteins, including single-pass receptor tyrosine kinases, cytokine receptors, and ion channels, functions through the folding and association of several polypeptide chains into specific quaternary structures. The functional role of oligomerization

in other membrane protein classes remains controversial as the observation of receptor associations is very sensitive to the experimental conditions and techniques<sup>1–4</sup>. Receptors from the largest class of G protein-coupled receptors (GPCRs) were often observed as

<sup>1</sup>Department of Biochemistry and Molecular Medicine, Université de Montréal, Montréal, QC H3T 1J4, Canada. <sup>2</sup>Institute for Research in Immunology and Cancer (IRIC), Université de Montréal, Montréal, QC H3T 1J4, Canada. <sup>3</sup>Interfaculty Institute of Bioengineering, Ecole Polytechnique Fédérale de Lausanne, Lausanne CH-1015, Switzerland. <sup>4</sup>Department of Infection and Immunity, Immuno-Pharmacology and Interactomics, Luxembourg Institute of Health, Esch-sur-Alzette, Luxembourg. <sup>5</sup>Amsterdam Institute for Molecules, Medicines and Systems (AIMMS), Division of Medicinal Chemistry, Faculty of Sciences, Vrije Universiteit, Amsterdam, The Netherlands. <sup>6</sup>Present address: Department of Structural Biology, Van Andel Institute, Grand Rapids, MI, USA. <sup>7</sup>These authors contributed equally: Justine S. Paradis, Xiang Feng. <sup>8</sup>These authors jointly supervised this work: Michel Bouvier, Patrick Barth.

 e-mail: [michel.bouvier@umontreal.ca](mailto:michel.bouvier@umontreal.ca); [patrick.barth@epfl.ch](mailto:patrick.barth@epfl.ch)

oligomers in electron microscopy, X-ray crystallography, and BRET studies<sup>5–11</sup>. However, when trapped as monomers in nanolipid disks, GPCRs, such as rhodopsin and  $\beta$ 2 adrenergic receptor, remained functional, binding and activating their primary intracellular signaling G proteins<sup>12,13</sup>. Structural and biochemical studies suggested that different GPCRs can self-associate through distinct transmembrane helical (TMH) interfaces. Computational modeling approaches based on molecular dynamics simulations have also identified different possible modes and lifetimes of GPCR associations<sup>14,15</sup> but the functional relevance of these oligomeric forms remains poorly understood<sup>5–7,16–22</sup>. For example, chemokine receptor CXCR4 signaling is linked to the formation of nanoclusters at the cell membrane<sup>23</sup>. Such nanoclusters are controlled by key structural motifs present at the receptor TMH surface but do not involve the receptor dimeric interface observed in X-ray structures<sup>10</sup>.

In principle, computational protein design techniques can probe and decipher the importance of protein associations by reprogramming protein-protein interactions or designing competitive binding inhibitors, but these approaches have mostly been applied to soluble proteins<sup>24–26</sup>. Applications to membrane proteins have been limited to the design of single-pass TMH associations<sup>27–29</sup>.

Here, we developed a computational approach for modeling and designing quaternary structures of multi-pass membrane receptors. Using this method and given that CXCR4 form homodimers that can be regulated by ligands<sup>10,11</sup>, we engineered the CXCR4 to associate into distinct oligomeric structures that recruited and activated intracellular signaling proteins differently. Altogether, our study reveals that quaternary structures constitute important unforeseen structural determinants of GPCR biased signaling and identified a common conformational switch at the dimer interface of several GPCRs that differentially control  $\beta$ -arrestin engagement versus G protein signaling. The approach is general and should prove useful for reprogramming cellular functions through designed receptor associations.

## Results

### Computational approach for modeling and designing multi-pass receptor oligomers

We developed an approach to model and design multi-pass membrane protein associations with precise quaternary structures, stabilities, and signaling functions (Fig. 1, Supplementary Fig. 1). We call the method QUESTS which stands for Quaternary receptor State design for Signaling selectivity. The method builds GPCR monomeric structures in distinct active and inactive states, docks them to identify possible modes of protomer associations into homodimers, and designs the binding interfaces to generate quaternary structures with distinct dimer stabilities, conformations, and propensity to recruit and activate specific intracellular signaling proteins. In this study, an active state model refers to a GPCR in an active state conformation modeled using a receptor structure bound to an agonist and G protein or an agonist and  $\beta$ -arrestin as templates.

We applied QUESTS to reprogram the homo-dimeric structure and function of CXCR4, a GPCR from the chemokine receptor family. We chose CXCR4 because it is a critical signaling hub involved in immune responses<sup>7,30</sup> and HIV infection, as well as a receptor for which multiple experimental lines of evidence supporting the formation of constitutive homo-oligomers and its regulation by ligands exists<sup>10,11</sup>.

We first modeled CXCR4 WT monomers in inactive and active states (Fig. 1, Supplementary Fig. 1). For instance, the active state model of CXCR4 was obtained from the active state structure of the homologous viral GPCR US28 (PDB 4XT1) using the method IPHoLD which integrates homology modeling and ligand docking<sup>31</sup>. The CXCR4 WT monomers in the inactive state were taken from the antagonist-bound CXCR4 WT structure (PDB 3ODU) after energy minimization of the X-ray coordinates. The CXCR4 WT monomers were assembled into inactive or active state dimers along different dimer binding interfaces involving TMHs 4, 5, and 6. We found that, in both the inactive and active states, the dimer WT models populated primarily an open-dimer

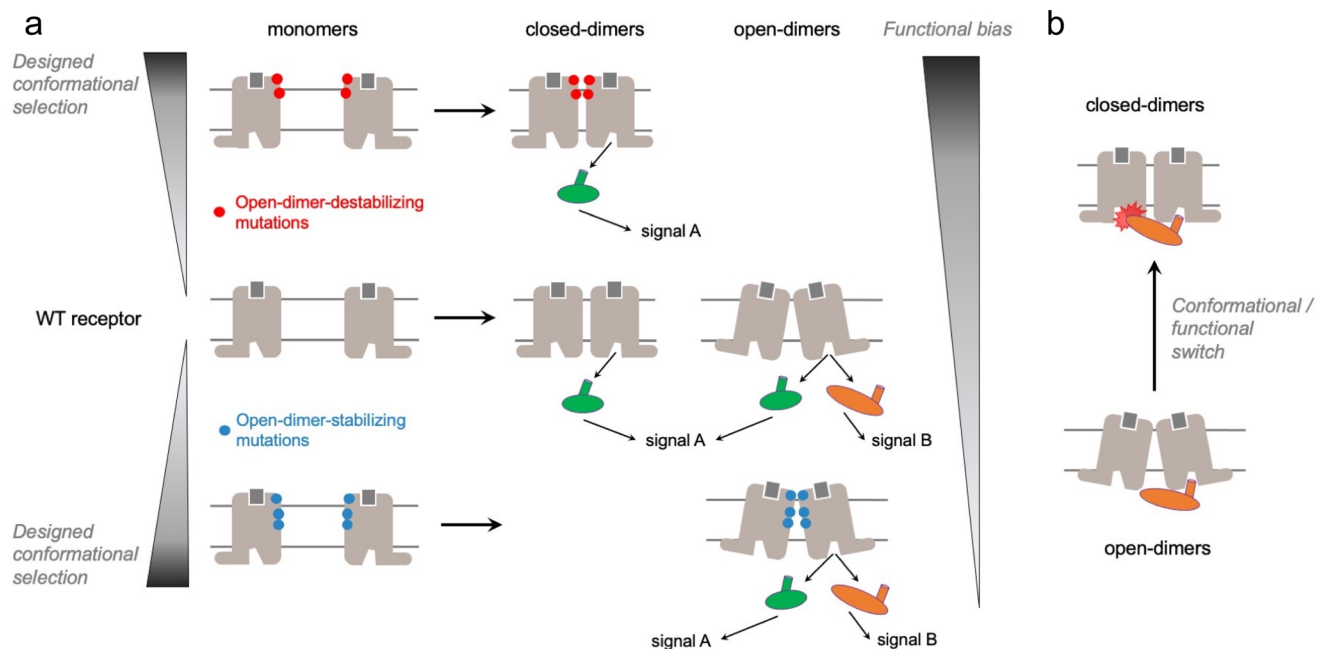


**Fig. 1 | Computational modeling and design of GPCR associations with reprogrammed structures and functions using QUESTS. a** Framework for the modeling and design of specific receptor quaternary active state conformations eliciting various degree of functional selectivity. The WT receptor modeled in the active state is assembled into dimers and then into ternary complex with G proteins (green) or  $\beta$ -arrestin (orange) to identify the distribution of quaternary conformations and their ability to recruit intracellular signaling proteins. The dimer

binding interface is redesigned to stabilize and/or destabilize specific quaternary conformations. This design strategy enhances the quaternary conformational selectivity of the receptor and reprograms the functional bias of the receptor oligomer (Supplementary Fig. 1, Methods). **b** Quaternary structural changes act as a functional switch as the closed-dimer conformation interferes with the binding of a GPCR monomer to  $\beta$ -arrestin.

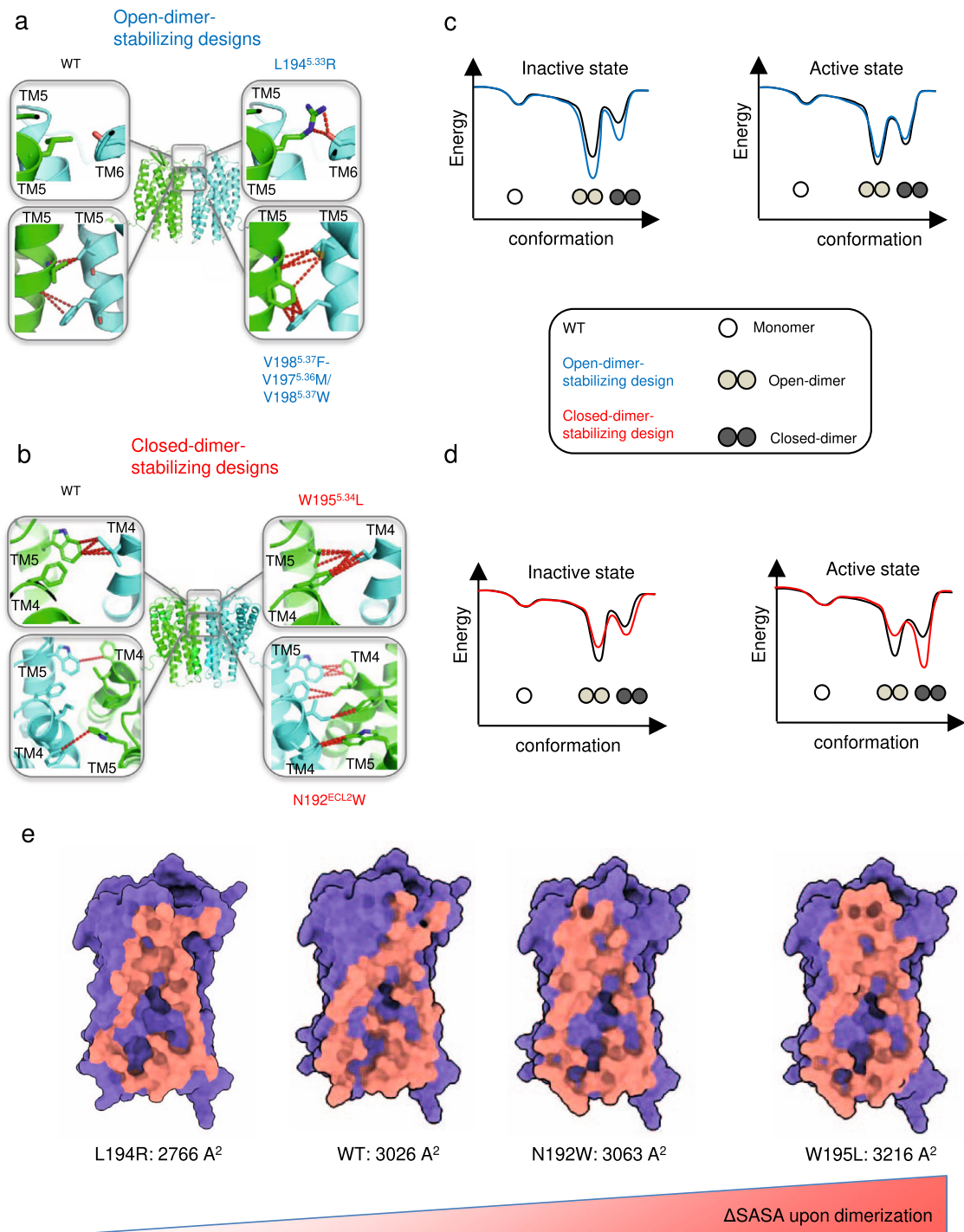


**Fig. 2 | Computational design of CXCR4 associations with specific conformations.** **a** Mutations designed to selectively stabilize the CXCR4 open-dimer conformation without affecting CXCR4 monomer stability were identified in the extracellular and TMH regions. **b** Mutations designed to selectively stabilize the CXCR4 closed-dimer conformation without affecting CXCR4 monomer stability were identified in the extracellular region. Key atomic contacts are represented as red dotted lines. **c** Schematic conformational energy landscapes of CXCR4 dimerization in the inactive and active states for the open-dimer stabilizing designs. **d** Schematic conformational energy landscapes of CXCR4 dimerization in the inactive and active states for the closed-dimer stabilizing designs. **c, d** The

dimerization energies reported in Supplementary Table 1 were used to plot the energy landscapes. The monomer energies and energy barriers between states are fictitious and were not predicted by our simulations. **e** Ranking of the CXCR4 variants based on changes in buried surface area upon dimerization ( $\Delta$ SASA) calculated from the predicted models in the active state. The  $\Delta$ SASA is reported for the most occupied dimer conformation for each variant: L194R open-dimer state, WT open-dimer state, N192W closed-dimer state, W195L closed-dimer state. Larger buried  $\Delta$ SASA are predicted to correlate with enhanced dimerization propensity (see Supplementary Table 2).

conformation similar to that observed in the antagonist-bound receptor X-ray structure but also, to a lesser extent, a distinct closed-dimer conformation (Fig. 2, Supplementary Table 1, Supplementary Fig. 2). The distribution between dimer conformations can be deduced

from the difference in binding energy (strength of association) at the distinct dimer interfaces (Supplementary Table 1). Interestingly, while the major open-dimer conformation remains very similar in both signaling states, the minor closed form differs by a slight rotation around

TMH5 between the inactive and active state conformations of the receptor (Supplementary Fig. 2).

To elucidate the function of these different quaternary structures, we then designed TMH and loop binding surfaces to selectively stabilize either the open-dimer or the closed-dimer conformation of the inactive and active state dimer models. QUESTS first searches for combinations of mutations and conformations that modulate the intermolecular interactions between the monomers without affecting the monomer's intrinsic conformational stability and functions. Any design that modifies the dimer binding energies as intended but significantly affect monomer stability is systematically discarded (see Methods). After each round of design, the CXCR4 monomers are assembled into dimers to predict the effects of the designed sequence-structure features on the distribution of quaternary structures in distinct signaling states. Lastly, the G protein Gi and  $\beta$ -arrestin are docked and assembled onto the designed CXCR4 active state dimers to predict whether the engineered receptors would effectively engage and activate these intracellular signaling proteins. The cycles of design, flexible docking and ternary complex assembly are repeated until the calculations converge to significant predicted reprogramming of the quaternary structure and functional selectivity of the designed CXCR4 oligomers (Fig. 1, Supplementary Fig. 1).

### Designing CXCR4 dimers with selective conformations and intracellular functions

From our *in silico* design screen, we first selected three engineered CXCR4s predicted to dimerize with greater propensity than CXCR4 WT in the open-dimer conformation (Fig. 2a, c, Supplementary Table 1). The designs involved key conformational lock motifs stabilizing the open-dimer conformation (Fig. 2a, c). The L194<sup>5.33</sup>K and the L194<sup>5.33</sup>R design introduced a set of strong and conformationally selective polar contacts between the extracellular sides of TMH5s of two protomers predicted to stabilize the dimer interface by 2.4 Rosetta Energy Units (REU) (Fig. 2a, Supplementary Table 1). The triplet design, formed by the V198<sup>5.37</sup>F-V197<sup>5.36</sup>M mutation on one protomer and the V198<sup>5.37</sup>W on the other protomer, encoded a new network of optimal hydrophobic contacts bridging the membrane-embedded core of the dimer-binding interface between TMH5s (Fig. 2a). When modeled in the active state, these designs primarily dimerized in an open conformation that could readily form tight active state complex structures with both Gi and  $\beta$ -arrestin (Fig. 1, Supplementary Table 1, Supplementary Fig. 3).

Conversely, we also engineered two binding surfaces predicted to stabilize the closed-dimer conformation (Fig. 2b, d, Supplementary Table 1). We selected these “closed-dimer-stabilizing” designs, because, unlike WT, they preferentially assemble into closed-dimer conformations that form tight active-state complex structures with Gi but not with  $\beta$ -arrestin (Fig. 2b, d, Supplementary Fig. 3). We found that steric hindrance prevents the optimal interaction of  $\beta$ -arrestin's finger loop in the intracellular binding groove of CXCR4 when the receptor occupies the closed-dimer conformation. Specifically, our models predict that regions of close contacts between the  $\beta$ -arrestin and the open-dimer CXCR4 (i.e. helix 8 of CXCR4 monomer 2 with the C-tip of  $\beta$ -arrestin, and ICL2 of CXCR4 monomer 1 with the C-loop of  $\beta$ -arrestin) would be disrupted in the closed-dimer conformation (Supplementary Fig. 4). Both designed interfaces (that we name W195<sup>5.34</sup>L and N192<sup>ECL2</sup>W design switches) involved distinct conformational switch motifs stabilizing the closed-dimer conformation, especially when the receptor occupies the signaling active state (Fig. 2b, Supplementary Table 1). The W195<sup>5.34</sup>L design switch increased the packing of TMH4 and 5 across the extracellular side of the binding interface, stabilizing the closed-dimer conformation through additional van der Waals contacts (Fig. 2b). The N192<sup>ECL2</sup>W design switch induced several conformational changes in a neighboring layer of residues buried at the

dimer interface, creating new key hydrophobic interactions stabilizing the closed form (Fig. 2b).

By simulating the association for the WT and the designed CXCR4 monomers, we identified important differences in the stability of the dimer conformations and hence in the distribution of the monomer and dimer forms in the inactive and active states of the receptor (Fig. 2b, d, Supplementary Tables 1, 2). Although QUESTS does not rigorously calculate free energies of dimerization, we could derive an apparent dimerization propensity score relative to WT for the different CXCR4 variants (Methods, Supplementary Table 2). The significant difference in dimerization propensities between the designs described below stemmed directly from the distinct calculated stabilities of the dimer conformations (Methods, Supplementary Table 1). In the inactive state, the “closed-dimer-stabilizing” N192<sup>ECL2</sup>W and W195<sup>5.34</sup>L designs formed weaker dimers while the “open-dimer-stabilizing” L194<sup>5.33</sup>R design formed stronger dimers than WT, suggesting that the “closed-dimer-stabilizing” designs would occupy more often the monomeric form in the inactive state. The reverse scenario was observed in the active state. While the dimerization propensity of the L194<sup>5.33</sup>R design was lower than WT, the W195<sup>5.34</sup>L design formed the most stable active state dimers among all variants. Interestingly, the dimerization propensities were consistent with the changes in receptor buried surface areas upon self-association (Fig. 2e), except for the L194<sup>5.33</sup>R design which stabilizes the dimer interface through strong polar interactions instead of VDW contacts (Fig. 2a).

Our calculations suggested also important differences in the distribution between dimer conformations (Fig. 2b, d, Supplementary Table 1). Concerning the WT receptor, we observed that the closed-dimer conformation was significantly more stable in the active state, indicating a relative shift toward the closed form in that state. By contrast, virtually no difference in the closed-dimer conformation stability between the inactive and active states was observed for the “open-dimer-stabilizing” designs (L194<sup>5.33</sup>R switch). The largest changes in dimer populations between inactive and active signaling states were observed for the “closed-dimer-stabilizing” designs (W195<sup>5.34</sup>L switch). Despite a significant stabilization of the closed-dimer conformation, the open dimer remained the most stable form in the inactive state and the W195<sup>5.34</sup>L variant still predominantly populated the open-dimer structure in that state. However, the distribution between open and closed conformation of the W195<sup>5.34</sup>L variant was reversed in the active state and the closed form became the most stable and dominant structure. Overall, the W195<sup>5.34</sup>L design was found to be most stable in the active state closed-dimer form (Supplementary Table 1).

### Designed CXCR4 receptors dimerize in distinct conformations

We validated the predicted designed oligomeric CXCR4 structures and functions using an ensemble of cell-based experiments.

We first measured constitutive and CXCL12 agonist-promoted CXCR4 dimerization in living HEK293T cells by BRET using CXCR4-RLuc and CXCR4-YFP constructs (Fig. 3a). A large constitutive BRET signal was observed for the WT receptor which, as previously reported<sup>10,11</sup>, further increased upon activation by agonist (Fig. 3a, Supplementary Fig. 5, Supplementary Fig. 6 for CXCR4 cell surface expression levels). This increase in BRET can be interpreted as a change in conformation within dimers and a shift toward the closed-dimer form or as an increase in dimer population upon activation that were both suggested by our calculations (Supplementary Table 1). Although both phenomena most likely contribute to the increase, their relative contribution cannot be determined from the BRET data or, to our knowledge, any other experimental approach. Consistent with the “open-dimer-stabilizing” designs associating in a similar open conformation than WT, the constitutive BRET signals measured for these designs (L194<sup>5.33</sup>K/L194<sup>5.33</sup>K, L194<sup>5.33</sup>R/L194<sup>5.33</sup>R,



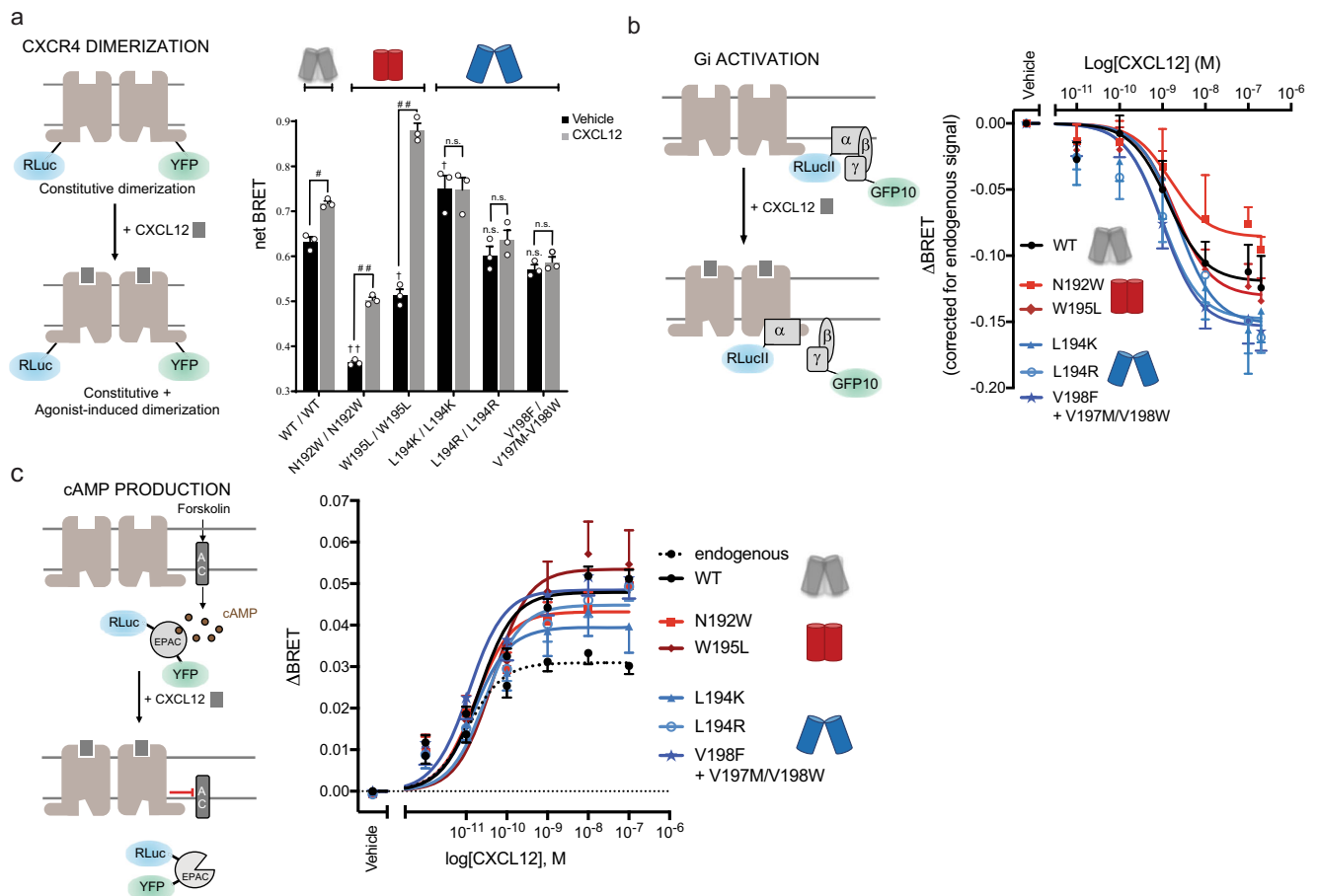


**Fig. 3 | CXCR4 association and Gi activation.** **a** (Left) Schematic representation of the CXCR4 dimerization BRET-based assay. (Right) CXCR4 association in HEK293T cells transfected with CXCR4-RLuc and its counterpart CXCR4-YFP, WT, or mutant as indicated. BRET<sub>480-YFP</sub> was measured after the addition of coel-h (10 min) and CXCL12 (15 min). Data shown represent the mean  $\pm$  SEM of three independent experiments and are expressed as net BRET (calculated by subtracting background luminescence). Statistical significance was assessed using a two-way ANOVA followed by a Šidák's multiple comparisons test: # $p = 0.007$ , ## $p < 0.0001$ , n.s. not significant  $p > 0.05$  are used to compare BRET values between basal to CXCL12-treated conditions and \* $p = 0.0004$ , \*\* $p < 0.0001$  are used to compare basal BRET values between the mutants. **b** (Left) Schematic representation of the BRET-based ligand-induced Gi activation assay. (Right) CXCL12-promoted Gi activation

measured by BRET in HEK293T cells transfected with HA-CXCR4, WT or mutant as indicated, G $\alpha$ i1-RLucII, G $\beta$ 1, and G $\gamma$ 2-GFP10. BRET<sub>400-GFP10</sub> was measured after the addition of coel-400a (10 min) and CXCL12 (3 min). **c** (Left) Schematic representation of the BRET-based EPAC sensor to measure cAMP production. (Right) CXCL12-promoted EPAC inhibition was measured by BRET in HEK293T cells transfected with HA-CXCR4, WT or mutant as indicated, and RLuc-EPAC-YFP. BRET<sub>480-YFP</sub>, reporting the conformation rearrangement of the EPAC sensor from an open to a closed conformation, was measured after the addition of coel-h (10 min) and CXCL12 (5 min). **b**, **c** CXCR4 mutations predicted to stabilize the open-dimer or the closed-dimer conformation are annotated with a blue or red dimer symbol, respectively. Data shown represent the mean  $\pm$  SEM of at least three independent experiments and are expressed as  $\Delta$ BRET (agonist-promoted BRET).

V198<sup>S.37F</sup>/V197<sup>S.36M</sup>-V198<sup>S.37W</sup>), were either similar to or slightly larger than WT. However, unlike what is seen for the WT receptor, we did not observe any significant BRET increase upon agonist stimulation. These results suggest that stabilization of the open-dimer conformation prevents further agonist-induced conformational changes across the binding interface and locks the receptor dimer in a constitutive open-dimer conformation, consistent with the lack of stabilization of the closed-dimer form upon receptor activation in our simulations (Supplementary Table 1). In the specific case of the L194<sup>S.33K</sup> design, the lack of BRET increase upon stimulation could also result in part from the designed receptors occupying more frequently the dimer state than the WT receptor, even without stimulus, as suggested by the significantly increased constitutive BRET signals measured for that design.

The BRET signals measured for the “closed-dimer-stabilizing” designs (N192<sup>ECL2W</sup>/N192<sup>ECL2W</sup>, W195<sup>S.34L</sup>/W195<sup>S.34L</sup>) without ligand stimulus were significantly lower than WT. These observations are consistent with the designs still predominantly occupying the open conformation in the inactive state (Supplementary Table 1) and

forming overall weaker dimers than WT (Supplementary Table 2) that may result in a greater proportion of receptor in the monomeric state. Upon agonist stimulation, however, we observed a larger increase in net BRET signal compared to WT, especially for W195<sup>S.34L</sup> in agreement with the large predicted changes in dimer conformation favoring the closed-state and increased dimerization propensity upon receptor activation (Supplementary Tables 1, 2). These results suggest that the “closed-dimer-stabilizing” receptors constitutively dimerize less than WT and display stronger propensity to associate in the closed-dimer form upon agonist stimulation.

Overall, we observed a consistent trend between predicted closed-dimer stabilization and increase in  $\Delta$ BRET upon activation (Supplementary Fig. 7). These results suggest that major conformational changes and population shifts towards the closed-dimer form can readily occur in the active state when triggered by strong switching mutations such as W195<sup>S.34L</sup>. Concerning the effects of the designs on dimerization, except for L194<sup>S.33R</sup>, we observed a qualitative trend between the calculated propensities and BRET measurements (Supplementary Table 2), which suggest that designed structural

interactions may impact the dimerization propensity as predicted by the design calculations.

In summary, the BRET measurements validate the designed CXCR4-dimer structures and indicate that receptor dimers with distinct strengths of associations and quaternary conformations can be rationally engineered using our approach.

### Designed CXCR4 receptors activate distinct intracellular signaling proteins

According to our calculations, the two classes of designed receptors should display distinct propensity to bind and activate intracellular signaling proteins. While the receptors dimerizing in the open conformation should recruit both Gi and  $\beta$ -arrestin, the receptors preferentially dimerizing in a closed conformation should couple strongly to Gi only.

To validate these predictions, we measured Gi activation and  $\beta$ -arrestin recruitment to CXCR4 using BRET-based assays in HEK293 cells. Consistent with the active state modeling, both classes of designed CXCR4 dimers were able to activate Gi similarly to WT, as measured by the agonist-induced dissociation of the heterotrimeric Gi protein subunits (Fig. 3b) and the inhibition of cAMP production (Fig. 3c). As shown in Supplementary Fig. 6d, HEK293 cells endogenously express a low level of CXCR4 that result in a background CXCL12-promoted cAMP inhibition that can easily be distinguished from the signal generated by the transfected WT or mutant receptors (Fig. 3c). No such background signal is observed in the BRET-based Gi activation or  $\beta$ -arrestin recruitment assays due to the lower level of amplification of these assays. Both assays clearly indicated that the mutations did not affect the ability of the receptor to activate Gi.

$\beta$ -arrestin recruitment was measured using BRET reporting directly the interaction between CXCR4-RLuc and  $\beta$ -arrestin-2-YFP (in HEK293 cells)<sup>32</sup> or ebBRET<sup>33</sup> monitoring the interaction between  $\beta$ -arrestin-2-RLuc and the lipid-modified rGFP-CAAX anchored at the cell membrane. Both assays consistently showed that the “open-dimer-stabilizing” designs recruited  $\beta$ -arrestin very effectively and similarly to WT upon agonist stimulus (Fig. 4a, Supplementary Fig. 8). On the contrary, and in agreement with our predictions, the “closed-dimer-stabilizing” designs had largely impaired  $\beta$ -arrestin recruitment abilities. Specifically, while  $\beta$ -arrestin-2 coupling to the N192<sup>ECL2</sup>W design was considerably reduced compared to WT, virtually no recruitment signals could be measured for the W195<sup>5,34</sup>L design (Fig. 4a, Supplementary Fig. 8). The differences in  $\beta$ -arrestin recruitment were not due to difference in the expression levels of the different mutants as they showed similar cell surface expression as assessed by ELISA (Supplementary Fig. 6). Given that phosphorylation of GPCRs is known to increase the affinity of  $\beta$ -arrestin for the active forms of receptors, we assessed the impact of W195<sup>5,34</sup>L on the agonist-promoted phosphorylation of CXCR4. As shown in Fig. 4b, despite a small reduction in the basal phosphorylation level, the same CXCL12-promoted phosphorylation was observed for WT- and W195<sup>5,34</sup>L-CXCR4, indicating that the loss of agonist-promoted  $\beta$ -arrestin recruitment is not due to a phosphorylation defect.

Consistent with the previously reported role of  $\beta$ -arrestin in ERK activation<sup>34</sup>, the W195<sup>5,34</sup>L design showed a reduced level of ERK phosphorylation compared to WT, suggesting that the scaffolding function supported by  $\beta$ -arrestin was affected (Fig. 4c). Because of a high background CXCL12-promoted ERK activity in HEK293 cells, the ERK assay was performed in U87.GM cells that lack endogenous CXCR4 in which WT- and W195<sup>5,34</sup>L-CXCR4 were heterologously expressed at equivalent expression levels (Supplementary Fig. 6e). These data show that the designed change in dimerization resulted into a functional outcome at the signaling level reflected by a blunted ERK response, a result that is consistent with the reduced  $\beta$ -arrestin recruitment observed for this mutant.

### New structural mechanism of GPCR-mediated biased signaling

Overall, our designs reveal an unforeseen structural mechanism of GPCR-mediated biased signaling. Molecular determinants of biased signaling identified so far were primarily encoded by specific sequence motifs and conformations of receptor monomers<sup>35</sup>. However, Gi-mediated CXCR4 signaling triggering important functions such as chemotaxis was recently found to depend on the formation of specific receptor nanoclusters at the cell surface<sup>23</sup>. These oligomers are controlled by specific structural motifs on the lipid-exposed intracellular surface of TMH6, that is remote from the dimer interface studied here (Fig. 5a). Mutations of the corresponding residues on TMH6 resulted in nanocluster-defective receptor variants with severely impaired Gi-mediated signaling, suggesting that this CXCR4 oligomerization surface constitutes a Gi bias signaling switch. On the other hand, our study demonstrates that the extracellular dimerization surface primarily constituted by TMH5 residues can control the selective recruitment of the other main class of GPCR signaling and regulating partners,  $\beta$ -arrestin. Since Gi coupling remains insensitive to the precise dimer structure mediated by TMH5 contacts, we propose that this binding surface constitutes a  $\beta$ -arrestin bias signaling switch. This is consistent with our modeling suggesting that the active close-dimer conformations prevent the engagement of the  $\beta$ -arrestin finger loop of the receptor by the cradle core of the receptor through steric hindrance (Supplementary Fig. 4).

Since the structural motifs identified at the surface of CXCR4 monomers control a key signaling pathway conserved in most GPCRs, we wondered whether similar binding surfaces could be identified in other receptors. We first performed a sequence alignment of CXCR4s from various organisms and found that the native residues at the designed dimerization hotspot positions were highly conserved in CXCR4s through evolution, supporting an important functional role for this region of the receptor (Fig. 5b). Strikingly, a similar analysis revealed that these positions are poorly conserved in other human chemokine receptors with the exception of W195<sup>5,34</sup> (Fig. 5b). Interestingly, while no other chemokine receptors have been crystallized in a dimeric form involving TMH5-mediated contacts, the position of W5.34 in CXCR1 (PDB 2LNL), CCR2 (PDB 5T1A), CCR5 (PDB 4MBS) and Y5.34 in chemokine-related US28 (PDB 4XT1) was found to be superimposable to that in CXCR4 (Fig. 5c). We also found conserved aromatic residues at position 5.34 in P2Y and other peptide-binding receptors which are known to dimerize (Fig. 5b).

Since a single mutation at the extracellular tip of TM5 (W5.34) was sufficient to disrupt  $\beta$ -arrestin recruitment at CXCR4, we wondered whether that particular position could also constitute a  $\beta$ -arrestin bias signaling switch in other class A GPCRs. To validate this hypothesis, we identified two additional GPCRs from the peptide-binding receptor subfamily that are known to dimerize, the  $\mu$ -opioid receptor ( $\mu$ OR) and the type-2 vasopressin receptor (V2R), that bear a tryptophan at position 5.34 or 5.33, respectively (Supplementary Fig. 9). We investigated the effect of mutating the native tryptophan at these positions to alanine to assess its role on the receptor signaling functions. Receptor signaling was measured using distinct BRET sensors monitoring  $\beta$ -arrestin and Go for  $\mu$ OR, and  $\beta$ -arrestin, and Gs for V2R (Fig. 6). While signaling through the G proteins was moderately affected by the W5.34/33A mutation in both receptors (V2R: 85% and  $\mu$ OR: 61% of WT efficacy, Fig. 6),  $\mu$ OR and V2R receptor mutants were more strongly impaired in  $\beta$ -arrestin signaling (<25% of WT efficacy, Fig. 6). These results indicate that the aromatic residue at position 5.34/33 preferentially controls the signaling efficacy through the  $\beta$ -arrestin pathway and plays the role of a signaling switch in receptors that belong to distinct peptide-binding GPCR families.

To better understand the structure-function underpinnings of the mutational effects and assess whether a common structural mechanism underlies the function of the identified switches in the studied

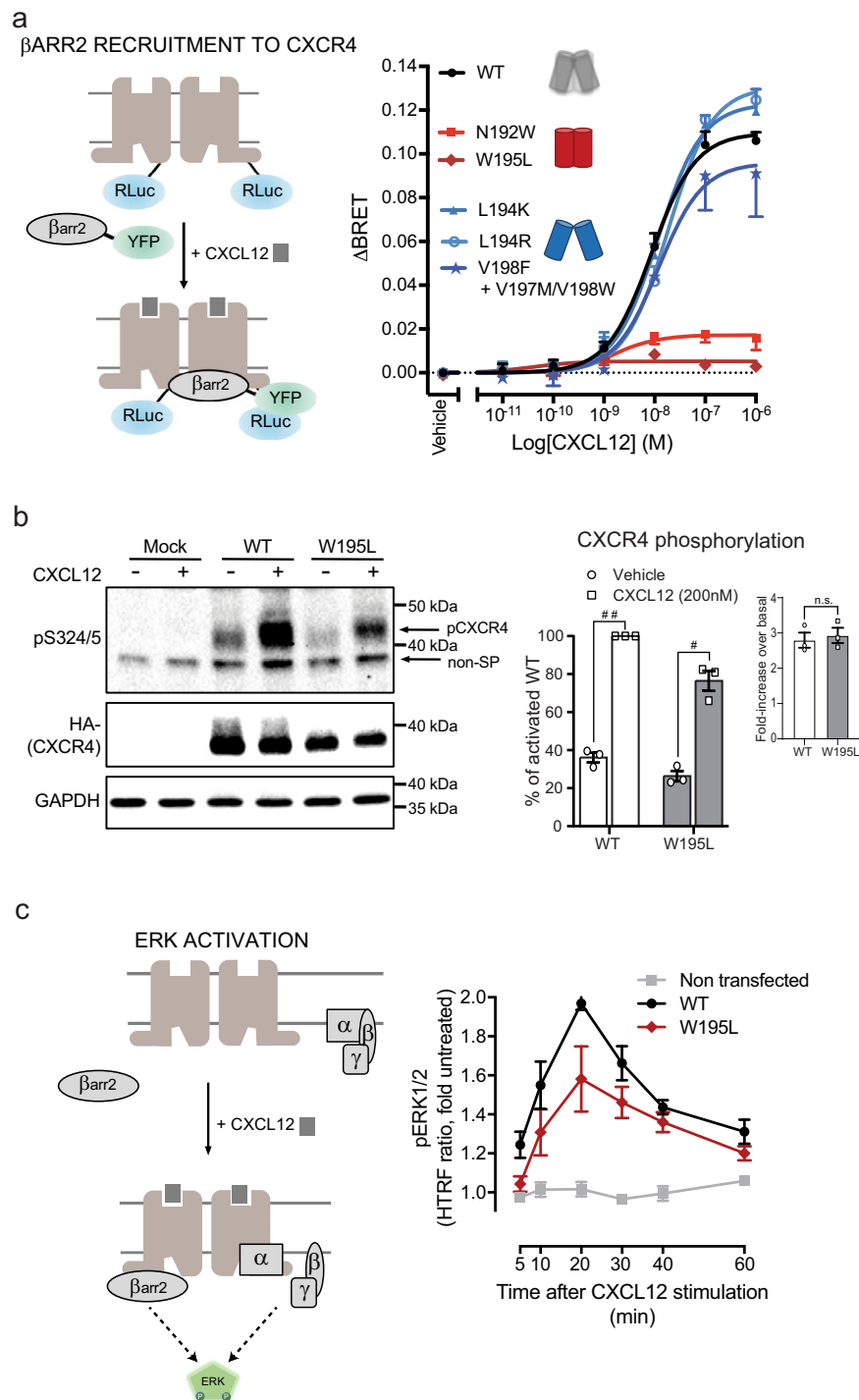


**Fig. 4 |  $\beta$ -arrestin recruitment and ERK activation.** **a** (Left) Schematic representation of the BRET-based ligand-induced  $\beta$ -arrestin-2 ( $\beta$ arr2) translocation assay. (Right) CXCL12-promoted  $\beta$ arr2 recruitment to CXCR4 measured by BRET in HEK293T cells transfected with CXCR4-RLuc, WT or mutant as indicated, and  $\beta$ arr2-YFP. BRET<sub>480-YFP</sub> between CXCR4-RLuc and  $\beta$ arr2-YFP was measured after the addition of coel-h (10 min) and CXCL12 (15 min). Data shown represent the mean  $\pm$  SEM of at least three independent experiments and are represented as  $\Delta$ BRET. **b** (Left) Phosphorylation at S324/5 of WT and W195<sup>S34L</sup> CXCR4 promoted by stimulation with 200 nM CXCL12 for 30 min detected using an anti pS324/5 antibody (pCXCR4 indicates the CXCR4-S324/5 phosphorylation band; non-SP correspond to a non-specific band). (Right) Quantification of phosphorylation

bands normalized as a function of the intensity of the total HA-CXCR4 detected using an anti-HA antibody. Shown in the inset is the fold increase in phosphorylation over basal levels. Data shown represent the mean  $\pm$  SEM of three independent experiments. Statistical significance was assessed using unpaired *t* test. \**p* = 0.001, \*\**p* < 0.0001, n.s. not significant *p* > 0.05. **c** (Left) Schematic representation of ERK activation by CXCR4. (Right) ERK phosphorylation in U87 stably expressing equivalent levels of WT and W195<sup>S34L</sup> CXCR4 induced by stimulation with 10 nM CXCL12 for the indicated times was monitored by HTRF. CXCR4 mutations predicted to stabilize the open-dimer or the closed-dimer conformation are annotated with a blue or red dimer symbol, respectively. Data shown represent the mean  $\pm$  SEM of at least three independent experiments.



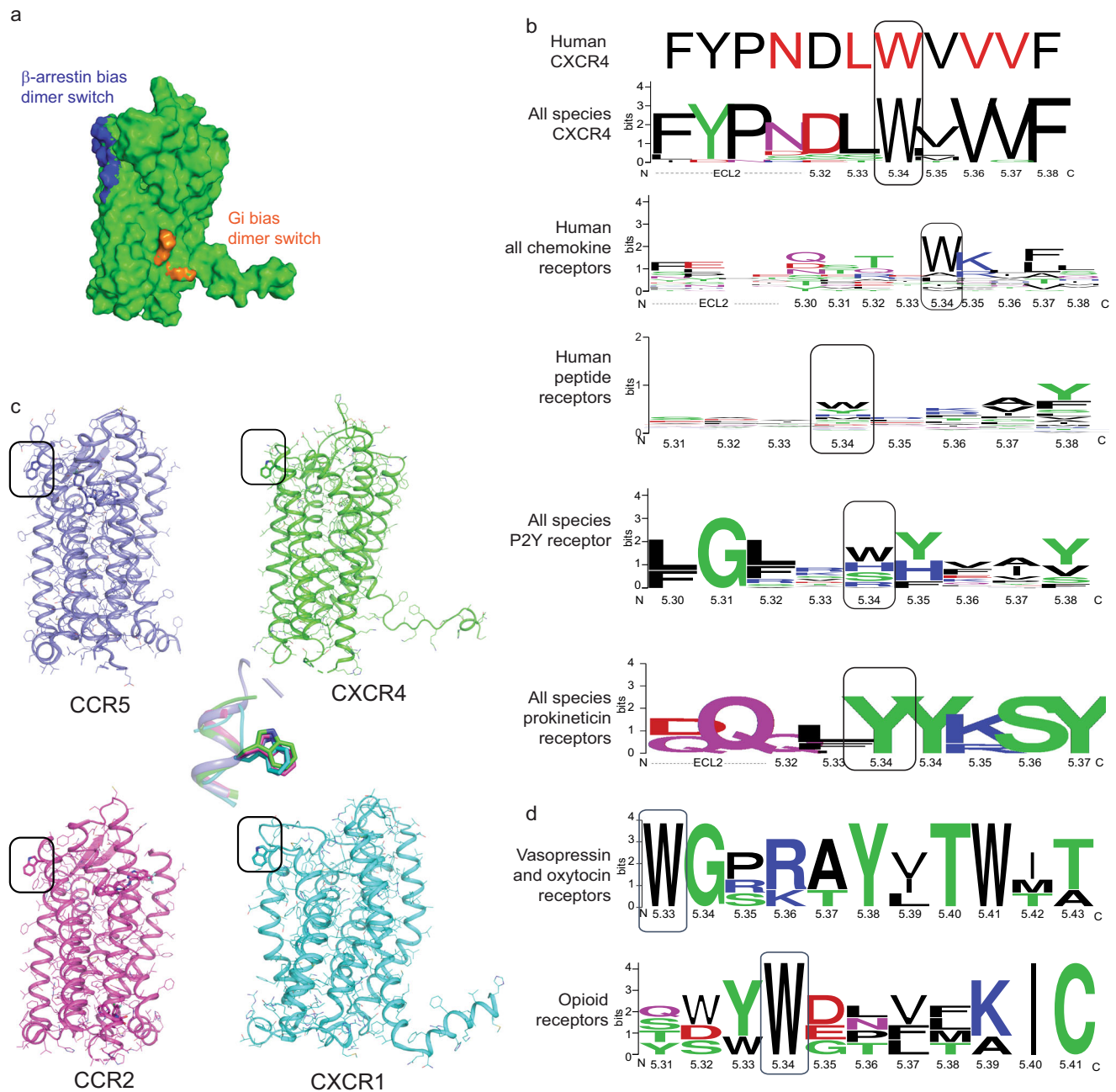


**Fig. 5 | Distinct quaternary structures selectively control G protein and  $\beta$ -arrestin recruitment.** **a** Surface representation of the CXCR4 inactive state monomeric structure highlighting the distinct oligomerization interfaces controlling either  $\beta$ -arrestin recruitment (extracellular side and TM core of TMH5, blue) or Gi activation and nanocluster formation<sup>23</sup> (intracellular side of TMH6, orange). **b** The hotspot binding sites controlling CXCR4 oligomerization through TMH5 (designed residues

in red) are poorly conserved in the chemokine receptor family, except for the  $\beta$ -arrestin signaling switch W5.34. Aromatic residues are highly enriched at position 5.34 of other dimerizing GPCR families. **c** Conserved position and conformation of W5.34 in human chemokine receptor X-ray structures. The superposition of W5.34 conformations is shown in the center. **d** Conservation of the  $\beta$ -arrestin signaling switch in the TM5 of vasopressin/oxytocin receptors and opioid receptors.

receptors, we investigated the structural impact of the tryptophan to alanine substitution. We focused our analysis on  $\mu$ OR, as a broad range of structural and functional evidence indicate that this receptor strongly homodimerizes in cell membranes<sup>36,37</sup>. In particular, a high-resolution structure of the murine  $\mu$ OR in the inactive state revealed a homodimer stabilized by an extensive binding interface between TMH5 and TMH6. Using our computational quaternary structure modeling approach, we modeled WT and W5.34 A  $\mu$ OR homodimers in active signaling complexes bound to either G protein Go or  $\beta$ -arrestin. Our simulations revealed that  $\mu$ OR in the active signaling state mainly

adopts a major “open” and a minor “wide-open” homodimer conformational state (Supplementary Fig. 10). The open-dimer form of  $\mu$ OR was found to strongly bind to  $\beta$ -arrestin, while the wide-open dimer interacted considerably less well with that protein (Supplementary Figs. 11, 12, Supplementary Table 3). By contrast, both homodimer conformations were able to strongly recruit Go (Supplementary Fig. 11, Supplementary Table 3). W5.34 was found at the dimer interface of all  $\mu$ OR homodimers but involved in different sets of interactions. Consequently, the W5.34 A mutation displayed distinct effects on the dimer structures, destabilizing the major open dimer

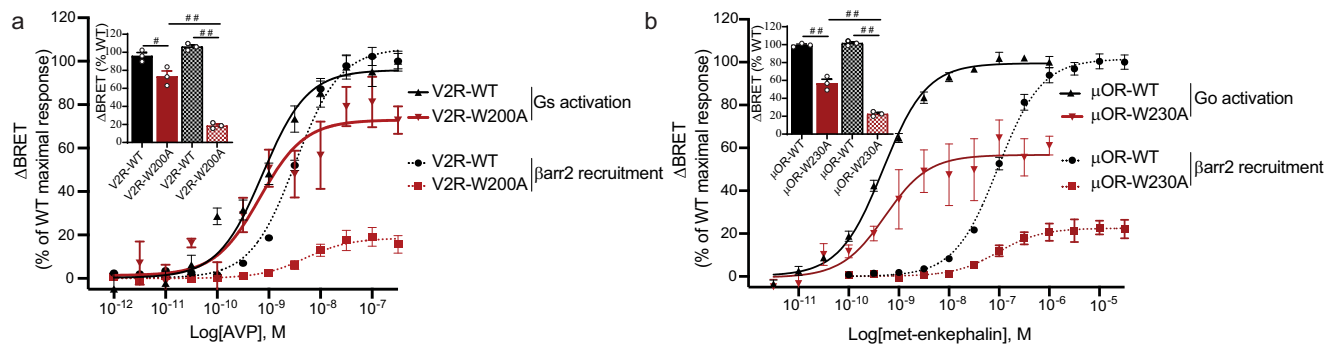


**Fig. 6 | W5.34/33 is a common biased signaling switch in dimerizing peptide-binding GPCRs. a, b** Ligand-promoted Gs (V2R) or Go ( $\mu$ OR) and  $\beta$ arr2 recruitment to the membrane in the presence of V2R-WT or V2R-W200<sup>S33A</sup> (a), and  $\mu$ OR-WT or  $\mu$ OR-W230<sup>S34A</sup> (b). Gs and Go activation were detected by monitoring the dissociation between  $\text{G}\alpha$  and  $\text{G}\beta\gamma$  by BRET whereas  $\beta$ -arrestin recruitment to the plasma membrane was assessed in cells transfected with rGFP-CAAX, WT, or mutant

receptors, as indicated, and  $\beta$ arr2-RlucII. Data shown represent the mean  $\pm$  SEM of three independent experiments and are represented as  $\Delta$ BRET normalized to the maximal response of the WT receptor. The insets represent the maximal agonist-promoted responses for G protein activation (solid bars) and  $\beta$ -arrestin-2 recruitment (checkered bars). Statistical significance was assessed using a one-way ANOVA followed by Tukey's multiple comparison test: # $p < 0.012$ , ## $p < 0.0001$ .

and stabilizing the minor wide-open form (Supplementary Table 3). The simulations corroborate the experimental observations and provide a structural explanation as to why W5.34 A preferentially decreases signaling through  $\beta$ -arrestin. Since no high-resolution structure of a dimer of V2R is available, similar simulations were not attempted on that receptor. Nevertheless, from the available agonist-bound monomeric V2R structure bound to Gs (PDB 7DW9) it is evident that W5.33 in V2R points in a very similar direction than W5.34 in CXCR4 and would be involved in a similar dimer interface than CXCR4 and  $\mu$ OR (Supplementary Fig. 9).

To further support our structural interpretations of the observed biased signaling, we performed structural predictions of the studied complexes using AlphaFold multimer (AF2)<sup>38,39</sup>. While AF2 was not able to predict the CXCR4-dimer conformation on its own, it did recapitulate our predicted conformations or the X-ray structure when these structures were given as template (Supplementary Fig. 13). AF2 predictions of  $\mu$ OR dimers converged also to our modeled conformations when provided a template. Concerning the G protein and  $\beta$ -arrestin-bound complex structures, we obtained good agreement between AF2 and our modeling approach. Even without template, AF2 recapitulated our  $\beta$ -arrestin-2 bound CXCR4 models. In fact, all AF2 models predicted the orientation of the  $\beta$ -arrestin-2 and the main interactions between the arrestin finger loop and the receptor observed in our model (Supplementary Fig. 14). Importantly, AF2 predicted the same steric hindrance between arrestin and the receptor in the "closed-state" dimer that we identified using our approach (Supplementary Fig. 15). Lastly, while the AF2 predicted Gi-orientation in the Gi-bound CXCR4 complex was slightly different than in our models, the bound conformation of the G protein and interactions with the receptor were not sensitive to the dimer conformation (Supplementary Fig. 15), consistent with our modeling calculations. Overall, the AF2 models support the quaternary structure-based mechanism of biased signaling that we uncovered and report in this study.

Overall, our findings imply that residues at position 5.34/33 control  $\beta$ -arrestin signaling of CXCR4,  $\mu$ OR, and V2R by acting as a bias switch at quaternary interfaces. While the 3 receptors are functionally unrelated, belong to 3 distinct receptor subfamilies, and couple to different G proteins, this specific mechanism may not universally apply to all GPCRs. We found 6 class A GPCR structures in the pdb that form an extensive and symmetric homodimer interface. Analysis of these structures suggests that receptors mainly self-associate through either TMHs 4, 5, and 6 (e.g., in CXCR4,  $\mu$ OR) or TMHs 1,2,7 and 8 (e.g. in rhodopsin, beta

1 adrenergic receptors), implying that the latter could use other functional selectivity switches to regulate distinct signaling properties. Nevertheless, our study provides solid evidence from 3 unrelated receptors belonging to one of the main class of structural dimers that functional selectivity switches can exist at a specific transmembrane helical dimer interface thus defining a new molecular mechanism of regulating GPCR signaling.

## Discussion

Membrane protein oligomers are ubiquitously observed in cell membranes and have been widely investigated using structural, spectroscopic, and mutagenesis approaches<sup>40</sup>. However, how specific self-associations and quaternary structures control selective protein functions has remained elusive for many classes of multi-pass membrane proteins, including GPCRs. We developed QUESTS, a general computational modeling, and design approach that enables the precise design of binding surfaces and interactions to perturb native or create novel receptor oligomeric structures and associated functions.

A large fraction of GPCRs can activate multiple signaling pathways. This promiscuity has proven a challenge for the development of selective therapeutics since drugs targeting the canonical extracellular ligand binding site of GPCRs often trigger several intracellular functions, beyond the therapeutically relevant one(s) leading to undesirable side-effects<sup>41</sup>. In this study, we uncovered and engineered hotspot dimerization conformational switches on the extracellular side of CXCR4 and  $\mu$ OR that controlled the precise receptor dimeric structure and the selective activation of intracellular signaling pathways. Interestingly, we also identified a biased signaling hotspot at the same location in another strongly homodimerizing peptide-binding GPCR, V2R, but for which a high-resolution dimer structure has not yet been determined. Altogether, the results suggest that specific positions at dimer interfaces can act as conformational switches to control biased signaling in GPCRs.

The extracellular locations of these biased signaling switches suggest that the sites are druggable. The signaling regulatory mechanism controlled by specific receptor oligomeric structures emerging from our study opens new avenues for selective pharmacological treatments that do not perturb receptor monomeric structures and associated signaling functions.

Overall, our approach should prove useful for designing multi-pass membrane protein associations with novel structures and functions, and expand protein design toolkits for engineered cell-based therapies and synthetic biology applications.

## Methods

### Modeling CXCR4 inactive state monomer and homodimer structures

The X-ray structure of the antagonist-bound human chemokine receptor CXCR4 homodimer (PDB 3ODU) served as a starting template for modeling the CXCR4 inactive state monomer. After removal of detergent and lipid molecules, the two receptor molecules were separated from the dimer structure and the region corresponding to the binding interface was relaxed in implicit lipid membrane environment (The RMSD between the relaxed structure and the starting antagonist-bound X-ray structure was 0.1 Å over C $\alpha$  atoms). The lowest energy relaxed CXCR4 monomer structure was selected as a representative model of the CXCR4 inactive state monomer.

The symmetric flexible docking mode of RosettaMembrane<sup>28</sup> involving inter-monomer rigid-body movements and intra-monomer conformational flexibility was then applied to model CXCR4 homodimer inactive state structures. 10,000 homodimer models were generated starting from the selected CXCR4 inactive state monomer model. The 10% lowest homodimer interface energy CXCR4 homodimer models were selected and then filtered by inter-protomer angles to select quaternary structures that had both optimal homodimer binding energies and proper membrane insertion. Specifically, the relative orientation of the monomers in the X-ray homodimer structure is characterized by an interhelical angle between helix 5 of 52 degrees which ensures optimal membrane embedding. Hence, all models where such angle was no larger than 85 degrees and no less than -50 degrees were considered compatible with proper embedding. Overall, 80% of the models selected by interface energy were kept after applying this relative orientation filter.

These homodimer models were then clustered by dimer-specific geometric parameters across the dimer binding interface (i.e.,  $\theta$  and  $d$ , as described in Supplementary Fig. 2) for major dimer orientation analysis. We used the hdbscan-clustering method, which is a density-based clustering method based on hierarchical density estimates<sup>42</sup>. A majority of the models clustered in two large families of distinct dimer conformations (i.e., closed or open) characterized by very different interhelical angles and distances between TMH5 as described in Supplementary Fig. 2. The lowest-energy structure from each cluster was selected as the representative model of each specific (i.e., closed or open) homodimer conformation.

### Quaternary structure assembly of CXCR4 active state dimer complexes bound to G protein or $\beta$ -arrestin

The general strategy for modeling G protein or  $\beta$ -arrestin-bound CXCR4 active state homodimers involved the following steps: First, the CXCR4 monomer was modeled in the active state conformation and then assembled into homodimers. Lastly, the G protein Gi and  $\beta$ -arrestin-2 were also modeled and assembled onto the CXCR4 active state dimers to generate an optimal signaling complex. The same procedure was applied to model the WT and designed CXCR4 quaternary structures.

**Modeling CXCR4 active state monomer structures.** We applied RosettaMembrane homology modeling method<sup>21,43</sup> to model the agonist-bound conformations of a CXCR4 active state monomer. We used the nanobody and chemokine-bound active state viral GPCR (PDB 4XTI, Sequence identity = 30%) as a template because it displayed the highest sequence homology to CXCR4 among active state GPCR structures. 50,000 models of CXCR4 monomer were generated and the 10% lowest-energy models were clustered based on C $\alpha$  RMSD. The cluster centers of the top 10 largest clusters were used to build models of active state CXCR4 homodimer.

**Modeling CXCR4 active state homodimer structures.** Active-state CXCR4 homodimer structures were modeled using the same approach

than for the inactive state models with the exception that 10 starting active state monomer models were considered. The symmetric flexible docking mode of RosettaMembrane<sup>28</sup> was applied on each monomer model, and, after filtering by interhelical angle, all homodimer models were pooled together prior to the final clustering step. The lowest interface energy decoy from the largest clusters were selected for modeling CXCR4-dimer- $\beta$ -arrestin-2 or CXCR4-dimer-Gi complexes.

**Modeling GPCR-bound  $\beta$ -arrestin-2 conformations.** Arrestin binding to GPCRs mainly involves 3 loops which undergo significant conformational changes upon receptor binding. Since  $\beta$ -arrestin-2 was never crystallized in complex with a GPCR, to increase the chance of identifying optimal CXCR4- $\beta$ -arrestin-2 binding modes, we modeled the receptor-bound conformations of  $\beta$ -arrestin-2 by homology to that of the close homolog arrestin-1 bound to Rhodopsin (Sequence identity = 60%, PDB 4ZWJ) using Rosetta homology modeling. 10,000 models were generated, and the lowest 10% energy models were clustered. The lowest-energy models of the largest clusters (containing at least 2% of the population) were used to generate CXCR4-dimer- $\beta$ -arrestin-2 complex structures.

**Assembling  $\beta$ -arrestin-2-CXCR4-dimer active state complexes.** A total of eight  $\beta$ -arrestin-2 models were selected for optimal docking assembly to each selected active CXCR4 homodimer models. Starting conformations were generated by aligning one subunit of the CXCR4 dimer to Rhodopsin receptor and  $\beta$ -arrestin-2 to visual arrestin in the Rhodopsin-arrestin X-ray structure (PDB 4ZWJ). 5000 models were generated by flexible docking perturbation of the starting structure to optimize the interaction between the different domains of  $\beta$ -arrestin-2 and the intracellular regions of the CXCR4 homodimers. The complexes with the lowest interface energy were selected as representative conformations of  $\beta$ -arrestin-2 bound to one CXCR4 homodimer structure model.

**Assembling Gi-CXCR4-dimer active state complexes.** The  $\alpha$ -subunit of the Gi protein (G $\alpha$ i)-CXCR4-dimer structure was modeled before the first X-ray structure of a GPCR-Gi complex was solved. The GPCR-bound active state conformation of the C-terminal domain of Gi (including the  $\alpha$ 5 C-terminal helix) was modeled from the Gs structure bound to the  $\beta$ 2 adrenergic receptor ( $\beta$ 2AR) (PDB 3SN6, Sequence Identity >40%). The C-terminal domain model of Gi was grafted onto the N-terminal domain of the GTPyS bound structure of Gi protein  $\alpha$ -subunit (PDB 1GIA) to model the full-length GPCR-bound conformation of G $\alpha$ i. 10,000 models were generated and the lowest-energy 10% models by total energy were clustered. The lowest-energy decoys in the largest clusters were used as representative active state G $\alpha$ i to assemble CXCR4-dimer-G $\alpha$ i complex structures.

The starting position of G $\alpha$ i for docking onto CXCR4 was generated by aligning G $\alpha$ i and CXCR4 to the  $\beta$ 2 adrenergic receptor and Gs protein  $\alpha$ -subunit, respectively in their bound active state structure (PDB 3SN6). 5000 models were generated through perturbation of the starting structures to refine the interaction between the downstream effector and CXCR4 models. The docked structures were filtered by interface energy (lowest 1% effector-interface energy) and clustered. The models with the lowest effector-docking interface energy in the largest clusters were selected as representative conformation for further analysis.

### Computational design of CXCR4-dimer conformations with distinct stabilities

Inactive and active state open-dimer and closed-dimer models of the WT receptor served as starting templates for all design calculations performed using the implicit lipid membrane model of RosettaMembrane<sup>28,44,45</sup>. Positions at the interface of the two protomers were systematically scanned in silico (-20 positions, 20<sup>20</sup> possible



combinations) to search for mutations that would stabilize the open-dimer or closed-dimer conformation without modifying significantly the stability of each monomer. This strategy ensured that designed mutations would solely affect the structural and functional properties associated with receptor dimerization. Hence, mutations were selected according to the quantity  $\Delta E_{interface}$  using the following equation:

$$\Delta E_{interface} = (E_{interface})_{design} - (E_{interface})_{WT} \quad (1)$$

where

$$E_{interface} = E_{dimer} - 2 * E_{monomer} \quad (2)$$

$$\text{providing } \Delta E_{monomer} = (E_{monomer})_{design} - (E_{monomer})_{WT} \quad (3)$$

remained minimal.

Any designed mutation that had minimal effects on  $\Delta E_{interface}$  (<1.0 REU) and/or significantly affected  $\Delta E_{monomer}$  (>1.0 REU) was systematically discarded. After each step of sequence selection, the structure of the designed binding interface was refined and optimized using a Monte Carlo Minimization protocol sampling all conformational degrees of freedom.

The distribution between dimer conformations for the final selected designs and the associated functional effects on the binding to G protein versus  $\beta$ -arrestin were obtained by performing a final round of docking simulations where designed monomers were assembled into GPCR dimers and into complex with G proteins or  $\beta$ -arrestin as described above for the WT receptor.

### Modeling $\mu$ OR active state dimer structures

Starting from the active state monomeric structure of  $\mu$ OR bound to the G protein Gi (PDB 6DDF), homodimer models of the WT receptor were obtained using the symmetric docking mode of RosettaMembrane described above using the same parameters than for CXCR4. Representative lowest-energy homodimer  $\mu$ OR models were selected to assemble Gi and  $\beta$ -arrestin complexes as described above for CXCR4. The bound Gi structure resolved in the 6DDF structure was used for docking onto  $\mu$ OR dimer models. Final models were selected and analyzed using the same unbiased geometric and energetic criteria as for CXCR4. The effect of the W5.34 A mutation was obtained by calculating the quantity  $\Delta E_{interface}$  after assembling the mutated monomers into GPCR dimers as described in the computational design section.

### Calculation of dimerization propensity

The docking simulations performed using the software Rosetta do not reliably calculate free energies of protein associations because they neglect conformational and configurational entropies for example and just provide the enthalpy of a static structure. Nevertheless, differences in dimerization propensities between receptor variants can be estimated from the dimer binding energy calculated for the selected open and closed-dimer conformation as follows. In absence of free energies for the monomer and dimer species, we define a reference state, that of the lowest-energy primary dimer conformation of the WT receptor, i.e. the open dimer:  $(\Delta E_{interface, O})_{WT}$ . We first calculate the difference in dimer binding energies for each variant and conformation from WT as follows:

$$(\Delta \Delta E_{interface, Y})_X = (\Delta E_{interface, Y})_X - (\Delta E_{interface, O})_{WT} \quad (4)$$

where X represents WT or any designed receptor variant and Y = O or C and corresponds to the open and closed conformation, respectively.

The Boltzmann factors describing the probability of a variant X to occupy the dimer state in a specific conformation  $((PD_Y)_X)$ , dimerization

propensity) relative to WT can be derived as follows:

$$(PD_Y)_X = \exp(- (0.5((\Delta \Delta E_{interface, Y})_X) / RT) \quad (5)$$

where the 0.5 factor roughly converts Rosetta Energy Units to kcal/mol. RT is the thermal scaling factor and equal to 0.593 kcal.mol<sup>-1</sup>.

The sum of the Boltzmann factors for the open and closed conformation are calculated in the inactive and active state (reported in Supplementary Table 2) and provides an indication whether a variant has a lower or higher propensity to occupy the dimer state than WT.

### Alpha-Fold predictions

The Alphafold2-multimer<sup>38</sup> algorithm implemented by ColabFold<sup>39</sup> was applied to generate Alphafold2 models. The ColabFold implementation enables to provide custom structural templates to the program. Steric clashes in AF2 models of CXCR4 bound to Gi or  $\beta$ -arrestin were calculated using the ChimeraX software<sup>46</sup>.

### Reagents and plasmids

CXCL12 was purchased from Cedarlane. Forskolin, isobutylmethyl xanthine (IBMX), AVP, and met-enkephalin were purchased from Sigma. The following plasmids were already described: HA-CXCR4<sup>47</sup>,  $\beta$ -arrestin-2-LucII<sup>48</sup>,  $\beta$ -arrestin-2-YFP<sup>49</sup>,  $G\alpha_{i1}$ -91RLucII<sup>47</sup>,  $G\alpha_{s}$ -117RLucII<sup>50</sup>,  $G\alpha_{oA}$ -91RLucII<sup>51</sup>, GFP10-G<sub>Y1</sub><sup>52</sup>, GFP10-G<sub>Y2</sub><sup>53</sup>, GFP10-EPAC-RLucII<sup>54</sup> and rGFP-CAAX<sup>33</sup>. The cloning of CXCR4-RLuc and CXCR4-YFP in pcDNA3.1 was previously described<sup>11</sup>. In the present study, CXCR4-RLuc and CXCR4-YFP were amplified and modified by PCR at the N-terminal end to add a myc epitope (EQKLISEEDL) or a HA epitope (YPYDVPDYA), respectively. Myc-CXCR4-RLuc and HA-CXCR4-YFP segments were then subcloned into pIREShyg3 (BsrGI/AflIII) and pIRESpuro3 (NheI/AflIII) respectively. The human  $\mu$ OR and V2R were amplified with a SNAP tag at their N-terminal (NEB) and subcloned in the pcDNA4/TO plasmid (Invitrogen). All the mutants were obtained by site-directed mutagenesis using the extension of overlapping gene segments by PCR technique and validated by sequencing.

### Cell culture and Transfections

Human Embryonic Kidney 293 T cells (HEK293T cells) were cultured using Dulbecco's Modified Eagle Medium (DMEM with L-glutamine from Wisent) supplemented with 10% vol/vol Fetal Bovine Serum (Wisent). The day before transfection, 600,000 cells were seeded in 6-well plates. Transient transfections were performed using Polyethylenimine 25 Kd linear (PEI, Polysciences) as transfection agent, with a 3:1 PEI:DNA ratio.

U87.MG cells stably expressing HA-CXCR4 and HA-CXCR4-W195<sup>5,34</sup>L mutant (U87.CXCR4 and U87.CXCR4-W195<sup>5,34</sup>L, respectively) were established by transfection of pIRES-HA-CXCR4 and pIRES-HA-CXCR4-W195<sup>5,34</sup>L and subsequent cell sorting for equivalent surface expression levels using Alexa Fluor 488-labeled anti-HA antibody 1:1000 (Biolegend, clone 16B12,). U87 cells were grown in Dulbecco's modified Eagle medium (Thermo Fischer Scientific) supplemented with 15% vol/vol fetal bovine serum and penicillin/streptomycin (100 Units/ml and 100  $\mu$ g/ml) (Thermo Fischer Scientific). U87.CXCR4 and U87.CXCR4-W195<sup>5,34</sup>L cell lines were maintained under puromycin (0.5  $\mu$ g/ml) selective pressure.

Cells were regularly tested for mycoplasma contamination (PCR Mycoplasma Detection kit, abm). If contamination was detected, cells were discarded and replaced from a frozen mycoplasma-free cell stock of lower passage.

### BRET measurements

Two different BRET configurations were used in this study: BRET<sub>480-YFP</sub> and BRET<sub>400-GFP10</sub>. BRET<sub>480-YFP</sub> uses RLuc as energy donor and YFP as the acceptor (excitation peak at 488 nm) and coelenterazine-h (coel-h, Nanolight Technology) was used as the substrate (emission peak at

480 nm). BRET<sub>400-GFP10</sub> uses RLucII as energy donor and GFP10 as the acceptor (excitation peak at 400 nm) and coelenterazine-400a (coel-400a, Nanolight Technology) was used as the substrate (emission peak at 400 nm). Enhanced bystander BRET (ebBRET) uses RLucII as energy donor, rGFP as the acceptor and is detected using the BRET<sub>480-YFP</sub> configuration and Prolume Purple as the substrate (NanoLight Technology). BRET was measured with a Mithras LB940 multimode microplate reader (Berthold Technologies) equipped with a BRET<sub>480-YFP</sub> filters set (donor 480 ± 20 nm and acceptor 530 ± 20 nm filters) or a Tristar microplate reader equipped either with a BRET<sub>480-YFP</sub> filters set (donor 480 ± 20 nm and acceptor 530 ± 20 nm filters) or a BRET<sub>400-GFP10</sub> filters set (donor 400 ± 70 nm and acceptor 515 ± 20 nm filters). All the BRET experiments were performed at room temperature.

**CXCR4 dimerization.** Cells were transfected with HA-CXCR4-YFP and myc-CXCR4-RLuc, WT or mutant, and seeded in 96-well plates (Cultuplate, PerkinElmer) coated with poly-L-ornithine (Sigma Aldrich) 24 h after transfection. The following day, cells were washed with Hank's Balanced Salt Solution (HBSS, Invitrogen) and incubated in HBSS supplemented with 0.1% BSA. Cells were treated with CXCL12 at the indicated times and concentrations. Coel-h (2.5 μM) was added 10 min before reading.

**G protein activation.** Cells were transfected with the receptor (CXCR4, V2R or μOR) and a three-component BRET-based biosensor: Gα1-RLucII (CXCR4), Gαs117RLucII (V2R) or Gαo-RLucII (μOR) and Gβ1, and Gy1-GFP10 (V2R and μOR) or Gy2-GFP10 (CXCR4). BRET was then monitored as described above using coel-400a as a substrate. The dissociation of the Gα and Gβ/Gy subunits after activation leads to a decrease in the BRET ratio.

**β-arrestin engagement (direct interaction).** Cells were transfected with CXCR4-RLuc and β-arrestin-2-YFP. BRET was monitored as described above using Coel-h as a substrate.

**β-arrestin engagement (ebBRET).** Cells were transfected with the receptor (HA-CXCR4, SNAP-V2R or SNAP- μOR), β-arrestin-2-RLucII, and CAAX-rGFP. BRET was monitored as described above using Prolume Purple (1.3 μM) as a substrate.

**cAMP accumulation.** Cells were transfected with HA-CXCR4 and the BRET-based biosensor GFP10-EPAC1-RLucII. BRET was then monitored as described above with the cells first washed with HBSS and then incubated in HBSS + 0.1% BSA containing 500 μM isobutylmethyl xanthine (IBMX), without or with 10 μM forskolin for 15 min, followed by agonist stimulation.

### CXCR4 phosphorylation

HEK293 cells were seeded in six-well plates and transfected with either HA-CXCR4-WT or HA-CXCR4-W195L. 48 h later, cells were washed with phosphate-buffered saline (PBS) and serum starved in HBSS for 2 h. Cells were then stimulated with 200 nM CXCL12 or vehicle for 30 min before washing with ice-cold PBS and lysed with RIPA lysis buffer (50 mM Tris-HCl pH 7.6, 150 mM NaCl, 1% NP-40, 0.5% sodium deoxycholate, 0.1% SDS complemented with Halt™ Protease Inhibitor Cocktail (Thermo Fischer) and PhosSTOP phosphatase inhibitor (Roche)). Cell lysates were cleared by centrifugation at 14 000 rpm for 15 min at 4 °C and the supernatant was mixed with 2X SDS sample buffer. Samples were then analyzed by electrophoresis on a 10% SDS-polyacrylamide gel, transferred to a PVDF membrane, and immunoblotted with the following antibodies: pS324/pS325-CXCR4 phospho-CXC Chemokine Receptor 4 rabbit 1:1000 (7TM antibodies), anti-HA 3F10 rat monoclonal 1:1000 (Roche) and anti-GAPDH rabbit monoclonal 1:5000 (Cell Signaling) antibodies. Membranes were then washed and incubated with HRP-coupled secondary donkey anti-

rabbit IgG (GE healthcare) or goat anti-rat IgG (Sigma) antibodies, and the images were acquired and analyzed using a Chemidoc Imaging System (Bio-Rad). The unprocessed scans of the Western blots are presented in Supplementary Fig. 16.

### ERK phosphorylation assay monitored by HTRF

U87, U87.CXCR4 and U87.CXCR4-W195<sup>5,34</sup>L cells were seeded in 96-well plates (1 × 10<sup>4</sup> cell/well). 72 h later, culture medium was replaced with FBS-free, phenol-red free DMEM. After 4-hour starvation, CXCL12 was added to cells at a final concentration of 10 nM and incubated for the indicated times. ERK phosphorylation was evaluated using a Homogenous Time-Resolved FRET (HTRF)-based Phospho-ERK (Thr202/Tyr204) cellular kit (Cisbio, 64AERPET). Cells were lysed for 30 min with the lysis buffer provided and incubated for 2 h with pERK1/2-specific antibodies conjugated with Eu<sup>3+</sup>-cryptate donor and d2 acceptor at recommended dilutions. HTRF was measured with Tecan GENios Pro plate reader equipped with 612 ± 10 (donor) and 670 ± 25 (acceptor) filters. HTRF ratio was calculated as follows:

$$\text{Ratio} = \frac{A_{670}}{D_{612}} \times 10000 \quad (6)$$

Where A<sub>670</sub> = emission at 670 nm (RFU) and D<sub>612</sub> = emission at 612 nm (RFU).

### Elisa

To control for the cell surface expression of HA-CXCR4, HA-CXCR4-YFP, and myc-CXCR4-RLuc, and their respective mutant receptors, ELISA were performed in parallel of BRET experiments, using an antibody directed at the extracellular epitope (HA or Myc). 24 h after transfection, cells were seeded in 24-well plates coated with poly-L-ornithine. The day of the experiment, media was removed and a solution of PBS with 3.7% paraformaldehyde was added for 5 min. Cells were then washed 3 times with Phosphate-Buffered Saline (PBS). Blocking solution (PBS + 1% BSA) was added for 45 min then replaced by PBS + 1% BSA containing HA mouse monoclonal 12CA5 antibody 1:1000 (Santacruz) or Myc-tag rabbit 71D10 mAb 1:1000 (Cell Signaling) for 45 min. After antibody addition, cells were washed three times with PBS and incubated 45 min with PBS + 1% BSA containing an HRP-tagged sheep anti-mouse or donkey anti-rabbit IgG antibodies 1:2000 (GE healthcare). After labeling, cells were washed three times with PBS and incubated with SigmaFastOPD (SigmaAldrich) at room temperature. Reaction was stopped using 3 N HCl, supernatant transferred in a 96-well plate, and reading was performed using a Spectramax multimode microplate reader (Molecular Devices) at 492 nm.

### Flow cytometry

Endogenous CXCR4 expression on the surface of HEK and U87 cells was monitored by flow cytometry using CXCR4-specific phycoerythrin-conjugated mAb 12G5 1:20 or the corresponding isotype control (R&D Systems) in a BD FACS LSR Fortessa cytometer (BD Biosciences). U87 was chosen as the cellular background for the absence of endogenous CXCR4 and ACKR3, as previously demonstrated<sup>55,56</sup>. U87 cells stably expressing the HA-tagged CXCR4 or variants thereof were obtained following puromycin selection and subsequent single-cell sorting using BD FACS Aria II cell sorter (BD Biosciences). The equivalent surface expression level was verified using an Alexa Fluor 488-conjugated anti-HA-tag mAb 1:1000 (Biolegend, clone 16B12). Flow cytometry data were analyzed using FlowJo V10 software.

### Data and statistical analysis

All data were analyzed using GraphPad Prism (GraphPad Software, Inc). Statistical significance between the groups was assessed with unpaired *t* test, a one-way ANOVA followed by Tukey's post hoc test, or a two-way ANOVA followed by Šidák's multiple comparisons test.

## Reporting summary

Further information on research design is available in the Nature Research Reporting Summary linked to this article.

## Data availability

The data supporting the findings in this study are present within the article and its Supplementary Information files, and are available from the corresponding authors upon request. All the biosensors can be obtained and used without limitations for academic non-commercial studies through regular Material Transfer Agreements and can be requested by email from Michel Bouvier. The following PDB entries were used for modeling: [3ODU](#), [4XTI](#), [6DDF](#), [7DW9](#), [4ZJW](#), [3SN6](#), and [1GIA](#). Source data are provided with this paper.

## Code availability

Examples with commands/inputs/outputs/code for running the symmetry docking, clustering analysis, Gi &  $\beta$ -arresting docking, and AlphaFold are provided in the github repository: <https://github.com/barth-lab/QUESTS>.

## References

1. Felce, J. H., Davis, S. J. & Klenerman, D. Single-molecule analysis of G protein-coupled receptor stoichiometry: approaches and limitations. *Trends Pharm. Sci.* **39**, 96–108 (2018).
2. Felce, J. H. et al. Receptor quaternary organization explains G protein-coupled receptor family structure. *Cell Rep.* **20**, 2654–2665 (2017).
3. Bouvier, M., Heveker, N., Jockers, R., Marullo, S. & Milligan, G. BRET analysis of GPCR oligomerization: newer does not mean better. *Nat. Methods* **4**, 3–4 (2007).
4. Milligan, G. & Bouvier, M. Methods to monitor the quaternary structure of G protein-coupled receptors. *FEBS J.* **272**, 2914–2925 (2005).
5. Huang, J., Chen, S., Zhang, J. J. & Huang, X. Y. Crystal structure of oligomeric beta1-adrenergic G protein-coupled receptors in ligand-free basal state. *Nat. Struct. Mol. Biol.* **20**, 419–425 (2013).
6. Manglik, A. et al. Crystal structure of the micro-opioid receptor bound to a morphinan antagonist. *Nature* **485**, 321–326 (2012).
7. Wu, B. et al. Structures of the CXCR4 chemokine GPCR with small-molecule and cyclic peptide antagonists. *Science* **330**, 1066–1071 (2010).
8. Liang, Y. et al. Organization of the G protein-coupled receptors rhodopsin and opsin in native membranes. *J. Biol. Chem.* **278**, 21655–21662 (2003).
9. Fotiadis, D. et al. Atomic-force microscopy: Rhodopsin dimers in native disc membranes. *Nature* **421**, 127–128 (2003).
10. Armando, S. et al. The chemokine CXCR4 and CC2 receptors form homo- and heterooligomers that can engage their signaling G-protein effectors and betaarrestin. *FASEB J.* **28**, 4509–4523 (2014).
11. Percherancier, Y. et al. Bioluminescence resonance energy transfer reveals ligand-induced conformational changes in CXCR4 homo- and heterodimers. *J. Biol. Chem.* **280**, 9895–9903 (2005).
12. Whorton, M. R. et al. A monomeric G protein-coupled receptor isolated in a high-density lipoprotein particle efficiently activates its G protein. *Proc. Natl Acad. Sci. USA* **104**, 7682–7687 (2007).
13. Whorton, M. R. et al. Efficient coupling of transducin to monomeric rhodopsin in a phospholipid bilayer. *J. Biol. Chem.* **283**, 4387–4394 (2008).
14. Meral, D. et al. Molecular details of dimerization kinetics reveal negligible populations of transient  $\mu$ -opioid receptor homodimers at physiological concentrations. *Sci. Rep.* **8**, 7705 (2018).
15. Mondal, S. et al. Membrane driven spatial organization of GPCRs. *Sci. Rep.* **3**, 2909 (2013).
16. Gahbauer, S. & Bockmann, R. A. Membrane-mediated oligomerization of g protein coupled receptors and its implications for GPCR function. *Front. Physiol.* **7**, 494 (2016).
17. Kobayashi, H., Ogawa, K., Yao, R., Lichtarge, O. & Bouvier, M. Functional rescue of beta-adrenoceptor dimerization and trafficking by pharmacological chaperones. *Traffic* **10**, 1019–1033 (2009).
18. Salahpour, A. et al. Homodimerization of the beta2-adrenergic receptor as a prerequisite for cell surface targeting. *J. Biol. Chem.* **279**, 33390–33397 (2004).
19. Han, Y., Moreira, I. S., Urizar, E., Weinstein, H. & Javitch, J. A. Allosteric communication between protomers of dopamine class A GPCR dimers modulates activation. *Nat. Chem. Biol.* **5**, 688–695 (2009).
20. Guo, W., Shi, L., Filizola, M., Weinstein, H. & Javitch, J. A. Crosstalk in G protein-coupled receptors: changes at the transmembrane homodimer interface determine activation. *Proc. Natl Acad. Sci. USA* **102**, 17495–17500 (2005).
21. Fung, J. J. et al. Ligand-regulated oligomerization of beta(2)-adrenoceptors in a model lipid bilayer. *EMBO J.* **28**, 3315–3328 (2009).
22. Yao, X. J. et al. The effect of ligand efficacy on the formation and stability of a GPCR-G protein complex. *Proc. Natl. Acad. Sci. USA* **106**, 9501–9506 (2009).
23. Martinez-Munoz, L. et al. Separating actin-dependent chemokine receptor nanoclustering from dimerization indicates a role for clustering in CXCR4 signaling and function. *Mol. Cell* **70**, 106–119 e10 (2018).
24. Das, R. & Baker, D. Macromolecular modeling with rosetta. *Annu Rev. Biochem.* **77**, 363–382 (2008).
25. Procko, E. et al. A computationally designed inhibitor of an Epstein-Barr viral Bcl-2 protein induces apoptosis in infected cells. *Cell* **157**, 1644–1656 (2014).
26. Silva, D. A. et al. De novo design of potent and selective mimics of IL-2 and IL-15. *Nature* **565**, 186–191 (2019).
27. Joh, N. H. et al. De novo design of a transmembrane Zn(2) (+)-transporting four-helix bundle. *Science* **346**, 1520–1524 (2014).
28. Wang, Y. & Barth, P. Evolutionary-guided de novo structure prediction of self-associated transmembrane helical proteins with near-atomic accuracy. *Nat. Commun.* **6**, 7196 (2015).
29. Yin, H. et al. Computational design of peptides that target transmembrane helices. *Science* **315**, 1817–1822 (2007).
30. Qin, L. et al. Structural biology. Crystal structure of the chemokine receptor CXCR4 in complex with a viral chemokine. *Science* **347**, 1117–1122 (2015).
31. Feng, X., Ambia, J., Chen, K. M., Young, M. & Barth, P. Computational design of ligand-binding membrane receptors with high selectivity. *Nat. Chem. Biol.* **13**, 715–723 (2017).
32. Angers, S. et al. Detection of beta 2-adrenergic receptor dimerization in living cells using bioluminescence resonance energy transfer (BRET). *Proc. Natl Acad. Sci. USA* **97**, 3684–3689 (2000).
33. Namkung, Y. et al. Monitoring G protein-coupled receptor and beta-arrestin trafficking in live cells using enhanced bystander BRET. *Nat. Commun.* **7**, 12178 (2016).
34. Luttrell, L. M. et al. Manifold roles of  $\beta$ -arrestins in GPCR signaling elucidated with siRNA and CRISPR/Cas9. *Sci. Signal.* **11**, eaat7650 (2018).
35. Wootten, D. et al. The extracellular surface of the GLP-1 receptor is a molecular trigger for biased agonism. *Cell* **165**, 1632–1643 (2016).
36. Manglik, A. et al. Crystal structure of the  $\mu$ -opioid receptor bound to a morphinan antagonist. *Nature* **485**, 321–326 (2012).
37. Vilardaga, J. P. et al. Conformational cross-talk between alpha2A-adrenergic and mu-opioid receptors controls cell signaling. *Nat. Chem. Biol.* **4**, 126–131 (2008).



38. Holgersen, E. M. et al. Transcriptome-wide off-target effects of steric-blocking oligonucleotides. *Nucleic Acid Ther.* **31**, 392–403 (2021).
39. Mirdita, M. et al. ColabFold: making protein folding accessible to all. *Nat. Methods* **19**, 679–682 (2022).
40. Kufareva, I. et al. A novel approach to quantify G-protein-coupled receptor dimerization equilibrium using bioluminescence resonance energy transfer. *Methods Mol. Biol.* **1013**, 93–127 (2013).
41. Manglik, A. et al. Structure-based discovery of opioid analgesics with reduced side effects. *Nature* **537**, 185–190 (2016).
42. McInnes, L., Healy, J. & Astels, S. hdbSCAN: Hierarchical density based clustering. *J. Open Source Softw.* **2**, 205 (2017).
43. Chen, K. Y., Sun, J., Salvo, J. S., Baker, D. & Barth, P. High-resolution modeling of transmembrane helical protein structures from distant homologues. *PLoS Comput. Biol.* **10**, e1003636 (2014).
44. Barth, P., Schonbrun, J. & Baker, D. Toward high-resolution prediction and design of transmembrane helical protein structures. *Proc. Natl Acad. Sci. USA* **104**, 15682–15687 (2007).
45. Chen, K. Y., Zhou, F., Fryszczyn, B. G. & Barth, P. Naturally evolved G protein-coupled receptors adopt metastable conformations. *Proc. Natl Acad. Sci. USA* **109**, 13284–13289 (2012).
46. Pettersen, E. F. et al. UCSF ChimeraX: Structure visualization for researchers, educators, and developers. *Protein Sci.* **30**, 70–82 (2021).
47. Quoyer, J. et al. Pepducin targeting the C-X-C chemokine receptor type 4 acts as a biased agonist favoring activation of the inhibitory G protein. *Proc. Natl Acad. Sci. USA* **110**, E5088–E5097 (2013).
48. Paradis, J. S. et al. Receptor sequestration in response to beta-arrestin-2 phosphorylation by ERK1/2 governs steady-state levels of GPCR cell-surface expression. *Proc. Natl Acad. Sci. USA* **112**, E5160–E5168 (2015).
49. Khoury, E., Nikolajev, L., Simaan, M., Namkung, Y. & Laporte, S. A. Differential regulation of endosomal GPCR/beta-arrestin complexes and trafficking by MAPK. *J. Biol. Chem.* **289**, 23302–23317 (2014).
50. Thomsen, A. R. B. et al. GPCR-G protein-β-arrestin super-complex mediates sustained G protein signaling. *Cell* **166**, 907–919 (2016).
51. Busnelli, M. et al. Functional selective oxytocin-derived agonists discriminate between individual G protein family subtypes. *J. Biol. Chem.* **287**, 3617–3629 (2012).
52. Galés, C. et al. Probing the activation-promoted structural rearrangements in preassembled receptor-G protein complexes. *Nat. Struct. Mol. Biol.* **13**, 778–786 (2006).
53. Gales, C. et al. Real-time monitoring of receptor and G-protein interactions in living cells. *Nat. Methods* **2**, 177–184 (2005).
54. Zimmerman, B. et al. Differential beta-arrestin-dependent conformational signaling and cellular responses revealed by angiotensin analogs. *Sci. Signal.* **5**, ra33 (2012).
55. Szpakowska, M. et al. Human herpesvirus 8-encoded chemokine vCCL2/vMIP-II is an agonist of the atypical chemokine receptor ACKR3/CXCR7. *Biochem. Pharm.* **114**, 14–21 (2016).
56. Szpakowska, M. et al. Mutational analysis of the extracellular disulphide bridges of the atypical chemokine receptor ACKR3/CXCR7 uncovers multiple binding and activation modes for its chemokine and endogenous non-chemokine agonists. *Biochem. Pharm.* **153**, 299–309 (2018).
- Luxembourg National Research Fund (Pathfinder “Interceptor” 19/14260467, INTER/FWO “Nanokine” grant 15/10358798, INTER/FNRS grants 20/15084569, and PoC “Megakine” 19/14209621) and F.R.S.-FNRS-Télévie (grants 7.4593.19, 7.4529.19 and 7.8504.20). J.S.P. had studentships from the ‘Groupe de Recherche Universitaire sur le Médicament’ and ‘la Faculté des Études Supérieures et postdoctorales de l’Université de Montréal’. R.E.J. was supported by a Marie Curie Postdoctoral Fellowship and received funding for this project from the European Union’s Horizon 2020 research and innovation programme under the Marie Skłodowska-Curie grant agreement No 588412. B.S. holds a studentship from the ‘Fond de Recherche du Québec-Santé’ (FRQ-S). B.M. had a fellowship from the ‘Fondation pour la Recherche Médicale (France)’. M.B. Holds a Canada Research Chair in Signal Transduction and Molecular Pharmacology. The authors thank Dr. Monique Lagacé for her critical reading of the manuscript.

## Author contributions

P.B., A.C., and M.B. designed the study; X.F., R.E.J., and P.B. performed the modeling and design calculations; J.S.P., B.M., B.S., M.S., M.H., N.D.B., and F.M.H. performed the experiments under the supervision of M.B., A.C., and M.J.S.; all authors analyzed the data; P.B., J.S.P., X.F., B.S., and M.B. wrote the manuscript. B.M., R.E.J., and B.S. made equal contributions.

## Competing interests

M.B. is the president of the scientific advisory Board of Domain Therapeutics, which licensed some of the BRET-based biosensors used in the present study for their commercial use. P.B. holds patents and provisional patent applications in the field of engineered T-cell therapies and protein design. The other authors declare no competing interests.

## Additional information

**Supplementary information** The online version contains supplementary material available at <https://doi.org/10.1038/s41467-022-34382-7>.

**Correspondence** and requests for materials should be addressed to Michel Bouvier or Patrick Barth.

**Peer review information** *Nature Communications* thanks the anonymous reviewer(s) for their contribution to the peer review of this work. Peer reviewer reports are available.

**Reprints and permissions information** is available at <http://www.nature.com/reprints>

**Publisher’s note** Springer Nature remains neutral with regard to jurisdictional claims in published maps and institutional affiliations.

**Open Access** This article is licensed under a Creative Commons Attribution 4.0 International License, which permits use, sharing, adaptation, distribution and reproduction in any medium or format, as long as you give appropriate credit to the original author(s) and the source, provide a link to the Creative Commons license, and indicate if changes were made. The images or other third party material in this article are included in the article’s Creative Commons license, unless indicated otherwise in a credit line to the material. If material is not included in the article’s Creative Commons license and your intended use is not permitted by statutory regulation or exceeds the permitted use, you will need to obtain permission directly from the copyright holder. To view a copy of this license, visit <http://creativecommons.org/licenses/by/4.0/>.

© The Author(s) 2022

## Acknowledgements

This work was supported by a Swiss National Science Foundation grant (31003A\_182263 and 310030\_208179), a Novartis Foundation for medical-biological Research grant 21C195, a Swiss Cancer Research grant (KFS-4687-02-2019), a National Institute of Health grant (1R01GM097207), funds from EPFL, and the Ludwig Institute for Cancer Research to P.B., and a grant from the Canadian Institute for health Research (CIHR) (Foundation grant #148431) to M.B. M.J.S. and A.C. were supported by the